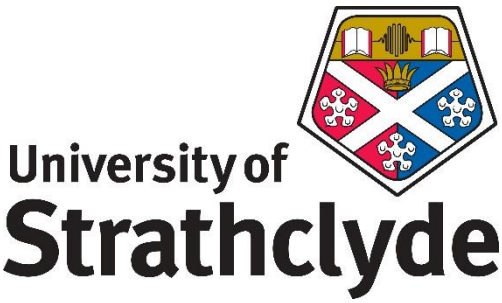

α_V Integrin Antagonists for the Treatment of Idiopathic Pulmonary Fibrosis

PhD Thesis

James Thompson

Abstract

Herein are described two investigations of α_v integrin antagonists for the treatment of Idiopathic Pulmonary Fibrosis (IPF). Previous studies have implicated several α_V-containing integrins as having an important role in the onset of fibrotic disease in several organs.

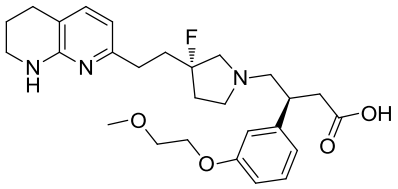

1

Figure 1 *Candidate molecule* ***1***

In the first of the projects described, the unusual properties of **1 (Figure 1)** have been investigated. Compound **1** is an $\alpha_V\beta_6$ antagonist, a candidate molecule for IPF. This molecule possesses greater permeability than its diastereomers, and it was hypothesised that this is the result of a conformational effect. In particular, the propensity for these, and related compounds, to form a transient intramolecular hydrogen bond (IMHB) when permeating, leading to shielding of the polarity of the molecule, has been investigated.

Several close analogues of **1** have been synthesised, which imply a conformational effect is present, and nuclear magnetic resonance (NMR) investigations, in particular using ^{15}N NMR, give evidence for IMHB formation. The ^{15}N NMR spectroscopic data gives a quantitative indication of the differing extent of IMHB formation between compounds. Other similar $\alpha_V\beta_6$ antagonists have been investigated using this approach, helping to validate this method, as their ^{15}N NMR shifts correlate with their permeability, relative to their lipophilicity. The results observed have been corroborated by computational calculations.

The extent of IMHB formation of a group of previously synthesised α_V integrin antagonists has been predicted using these calculations, and ^{15}N NMR measurements have been compared to the predictions. The success of these predictions shows that, to an extent, it is possible to predict the extent of IMHB formation, which will help

future medicinal chemistry efforts where designing passively permeable compounds is a challenge.

In the second project, structure-activity relationship (SAR) studies on a series of tetrahydroazepine compounds as $\alpha_V\beta_1$ integrin antagonists were performed **(Figure 2)**. The $\alpha_V\beta_1$ integrin appears to have a role in tissue fibrosis, although a relative paucity of investigations on this integrin have been carried out, largely due to the lack of selective tool compounds available.

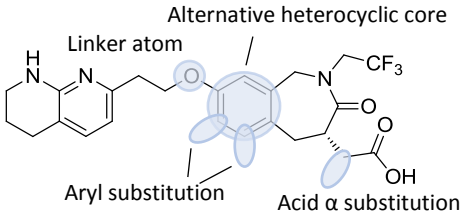

***Figure 2** The areas modified on the series of $\alpha_V\beta_1$ integrin antagonists*

Beginning from a previous series of orally bioavailable $\alpha_V\beta_3$ and $\alpha_V\beta_5$ selective compounds, the aims of this work were to obtain potency at the $\alpha_V\beta_1$ integrin, whilst moving the series into previously unexemplified chemical space, and ideally to also obtain selectivity over the other integrins, particularly $\alpha_V\beta_3$ and $\alpha_V\beta_5$. This work has been computationally guided, using an $\alpha_V\beta_1$ homology model to first rationalise the potency of compounds, then latterly to design new analogues.

A group of analogues with different aromatic cores and different linker atoms have been synthesised, each with a bespoke route. It has been found that it is possible to include heterocycles within the core of the molecule, but changing the ether linkage to the chain to a carbon atom is not tolerated. The potency of these compounds could be rationalised by evaluation of the docked conformations of these compounds in the homology model.

Consequently, the docking model was used prospectively, in order to design compounds that were selective for $\alpha_V\beta_1$ over $\alpha_V\beta_3$, by comparing the receptor of the $\alpha_V\beta_3$ crystal structure with the $\alpha_V\beta_1$ homology model. Late-stage modifications were carried out to rapidly generate a range of substitution at two different positions. Unfortunately, however, selectivity for the $\alpha_V\beta_1$ has remained elusive, and this part of the work has highlighted the limitations of the use of homology model docking in ligand design.

Author declaration

This thesis is the result of the author's original research. It has been composed by the author and has not been previously submitted for examination which has led to the award of a degree.

Signed: Date:

Acknowledgements

I owe a huge debt of thanks to John Pritchard for his continual support, guidance and friendship as my supervisor throughout my time at GSK, and for his thoughtful suggestions and ideas. I would also like to thank Billy Kerr for his enthusiastic supervision, careful proof reading of my reports, and for an enjoyable and useful secondment to his laboratory. I am grateful to both Billy and Harry Kelly for the opportunity to join the collaborative PhD programme.

My thanks go to Stephen Richards for his tremendous help with NMR spectroscopy, particularly for the ^{15}N NMR work. He has shown real generosity with his time in supporting my projects. I am also indebted to all those who have helped me with the computational work, in particular Anna Gruszka and Peter Pogány, who have been very patient in teaching me to use the software and for much troubleshooting. I am grateful to those who have run biological and physicochemical assays for me, in particular James Rowedder and Iain Reid, and to those who have provided technical support.

I am also thankful to all those I have shared a lab with during my studies; for many tips and tricks passed on, many helpful and creative suggestions to solve synthetic problems, and for their company in the lab.

Finally, to my wonderful wife Maria, whose extraordinary kindness, patience and love have enabled me to devote myself to this work in a way that I could not have done without her.

"Great are the works of the Lord; studied by all who delight in them" Psalm 111:2

Table of Contents

Abbreviations

Ac – Acetyl

ALK5 – Activin receptor-like kinase 5

AMP – Artificial membrane permeability

Aq – Aqueous

AUC – Area under the curve

BINAP – 2,2'-Bis(diphenylphosphino)-1,1'-binaphthyl

Boc – *tert*-Butyloxycarbonyl

Br – Broad

Bu – Butyl

Calc – Calculated

CHI – Chromatographic hydrophobicity index

Cl – Clearance

cm^{-1} – Reciprocal centimetre

CMBP – (Cyanomethylene)tributylphosphorane

COD – 1,5-Cyclooctadiene

COSY – Correlation spectroscopy

CSD – Cambridge structural database

d – Doublet

DBA – Dibenzylideneacetone

DCA – Dicyclohexylamine

de – Diastereomeric excess

DFT – Density functional theory

DIPEA – *N,N*-Diethyl-*N*-isopropylpropan-2-amine

DMA – *N,N*-Dimethylacetamide

DMAP – 4-Dimethylaminopyridine

DMF – *N,N*-Dimethylformamide

DMSO – Dimethyl sulfoxide

ECM – Extracellular matrix

ee – Enantiomeric excess

ESI – Electrospray ionisation

Et – Ethyl

F – Oral bioavailability

FDA – Food and Drug Administration

FVC – Forced vital capacity

g – Grams

GSK – GlaxoSmithKline

h – Hours

HATU – 1-[Bis(dimethylamino)methylene]-1H-1,2,3-triazolo[4,5-b]pyridinium 3-oxide hexafluorophosphate

HBD – Hydrogen bond donor

HMBC – Heteronuclear multiple bond correlation

HMDS – Hexamethyldisilazide

HPLC – High performance liquid chromatography

HRMS – High resolution mass spectrometry

HSQC – Heteronuclear single quantum coherence

HTS – High throughput screening

Hz – Hertz

IMHB – Intramolecular hydrogen bond

IPF – Idiopathic pulmonary fibrosis

IR – Fourier transform infra-red spectroscopy

IV – Intravenously

J – Coupling constant

LAP – Latently-associated peptide

LCMS – Liquid-chromatography mass spectrometry

LPA – Lysophosphatidic acid

m – Multiplet

M – Concentration in moles / dm^3

mTOR – Mammalian target of rapamycin

MDAP – Mass-directed auto-preparative HPLC

MDCK – Madin-Darby Canine Kidney

Me – Methyl

Mg – Milligrams

min – Minutes

ml – Millilitres

mmol – Millimoles

MOE – Molecular operating environment

mp – Melting point

MS – Molecular sieves

NBS – *N*-Bromosuccinimide

NIS – *N*-Iodosuccinimide

NFSI – *N*-Fluorobenzenesulfonamide

nm – Nanometre

NMR – Nuclear magnetic resonance

nOe – Nuclear Overhauser effect

pH – (-Log) value of $[H^+]$

PI3K – Phosphatidylinositol-3-kinase

pIC_{50} – Log value of concentration of inhibitor required to inhibit cellular activity by 50 %

PK – Pharmacokinetic

PMB – *para*-Methoxybenzyl

PO – *Per os*

Pr – Propyl

q – Quartet

quint – Quintet

RGD – Arginine – glycine– aspartic acid tripeptide sequence

RMSD – Root mean square deviation

ro5 – Lipinski's rule of five

rt – Room temperature

s – Singlet

SAR – Structure-activity relationship

SDL – Specificity-determining loop

α-SMA – α-Smooth muscle actin

SMAD - The combination of *Caenorhabditis elegans SMA* and the *Drosophila MAD*, 'mothers against decapentaplegic' genes

t – Triplet

$T_{1/2}$ – Half-life

t_R – Retention time

TBAB – Tetrabutylammonium bromide

TBAF – Tetrabutylammonium fluoride

TBME – *tert*-Butyl methyl ether

TBS - *tert*-Butyldimethylsilyl

TEMPO – (2,2,6,6-Tetramethylpiperidin-1-yl)oxyl

TFA – Trifluoroacetic acid

TGFβ – Transforming growth factor β

THF – Tetrahydrofuran

TLC – Thin-layer chromatography

TPSA – Topological polar surface area

UV – Ultraviolet radiation

VCD – Vibrating circular dichroism

Chapter 1: Introduction to IPF, integrins and RGD mimetics

1.1 Nature and incidence of pulmonary fibrosis

Nearly 45 % of deaths in the developed world are the result of a chronic fibroproliferative disease, the excessive scarring of tissue.[1] However, explorations of the mechanism and causes of the disease have only begun to be investigated relatively recently. All fibrosis follows a similar sequence of events, namely primary injury to the cell, followed by the activation of effector cells, resulting in the elaboration of extracellular matrix (ECM) proteins, followed by further deposition of ECM proteins and their chronic production.[2] This build-up of ECM, primarily collagen, leads to increased tissue stiffness, and gradual loss of function, which may eventually result in organ failure.

The initial injury event could be exposure to a toxic substance, such as smoking or asbestos,[3] or from a physical impact. Unlike in the case of fibrosis of other organs,[4] the scarring caused in idiopathic pulmonary fibrosis (IPF) is seemingly irreversible, and destruction of the architecture in the periphery of the lungs means that transplant is the only means by which patients regain proper lung function. However, this is only possible for a minority of patients due to a lack of available donors,[2] and those who have undergone lung transplant only survive for an average of three years after transplantation.[5] Honeycombing of the lung occurs (shown by the high resolution computed tomography image in **Figure 3**),[6] and fibrotic deposits in the interstitial space in the lung, combined with epithelial cell apoptosis, gradually reduces lung function.[7] The symptoms of the disease are a dry cough, clubbing of the tips of fingers and toes, and dyspnoea.[8] The disease can remain asymptomatic for 2

– 3 years, and diagnosis is often only made 6 – 24 months after the onset of symptoms.[9] However, it is anticipated that novel treatments for IPF will result in earlier diagnosis, in conjunction with refinement of the diagnostic criteria.[10]

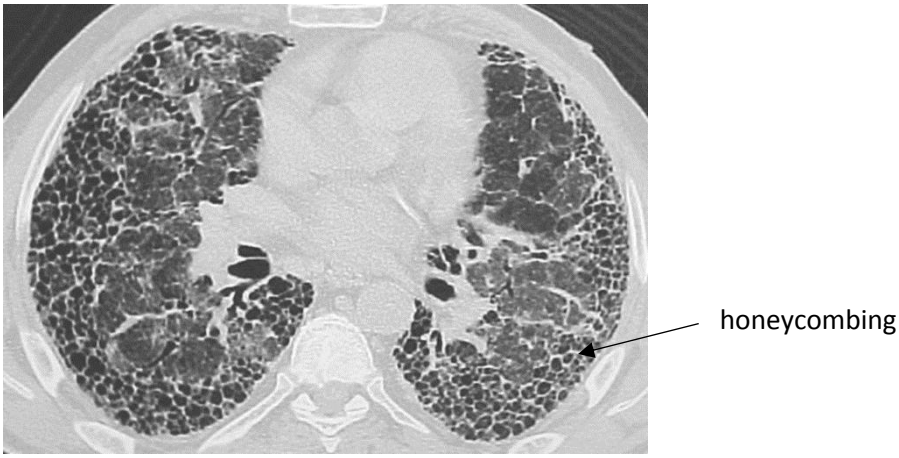

Figure 3 *A high resolution computed tomography image of a severe case of IPF. The honeycombing effect is noticeable as the rigid, collagen rich parts appear in white. Reproduced with permission from the authors.*[6]

The incidence of IPF is greater in men than in women,[11] and environmental, genetic and age factors are all considered to have a role in the likelihood of contracting the disease. The median age of onset is 50 – 60 years,[11] and ex-smokers represent a significant proportion of those with IPF. Histopathological patterns exhibited by sufferers of IPF, which includes interstitial pneumonia amongst other interstitial lung diseases, are varied in how much fibrosis and inflammation is presented. Some of these patterns are of unknown aetiology, and so the disease is termed idiopathic.[12] IPF affects 4.6 people per 100,000 in the UK, and the incidence rate of the disease more than doubled between 1990 and 2003,[13] although the disease is likely to be more common than has been previously reported.[14] The median survival rate in patients is only 3 – 5 years,[13,15] indicating a significant unmet need that, coupled with the significant health-care burden of suffers who need daily oxygen support, demands continued effort in the search for treatments. In addition to this, the annual cost of IPF to the US healthcare system, excluding the cost of medication, is estimated to be close to $2 billion, indicating the significant financial burden of the disease.[16]

1.2 Pathways and mechanisms involved in the fibrotic response

In general, when a tissue sustains damage, a cascade of events is initiated in order to repair the damaged organ. Fibrotic disease arises from an over-exuberant and unceasing response to this stimulus, gradually causing distortion of the architecture of the organ and loss of function. However, in IPF, the pathogenesis of the disease remains only partially understood.[17] Epithelial cell apoptosis is a hallmark of IPF,[18] and so it is possible that damage to epithelial cells induces the fibrotic response, but conclusive determination of this is hindered by the technical challenge of studying the cells, and by the fact that patients tend to present with the disease only once it is well established and they are unwell.[2,9] Due to the unknown aetiology of the disease, determination of the biological pathways implicated in fibrosis has been limited largely to animal models, which may not be fully illustrative of the situation in IPF patients. Despite this, all fibrotic disease is characterised by accumulation of mesenchymal cells of altered function, enhanced inflammation, and persistent myofibroblast activation, amongst other features.

The deposition of ECM proteins as a result of sustained myofibroblast activation is the ultimate cause of deterioration in the breathing capacity of IPF patients. These ECM proteins, particularly collagen, cause the tissue to stiffen, which further promotes the rest of the fibrotic sequence. The ECM produced in a fibrotic organ differs from that found in healthy tissue, and several of these differences also promote organ dysfunction, such as producing more heavily cross-linked collagen and altering the behaviour of local cells and growth factors. This insoluble, cross-linked collagen is the cause of the loss of tissue function as, particularly in the case of pulmonary fibrosis over the fibrosis of other organs, the delicate and highly flexible tissue structure on the surface of the lung is relied upon for a high surface area on which gas exchange can occur. When this occurs, a positive feedback loop is formed because transforming growth factor-β (TGFβ), a key cytokine involved in the

upregulation of activated fibroblasts, is both better activated by integrins, and itself more efficiently activates fibroblasts to their myofibroblast form in more rigid tissue.[19,20] In addition to this, a further feedback loop is formed as mechanical tension in the surrounding matrix may demote myofibroblast apoptosis and loss of antiproliferative reponse.[21,22]

Myofibroblasts are the most important of several cell types which form in large quantities in fibrotic tissue. They are responsible for the increased secretion of collagen which stiffens the tissue. A clear histological marker of the disease is the formation of fibroblastic foci in the lung, where fibroblasts accumulate.[23] Upon activation of the fibroblasts to myofibroblasts by TGFβ (and other cytokines), they release α-smooth muscle actin (α-SMA), which confers higher contractile activity to the cells.[24] This is important in a healthy cell as it aids wound closure. There, however, is no evidence for injured epithelial cells themselves undergoing transition to myofibroblasts.[25]

TGFβ is a family of cytokines containing 3 isoforms, TGFβ1, -2, and -3, though TGFβ1 has received the most attention in the case of fibrogenesis in IPF.[26] TGFβ is secreted by nearly all cells and is stored outside the cell, bound to the ECM. Before activation, the TGFβ is bound to the latency associated protein (LAP), which is itself bound to another protein, the latent TGFβ binding protein. Binding to these proteins prevents the TGFβ from binding to its receptors so it remains unactivated.[27] Upon injury, TGFβ is activated by the disassociation of the LAP **(Figure 4)**. Active TGFβ then causes a signalling cascade, binding to its receptor on nearby cells, leading to the phosphorylation of SMAD-2 and SMAD-3 proteins (SMAD derives from the combination of *Caenorhabditis elegans SMA* and the *Drosophila MAD*, 'mothers against decapentaplegic' genes),[28] which then recruit SMAD-4 to form a complex which enters the cell nucleus and results in the transcription of mRNAs. These mRNAs are responsible for fibroblast activation and proliferation, and inhibition of matrix-

degrading enzymes, amongst others.[29,30,31,32] Therefore, such transcription pathways have been the focus of some attempts to block myofibroblast differentiation.[33]

In rat studies, transient over-expression of activated TGFβ has been shown to cause the formation of collagen.[34] However, TGFβ is a key regulator of all cells, one role that it plays being the reduction of inflammation. Consequently, systemic modulation would likely result in many side effects. Global TGFβ disruption in mice has been shown to cause multifocal inflammatory disease,[35] therefore a compartment-specific regulation of TGFβ would be necessary were it to be targeted therapeutically. Unsurprisingly, therefore, molecules which attempt to block TGFβ, such as activin receptor-like kinase 5 (ALK5) inhibitors, which inhibit the TGFβ1 receptor directly, or antibodies, have failed to reach clinical testing due to safety concerns.[2,32]

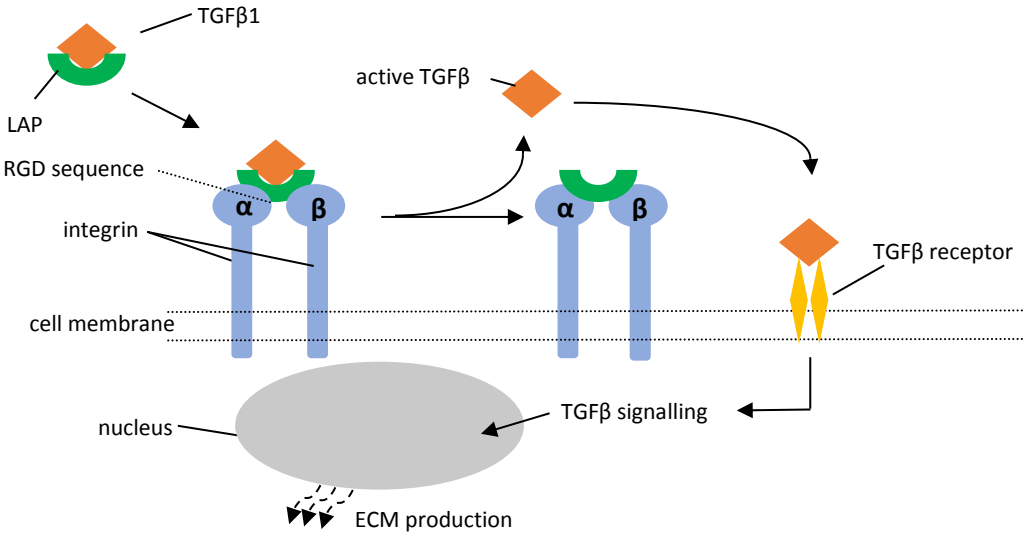

Figure 4 *Role of integrins in the pathway of TGFβ activation and signalling in IPF*

Inflammation is ubiquitous in cells undergoing a fibrotic response, and is considered to have an important role to play.[36] However, unlike treating fibrosis of other organs,[37] anti-inflammatory drugs have proved to be ineffective in the treatment of idiopathic pulmonary fibrosis, which indicates that other physiological responses to cell injury may be more significant, despite some level of inflammation being a feature of the disease.[19] It has been argued that the inflammation present is a result,

rather than a cause, of the change in local microenvironment.[38] Animal models indicate that the onset of fibrosis by over-expression of TGFβ in lung cells is not initially accompanied by inflammation, and rather that this occurs only after some time, subsequent to the formation of the fibrotic microenvironment.[39] However, it may be that an inflammatory response is present upon initial injury, but by the time the disease is identified, the tissue has 'switched off' the classical inflammatory response, leaving the chronic repair cycle continuing.

1.3 Integrins and their role in TGFβ activation

Bound, inactive TGFβ may be cleaved from LAP to give the active form, either *via* proteolytic cleavage,[40] or by the exertion of mechanical force exerted by adjacent cells, mediated by integrins **(Figure 4)**.[27] Integrins are heterodimeric transmembrane proteins **(Figure 5)** which were first known as cell adhesion molecules, but more recently have been implicated in other cell functions, particularly cellular signalling. They act as transmembrane receptors and facilitate cell-cell and cell-ECM interactions, and function as 'molecular hooks' for the cell. Their role in signalling in the cell involves interactions of the intracellular region of the integrin with receptor tyrosine kinases, which can result in growth, division, differentiation, and apoptosis of the cell.[41]

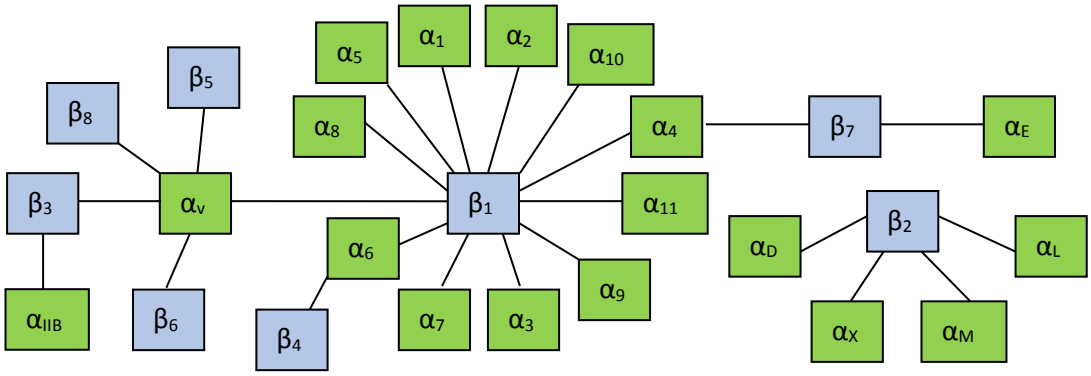

Figure 5 *The family of integrins, indicating which α and β subunits are found together*

There are 18 different α subunits and 8 β integrin subunits known, and in humans 24 combinations of these are known **(Figure 5)**. TGFβ1-LAP contains an arginine-glycine-aspartic acid (RGD) sequence of peptides, to which a subset of the integrin family is able to bind. So-called RGD-integrins are those which recognise and bind to the RGD sequence, and there are 8 integrins in this subset, namely $\alpha_V\beta_1$, $\alpha_V\beta_3$, $\alpha_V\beta_5$, $\alpha_V\beta_6$ **(Figure 6)**, $\alpha_V\beta_8$, $\alpha_{IIb}\beta_3$, $\alpha_5\beta_1$, and $\alpha_8\beta_1$ integrins.[42] This has been verified by crystal structures of $\alpha_{IIb}\beta_3$, $\alpha_5\beta_1$, $\alpha_V\beta_6$, and $\alpha_V\beta_3$ integrins complexed to RGD ligands, which showed that binding occurs by the same set of interactions.[43,44,45,46] This implies that integrins have a role in regulating the activity of TGFβ, by activating it when they bind to the TFGβ1-LAP complex.

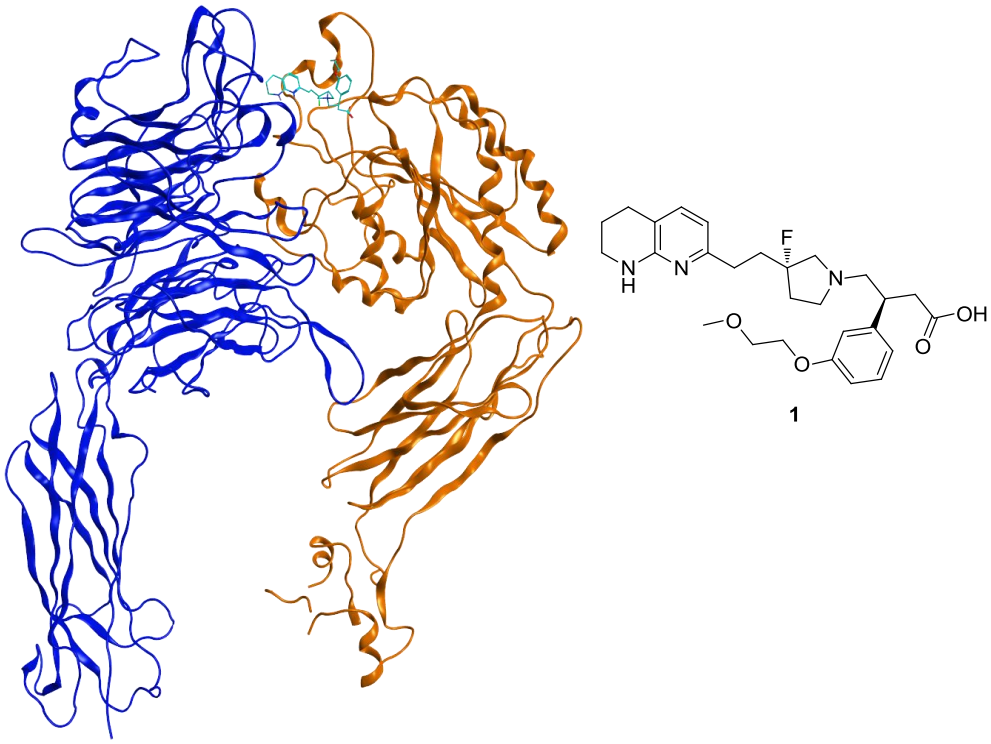

Figure 6 *A crystal structure of the $\alpha_V\beta_6$ integrin, with the α_v (blue) and β_6 (orange) sides binding antagonist **1***

Two α_v antagonists, namely Intetumumab, an antibody, and Cilengitide **(2, Figure 7)**, have recently been in clinical development for cancer and glioblastoma respectively, and both were well-tolerated.[47,48] This is encouraging evidence for the credibility of RGD integrin antagonists as drugs.

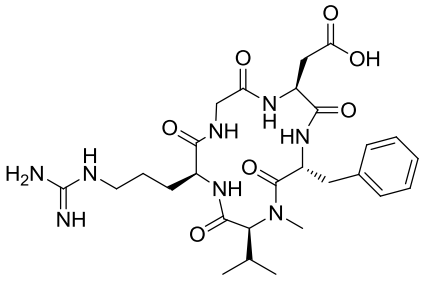

2

Figure 7 *Cilengitide* ***(2)****, an integrin antagonist that has previously undergone extensive clinical investigation*

1.4 $\alpha_V\beta_6$ Integrin target validation

There is strong evidence to suggest that the $\alpha_V\beta_6$ integrin, in particular, has a role in the initiation and progression of IPF.[49] The $\alpha_V\beta_6$ integrin is only expressed on the surface of epithelial cells, and its production is significantly upregulated following an injury to the cell.[50] In fact, TGFβ has been found to induce $\alpha_V\beta_6$ expression on epithelial cells in a guinea pig, which results in another positive feedback loop, accelerating fibrogenesis.[51] Therefore, $\alpha_V\beta_6$ integrin inhibition could offer a method of manipulating TGFβ specifically where a cell injury has occurred, avoiding the aforementioned problems associated with systemic regulation of TGFβ. This is supported by evidence that mice deficient in the $\alpha_V\beta_6$ integrin are protected from bleomycin-induced pulmonary fibrosis, due to reduced TGFβ1 activation.[27] Furthermore, it has been found that β_6 inhibition by genetic knockdown or anti-$\alpha_V\beta_6$ antibodies is protective in radiation-induced models of pulmonary fibrosis.[52] Genetic evidence also indicates the importance of $\alpha_V\beta_6$ in TGFβ activation in mice, where the lungs of bleomycin-induced mice without β_6 show lower induction of TGFβ-inducible genes than normal bleomycin-induced mice.[53] This evidence, amongst other validation, means that $\alpha_V\beta_6$ is a relatively well-established target for pulmonary fibrosis. It has, therefore, been the target of a small molecule medicinal chemistry programme within our laboratories, which will be outlined below.

1.5 $\alpha_V\beta_1$ Integrin target validation

In comparison to $\alpha_V\beta_6$, the $\alpha_V\beta_1$ integrin remains a relative unknown in terms of its role in the pathogenesis of IPF, despite being discovered over 25 years ago.[54,55] Several factors contribute to this, firstly because mice lacking β_1 on fibroblasts do not survive, hindering *in vivo* knockout studies.[56] Secondly, because the individual α and β subunits are represented many times across the integrin family (12 for β_1, 5 for α_V), development of an $\alpha_V\beta_1$ specific antibody has been hindered and has thus far proved elusive.

For these reasons, target validation work for this integrin has been limited to experiments which attempt to rule out the role of other similar integrins in causing the observed pharmacology, thus leaving $\alpha_V\beta_1$ as the only integrin left which could be responsible. An example would be an experiment where the deletion of all α_V integrins on tissue fibroblasts in mice resulted in protection from fibrosis, but individual deletion of the $\alpha_V\beta_3$, $\alpha_V\beta_5$, and $\alpha_V\beta_8$ integrins did not.[57] Though $\alpha_V\beta_1$ is the only other RGD integrin known to be expressed on fibroblasts, this observation does not unequivocally show that $\alpha_V\beta_1$ is responsible for fibroblast activation. This is because other non-RGD integrins could be responsible for the observed response, or alternatively α_V integrin redundancy (where the deletion or loss of one integrin causes another integrin to take up the role or perform the process of the deleted integrin) could be taking place, since many of the integrins perform similar roles.

The recent publication of a selective small molecule antagonist of $\alpha_V\beta_1$ by Sheppard and DeGrado was hoped to enable more reliable validation.[57] A small molecule inhibitor **(3, Figure 8)** was reported, with exquisite selectivity over other RGD integrins. It was found that $\alpha_V\beta_1$ does bind to LAP, and in cells engineered to express $\alpha_V\beta_1$ the reported small molecule was able to reduce the activation of TGFβ in these cells. The same group also reported a role for $\alpha_V\beta_1$ in liver fibrosis.[56] These

publications led to interest in $\alpha_V\beta_1$ from our laboratories involving the initiation of our own medicinal chemistry work towards a selective $\alpha_V\beta_1$ antagonist.

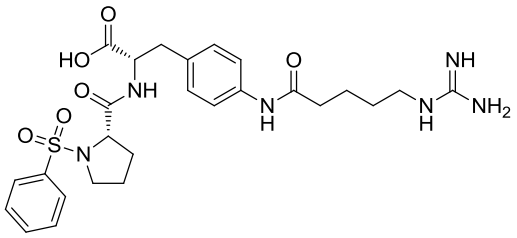

3

***Figure 8** Compound **3**, reported to be an exquisitely selective $\alpha_V\beta_1$ integrin antagonist*

However, when DeGrado and Sheppard's small molecule was reassessed by our laboratories, the compound was not found to be as selective over other integrins as had been originally reported.[58] The true affinity of the compound for a larger group of integrins was measured using our radioligand binding assay,[59] and it was found that although this specific small molecule was highly selective over the other α_V integrins, it was in fact only 21-fold selective over $\alpha_5\beta_1$, and was found to be almost equipotent at $\alpha_4\beta_1$. Therefore, it is not possible to attribute the results of the DeGrado and Sheppard *in vivo* experiments to the blockade of $\alpha_V\beta_1$, as the response may be due to other integrins which had not been considered within this previously published study.

This new evidence does not rule out $\alpha_V\beta_1$ as a target for the treatment of fibrosis, rather it indicates that further work is required to confirm the role that it has to play. In particular, these results highlight the importance of a genuinely selective antagonist for $\alpha_V\beta_1$, be that an antibody or a small molecule, in order to more effectively probe the target.

In our own laboratories, antibody work has been carried out which also indicates, though not incontrovertibly, a role for $\alpha_V\beta_1$ **(Figure 9 and Figure 10)**.[60] **Figure 9(a)** indicates that use of an anti-α_V antibody (17E6) causes reduction in TGFβ in a dose dependent manner, to a similar extent to the ALK5 inhibitor, a TGFβ antagonist

(percent response relative to the ALK5 inhibitor). The same is observed for an anti-β_1 antibody (4B4) **(Figure 9(b))**.

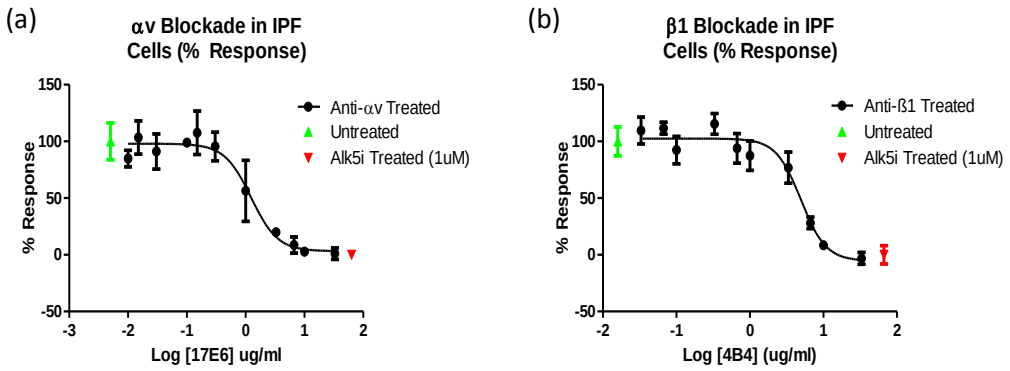

Figure 9 *The dose-dependent response of Mink lung epithelial cells (modified to express the luciferase reporter gene) cocultured with IPF lung fibroblasts to a dose of (a) an α_V selective antibody (17E6), and (b) a β_1 selective antibody (4B4). The experiments indicate a role for both an unidentified α_V integrin and an unidentified β_1 integrin in the activation of TGFβ. Both responses are measured relative to an ALK5 inhibitor, which directly inhibits TGFβ.*

These results indicate a role for an unidentified α_V integrin, and for an unidentified β_1 integrin. A secondary experiment involved initial addition of an anti-β_1 antibody and subsequent addition of a gradually increasing dose of an anti-α_V antibody **(Figure 10(a))**. A dose response curve was not observed as the dose of anti-α_V antibody was elevated, which implies that the response seen in the last experiment was not due to any α_V integrin that is not $\alpha_V\beta_1$. **Figure 10(b)** shows the same experiment in reverse, with the same result, indicating that the response is not due to any β_1 integrin that is not $\alpha_V\beta_1$. Whilst this is positive in indicating that $\alpha_V\beta_1$ may be significant, this experiment assumes that there is a greater response possible in the extent of TGFβ activation after the initial antibody blockade, which may not be the case. If this was not the case, then no further dose response curve would be possible. There is, therefore, still uncertainty in the conclusions that may be drawn from these results.

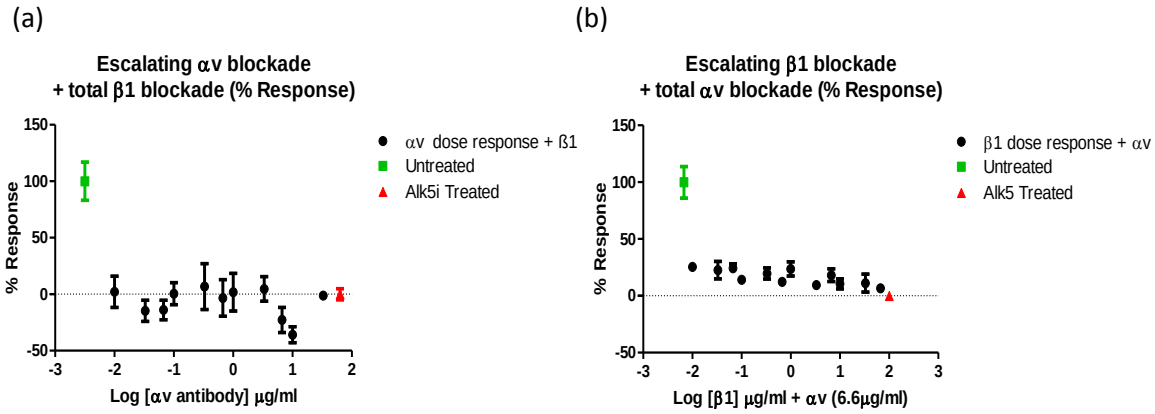

Figure 10 *The dose-dependent response of Mink lung epithelial cells (modified to express the luciferase reporter gene) cocultured with IPF lung fibroblasts to a rising dose of (a) an α_V selective antibody, with the cells having been pre-dosed with an antibody to give total β_1 blockade, and (b) a rising dose of a β_1 selective antibody, with the cells having been pre-dosed with an antibody to give a total α_V blockade. In neither case was a dose-dependent response observed. This implies that the results of the previous experiments were not due to any α_V integrins other than $\alpha_V\beta_1$, or any β_1 integrins other than $\alpha_V\beta_1$ integrins.*

Based on this evidence, clearly there is interest in an $\alpha_V\beta_1$ selective small molecule antagonist, both from the point of view of validating the target and elucidating the role that it plays in the fibrotic response. Moreover, it does appear that, from a therapeutic point of view, $\alpha_V\beta_1$ may well have a role to play in the activation of fibroblasts by TGFβ.

1.6 Current treatments for IPF

1.6.1 Marketed treatments

At present, only two drugs are available as treatment for IPF, and these drugs slow the rate of decline, rather than being curative. Currently, the only curative treatment is lung transplant which, as mentioned, is only available to very few patients. This is because very few qualify on the grounds of advanced age, having significant co-morbidities, a lack of donors, and due to the complexity of the surgery.[61] Oxygen therapy is the most common treatment, alongside *N*-acetyl cysteine which is often

prescribed to reduce the build-up of mucus in patients' lungs.

Both of the drugs marketed to treat the disease were approved by the Food and Drugs Administration (FDA) in 2014, although the short median survival rate demonstrates that prospects for patients are still relatively poor. The first, Nintedanib (Ofev) **(4), (Figure 11)**, inhibits angiokinase receptors,[62] and the second, Pirfenidone **(5)**, has been shown to reduce TGFβ,[63] inhibit proinflammatory cytokines, and scavenge for hydroxyl radicals.[64,65]

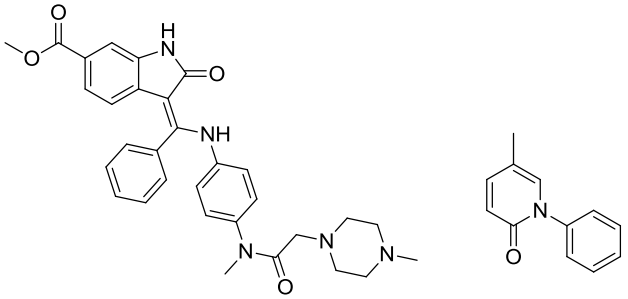

Figure 11 *Two marketed treatments for IPF. Nintedanib (**4**, left) and Pirfenidone (**5**, right)*

The dosing regimen for Nintedanib **(4)** is 100 mg or 150 mg twice daily, and common side effects include nausea, vomiting and abdominal pain.[66] For Pirfenidone **(5)**, the dose rises to 800 mg three times per day over the first two weeks of treatment, and has a wide range of possible side effects. These include constipation, diarrhoea, dizziness, insomnia, gastrointestinal issues, photosensitivity and vomiting.[67] Both drugs are only given to patients whose lung function is within a certain range (50 – 80 % forced vital capacity (FVC, the total amount of air that a patient can exhale during a forced breath)), and treatment is withdrawn if the condition of the patient continues to decline (defined as a reduction of more than 10 % in FVC) in the first 12 months. These side effects, restrictions on use, and the high dose of Pirfenidone, make these treatment options undesirable. However, another significant drawback to these drugs is since they only slow the progression of the disease rather than improve the health of the patients, patients do not feel any better as a result of taking

the medication. This has a negative effect on patient compliance and morale. Clearly, an improved method of treatment is required.

1.6.2 Other therapeutic approaches under investigation

Given the inadequacies of current medication for IPF suffers, and the valuation of peak sales of a new drug of around $2 billion per annum,[19,68] there is currently greater interest than ever before in the development of treatments for IPF. This is demonstrated by the large number of potential treatments currently undergoing clinical trials, targeting the disease by a wide range of approaches.[61] While exhaustive description of these approaches is beyond the scope of this introduction, a few potential approaches are mentioned. These include the humanized monoclonal antibody BG00011 (STX-100), an $\alpha_V\beta_6$ integrin antagonist which is currently in phase II clinical trials to assess its efficacy in IPF patients.[69] Clearly, the progress of this asset in the clinic is of particular interest to our laboratories, as it also targets the $\alpha_V\beta_6$ integrin, and so the efficacy and safety profile of this compound in patients are expected to be an important indicator of the validity of this target.

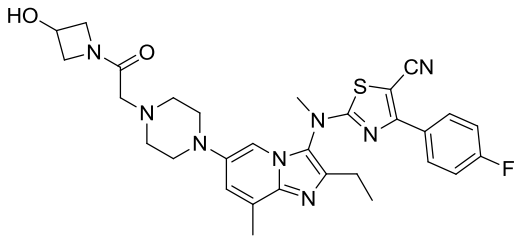

6

Figure 12 *Autotaxin inhibitor* ***6****, currently being evaluated clinically for the treatment of IPF.*

Additionally, GLPG1690 **(6**, **Figure 12)** an autotaxin inhibitor, has recently entered a phase III study, having been well-tolerated in phase I and found to stabilise FVC in phase II.[70,71,72] Autotaxin is an enzyme which converts lysophosphatidylcholine into

lysophosphatidic acid (LPA), a pleiotropic lipid which is involved in fibroblast recruitment and survival,[73] as well as TGFβ activation.[74] It is thought that the particular shape of **6** allows it to occupy the T-shaped autotaxin binding site in such a way as to both block LPA formation and LPA delivery. This may explain the superior efficacy of **6** over other autotaxin inhibitors.[71]

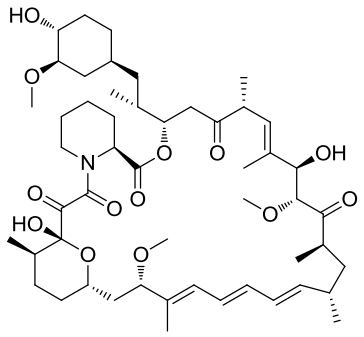

7

Figure 13 *Rapamycin* ***(7)*** *is an mTOR inhibitor being investigated for the treatment of IPF*

Several lipid kinases, such as mammalian target of rapamycin (mTOR) and phosphatidylinositol-3-kinase (PI3K), have been targeted for IPF. Rapamycin **(7, Figure 13)**, a marine macrolide, is a potent inhibitor of mTOR, and was first investigated clinically as an immunosuppressant for the recipients of organ transplants.[75] However, more recently, mTOR has become an attractive target for the treatment of fibrotic diseases,[76] and **7** is currently under investigation in a phase II study for the treatment of IPF.[77] The mTOR kinase forms two different complexes, mTORC1 and mTORC2 (**7** was found to be an inhibitor of mTORC1), both of which are involved in the pro-fibrotic signalling cascade downstream of the release of TGFβ. This validation work has also led to preclinical work in our laboratories on a small molecule mTOR inhibitor for the treatment of IPF.[78,79] An inhibitor of both PI3K and mTOR, Omipalisib **(8, Figure 14)** has been shown to be effective in reducing fibroblast response,[76] and has been tested in a phase II study with IPF patients.[80]

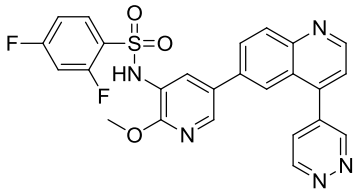

8

***Figure 14** Omipalisib **(8)**, an inhibitor of PI3K and mTOR kinases*

In addition to these approaches, several antibiotic therapies are currently being trialled, since the initial injuries that are thought to precede the fibrotic response may be the result of viral or bacterial action. One example of this is a phase III trial comparing the use of either co-trimoxazole (a combination of trimethoprim **(9)** and sulfamethoxazole **(10)**) or doxycycline **(11)** to the current standard care, which is currently recruiting patients **(Figure 15)**.[81]

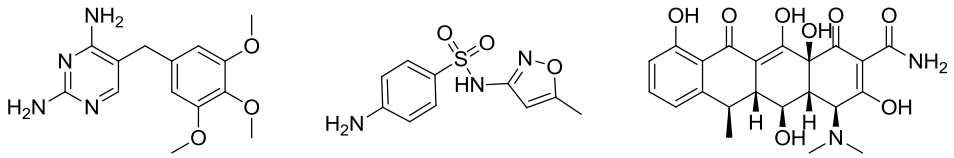

9 **10** **11**

***Figure 15** Co-trimoxazole (a combination of **9** and **10**) and **11**, antibiotics investigated to treat IPF*

Beyond these small molecule approaches, antibodies which target the connective tissue growth factor (observed at higher levels in IPF patients)[82] have been investigated, of which Palrevlumab is one such example, which successfully reduced FVC decline in a phase II study.[83] Another antibody-based approach has been to target the lysyl oxidases, which stiffen the matrix deposited in fibrosis,[84] for example Simtuzumab, which was studied in phase II, but abandoned on efficacy grounds.[85]

This plethora of approaches still only represent a subset of those attempting to achieve disease modification in IPF sufferers. In all, a 2018 review listed 19 therapies currently under investigation in phase II or III clinical trials.[61]

1.6.3 The work of our laboratory

Specific studies within our laboratory have focused on the production of α_V integrin antagonists. Currently, two $\alpha_V\beta_6$ selective RGD mimetics from our laboratories have undergone or are approaching clinical trials, namely **12** and **1 (Figure 16)**.[86] Molecule **12** is an inhaled compound with a pIC_{50} value of 8.4 for $\alpha_V\beta_6$ and 5.9-7.7 for the other α_V integrins in cell adhesion assays, which has recently undergone phase IIA clinical trials.[87,88,89] Molecule **1** is an orally dosed compound with a pIC_{50} value of 7.9 for $\alpha_V\beta_6$ and 6.4-7.5 for the other α_V integrins, as measured in the cell adhesion assay.[90] Compound **1** has recently completed preclinical toxicological investigations.

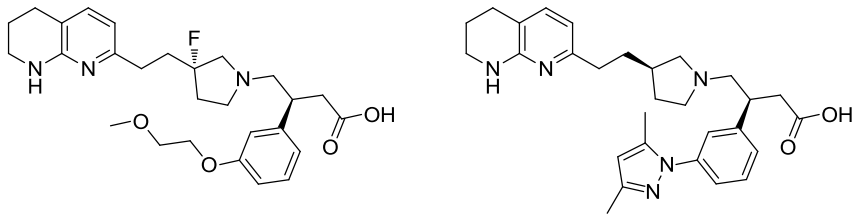

Figure 16 *Compounds **1** and **12**, two small molecules produced within our laboratories, that are currently approaching or that have recently undergone clinical trials for IPF*

In both cases, RGD-integrin inhibition has been achieved by mimicking the structural motif of the RGD sequence, and many such compounds have been published.[91] From the crystal structure of the protein bound to **1** it is known that the α unit binds to the arginine, or its mimetic **(Figure 17)**. As had been intended, the arginine mimetic, which in this case is a protonated tetrahydronaphthyridine group, binds to the α side of the integrin *via* a salt bridge with the aspartic acid residue. The aspartic acid, or its mimetic, binds to the β unit of the integrin, and the same bound crystal structure indicates that this is indeed the case, where the acid coordinates both to a magnesium ion, and to hydrogen bond donors on the backbone. Since such compounds require both an arginine mimetic, which is often basic, and an aspartic acid mimetic, which is usually a carboxylic acid, these inhibitors require highly polar groups to be incorporated.

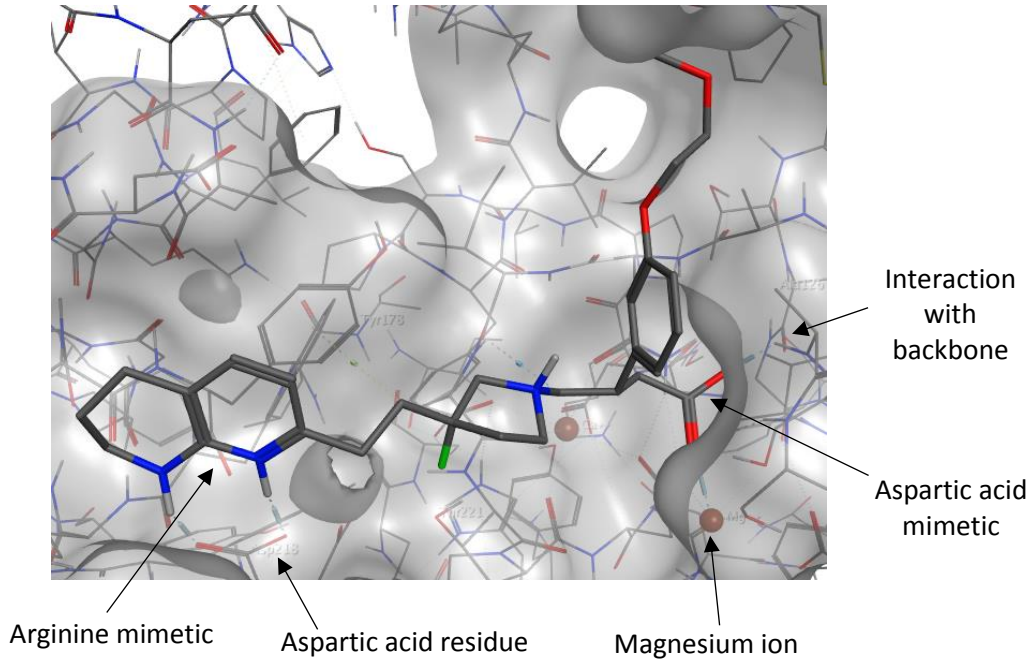

Figure 17 *A part of the crystal structure of **1**, showing the aspartic acid residue of the α_V side of the integrin bound to the arginine mimetic by a salt bridge, and the magnesium ion bound to the aspartic acid mimetic in the β_6 integrin side of the receptor, as well as to the protein backbone.*

There is a close homology between the different α_V integrins. As a result, despite the small molecule crystal structures of several integrins having been published, designing selective compounds is a challenge. Furthermore, the SAR of the potency of inhibitors at different α_V integrins is often very complex, where subtle modifications cause relatively large changes in the selectivity profile. This indicates that, although the key ionic interactions of the ligand with the receptor are obvious, understanding the precise modes of binding within each integrin binding site is not trivial.[92] Accordingly, work within our laboratory has aimed to explore the SAR of inhibitors of all α_v integrins, in order to find a potent and selective $\alpha_V\beta_6$ inhibitor with appropriate pharmacokinetic (PK) properties.

This work began with the development of a compound for inhaled dosing, eventually leading to the development of **12**. An inhaled compound was sought in the first instance, because as stated above, inhibitors of RGD integrins require ionisable functional groups, and so are often highly polar compounds. As will be explained in

more detail below, highly polar compounds are not usually able to diffuse through the non-polar centre of a cell membrane, which is a requirement for an orally-dosed drug (assuming that active transport is not aiding the permeability of the compound, which is unpredictable). Therefore, the high polarity of RGD mimetics was thought to preclude the development of an oral drug, hence the initial development of the inhaled compound **12**. However, during the development of **12**, it was found that some compounds did, surprisingly, possess some passive permeability, which initiated the development of an oral series of compounds, eventually culminating in the development of **1**.

Chapter 2: Investigating the chameleonic properties of 1 and its analogues

2.1 Introduction to membrane permeability

For an orally-dosed drug, the active compound must be well-absorbed in order to reach the site of action at sufficiently high concentration to be efficacious, whilst keeping the dose to a minimum. This is paramount in ensuring an adequate therapeutic window, and it reduces one cause of off-target toxicity, namely variable absorption between different individual patients. In order to reach the site of action, an orally-dosed medicine must first permeate into the blood from the digestive tract, then from the blood into the tissue where it is to act. Clearly, therefore, permeability plays a crucial role in drug absorption and efficacy.

Although it has been proposed that all permeability is mediated by active transporters,[93] this remains controversial and most would still propose that diffusion-controlled, 'passive' permeation of molecules through phospholipid bilayers still plays a significant role in the overall permeability of compounds. Additionally, reliance upon active transport of a drug has its downsides, namely that the expression of transporters varies between individual patients, and the extent of transport can be affected by other drugs in the system which may also be substrates for that particular transporter.

The two principal means of passive permeation of a compound are the transcellular and the paracellular routes. Transcellular permeation involves, either actively or passively, the passage of a compound into the cell, across the membrane, whereas paracellular transport refers to the crossing of the boundary between the cells

themselves. Paracellular transportation allows for small, hydrophilic compounds to be absorbed.

In the case of transcellular transport, which is thought to predominate for orally-dosed drugs with high oral bioavailability, the molecule must pass through a membrane, a bilayer of compounds such as phosphotidylcholine **(Figure 18)**. These amphiphilic molecules consist of polar 'head' groups, in this case the phosphate and ammonium end, which point out towards the aqueous media on both sides of the membrane, and lipophilic 'tail' groups, the alkyl chains, which point in towards each other, forming a non-polar centre to the membrane **(Figure 18)**. If a compound is too lipophilic, it will not be permeable, as it will not diffuse out of the lipophilic centre into the aqueous medium. However, if it is too hydrophilic, it is not energetically favourable to diffuse into the non-polar bilayer, and so it is also impermeable as it remains embedded in the membrane.

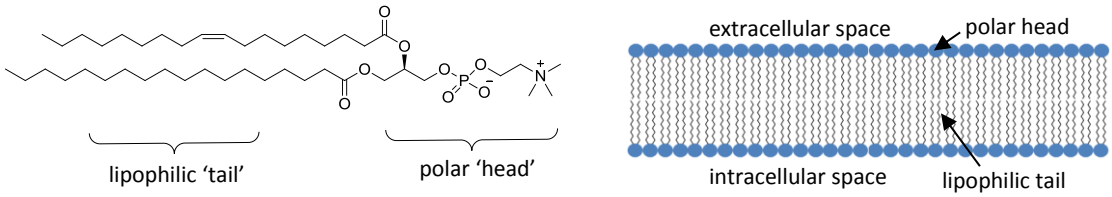

Figure 18 *Left, phosphotidylcholine, a major constituent of phospholipid membrane. Right, a schematic representation of a bilayer.*

2.1.1 The permeability of ampholytic compounds

The pH partition hypothesis, according to which only neutral and non-polar molecules show passive transcellular permeability, is a prominently held concept associated with biological permeation.[94] This implies that ionic species should not be permeable, when measured in an artificial membrane permeability (AMP) assay. It is the permeability of zwitterions which is most relevant within this project, and these represent a more complex case.

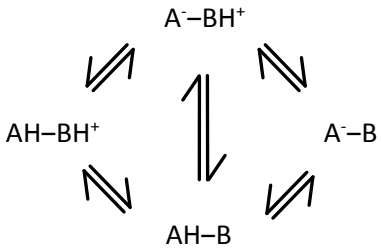

Figure 19 *The equilibria between the possible species of an ampholyte in a protic solution. A represents the acidic group in the molecule, B represents the basic group.*

Ampholytes are molecules which contain both acidic and basic functional groups, and thus are capable of existing in multiple charge states **(Figure 19)**.[95] As well as the individual, measurable pK_a and pK_{aH} values of the groups on the molecule, other equilibria exist between these different possible forms which are not directly measurable. If the difference between the pK_a and pK_{aH} values is more than 5 units, then the species AH–B will not exist, so the above diagram is simplified to just two equilibria. However, in the case of RGD mimetics, the carboxylic acid group has a pK_a of approximately 4.5, and the arginine mimetic (the tetrahydronaphthyridine in the case of **1** and its analogues) usually has a pK_{aH} of 8.5 or less, therefore this represents the more complex case, where $A^-–BH^+$ and AH–B will coexist to varying extents depending on the environment, as depicted in **Figure 20**. From this point, species which are of the form $A^-–BH^+$ will be referred to as the zwitterionic or ionic tautomer, and species which are of the form AH–B will be referred to as the neutral tautomer.

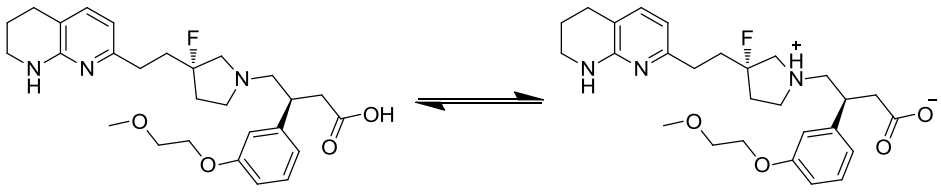

Figure 20 *Tautomerisation of **1** between its unionised form and one possible zwitterionic form*

In the case of **1** and its analogues, the situation is further complicated by the presence of a second basic group. The pK_a of the acid group is 4.1, and the pK_{aH}s of the two nitrogens are 7.3 and 8.3, respectively **(Figure 21)**. Therefore, at physiological pH of

just over 7, the acid group is expected to be almost completely deprotonated, the pyrrolidine nitrogen is expected to be predominantly (approximately 90 %) protonated, and the tetrahydronaphthyridyl nitrogen is expected to be a near-equal mixture of both protonation states. This is summarised by the graph in **Figure 22**.

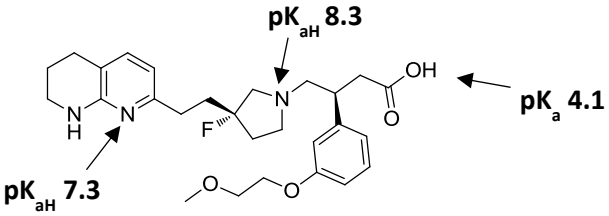

Figure 21 *The ionisable groups on* ***1***

It is necessary to consider a pH range, however, because in the stomach the pH is around 1-2,[96] whereas in the small intestine, where drug absorption is considered to principally occur, the pH is approximately 6, increasing gradually to around 7 at the end of the gastrointestinal tract.[97] The blood is pH 7.4. However, what may be surmised from this graph is that a mixture of protonation states will be present at these physiological pHs.

As has been stated, neutral and non-polar molecules were historically considered to be the only compounds capable of passive permeation and, indeed, for some studies on the permeation of ionisable molecules, it has been assumed that the neutral form will be the one which permeates.[98]

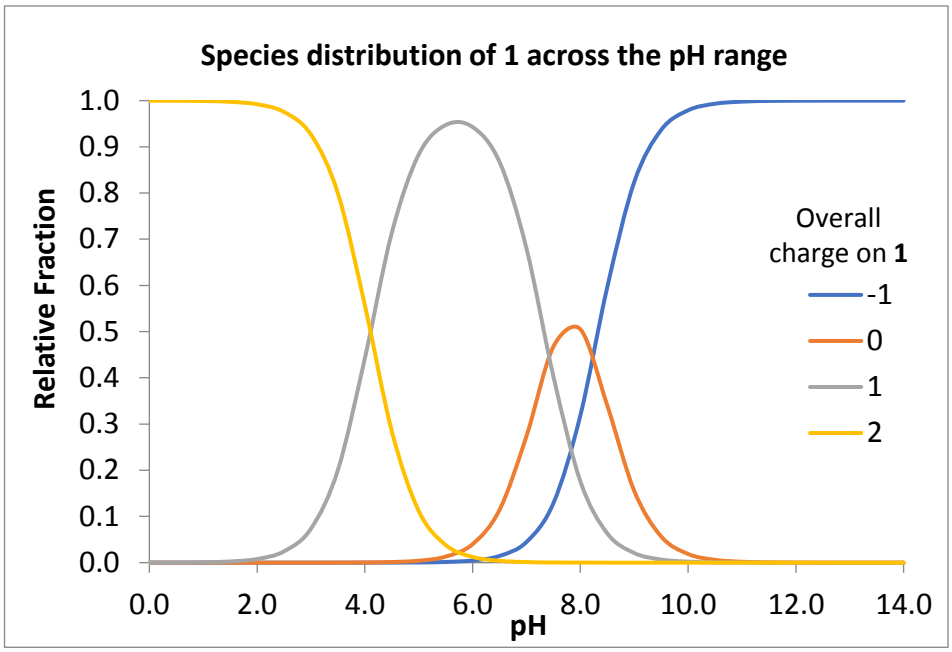

Figure 22 *Graph showing the probability of the different ionisable groups of **1** being protonated across the pH range*

2.1.2 Introduction to Lipinski's rules, molecular chameleons and IMHBs

Clearly, permeability is not the only property necessary for a drug to obtain good oral bioavailability. Rather, a balance of different properties are necessary, which have been grouped together to give rise to the rather nebulous term of 'drug-likeness'.[99] Essentially, this term has been intended as a guide for suggested limits on the designed properties of a drug such that it has sufficient potency whilst maintaining membrane permeability, aqueous solubility, low clearance, and metabolic stability, which are likely to give rise to high oral bioavailability. There is a tension between the minimum lipophilicity required to obtain both good potency (which is often driven in large part by hydrophobicity and, therefore, lipophilicity) and good membrane permeability, and the negative effects of lipophilicity, namely reduced aqueous solubility, increased clearance, partly due to metabolic instability, and risk of off-target toxicity.[100]

Such limits to maintain 'drug-likeness' have been conventionally defined using Lipinski's 'rule of 5' (ro5), which was initially introduced in the context of assessing

high throughput screening (HTS) hits.[101] The ro5 requires that for a drug to have high oral bioavailability, it should not have more than one property outside of the following guidelines: maximum molecular weight of 500, maximum hydrogen bond donor count of 5, maximum hydrogen bond acceptor count of 10, and a logP no greater than 5. It has been shown since that molecular weight is not in itself a significant factor, rather that it correlates with other factors which are significant, including others on Lipinski's list.[102]

Though it could be argued that these guidelines have, at times, been adhered to more strictly than they should have been, they have nonetheless provided useful guidance. It has recently been shown that should the same empirical analysis that was done by Lipinski to form his rules be carried out on a modern set of drugs, Lipinski's maxima would, except for the case of molecular weight, remain almost unchanged.[99] Additional, later parameters such as topological polar surface area (TPSA) not exceeding 140 $Å^2$ and the number of rotatable bonds not exceeding 10 were introduced to provide further filtering.

In spite of the presence of these guidelines, there has been a recent increase in the requirement of some drugs to have properties which fall well outside of the space recommended by Lipinski. This is a result of some drug targets having active sites that are larger or flatter, or with fewer sites for possible polar interactions with ligands. This has led to the need for, and the rise in prominence of, 'beyond rule of 5' drugs.[103] Many such drug compounds are macrocycles, and they are thought to gain an advantage through their enhanced ability to adopt conformations in which several polar groups are internally complemented and, therefore, buried and no longer solvent exposed.[104,105] This transient reduction in polarity allows for compounds to permeate membranes, despite containing a greater number of hydrogen bond donors and acceptors than would ordinarily be associated with good permeability. These polar groups are essential for the molecule to have sufficient solubility, which is also necessary for good oral bioavailability. In this way, these compounds are able

to act as 'chameleons', where they are able to appear either more or less lipophilic depending on their environment.

Indeed, it has been postulated that such chameleonic behaviour is essential for drugs with molecular weight greater than 700, in order for them to be able to obtain sufficiently low polar surface area to maintain cell permeability, unless active transporters are responsible for their absorption instead.[105,106]

The most significant means by which a molecular chameleon can shield its polarity is through the formation of intramolecular hydrogen bonds (IMHB). This area of research is most mature for cyclic peptides and macrocycles, where conformational rigidity simplifies the analysis.[107] Indeed, for cyclic peptides it has been shown that passive permeability correlates with the ability to form IMHBs which are able to shield the polarity of the molecule.[108]

These interactions have been the means by which certain molecules found in nature have unexpectedly been shown to possess oral bioavailability, such as fungal natural product cyclosporine A **(13, Figure 23)**, which is an example of such a 'beyond ro5' drug, and is marketed as an immunosuppressant for several indications. Compound **13** has been found to adopt an IMHB-containing conformation in a non-polar environment, and an 'open' conformation, without IMHB formation, in water and when bound to its receptor.[109,110]

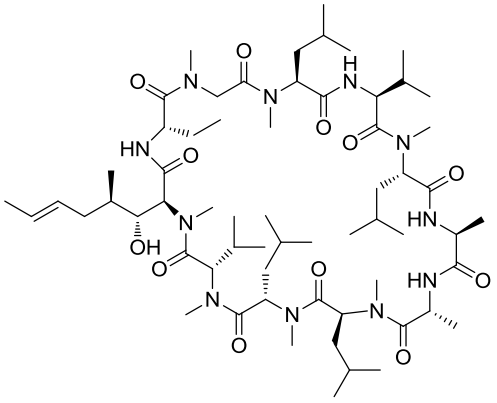

13

Molecular weight	1203
Hydrogen bond donor count	5
Hydrogen bond acceptor count	12
clogP	14.4

Figure 23 *Cyclosporine A* ***(13)****, a natural product derived from a fungus, which is marketed as an immunosuppressant for several indications. The Lipinski parameters are also shown, indicating that this compound is in chemical space 'beyond ro5'.*

Though only considered essential for these 'beyond ro5' drugs, chameleonic properties are desirable for compounds of any size, as they allow for a greater level of polarity to be contained within the molecule, which may be important for solubility and metabolic stability, potency or selectivity. In the case of the highly polar integrin binding site, this may be a key advantage in developing orally bioavailable RGD mimetics with sufficient polarity for potency. Additionally, although **1** and its analogues are in agreement with Lipinski's rules, their rotatable bond count (13 in the case of **1**) exceeds the limit that has been broadly set. This is largely due to the elongated nature of the integrin binding site, as the ligand must span between the α and β portions. For these reasons, our laboratories had initially anticipated that it would be very difficult to design an orally bioavailable RGD mimetic, but chameleonic behaviour may be the phenomenon which allows for even such flexible, polar compounds to still be permeable.

Elsewhere, in a relatively early example of such a study, a pair of morphine-substituted glucuronides were shown to be more lipophilic than expected, and force field calculations suggest that they exist in an equilibrium between a hydrophilic extended form which predominates in aqueous compartments, and a lipophilic, hydrogen bonded form which predominates in less polar organic media **(Figure 24)**.[111]

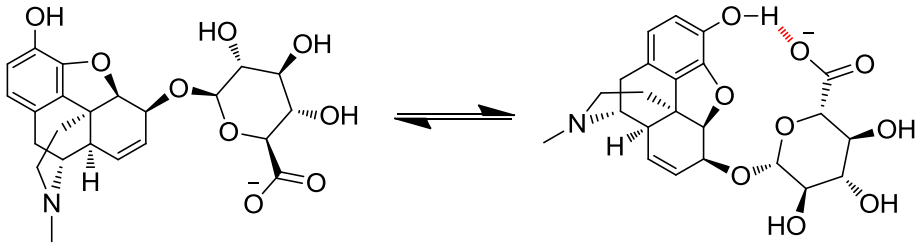

Figure 24 *The equilibrium between the elongated (left) and folded (right) forms of morphine 6-glucuronide. The folded form possesses an IMHB between the phenol and the glucuronic acid. This is thought to account for the increased lipophilicity of this morphine glucuronide, compared to a structural isomer which is less able to assume a folded conformation.*

More recently, there has been a dramatic increase in the number of publications highlighting the importance and use of IMHBs within drug discovery.[109, 112] In one recent study, the properties of a group of eight stereoisomers **(Figure 25)**, all *T. cruzi* growth inhibitors, were compared. It was found that when the C_8 and C_9 substituents on the oxazocinone ring are in a *trans* relationship, the compounds were noticeably more permeable than when they were *cis*. The IMHB indicated by the red line was identified using NMR spectroscopy and conformational searches.[113]

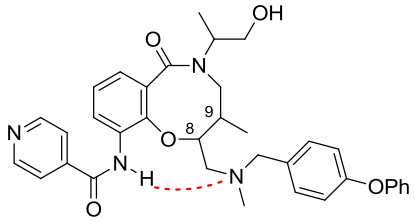

Figure 25 *A group of stereoisomers, all T. cruzi inhibitors, which display differing extents of IMHB formation. When C_8 and C_9 are in a trans relationship, the IMHB interaction indicated by the dotted line is observed by NMR.*

In another recent example of the identification of IMHBs and their ability to improve the oral bioavailability of compounds, a CCR2 antagonist **(14**, **Figure 26)** required a polar side chain for sufficient selectivity for the target, but compounds with a polar side chain were not permeable. However, the incorporation of an amide in the side chain allowed for IMHBs (shown in the figure as red lines) which shielded the additional polarity, leading to superior oral bioavailability. The IMHB was observed using crystal structures and spectroscopically, with NMR. Upon protonation of the amine group in the aqueous compartment, the compound could then change to a

different conformation which was optimal for binding, thus showing chameleonic behaviour.

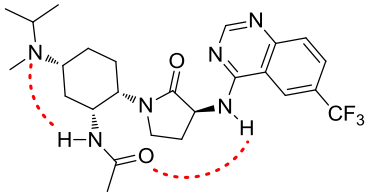

14

Figure 26 *CCR2 antagonist, capable of IMHB formation (shown by red dotted lines) when permeating, the subsequent protonation and conformational switching to the active conformation.*

A final example is that of a group of macrocyclic compounds, where range of phenyl ring-containing side chains were added to an amide-containing compound in an attempt to design in an NH-π interaction that would shield the amide polarity.[114] This last example is a rare case where there has been an attempt to design chameleonic behaviour into the compound rather than to just retrospectively detect it.

2.2 Observation of the permeability of 1 and its stereoisomers

During the development of **1**, it was found that its different stereoisomers **(Figure 27)** exhibit variability in potency and in membrane permeability between them **(Table 1)**.[115] This is apparent as a difference in both the cell permeability assay, measured in Madin-Darby Canine Kidney (MDCK) cells, and in the AMP assay.

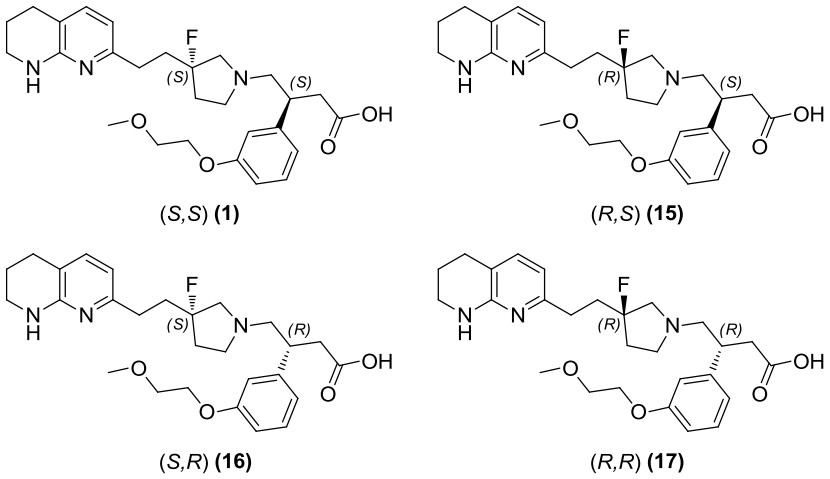

Figure 27 *The four stereoisomers of* ***1***

The (*S,S*) isomer, **1**, shows a similar potency to the (*R,S*) isomer **(15)**, but (*S,R*) **(16)** and (*R,R*) **(17)** show a reduction in potency of several log units. The absolute stereochemistry of the benzyl stereocentre appears to be important for the potency of the compound, whereas the combination of both stereocentres defines the permeability, according to the MDCK permeability (though the MDCK permeability of **17** has not been measured).

Compound	**1**	**15**	**16**	**17**
Configuration of stereocentres	(*S,S*)	(*R,S*)	(*S,R*)	(*R,R*)
Inhibition of $\alpha_V\beta_6$ integrin in cell assay (pIC_{50})	7.9	7.7	6.2	5.4
MDCK epithelial cell permeability / nm s^{-1}	87	19	32	-
Mean artificial membrane permeability / nm s^{-1}	132 (n = 8)	130 (n = 1)	72 (n = 4)	300 (n = 1)

Table 1 *A summary of the variable activity and permeability of* ***1*** *and its stereoisomers*

The AMP data also supported this observation, although it perhaps warrants more explanation. The focus of the analysis was on the comparison of **1** with **16**, rather than with **15** or **17**, because significant amounts of **16** were available as a by-product from the scale up of candidate **1**. **Table 1** shows the AMP data collected for the compounds at the time of writing, but **Table 2** shows the AMP data available for **1**

and **16** when the hypothesis for the permeability difference between the compounds was first made. **Table 2** shows a three-fold difference in permeability between **1** and **16**. However, since the AMP assay is known to have some variability associated with it, as evidenced by the wide range of values of permeability measured for **1 (Table 2)**, repeats of the AMP were made for **1** and **16**, giving the new mean values shown in **Table 1**, where the permeability difference between **1** and **16** is closer to two-fold.

Compound	**1**	**16**
Configuration of stereocentres	(*S,S*)	(*S,R*)
Mean artificial membrane permeability when the hypothesis was made / nm s^{-1}	156 (n = 5)	57 (n = 1)
AMP range when hypothesis was made / nm s^{-1}	68 – 280	-

Table 2 *The mean and ranges of the AMP permeability of **1** and **16** when the hypothesis was initially made*

In light of this variability in the assay (normally assumed to vary by ±30 nm s^{-1}, but clearly exhibiting a greater variability in the case of **1**, **Table 2**), a further ten identical samples of **1** on the same plate in the assay had their permeability measured,[116] and the results are summarised in **Table 3**.

AMP / nm s^{-1}
130
110
130
170
170
130
130
120
120
140

Table 3 *Additional AMP data for **1**, all run together and with the same sample, in order to test the variability of the assay*

These new data points support the notion that the assay will normally vary by ±30 nm s^{-1}, though the mean value of the new 10 data points is 135 nm s^{-1}, which,

encouragingly, is close to the previous mean of 132 nm s^{-1}. These additional data points suggest that although significant variability was initially observed in the AMP data for **1** initially, the mean data obtained may be relied upon.

It is this variability which is thought to explain the AMP values for **15** and **17**. Upon first examination, the AMP value of 130 nm s^{-1} for **15** appears to be very close to the mean for **1**, but it is anticipated that if more repeat measurements were made, this would value would fall to close to that of **16**, since enantiomers are not expected to differ significantly in this assay. Additionally, the MDCK permeability of **15** is similar to that of **16 (Table 1)**. Likewise, the value of **17** is much higher than for **1**, but this would be expected to be reduced to a value similar to **1** if more repeat measurements were carried out.

Resource constraints have precluded these additional data points from being collected, but this example clearly shows the significant variability of these AMP values. Unfortunately, due to resource limitations, it has not been possible to measure the MDCK permeability of some of the compounds synthesised herein, and so the AMP value must be used, though the variability of this value is acknowledged. This reduces the certainty with which conclusions can be drawn using these values alone. For compounds **1** and **16**, however, the additional repeats of the AMP measurement meant that there is increased confidence in these values, and the difference measured is thought to be genuine, particularly given the results of the other assays.

Compound	**1**	**15**	**16**
Configuration of stereocentres	(*S,S*)	(*R,S*)	(*S,R*)
Dose-adjusted oral rat AUC* / ng h mL^{-1}	795	101	-
Cell concentration assay PΔC	0.25	-	0.12

Table 4 *The rat AUC and cell concentration assay values for **1**, **15**, and **16**.*Compound **1** was dosed at 1.97 mg / kg, whereas compound **15** was dosed at 1.01 mg / kg, so the measured mean for **1** has been divided by 2. Both values are the mean of three test occasions. The PΔC result in the concentration assay is the log([concentration of compound in cells]/[concentration of compound in a no cell control])*

Further comparisons between the stereoisomers are shown in **Table 4**. Due to its lower integrin affinity, compound **16** was not dosed *in vivo*, but its more potent enantiomer **15** was.[117] For compound **1**, the compound was dosed both orally and intravenously (IV), allowing for the calculation of the oral bioavailability of the compound.[117] However, isomer **15** was only dosed orally to the animal (without an accompanying IV dose as a separate part of the experiment), so the oral bioavailability could not be measured, as IV data is required to calculate the oral bioavailability. This precluded a direct comparison of the oral bioavailability of the two compounds. Additionally, since the clearance of the compound is measured during the IV dosing of the animal, the clearance of compound **15** was not measured.

Table 4 shows the area under the curve (AUC), which corresponds to the total exposure of the drug in the bloodstream of the animals after the oral dose. The two compounds were dosed at different amounts, and so the AUC value has been adjusted to accommodate this. In comparing the two values, it must also be assumed that the clearance of the two compounds is the same, which is not known as the IV leg was not measured for **15**. In spite of these caveats, the nearly eight-fold difference in the values indicates that even if the clearances differ slightly, and there is further uncertainty introduced by adjusting for the different dosing, **1** is significantly better absorbed than **15**. This points to a superior permeability of **1**.

The final assay measurement used to compare the permeability of **1** and its diastereomers was the cell concentration assay, which measures the intracellular concentration of compounds dosed *in vitro*. Compound **1** was found to have a higher concentration than **16**, and the PΔC value is a logarithm of the ratio of the intracellular concentration and a no-cell control.[118] Therefore, the difference in measured values corresponds to an approximately 40 % higher concentration within the cell for compound **1**.

In summary of all the different assay results comparing the permeability of these compounds, the experiments suggest differing extents of permeability discrepancies

between **1** and its diastereomers **15** and **16**, but, in all cases, the candidate compound **1** was found to be significantly more permeable. The fact that this result was replicated across four different types of experiments suggests that the difference is genuine.

One valuable additional piece of evidence to corroborate the observed difference between the permeability of **1** and **16** was that during the development of **1**, it was found that similar fluoropyrrolidine-containing analogues to **1** showed a similar pattern of permeability between the diastereomers,[115] suggesting that this might be the result of a specific phenomenon rather than just a quirk of the assay data for this particular substrate.

2.3 The hypothesis for the unusual permeability observed

The obvious explanations for the difference in permeability between the diastereomers are either a difference in lipophilicity or a difference in pK_a and pK_{aH} values between the two diastereomers. However, **Table 5** shows that there is only a very small difference in these values, which was thought to be too small to account for the difference in permeability.

Compound	ChromlogD	pK_a and pK_{aH}s
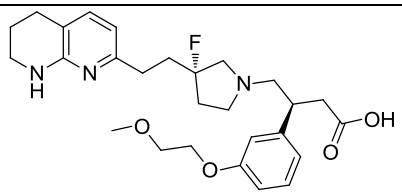 **1**	2.93	8.33, 7.33, 4.10
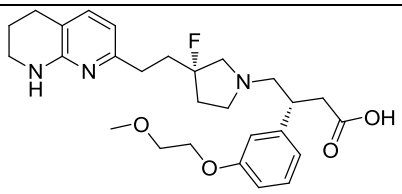 **16**	2.89	8.30, 7.17, 3.97

***Table 5** The measured lipophilicity values and pK_a and pK_{aH} values for **1** and **16**.*

Therefore, the difference in permeability between **1** and its diastereomers is proposed to arise as a result of the different conformations that the molecules prefer in a lipophilic environment, such as is found in a lipid bilayer. It is hypothesised that **1** is able to more readily adopt conformations in lipids that mask the polarity of the molecule and enable it to pass through the membrane, and that these conformations are less accessible to its diastereomers, explaining the lower permeability that is observed. In particular, it was proposed that **1** could form IMHBs, allowing for masking of the polarity of the compound, and **16** could either not form them at all, or not form these interactions to the same extent that **1** is able to.

2.4 Aims and approach of the investigation

It is proposed that this hypothesised conformational effect can be investigated spectroscopically, computationally, and by synthesising tool compounds to assess the effect of structural changes on the permeability. The aim is to confirm whether there is a conformational effect, and whether this is responsible for the difference in

permeability. If the effect can be identified, then it is envisaged that it would be possible to assess whether this effect is also true for other RGD integrin antagonists. If the phenomenon is observed across a range of $\alpha_V\beta_6$ inhibitors then, ideally, a means of predicting how pronounced the effect is for different prospective targets would be sought, in order to use this as a predictive tool for triaging compounds as part of targeting superior physicochemical properties. These superior properties are expected to arise as a result of gaining extra lipophilicity 'for free' by means of this chameleonic behaviour.

Firstly, considering the synthetic approach, the pyrrolidine ring in **1** limits the flexibility of the molecule and may reduce the likelihood of the proposed interaction between the polar groups in the molecule. In order to maximise the chance of such an interaction being seen, analogues of **1** with maximum flexibility, **18** and **19 (Figure 28),** will be synthesised, as tools for comparison with **1**, giving a baseline value for the permeability.

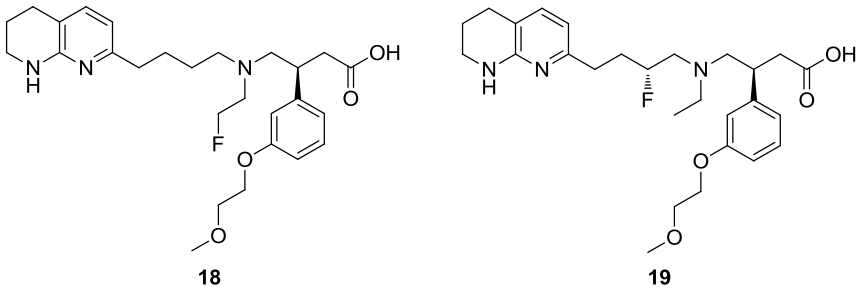

***Figure 28** More flexible analogues of **1** with a linear amine chain instead of a pyrrolidine moiety*

In addition to these compounds, it was proposed that if one or more of the polar groups on the compound was removed, then it may also affect the conformation that the compound is able to adopt, which may show an observable difference in terms of the permeability of the compounds. This would also be investigated.

In terms of the spectroscopic approach, NMR, vibrating circular dichroism (VCD) and IR were all tools proposed to be useful in investigating the conformation of these

compounds, with NMR anticipated to provide the most detailed insight, through the use of nuclear Overhauser effect (nOe) signals to calculate through-space distances.

It was intended that computational investigations could be used to corroborate the other evidence for the conformations that **1** and related compounds take. In particular, if these calculations could be validated, then the computational methods were envisaged to be the means by which this investigation could be most useful, namely that such properties could be forecast *in silico* for compounds that had not yet been synthesised.

2.5 Results and discussion: Synthetic work

2.5.1 Synthesis of linear analogues 18 and 19

Beginning with the synthesis of **18** and **19** to assess the effect of increasing the flexibility of the linker towards the formation of a 'permeable conformation', synthetic routes to both compounds were planned. Building on previous work within our laboratory,[87] **Scheme 1** shows the proposed disconnections to fluoroethyl analogue **20**. A final ester hydrolysis was proposed to furnish the final compound from **21**, preceded by a late stage asymmetric rhodium-catalysed Miyaura–Hayashi 1,4-addition of a boronic acid to ester **22** to yield the *meta*-substituted phenyl ring.[119,120]

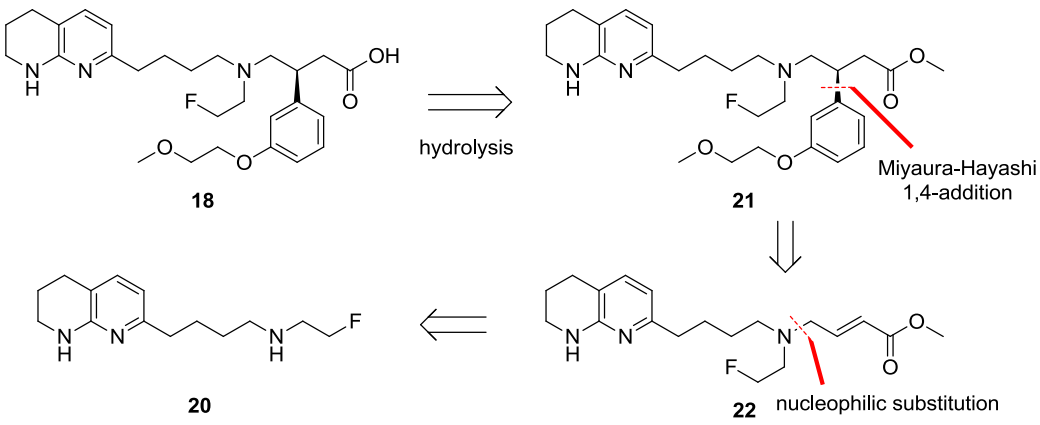

Scheme 1 *Retrosynthetic analysis of* ***18***

A simple base-catalysed nucleophilic substitution was envisaged to add the crotyl ester to **20**. It was proposed that fragment **20** could be obtained by reduction of amide **23**, itself accessible from reduction of compound **24 (Scheme 2)**. This could then be disconnected back to ester **25**, which could be accessed directly from available starting materials 2-amino nicotinaldehyde **(26)** and ethyl 5-oxoethanoate **(27)**.

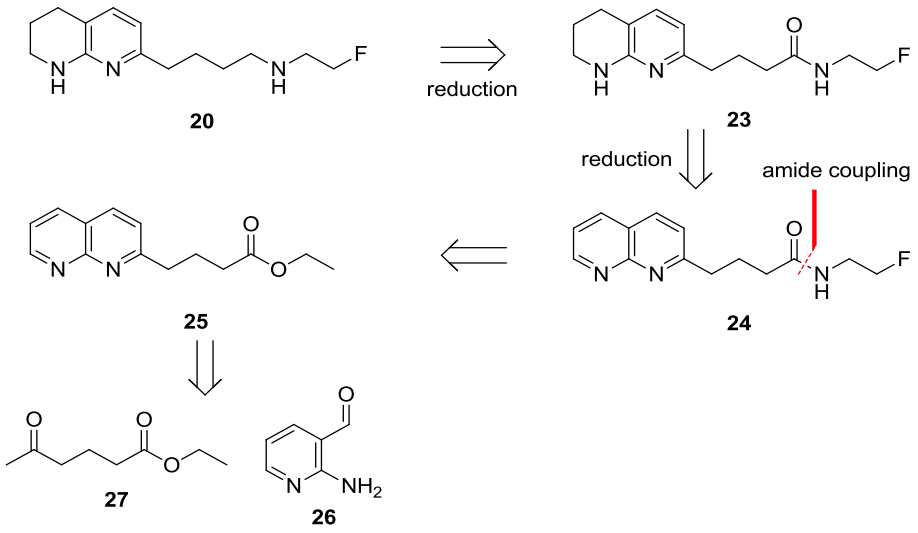

Scheme 2 *Retrosynthetic analysis of* ***20***

For more synthetically challenging analogue **19**, where the fluorine atom now forms a stereocentre in the carbon chain, it is envisaged that the final compound **19** could be disconnected in a similar fashion to the fluoroethyl analogue **18**, back to secondary amine **28 (Scheme 3)**.

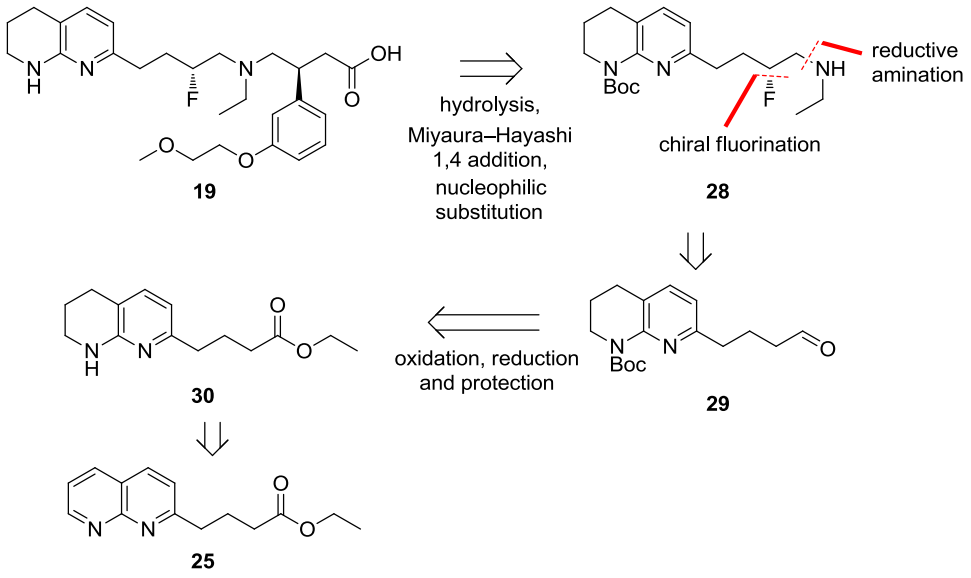

Scheme 3** Proposed disconnections of **19** back to common intermediate **25

It was proposed that chiral fluorination and reductive amination of aldehyde **29**, building upon the original work of MacMillan,[121] would furnish amine **28**. Aldehyde **29** could itself be accessed *via* manipulation of the carbonyl oxidation state and protection of the naphthyridyl nitrogen atom, in the forward sense, of tetrahydronaphthyridine **30**. This species could be accessed from naphthyridine **25**, which is common to the route for the other proposed analogue **18**.

Therefore, the synthesis of compound **18** was commenced. Starting from commercially available **26** and **27**, known ester **25** was accessed directly *via* a Friedländer reaction **(Scheme 4)**.[122]

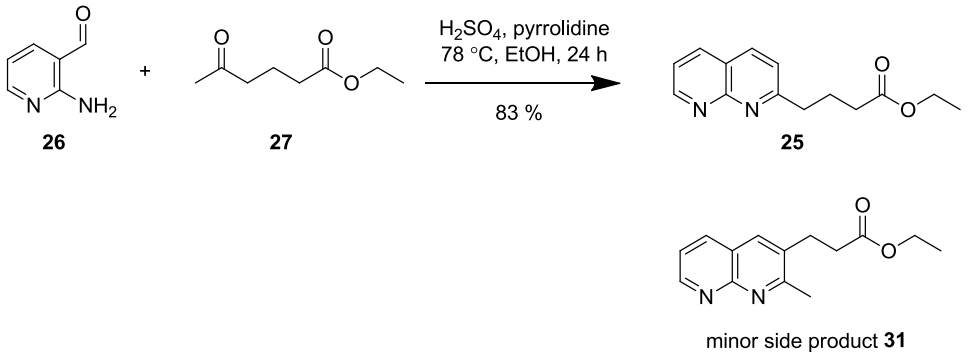

Scheme 4** The Friedländer synthesis of naphthyridine **25

A minority of the unwanted 2,3-disubstituted naphthyridine side-product **31** was

formed, although the addition of pyrrolidine-derived amines has been shown to increase the selectivity for the mono 2-substituted product,[123] and the two regioisomers were separable by column chromatography to give **25** in 83 % yield. The unwanted regioisomer was not isolated in this case.

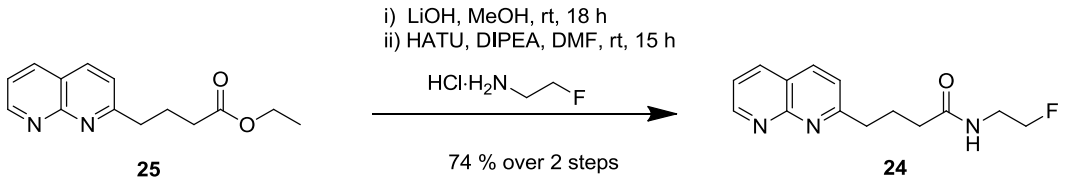

Scheme 5 Synthesis of amide ***24***

The formation of amide **24** was achieved by base-catalysed hydrolysis of ester **25**, with the resulting lithium salt used directly in an amide coupling, using 1-[bis(dimethylamino)methylene]-1H-1,2,3-triazolo[4,5-b]pyridinium3-oxide hexafluorophosphate (HATU) as a coupling agent, to furnish amide **24 (Scheme 5)**. Attempts to isolate the intermediate acid in good yield were hampered by the significant solubility of the product in H_2O, so the HATU coupling was performed directly on the crude product of the hydrolysis reaction, after concentration of the reaction mixture *in vacuo*, as has been previously reported.[124]

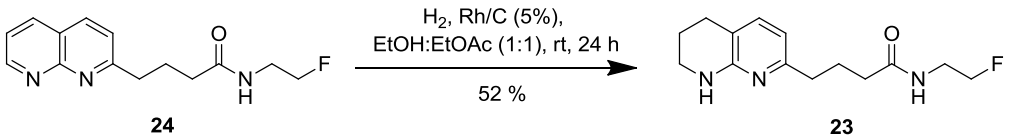

Scheme 6 *Hydrogenation of naphthyridine* ***24***

Building upon previous work in our laboratories,[125] the requisite hydrogenation showed selectivity for the desired side of the naphthyridine **(Scheme 6)**, when performed at ambient pressures and temperature, to yield tetrahydronaphthyridine **23**. The disappointing yield obtained is attributed to product insolubility during the filtration through Celite® during work-up.

With tetrahydronaphthyridine **23** in hand, it was anticipated that reduction with $LiAlH_4$ would quickly yield amine **20**, but this reaction led to the loss of fluorine and

possible formation of β-hydroxylamine **32 (Scheme 7)**, identified by NMR and liquid chromatography-mass spectrometry (LCMS).

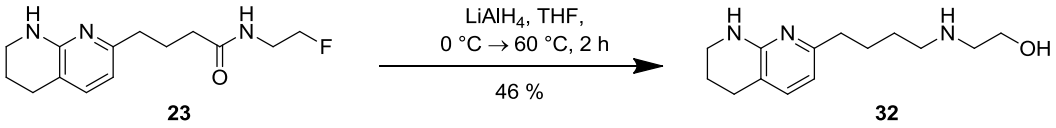

Scheme 7 Unwanted defluorination of tetrahydronaphthyridine 23

Formation of product **32** is proposed to occur *via* formation of an oxazolidine species that is subsequently opened upon addition of a second hydride nucleophile. Instead, borane was used to furnish amine **20 (Scheme 8)**, as has been used elsewhere in reducing the β-fluoroamide motif.[126]

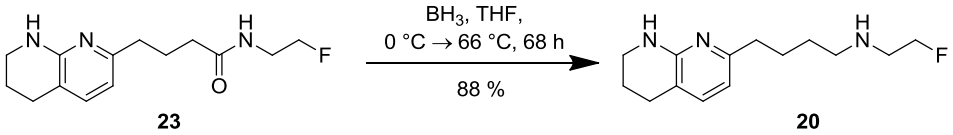

Scheme 8 Successful reduction of amide 23

This reaction proceeded very cleanly and did not require purification after the borane complexes were cleaved with NaOH in the work up. Indeed, such borane complexes are stable enough to use borane as a protecting group for 2-amino pyridines.[127] When this reaction was attempted on naphthyridine **24** before hydrogenation, amine **20** was also obtained directly, but in low yield and mixed with several other products.

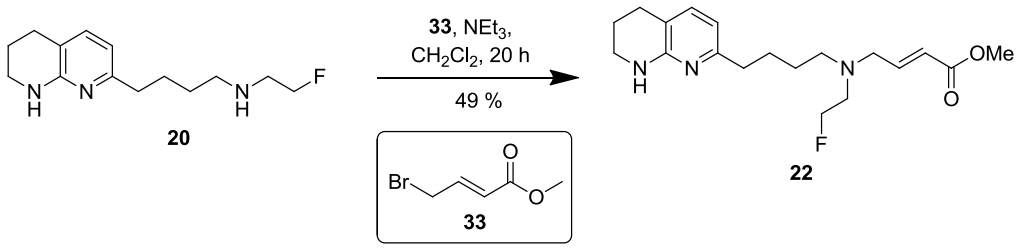

Scheme 9 Alkylation of amine 20

Work towards the synthesis of **18** continued with the alkylation of amine **20** *via* a S_N2 nucleophilic addition of bromide **33 (Scheme 9)**. The reaction proceeded cleanly to give the product, enoate **22**. The product was purified using high performance liquid

chromatography (HPLC). It should, however, be noted that the crude product after work-up was also competent in the subsequent cross coupling step.

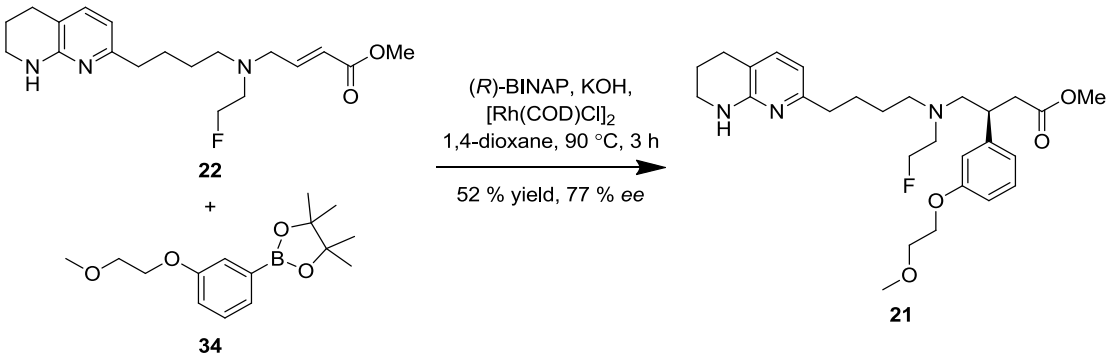

Scheme 10 *Rhodium-catalysed 1,4 addition of boronic acid **34** to **22***

Following this, the crucial asymmetric 1,4-addition of boronic ester **34** was attempted using a rhodium 1,5-cyclooctadiene (COD) chloride dimer catalyst, with the addition of an aqueous base to improve conversion and (*R*)- 2,2'-bis(diphenylphosphino)-1,1'-binaphthyl (BINAP) as the source of chiral bias.[120] The reaction proceeded as envisaged to form methyl ester **21 (Scheme 10)**. Despite being the subject of previous optimisation by co-workers in our laboratories,[128] this reaction exhibits a variety of yields, depending on the boronic acid or ester used. This was attributed to competing side reactions, such as metal-mediated elimination of the crotyl ester from **22** to re-form amine **20**, and protodeborylation of the boronic ester starting material, as observed by LCMS. The reaction occurred with satisfactory enantiomeric excess (*ee*) of 77 %, and a preparative chiral separation (carried out by co-workers Hortense and Hindley) followed to yield **21** as a single enantiomer.[129] The racemate, for use as an HPLC standard in the chiral separation, was prepared using racemic BINAP.

A small group of other boronic esters were coupled to crotyl ester **22** in order to generate a few analogues to provide some SAR around the linear 2-fluoro ethylamine motif and,[130] during hydrolysis of the resulting methyl esters to the final compound acids, it was found that basic conditions for the hydrolysis and purification led to partial degradation of the products. So, for the hydrolysis of ester **21**, an acid-

catalysed hydrolysis was performed instead, followed by reverse phase purification using a formic acid modified aqueous component to furnish final compound **18 (Scheme 11)** as a formic acid salt with no instability issues.

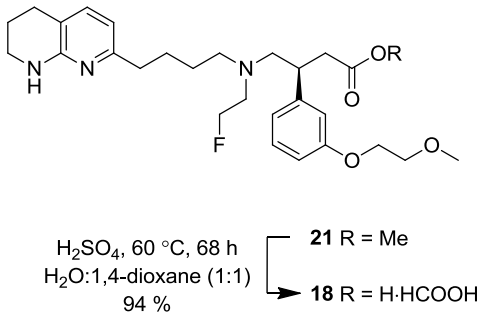

Scheme 11** Acid-catalysed hydrolysis of **21** to furnish **18

The proposed route towards β-fluoroamine analogue **19** was chosen such that it bore resemblance to the route to fluoroethyl analogue **18**, in order to expedite the synthesis. As such, ester **25**, already in hand from that previous work, was used as a starting point.

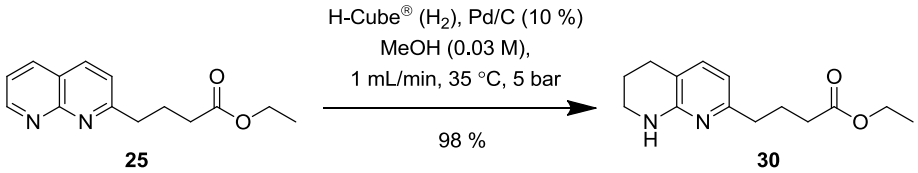

***Scheme 12** Selective hydrogenation of naphthyridine **25** using flow chemistry in the H-Cube®*

Ester **25** was conveniently and selectively reduced using the H-Cube® (a flow hydrogenation apparatus which generates H_2 *in situ*, and uses a cartridge of the desired catalyst) to furnish tetrahydronaphthyridine **30 (Scheme 12)**. Interestingly, in a traditional batch process in the presence of hydrogen, rhodium catalysis has been found by our laboratory to give the highest selectivity in reduction,[125] but a rhodium catalyst was not found to be as selective when the reaction was conducted using flow chemistry. Instead, a palladium catalyst was found to provide exquisite selectivity for the desired tetrahydronaphthyridine isomer **30.**

Following this, **30** underwent *tert*-butyloxycarbonyl (Boc) protection to give **35**, followed by reduction of the ester group to the corresponding alcohol **36 (Scheme 13)**. Following literature precedent,[131] the Boc protection of this electron-deficient amine was achieved, conveniently, without the use of either solvent or catalyst.

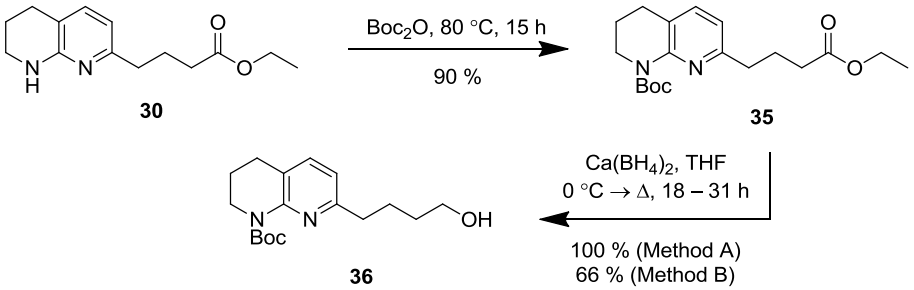

Scheme 13** Preparation of alcohol **36

Surprisingly, when Boc protection was performed on alcohol **36**, having already been reduced, the alcohol unit was found to react before the amine with Boc_2O. Ordinarily, the higher energy nitrogen lone pair compared to oxygen would make it more reactive to electrophiles. Therefore, this chemoselectivity indicates the extent to which the tetrahydronaphthyridine amine donates electron density into the electron-poor aromatic ring, thus lowering the energy of the nitrogen lone pair. Calcium borohydride, easily prepared from sodium borohydride and calcium chloride, provides a suitably reactive reducing agent to perform ester reduction.[132] On one occasion, the product was obtained quantitatively, when no purification was carried out, but was obtained in 66 % yield on another occasion, when the material was purified after the reaction did not go to completion.

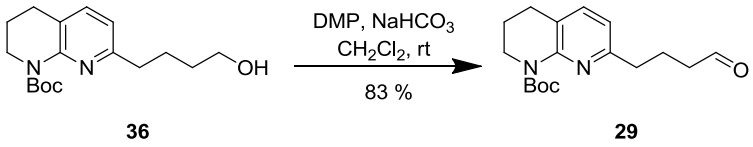

Scheme 14** Oxidation of **36** to **29

For the sake of convenience, Dess-Martin periodinane was the oxidising agent chosen for the oxidation of **36** to the corresponding aldehyde **29 (Scheme 14)**. Schreiber has

noted that the addition of a catalytic amount of H_2O to the oxidation accelerates the reaction cycle,[133] as the presence of a more strongly electron-donating hydroxyl group on the hypervalent iodine centre is able increase the dissociation rate of the final acetate group, liberating the final product. A drop of H_2O, therefore, was added to the reaction, which proceeded in 83 % yield.

With aldehyde **29** in hand, installation of the crucial β-fluoroamine moiety could proceed. MacMillan's original chiral α-fluorination chemistry with his imidazolidinone organocatalysts **37** and **38 (Figure 29)** has been applied to the formation of the β-fluoroamine moiety directly in a limited number of cases.[121,134]

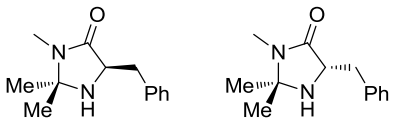

Figure 29 *Both enantiomers of MacMillan's imidazolidinone catalyst*

Though very high enantiomeric excesses have been reported, the presence of a tetrahydronaphthyridine group represents an extension of the scope of the reaction beyond that which has currently been reported. Both two-pot and one-pot tandem fluorination-reductive aminations have been reported with many more examples given for the former **(Scheme 15)**. Both begin with reaction of the chiral enamine (which forms between the aldehyde and organocatalyst) with *N*-fluorobenzenesulfonamide (NFSI).

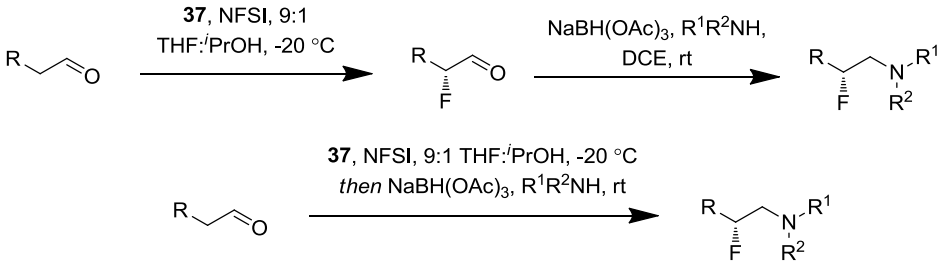

Scheme 15 *One-pot and two-pot sequences for the formation of β-fluoroamines*

In order to minimise the possibility of racemisation of the intermediate fluoroaldehyde, and for the sake of synthetic convenience on a small scale, the one-

pot procedure was chosen. The orientation of the fluoro stereocentre created was not thought to be a significant consideration at this stage, so the (*R*)-enantiomer of MacMillan's catalyst **37** was utilised, though it is envisaged that fluorine could be installed in the opposite sense straightforwardly using the (*S*)-enantiomer **38** instead. The amine initially chosen for the reductive amination was ethylamine, in order to form the *N*-ethyl species **28 (Figure 30)**.

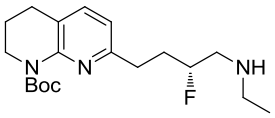

28

Figure 30 *Desired amine* ***28***

However, when ethylamine was used, no reductive amination was observed by LCMS. Therefore, *N*-benzylethylamine was used instead, as most of the amines exemplified in the original work were secondary amines. Gratifyingly, this approach yielded the desired β-fluoroamine **39** with pleasing enantio-enrichment, despite a disappointing yield **(Scheme 16)**. For chiral analysis, the reaction was carried out with pyrrolidine as the catalyst instead of **37** to give *rac*-**39** as an HPLC standard. Although it has not been possible to form crystals of intermediate **39**, tentative assignment of the stereocentre has been made based on the literature precedent.[134] Attempts to obtain crystalline material have included the hydrolysis of the Boc group of **39** and replacement with a *para*-nitrophenyl amide group, but this has still not resulted in crystalline material, presumably because of the high flexibility of the compound. For the same reason, VCD modelling is not anticipated to yield conclusive results.

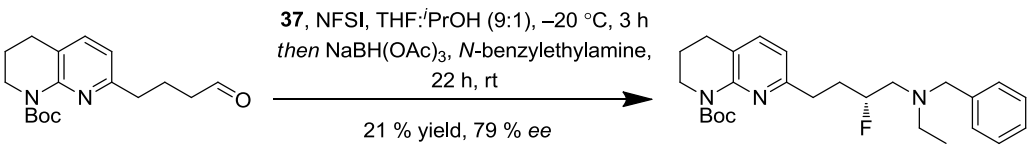

29 **39**

Scheme 16 *Formation of fluoroamine* ***39***

This reaction has not yet been the subject of any optimisation, and the alternative two-pot procedure has not yet been attempted. It is envisaged that a significant improvement could be made to the yield should such optimisation be performed. Separately, the *N*-methyl analogue **40 (Figure 31)** was also successfully synthesised by the author using the same approach, as previous SAR studies had indicated that this might be a potent compound.[135]

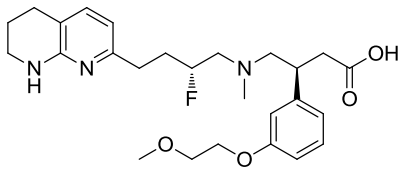

40

Figure 31 *N-methyl analogue* ***40***

With the fluorine atom successfully introduced, the benzyl group on **39** required removal in order to continue the synthesis analogously to the 2-fluoroethyl series, with addition of the crotyl ester. Rationally, initial attempts were made to remove this protecting group using hydrogenation. However, the presence of the aromatic tetrahydronaphthyridyl group meant that particularly forcing conditions could not be used, because of the likely regioselectivity issues. Attempts to remove the protecting group using both traditional hydrogenation conditions and using flow hydrogenation with the H-Cube® caused the formation of unwanted side products, therefore methodology introduced initially by Olofson for mild debenzylation with α-chloroethyl chloroformate **41** was employed instead to form **42 (Scheme 17)**.[136]

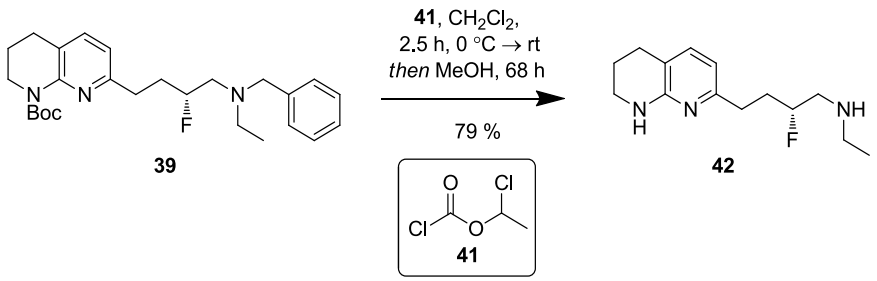

Scheme 17 *Mild debenzylation of N-benzyl amine* ***39***

This little-known transformation is believed to proceed *via* the mechanism outlined in **Scheme 18.** The tertiary nitrogen in **39** quaternises, then the benzylic group is preferentially removed by the chloride ion, due to the greater ability of the adjacent phenyl group to more readily stabilise the transition state compared to removal of the ethyl group. This yields carbamate **43**, at which point the CH_2Cl_2 is removed and the reaction is stirred in MeOH.

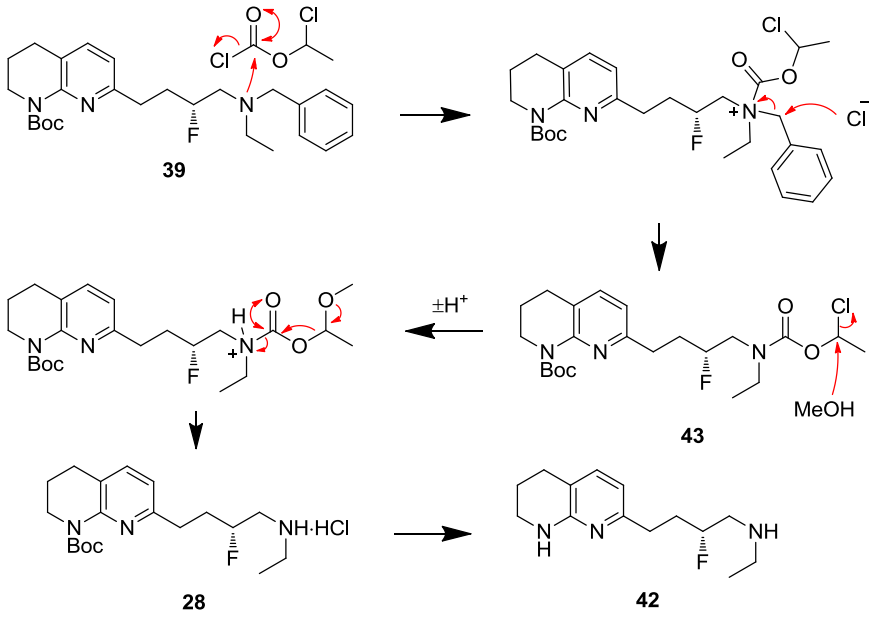

Scheme 18 *Mechanism of debenzylation, and subsequent Boc deprotection of* ***39****.*

This causes decomposition of **43** to form a hydrochloride salt of **28** and carbon dioxide, an entropic driver of this reaction. Particularly conveniently in this case, the formation of acid in this fragmentation causes subsequent Boc deprotection *in situ* to furnish desired amine **42**.

The same steps were then employed from this point in the synthesis as were used in the synthesis of **18 (Scheme 19)**. Crotyl ester **44** was furnished and subsequently arylated *via* 1,4-addition with boronic ester **34**.

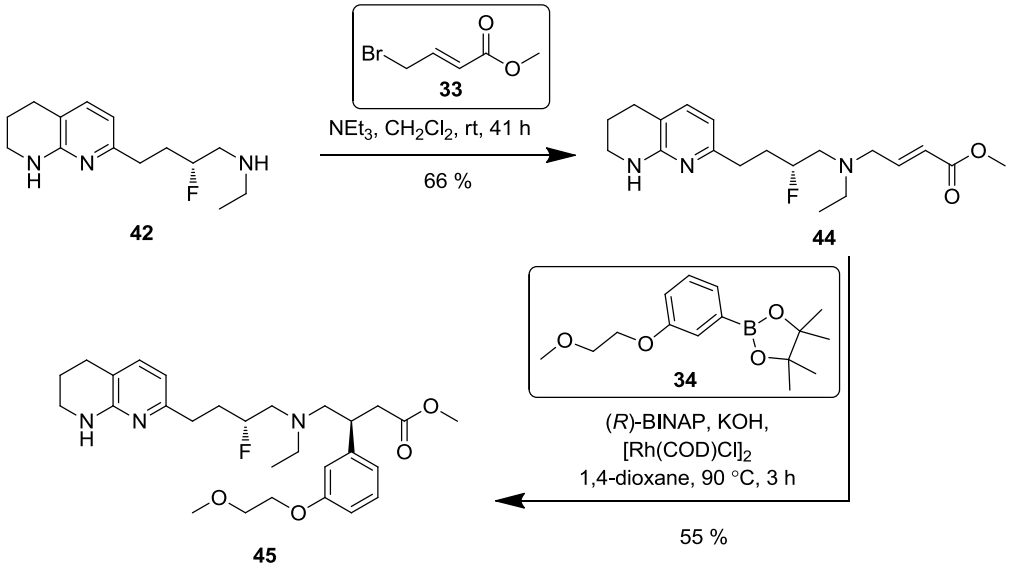

Scheme 19 *Preparation of methyl ester* ***45***

Ester **45** subsequently underwent chiral purification, followed by acid-catalysed hydrolysis and acidic purification conditions to furnish final compound **19 (Scheme 20)**.

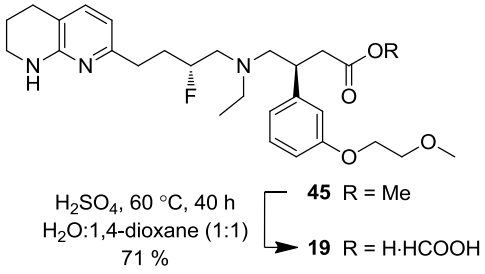

Scheme 20 *Hydrolysis of methyl ester* ***45*** *to furnish* ***19***

The AMP of compounds **18** and **19** were subsequently measured, along with the pK_a and pK_{aH} values. The results are shown in **Table 6**.

Compound	ChromlogD	AMP / nm s^{-1}	pK_a and pK_{aH}s
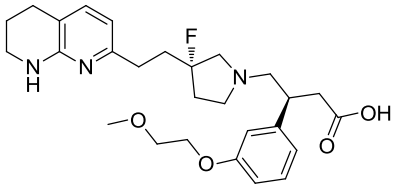 **1**	2.93	132 (n = 8)	8.33, 7.33, 4.10
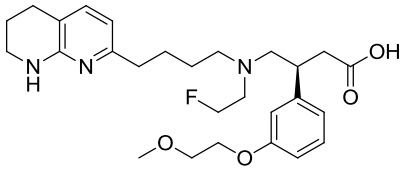 **18**	3.20	260 (n = 1)	8.36, 7.32, 3.69
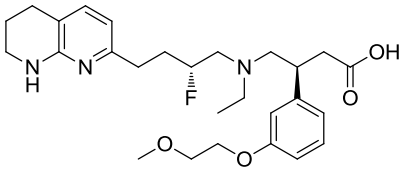 **19**	3.16	310 (n = 1)	8.41, 7.22, 3.49

Table 6 *The measured ChromlogD, AMP and pK_a and pK_{aH} values for **18** and **19**, compared with **1***

Pleasingly, the measured pK_a and pK_{aH} values for compounds **18** and **19** were very close to those of **1**. It had been hypothesised that the increased flexibility of **18** and **19** would give them the greatest possible chance of IMHB formation, therefore increasing the AMP. The measured AMP values were, indeed, much higher than that of **1**. Since only one AMP data point was measured for each compound, and given the variability of the AMP values exemplified by the stereoisomers of **1** (**Table 1**, page 30), caution must be taken with these values. However, it is likely that these values do indicate a real increase in the permeability of these compounds compared to **1**, as the disparity in AMP with **1** is significant. There was, unsurprisingly, also an accompanying increase in the lipophilicity, as measured by the ChromlogD, which is likely to also increase the AMP. The increase in AMP is not, therefore, the unequivocal result of an increased propensity to form IMHBs, because according to the pH

partition hypothesis, these compounds are also likely to be more permeable on the grounds of their lipophilicity.

2.5.2 Synthesis of tool compounds 46, 47, 53 and 54

In addition to the linear analogues **18** and **19,** the synthesis of some other analogues of **1** was targeted. More specifically, it was envisaged that removing the ether side chain of **1** would allow analysis of whether or not the ether chain had a role to play in contributing to the permeability difference between **1** and **16**. Therefore, analogues **46** and **47 (Figure 32)** were synthesised.

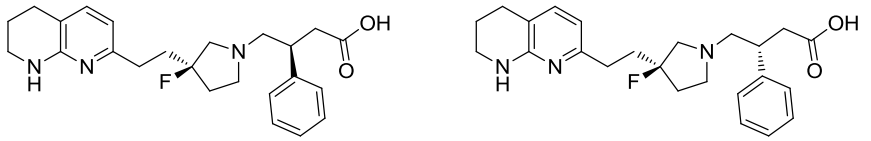

46 **47**

Figure 32 *Analogues of **1** without the ether side chain*

In fact, these compounds have the opposite stereochemistry to **1** at the fluoro position. This was simply due to the availability of advanced intermediate **48 (Figure 33)**, which was accessible within our laboratories, as an unwanted enantiomer isolated during the large-scale synthesis of **1**.[137]

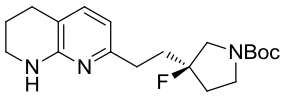

48

Figure 33 *Advanced intermediate **48***

The permeabilities of the two proposed diastereomers may still be compared with those of **1** and **16**, because the identity of the enantiomer is not thought to significantly affect the AMP.

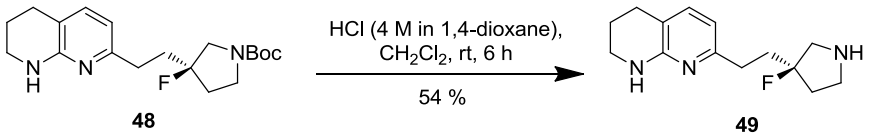

Scheme 21 *Boc deprotection of **48** to yield secondary amine **49***

Deprotection of **48** gave **49 (Scheme 21)** and, with amine **49** in hand, **46** and **47** could then be formed *via* the now familiar alkylation (to give **50**), 1,4-addition, and hydrolysis steps **(Scheme 22)**.

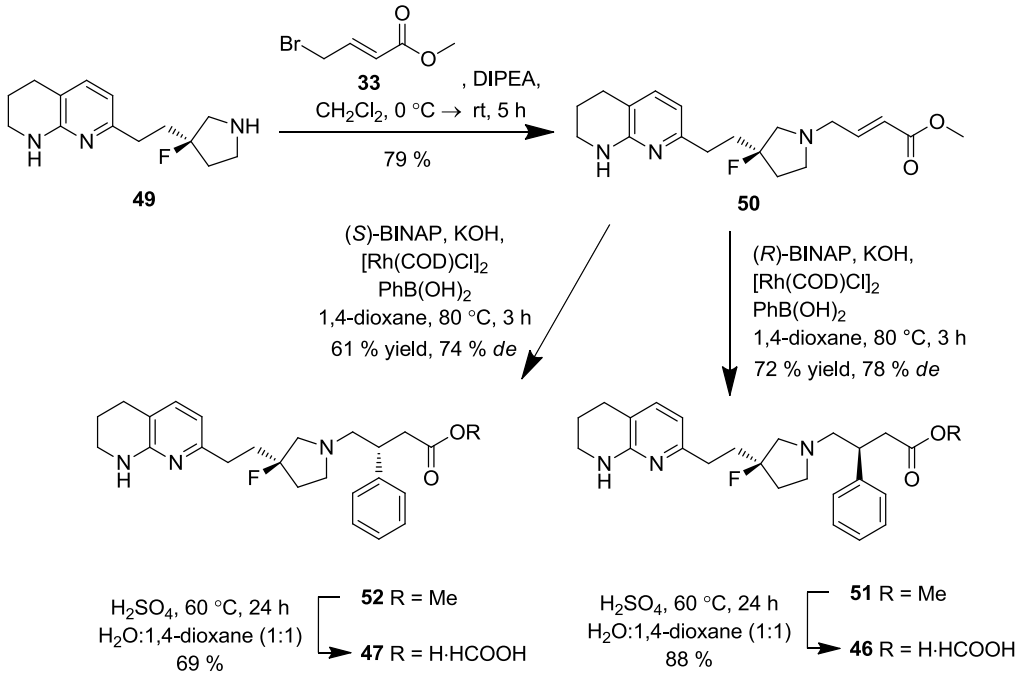

Scheme 22 *Synthesis of diastereomeric analogues of **1**, without the ether side chain*

With **50** in hand, choice of the two enantiomers of BINAP gave access to **51** and **52**. Conveniently, as **48** was received as a single enantiomer, the diastereomeric excess (*de*) of compounds **51** and **52** could be determined using ^{19}F NMR. After hydrolysis to give **46** and **47**, these compounds were subsequently sent for biological test to measure the permeability of the two diastereomers.

Compound	ChromlogD	AMP / nm s^{-1}	TPSA / $Å^2$
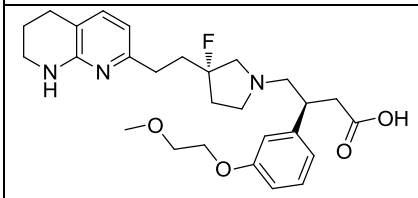 **1**	2.93	132 (n = 8)	83.9
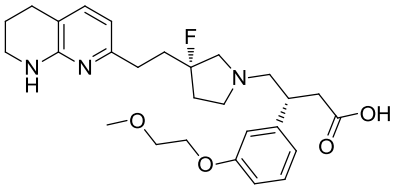 **16**	2.89	72 (n = 4)	83.9
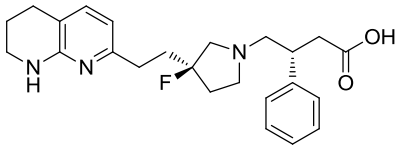 **47**	2.70	320 (n = 1)	65.5
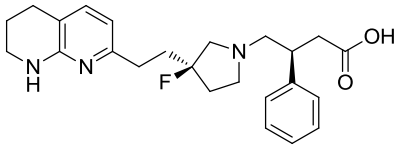 **46**	2.60	250 (n = 1)	65.5

Table 7** Permeability and TPSA data for compounds **46** and **47** in comparison with **1** and **16

Interestingly, both **46** and **47** were more permeable than **1** and **16 (Table 7)**, despite having a lower lipophilicity, which appears to contradict the pH partition hypothesis (which suggests that permeability correlates with lipophilicity). This result may indicate a greater propensity for these compounds to coil up compared to **1** and **16**, thereby gaining unexpectedly enhanced permeability. However, in this particular case, it is pertinent to consider the topological polar surface area (TPSA) of the compounds. This is especially relevant in this case, as removal of the ether side chain appreciably reduces the polar surface area of the compound, which is known to have a positive influence on the permeability of the compound.[138] This change in TPSA is anticipated to be partially responsible for the comparatively high permeability of these compounds.

Given the uncertainty associated with the AMP values, it is not possible to draw firm conclusions from the difference in AMP between **46** and **47**, although diastereomer **47**, with the same relative stereochemistry as **1**, does have a higher AMP than **46**. If this difference was real, it would imply that the effect causing the difference in permeabilities of **1** and **16** does not involve the ether side-chain, since the effect is exhibited without it present in the molecule.

In addition to this, a further diastereomeric pair of compounds were synthesised. In **53** and **54 (Figure 34)**, the phenyl ring has been chosen as a simple alternative to the tetrahydronaphthyridine group, in order to test the significance of the nitrogen atoms in that part of the molecule in the formation of possible intramolecular interactions which could influence the permeability of **1**.

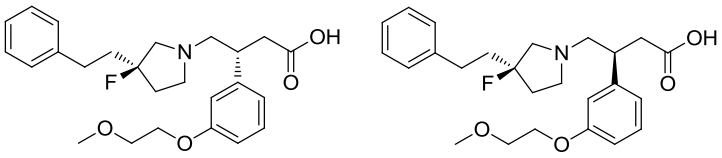

53 **54**

Figure 34 *A diastereomeric pair of compounds synthesised in order to investigate the importance of the naphthyridyl nitrogen atoms in IMHB formation*

The synthesis of these compounds began with intermediate **55 (Figure 35)**, also available from the scale-up synthesis of **1** for use in pre-clinical studies.[139] Although it has the opposite stereochemistry to **1** at the fluoropyrrolidine, like intermediate for **48** for the synthesis of **46** and **47**, the permeability of the resulting diastereomers (**53** and **54**) may still be compared.

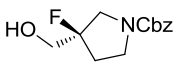

55

Figure 35 *Intermediate **55**, available from the scaled-up synthesis of candidate **1**.*

Phosphonium bromide **56** was prepared from benzyl bromide (**Scheme 23**), and it was envisaged that this could be used to append the phenyl ring to the fluoropyrrolidine ring in **53** and **54**.

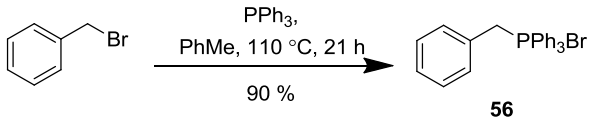

Scheme 23 *Preparation of phosphonium salt* ***56***

With **56** in hand, alcohol **55** was oxidised to the corresponding aldehyde, which was then reacted with the resulting ylide from phosphonium salt **56** to give vinyl species **57** as a mixture of geometric isomers (**Scheme 24**).

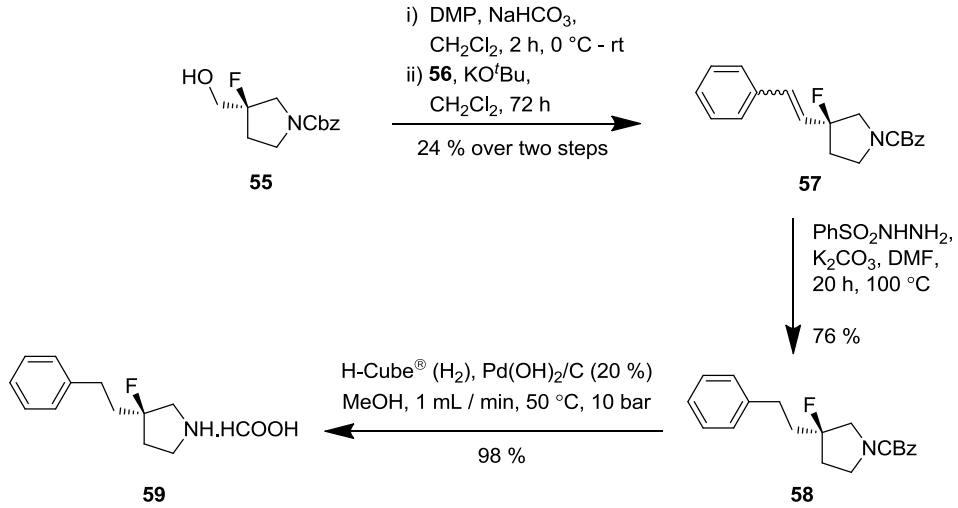

Scheme 24 *Preparation of intermediate* ***59***

Diimide reduction of **57** with benzenesulfonyl hydrazide furnished compound **58**, which was subsequently deprotected to yield secondary amine **59**.

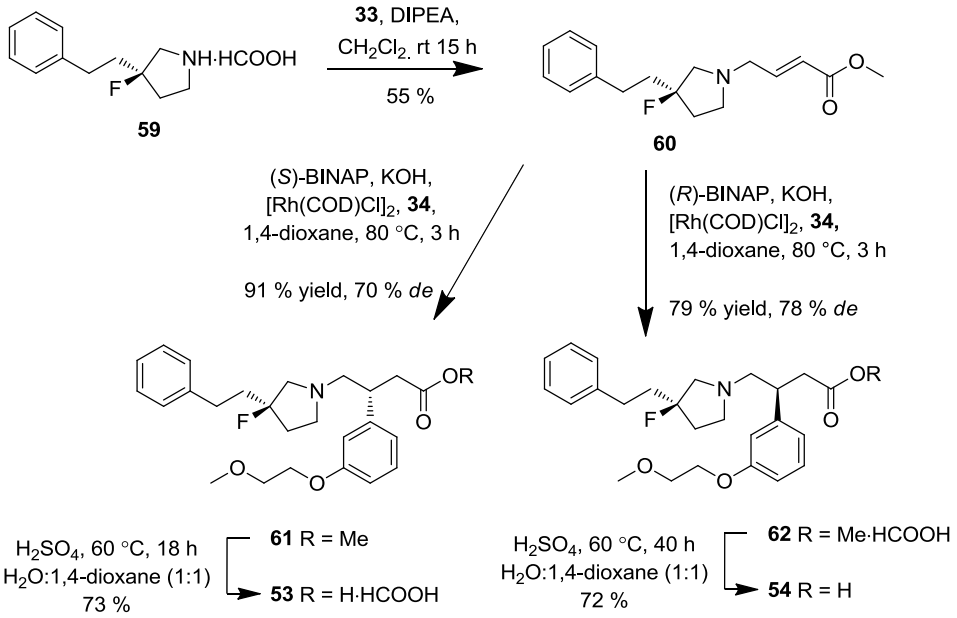

Scheme 25 *Synthesis of phenyl analogues **53** and **54***

Having prepared **59**, compounds **53** and **54** could be prepared by the usual route, *via* crotyl ester **60** and methyl esters **61** and **62 (Scheme 25)**. The AMP of these two compounds is shown in **Table 8**.

Compound	ChromlogD	AMP / nm s^{-1}	TPSA / $Å^2$
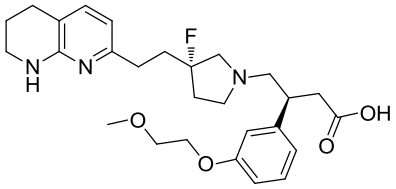 **1**	2.93	132 (n = 8)	83.9
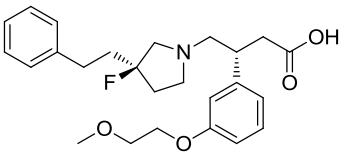 **53**	3.46	140 (n = 1)	59.0
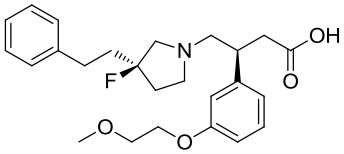 **54**	3.45	120 (n = 1)	59.0

Table 8 *Permeability and TPSA data for compounds **53** and **54***

Analogues **53** and **54** show a slight difference in permeability between one another, but it falls within the error of the assay and so no conclusions can be drawn from this difference. It seems possible, therefore, that removal of the hydrogen bond donor and acceptor of the tetrahydronaphthyridine moiety has removed a group that the molecule had been using in shielding its polarity, thus rendering both diastereomers **53** and **54** comparable in permeability. This notion is supported by the fact that when comparing analogues **53** and **54** to **1**, the AMP is comparable in spite of **53** and **54** having significantly higher ChromlogD, which would ordinarily be associated with a higher AMP. This is particularly striking given that the TPSA of these analogues are significantly lower than **1**, which would also ordinarily lead to increased permeability for these compounds. These data suggest that **53** and **54** may be in some way at a conformational disadvantage to **1** when permeating, since the additional lipophilicity does not aid their permeability, which would support the idea of IMHB formation in **1** and **16**. It also suggests that any interaction of the acid and the pyrrolidine nitrogen may be of lower importance than an interaction between the acid and tetrahydronaphthyridine group.

It is important not to draw conclusions beyond what that data suggests (especially as the AMP data is variable), however what is indicated by the results from the synthesis and evaluation of analogues **46**, **47**, **53**, and **54** is that AMP does not correlate with ChromlogD as would normally be expected. Whilst always expecting a very close correlation between these values under all circumstances is not reasonable, when considering compounds which are so similar to one another, they would be expected to correlate. Therefore, this indicates that other effects are involved in the permeability of these compounds, such as their conformations.

2.6 Results and discussion: Spectroscopic evaluation

2.6.1 ^{1}H NMR analysis

Encouraged that **1** and its analogues may indeed be capable of IMHB formation when permeating, and in an attempt to evaluate the conformations of **1** further, spectroscopic evaluation of **1** was carried out, first using ^{1}H NMR spectroscopy. Spectroscopic analysis indicated that one conformation predominated, which increases the likelihood of finding a distinct conformation. $CDCl_3$ is an appropriate solvent because it has a dielectric constant of 4.8, similar to that found at the centre of a bilipid layer.[140] Analysis of the correlation spectroscopy (COSY), heteronuclear multiple bond correlation (HMBC) spectroscopy, heteronuclear single quantum coherence (HSQC) spectroscopy, and nOe spectroscopy allowed the 'time averaged' conformation represented by the NMR data to be found.[141] The strength of the nOe signals could be quantified (this work was carried out by co-worker Upton), and the conformation, specifically around the pyrrolidine ring and benzylic stereocentre, could be estimated. The conformation of the core of **1** that resulted is shown in **Figure 36**.

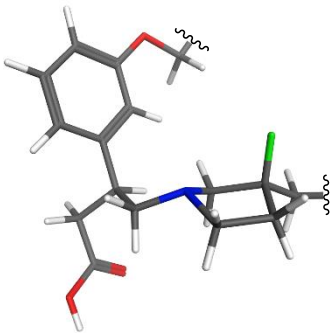

Figure 36 *The average conformation of the core of **1** by NMR. Full details of the nOe distances are included in the experimental section*

This truncated conformation of **1** indicated that it is not possible that the pyrrolidine nitrogen and the acid group are forming an IMHB, as the acid points away from this

cyclic amine. This was important information, as the small molecule crystal structure of a salt of **1**, which had been obtained prior to the commencement of this investigation, had displayed an interaction between the pyrrolidine nitrogen and the carboxylic acid (**Figure 48**, page 78), and so it was thought that this could be the type of IMHB observed for **1** in solution.

Unfortunately, however, the nOe data did not give any information about the conformation of the rest of the molecule, so it was not possible to deduce whether the acid group is engaged in an IMHB with the α-binding end of the molecule, or rather pointing into solvent. It seems unlikely that the acid group would extend out into solvent in a non-polar solvent such as $CDCl_3$, but unfortunately ^{1}H NMR is unable to give any more information.

Unfortunately, it has also not been possible to perform the same analysis of the NMR spectrum of **16**, as in this spectrum more of the proton shifts are overlapping, so assignment of the diastereotopic protons has not been possible. Therefore, a conformation has not been generated. This means that the time-averaged NMR conformation of **1** in deuterated chloroform may not be compared and contrasted with that of **16**, although it is noteworthy that the ^{1}H NMR spectra of **1** and **16** did appear to be significantly different from one another.

2.6.2 ^{15}N NMR analysis

Prompted by the use of chemical shift indexing for amide NH bonds to analyse IMHB formation in peptides,[142,143] it was proposed that a similar technique could be used to analyse the NH bonds in **1**. Although such a technique was not found, during these deliberations it was highlighted that ^{15}N NMR is a potentially powerful and significantly underused tool for probing the structure and conformation of compounds.[144]

The sensitivity of ^{15}N NMR is extremely low on account of its very low natural abundance (0.37 %) and low magnetogyric ratio, giving it a relative sensitivity approximately 50 times smaller than that of ^{13}C NMR.[144] This necessitates indirect detection of the nuclei, namely using ^{15}N HMBC spectra, in order to measure the shift, so that the much larger magnetogyric ratio of the protons may be utilised to increase the sensitivity.

In spite of these challenges in detection, the spectra are very useful, as the chemical shifts of protonatable sp^2-hybridised nitrogen atoms vary greatly depending on their state of protonation. As an illustration, the chemical shift of the nitrogen in pyridine itself is approximately 310 ppm, while fully protonated pyridine has a shift of approximately 200 ppm **(Figure 37)**. This upfield shift of approximately 100 ppm upon protonation has been observed for many sp^2-hybridised nitrogen-containing rings and functional groups.[145,146]

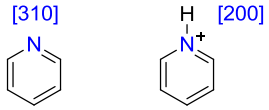

Figure 37 *The ^{15}N NMR shifts of pyridine and protonated pyridine, measured by ^{15}N HMBC spectroscopy*

As the protonation/deprotonation process is rapid on the NMR timescale, the observed shift of a pyridine nitrogen can be viewed as indicative of the level of protonation in solution, particularly as the study by Semenov referenced above showed an approximately linear relationship between the amount of acid added to a heterocycle in solution and the change in shift of the nitrogen atom (up to one equivalent of acid).[145] This makes it possible to assess the degree of protonation of sp^2-hybridised nitrogen atoms in solution.

It is not possible to perform the analysis to the same extent with sp^3-hybridised nitrogen atoms, and in fact these show a small downfield shift upon protonation (of approximately 10 ppm). Natural bond orbital analysis has shown that this strikingly different behaviour is the result of the lone pair on the nitrogen atom.[145]

More specifically, the total nuclear screening, which is responsible for the observed NMR shift is the sum of the local diamagnetic screening, the local paramagnetic screening, and additional screening from sources other than the nucleus, such as solvent effects.[147] The diamagnetic screening dominates for proton chemical shifts, and is directly related to electron density, as it arises from magnetically derived local electronic circulations around the nucleus. The additional screening sources are usually minor.

The local paramagnetic term, σ^p, which has a deshielding influence, unlike the diamagnetic component of the screening, is most significant in the case of ^{15}N NMR. Its significance in the present case may be explained by **Equation 1** below.[147]

$$\sigma^{\mathrm{p}} \propto \frac{1}{\Delta \mathrm{E}} \langle \frac{1}{\mathrm{r}^3} \rangle \sum Q$$

Equation 1 *The relation of the paramagnetic contribution (σ^p) to the total nuclear screening to the excitation energy between the ground and excited states (ΔE), the orbital radius of the electrons influencing the shift (r), and the charge density of bonding electrons (Q).*

In nitrogen-containing heterocycles such as pyridine, there are low-lying excited states into which the nitrogen lone pair may be excited (hence ΔE is small).[148] Additionally, the sp^2 hybridisation of the nitrogen results in larger s character of the nucleus compared to an sp^3 nitrogen, meaning a smaller value for r. Thirdly, multiple bonding to the nitrogen is present, therefore the contributions to *Q* are large. These factors result in a large contribution of σ^p to the total nuclear screening, and therefore the dominance of this effect in the ^{15}N shift of sp^2 nitrogen nuclei.

Once the nitrogen lone pair is protonated, this deshielding paramagnetic contribution to the overall NMR shift of the nucleus is much reduced. This is as a result of the occupation of the nitrogen lone pair in a bonding interaction with the proton, which precludes excitation of that lone pair into excited states (ΔE is significantly increased). This effect is much more significant than the deshielding influence of the positive charge (which affects the diamagnetic contribution to the

overall shift), resulting overall in the significant upfield shift of the ^{15}N NMR shift signal.[146]

In contrast, with an sp^3-hybridised nitrogen atom the lone pair has no low-lying excited states (large ΔE), the electrons are held further from the nucleus (larger r), and the multiple-bond character at the nitrogen is less (smaller Q), so the paramagnetic contribution to the overall shielding is very small. As a consequence, there is no significant change in shielding from the lone pair, as in the sp^2 case, upon protonation. Consequently, the deshielding influence of the positive charge on the sp^3 nucleus (a diamagnetic contribution) when protonated is the most important contribution, leading to a relatively small downfield change of the shift.

Without this sensitivity to the change in protonation, it is not possible to analyse the extent of protonation for sp^3 nitrogen atoms using ^{15}N NMR with the same sensitivity as for their sp^2 counterparts .[149] Instead, the shift of α-methylene groups to the sp^3 amine are often compared to a matched pair where the amine may not become protonated, to assess whether significant positive charge has built up on the nitrogen nucleus, since the shifts of the neighbouring protons are affected by this charge.

Optimistic that this approach could be applied to the case of the sp^2 nitrogen atoms in **1** and **16**, both compounds were repurified using an HPLC method with an ammonium carbonate modifier, in order to obtain both compounds in their free base form, without an acid which could interfere with the results. Again, using $CDCl_3$ as the solvent, **1** and **16** had their ^{15}N HMBC spectra measured, along with their corresponding methyl esters **63** and **64**, to use as controls. All ^{15}N spectra were acquired by co-worker Richards.[150] **Figure 38** shows the shifts of the pyridyl nitrogen atoms in each compound.

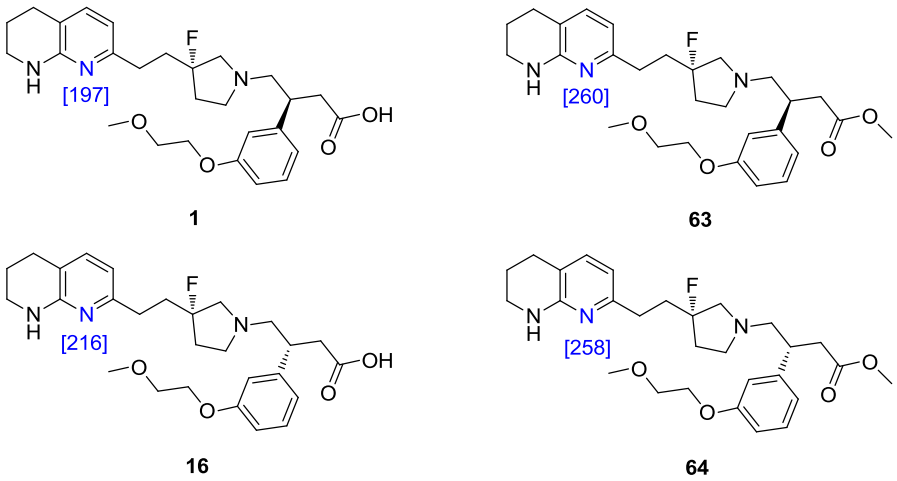

Figure 38 *The ^{15}N NMR shifts of compounds **1**, **16**, **63**, and **64**.*

It was immediately apparent that for both **1** and **16**, the ^{15}N shift of the aromatic nitrogen was significantly reduced compared to the corresponding methyl esters, which were within a few ppm of one another. This indicates that in both cases, there is a greater degree of protonation in the zwitterionic final compounds compared to their methyl ester analogues. It is assumed in the cases of the methyl esters, since no labile protons are present on the molecule, that these N shifts represent the completely non-protonated form.

It is essential to consider what the possible source of the protonation of the tetrahydronaphthyridine group is for compounds **1** and **16** since the shift of the nitrogen by ^{15}N NMR would not differentiate between protonation as a result of normal tautomerisation between the zwitterionic and neutral forms of the compound. Although it is anticipated that in a non-polar solvent such as $CDCl_3$ the zwitterionic form would not exist,[95] it is important to rule out such behaviour. Fortunately, in the case of compounds such as **1** and **16**, the tetrahydronaphthyridine moiety is not the most basic functional group in the molecule, rather it is the fluoropyrrolidine which has a pK_{aH} approximately 1 unit higher than that of the tetrahydronaphthyridine group. The fluoropyrrolidine, therefore, would be expected to protonate before the tetrahydronaphthyridine group.

When comparing the ^{1}H NMR spectra of **1** with **63**, it was evident from the shifts of the methylene protons surrounding the fluoropyrrolidine nitrogen (fully assigned spectral data is included in the experimental section), that there is no significant difference in protonation between the group in the two different compounds. Therefore, if the fluoropyrrolidine nitrogen is not protonated through zwitterionic tautomerisation in **1**, the aromatic nitrogen is not expected to be protonated *via* traditional zwitterionic tautomerisation behaviour either.

The other source of protonation that it is important to rule out is the *inter*molecular protonation of **1** by another molecule of itself. Crucially, a spectrum of **1** in $CDCl_3$ spiked with the corresponding methyl ester **63** showed no change in the shifts of the pyridyl nitrogens observed for either the acid or the ester. This spectrum clearly demonstrated the protonation activity to be an entirely *intra*molecular process, as the chemical shifts for both acid and ester were preserved in the mixture. Had there been any *inter*molecular protonation taking place, an averaging of the observed shifts would have been expected based on the very close similarity of the two compounds.

Having ruled out the observations as being a result of either intermolecular behaviour or zwitterionic tautomerisation, it does indeed appear that the reduced ^{15}N shift is as a result of partial intramolecular protonation, therefore IMHB formation, in **1** and **63**. Excitingly, the sensitivity of the technique, in that the ^{15}N signal varies by approximately 100 ppm depending on the extent of protonation, means that the value of the shift can not only give an indication of whether or not an IMHB is formed, but also give an indication of the level of protonation, therefore the extent of IMHB formation. There is a 20 ppm difference between the shifts of the N in **1** compared to **16**, which is indicative of a significantly greater quantity of protonation at the tetrahydronaphthyridyl nitrogen in **1** compared with **16**. This indicates a greater extent of hydrogen bonding in **1**, which was what was hypothesised to give the improved membrane permeability compared to **16**. This result is very significant, as

this spectroscopic method appears to be capable of not only identifying but also quantifying the extent of IMHB formation in these compounds.

Another important experiment was to run the ^{15}N NMR experiment for both **16** and **64** in deuterated DMSO, the results of which are shown in **Figure 39**. In this case, the ^{15}N shift of the pyridyl nitrogen atoms are the same in both **16** and **64**, indicating that in this solvent, no IMHB formation is taking place. This is in line with the hypothesis that it is only the relative hydrophobicity of a lipid bilayer, or $CDCl_3$, which promotes the formation of IMHBs, and so in a polar solvent such as DMSO this is not observed.

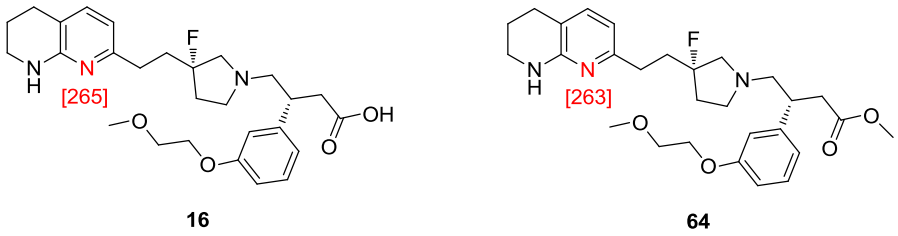

16 **64**

Figure 39 *^{15}N NMR shifts of compounds **16** and **64**, measured in deuterated DMSO, with the pyridyl nitrogen atoms showing an almost identical ^{15}N shift, indicating no IMHB formation in this solvent*

In order to better understand the behaviour of these compounds in relation to their ^{15}N shifts, a group of tool compounds was synthesised. Firstly, compounds **65** and **66** were chosen, based on the ability of **65** to form a six membered ring containing a hydrogen bond, compared to **66** which cannot. From a stock of **67** in our laboratories from a previous scale up campaign, compound **65** was prepared by Boc deprotection with trifluoroacetic acid (TFA), whilst methyl ether **66** was prepared by *O*-methylation to give **68**, followed by subsequent Boc deprotection **(Scheme 26)**.

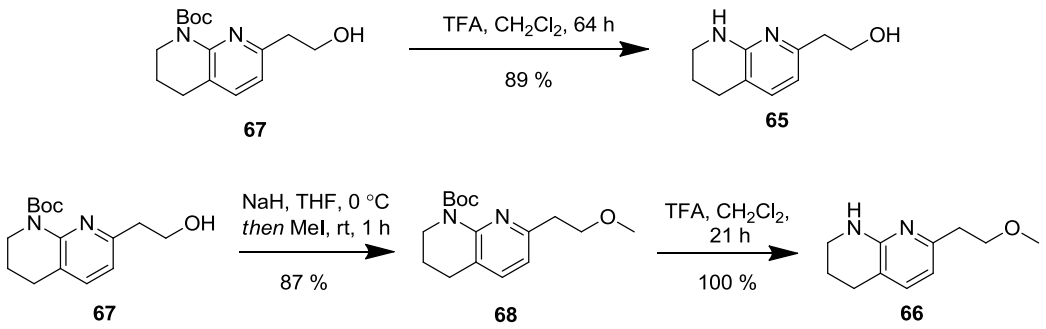

67 **65** **67** **68** **66**

Scheme 26 *The preparation of **65** and **66** for ^{15}N NMR analysis*

^{15}N NMR analysis of **66** showed a very similar result to that seen with the methyl esters of **1** and **16**, with approximately 260 ppm appearing to be an approximate baseline for the tetrahydronaphthyridine group. A small difference in the shifts between **65** and **66** was observed, but it is noted how much smaller of a difference this is compared to in the fully elaborated compounds **(Figure 40)**. It is possible that this is due to a reduced ability for the hydroxyl group of **65** to donate its proton to the aromatic nitrogen compared to a carboxylic acid group, or due to a difference in pK_{aH} value of the tetrahydronaphthyridine group in this example. However, it seems more likely that the smaller difference arises as a result of the fact that a hydroxyl group is more easily tolerated by the surrounding $CDCl_3$ solvent molecules compared with a more polar carboxylic acid group. Therefore, it is anticipated that there would be a decreased driving force for the formation of a hydrogen bonded ring (given the entropic costs of such an interaction) for the masking of a hydroxyl group in **65** compared with a carboxylic acid group as in compound **1**.

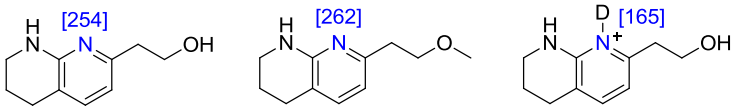

*Figure 40 ^{15}N NMR shifts of compounds **65** and **66***

Additionally, in order to set a lower bound for the shift of the tetrahydronaphthyridine group with complete protonation of the nitrogen, to a sample of **65** was added DCl in order to completely acidify the sample. The resulting shift of 165 ppm **(Figure 40)** confirms that there is a range of approximately 100 ppm between no protonation and complete protonation of the nitrogen. Since the shift changes approximately linearly with the amount of protonation at the nitrogen atom,[145] then it appears that a percentage amount of protonation of the N atom as a result of IMHB formation could be determined using this method.

In order to make a comparison with the corresponding compound with a carboxylic acid group present, compounds **69** and **70** were prepared **(Scheme 27)**. Reaction of

2-methyl-1,8-naphthyridine **(71)** with diethyl carbonate, followed by reduction using a rhodium catalyst furnished ester **69**, a portion of which was then hydrolysed to give **70**.

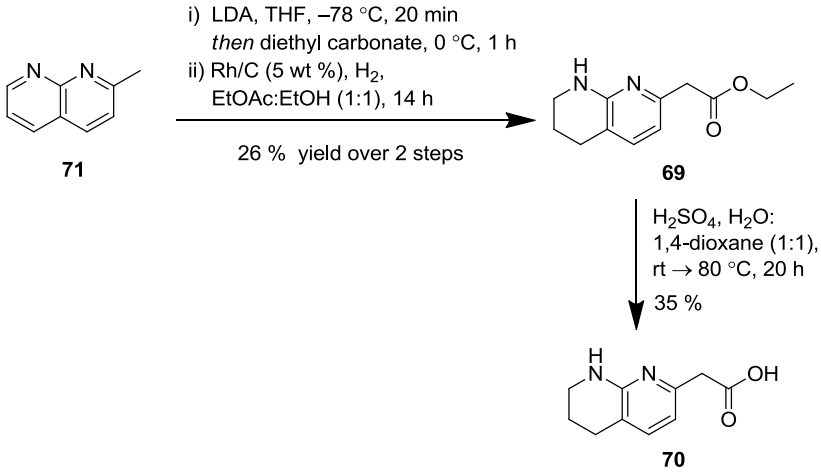

Scheme 27 *The synthesis of ester **69** and carboxylic acid **70***

Comparing acid **70** and ethyl ester **69** to the corresponding hydroxyl and ether pair **65** and **66**, the difference in N shift is much more pronounced. Indeed, compound **70** looks close to fully protonated **(Figure 41)**. This perhaps is not a surprise given that this compound is perfectly oriented for a hydrogen bond and is likely to have an increased driving force for its formation compared to alcohol **65**.

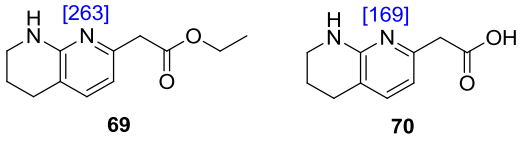

Figure 41 *The ^{15}N NMR shifts of compounds **69** and **70***

An example was sought whereby the formation of an IMHB was not possible geometrically. This led to the synthesis of **72** and **73 (Scheme 28)**, chosen because, conveniently, the starting material **31** was available as an unwanted side product during the Friedländer synthesis of **25**. In fact, **31** could be accessed in improved yield using alternative Friedländer conditions, using NaOH as the base. Subsequent reduction provided access to ester **72**, which was then hydrolysed to yield acid **73**. This product was only obtained in very low yield, because the product was highly

insoluble, and it was necessary to purify these compounds by HPLC in order to ensure that the pH of the final compound was controlled. In order to load the crude product of **73** onto the HPLC, only a small portion could be taken, hence giving only a very low isolated yield after purification.

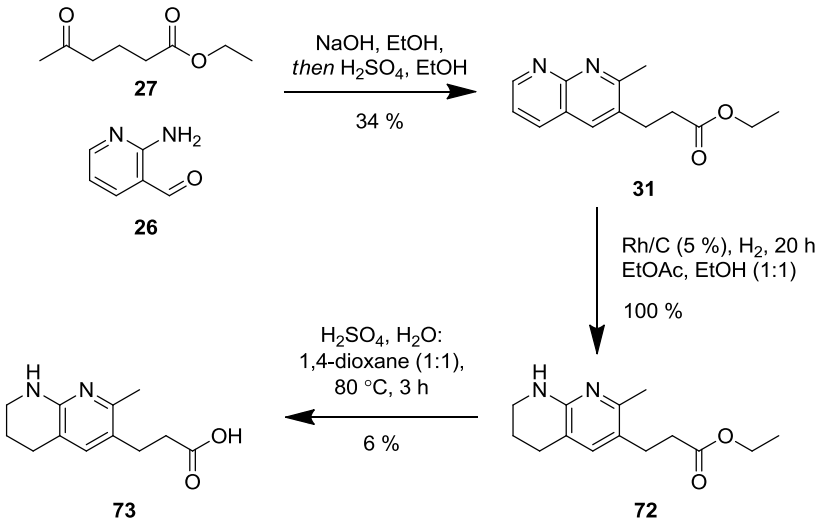

Scheme 28** The preparation of **72** and **73** from **31

The solubility of acid **73** was remarkably different from all the other tool compounds synthesised, and it was only very sparingly soluble in chloroform, requiring significant heating and sonication to give sufficient solubility for a weak spectrum to be obtained.

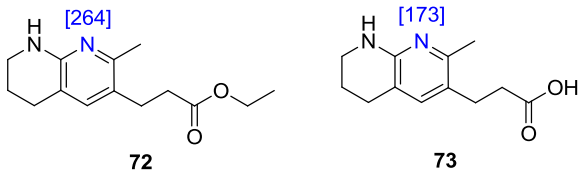

Figure 42** The ^{15}N NMR shifts of **72** and **73

Somewhat surprisingly, **73** showed nearly full protonation **(Figure 42)**, despite appearing to be unable to form an IMHB. However, subsequent measurement of the pK_{aH} of the tetrahydronaphthyridine group of this molecule indicated that the pK_{aH} is 8.47, which is one unit higher than in **1**, where the presence of a more basic group in the molecule reduces the basicity of the pertinent sp^2-hybridised nitrogen. This greater difference in pK_a between the acidic and the basic groups in the molecule

means that there is a greater driving force for the molecule to exist as the zwitterionic tautomer **(Figure 43)**.

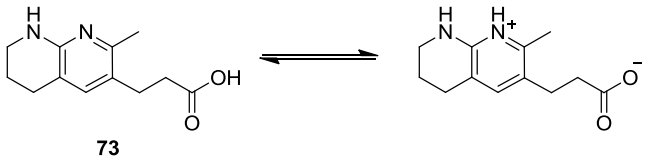

73

Figure 43 *The tautomerisation of* ***73*** *between its neutral and zwitterionic forms*

The N shift of the compound may, therefore, be explained by the molecule behaving as a zwitterion rather than as a neutral molecule. Whilst this is merely speculation, it is supported by the drastically different physical properties of the compound in comparison to all the other analogues, which are highly soluble in $CDCl_3$. It may be that without the opportunity for IMHB formation, the alternative zwitterionic form becomes more thermodynamically favourable. This example does serve as a reminder, however, of the complexity of these compounds when considering their ^{15}N NMR shifts, since there are several means by which protonation of the nitrogen may occur.

Buoyed by the productivity of this approach, ^{15}N HMBC analysis of a simplified analogue of **1** was carried out. Compound **74** was designed as a part of the 'back-up' programme, to have very similar properties to **1 (Table 9)**, but to be more synthetically tractable.[151]

Compound	ChromlogD	pK_a and pK_{aH}s	AMP / nm s^{-1}	MDCK permeability/ nm s^{-1}
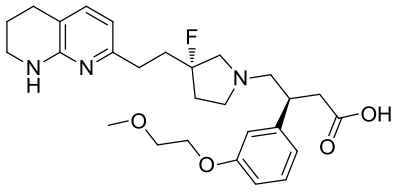 **1**	2.93	8.33, 7.33, 4.10	132 (n = 8)	87
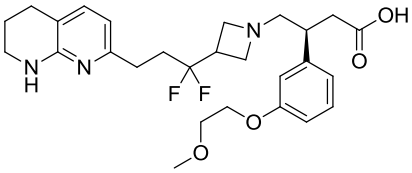 **74**	2.95	8.42, 7.42, 3.86	88 (n = 3)	37

Table 9 *A comparison of the properties of **1** and **74***

Despite only differing slightly in the design of the core, and having very similar ChromlogD, and pK_a and pK_{aH} values, compound **74** suffers from reduced permeability, measured by both AMP and MDCK cell assays, compared to **1,** and the oral bioavailability in rat is also lower. Compound **74** has AMP and MDCK permeability values close to those of **16**, and so makes an interesting case for measurement of the ^{15}N NMR spectrum, since it would be predicted that **74** is less capable for forming an IMHB in a lipid environment, possibly due to increased rigidity of the core.

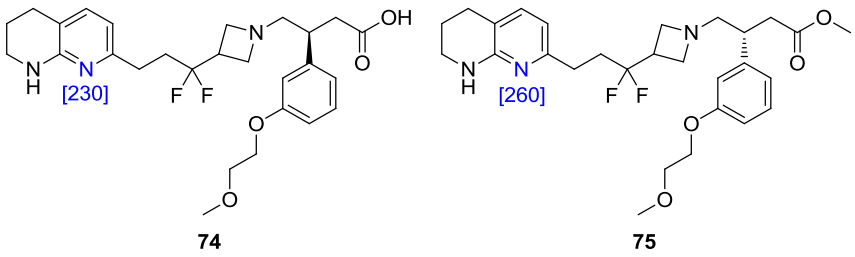

Figure 44 *The ^{15}N NMR shift of **74**, indicating a reduced level of IMHB formation (over methyl ester **75**, measured for the enantiomer due to limited compound availability) compared with **1** and **16***

Indeed, measurement of the ^{15}N NMR of **74 (Figure 44)** found that there was a lower level of protonation on the aromatic nitrogen compared with both **1** (N shift of 197) and **16** (N shift of 216), whilst the methyl ester analogue **75** (spectrum measured on

the enantiomeric compound due to limited compound availability) was almost identical to methyl esters **63** and **64**. This implies that **74** forms an IMHB appreciably less effectively, and this may explain why it suffers from reduced permeability. In an effort to further test the model, linear analogues **18** and **19** had their ^{15}N NMR spectra measured. The results are shown in **Figure 45**.

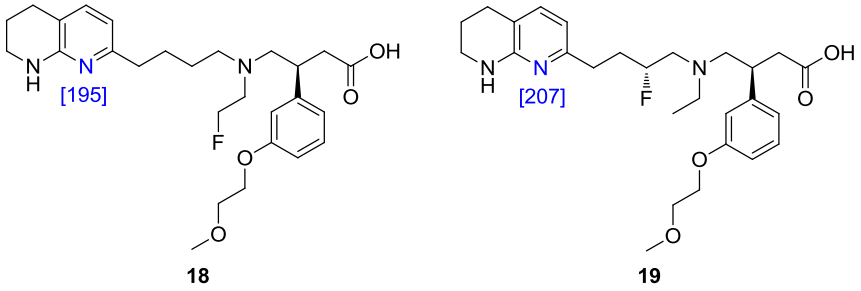

Figure 45** The ^{15}N NMR shift of linear analogues **18** and **19

In both cases, the N shift of around 200 indicates a high level of N protonation, therefore a significant amount of IMHB formation, as had been proposed for these more flexible analogues. In the case of **18**, the N shift is slightly lower than that of **1**, indicating a similar or potentially even greater amount of IMHB formation than in **1**, whereas the N shift of 207 for **19** indicates a slightly less tightly hydrogen bonded conformation, but nonetheless still indicating a greater extent of hydrogen bonding than in **16**. These values may go some way towards rationalising the high measured AMP values of these compounds, though the N shift does not seem to indicate a significantly greater amount of IMHB formation compared with **1**. The additional permeability may, therefore, be as a result of the increased lipophilicity of **18** and **19** as compared to **1**.

Seeking to extend this approach to other series of $\alpha_v\beta_6$ integrin antagonists synthesised within our laboratories, compounds **76** and **77** were considered **(Figure 46)**.

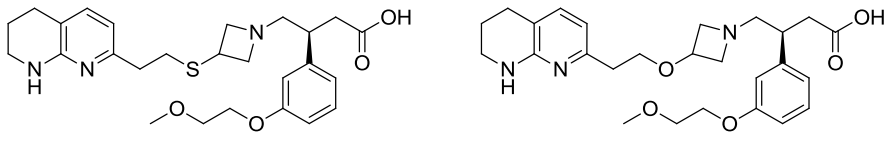

76 **77**

Figure 46 *Compounds **76** and **77**, developed more recently within our laboratories.*

A supply of **76** was available from within our laboratories,[152] whereas **77** had to be synthesised from late-stage intermediate **78**, which was itself available from previous synthetic work within our laboratories.[152] Oxygen-linked azetidine **77** was obtained *via* the familiar sequence of Miyaura-Hayashi coupling with boronic ester **34**, followed by hydrolysis **(Scheme 29).** The low yield is attributed to the formation of an impurity during the cross-coupling step, which was difficult to separate from the final compound.

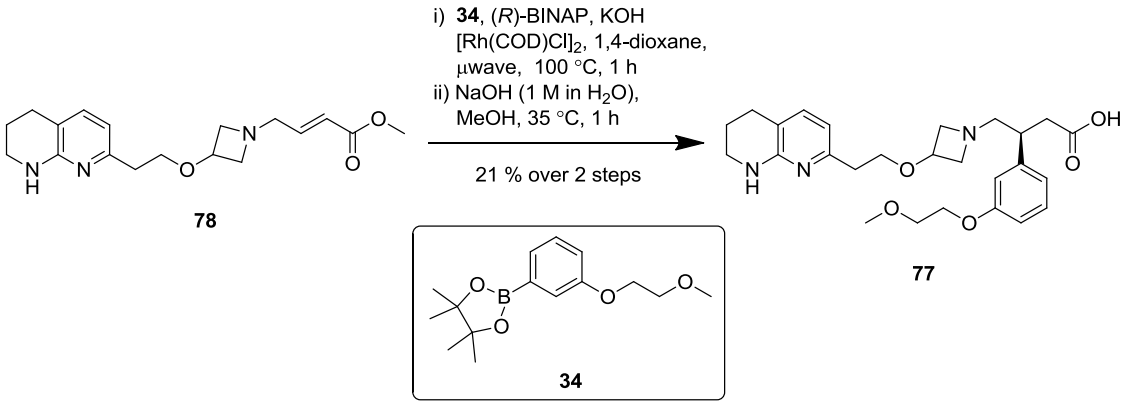

78 **77** **34**

Scheme 29 *The synthesis of **77** from **78**, using boronic ester **34** as the coupling partner in the cross coupling reaction.*

The chromatographic lipophilicities and permeability of **76** and **77** are shown alongside those of difluoroazetidine **74** in **Table 10**, and the measured pK_a and pK_{aH} values shown indicate that the different electron withdrawing groups all result in similarly basic azetidine nitrogen atoms.

Compound	ChromlogD	pK_a and pK_{aH}s	AMP / nm s^{-1}	MDCK permeability/ nm s^{-1}
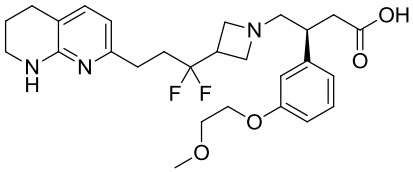 **74**	2.95	8.42, 7.42, 3.86	88 (n = 3)	37
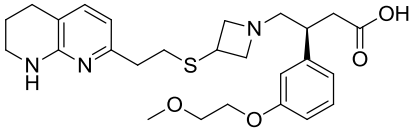 **76**	2.41	8.62, 7.21, 4.29	72	36*
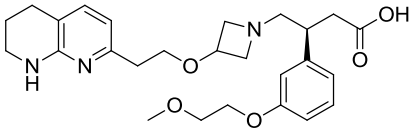 **77**	2.04	8.54, 7.09, 3.97	< 3	5

Table 10 *The lipophilicities, pK_a and pK_{aH} values, and permeabilities of azetidine analogues **74**, **76**, and **77**. *This datum was measured on an unequal mixture of enantiomers of **76**.*

However, these different groups (the CF_2, S, and O linker groups) possess differing levels of lipophilicity, which result in a range of lipophilicities for the overall compounds. Because the of pH partition hypothesis, it is anticipated that the more lipophilic compounds will be more permeable, and so the direct comparison of the permeability of these compounds is hampered.

In order to correct for the difference in lipophilicities, **Table 11** shows the ChromlogD values for the compounds, subtracted by the logarithm of the values of the AMP and MDCK permeabilities of the compounds. These values are intended to correct for the permeability differences between the compounds, and the higher (less negative) numbers indicate a more permeable compound, adjusted for the lipophilicity. The values calculated using the AMP data indicate that compound **76** is more permeable than **74**, and **77** is less permeable. The MDCK permeability-derived value indicates that **74** and **77** are similarly permeable.

Compound	log(AMP) – ChromlogD	Log(MDCK) – ChromlogD
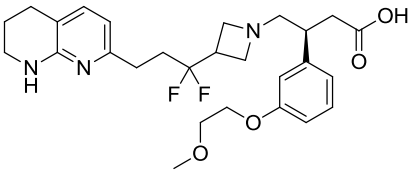 **74**	– 1.01	– 1.39
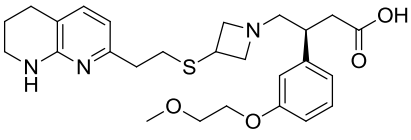 **76**	– 0.55	– 0.85
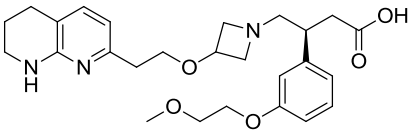 **77**	– 1.56*	– 1.35

Table 11 *The lipophilicity-adjusted permeabilities of azetidine analogues **74**, **76**, and **77**. *This datum is uncertain as the AMP value from which it derives is < 3, rather than a measured value.*

In order to give context to the values in **Table 11**, the same data manipulations have been carried out for compounds **1**, **16**, **18** and **19**, and are shown in **Table 12**.

Compound	log(AMP) – ChromlogD	Log(MDCK) – ChromlogD
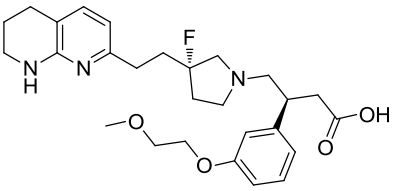 **1**	– 0.81	– 1.05
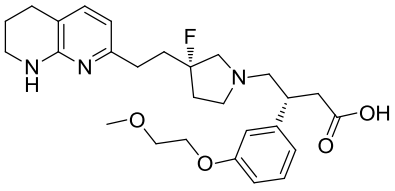 **16**	– 1.03	–1.38

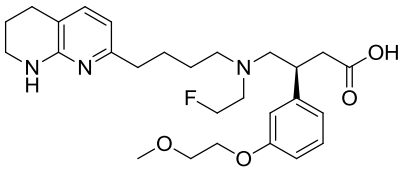 **18**	– 0.67	–
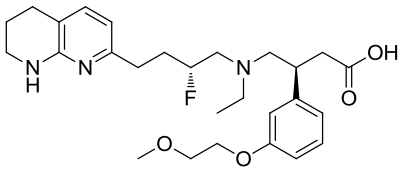 **19**	– 0.78	–

Table 12 *The lipophilicity-adjusted permeabilities of compounds **1, 16, 18** and **19***

Comparing the data from both **Table 11** and **Table 12**, for compounds **16** and **74**, which were considered to be less permeable than **1**, the log(AMP) – ChromlogD and log(MDCK) – ChromlogD values are close to one another, and are more negative than those of **1**, as anticipated, as this corresponds to a lower permeability for their lipophilicity. In comparison, the linear analogues **18** and **19**, for which only the AMP-derived data was available, had less negative values, indicating a greater normalised permeability.

The thioether-linked azetidine **76** had superior values for both metrics even of that of **1**, and so it was anticipated that this compound would be able to effectively form IMHBs. In contrast, ether-linked azetidine **77** appeared to be less permeable, given its polarity, and so was not expected to form IMHBs to such an extent. When the ^{15}N NMR of **76** and **77** were then measured, it was pleasing to observe the expected pattern of IMHB formation according to the shift of the sp^2 nitrogen atoms of these compounds **(Figure 47)**. According to the ^{15}N shift, compound **76** forms IMHBs with a similar efficiency as **1**, or linear compounds **18** and **19**, which is in agreement with the prediction of the lipophilicity-adjusted permeability. Ether-linked compound **77** forms IMHBs less effectively, with a ^{15}N shift similar to that of the difluoroazetidine analogue **74**, which was considered less permeable in the earlier analyses.

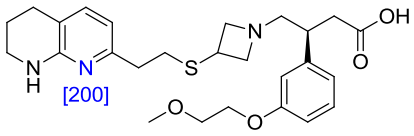

76

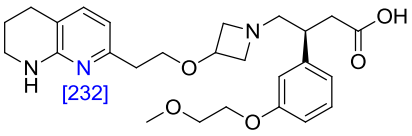

77

Figure 47 *The measured ^{15}N NMR shifts of **76** and **77**, in line with predictions*

Since the pK_a and pK_{aH} values for these two compounds are similar to those compounds which have already been considered, it appears that considering the lipophilicity-adjusted permeability of the compounds is a reasonable, albeit crude, method of comparing the permeability of compounds with different lipophilicities. This comparison relies on the compounds being differentiable in the permeability assays, and so would not be productive if both compounds registered minimal or maximal results within the assay. However, in this case it has successfully enabled compounds from multiple different lead series within our laboratories to be compared in the relative permeability, and pleasingly the ^{15}N NMR shifts measured for these compounds has been in line with predictions. The impact of this approach having predictive use would be especially significant and so obtaining this goal remained an important objective within the project.

2.6.3 IR and VCD analysis

Given the success of NMR in elucidating the conformations involved in the making **1** more permeable, it was hoped that solution-phase IR and VCD spectroscopy could shed further light on the behaviour of these compounds. The spectra of both for **1** and **16** were measured by co-worker He.[153] Under normal circumstances these measured spectra could then be compared to spectra calculated from the computationally generated conformations of the compounds, and therefore used to corroborate the computationally proposed conformations.

Unfortunately, the standard concentration at which the IR and VCD spectra are measured in the VCD workflow within our laboratories is very high in order to give a strong spectrum. However, ampholytic compounds such as **1** and **16** in non-polar solvents such as $CHCl_3$ at these concentrations are likely candidates for intermolecular interactions, and self-association to form aggregates such as dimers. Therefore, although the spectra were measured for **1** and **16**, these spectra measured at these concentrations were deemed not to provide sufficiently reliable data. Accordingly, this approach was not pursued further.

2.7 Results and discussion: Computational investigations

It has been commonplace in the literature, when assessing IMHB formation, to use molecular crystal structures to determine if a specific molecular framework is capable of forming IMHBs.[107] Whilst the conformations observed in crystal structures are low energy conformations, they are by no means the most relevant conformations when considering solution-phase conformations of molecules, where the environment is significantly different. Often, as is the case for **1**, the molecules are crystallised as salts, which changes the ionic state of the molecule and so significantly affects the conformation. **Figure 48** shows the crystal structure of the 2-methyl maleic acid salt of **1**, obtained by co-worker Copley within our laboratories.[154] In this crystal structure, the molecule takes an extended conformation, which is unlikely to be observed in the solution phase, in non-polar solvents. It is interesting to note that the carboxylate anion interacts with the pyrrolidyl N–H. Indeed, and as mentioned previously, this crystal structure led to the supposition that there might be an IMHB formed between the carboxylic acid group and the pyrrolidyl nitrogen in solution. However, this notion was dispelled by the ^1H NMR spectrum of **1** in $CDCl_3$ (**Figure 36**, page 58).

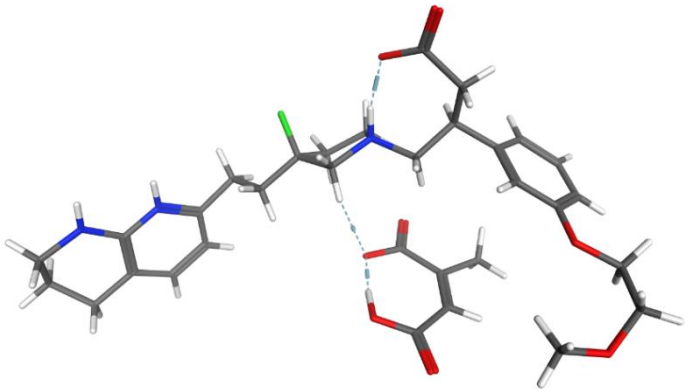

Figure 48 *The crystal structure of the 2-methyl maleic acid salt of **1**, displaying an intramolecular hydrogen bonding interaction between the pyrrolidyl N-H and the carboxylate*

However, when more than one molecule of **1** is considered in the crystal structure **(Figure 49)**, it is clear that the tetrahydronaphthyridine group is engaged in a hydrogen bonding interaction with the carboxylate group, but that it is an intermolecular hydrogen bond which forms. This case provides a good example of the drawbacks of using a crystal structure to assess the likelihood of IMHB formation in solution. That is because, in this case, the tetrahydronaphthyridine does form hydrogen bonds, but to a neighbouring molecule. There is, therefore, a clear driving force for this moiety to form hydrogen bonds, but there is no neighbouring molecule present in a dilute solution, so the only hydrogen bonding interaction that it could form would be intramolecular in nature.

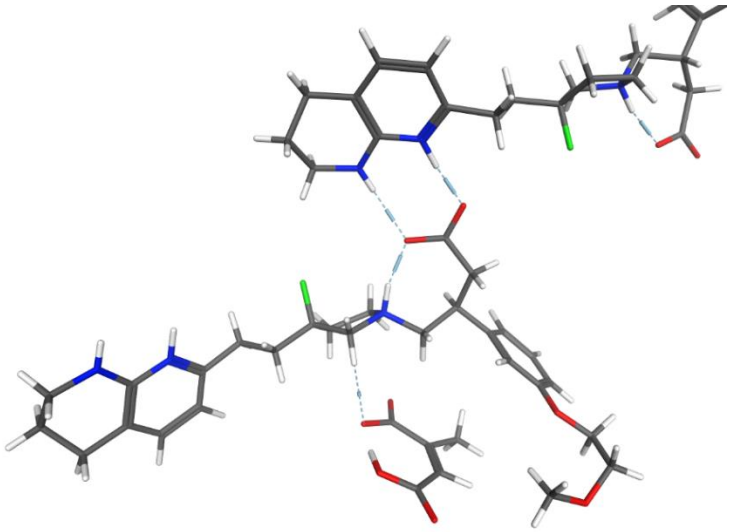

Figure 49 *Two molecules of the crystal structure of the 2-methyl maleic acid salt of **1**, displaying a hydrogen bonding interaction between the tetrahydronaphthyridine and the carboxylate of another molecule, as well as the IMHB shown in **Figure 48***

If possible, therefore, the preferred approach is to model the molecule computationally, as though it were in the solution phase, rather than relying on one or two conformations observed crystallographically. In other previous studies, conformational searches have been carried out in a vacuum, but this too is a significant oversimplification which overstates the likelihood of a compound adopting an IMHB-containing conformation,[138] as there are no solvent molecules to screen the charge of polar groups, and should be avoided if possible.

2.7.1 Determination of the best computational approach

During any computational investigation, it is important to always find the correct balance between having a sufficient level of theory to describe the system in question in such a way as to be able to rationalise what is observed experimentally, but also to avoid such a complicated modelling approach that the calculations are prohibitively slow and resource-intensive. In light of this, in this project the computational modelling was started with a molecular mechanics approach using MOE, which had been reported as the optimal software for searching low energy conformations of larger, more flexible drug-like molecules.[155]

The intention was to find the lowest-energy conformations of compounds **1** and **16** in a medium resembling a lipid bilayer, in order to establish whether any lowest, or accessibly low-energy conformations, displayed IMHB formation. In similar work on cyclic peptides, it was assumed that in water the molecules adopt many interconverting conformations, whereas in a low dielectric organic solvent, one low energy conformation dominates during membrane permeation.[108]

The lipid bilayer can again be mimicked by the use of chloroform as the solvent. However, unlike in the NMR experiments, the solvent is only implicit in the calculations rather than using explicit solvent molecules, since to use an explicit

solvent model in these calculations would add unnecessary complexity to the calculations. Such an approach is also unnecessary, since *in vivo,* the permeating compound is not interacting with chloroform molecules, but rather the phospholipid.

Initially, the conformation searches of **1** and **16** were carried out in MOE using the in-built conformer generation feature, using a LowModeMD searching method. These were carried out without a lower limit on the minimum root mean squared deviation (RMSD) between the heavy atoms of two different conformations, meaning that no two conformations that differed at all were judged the same. The benefit of this approach is that conformational space is very well-covered, but the drawback is that this method generates 5000 – 10000 conformations for each compound, which is an unmanageably large number. Additionally, if quantum mechanical optimisation of this large number of conformers were carried out, they would collapse into a much smaller number of conformers, since in reality there are fewer local minima on the potential energy surface than this number of conformers suggests. When visually comparing the lowest-energy conformers of **1** and **16** generated using this approach, no apparent difference was observed, and no IMHBs were observed.

One benefit of generating such a large number of conformers is if they are used to form a Boltzmann distribution, then this distribution is less likely to be skewed by a few particular conformers as compared to if a much smaller set of conformations was used to generate the distribution.

As a result, this set of conformers was treated similarly to how Over had treated a set of conformers of diastereomeric macrocycles that differed in their membrane permeability.[156] Within this published study, eight clusters were defined based on the patterns of IMHBs (defining a maximum distance of 2.6 Å between the two atoms for an IMHB to be present), and then the Boltzmann weighted microstate probability of each cluster being present was calculated, using the energy of the lowest-energy conformation of each cluster. From this, it was shown that one diastereomer was more likely to form IMHBs than another, thus explaining the improved permeability

of one over the other. Because the compounds being analysed were macrocycles, they possessed far fewer possible conformations compared to **1** and **16**, because of their increased rigidity.

Initially, this same approach was taken for **1** and **16**, defining possible hydrogen bonding interactions between the ether chain, acid, tetrahydronaphthyridine, and pyrrolidine groups. However, this led to a probability distribution where the formation of no intramolecular hydrogen bonding interactions was the overwhelmingly most likely probability. It was noted that in the approach adopted by Over, the minimum energy conformation for each cluster was optimised using density functional theory (DFT) in Jaguar® software before Boltzmann microstate weighting took place to form the probability distribution. When the low energy conformations of **1** and **16** were recalculated using DFT in Gaussian software (BLYP, STO-3G level of theory), there was found to be a significant re-ranking of the energies of the compounds. When the single point energy for all of the conformers of **1** and **16** were recalculated using this approach, a process which took over six weeks for each set of conformations, the resulting Boltzmann-weighted probability distributions looked starkly different, with **1** now most likely to exist with an IMHB between the acid and the tetrahydronaphthyridine groups, and **16** most likely to be in an open conformation.

Unfortunately, even this higher level of theory is considered too primitive to be appropriate for modern DFT calculations, as STO-3G is a minimal basis set. This means that it only contains sufficient functions to accommodate the electrons of the atoms, and the functions are all spherical and atom-centred, meaning that the model is inadequate for accurately describing bonds.[157]

To overcome these shortcomings, split-valence basis sets were developed, in which core orbitals are described by one set of Gaussians, and valence orbitals are described by two Gaussians. Such an example is the 6-31G basis set, with the basis function for each of the core orbitals built up from the linear combination of 6 Gaussian functions,

and each valence orbital built up of 2 basis functions, with the 'inner' one built from 3 Gaussians, and the 'outer' built from one Gaussian.[158] The introduction of polarisation functions has overcome the 'atom-centred' shortcoming of the original STO-3G basis set, where main group elements are assigned d-type functions and hydrogen atoms can also be given p-type functions.[159] These allow for electrons to be distributed away from the nuclei, akin to in an orbital hybridisation model, and are denoted by an asterisk (* (when only main group elements are assigned extra functions) or ** (where hydrogen atoms are also assigned additional functions)) when describing the basis set.[159] This is important in cases where hydrogen atoms can act as bridging atoms, such as in IMHB.

In addition to improvements to the basis set, the BLYP functional has also been surpassed by the B3LYP functional,[160,161] which is superior in that it considers the exchange terms from the Hartree-Fock approximation. A final improvement has been to include a dispersion correction to better account for London dispersion forces,[162] giving a functional termed B3LYP-D3. This correction is particularly important for weak interaction forces, such as pi stacking and IMHB formation, hence its utility here.

Therefore, the level of theory of the quantum chemical calculations was raised to the B3LYP-D3, 6-31G** level of theory. This level of theory comes at much greater computational expense, and so it was not possible to consider such a large set of conformations with this approach. Therefore, a different conformational search was required which would limit the number of conformations generated, in order that a more manageable set could be optimised using the quantum calculations.

In order to do this conveniently in one programme, MacroModel was used in Maestro, rather than MOE, for the conformation search.[163] Redundant conformations were removed by only considering two structures as different if the maximum atom deviation of any pair of corresponding atoms was greater than 0.5 Å. The resulting conformations (typically 200 – 400) were then further clustered

according to the RMSD of the heavy atoms, and either the optimal number of clusters was calculated (typically 20 – 30), or 25 was set as the chosen number of clusters. These clusters were then represented by the conformer closest to the centroid of each cluster, and these representative conformers were optimised using Jaguar in Maestro,[164] at the B3LYP-D3, 6-31G** level of theory.

Vibrational frequencies of the optimised structures were calculated, in order to establish whether the structures were at minima or saddle points on the potential energy surface, and in order to calculate thermodynamic quantities. These were combined with the energies of the optimised structures to generate a free energy value for the conformations, which were compared.

This allowed for an approach which was designed to sample the conformational space as widely as possible before optimisation using DFT on a manageable number of structures, such that the results can be obtained within a few days, and with a level of theory thought to account for the subtlety of the problem. The drawback of this approach is that it is not appropriate as a means for creating a Boltzmann distribution of the possible conformations of a compound. The reason for that is that unlike the simple approach taken initially, the conformation and energy of all possible conformers cannot be calculated at this higher level of theory in a timely manner, which would be required in order to generate a Boltzmann distribution. Instead, this approach aims only to find the lowest-energy conformer of the compounds. However, if there were other low-energy conformers at accessible energies from the ground state, it is reasonable to expect that these will also be found by the latter approach. This may be useful, if they show distinct conformational preferences compared to their corresponding ground state conformation.

Following initial guidance and training from co-workers Gruszka and Pogány within our laboratories, the computational studies described herein, for both chapters 2 and 3, were performed by the author. For additional information, see the experimental section and the associated USB drive for the resulting conformations.

2.7.2 The calculated conformations of 1 and 16.

When the approach explained above was applied to **1**, the lowest free energy conformation generated is shown in **Figure 50**. Pleasingly, this structure exhibits an interaction of the sort that was predicted initially, namely an interaction between two polar groups in the molecule, such that these groups are partially masked from the environment. It is thought that the formation of the double hydrogen bond would confer additional stability to the conformation, though this is clearly still a dynamic hydrogen bond, since in the crystal structure the bound conformation is linear.

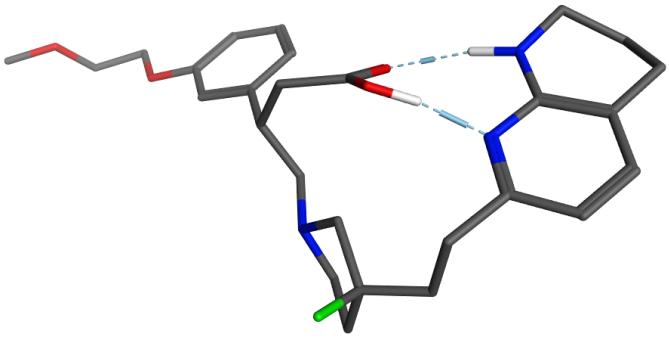

Figure 50 *The lowest-energy conformation of **1**, displaying a doubly hydrogen bonded interaction between the acid group and the tetrahydronaphthyridine group*

Having found that **16** also showed IMHB character according to the ^{15}N NMR, it was hoped that this would be reflected by the lowest-energy conformation of **16**. When **16** was minimised, it was not possible to obtain a structure without negative vibrational frequencies even after several reoptimisations, and these negative frequencies were always found to be associated to the flexible ether chain. This is thought to be because the potential energy surface is flat for conformations involving the rotation of this group, as it has little bearing on the energy of the compound. Since this group points away from the IMHB that is formed and so is not involved in the important interaction of the molecule, this was thought not to be an issue, and this conformation was used despite not being a global minimum conformation. **Figure 51** demonstrates that **16** did, indeed, show an IMHB.

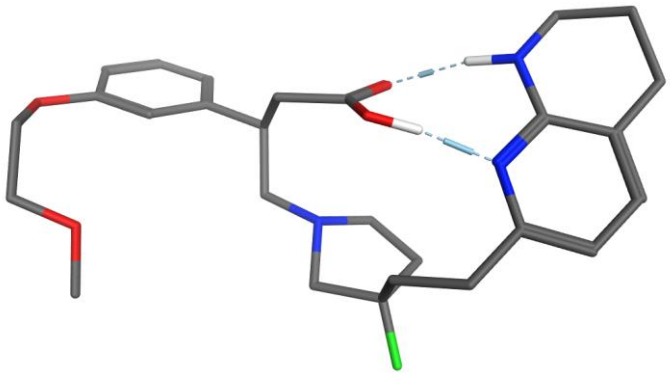

Figure 51 *The lowest-energy conformation of **16**, also displaying a doubly hydrogen bonded interaction*

Given that the hypothesis surrounding the IMHB formation of these compounds had arisen from the observation of the differing permeabilities of **1** and **16**, and given that this difference had been observed experimentally in the ^{15}N NMR spectra, it was envisaged that this difference could be apparent computationally. Both compounds appeared to have a similar-looking IMHB in the lowest-energy conformation, and when the bond angles and bond distances of the IMHBs for both compounds were measured **(Figure 52)**, it was found that the angles of the IMHBs measured were very similar.

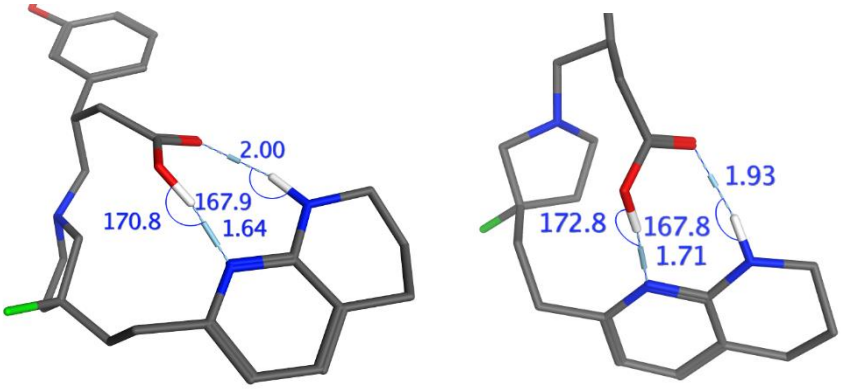

Figure 52 *Left, the lowest-energy conformation of **1**, and Right, the lowest-energy conformation of **16**, both with the bond angles and distances (measured in Å) labelled for the IMHBs*

The bond distance for the IMHB between the carboxylic acid hydrogen and the pyridyl nitrogen, thought to be the more important of the IMHB interactions due to the acidity of this hydrogen, was lower for **1** than for **16**, by 0.07 Å, which would confer

greater stability to the IMHB in **1**. However, the difference is so small that it is not thought to be significant.

When these two conformations were imported to MOE, the partial charges were calculated using the AMBER 94 forcefield, and these charges were used to calculate the accessible hydrophobic surface area (ASA_H) and accessible polar surface area (ASA_P) of the compounds, and the fraction of the surface area that is polar (FASA_P). These results are shown in **Table 13**.[165]

	ASA_H / Å^2	ASA_P / Å^2	FASA_P
1	693	94	0.120
16	659	85	0.115

Table 13 *The 3D accessible surface areas of **1** and **16** that are hydrophobic and polar in nature, and the fraction polar surface area*

These results appear to indicate that **16** is less polar than **1** in terms of exposed polarity, but in fact that is likely to simply be a result of the ether chain of **1** being more linear in the lowest-energy conformation than for **16** (for which the lowest-energy conformation of the ether chain is not known as the calculations would not converge to a global minimum for this compound). When the ether chain is more linear, it exposes more polar surface area, skewing this result. Accordingly, the outputs detailed in **Table 13** were deemed to be of lowered overall utility and importance. It is noteworthy, however, that an open conformation of **1** has an FASA_P of approximately 0.2, which is noticeably higher than these IMHB-containing low-energy conformers.

2.7.3 Analysis of the conformations of 18, 19, 74, 76 and 77

From that communicated above, it may be that the theoretical studies are not able to differentiate between the two different extents of IMHB formation that **1** and **16** undergo in the same way that the ^{15}N NMR could. In order to further test this, the lowest-energy conformation for simplified analogue of **1**, **74**, was calculated, as it had shown an apparently reduced propensity for forming IMHBs compared to **1** and **16** (page 84-85).

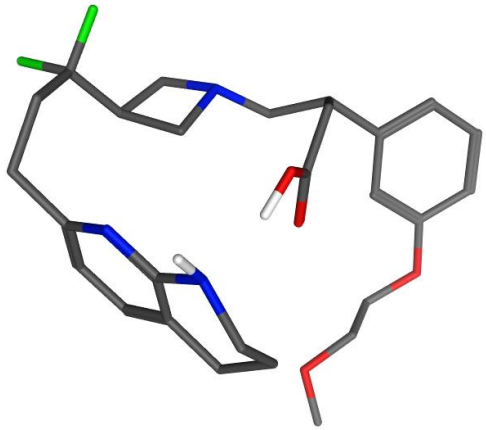

Figure 53 *The lowest-energy conformation of **74**, displaying a weaker interaction between the acid and the tetrahydronaphthyridine group. The rigidity of the core is evident in this case*

When the lowest free energy conformation of **74** was measured, there was indeed a lesser extent of IMHB formation indicated. **Figure 53** indicates that the lowest-energy conformer is proposed to have an interaction with the aliphatic nitrogen atom on the tetrahydronaphthyridine group, which is anticipated to be less stabilising than an interaction with the aromatic nitrogen, which would require a tighter coil of the compound for an interaction to take place. This is thought to explain the lesser extent of IMHB formation evident by ^{15}N NMR.

A further piece of evidence to corroborate this conformation resulted when an analogue of **74** was reacted with benzyl glucuronate **(79, Figure 54)** and HATU by a co-worker in an attempt to form the corresponding glucuronide. In this instance, the

corresponding macrocyclic lactam (with an amide bond formed between the carboxylate and the sp^3 tetrahydronaphthyridine nitrogen) was unexpectedly isolated.[166]

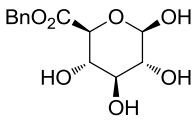

79

***Figure 54** Benzyl glucuronate **(79)**, which was reacted with HATU and a close analogue of **74**, leading to the formation of a macrocycle*

This macrolactonisation is incontrovertible evidence of the coiling of these compounds, and the reaction at the aliphatic tetrahydronaphthyridine atom agrees with the computed conformation of **74** in $CHCl_3$, where the acid group is oriented towards this nitrogen atom.

Linear analogues **18** and **19** were also assessed computationally. Both compounds are expected to have tightly hydrogen bonded structures, based on the ^{15}N NMR data. The minimum energy conformation of **18** is shown in **Figure 55**. This calculation, and that of linear analogue **19**, suffered from the same uncertainty over the exact position of the ether chain as **16**.

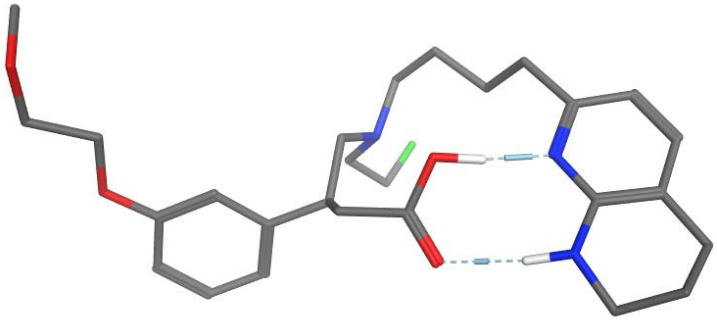

***Figure 55** The minimum energy conformation of linear analogue **18**, showing a double hydrogen bonding interaction*

As shown in **Figure 55**, **18** shows the double hydrogen bonding that was observed for **1** and **16**, which is not surprising given that this compound possessed the lowest aromatic ^{15}N shift of all of the full $\alpha_V\beta_6$ antagonists measured (195 ppm). When **19**, the linear analogue with the fluorine atom in the chain, was computed, it was found the compound preferred a single hydrogen bonding interaction **(Figure 56)**.

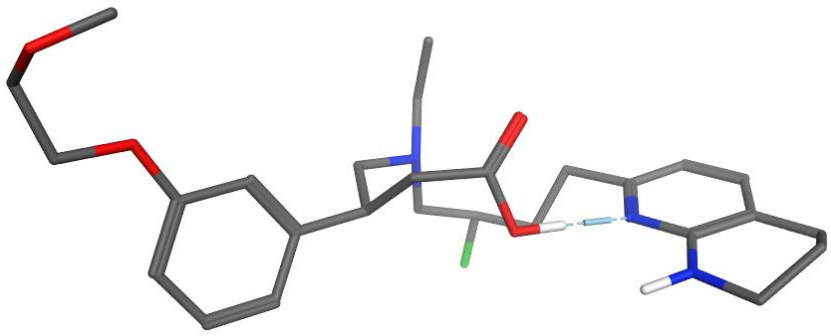

Figure 56 *The minimum energy conformation of linear analogue **19**, showing a single hydrogen bonding interaction*

It came as a surprise that this appears to be the lowest-energy conformation of **19**, as this appears to shield the polar functionality in the compound less effectively, but it may be a result of the pronounced conformational effect that can occur from having fluorine substitution in such a chain.[167]

Figure 57 shows the angle and lengths of the hydrogen bonds in **18** and **19**. The hydrogen bonds of **18** are straight and short, supporting the low ^{15}N shift (195 ppm). For **19**, which has a ^{15}N shift of 207 ppm for the aromatic nitrogen, it is a surprise that the IMHB between the acid and the tetrahydronaphthyridine only involves one of the hydrogen atoms, but this H bond is extremely linear and it is short, so it is likely to be strong. This may be enough to also bring the ^{15}N shift below that of **16** (216 pm).

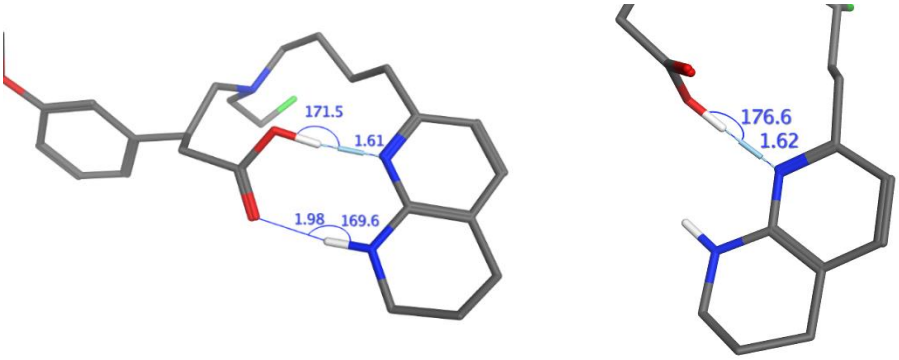

Figure 57 *The angles and lengths of the hydrogen bonds in **18** (left) and **19** (right)*

Finally, the lowest-energy conformations of thioether-linked azetidine **76** and ether-linked azetidine **77** were assessed. The ether-linked compound **77** had a ^{15}N NMR shift very similar to that of the difluoroazetidine compound **74**, and appeared to be less permeable than **1**, even when considering its lower lipophilicity (**Table 11**, page 74). Given that the ^{15}N shift of the sp^2 nitrogen atom was very similar to that of **74**, a similar conformation was anticipated. Pleasingly, this was indeed found to be the case, as shown in **Figure 58**. Visually, the interaction of the acid and tetrahydronaphthyridine groups for this compound is similar to that exhibited by the lowest-energy conformation of **74**, shown in **Figure 53**, in spite of differing azetidine conformations.

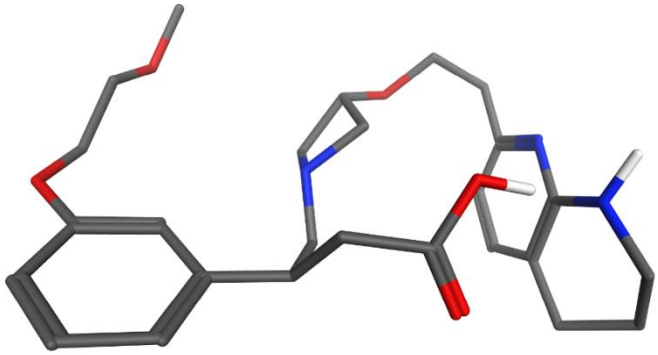

Figure 58 *The lowest free energy conformation of **77**, displaying similar IMHB characteristics as CF_2-linked analogue **74**.*

Lastly, thioether-linked compound **76** was assessed. From the outset of the modelling work, this compound was expected to be more demanding to model accurately than the others, because of the presence of the sulfur atom in the molecule. For neutral molecules containing second row elements such as sulfur, bond geometry is not particularly affected by the incorporation of diffuse functions to the DFT.[168] However, for energy calculations of such compounds, and in particular when considering non-covalent interactions of such molecules, adding diffuse functions is of significant benefit to the accuracy of the results.[169,170] Diffuse functions aid the description of electron density further from the nucleus of the atoms, as is particularly important for larger, more polarisable molecules, and in non-covalent interactions. These diffuse functions are denoted by + or ++ when describing the basis set used (where

++ denotes diffuse functions on all atoms, and + denotes diffuse functions on all atoms except hydrogen).

Therefore, with the intention of accommodating these additional considerations, the level of theory used for the geometry optimisation calculations for **76** was raised to B3LYP-D3, 6-31++G**. This change resulted in the geometry optimisation calculations for the 25 representatives of the clustered conformations taking over a week, unlike the others which take one or two days. The resulting lowest-energy conformation of **76** is shown in **Figure 59**.

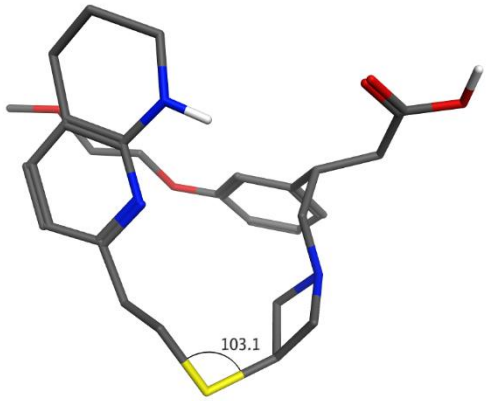

Figure 59 *The lowest-energy conformation of **76**, which, unexpectedly, does not indicate IMHB formation. The C-S-C bond angle is, notably, significantly closer to 90 ° than the C-O-C ether linkage in **77***

Unexpectedly, even utilising the higher level of theory, the lowest-energy conformation of **76** indicates no hydrogen bonding. This came as a surprise, given both the permeability measurements for this compound, and the ^{15}N NMR shift. If the diffuse functions were not added to the calculation, it also did not calculate a hydrogen bonding conformation as lowest in energy. In fact, the same conformation (that shown in **Figure 59**) was found to be lowest in energy using both methods.

Although it was disappointing that the calculation did not appear to be capable of rationalising the measured results for this compound, it had been initially anticipated that this compound would represent a more challenging case to model computationally, because of the presence of the second-row main group element, and that was indeed found to be the case.

One means of increasing the likelihood of successfully finding the lowest-energy conformation is to repeat the analysis with a larger number of starting conformations, in order to give more starting points to the optimisation. However, since the addition of the diffuse functions in the geometry optimisation of this compound significantly increases the time required for the calculation, this approach was not considered for this compound.

Although unsuccessful in rationalising the IMHB behaviour observed spectroscopically, the conformation of **76** in **Figure 59** does display the distinct C-S-C bond angle in the thioether linker, which is approaching 90 °. This is a noticeably different angle to that of ether analogue **77**, shown with the angle labelled in **Figure 60.**

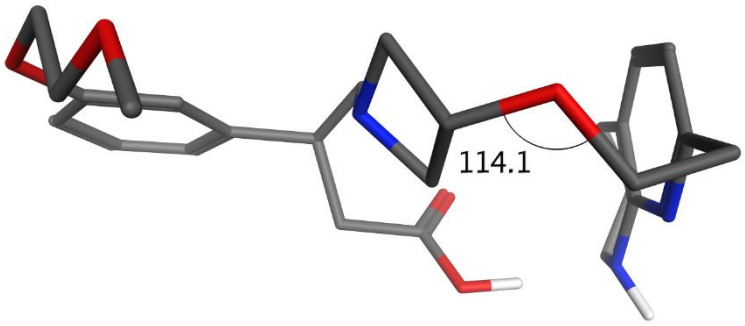

***Figure* 60** *The lowest-energy conformation of **77**, shown in such a way as to indicate the more linear C-O-C ether linkage*

The difference in the ether and thioether angles helps to rationalise why two compounds that are ostensibly so similar in structure are found to display noticeably different physicochemical and conformational properties, since the different bond angle is anticipated to allow two compounds to access different conformations.

Overall, in summary of the computational results obtained thus far, there is a broad agreement between these results and those obtained spectroscopically and observed in the permeability assays. It must be stated that a visual assessment of the lowest-energy conformation of each compound does not appear to be sufficient to explain the stability of the hydrogen bonded conformation, for example where **19** was

expected to form a doubly hydrogen bonded conformation. However, it may be too simplistic to expect the different extents of hydrogen bonding in these compounds to always be differentiable using this computational approach, which requires many assumptions to be made. Additionally, in the case of thioether **76**, the method is clearly deficient as a low-energy conformation where IMHB formation is observed was not found. It should be stated that the significant flexibility of these compounds, in particular the methoxy-ethoxy side chain, further hinders the determination of the lowest-energy species. It is expected that the lowest-energy conformation is determined by a fine balance between energetically unfavourable strain in the coiled structure, and favourable IMHB formation. This is likely to be the reason for the large difference between the energetic order of conformers found by the quantum mechanical approach and the order found using the simpler molecular mechanics calculation.

One additional reason anticipated to hinder this approach relates to the possible presence of other low-energy conformers which are also accessible at room temperature in solution. Unfortunately, this computational approach aims to find the lowest-energy conformation but not necessarily all possible conformations. Therefore, it may be that for some of these compounds there exists other low-energy conformers which show a greater or lesser extent of IMHB. It may only be if such a Boltzmann-weighted ensemble of conformations was generated, such as had been done when the calculations were only being carried out more simply using molecular mechanics, that the computational work would have enough nuance to determine accurately the differing strengths of hydrogen bonding interactions. Nonetheless, this approach has, in most cases, successfully rationalised and corroborated what has been observed spectroscopically and in the permeability assays.

2.8 Results and Discussion: Lipophilicity measurements

2.8.1 Introduction to ΔlogD

Confident that the synthetic, spectroscopic, and computational investigations had successfully identified the formation of IMHBs in **1**, and been able to differentiate between the different extents of IMHB formation in different analogues and stereoisomers, physicochemical investigations were then carried out. The purpose of these investigations was to both consider further the lipophilicity of the compounds, particularly of **1** and **16**, and also to investigate another method described in the literature for the identification of IMHB formation.

A small group of recent publications have advocated the used of water-hydrocarbon partitioning experiments, akin to traditional logP and logD measurements, to identify IMHBs, whereas logD and logP are usually measured as the partition of compounds between octanol and water. The usual partition between octanol and water can overestimate the lipophilicity of polar compounds, because of the ability of octanol to form hydrogen bonds to the solute, unlike in hydrocarbon solvents where no hydrogen bonding is possible.

This has included the partition of compounds between water and 1,9-decadiene,[100] and between water and toluene.[171, 172] It is proposed that the difference between the measured $\log P_{octanol/water}$ of a compound and the $\log P_{hydrocarbon/water}$ is diagnostic for IMHB formation. This difference, termed ΔlogP ($= \log P_{octanol/water} - \log P_{hydrocarbon/water}$), is expected to be smaller for compounds which can form IMHBs because $\log P_{hydrocarbon/water}$ is greater for compounds with IMHBs, as the compound is capable of taking a more hydrophobic conformation as a result of the IMHB formation, hiding the polarity of the compound in the solvent without any hydrogen bond acceptors.

This leads the compound to partition more favourably into the hydrocarbon than a similar compound with no intramolecular interactions.

Initially, these measurements were made using a traditional shake flask approach,[171] but this method has, as for all logP and logD measurements, been surpassed by UV and potentiometric titrations, carried out using instruments such as the Sirius T3.[172,173] This method is higher throughput and significantly less labour-intensive. This machine enables logP or logD measurements to be made across the pH range, which provides important lipophilicity information for ionisable molecules.

In the original publication describing this method,[171] matched pairs of compounds were chosen, one of which was capable of forming an IMHB, the other of which was not. The logPs of the compounds were then measured in octanol/water and toluene/water, and the $\Delta logP_{octanol/toluene}$ value was calculated. The only interpretation of the data that was made was that, of the compound in the pair that could form the IMHB, the $logP_{toluene/water}$ was larger, relatively, than the compound that could not, therefore the $\Delta logP_{octanol/toluene}$ value was smaller (or more negative). An example pair, compounds **80** and **81**, from the publication are shown in **Figure 61**.[171] Compound **81** can form an IMHB, whereas **80** cannot. In this case, there is a clear difference between the two $\Delta logP_{octanol/toluene}$ values, with the expected pattern observed, whereby the compound which can form IMHBs has a lower value.

80 ΔLogP = 1.96

81 ΔLogP = 1.14

Figure 61 *An example matched pair from the publication first detailing the use of $\Delta logP_{toluene/water}$ to identify IMHBs. The lower value for compound **81** indicates a greater extent of IMHB formation.*

However, in some other cases in the publication, the expected pattern for the matched pair was not observed, though some of the structures of the compounds in the pairs were not very similar to one another (perhaps as a result of limited access to the optimal compounds).[171]

A later publication suggested that for compounds for only one hydrogen bond donor (HBD), the $\Delta logP_{octanol/toluene}$ should be close to zero, but considered a value of 0.5 as still being close to zero, due to the errors associated with the measurements.[172] However, for more complex molecules, where some HBDs may be involved in IMHBs and others are not involved, there is significant uncertainty about what value would constitute the formation of IMHB interactions, stating that other techniques are required to confirm the presence or absence of interactions.

A third publication advocates the use of 1,9-decadiene as a solvent for use in logD measurements, because the $logD_{1,9\text{-decadiene/water}}$ value had the closest correlation with the logarithm of the MDCK permeability values for the set of compounds tested.[100] Consequently, the $logD_{1,9\text{-decadiene/water}}$ partition would also be investigated for **1** and **16,** in addition to $logD_{toluene/water}$.

Since compounds **1** and **16** are so similar to one another, the approach taken in the first publication, where a matched pair are compared, seemed to be a reasonable approach.

In addition to the analysis of the $\Delta logP_{octanol/toluene}$, or $\Delta logD_{octanol/toluene}$ in the case of **1** and its analogues, the lipophilicity values obtained are of interest to compare to the chromatographic lipophilicity values (ChromlogD) obtained for each of the compounds. The ChromlogD values for **1**, **16**, and **74** are almost identical, which implies that ChromlogD is not able to determine a lipophilicity difference which results from the formation of a dynamic IMHB. These measurements will further support the current work and give important insights into the possible limitations of ChromlogD as a measure of the lipophilicity of a compound.

The ChromlogD is derived from a chromatographic retention time, where the sample elutes on an HPLC column in H_2O with an increasing concentration of MeCN (outlined fully in section 4.5.5). This method has a close correlation with measured logD values within the lipophilicity range being considered here.[174] However, it appears that

IMHB interactions cannot be determined using this method. This is thought to be because this method involves the adsorption of the compound onto the stationary phase, and the solvent is monophasic and always has a significant aqueous component. Therefore, the non-polar solution-phase conformations of these chameleonic compounds may not be able to form.

It is envisaged that although the ChromlogD measurement cannot detect the changes that arise as a result of this chameleonic behaviour, the logD measurements made using the partition, with the Sirius T3 instrument, may be able to.

2.8.2 LogD and ΔlogD results

Using the Sirius T3 instrument as described, the logD of compounds **1** and **16** were measured across the pH range. The resulting logD values for the two compounds are shown in **Figure 62**.

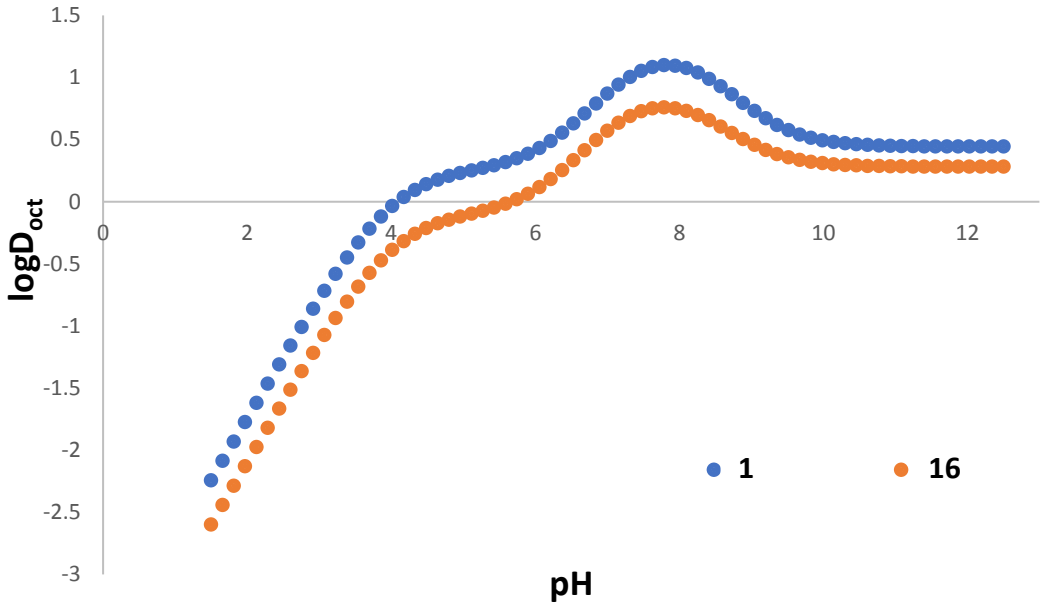

Figure 62 *The logD of **1** and **16**, measured as their partition between octanol and water, using a Sirius T3 instrument*

What is clear from this graph is that, as measured by this approach, compound **1** is more lipophilic than compound **16**. This difference is noteworthy given that the ChromlogD values of the two compounds were almost identical. The discrepancy in lipophilicity between the two compounds is at its most noticeable at the physiologically relevant pH range of between 6 and 8. This implied that the difference in the lipophilicities between the two compounds is a result of the IMHB formation, helping **1** to partition into the more lipophilic phase in a superior manner to **16**. This difference is not detectable using the ChromlogD method, as anticipated, since the chromatographic method does not have a hydrophobic phase. This highlights a potentially important deficiency of the ChromlogD method, which may not be able to adequately detect the presence of lipophilicity-altering intramolecular non-covalent interactions which occur when compounds are in solution. However, as it is a high-throughput, convenient method, it is nonetheless appropriate in most scenarios.

Having detected a difference in the $logD_{octanol}$ values for the two diastereomers, attention was then turned to the $logD_{toluene}$ results. Since, as mentioned above, 1,9-decadiene had garnered some interest as a useful solvent for correlations with permeability, it was briefly investigated as an alternative hydrocarbon solvent. However, issues with compound solubility arose, and it was not investigated further. Since the ChromlogD values for the compounds being considered were measured at pH 7.4, this was the pH initially chosen at which to examine the $logD_{toluene}$.

	1	**16**
ChromlogD (pH 7.4)	2.93	2.89
$logD_{octanol}$ (pH 7.47)	1.05	0.73
$\Delta logD_{octanol/toluene}$ (pH 7.47)	0.68	0.79

Table 14 *Various lipophilicity measurements of **1** and **16***

Table 14 shows the measured ChromlogD and logD (measured using the Sirius T3) values for compounds **1** and **16**, at the chosen pH. As mentioned above, the difference in the logD between the compounds is at its greatest at this approximate pH, and the difference of around 0.3 in the logD values corresponds to a concentration of **1** in the organic phase that is approximately twice that of **16**.

Thirdly, **Table 14** shows the $\Delta logD_{octanol/toluene}$ value for compounds **1** and **16** at pH 7.47 (the closest pH to 7.4 at which the Sirius T3 collects a data point). Pleasingly, the anticipated relationship between the two compounds was observed, whereby the lower value for the $\Delta logD_{octanol/toluene}$ of **1** suggests that, relative to compound **16**, it is better-able to partition into toluene, and therefore expected to be superior in its ability to shield its polar groups with IMHBs. In the example shown in **Figure 61** (page 95), the difference in $\Delta logD_{octanol/toluene}$ values for the two compounds is 0.8, and that is when comparing two compounds, one of which cannot form any IMHB. Since both **1** and **16** are anticipated to form IMHBs, but **1** is simply thought to do so to a greater

extent, the anticipated $\Delta logD_{octanol/toluene}$ was expected to be smaller, since the effect is more subtle. Therefore, the $\Delta logD_{octanol/toluene}$ difference of 0.11 between the values for **1** and **16** was in line with expectation. This very pleasing result suggested that even for this more challenging case, compared with those outlined in the publication,[171] this relatively recently developed metric has value in determining IMHB formation. Establishment of a method by which to make these measurements was also of value for use more widely in our laboratories, particularly since these results have highlighted the potential limitations of the use of ChromlogD in some scenarios.

Seeking to build on these results, the linear analogues and azetidine-containing analogues investigated spectroscopically and computationally were assessed **(Table 15)**.

Compound	ChromlogD	$logD_{octanol}$ (pH 7.47)	$\Delta logD_{octanol/toluene}$ (pH 7.47)
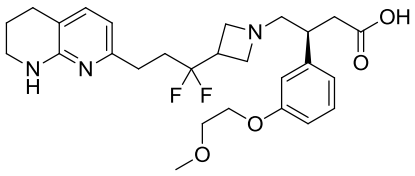 **74**	2.95	0.93	0.71
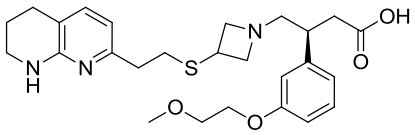 **76**	2.41	0.44	0.50
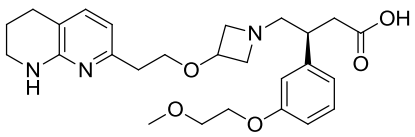 **77**	2.04	0.47	0.16

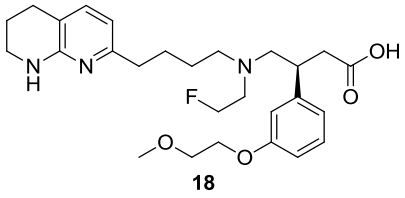 **18**	3.20	0.75	0.11
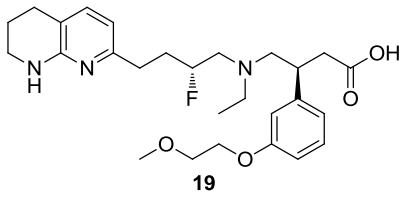 **19**	3.16	1.44	0.44

Table 15 *The lipophilicities and $\Delta logD_{octanol/toluene}$ values of several other analogues*

These latter results were not as straightforward to rationalise as those obtained for compounds **1** and **16**. Difluoroazetidine **74** forms IMHBs to a lesser extent than **1** and **16**, and so was envisaged to have a lower $logD_{octanol}$ and higher $\Delta logD_{octanol/toluene}$ than either of these compounds, but the values for both fall between that of **1** and **16**. Thioether **76** was, as expected, less lipophilic according to the $logD_{octanol}$ measurement, and the lower value for the $\Delta logD_{octanol/toluene}$ compared to **1** and **16** is indicative of significant IMHB formation, which was expected for this compound given its ^{15}N NMR shift. Ether-linked azetidine **77**, however, also gave unexpected results. The compound was thought not to form significant IMHBs based on the ^{15}N NMR and the permeability, but it had a higher-than-expected $logD_{octanol}$ and lower $\Delta logD_{octanol/toluene}$. It was the data collected for **18** and **19** which cast real aspersions over the quality of the data generated using this method. These compounds were expected to yield values of $logD_{octanol}$ and $\Delta logD_{octanol/toluene}$ that were very similar to one another, as their ChromlogD values, ^{15}N NMR values, and structures are very similar to one another. However, **Table 15** shows a marked difference between the compounds for both metrics.

It is not clear at this stage whether the method is robust, but the data collection for some of the compounds has gone awry, or whether there is too much error associated with the values obtained for it to be able to detect the subtle effects under consideration in this present study. It is certainly the case that these zwitterionic,

dibasic compounds, represent far more complex cases than the compounds already investigated in the literature using this approach. Additionally, these compounds are also more complex than those ordinarily measured using the Sirius T3. One previous published study using the $\Delta\log P_{octanol/toluene}$ suggested that the experimental error associated with measuring partitions means that an error of 0.5 for the logD measurements is reasonable.[172] Whilst no data is supplied in support of this value, it does also cast doubt over whether this approach is capable of discerning between different compounds' ability to form more subtle non-covalent interactions.

A more extensive study of the associated errors and the scope of this method is required, both within this project and also more widely in the literature, where there remains a paucity of examples of its use. Unfortunately, that has been beyond the scope of this present study. Such work might reveal more uses of this data in rationalising or predicting the permeability of compounds. One possible example of this would be that the collection of logD data across the entire pH range may be exploited. This would allow, for example, for the comparison of the lipophilicity of the compounds at a particular pH to be made. For example, the $\log D_{octanol}$ values for **1**, **16** and **74** may be compared at a lower pH, which may be more relevant for the absorption of compounds in the earlier part of the intestinal tract. These lipophilicities are shown in **Table 16**, and the observed pattern is in line with the relative lipophilicities for these compounds that might be envisaged based on the permeability (and the ^{15}N NMR shifts) of the compounds. However, this observation would also require significant validation from a larger test set to determine its applicability more broadly. This is also beyond the scope of this project.

	1	**16**	**74**
$\log D_{octanol}$ (pH 6.53)	0.63	0.33	0.27

Table 16 *The $\log D_{octanol}$ values of three analogues at a lower pH, which might be more relevant for the absorption of compounds in vivo*

This part of the investigation has, therefore, indicated that this means of investigating IMHBs may be of use in this case, but further work to determine the error of the measurements and the breadth of applicability of the method is required.

2.9 IMHB predictions

2.9.1 Outline of the method

Now confident that the compounds investigated form IMHBs, and to differing extents relative to each other, the aim was to see whether this knowledge, and the means of identifying these interactions (namely the ^{15}N NMR spectroscopy) could be applied. The ^{15}N NMR spectroscopy had been used to successfully rationalise the permeability of analogues from more recent series of $\alpha_V\beta_6$ integrin antagonists developed within our laboratories (**Figure 47,** page 76). The NMR shifts of these compounds (**76** and **77**) were successfully predicted based on the permeability data for these compounds. This led to the notion that it might be possible to predict the extent of IMHB formation in compounds. However, to do so using the ^{15}N NMR data still requires the compounds to be synthesised, and therefore the permeability can simply be tested for these compounds.

Much more valuable would be a scenario where the prediction of the extent of IMHB formation, and therefore the cases in which this has an advantageous effect on the permeability of the compound, could be predicted without having to carry out the synthesis of the compound. In order to do this, the *in silico* conformational analysis would be required to predict the extent of IMHB formation. Based on the evidence of the quantum chemical calculations carried out on the various analogues thus far, it appears that in most cases, the calculated lowest-energy conformations are,

broadly speaking, a correct reflection of the extent of IMHB formation in chloroform, according to the ^{15}N NMR.

This approach would be of particular value to synthetic chemists, both those working on $\alpha_V\beta_6$ integrin antagonists and those working on other projects, because if these interactions, which improve the permeability of the compounds, can be identified without having to synthesise the compounds, then they could be designed into future analogues during a series. This would have the potential to allow chemists working on series where obtaining sufficiently permeable compounds without the addition of too much lipophilicity is difficult, to design in these chameleonic properties, in order to improve the permeability without additional lipophilicity. Since the quantum chemical calculations can be carried out in one or two days, and at limited computational expense, then clearly it would be far less expensive and more expeditious to calculate whether a prospective target for synthesis is likely to possess these chameleonic properties than to have to synthesise and test it.

In order to test this predictive power of the conformational searches, an experiment was designed whereby the lowest-energy conformations of a diverse group of $\alpha_V\beta_6$ integrin antagonists would be calculated, then assessed to see the extent of IMHB formation in the lowest-energy conformation. Based on this, the ^{15}N NMR shift of the sp^2 nitrogen atom on the tetrahydronaphthyridine group would be predicted, and then once the prediction had been made, the ^{15}N NMR shift of the compound in $CDCl_3$ would be measured.

The conclusion from the computational investigations made in section 2.7 (Page 77) was that there was a general agreement between the measured and calculated conformations, but that this computational approach was not necessarily capable of differentiating between small differences in the conformations. An example of this was that the calculated conformations of **1** and **16** were, in terms of IMHB formation, the same, despite a 19 ppm difference between the measured ^{15}N NMR shifts **(Figure 38)**. In addition, the conformational searching and geometry optimisation of

thioether-linked azetidine compound **76** was not able to find a lowest energy conformation where the anticipated IMHBs interactions were observed.

In light of these limitations, the prediction experiment outlined above was not expected to be sensitive to small changes in the IMHB strength within these compounds. Therefore, in recognition of this, the predictions were fitted into the traffic light system outlined below in **Figure 63**.

Figure 63 *The traffic light system used to bin the selected compounds according to the extent of IMHB observed for the lowest-energy conformation*

In this simplified prediction, the lowest-energy conformer of the compounds were visually analysed and, if a double hydrogen bond was observed between the acceptor-donor pairs of the carboxylic acid and tetrahydronaphthyridine (as in the case of, for example, **1**, **Figure 50**, page 84), the compound was assigned 'green'. The ^{15}N NMR shift assigned to correspond to these compounds was < 220 ppm. This was chosen because compounds **1** and **16** both displayed this doubly interacting IMHB, and the higher of the shifts of those two compounds was 217 ppm. Therefore, in order to make the boundary a round number, any shift less than 220 ppm was anticipated for those in the green category.

Any compounds which implied the formation of some IMHB formation, but not the double hydrogen bonding interaction observed for **1**, were assigned into the yellow category. Compounds such as **74** (**Figure 53**, page 87) and **77** (**Figure 58**, page 90) displayed this behaviour, and since the ^{15}N NMR shifts of these compounds was approximately 230 ppm, the range of shifts for which the compounds would be assigned into the yellow category was 220-240 ppm. Given that the unprotonated ^{15}N NMR shift of the tetrahydronaphthyridine group is approximately 260 ppm, the

upper limit of 240 ppm for the yellow category then means that the yellow category, which spans 20 ppm, spans a similar range to the red category (δ > 240 ppm), which was for those compounds where no IMHB formation was indicated by the lowest-energy conformer.

When it came to the selection of compounds for which to make the predictions, the wide range of chemotypes which have been investigated within our laboratories has been exploited. For a range of analogues, with a variety of structures, there was sufficient solid material available for ^{15}N NMR measurement. Unlike the compounds considered so far in this work, not all of the compounds being assessed were developed as orally-dosed compounds, so several of these compounds were not designed, necessarily, to possess passive permeability. Therefore, the permeability of the compounds was not considered, instead only the ^{15}N NMR measurement, when considering whether these compounds form IMHBs or not.

2.9.2 Outcome of the predictions

Once the compounds were chosen, the predictions were made in groups of five. The first five compounds are shown in **Table 17**. Using the same approach as previously, the conformations of these compounds were calculated, and although the vast majority of the lowest-energy conformations are not included in the main text here for the sake of brevity, they have been included in the electronic supporting information. Similarly to the situation for compound **16**, for a few of the compounds, the lowest-energy conformation found was a saddle point rather than a global minimum, but the parts of the molecule implicated in these negative vibrational frequencies were not thought to be of high importance in the formation of IMHBs, and so for the sake of retaining a simple and time-efficient computational approach, these conformations were used in spite of these discrepancies. Based on the low-

energy conformations found in each case, the compounds were assigned to a group based on the traffic light system.

Compound	Predicted ^{15}N NMR colour category	Measured ^{15}N NMR / ppm category
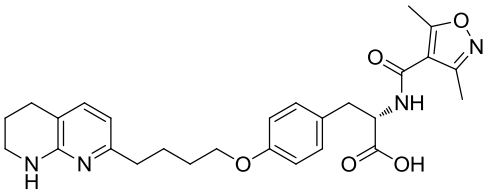 **85**		168 – ionic tautomer
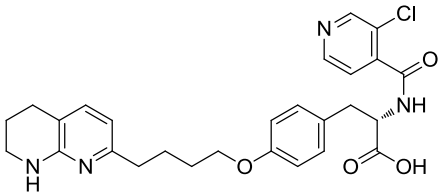 **86**		167 – ionic tautomer
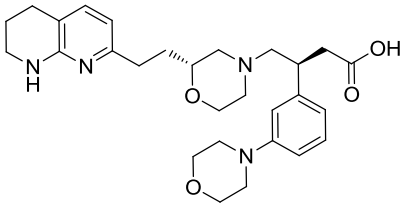 **82**		190
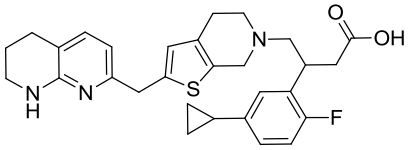 **84**		Could not be measured
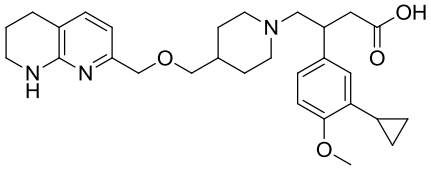 **83**		255

Table 17 *The predicted categories, and measured values and categories for the ^{15}N NMR shifts of the first group of compounds, measured in $CDCl_3$.*

Pleasingly, for compounds **82** and **83**, the predicted and measured extent of IMHB formation was in the same colour category, suggesting that there is predictive potential for this method. For compound **84**, unusually, the sp^2 nitrogen atom was not observable in the ^{15}N HMBC spectrum, so the prediction could not be checked using this approach. The ^{15}N peak is detected indirectly, *via* the coupling of the nitrogen nuclei to the nearby protons. In the case of the 2-substituted tetrahydronaphthyridines in the $\alpha_V\beta_6$ integrin antagonists, it is usually the benzylic methylene group that is used for detection. Therefore, in this case, it may be that the N signal is broadened in this case, possibly due to restricted rotation between the two aryl rings.

For the other two cases in this group, tyrosine-derived analogues **85** and **86** both measured remarkably low ^{15}N shifts, despite the predictions being for them to occupy the yellow and red categories respectively. These ^{15}N NMR shifts are reminiscent of when the tool compound **73** was tested (**Figure 42**, page 68), where the compound appeared to exist in solution as its fully ionic tautomer (**Figure 43**, page 69). This indicates that these compounds are, too, anticipated to exist as the fully ionic tautomer. In the case of **73**, the absence of any other basic group made the tetrahydronaphthyridine group more basic, which is expected to increase the driving force for formation of the ionic tautomer of the zwitterion. The same expected to be true for compounds **85** and **86**, and so this is anticipated to explain this behaviour. It is interesting to note that these compounds were designed originally within our laboratories as compounds for inhaled dosing, and so membrane permeability was neither desired not obtained for these compounds. The NMR results, which imply that these compounds exist as the ionic tautomer in a low dielectric constant solvent, may go some way towards explaining this lack of permeability for these zwitterions. For this analysis, however, the permanently zwitterionic form for the compounds means that the predictions that were made did not apply, because these were made

for the neutral form of the molecule, and the extent of IMHB formation cannot be measured if the sp^2 nitrogen remains fully charged throughout.

With mixed results for this initial group of compounds, the next set of five compounds were predicted and measured. The results obtained are shown in **Table 18**.

Compound	Predicted ^{15}N NMR colour category	Measured ^{15}N NMR / ppm category
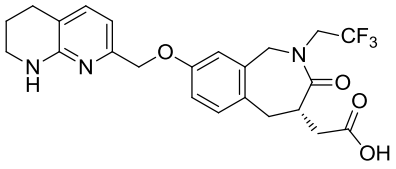 **91**		205
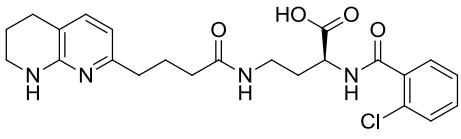 **90**		171 – ionic tautomer
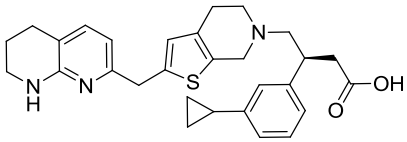 **87**		235
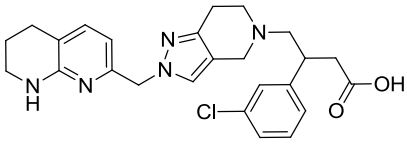 **88**		234
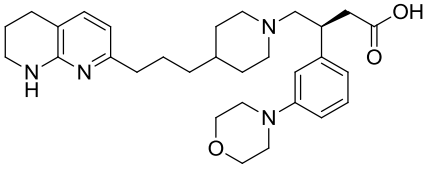 **89**		251

Table 18 *The predicted categories, and measured values and categories for the ^{15}N NMR shifts of the second test group.*

Pleasingly, for compounds **87**, **88**, and **89**, the prediction was successful. Compound **90** was, like compounds **85** and **86** found to be fully protonated and therefore expected to exist in its ionic tautomer. Again, this compound was part of a series of compounds designed for inhaled dosing, and did not show any permeability. Compound **91** was the only compound of the ten compounds in the first two test groups where the prediction had been unsuccessful in assigning the compound to the correct group for IMHB formation (other than where in the cases where the ionic tautomer was present and so the prediction was not appropriate). Compound **91** was not grouped correctly, and reoptimisations with representatives of 100 clustered conformers rather than 25 as usual, still gave the same lowest-energy conformation. A single IMHB interaction was predicted, but a low N shift was observed. This disparity may be the result of imperfect computational modelling or perhaps more likely it is a drawback of the non-quantitative approach to assessing the extent of IMHB formation. For example, linear compound **19** was expected to form a strong IMHB, but was only found to have a single interaction (**Figure 56**, page 89). Compound **91** might be a similar case.

Buoyed by the overall success of the first ten predictions, the final five compounds were assessed **(Table 19)**.

Compound	Predicted ^{15}N NMR colour category	Measured ^{15}N NMR / ppm category
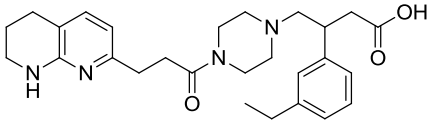 **92**		201
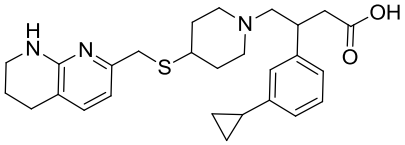 **93**		249

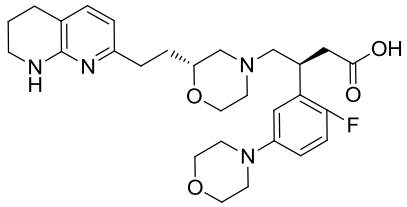 **94**		187
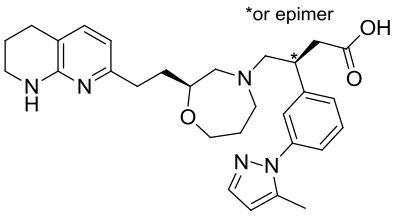 *or epimer **95**		199
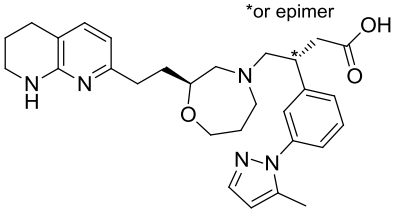 *or epimer **96**		190

Table 19 *The predicted categories, and measured values and categories for the ^{15}N NMR shifts of the third test group.*

Clearly, this group was less successful at predicting the extent of IMHB formation using this method. Computationally, piperazine-containing compound **92** indicated no IMHB formation to the tetrahydronaphthyridine, instead showing IMHB formation to the piperazine nitrogen from the carboxylic acid **(Figure 64)**. Whilst this would result in the shielding of the polarity, it would not be expected to result in the low value observed for the ^{15}N NMR shift of the sp^2 nitrogen.

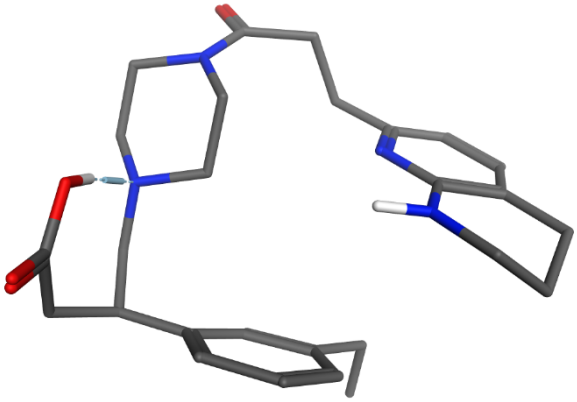

Figure 64 *The calculated lowest-energy conformation of **92**, with hydrogen bonding predicted between the piperazine nitrogen and the acid, rather than with the tetrahydronaphthyridine*

In an attempt to find a conformation that explained the measured NMR shift, the geometry optimisation was repeated with 100 conformations of **92**. However, a similar conformation to that shown in **Figure 64** was obtained, with the same hydrogen bonding interaction. Upon examination of the starting conformations for the optimisation generated by the MacroModel conformation search, it appears that many of these conformers had this interaction present. Therefore, it seems likely that, although this interaction is not the global energy minimum that results in the observed ^{15}N shift, the optimisation procedure was never able to locate the lowest-energy conformer as the carboxylic acid was always occupied in this alternative low-energy arrangement.

Based on the results for thioether-containing azetidine compound **76 (Figure 59**, page 91) thioether-containing compound **93** was anticipated to represent a challenging case for this method. The lower level of theory (without the use of diffuse functions) approach was chosen to avoid the approach becoming excessively long-winded, computationally intense, and unwieldy to a medicinal chemist seeking to utilise this approach. The method was, however, able to successfully predict the extent of IMHB formation for this compound. Given the lack of success in rationalising the thioether-containing azetidine **76**, this result may merely be the result of serendipity.

For morpholine-containing compound **94** and oxazepane **95**, the usual conformer search method found conformers in the red and yellow categories, respectively, for the two compounds. This was in contrast to the measured values for both **(Table 19)**, but when the optimisation was repeated, starting with 100 conformations for each compound, a lowest-energy conformation in the green category was found in both cases, agreeing with experiment. For the diastereomer of oxazepane **95**, compound **96** (these compounds had been chosen to make an interesting comparison to the case with fluoropyrrolidine-containing diastereomers **1** and **16**), the calculated lowest-energy conformation was in the red category when the optimisation was carried out with 25 conformations, but when it was repeated with 100 conformations, it was in the yellow category. Therefore, the additional computational expense, on this occasion, did not result in agreement with experiment, but it was able to make the prediction closer to what was observed.

In summary of these IMHB predictions, therefore, the first two groups of five compounds are illustrative of the enormous potential of this approach, in being able to quickly determine the likelihood of these compounds to form IMHBs, which are expected to result in superior permeability for these compounds, without the addition of any lipophilicity. In three of the cases, the revelation that the compounds appear to exist as their zwitterionic tautomer in solution means that this spectroscopic means of analysis is not appropriate. Though these compounds could not be analysed using this prediction, the observation that these compounds exist in their ionic form even in a low-dielectric solvent such as $CHCl_3$ tallies with their lack of membrane permeability (and solubility), as a part of series of compounds designed for inhaled dosing. Whilst the ^{15}N NMR could not be measured for one compound **(84)**, in five of the other six cases, the approach successfully predicted the extent of IMHB formation. This is particularly notable as these compounds often required ten or more synthetic steps to prepare, so the ability to predict their IMHB formation before synthesis is thought to be highly valuable.

Though the method was successful for compound **93**, the third group of compounds assessed is illustrative of the potential limitations of any computational investigation. For compound **92**, the presence of another hydrogen bond acceptor close to the carboxylic acid appears to preclude discovery of any conformations with an IMHB between the acid and tetrahydronaphthyridine groups. This may be a weakness of the conformational sampling method. For compounds **94**, **95**, and **96**, the initial search and optimisation with 25 representative conformations did not yield a conformation that agreed with experiment, but optimisation of sets of 100 conformers improved the predictions. In two of the cases, the predicted conformation was now in line with experiment. In the third case, the prediction was improved but still did not give a predicted conformation in the assigned category. These results are an accurate reflection of the aforementioned balance which must always be struck in any computational work; namely, that additional computational expense will always lead to superior results. It is, therefore, a case of weighing the importance of this additional computational demand. In these latter cases, clearly it is required for the correct prediction to be made. Overall, however, these predictions have shown, that with refinement, this could be a very valuable tool in predicting chameleonic behaviour which enhances permeability.

2.10 Conclusions and future work

2.10.1 Conclusions

The initial aim of this project was to embark upon a multifaceted study that could lead towards an explanation for the unusual permeability of **1** and its analogues, prompted by the significant permeability difference observed for two diastereomeric compounds, **1** and **16**. Since this difference could not easily be explained by a

difference in the ChromlogD or the pK_a or pK_{aH} values, it was believed that a conformational effect could be at play.

Initially, in order to investigate this effect, two linear analogues, **18** and **19,** were synthesised **(Figure 65)**. It was thought that since these compounds would be more flexible than **1**, any potential IMHB would be facilitated, and the permeability might be further enhanced.

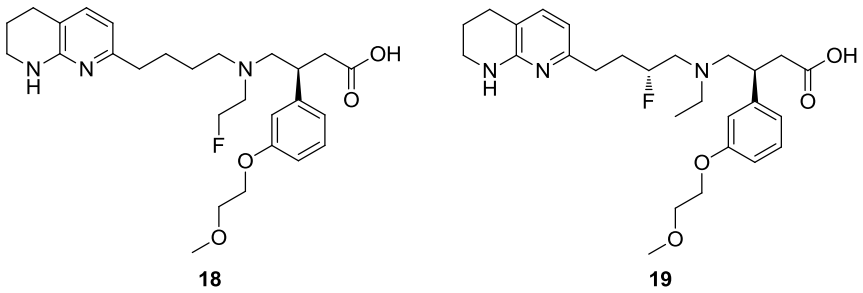

*Figure 65 Linear analogues **18** and **19***

Pleasingly, this was found to be the case, as both **18** and **19** were highly permeable in the AMP assay. They were, however, also slightly more lipophilic than **1**, which may also contribute to the elevated permeability. Furthermore, though it is not the focus of this work, these compounds were highly selective for the $\alpha_V\beta_6$ integrin over other RGD-recognising integrins.

When truncated analogues of **1** and **16** were synthesised **(Figure 66)**, it was found that in spite of the structural similarity of these compounds with **1**, there is not the expected relationship between lipophilicity, measured by ChromlogD, and AMP with these compounds, further confirming that there is an underlying conformation effect having a role.

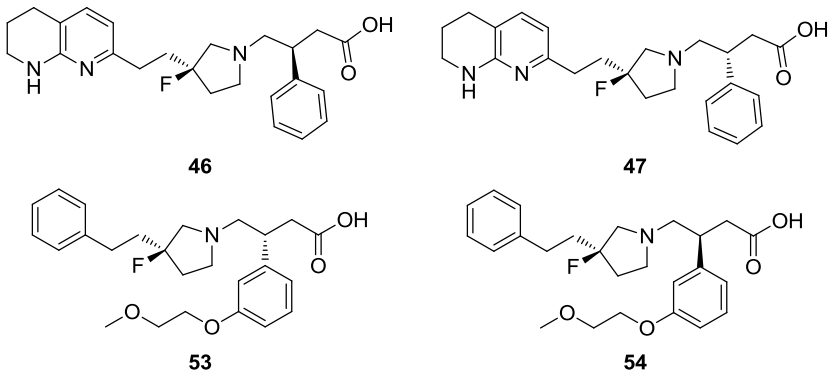

Figure 66 *Truncated analogues of **1**, to analyse the importance of particular functional groups*

Building on this, the conformation of **1** was assessed in chloroform, taken to be a good mimic of a lipid bilayer. Quantitative nOe analysis of the spectrum of **1** showed that the acid was not interacting with the nearby pyrrolidine nitrogen, as had been anticipated. However, ^{1}H NMR was not able to determine anything related to the conformation of the two ends of the molecule.

To our delight, it was found that ^{15}N NMR could be used to directly indicate the degree of protonation on the aromatic nitrogen of the tetrahydronaphthyridine group, as the shift is very sensitive for aromatic nitrogen atoms. This was investigated with the synthesis of a group of tool compounds. Furthermore and more importantly, it was found that there was more evidence of intramolecular protonation of the nitrogen atom in **1** than in **16 (Figure 67)**, but compared to the corresponding methyl esters (**63** and **64**) both appeared to show IMHB formation.

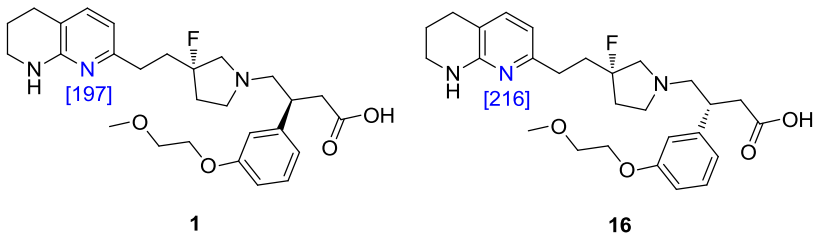

Figure 67 *The ^{15}N shifts of the pyridyl nitrogen atoms of **1** and **16**, indicating a greater extent of IMHB formation in **1**.*

A key experiment was to record a spectrum of **1** with methyl ester **63** in the same sample, where two distinct sets of peaks were measured for **1** and **63**, unchanged

from when the pure samples were measured. This indicated that these observations did not arise from an intermolecular effect. This technique was then applied to simplified analogue of **1**, **74 (Figure 68)**, which has similar measured physical properties to **1** but is less permeable.

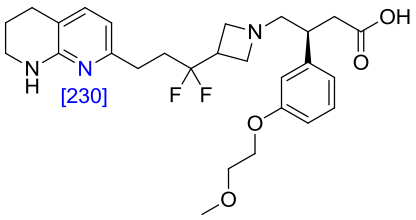

74

Figure 68 *The ^{15}N shift of **74,** thought to exhibit a lesser extent of IMHB formation than the corresponding fluoropyrrolidines.*

Indeed, it was found that the ^{15}N shift of the aromatic nitrogen atom in **74** was less engaged in IMHB formation than for **1** and **16**, in line with the measured permeability data. This approach was then applied to the two linear analogues **18** and **19**, and these were also found to engage significantly in hydrogen bonding, as predicted. This method is considered especially valuable because it appears to be sensitive enough to determine the strength of the hydrogen bonding character, and it is practically straightforward to carry out. Two similar analogues from more recent series of $\alpha_V\beta_6$ integrin antagonists, **76** and **77 (Figure 69)**, were predicted to have a greater, and lesser extent of IMHB formation respectively, based on their lipophilicity-adjusted permeability. The ^{15}N shifts of these compounds were, pleasingly, found to be in line with what had been anticipated.

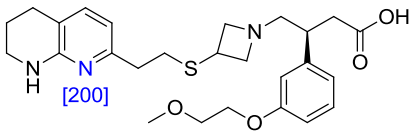

76

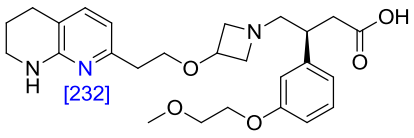

77

Figure 69 *The ^{15}N NMR shifts of compounds **76** and **77**, which were in line with predictions*

Having established a spectroscopic method of determining the formation of IMHBs, it was believed that this could be corroborated with computational work. Various approaches have been taken in order to provide insights into the lowest-energy

conformation of the compounds, eventually settling on a quantum chemical method of reduced throughput, but with, it is believed, the level of theory required to assess a subtle interaction such as an IMHB. Using this method, the lowest-energy conformations of **16** and **1** have been calculated, and as hoped, both exhibit hydrogen bond formation. However, these calculations do not seem to be able to differentiate between the differing strengths or stabilities of these two hydrogen bonded conformations, which may be a result of not finding the full ensemble of conformations, rather just looking for the single lowest. This means that other conformations which were not found might be contributing to the average conformation in solution. It may simply also be a limitation of only using a visual assessment of the conformation to determine the strength of the interaction.

The conformations of similar compounds **18**, **19**, **74**, **76**, and **77** were also calculated and also showed a broad agreement with the experimental results. However, in the case of sulfur-containing compound **76**, the conformational search did not find a conformation with an IMHB.

Having established that the IMHBs do form for these compounds, validation was sought for a recent physicochemical parameter for determining IMHB formation, namely the $\Delta\log D_{octanol/toluene}$. The initial comparison of **1** and **16** gave the expected results and the method successfully determined which was better-able to engage in IMHB interactions. Additionally, their measured $\log D_{octanol}$ values differentiated between the compounds where the ChromlogD values had been unable to, indicating a limitation of the ChromlogD measurement for the identification of non-covalent interactions.

However, measurement of the $\log D_{octanol}$ and $\Delta\log D_{octanol/toluene}$ for the other analogues examined using ^{15}N NMR cast doubt upon the utility of this method. The results were not in line with expectations from the other experiments, and it is not clear whether this is as a result of error within the measurements, or a lack of applicability of this approach to these dibasic zwitterionic compounds. More

validation of this approach is required, though this work has enabled the establishment of an approach within our laboratories for the experiments to be carried out.

Since the ^{15}N NMR shifts appeared to be a good indicator of the relative permeability of the compounds, and the computational calculations were in general agreement with the extent of IMHB formation observed, these methods were then combined to assess the ability of the computational approach to predict the formation of IMHBs in compounds not yet synthesised. This was intended to mimic the use of this approach as a triage for use in the design of future compounds.

In order to expedite this process, instead of designing and actually synthesising a set of compounds, the significant variety of $\alpha_V\beta_6$-targeting compounds synthesised within our laboratories were exploited. A diverse group of compounds were chosen, each with the tetrahydronaphthyridine group present, so that the extent of IMHB formation could be measured spectroscopically. The conformational search and quantum chemical optimisations were carried out, and the compounds were assigned to a red, yellow, or green category based on the predicted extent of IMHB formation.

In a few cases, the compound appeared to exist in its ionic form in solution, and so the prediction could not be validated using the ^{15}N NMR shift. Apart from these, in a high number of cases, the calculations were successfully able to predict the extent of IMHB formation in the compounds. In a few cases, the lowest-energy conformation found using the optimisation of 25 conformers of a compound was unsuccessful in predicting the IMHB formation, but when the analysis was repeated with 100 conformations, it was successful. This highlights the important balance between minimising computational expense for the predictions, but having sufficient expense for accuracy to be maintained.

In general, these predictions were a success and highlight the appreciable potential of this simple procedure, whereby complex molecules such as these can have their chameleonic behaviour predicted before synthesis, thereby avoiding lengthy and challenging synthetic routes. This is anticipated to aid future medicinal chemistry work, both for $\alpha_V\beta_6$ integrin inhibitors and more widely for other compounds where chameleonic behaviour would enhance the profile of the compounds, by increasing permeability or solubility without affecting the overall lipophilicity of the compounds.

At the outset, the initial aim was to determine whether **1** is able to form IMHBs, and whether it is superior in its ability to do so compared to its diastereomer, **16**. Several different methods (synthetic, spectroscopic, and computational) have been used to indicate this is indeed the case. Crucially, ^{15}N NMR has been shown to be capable of determining the extent of IMHB formation in a solution of deuterated chloroform, chosen to mimic the lipid bilayer. The computational work has then been used to show that it is possible to exploit this behaviour predictively, in order to enable this means of enhancing the properties of a drug molecule to be designed into future analogues. This is expected to be a valuable tool to medicinal chemists working on any sort of orally-dosed medicine.

2.10.2 Future work

In spite of the successes of the computational aspects of this work, it would still benefit from further refinement. The predictive work was successful in showing that the computational approach led to the correct prediction of IMHB formation. It involved carrying out the conformational search, followed by the clustering of the conformers and then optimisation of a representative of each cluster using DFT. Whilst this was generally a success, in several cases, more conformers had to be optimised in order to correctly find the correct lowest-energy conformer. There is,

therefore, scope for improvement of this approach, whether that would involve changing the way that the conformations for the optimisation are generated so as to increase the likelihood of leading to the global minimum on the potential energy surface, or settling upon the correct number of conformations required to successfully find this minimum in most cases.

Another limitation of the current approach is that, at present, the extent of IMHB formation is defined by a simple visual assessment of the arrangement of the lowest-energy conformer of the compound. In one way this is advantageous, as it is does not require any additional computational procedures once the lowest-energy conformation has been found, making the approach accessible more widely to medicinal chemists. However, it is not a quantitative means of assessing the strength of the IMHB formation. An example of the drawback of this is displayed in **Figure 56** (page 89), where the ^{15}N NMR shift of **19** indicates strong IMHB formation, but the lowest-energy conformation indicates only a single hydrogen bonding interaction between the tetrahydronaphthyridine and the acid groups (albeit a short bond). It may be that this interaction is indeed as strong as the double hydrogen bonds displayed in similar analogues, but a visual assessment cannot determine that. If an additional means of calculating the strength of that interaction could be incorporated, it would enhance the analysis. One means of doing this might be to make an *in silico* calculation of the ^{15}N NMR shift, and compare this to the experimental result, as it is more quantitative.

The other key area for further work is the further validation of the logD measurements made *via* the partition of the compounds between two solvents. The method was initially successful in corroborating the other results with regards to diastereomers **1** and **16**. However, relatively few examples have been tested, both within this work, but also in the literature, and so it is not clear how widely applicable, and, more importantly, how sensitive and accurate this approach is.

The repetition of a large group of compounds used in the published work on this approach is required to see whether the results can be repeated, and how much error is associated with the values. This method could be a useful tool within our laboratories, but further work is required to conclusively determine its use within this field.

Beyond these improvements to the methods used, it would be highly interesting to apply aspects of this approach, be that the retrospective identification of IMHBs using ^{15}N NMR, or the prediction of IMHB formation using the computational method, to other medicinal chemistry series beyond integrin antagonists. Hydrogen bonding to sp^2 nitrogen atoms is commonplace in medicinal chemistry and so it is foreseeable that many programmes could benefit from such interactions shielding the polarity of the compounds. If the compounds were not zwitterions, this would also simplify their analysis, since the $\alpha_V\beta_6$ antagonists have represented a complicated case, synthetically, computationally, and spectroscopically, throughout.

Chapter 3: SAR exploration of an orally bioavailable template for the $\alpha_V\beta_1$ integrin

3.1 Introduction to the benzazepine series

In light of the recent interest in $\alpha_V\beta_1$ as a target for IPF, in 2016 work was undertaken in our laboratories to find a small molecule that was selective for $\alpha_V\beta_1$ over the other integrins. Two different series were established, both of which were identified by cross-screening compounds from historical integrin antagonist programmes. The first of these was a series which had been adapted from previous work towards a selective antagonist for the $\alpha_4\beta_1$ integrin, which has been targeted for various indications including multiple sclerosis.[175]

The second of the series on which work was undertaken was based on a group of dual $\alpha_V\beta_3$ and $\alpha_V\beta_5$ inhibitors, which were originally developed for osteoarthritis, rheumatoid arthritis, and macular degeneration. The original medicinal chemistry efforts led to compounds **97** and **98 (Figure 70)**.[176]

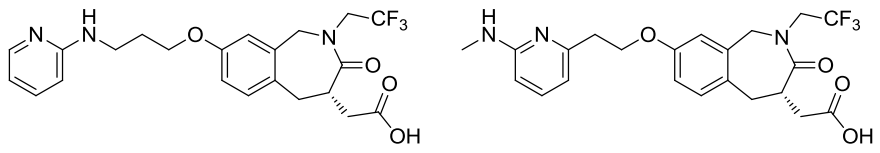

97 **98**

Figure 70 *Compounds **97** and **98**, both of which were candidate-selected for the treatment of arthritis*

These compounds were developed within SmithKline Beecham laboratories prior to a merger to form GSK, and had originated from a group of 1,4-benzodiazepine compounds, as this motif was found to be a good non-peptidic mimetic for the glycine-aspartic acid amino acid sequence **(Scheme 30)**. Compounds such as **99**,

containing the 1,4-benzodiazepine motif were published widely as $\alpha_V\beta_3$ antagonists,[177] and the benzazepine motif was first used for binding to the $\alpha_{IIb}\beta_3$ integrin, in compounds such as **100**.[178] Several alternative arginine mimetics to the benzimidazole group were explored,[179] before aminopyridines were found to be a potent unit.[180] These advances culminated in the discovery of **97** and **98 (Scheme 30)**.[176]

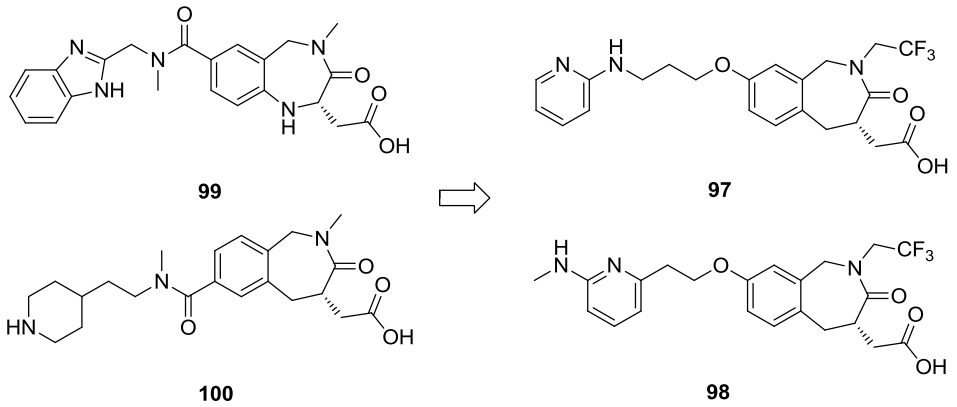

*Scheme 30 The discovery of **97** and **98** from **99** and **100***

Table 20 shows the properties of compounds **97** and **98**. Both compounds showed high potency at $\alpha_V\beta_3$ and $\alpha_V\beta_5$, with a lower potency at $\alpha_V\beta_1$. Both compounds were found to possess moderate to good oral bioavailability (F) despite not showing passive permeability (moderate F corresponds to approximately 30 – 60 %, good oral bioavailability corresponds to > 60 %,[181] passive permeability is measured using the AMP assay). Presumably, this can be attributed to active transport of these compounds. Additionally, the ChromlogD values for both compounds are in the desired range for an oral drug, as the ChromlogD values are adjusted so as to be approximately 2 units higher than the logD value for the compound would be.[174] That would put these compounds into a reasonable lipophilicity space with regards to clearance and solubility.[182] This was indeed found to be the case, with low to moderate plasma clearances (Cl) for **97** and **98**, and a long half-life ($T_{1/2}$) for **97**.[176] In general, a $T_{1/2}$ of several hours, and a low Cl, is preferable to reduce the frequency of dosing of the compound that is required as compared to a compound with a shorter

$T_{1/2}$, but $T_{1/2}$ should not be so long (or Cl so low) as to result in unwanted accumulation of the compound in the body. That is because this is likely to result in unwanted toxicity, and can complicate read-outs from clinical trials.[183]

	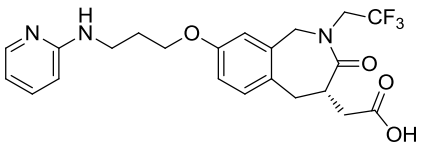 **97**	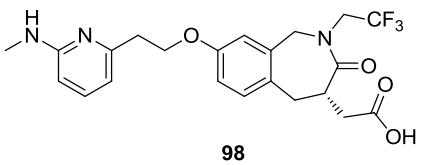 **98**
$\alpha_V\beta_1$ pIC_{50}	6.7 (n = 4)	7.3 (n = 9)
$\alpha_V\beta_3$ pIC_{50}	8.2 (n = 10)	8.6 (n = 5)
$\alpha_V\beta_5$ pIC_{50}	8.3 (n = 9)	8.7 (n = 7)
$\alpha_V\beta_6$ pIC_{50}	<5* (n = 11)	<5** (n = 5)
ChromlogD	2.23	2.28
AMP / nm s^{-1}	12	30
$T_{1/2}$ / min	360	53
Cl_p / mL min^{-1} kg^{-1}	16	25
F (rat) / %	34	72

Table 20 *The potency and PK properties of **97** and **98**. These PK data are from the original publication disclosing these compounds, whereas the integrin potency data and ChromlogD and AMP values are measured in the current assays of our laboratories.*One data point at 6.9 has been collected, but this has been ignored as an anomaly as the other measurements are all >5. **two further data points have been measured at 5.3 and 5.4, but these have been omitted as the <5 values cannot be used to form an average with these.*

These promising oral PK properties made **97** and **98** suitable for development as clinical candidates. However, **98** was found to cause vascular toxicity in mice, and so the development of the compound was halted.[184] Compound **97** was found to have a lack of efficacy in animal models of osteoarthritis,[185] and during safety studies, compound **97** was found to have an effect on organic acid transport, affecting bilirubin levels, so further development of this compound was also stopped.[186]

It is notable that the enantiomer of **97 (*ent*-97)** showed a 30-fold reduction in potency at $\alpha_V\beta_3$ compared to **97** when measured in an historic $\alpha_V\beta_3$ cell adhesion assay, as well as an approximately 20-fold reduction in half life and only 4 % oral bioavailability **(Table 21)**.[176] Given this disparity in potency, it is assumed in this series that only the

(*S*)-enantiomer of the compound is significantly active.

	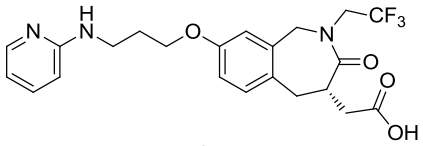 **97**	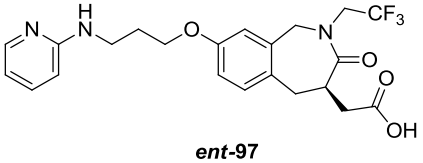 ***ent*-97**
$\alpha_V\beta_3$ pIC_{50}	7.9	6.4
$T_{1/2}$ / min	360	19
Cl_p / mL min^{-1} kg^{-1}	16	60
F (rat) / %	36	4

Table 21 *A comparison of the profiles of* ***97*** *and* ***ent-97****, based on previously published assay data.*

3.1.1 The synthesis of 97 and 98

During the previous studies, the synthetic route to these compounds as developed by the medicinal chemistry team was published **(Scheme 31)**.[176] The route centres around the installation of the itaconate group *via* Heck reaction of bromide **101** with dimethyl itaconate **(102)**,[187] and azepine formation *via* cyclisation of **103** to give mono-ester **104**. This Heck reaction was found to be selective for the *E* alkene isomer.

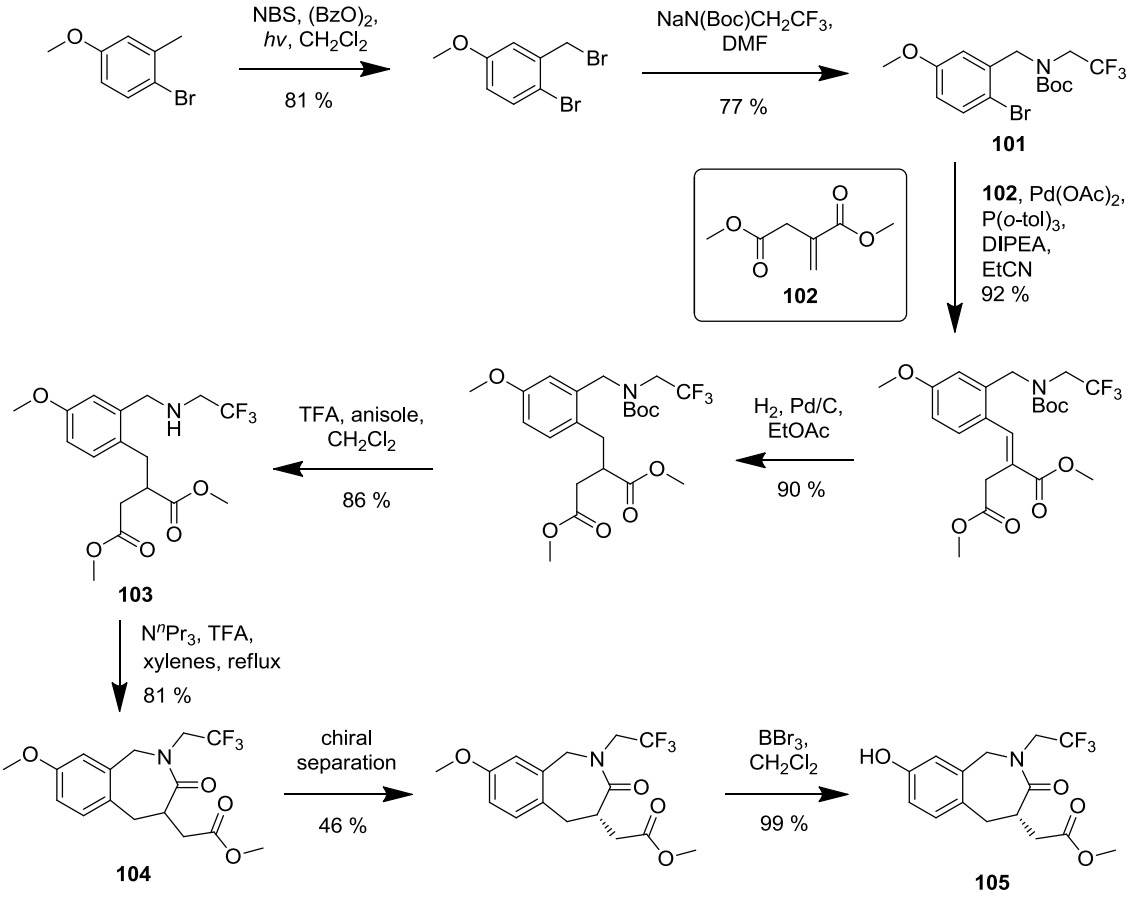

Scheme 31 *The medicinal chemistry route to intermediate* ***105***

Chiral separation of the enantiomers of **104** and subsequent methyl ether deprotection gave intermediate **105**, which was coupled to alcohol **106** *via* Mitsunobu reaction **(Scheme 32)**.[188] Deprotection steps then gave **97**.

Since **97** and **98** were also investigated clinically, the synthetic routes had to be scaled up significantly to allow sufficient compound to be produced for the safety studies and trials. This led to the development and publication of a process chemistry route to **98**, which is outlined in **Appendix A**.[189]

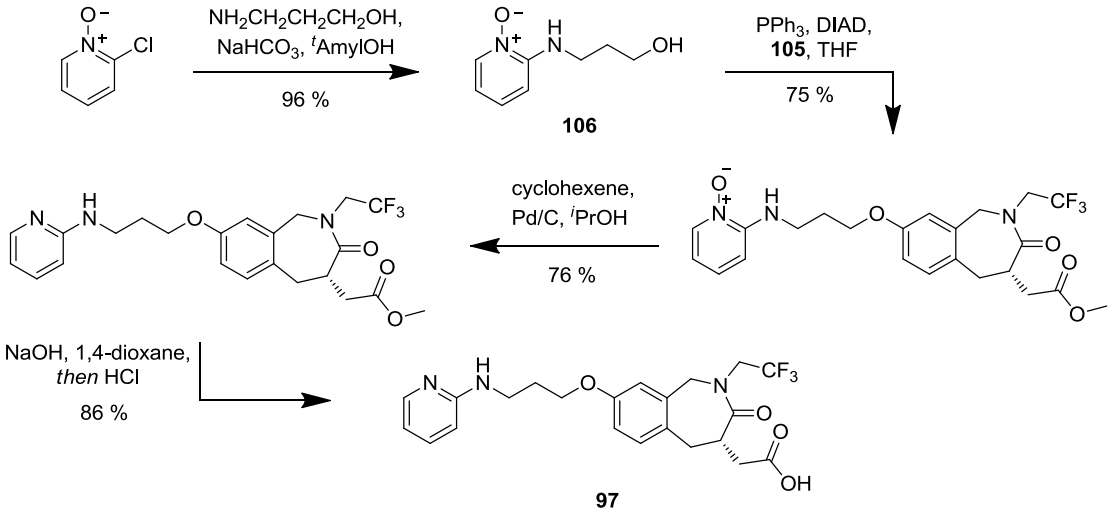

Scheme 32 *The completion of the synthesis of* ***97***

3.2 Previous work in our laboratories

Given the promising profiles of **97** and **98**, the aim was to use these compounds as a starting point for a series of compounds which would inhibit $\alpha_V\beta_1$. It was anticipated that, if structural similarity to these compounds could be maintained, then these compounds would also be likely to possess good PK properties and oral bioavailability. This was in contrast to the other series undergoing development, which had been developed from a series targeting $\alpha_4\beta_1$, in which the compounds showed high selectivity for $\alpha_V\beta_1$, but had undesirable PK properties.[190]

The first part of the molecule which was changed was the aminopyridine moiety. Since the initial development of these compounds, the tetrahydronaphthyridine group has become the near-ubiquitous α_V-binding group of choice, therefore this seemed an obvious alteration to make to the original compounds. This led to the synthesis of analogue **107**, the profile for which is shown in **Table 22**.[191]

	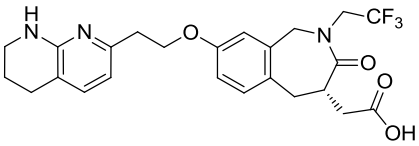 **107**	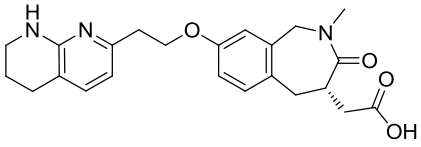 **108**
$\alpha_V\beta_1$ pIC_{50}	8.3 (n = 4)	8.2 (n = 6)
$\alpha_V\beta_3$ pIC_{50}	8.6 (n = 3)	8.8 (n = 4)
$\alpha_V\beta_5$ pIC_{50}	8.5 (n = 2)	8.4 (n = 1)
$\alpha_V\beta_6$ pIC_{50}	5.5 (n = 4)	5.4* (n = 4)
ChromlogD	2.67	1.89
AMP / nm s^{-1}	<10	<10
$T_{1/2}$ / min	72	246
Cl_b / mL min^{-1} kg^{-1}	75	15
F (rat) / %	22	39

Table 22 *The measured properties of compounds **107** and **108**, with the tetrahydronaphthyridine group replacing the aminopyridine group in **97** and **98.** *On one test occasion, this value was measured at < 5 but this is not included in the mean.*

Use of the tetrahydronaphthyridine group led to an immediate increase in potency at $\alpha_V\beta_1$ to 8.3. Though the $\alpha_V\beta_3$ and $\alpha_V\beta_5$ potency of this compound did not change significantly as measured by the integrin cell adhesion assay, this may be due to the fact that a pIC_{50} of approximately 8.5 is the maximum possible potency measurable with this assay set up. Therefore, the $\alpha_V\beta_3$ and $\alpha_V\beta_5$ potency is expected to have increased more, but this is not measurable in the assay.

In some historical series, the trifluoroethyl group on the amide nitrogen had been truncated to a methyl group without any significant loss in potency,[176] so compound **108** with the *N*-methyl amide was also prepared.[191] This was found to be equipotent with **107** in several different integrin cell assays and, in fact, showed superior pharmacokinetics to **108**, with lower blood clearance (Cl_b, where 14.5 represents a low-to-moderate clearance rate) and a longer $T_{1/2}$, though both compounds were found to be moderately orally bioavailable. Similarly to compounds **97** and **98**, these compounds possessed no measurable AMP, but in this case, the active transport of these compounds was confirmed, with these compounds found to be substrates for an organic anion transporter peptide.[192]

Compounds **107** and **108** were, therefore, a promising starting point in the medicinal chemistry work on this series, and were considered the 'lead compounds' at this stage. If this series were to be developed into a tool compound for $\alpha_V\beta_1$ target validation, several log units of selectivity would be required over other integrins. If, however, this series was to lead to a compound to be used for the treatment of fibrosis, then only sufficient selectivity would be required for pharmacology resulting from the antagonism of the $\alpha_V\beta_1$ integrin to predominate. This might, in the first instance, amount to one log unit of selectivity in potency over the other integrins, in order to initially validate the approach, showing that the series has potential for further development.

3.2.1 Existing patent literature

One of the key requirements of the new series of compounds was to avoid conflict with previously-declared intellectual property, with several patents having been published on the benzazepine and 1,4-benzodiazepine cores. Initially, in 1997, one parent forerunner company to GSK published two patents which contained a very broad scope.[193,194] These patents are now out of date, but were followed up by another patent of broad scope in 2002,[195] and a further patent containing benzimidazoles and imidazoles as the α_V-binding group.[196] In 2001 and 2002, two single-compound patents for $\alpha_V\beta_3$ compounds for the treatment of osteoporosis were published.[197,198] A final patent published by the same parent forerunner company to GSK was published in 2003, containing a group of compounds all with the same benzazepine core as **97** and **98**.[199] In terms of competitor patent literature, Merck published their own patent containing benzazepine and 1-4,benzodiazepine compounds as α_V receptor antagonists in 2001, including exemplification of the tetrahydronaphthyridine group as the α_V-binder.[200] A more recent patent published by Ube industries in 2010 of $\alpha_V\beta_3$, $\alpha_V\beta_5$, and $\alpha_V\beta_6$ antagonists includes examples with

the same benzazepine core as **97** and **98**, but a fused imidazole-piperazine as the α_V-binder.[201]

Motivated by a desired to explore chemical space beyond what had previously been exemplified, it was desired to substitute the phenyl ring of the benzazepine motif for a heterocycle, without significant deviation from the properties that had initially been attractive for **97** and **98**, and latterly **107** and **108**. Additionally, one of the 1997 patents was the only such publication to include heterocycles in this part of the molecule within the scope of the patent, and such compounds have not been exemplified in the patent literature thus far.

The drawback of modulation of this part of the molecule is that such core modification requires a bespoke synthesis for each compound, as it is not possible to install this aromatic ring in later in the synthesis. However, since no examples exist of this part of the molecule being changed in the literature, this was considered a very good opportunity, and so work was undertaken in our laboratories to access such compounds. The other part of the molecule which underwent initial investigation in our laboratories was the substituent on the amide nitrogen atom, as it was felt that a library of compounds with substitution at this position would be readily accessible synthetically.

3.2.2 Construction of an $\alpha_V\beta_1$ homology model

In order to prioritise the synthetic targets, and to rationalise the SAR that was observed, a computational model was required. No crystal structure of the $\alpha_V\beta_1$ integrin has been published, so in order to still be able to model the binding site, a homology model has been created in previous work within our laboratories.[202] It was developed by combining two proteins with established crystal structures, namely the $\alpha_V\beta_3$ and $\alpha_5\beta_1$ integrins.[44,203] The amino acid sequences of the proteins were

superposed, and the relevant α_V or β_1 domains of the integrin could then be kept to form the homology model for the $\alpha_V\beta_1$ binding site. Both proteins had been crystallised using small RGD-containing peptide sequences. These docking grids could then be used for docking ligands into using Glide on Maestro.[204] The homology model was created by co-worker Pal, and the docking studies were carried out by the author.

When compounds **97** and **98** were docked into the model, both were shown to bind in a similar fashion to one another **(Figure 71)**. The benzazepine of the compounds are slightly tilted compared to one another, but in both cases the linker chain to the α_V binder is linear and in a low-energy conformation. In the same way as for the $\alpha_V\beta_6$ antagonist **1** (**Figure 17**, page 18), the α_V-binding end of the molecule forms a salt bridge with the aspartate residue, and the carboxylate group binds to the magnesium ion in the β_1 domain of the protein. Whenever docking was carried out, the compounds were prepared for docking using LigPrep, and docked using Glide. If a satisfactory pose could not be obtained at the first attempt, the resulting conformation was re-docked using Glide.

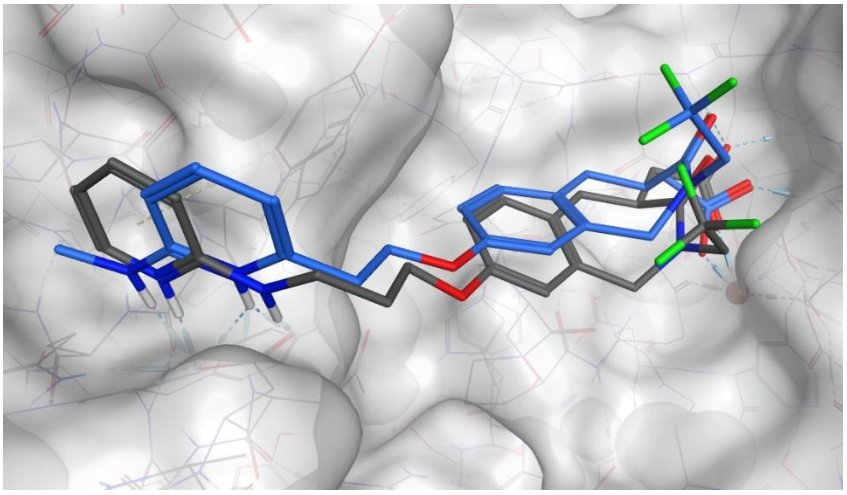

Figure 71 *Compounds **97** (grey) and **98** (blue) docked into the $\alpha_V\beta_1$ homology model. Both compounds appear to bind similarly to one another, though the two aryl cores of the molecule are tilted compared to one another. The aspartic acid residue and magnesium ion are visible, coordinating to the aminopyridine moiety and carboxylate group respectively.*

Though a similar homology model approach has been used by DeGrado in the rational design of $\alpha_V\beta_1$-selective compounds,[57] an important aspect of this project was to establish whether this computational model could rationalise observed ligand potency, and also be used predictively in compound design, as this approach had not been used before the outset of this project, when the previous SAR detailed below was established.

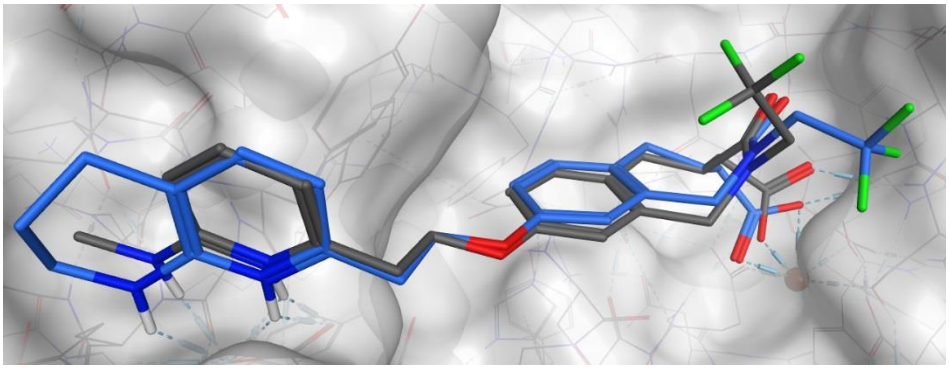

Figure 72 *Compound **107** (in blue) docked into the $\alpha_V\beta_1$ homology model, overlaid onto the docking of **98**, shown in grey. Both compounds appear to bind in a very similar pose.*

When compound **107** was docked into the homology model, it was found to overlay very closely with **98 (Figure 72)**. Both of these compounds have the chain linking the α_V and β_1 domains in an all-trans conformation, which is the lowest-energy arrangement. This is an indication that these compounds are a good fit for the binding site. Since **107** and **108** and were the lead compounds for the series at the outset, one of these compounds will be included in the figures of the docked compounds in order to provide comparison with the compound.

When *N*-methyl analogue **108** was docked, it was found to overlay very closely with **97 (Figure 73)**. Compound **97** was rotated with respect to **98** when they were overlaid in **Figure 71**, but **108** is highly potent when measured in the assay.

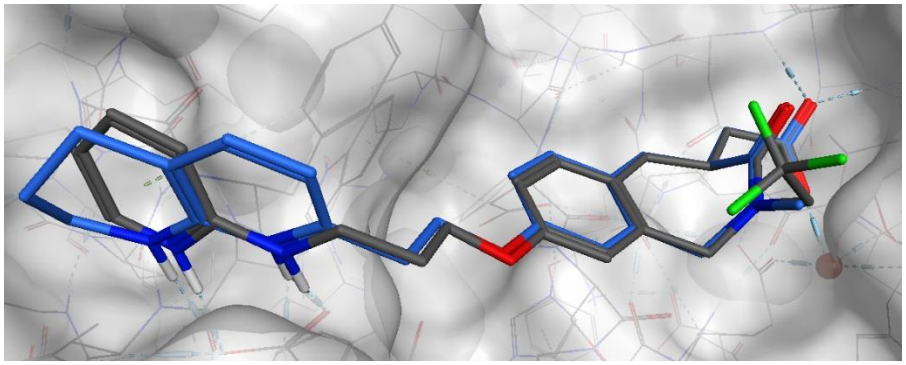

Figure 73 *Compound **108** (in blue) docked into the $\alpha_V\beta_1$ homology model, overlaid onto the docking of **97**, shown in grey. Both compounds appear to bind in a very similar pose.*

Therefore, when comparing the two lead compounds **107** and **108** it is notable that the azepine is twisted slightly in compared to **107 (Figure 74)**. In the $\alpha_V\beta_1$, the measured cell potency is almost equal **(Table 22)**, implying that the aromatic core might not make key interactions, instead just placing the carboxylate and tetrahydronaphthyridine group in the requisite positions. Therefore, such rotation of this part of the molecule may, in these circumstances, not affect the potency.

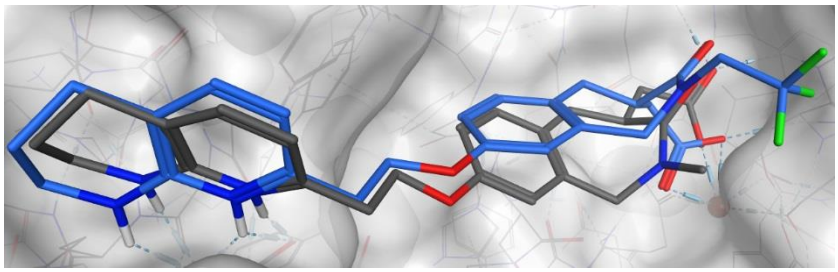

Figure 74 *Compound **108** (in grey) docked into the $\alpha_V\beta_1$ homology model, overlaid onto the docking **107** (in blue). The chain conformations are similar, but a twisting of the azepine ring is observed*

In addition to the docking of prospective targets into the $\alpha_V\beta_1$ homology model, the $\alpha_V\beta_3$ crystal structure from which the homology model was constructed can also be used for docking, to determine whether a compound is likely to be selective or not. Compound **3**, developed within the DeGrado laboratories, seemed an appropriate compound on which to test this prospect, since it had been found to be exquisitely selective for $\alpha_V\beta_1$ over other RGD-integrins. Also assessed was compound **109 (Figure**

75, developed within our laboratories,[205] which had been found to be highly selective for $\alpha_V\beta_1$ (though not as selective as **3**).

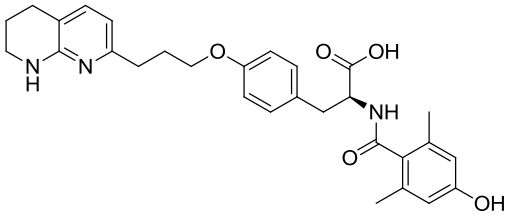

109

***Figure 75** Compound **109**, which was found to also be selective for $\alpha_V\beta_1$ over other RGD-integrins*

Figure 76 shows **3** docked into the homology model, with extraordinary shape complementarity in the so-called specificity-determining loop (SDL), which is above the magnesium ion in **Figure 76**.

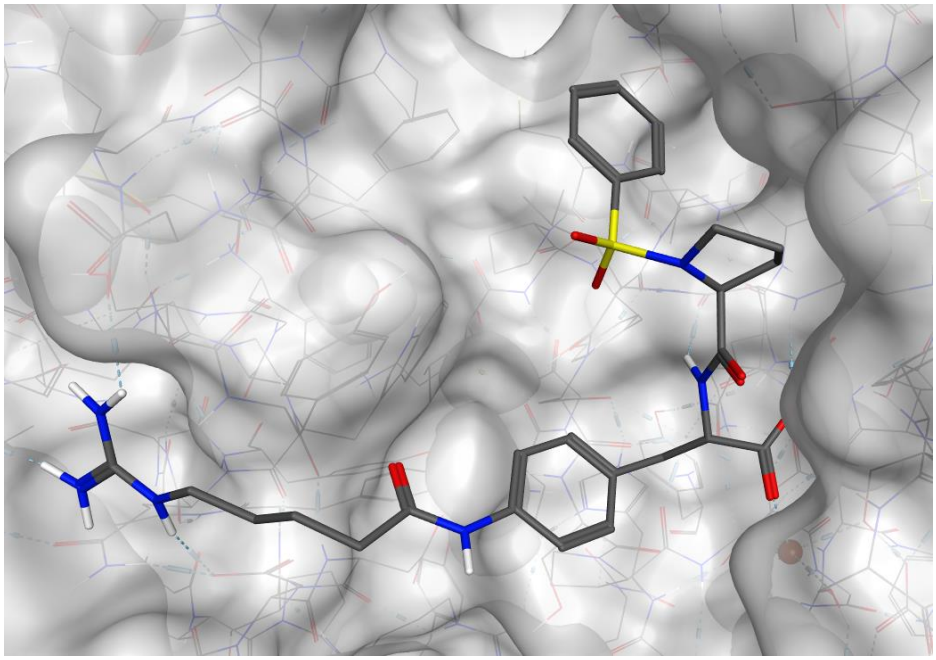

***Figure 76** Compound **3** docked into the $\alpha_V\beta_1$ homology model, showing exceptional shape complementarity in the SDL.*

When compound **3** was docked into the $\alpha_V\beta_3$ crystal structure **(Figure 77)**, the exquisite selectivity for these compounds became apparent. The compound fits poorly in the receptor, and in particular, the proline-sulfonamide is not accommodated in the SDL.

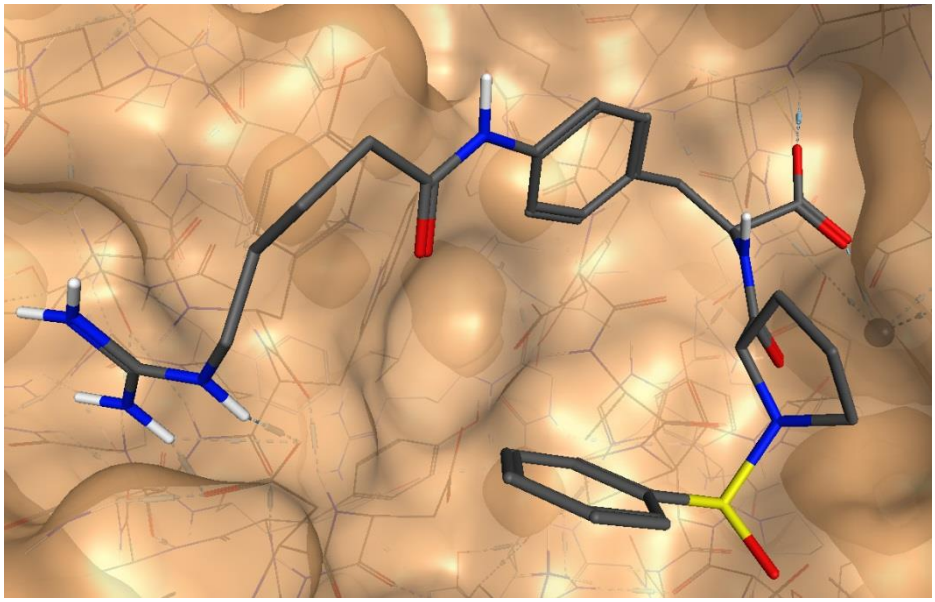

Figure 77 *Compound **3** docked into the $\alpha_V\beta_3$ crystal structure, with an extremely poor fit, and no possibility of the sulfonamide being accommodated in the SDL.*

Likewise, when compound **109** from our laboratories was docked into the two models **(Figure 78)**, the selectivity also appears to derive from the accommodation of the side (or lack thereof) in the SDL of the $\alpha_V\beta_1$ integrin compared to $\alpha_V\beta_3$.

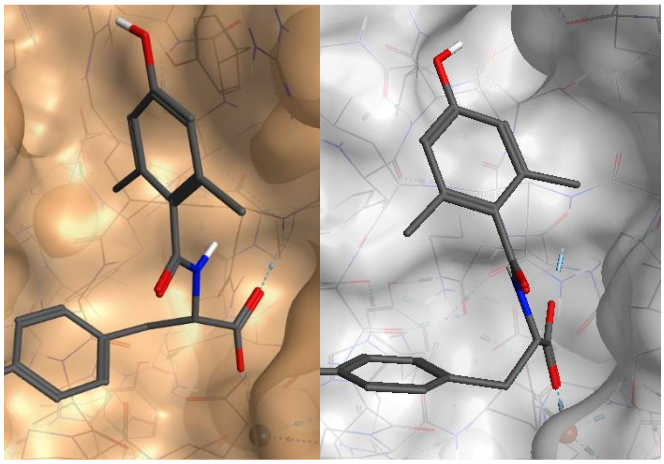

Figure 78 *Compound **109** docked into the $\alpha_V\beta_3$ crystal structure (left) and the $\alpha_V\beta_1$ homology model (right). Only the β-binding portion is shown in both cases. In the $\alpha_V\beta_1$ docking, the substitutions on the aryl ring in the SDL are able to fill the pockets created, whereas in the $\alpha_V\beta_3$ docking, the compound cannot fit. This is thought to account for the selectivity of the compound.*

The side chain of **109** is, however, still able to access the SDL part of the pocket in the $\alpha_V\beta_3$ crystal structure, unlike for compound **3**, which may explain why **3** has superior selectivity over **109**.

The ability of this docking approach to rationalise the selectivity of previously developed $\alpha_V\beta_1$ selective compounds **3** and **109** was promising for its utilisation in this study. What was also clear, however, was that the selectivity of these compounds derives from the compounds' ability to effectively occupy the SDL. In the series of compounds under investigation in this work, beginning with **107** and **108**, this pocket was not occupied, and so alternative, novel means of obtaining selectivity would be sought.

3.2.3 Summary of previous SAR from our laboratories

Building on the findings of **108**, which retained potency at $\alpha_V\beta_1$ compared to **107**, further modifications of the alkyl group on the amide nitrogen were made.[206] The majority of these analogues were synthesised by first accessing the unalkylated analogue **110**, which was then alkylated by deprotonation of the amide hydrogen by sodium hydride, followed by addition of the appropriate alkyl halide **(Scheme 33)**.

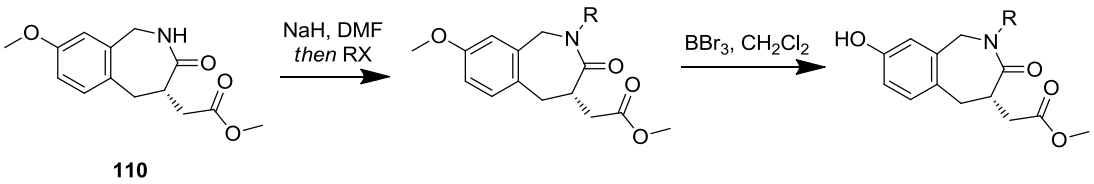

110

Scheme 33 *The alkylation of intermediate **110** with the corresponding alkyl halide, followed by deprotection to give the corresponding phenol. This was then subject to Mitsunobu reaction and then ester hydrolysis to furnish the final compounds*

However, the hindered nature of the azepine and the low nucleophilicity of the amide anion meant that only a small group of primary alkyl halides reacted in this manner, limiting the compounds that could be synthesised using this approach. However, a more labour-intensive approach could be utilised to synthesise more sterically demanding primary and secondary alkyl halides, namely to use the desired alkyl amine in a reductive amination with aldehyde **111 (Scheme 34)**.[206]

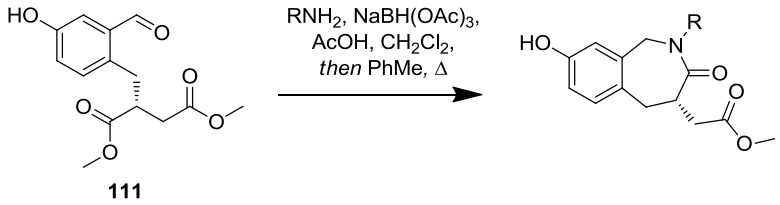

Scheme 34 *The alternative method for forming N-alkylated analogues of* ***110***

By these methods, a small group of analogues with varying *N*-alkyl substitutions were synthesised, which are summarised in **Table 23** below. [206]

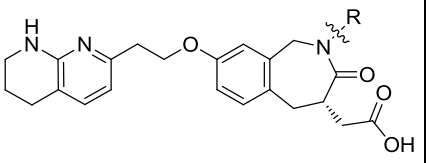			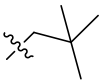	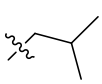	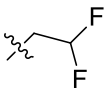
$\alpha_V\beta_1$ pIC_{50}	8.0 (n = 3)	8.1 (n = 2)	8.1 (n = 3)	8.2 (n = 3)	8.3 (n = 3)
$\alpha_V\beta_3$ pIC_{50}	8.5 (n = 3)	8.7 (n = 2)	8.3 (n = 3)	8.6 (n = 3)	8.7 (n = 3)
$\alpha_V\beta_5$ pIC_{50}	8.5 (n = 1)	-	8.4 (n = 1)	8.8 (n = 1)	8.8 (n = 1)
$\alpha_V\beta_6$ pIC_{50}	<5.0** (n = 2)	<5.0 (n = 2)	<5.0 (n = 3)	5.3* (n = 2)	5.3* (n = 2)
ChromlogD	2.19	2.46	3.46	2.84	2.55

Table 23 *The cell adhesion assay potency data for various N-alkyl substitutions. Whilst a range of lipophilicities were observed, there was no effect on potency at $\alpha_V\beta_1$ or selectivity over other integrins. Where R is Et, the compound was prepared as a racemate.*On one test occasion for each, < 5 measured. This value is not included in the mean. **On one test occasion, 5.1 measured.*

It was hoped that substitution of the *N*-alkyl group would lead to a reduction in potency at $\alpha_V\beta_3$ and $\alpha_V\beta_5$. However, as **Table 23** shows, a group of small alkyl substitutions did not show any effect on potency at any of the integrins that were tested. Based on the homology model, it appears that this may be because this part of the binding pocket is more solvent-exposed, and so any group with a methylene linker is able to orient the bulky group away from the protein. If more significantly hindered groups are accessed in future, this vector may yet prove productive in giving selectivity. These compounds do, however, show a range of lipophilicities, without

any effect on potency. Therefore, this vector appears to be a promising handle through which the physicochemical properties of the compound may be varied without affecting the potency, should that approach be required.

Changes were also made to the length of the alkyl chain connecting the tetrahydronaphthyridine to the benzazepine, but increasing or reducing the length by one carbon caused loss of $\alpha_V\beta_1$ activity by 2 log units in both cases. Modification of the length did not appear to be a likely source of selectivity, because the $\alpha_V\beta_1$ activity suffered more significantly as a result of changing the length of the linking chain than was observed for the $\alpha_V\beta_3$ and $\alpha_V\beta_5$ integrins.

As previously mentioned, it was desired to change the phenyl core of the molecule to different heterocycles, since these have not been exemplified in any patent literature. Therefore, pyridyl analogues **112** and **113** were prepared **(Figure 79)**.[207] These compounds were prepared as racemates, for the sake of synthetic tractability.

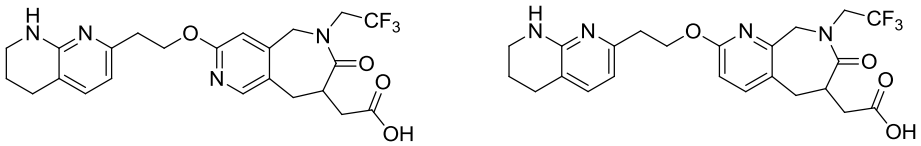

112 **113**

Figure 79 *Analogues **112** and **113**, containing a pyridine heterocycle in the core*

In the case of **97**, it was found that the enantiomer was 30-fold less potent at $\alpha_V\beta_3$, and other previous work in our laboratories has indicated that the enantiomers of these compounds would be significantly less active.[191] When one enantiomer of a compound is more than an order of magnitude greater in potency than its enantiomer then, within the error of the assay, the distomer may be considered not to contribute to the overall pIC_{50} of the compound. Therefore, the potency of the racemate is likely to be approximately half that of a sample of the single enantiomer, which corresponds to a reduction in pIC_{50} of approximately 0.3. Therefore, the measured cell adhesion potency of a racemate is assumed to be 0.3 units lower than the potency of the single enantiomer. It is possible to separate the enantiomers using

chiral chromatography, but since the throughput of this method is low, this is reserved for particular compounds of interest later in development.

	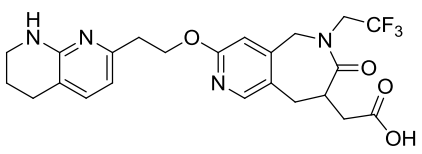 **112**	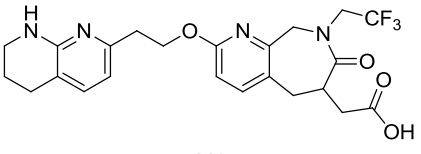 **113**
$\alpha_V\beta_1$ pIC_{50}	7.1 (n = 3)	7.7 (n = 8)
$\alpha_V\beta_3$ pIC_{50}	8.4 (n = 3)	8.4 (n = 4)
$\alpha_V\beta_5$ pIC_{50}	8.6 (n = 1)	8.6 (n = 3)
$\alpha_V\beta_6$ pIC_{50}	< 5 (n = 3)	5.6 (n = 3)
ChromlogD	1.55	2.38

Table 24 *The integrin cell assay data for racemic pyridyl analogues **112** and **113**. Regioisomer **112** shows a loss in cell potency at $\alpha_v\beta_1$ by approximately one log unit, whilst regioisomer **113** retains similar $\alpha_v\beta_1$ potency to phenyl analogue **107**, when considering that **113** was tested as a racemate.*

The integrin cell adhesion assay data for **112** and **113** is shown in **Table 24**. A reduction in potency at $\alpha_V\beta_1$ was observed for analogue **112**, without any reduction in potency at $\alpha_V\beta_3$ and $\alpha_V\beta_5$. More promisingly, regioisomeric analogue **113** appears to nearly maintain potency at $\alpha_V\beta_1$ (when considering that **113** was tested as a racemate), though there does not appear to be improved selectivity over the other α_V-containing integrins.

Encouragingly, when **113** was docked into the homology model, the docked conformation overlaid closely with **107 (Figure 80)**. This rationalises the fact that the two compounds are equipotent in the $\alpha_V\beta_1$ assay, when considering that **113** was tested as a racemate and the single enantiomer is anticipated to have a pIC_{50} 0.3 log units higher than the racemate.

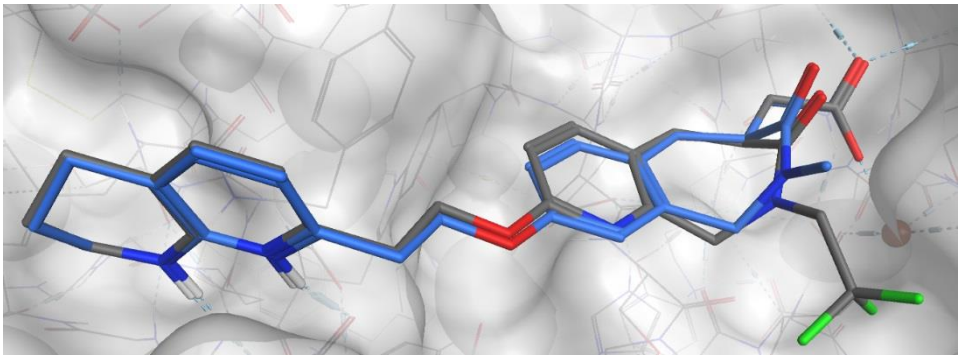

Figure 80 *The docked conformation of **113** (in grey), overlaying with **108** in blue. This successfully rationalises the equipotency of the two compounds in the $\alpha_V\beta_1$ assay (accounting for **113** being tested as a racemate)*

In comparison, **112** was found to have a lower potency in the assay, and this may be rationalised by the conformation that the compound takes when docked into the homology model **(Figure 81)**. Though most of the docked conformation appears to sit very similarly to the lead **107**, it is noticeable that the linking chain in **112** is puckered out of the plane, no longer in the energetically favoured all-*trans* conformation with respect to the aryl core.[208]

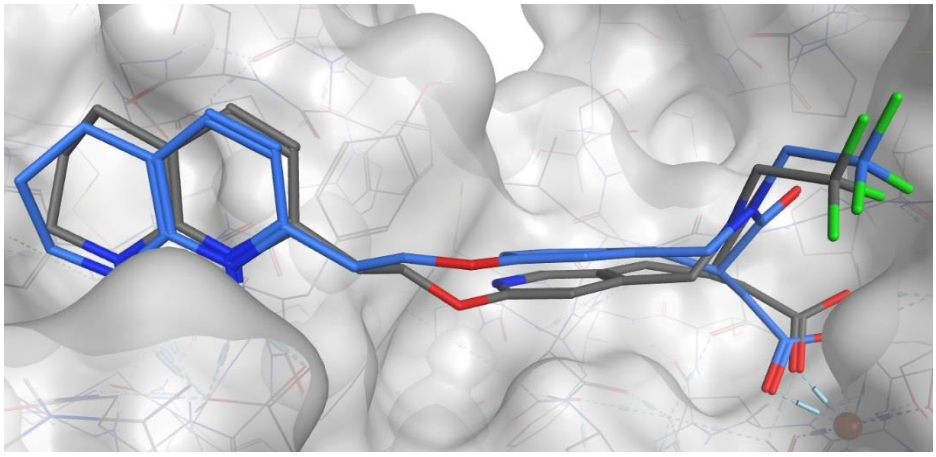

Figure 81 *The docked conformation of **112** (in grey), overlaid onto **107** in blue. Though most of the conformation overlays well, there is a notable puckering of the alkyl chain*

Inlaid into the graph of **Figure 82** is the measured dihedral angle of **112**. The graph shows the frequency of different dihedral angles for the searched substructure (also inlaid, with the atoms used for dihedral angle calculation shown in red) in the Mogul database.[209] The Mogul results suggest that a dihedral angle of 180 ° would be

preferred, which would give the favoured flat structure like for lead compound **107**. This suggests that this angle cannot be accommodated in this case, since it would otherwise be favoured. One possible explanation is that if the group sat in the same geometry as **107**, the position of the pyridyl nitrogen atom would result in the nitrogen lone pair pointing towards the middle of the aromatic electron density of the nearby phenylalanine residue, as visible in **Figure 81**, which would not be favoured.

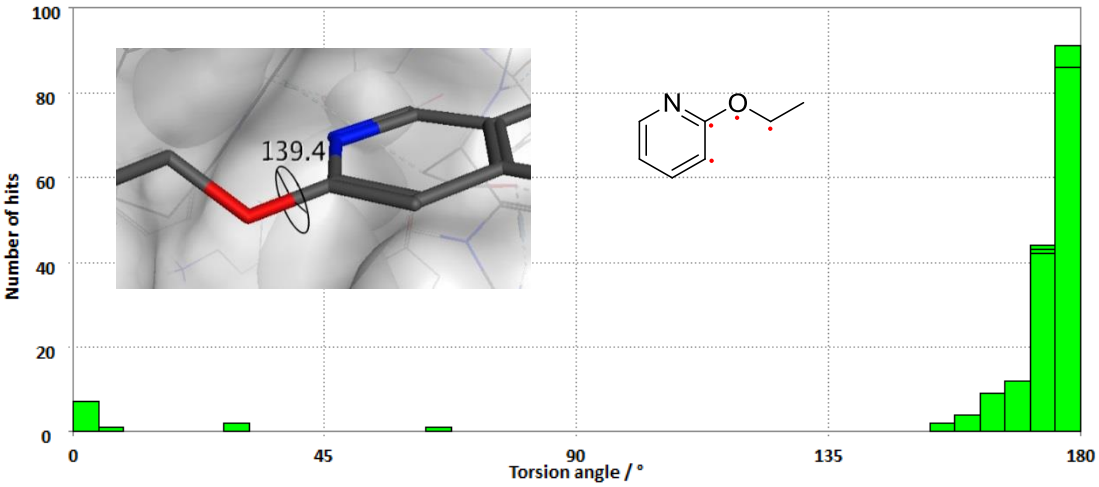

*Figure 82 The graph shows the distribution of dihedral angles in the Mogul database for the substructure search shown (inlaid, right). Inlaid, left is shown the dihedral angle for the docked conformation of **112***

In summary of the medicinal chemistry efforts on this series prior to the work described herein, the $\alpha_V\beta_1$ potency had been improved by the use of the tetrahydronaphthyridine group in the place of the aminopyridine moiety. It had been found that changing the length of the linker between the α_V-binding group and the β_1-binding group is unproductive for $\alpha_V\beta_1$ activity and selectivity, as the $\alpha_V\beta_3$ and $\alpha_V\beta_5$ integrins appear to be less length-specific than $\alpha_V\beta_1$. A small group of small alkyl substitutions were made in place of the CH_2CF_3 group, and these were not found to modulate the potency of the compounds, though this vector does appear a useful handle through which to modulate the physicochemical properties of the compounds. A small number of core changes were also made, where substitution of the phenyl ring with a pyridyl ring led to a loss of potency for one regioisomer **(112)**, and a compound of similar potency for another regioisomer **(113)**. It seemed,

therefore, that selectivity for $\alpha_V\beta_1$ might be difficult to obtain in this series, although several changes both to the core of the compound and the outer substituents were accommodated without a loss in activity.

3.3 Opportunities for further development of 107 and project aims

Building upon the previous work of our laboratories it was envisaged that a greater understanding of the SAR could lead to further increases in $\alpha_V\beta_1$ potency, and selectivity over the other integrins. **Figure 83** indicates possible areas for modification on compound **107**, in addition to the areas already considered.

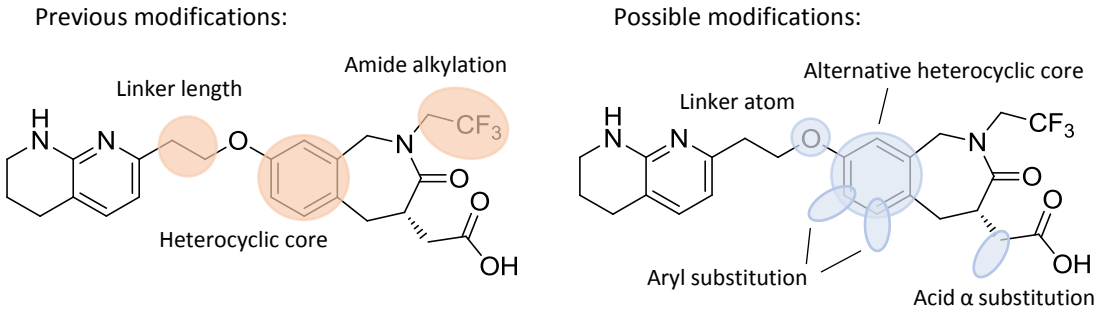

Figure 83 *The possible areas for modification on compound* ***107*** *that had already been investigated, and those not yet investigated*

The aim of this study was to continue to investigate this series of compounds as $\alpha_V\beta_1$ integrin antagonists, preferably with selectivity over other integrins. Whilst two analogues containing a pyridyl core had been synthesised, a number of other possible heterocycles were yet to be investigated. Additionally, it was of interest to investigate the atom linking the benzazepine with the linking chain, since changing the linker atom is likely to affect the preferred conformation of the chain. It was also hypothesised that alkylation next to the acid group or on the aryl core could confer

selectivity over the other integrins, and so it was intended that compounds with various substitutions at these positions would be prepared.

It was proposed that a group of potential heterocycles for the core of the compound could be accessed and assessed for their suitability, ideally finding several previously unexemplified cores with potency similar or superior to the current phenyl substituted lead compounds **107** and **108**. The best linker atom between the two halves of the compound would also be found, assessing carbon for its suitability. Finally, further alkyl substitution was planned, to target additional degrees of selectivity over other integrins in this series, given the lack of genuinely selective small molecule $\alpha_V\beta_1$ integrin antagonists. One of the most attractive features of this series at the outset of the work was the physicochemical properties and oral bioavailability of the compounds, and so the intention was to retain these properties in the analogues synthesised. Additionally, the physicochemical handle of the amide nitrogen could be used to modulate the lipophilicity in such a way as to remain in a similar physicochemical space to the lead compounds, should that be required.

3.4 Results and discussion: Core and linker investigations

3.4.1 Thiophene-containing analogues

First seeking to find other heterocycles that could be accommodated in the core of the molecule, it was immediately apparent that this would require bespoke syntheses of the different heterocyclic targets, since it is very difficult to envisage how the heterocycle could be built up after the tetrahydroazepine ring. A thiophene is a known bioisostere for a phenyl ring,[210] and so compound **114,** shown in **Figure 84**, was the first target chosen for synthesis.

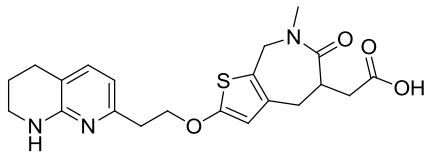

114

Figure 84 *Thiophene **114** was the first azepine compound chosen for synthesis*

This core was anticipated to have a significantly different vector for the attachment of the α_V-binding end of the molecule, particularly with this choice of thiophene regioisomer, since the sulfur atom is larger than the carbon atom. However, very little was known about whether this would have a positive or negative effect on the potency. Additionally, the methyl substituent on the amide nitrogen atom was chosen, on the basis that for compound **108**, no drop in potency or selectivity was compared in comparison with **107**, and so the simpler and smaller of the groups was chosen.

Retrosynthetically, inspiration was taken from the route to **97 (Scheme 31)**. An intramolecular amide coupling was envisaged to furnish the methyl ester of the final compound **114**, followed in a retrosynthetic sense by the union of alcohol **67** and 2-bromothiophene **115** *via* Ullmann coupling **(Scheme 35)**. It was envisaged that **115** could be obtained from alkene **116**, through reduction and electrophilic halogenation.

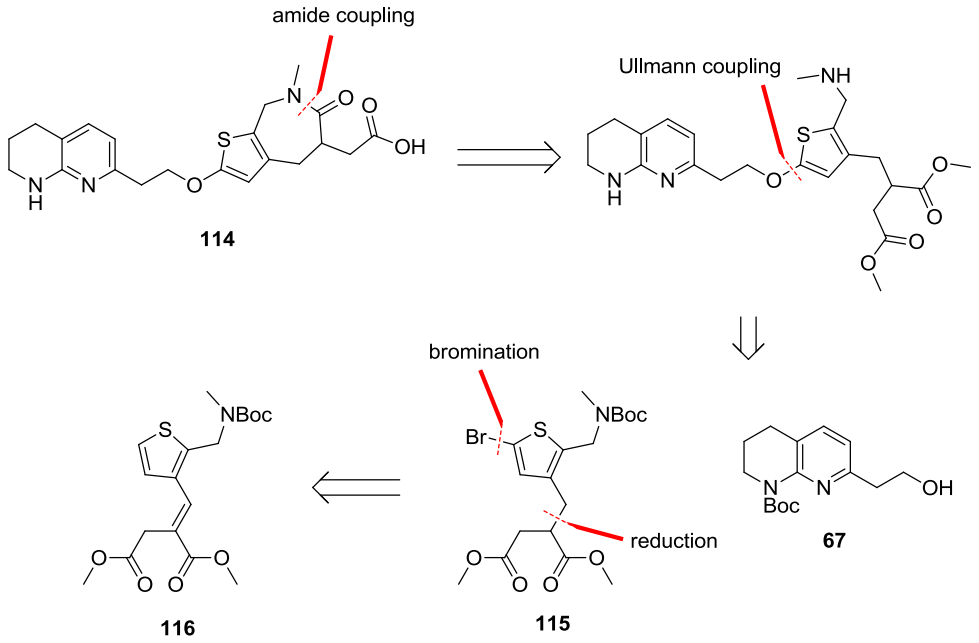

*Scheme 35 Retrosynthetic analysis of thiophene **114**, with an Ullmann coupling of **67** and **115** envisaged, followed by an intramolecular amide coupling akin to that used in the synthesis of **97***

Scheme 36 outlines the strategy for the preparation of alkene **116**. As in the synthesis of **97**, the Heck coupling of bromide **117** and dimethyl itaconate **102** was envisaged as the key carbon-carbon bond forming step. Protected amine **117** could then be prepared from acid **118**.

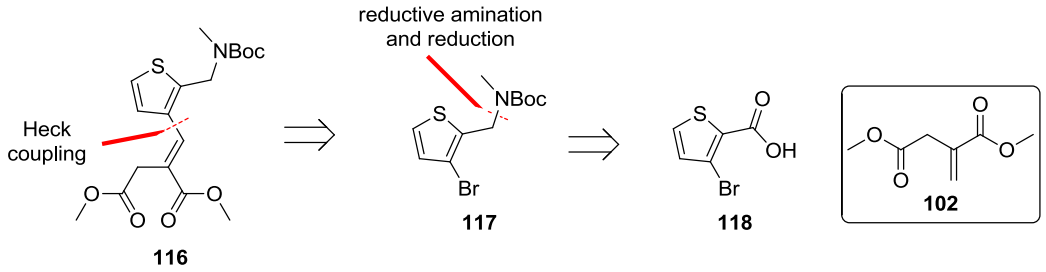

*Scheme 36 Retrosynthesis of **116** to commercially available acid **118**, via Heck reaction of **117** with dimethyl itaconate **(102)***

Therefore, synthetic work on **114** began with commercially available bromide **118 (Scheme 37)**. Amide coupling of the Weinreb salt with HATU afforded Weinreb amide **119**, which was smoothly transformed into aldehyde **120** *via* reduction with $LiAlH_4$. Subsequent reductive amination to amine **121** required sodium borohydride in

addition to sodium acetoxyborohydride for the reduction, presumably due to stabilisation of the resulting iminium ion by the aromatic ring, reducing the electrophilicity. The requirement for sodium borohydride in the reductive amination of thiophene-2-carbaldehydes has been widely reported elsewhere.[211] Boc protection gave bromide **117** in good yield, employing imidazole in the work up to remove unreacted Boc_2O. After reaction with imidazole, washing with a diluted acid removes the resulting imidazolocarbamate, and the regenerated imidazole is also washed into the aqueous phase.

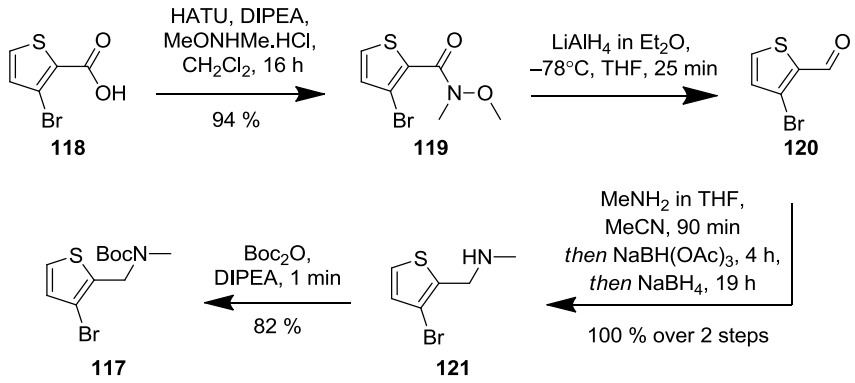

Scheme 37 *The preparation of bromide **117** from **118***

With bromide **117** in hand, the key Heck reaction could be carried out. The same conditions were used as had been employed in the medicinal chemistry route to **97**, and gave the product in moderate yield, in solely the *E* geometry. This geometry was confirmed by the observation of a correlation between the C_4 aryl proton and the itaconate methylene protons **(Scheme 38)**. Following this success, it was envisaged that the order of the steps might be altered to enable the Heck coupling of aldehyde **120** to **102**, in order to avoid the protection step and to enable the installation of a varied of different alkyl groups to the amine. Unfortunately, these attempts were unsuccessful.

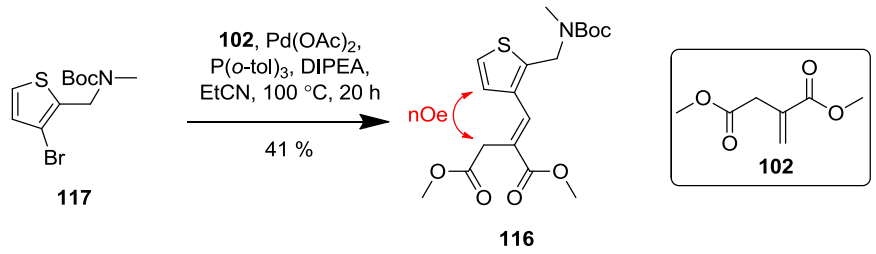

*Scheme 38 The reaction of **117** with dimethyl itaconate **(102)** to form **116**, with alkene geometry confirmed by nOe measurements*

The reduction of alkene **116** to **122** proved to be challenging. It was possible to carry out the reduction using the H-Cube® apparatus at high temperature and pressure, when the solution was passed through the machine a high number of times and at high dilution. This made this approach inappropriate for scale-up, therefore the diimide reduction with benzenesulfonyl hydrazide was used to complete the conversion to **122** when performed at a larger scale **(Scheme 39)**.

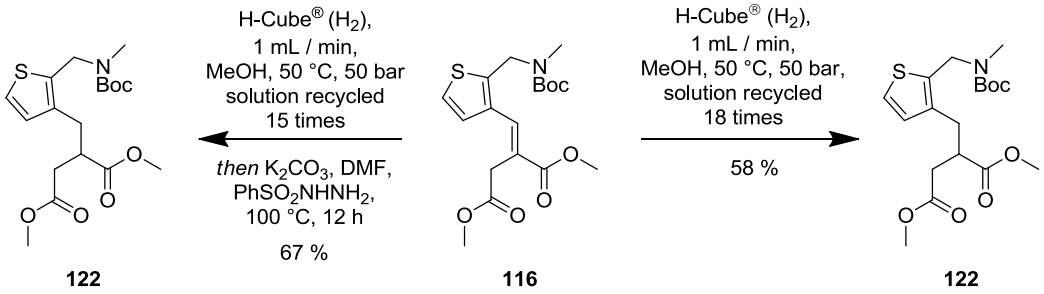

*Scheme 39 The reduction of **116** to **122**, which proceeded smoothly in the H-Cube® (flow H_2 generation) on small scale, but required diimide reduction to complete the reaction on a larger scale*

Additionally, it appeared that over time the catalyst cartridge on the H-Cube® was deactivated when operating on a larger scale, implying possible poisoning by the substrate or an impurity. This was another reason that the diimide reduction was appropriate, though the highly stable conjugated, triply substituted, double bond was less reactive in this process, meaning that a large number of equivalents of benzenesulfonyl hydrazide were required for the reaction to go to completion.

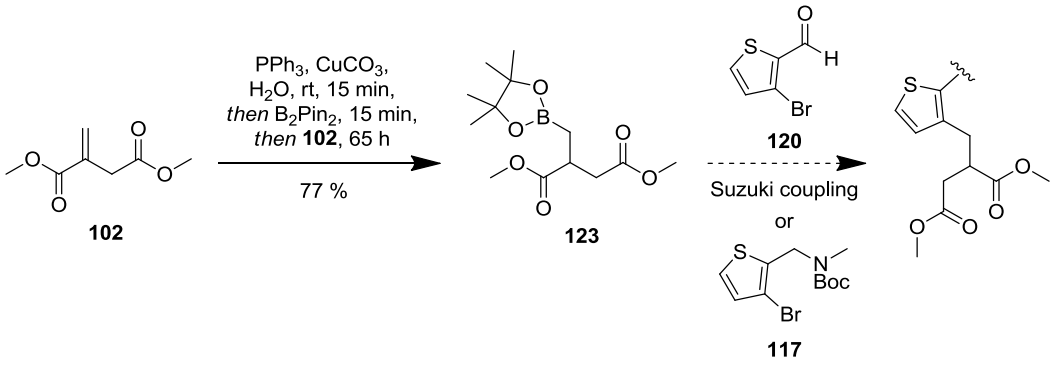

Scheme 40 *The borylation of itaconate* ***(102)****, proposed to lead to Suzuki coupling of the diester to the aryl bromide group*

In light of the difficulty encountered in reducing the double bond of **116**, an alternative approach was investigated **(Scheme 40)**. This involved the preparation of alkylborane **123** from **102**, which proceeded smoothly in a copper-mediated addition reaction in H_2O,[212] in the hope that this could be coupled *via* Suzuki reaction to bromide **117** or **120**. This would avoid the need for a reduction step, and also remove the requirement for the Heck reaction, which proceeds in only moderate yield.

The Suzuki reaction of 3-bromothiophenes with alkyl boronates has been reported,[213] using palladium and the RuPhos catalyst.[214] Additionally, the SPhos ligand has been used with tris(dibenzylideneacetone)dipalladium (Pd_2DBA_3) in the Suzuki reaction of alkyl boronates and aryl bromides with an *ortho*-aldehyde substitution.[215,216] Therefore, these conditions were chosen for the coupling reaction **(Scheme 41)**. Unfortunately, on the aldehyde substrate **(120)** and amine **(117)** substrates, neither reaction was productive. Although a trace amount of product was observed with the RuPhos conditions on amine **117**, no product was isolated.

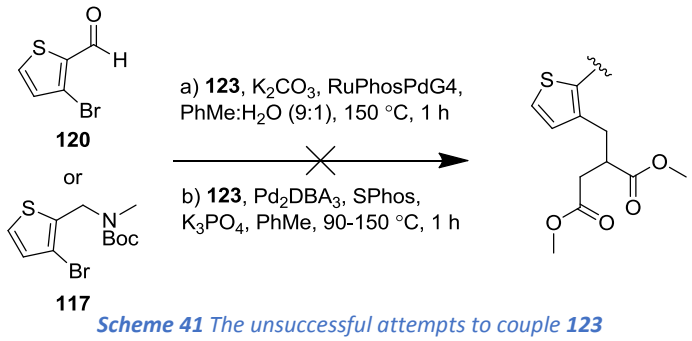

Scheme 41 *The unsuccessful attempts to couple* ***123***

As Molander has reported the utility of alkyl potassium trifluoroborate salts in sp^3 Suzuki couplings,[217] **123** was converted to the corresponding trifluoroborate **(124)** using a procedure that avoids the use or production of hydrogen fluoride **(Scheme 42)**, and the product used without further purification.[218]

Scheme 42 *The conversion of pinacol ester **123** into trifluoroborate **124**. The high yield is attributed to residual unreacted starting material*

This material was then used in a screen of conditions for the reaction detailed in **Scheme 43**. Two solvent mixtures and two bases were used, with six palladium precatalysts frequently used in sp^2-sp^3 Suzuki reactions. Unfortunately, only a trace amount of product was observed by LCMS in three of the cases, and not in sufficient quantity to warrant further investigation. So, this novel transformation was not successful, and the Heck and reduction sequence was continued to be used.

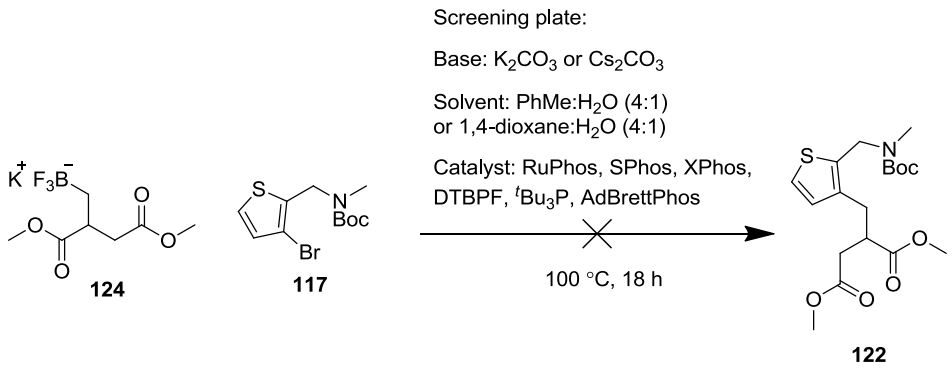

Scheme 43 *The unsuccessful screening of 24 reaction conditions for the Suzuki coupling of Molander salt **124** and bromide **117** to form **122***

After reduction, **122** underwent bromination using *N*-bromosuccinimide (NBS) **(Scheme 44)**. This reaction, whilst providing a moderate yield, suffered from overreaction, with bromination α to the nitrogen and subsequent imine hydrolysis yielding the corresponding aldehyde as a side product, although only traces were isolated for identification.

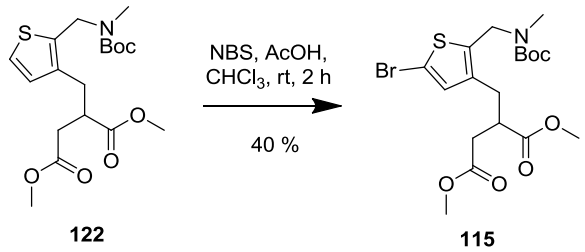

Scheme 44 *The bromination of* ***122***

With bromide **115** in hand, investigation of the key Ullmann coupling could take place. However, several attempts at coupling **115** and **67**, using **125** as a ligand, were unsuccessful in forming **126 (Scheme 45)**.

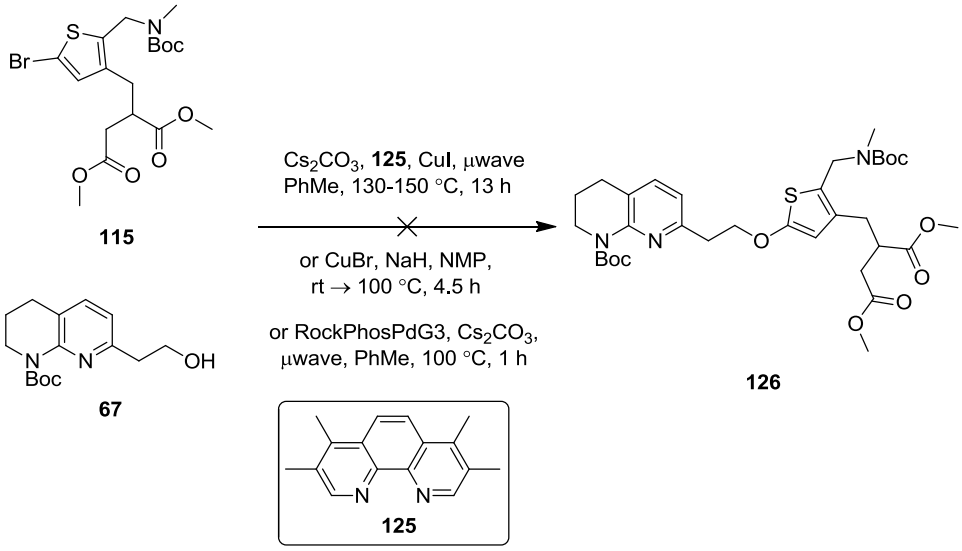

Scheme 45 *Several unsuccessful attempted etherifications of* ***67*** *and* ***115***

Traditional Ullmann conditions were unproductive, as were deprotonation of **67** with sodium hydride and subsequent heating with CuBr. Additionally, etherification with RockPhosPdG3 was attempted,[219] also without success. In the hope that a 2-iodothiophene would show enhanced reactivity in cross-coupling reactions compared to bromide **115**, iodide **127** was prepared using *N*-iodosuccinimide (NIS) instead **(Scheme 46)**. This approach also avoided unwanted over-reaction, as the less reactive NIS did not iodinate in the benzylic position, leading to superior yields.

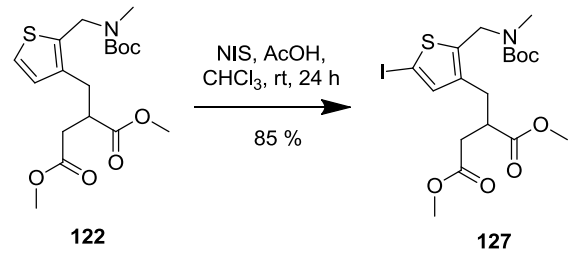

Scheme 46 Iodination of 122 using NIS

Ullmann coupling of **127** to alcohol **67** was attempted using the first conditions shown in **Scheme 45** without success, so the alcohol substrate was simplified, first to **128** then **129**, which was derived from **128 (Scheme 47)**. Neither of these substrates were competent coupling partners for **127**.

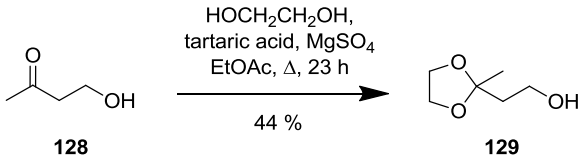

Scheme 47 Protection of 128 as an acetal. Neither substrate coupled to iodide 127 using Ullmann conditions

Borylation of the iodide was also attempted, in order to oxidise to the alcohol and attempt a Mitsunobu reaction to couple alcohol **67**, however the borylation (using ligand **130**) was not successful. Simpler Weinreb amide substrate **119** was chosen for two additional trial borylations, but neither afforded any product **(Scheme 48)**.

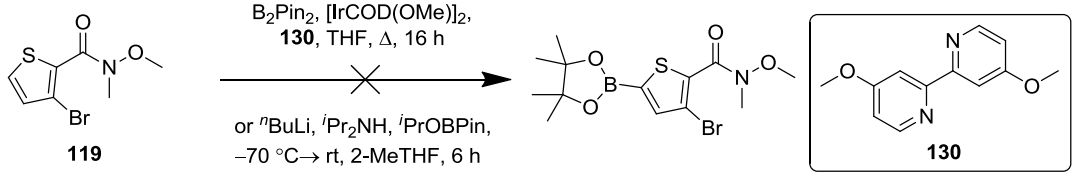

Scheme 48 Unsuccessful borylations of 119

Unable to couple the α_V binder to the thiophene, attention was turned instead to formation of the azepine ring. In the synthesis of **97**, a TFA-catalysed cyclisation furnished the desired 7-membered ring in good yield when refluxed in PhMe (**Scheme 31**, page 127). Therefore, these conditions were first attempted, following the TFA-mediated deprotection of **122 (Scheme 49)**.

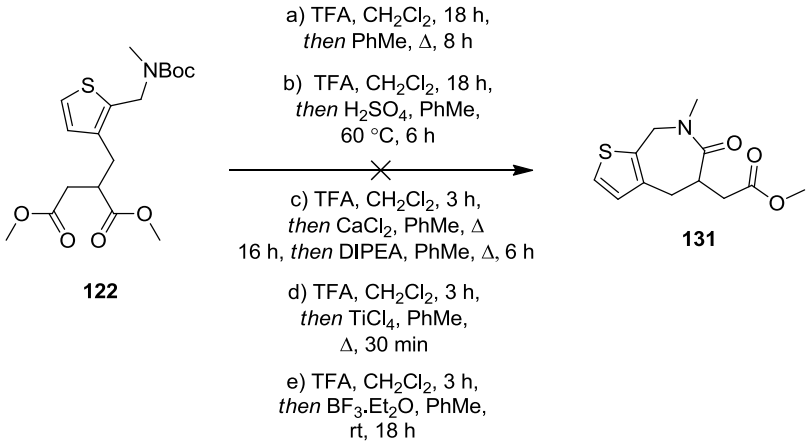

Scheme 49 Unsuccessful attempts at cyclising 122

Scheme 49 outlines a range of conditions under which the cyclisation was attempted, involving a range of acids and Lewis acids, and basic conditions. After the initial Boc deprotection, the CH_2Cl_2 was concentrated using a flow of nitrogen gas, so it is anticipated that some residual TFA remained at this stage, which is important in the subsequent reaction. According to the Cambridge Structural Database,[220] the S-C-C bond angle in an unsubstituted thiophene is 109 °, meaning the C-C-H_2 bond angle is likely to be approximately 125 ° **(Figure 85)**. The C-C-C bond angle is 114 °, meaning the C-C-H_3 bond angle is approximately 123 °.

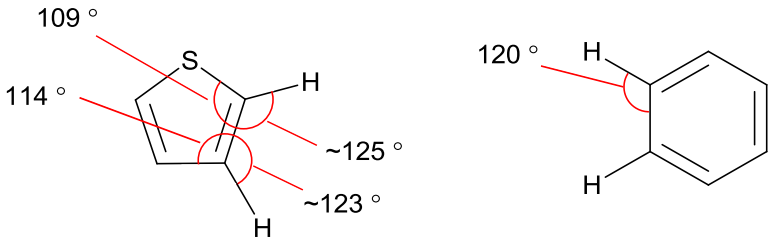

Figure 85 The bond angles of thiophene and benzene

These values are slightly larger than in benzene, meaning that in comparison to the cyclisation of **97**, it is anticipated that more strain energy must be overcome in forming the azepine. It was this rationale which led to the cyclisation being run in the microwave and at a higher temperature. Heating at 175 °C for 1 h was insufficient to

cause cyclisation, but 200 °C for 100 min was successful in inducing cyclisation to the azepine **(Scheme 50)**.

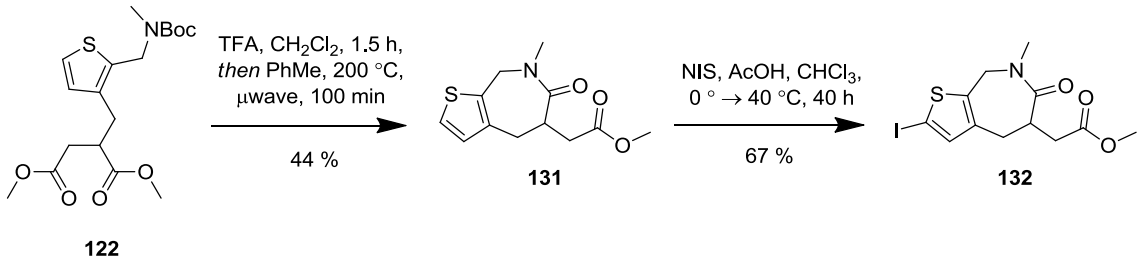

*Scheme 50 The cyclisation and iodination of **122** to give **132***

Initial reactions at this temperature led to a significant number of side reactions, but this was reduced when the solution was purged with nitrogen gas to remove oxygen from the solution prior to heating, leading to formation of the product in moderate yield. With **131** in hand, iodination was carried out to give **132**. Then, the Ullmann reaction could be retried with **132**. Unfortunately, this was still unsuccessful, even on simplified substrate **129**. Miyaura borylation of iodide **132** was also unsuccessful.[221]

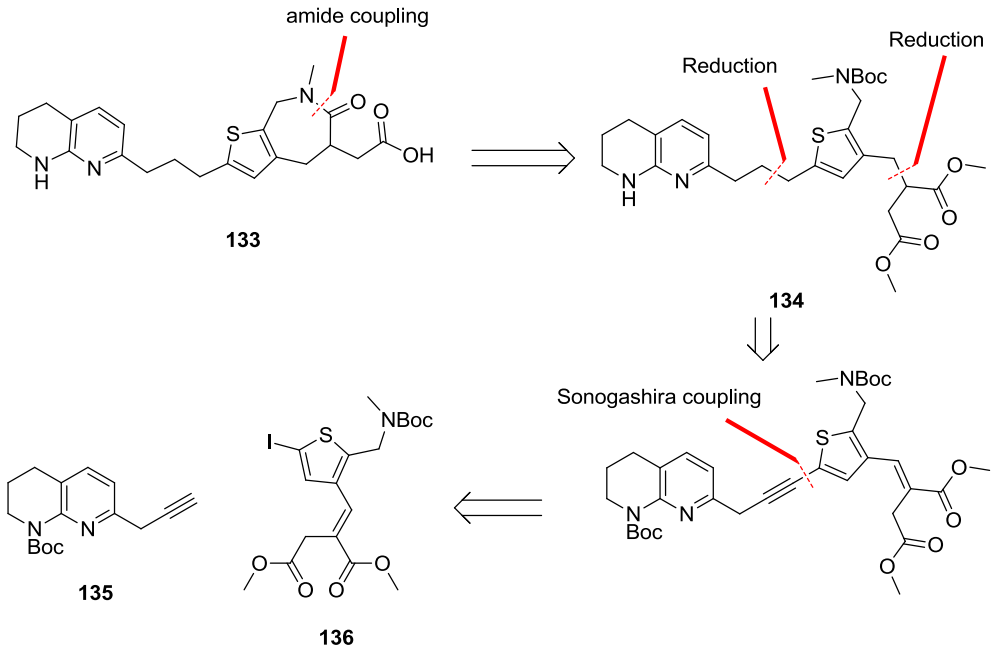

*Scheme 51 The retrosynthetic analysis of **133** to **135** and **136***

Unable to perform the required etherification for target **114**, attention was turned to carbon-linked analogue **133 (Scheme 51)**. This compound was also a high priority to synthesise, because it also enabled investigation of the linker atom. The retrosynthesis of this compound is outlined in **Scheme 51**.

Having established a method of azepine formation, and reduction of the stubborn tri-substituted double bond, it was envisaged that **133** could be disconnected back to **134**, which could arise from the Sonogashira reaction between alkyne **135** and iodide **136.**[222] Compound **136** was readily furnished in the usual manner **(Scheme 52)**.

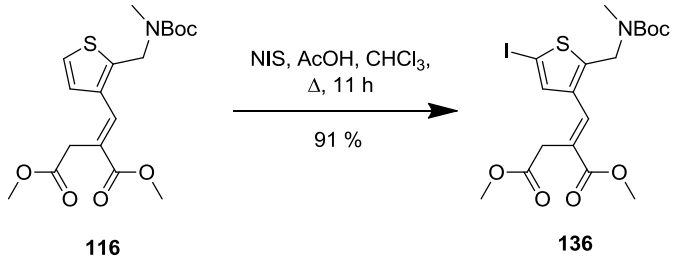

Scheme 52** The iodination of **116

The preparation of **135** was then investigated **(Scheme 53)**. Initially, a Seyferth-Gilbert homologation of aldehyde **137** was envisaged,[223,224] but various oxidation conditions were not successful on substrate **67**. These included DMP oxidation, manganese dioxide oxidation, and a bleach and (2,2,6,6-tetramethylpiperidin-1-yl)oxyl (TEMPO) oxidation. Alcohol **67** was already known to be difficult to oxidise, with previous work in our laboratories also proving unsuccessful.[207] This may be due to the formation of a six-membered ring as a result of a hydrogen bond between the hydroxyl group and the sp^2 nitrogen atom, affecting its properties in some way.

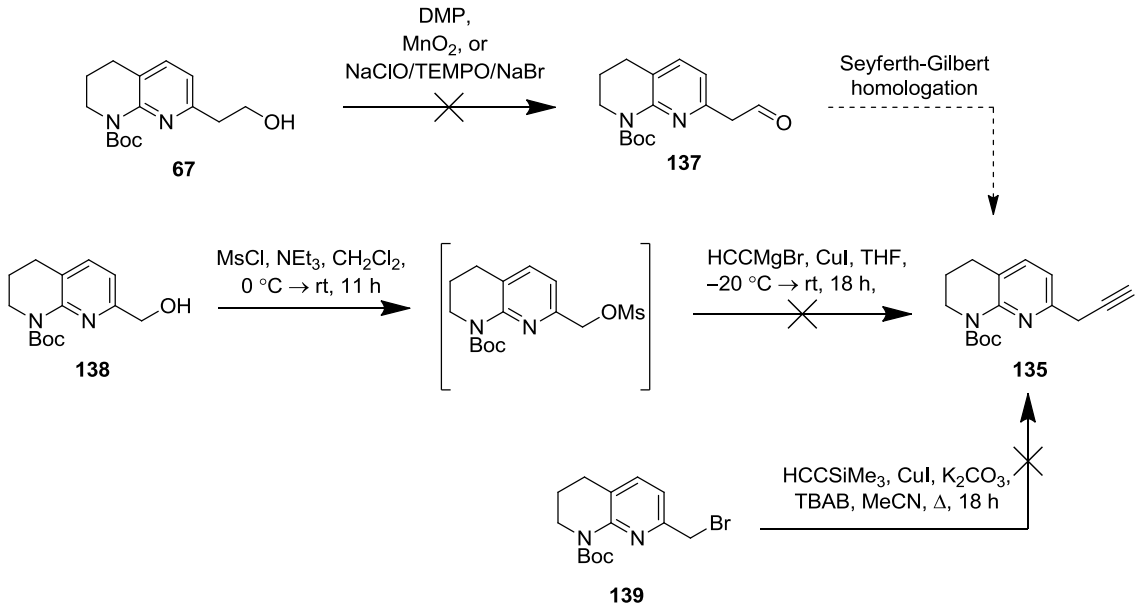

Scheme 53 *Attempts to synthesise **135**, hindered by inability to oxidise alcohol **67** and the failure of copper iodide mediated alkynylations*

As an alternative, alcohol **138** was mesylated successfully, but subsequent attempts to alkynylate using ethynyl Grignard and copper iodide were unsuccessful, only leading to bromide **139**. Bromide **139** was itself also unreactive in a similar procedure involving ethynyl trimethyl silane, copper iodide and tetrabutylammonium bromide (TBAB). In light of these findings, an alternative approach was considered **(Scheme 54)**.

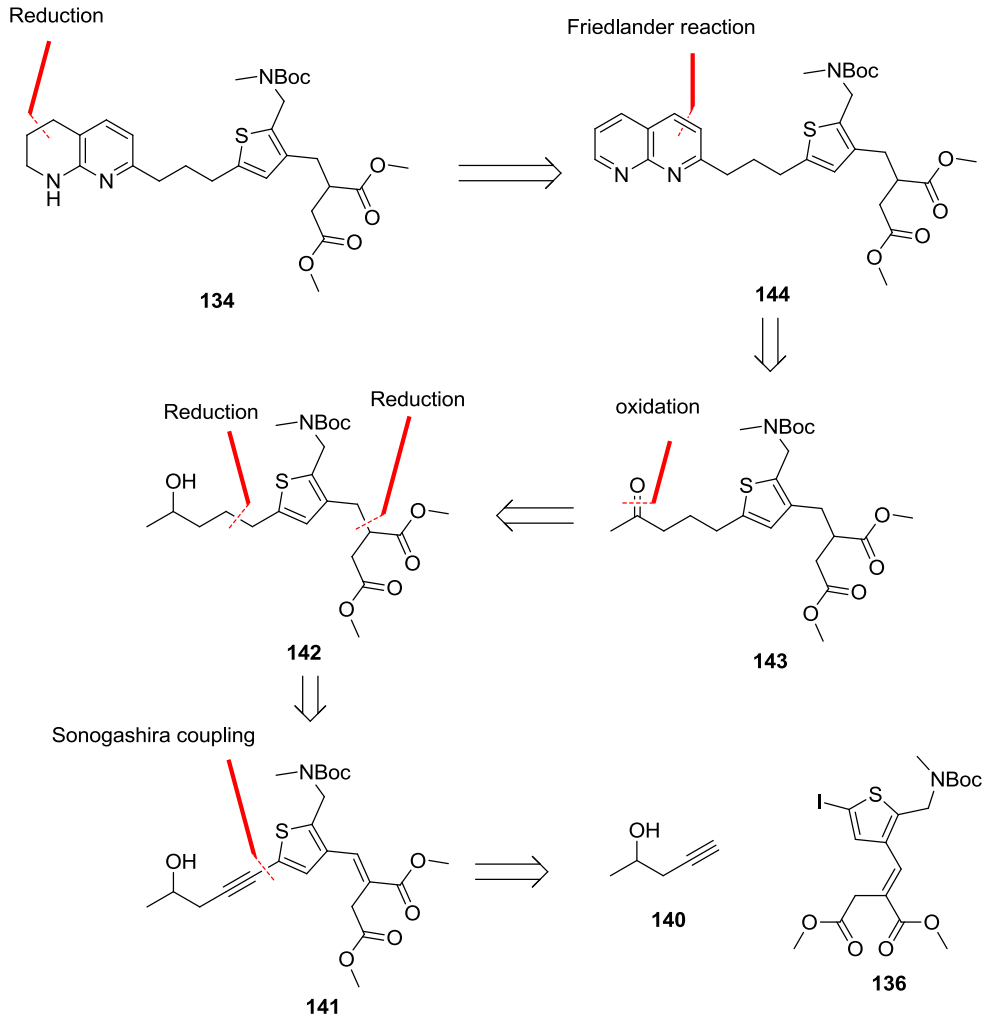

Scheme 54 *An alternative retrosynthesis of* ***134****, beginning with pentynol* ***140***

Beginning, in a forward sense, with the Sonogashira reaction of pentynol **140** and iodide **136** to give **141**, subsequent reduction to give **142** would avoid interference in the oxidation to **143** to follow. Formation of the tetrahydronaphthyridine group could then be carried out as usual to give **144**, which would then undergo selective reduction to give **134**. Indeed, this route proceeded as planned, first with Sonogashira coupling to yield **141** and subsequent reduction to **142 (Scheme 55)**.

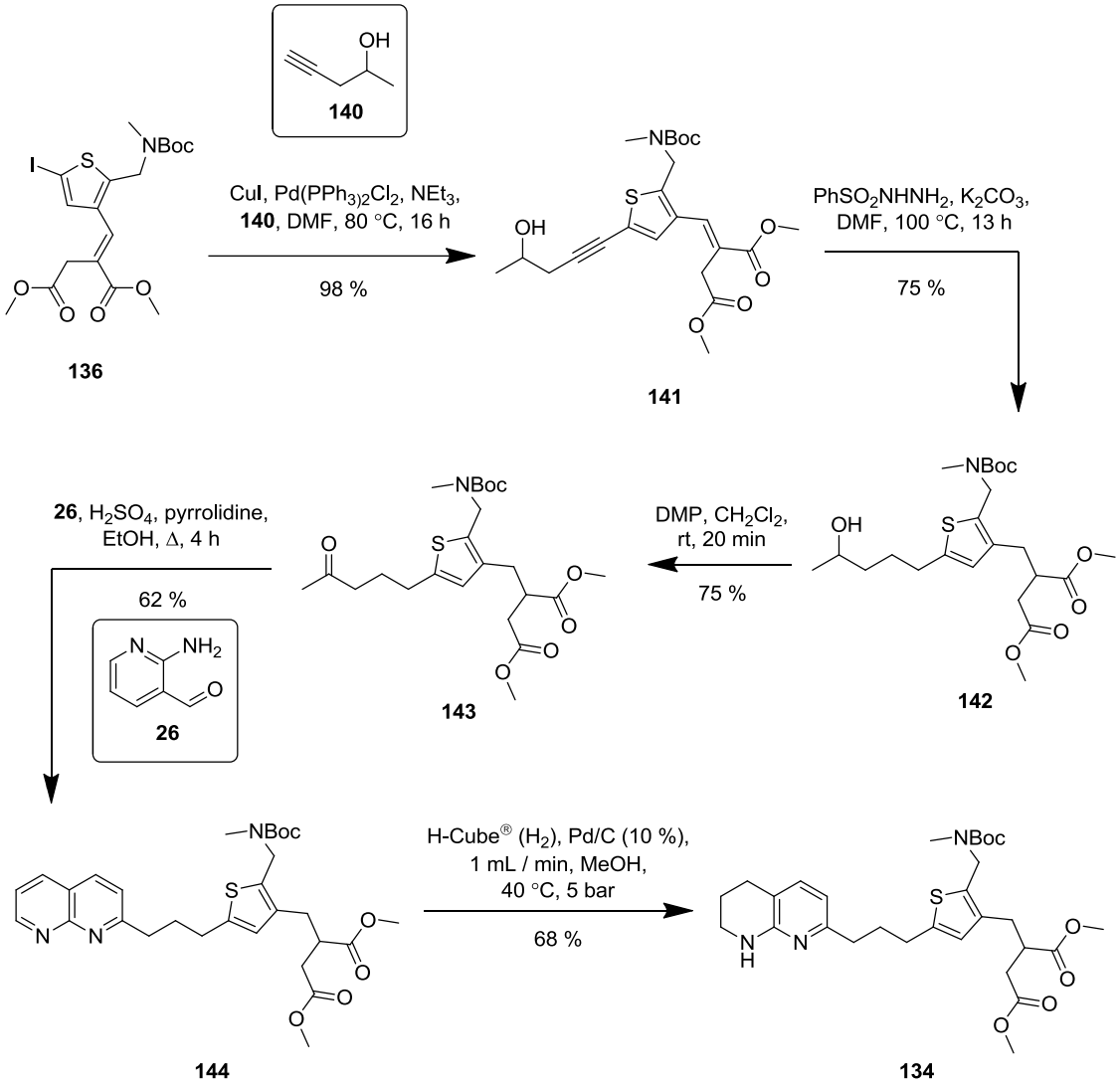

Scheme 55 *The forward synthesis of* ***134*** *from* ***136***

Unfortunately, this reduction remained as capricious as before, and only 80 % conversion to the product was obtained. The side-product had undergone alkyne reduction but not the reduction of the alkene moiety. This side-product was not separable and so **142** was an inseparable mixture in a 4:1 ratio with this side-product. This side-product persisted during the following reactions, although some was gradually removed in purification. After DMP oxidation followed by Friedländer reaction with **26**, ketone **143** then naphthyridine **144** were both afforded in a 13:1 ratio with the corresponding unsaturated side-product.

In spite of the presence of this impurity, these transformations proceeded as planned and furnished advanced intermediate **134** as a pure compound, with reduction of the naphthyridine group also converting the unwanted impurity to **134**. With **134** in hand, attention could be turned to the deprotection and azepine cyclisation **(Scheme 56)**. Having established that excluding oxygen from the reaction leads to a cleaner cyclisation at high temperature, nitrogen gas was bubbled through the solution in PhMe for 30 mins before sealing the reaction and heating it in the microwave. This successfully furnished **145**, which was then hydrolysed under basic conditions. Acidic conditions, unfortunately, led to the hydrolysis of the azepine amide to yield ring-opened product, but sodium hydroxide led to the desired product **133**.

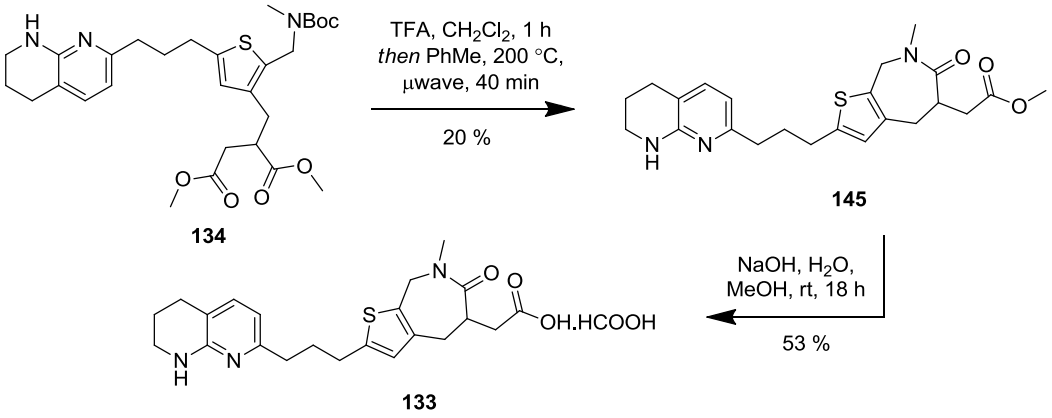

Scheme 56** The preparation of **133

With **133** in hand, this compound could be submitted for testing in the integrin cell adhesion assay. The results of these tests are summarised in **Table 25**.

	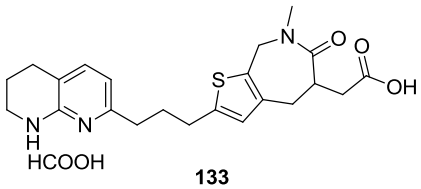 **133**
$\alpha_V\beta_1$ pIC_{50}	5.5 (n = 3)
$\alpha_V\beta_3$ pIC_{50}	7.3 (n = 3)
$\alpha_V\beta_5$ pIC_{50}	7.7 (n = 2)
$\alpha_V\beta_6$ pIC_{50}	5.8 (n = 3)
ChromlogD	2.04

Table 25 *The cell potency data for* ***133****, showing a lack of potency at* $\alpha_V\beta_1$

Unfortunately, the potency at $\alpha_V\beta_1$ was significantly reduced in comparison to **107** and **108**. This compound was then assessed in the homology model **(Figure 86)**, and it was found to not be at all well accommodated in the binding pocket, with the chain linking the two binding domains pulled into a highly strained conformation. This high energy conformation is thought to rationalise the low potency of this compound in the $\alpha_V\beta_1$ assay.

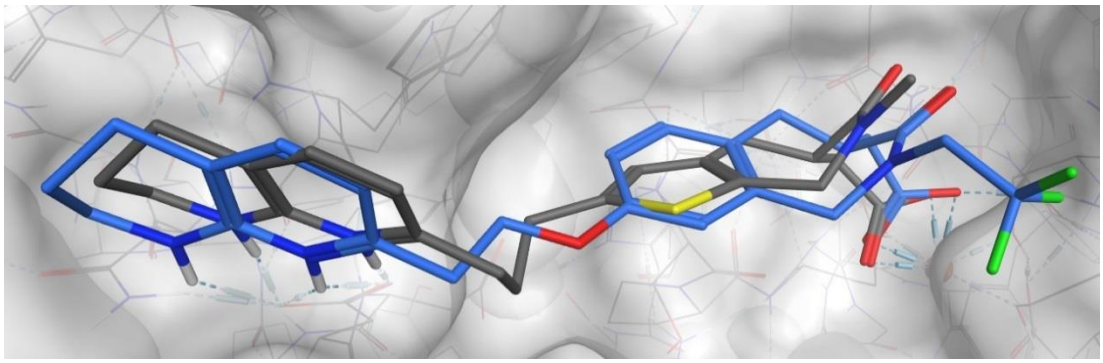

Figure 86 *The docked conformation of* ***133*** *(in grey), overlaid onto* ***107*** *in blue. The significantly different vector of the alkyl chain from the thiophene results in a very strained chain conformation which is thought to explain the lower potency in the assay*

Having found the potency of **133** to be significantly lower than **107**, work was commenced on regioisomeric thiophene **146 (Figure 87)**.

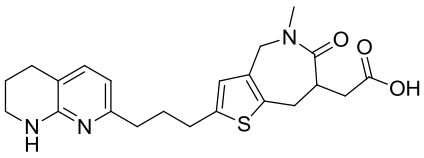

146

Figure 87 *Regioisomeric thiophene **146**, hoped to provide a better vector for the linker chain than **133***

Compound **146** was expected to provide a vector for the carbon chain linker that is more similar to the lead **107**, and therefore a more potent compound was envisaged. With regards the synthesis of **146**, having developed a route to **133,** it was anticipated that an analogous route could be used, as long as the electronic differences between the α and β positions of the thiophene intermediates do not preclude use of the same chemical transformations. Pleasingly, this was found not to be the case; **Scheme 57** displays the route to intermediate **147**.

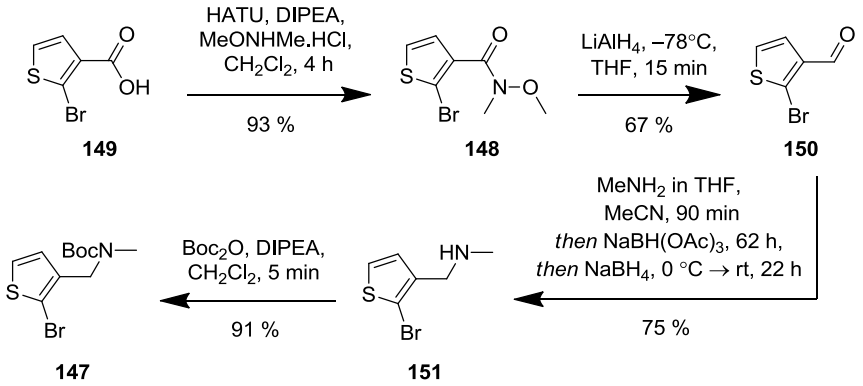

Scheme 57 *The preparation of **147** from commercially available starting material **149***

Weinreb amide **148** was prepared from commercially available acid **149**, followed by reduction to afford aldehyde **150**. Reductive amination to give **151**, followed by Boc protection furnished **147** for investigation of the Heck reaction. The Heck reaction of **147** with **102**, using the same procedure as for the 3-bromo regioisomer **117,** gave only a 4 % yield, but the Heck reaction of *tert*-butyl acrylate and aldehyde **150** has been reported using tetrabutylammonium bromide (TBAB) and an inorganic base, termed the 'Jeffery conditions'.[225,226] Therefore, these conditions were used in the cross coupling of **147** and **102**, which proceeded in an improved, albeit still moderate, yield **(Scheme 58)**. After Heck coupling, **152** was iodinated to give **153** as a single

geometric isomer, which was assumed to be the *E*-isomer by analogy with **116** and in the synthesis of **97** (where only one regioisomer was observed), although this could not be confirmed by nOe in this case.

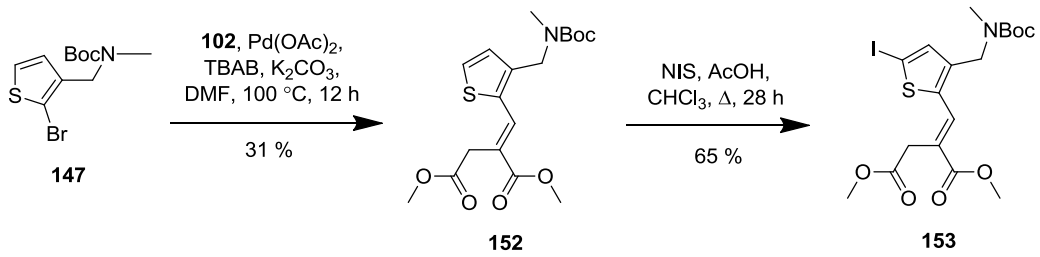

Scheme 58 *The Heck reaction of **147** and **102**, using alternative, ligand-free conditions. This was followed by iodination using the normal procedure*

Subsequent elaboration of **153** went smoothly **(Scheme 59)**, beginning with Sonogashira coupling of **153** and **140** to give **154.** However**,** material throughput was still greatly hindered by the inadequate reduction of **154** to **155**, requiring a great excess of benzenesulfonyl hydrazide and potassium carbonate. Nonetheless, alcohol **155** was obtained in adequate quantity for oxidation to **156**, followed by Friedländer naphthyridine synthesis to give **157** which was reduced to give **158**.

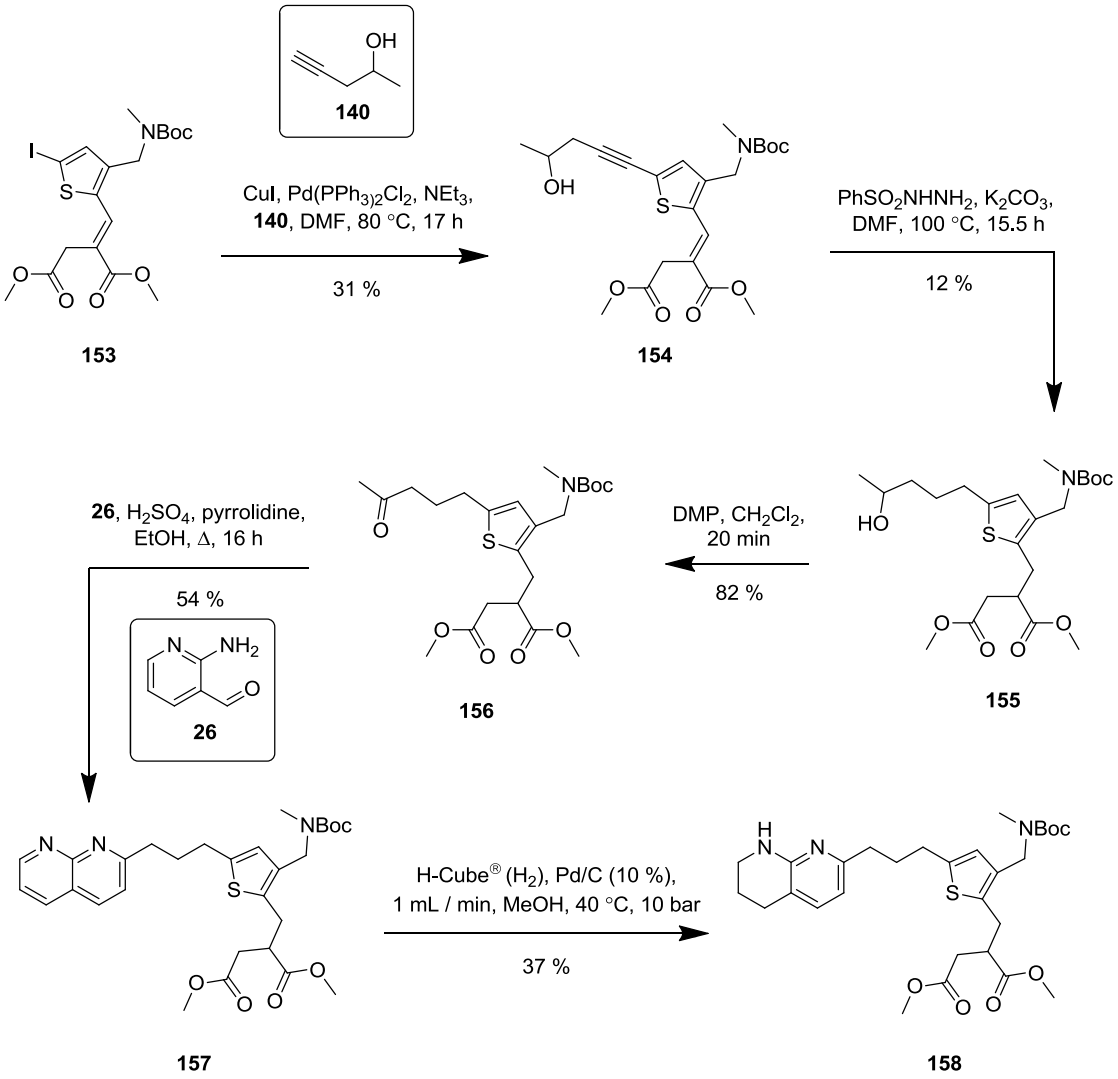

Scheme 59 *The route to tetrahydronaphthyridine **158** from iodide **153**, with the reduction of **154** to **155** proving a hindrance*

The deprotection and cyclisation of **158** to form the azepine **159** was carried out in the same manner as previously **(Scheme 60)**. After hydrolysis, **159** gave compound **146**. Several steps in this route took place in disappointing yield, but sufficient material was obtained for the compound to be tested, the results of which are shown in **Table 26**, compared with the regioisomer **133**.

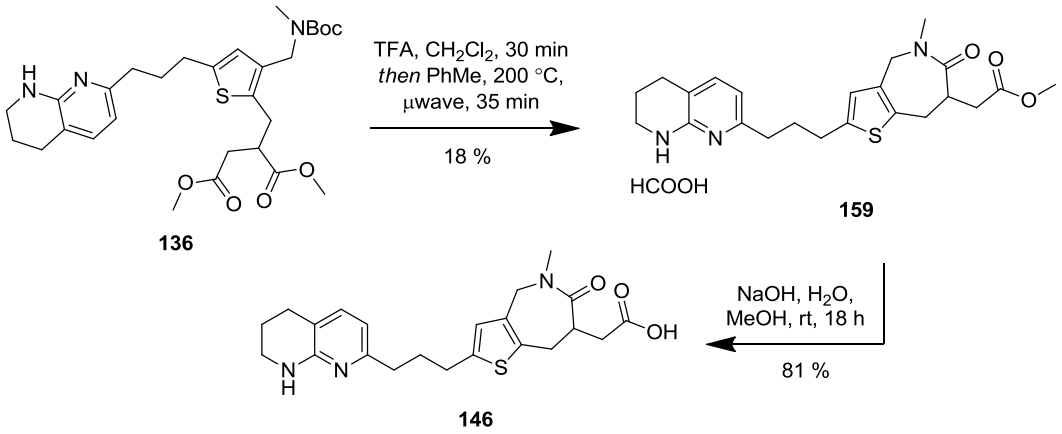

Scheme 60 *The preparation of* ***146*** *by azepine cyclisation and then ester hydrolysis*

The potency of **146** shows a log improvement in potency over **133**, but still a much lower potency than the lead compound in the series. When assessed in the homology model **(Figure 88)**, **146** does not appear to take a very low energy conformation in the binding site, though the conformation of the chain is improved in comparison to **133**, as had been expected. This helps to explain the improved, though still inadequate, potency of **146**.

	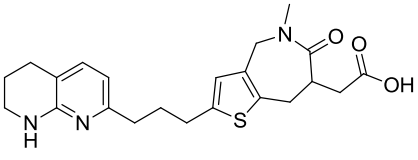 **146**	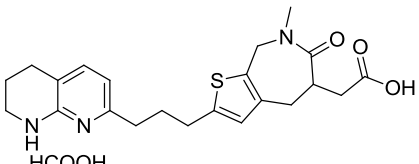 **133**
$\alpha_V\beta_1$ pIC_{50}	6.5 (n = 4)	5.5 (n = 3)
$\alpha_V\beta_3$ pIC_{50}	8.0 (n = 3)	7.3 (n = 3)
$\alpha_V\beta_5$ pIC_{50}	8.3 (n = 3)	7.7 (n = 2)
$\alpha_V\beta_6$ pIC_{50}	< 6 (n = 1)	5.8 (n = 3)
ChromlogD	2.00	2.04

Table 26 *The measured cell adhesion assay potency data for* ***146*** *compared with regioisomer* ***133***

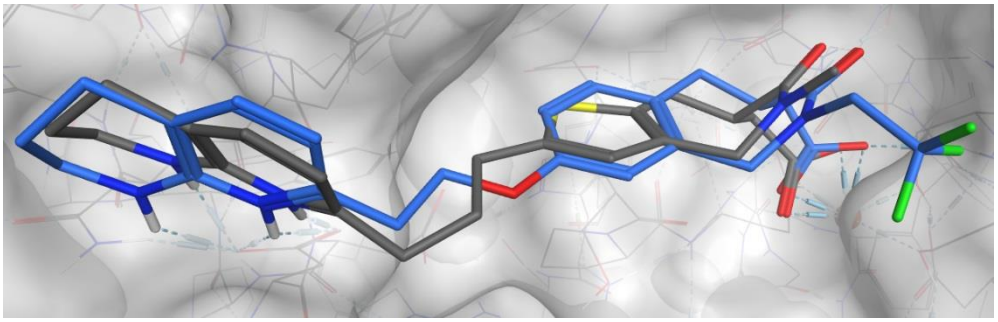

Figure 88 *The docked conformation of* ***146*** *in grey, overlaid with the lead* ***107****. This compound does not appear to be a very good fit, though the alkyl chain arrangement for this thiophene regioisomer is superior to* ***133****, potentially explaining the greater potency of* ***146.*** *The azepine of* ***146*** *is twisted downwards, similarly to N-methyl benzazepine* ***108****.*

At the time of synthesis of these compounds, the homology model had not been available for use predictively, so it was thought that the change in vector with the thiophene compounds might require a longer linker. Therefore, the analogue of **146** with a four carbon alkyl chain linking the two binders **(160, Figure 89)** was synthesised to investigate this.

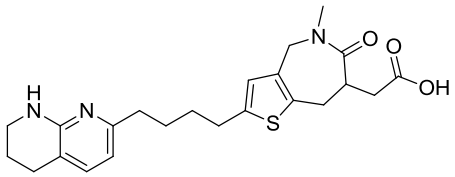

160

Figure 89 *Analogue* ***160****, with four carbon atoms in the chain*

Unlike for the three-carbon analogues, it was envisaged that this analogue could be prepared *via* a more convergent synthesis, disconnecting the molecule to **161**, then **162**, then back to alkyne **163** and iodothiophene **164 (Scheme 61)**. It was hoped that, in comparison to the 3 carbon alkyne **135,** which could not be prepared, the extra carbon atom between the alkyne and aromatic ring might improve the chemistry involved in the preparation of **163**.

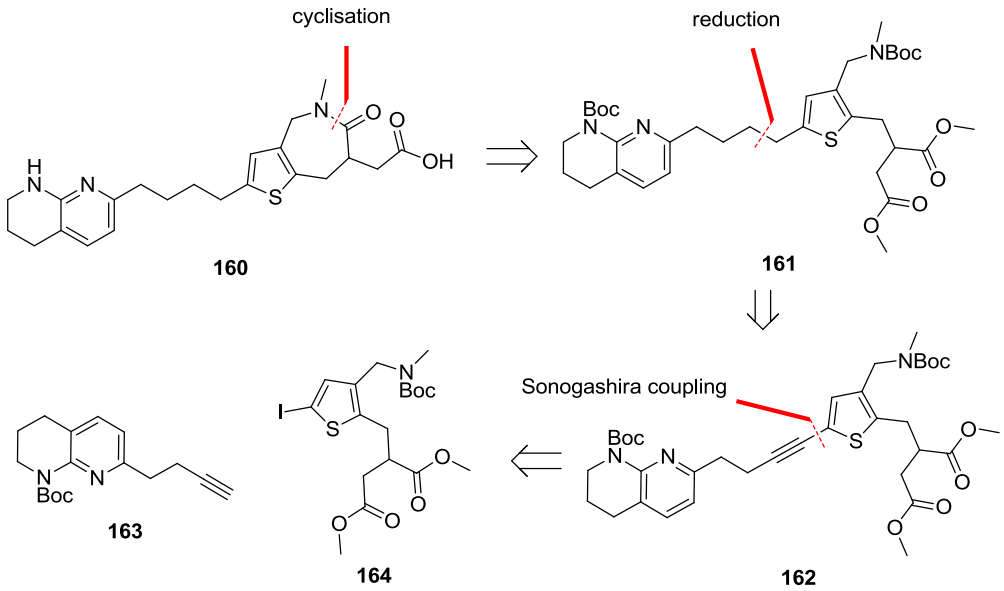

*Scheme 61 The retrosynthesis envisaged for **160**, back to **163** and **164***

Sonogashira reaction of **163** and iodide **164** would furnish **162**, which could then be reduced to **161** and cyclised and deprotected to form **160**. Pleasingly, the synthesis of alkyne **163** proceeded as planned **(Scheme 62)**.

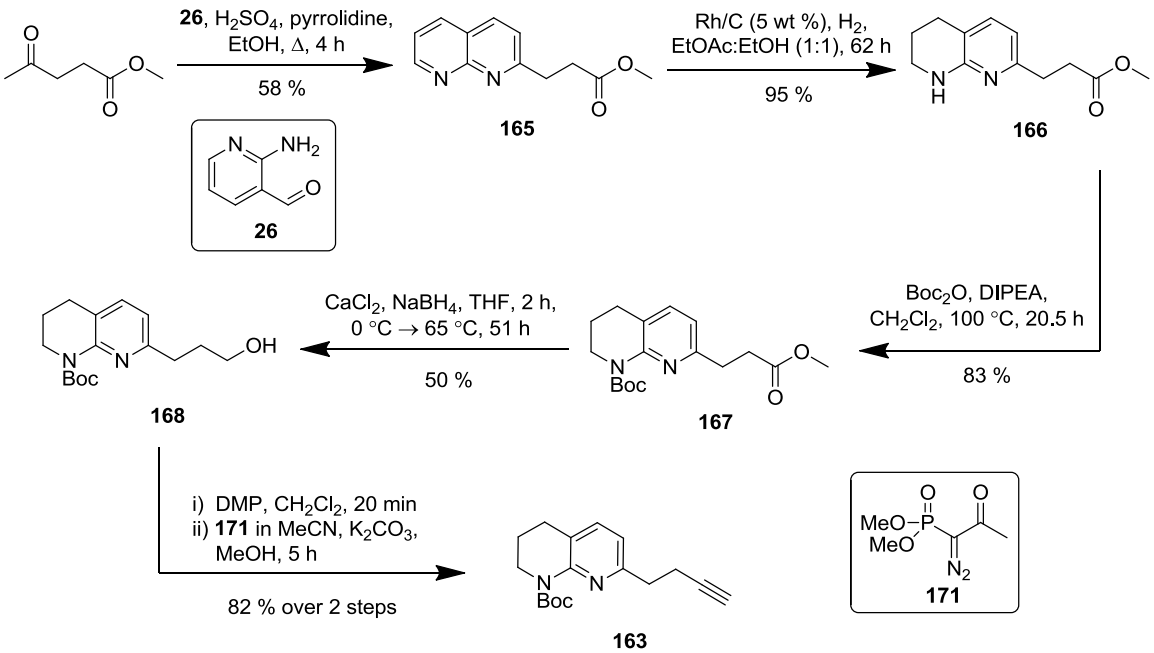

*Scheme 62 The preparation of **163***

The familiar sequence of Friedländer reaction (affording **165**), followed by reduction to **166** then protection led to **167**, followed by reduction with calcium borohydride to give alcohol **168**.

The aldehyde **169** resulting from DMP oxidation of alcohol **168** was stable to the work up conditions, but did not elute when it was purified by column chromatography. It is suspected that an acid-catalysed cyclisation of the product is able to take place on the acidic silica, leading to a highly polar, charged compound **170 (Scheme 63)**. Although this has not been isolated, similar behaviour has been reported by others with similar substrates.[122]

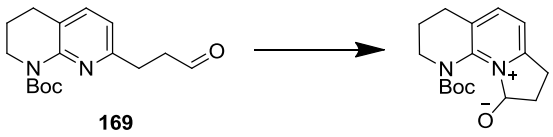

Scheme 63 *The suspected cyclisation of aldehyde **169** upon purification on silica to form ionic compound **170**, which was not isolated*

In order to overcome this, the aldehyde **169** was reacted directly after aqueous work up, without further purification. The Seyferth-Gilbert homologation reaction, using the Bestmann-Ohira reagent **171**, still proceeded smoothly to yield **163** in very good yield.[227] In order to provide coupling partner **164** for alkyne **163**, the challenging reduction of **152**, a common intermediate from the synthesis of **146**, to **172** was still required **(Scheme 64)**.

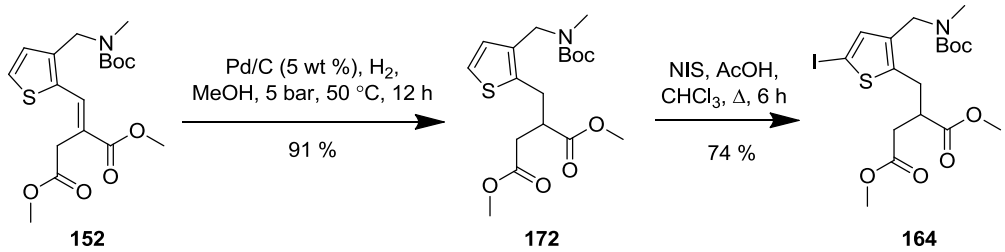

Scheme 64 *The successful reduction of **152** to **172**, followed by iodination to form **164***

Fortunately, at this time a range of equipment for high pressure batch hydrogenation reactions became available for use, and so the reduction could be performed at

elevated reaction temperatures and pressures. This provided a means of reducing the stubborn double bond of **152** in much higher yield and a much more facile manner, allowing for the access of **172**. Compound **172** was subsequently iodinated to give **164**.

With both fragments in hand, union of **163** and **164** could be performed *via* a Sonogashira reaction, affording **162** in a moderate yield, as an inseparable mixture with an unidentified impurity, in a 5:1 ratio by NMR **(Scheme 65)**. After reduction using the H-Cube® to give **161**, this impurity was removed. Upon cyclisation of **161** in a microwave reactor, some hydrolysis to give **160** was observed, so the material was hydrolysed completely to give product **160** under basic conditions in a moderate yield over the two steps, without isolation of the intermediate ester.

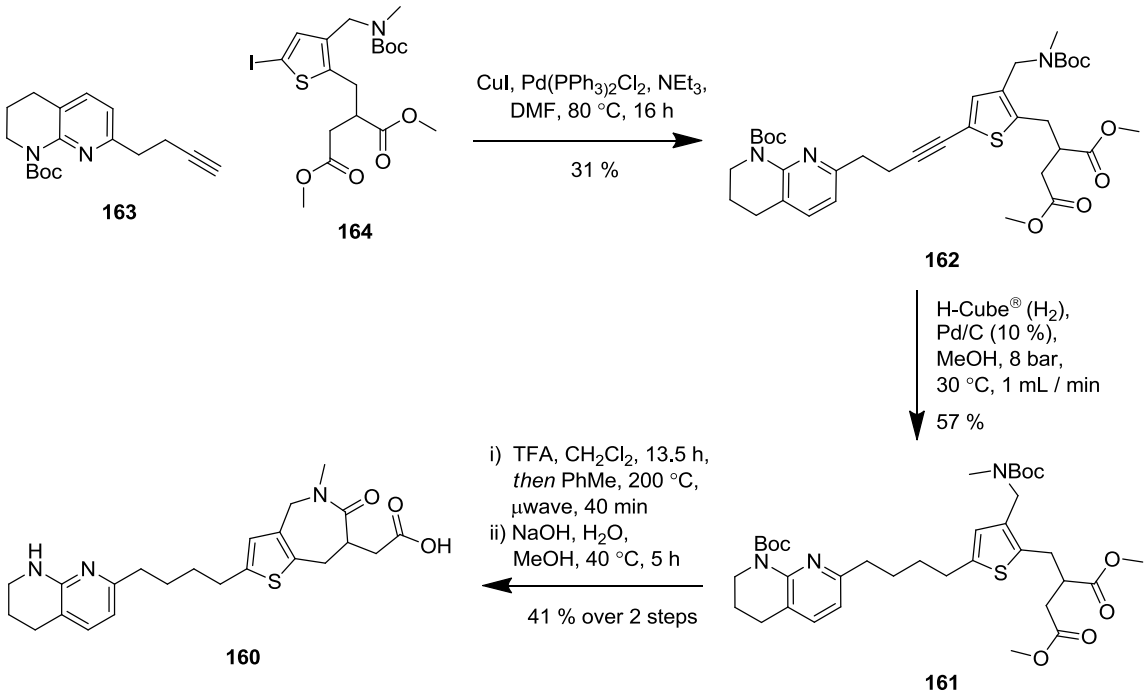

Scheme 65 *The Sonogashira reaction of **163** and **164**, followed by elaboration to final compound **160***

Compound **160** was then tested in the integrin cell assays **(Table 27)**, and the $\alpha_V\beta_1$ potency was lower than for the analogue with three carbon atoms in the linker chain.

Indeed, the cell potency was lower for all integrins measured, indicating that the molecule is simply too long for the receptor.

	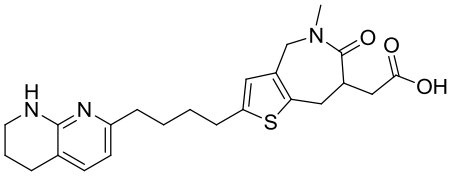 **160**	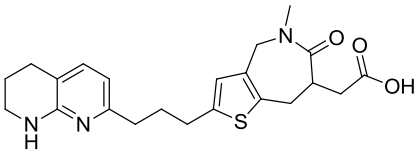 **146**
$\alpha_V\beta_1$ pIC_{50}	6.0 (n = 2)	6.5 (n = 4)
$\alpha_V\beta_3$ pIC_{50}	7.8 (n = 2)	8.0 (n = 3)
$\alpha_V\beta_5$ pIC_{50}	7.5 (n = 4)	8.3 (n = 3)
$\alpha_V\beta_6$ pIC_{50}	< 6.0 (n = 2)	< 6 (n = 1)
ChromlogD	2.46	2.00

Table 27 *The assay data for* ***160,*** *compared with three carbon analogue* ***146***

With access to the homology model, the reason for the reduced potency of **160** is clearly as a result of the elongated nature of the compound **(Figure 90)**. In order to bind to the aspartate and magnesium residues, the linker chain must coil in an unfavourable fashion, and the azepine is forced in closer to the surface of the protein.

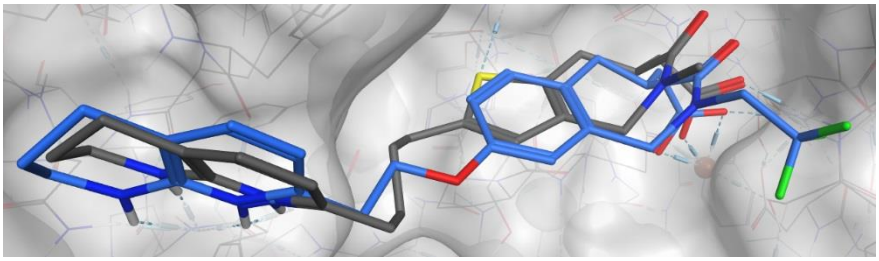

Figure 90 *The docked conformation of* ***160****, overlaid with the docking of* ***107****. The four-carbon chain is too long to be accommodated in the binding side*

Since the receptor in the homology model is rigid, but in reality, the protein is flexible, it is possible that the receptor can flex to partially accommodate this additional size. This may explain why the compound still possesses moderate potency.

Having established that the carbon-linked thiophene analogues would not provide adequate potency at the desired integrin, it became essential to delineate whether the reduction in potency was a result of the vector provided by the five-membered heterocycle in the core, or as a result of the carbon linker in the chain. Therefore, work was recommenced on an oxygen-linked thiophene analogue **173**, with an all carbon analogue **174** also becoming a priority target **(Figure 91)**.

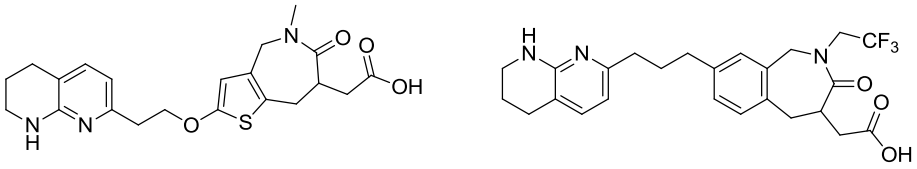

***Figure 91** Targets **173** and **174**, designed to test the requirement of the six membered ring in the core and the oxygen atom in the linker*

Having observed that the carbon-linked thiophene regioisomer with a vector for the linker most similar to lead compound **107** was preferred, this oxygen-linked thiophene regioisomer was now the target rather than the previously sought molecule **114**. Since **173** is a regioisomer of the original target **114**, it was hoped that a similar approach could be taken, although **114** had not been successfully accessed, so further development would be required. All-carbon analogue **174** had originally been a target of interest during the original work on this series, but had not proven synthetically accessible. However, having developed a synthesis of compounds **133** and **146** with a three carbon linker, it was envisaged that a similar route could be used in the synthesis of **174**.

With iodide **164** already accessed, and previously commercially available alcohol **67** in hand, the most practical approach to synthesising **173** would be the etherification of these fragments to give **175 (Scheme 66)**.

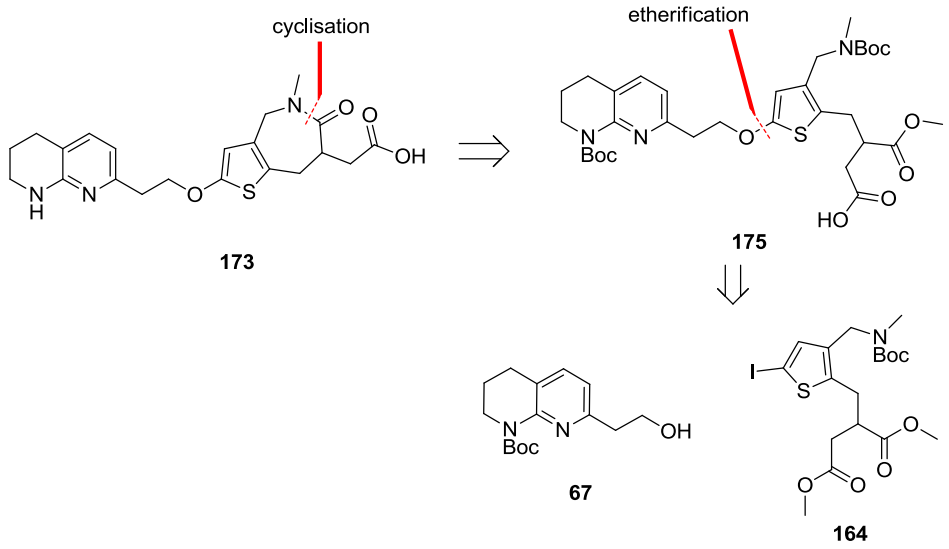

Scheme 66 *The proposed retrosynthesis of* ***173****, relying on the challenging etherification of* ***67*** *and* ***164***

With Ullmann chemistry proving unproductive when attempting to synthesise **114**, attention was turned back to using Buchwald's palladium-catalysed etherification approach.[228] Unfortunately, even when alcohol **67** was used as a co-solvent in the reaction, with 20 equivalents present, the coupling of **67** and **164** was not observed **(Scheme 67)**.

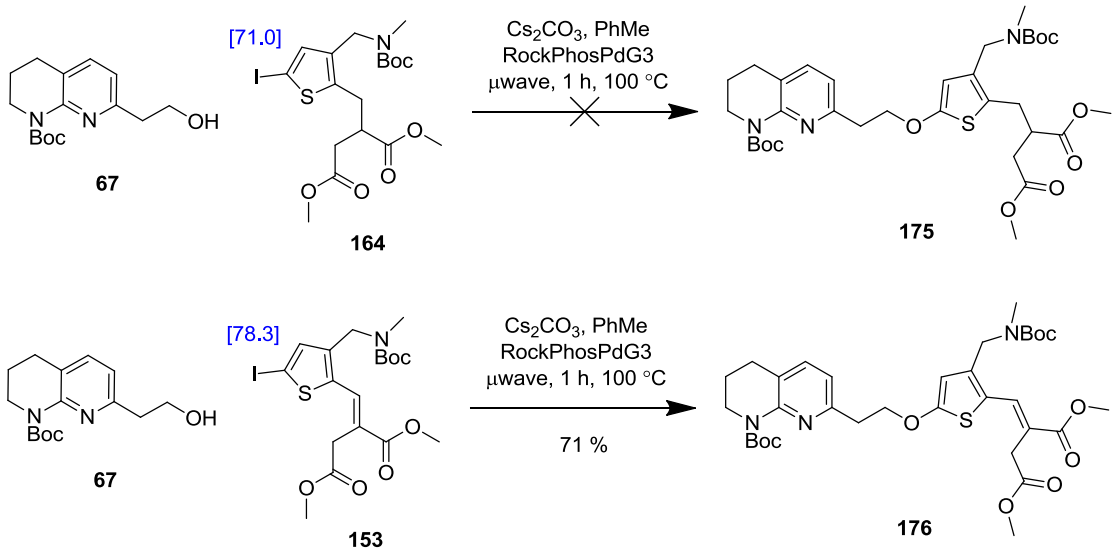

Scheme 67 *The etherification reactions of* ***164*** *and* ***153*** *with alcohol* ***67****, which was successful in the case of alkene* ***153****. The values shown in blue, in square brackets, are the* ^{13}C *NMR shifts of the carbon atom bonded to the iodine atom in each compound.*

However, it was postulated that the unsaturated form of **164**, namely previously prepared intermediate **153**, might be more reactive, as the electron-withdrawing ester is bought into conjugation with the aryl ring in **153**, resulting in a less electron-rich ring which might undergo oxidative addition more readily. The difference in electron density on the carbon of the carbon-iodine bond of **153** and **164** is indicated by the increased ^{13}C NMR shift of the atom, which is higher, therefore less electron-rich, for alkene **153 (Scheme 67)**. It is noteworthy that both ^{13}C NMR shifts are significantly lower than for iodobenzene, which has a reported ^{13}C NMR shift of 94.4.[229] This indicates how electron-rich this position of the thiophene ring is, and hence why addition into the carbon-iodine bond is a challenge. Pleasingly, iodide **153** was indeed found to be a competent coupling partner in this reaction, yielding **176** in good yield.

Having completed the challenging etherification step, **176** could be elaborated to the final compound. The reduction of **176** proceeded at 5 bar in 10 h, but the reaction did not go to completion, so required filtration to remove the catalyst, followed by the addition of fresh catalyst and re-subjection to the reaction conditions, upon which full reduction occurred. This is indicative of catalyst poisoning, which may have also hindered the reduction of previous similar substrates. These reaction conditions

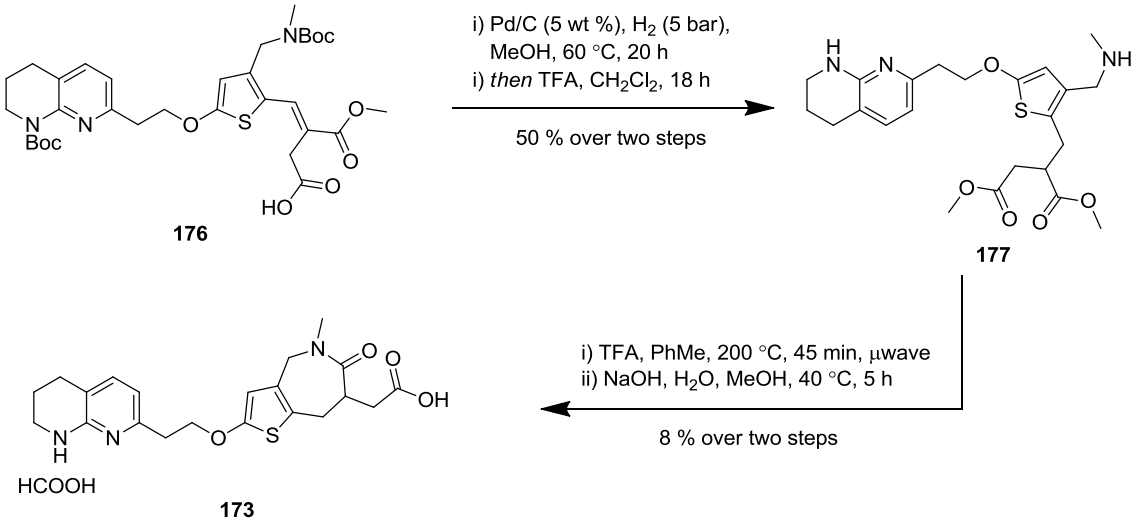

Scheme 68 *The completion of the synthesis of* ***173***

led to partial removal of the Boc group, so the rest of the Boc group was cleaved with TFA to give **177 (Scheme 68)**.

Compound **177** was then subjected to the cyclisation conditions, which was very low yielding. This was thought to be a result of the elimination of 2-vinyl tetrahydronaphthyridine which was observed by LCMS of the reaction mixture. It was also found that the product was destroyed if left exposed to the reaction conditions for too long. Because of these stability concerns, the product of the cyclisation was hydrolysed under basic conditions immediately after purification, to yield **173** as a formic acid salt (as a result of purification using a formic acid modified aqueous phase). The potency of **173** was then measured **(Table 28)**.

	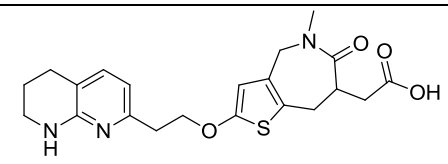 HCOOH **173**	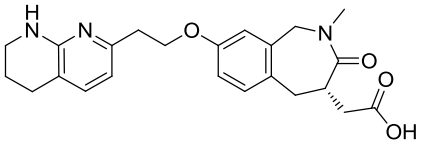 **108**
$\alpha_V\beta_1$ pIC_{50}	6.4 – 7.9* (n = 3)	8.2 (n = 6)
$\alpha_V\beta_3$ pIC_{50}	8.1 (n = 4)	8.8 (n = 4)
$\alpha_V\beta_5$ pIC_{50}	8.3 (n = 2)	8.4 (n = 1)
$\alpha_V\beta_6$ pIC_{50}	6.4 (n = 3)	5.4 (n = 4)
ChromlogD	1.97	1.89

Table 28 *The measured cell adhesion assay data for **173**, compared to **108**. *A range is given for this data point, since the first test occasion gave a potency value of 7.9, but the two later test occasions gave much lower potency. It is not possibly to verify, but it is postulated that this could be due to compound instability.*

Table 28 shows a comparison with **108**, which shows similar potency across the measured integrins, and a similar lipophilicity. Pleasingly, the $\alpha_V\beta_1$ cell potency of **173** was found to be equipotent with the lead compounds **107** and **108** on the first test occasion ($\alpha_V\beta_1$ pIC_{50} = 7.9), when considering that it was tested as a racemate. When the sample was retested six months later, the two subsequent potency values were over 1 log unit lower in potency. These samples were the last of the material synthesised, so it was not possible to check the purity of the material tested. Given

the aforementioned stability concerns with this compound, it is thought likely that the reduction in potency is due to instability of the compound when stored in DMSO, though this has not been possible to verify.

When docked into the homology model **(Figure 92)**, **173** was found to sit more favourably than the carbon linked thiophene analogues, with a low energy conformation of the chain.

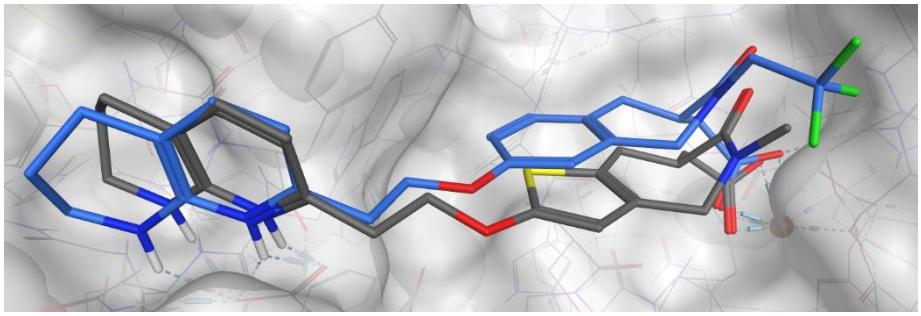

Figure 92 *The docked conformation of **173** in grey, overlaid with the docking of **107** (in blue). **173** shows a low energy conformation of the chain, but twisting of the azepine in comparison to **107***

The β_1-binding domain was found to dock differently to **107**, but when compared with **108** in the docking model, the two compounds appear to bind more similarly **(Figure 93)**. This result, and those previous compounds whose potency has been successfully rationalised using the model, provide further validation to the use of the homology model in guiding the project.

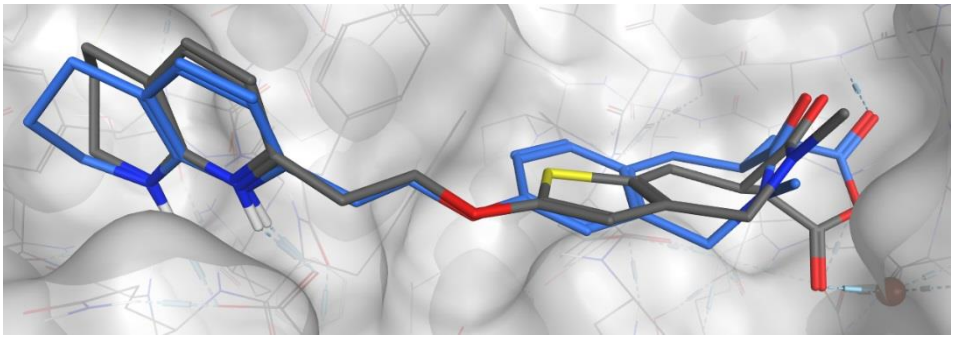

Figure 93 *The docked conformation of **173** in grey, overlaid with the docking of **108** (in blue). The azepine position is similar for these two compounds.*

It is noticeable that the vectors on the unsubstituted aryl and methylene positions of the thiophene-azepine of **173** differ from those corresponding positions in **108**. This is promising, because future substitutions in this position would probe the surrounding space differently for the two compounds, which has the potential to make selectivity over other integrins more achievable. This result implies that the linker atom is responsible for the compound finding a low energy, *trans*-conformation of the linker chain in the binding site.

3.4.2 The preparation and analysis of 174 and 190

In spite of this success, direct comparison of **107** with the all carbon chain analogue **174** was still desired in order to fully elucidate the effect of a carbon linker with a six-membered aromatic group in the core. The trifluoroethyl-substituted amide was chosen, so that it could be directly compared to the lead compound **107**.

Therefore, the synthesis of **174** was planned **(Scheme 69)**. During the previous work in our laboratories, it had not been possible to synthesise this compound, but in light of the development of a route to the carbon-linked thiophene compounds **133** and **146**, it was envisaged that the same approach could be taken in this case. Retrosynthetically, **174** could lead to **178**, which itself could arise from **179** *via* the familiar Friedländer and reduction sequence. Oxidation of alcohol **180** was envisaged to lead to **179**.

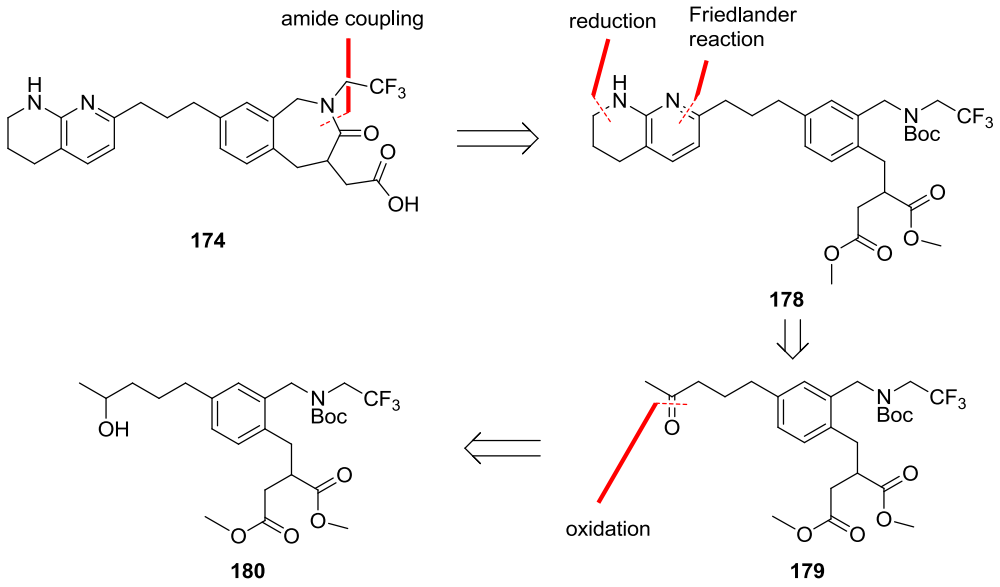

*Scheme 69 The proposed disconnections of **174** to alcohol **180***

It was believed that this route could begin with commercially available acid **181 (Scheme 70)**. Reduction to aldehyde **182** could precede reductive amination and protection to give **183**. It was envisaged that amine **183** could then undergo a chemoselective Sonogashira reaction, followed by a Heck reaction, to give **184**. Reduction of the alkene and alkyne could then be achieved simultaneously to give **180**. Therefore, the route to **174** was begun, starting with **181 (Scheme 71)**.

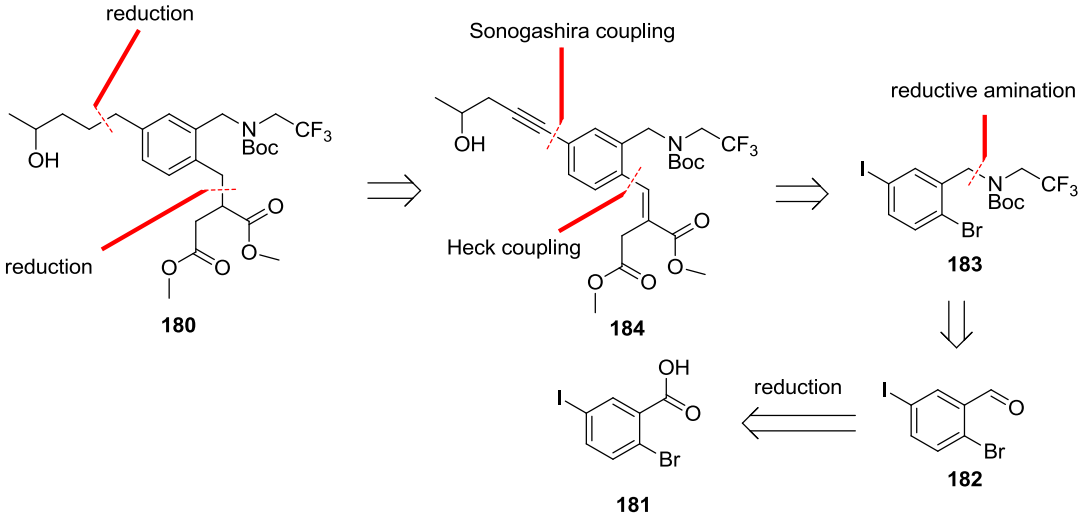

*Scheme 70 The proposed disconnections of **180** to commercially available **181***

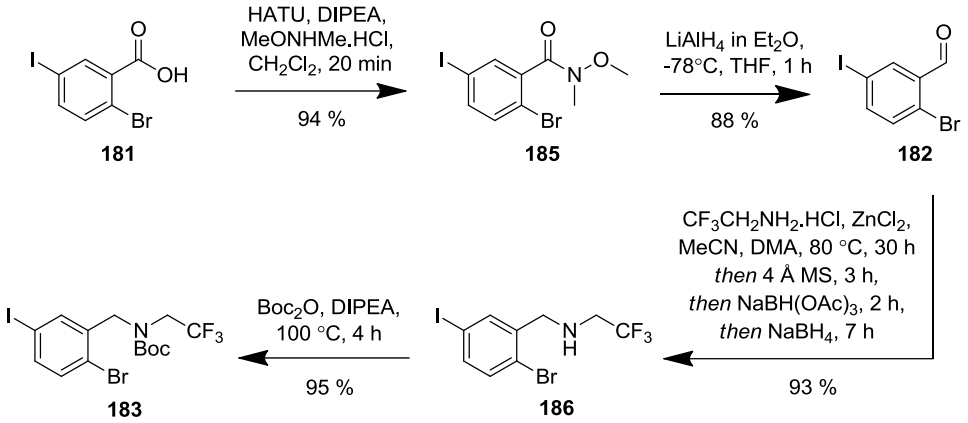

Scheme 71 *The preparation of **182** via Weinreb amide **185**, followed by reductive amination and protection to give **183***

In the same manner as for the thiophene compounds, reduction of the acid to the aldehyde was completed *via* amide coupling to form Weinreb amide **185**, followed by reduction to **182** with $LiAlH_4$. Zinc chloride and *N,N*-dimethylacetamide (DMA) were added to aid the iminium formation step of the reductive amination for the electron-poor amine $CF_3CH_2NH_2$, in the same way as they had been in the synthesis of **98 (Scheme 100, Appendix A)**, but only when activated molecular sieves (MS) were added was the iminium formation completed. After reduction of the iminium to give **186**, Boc protection straightforwardly furnished **183**. With **183** in hand, the key Sonogashira and Heck sequence could be investigated.

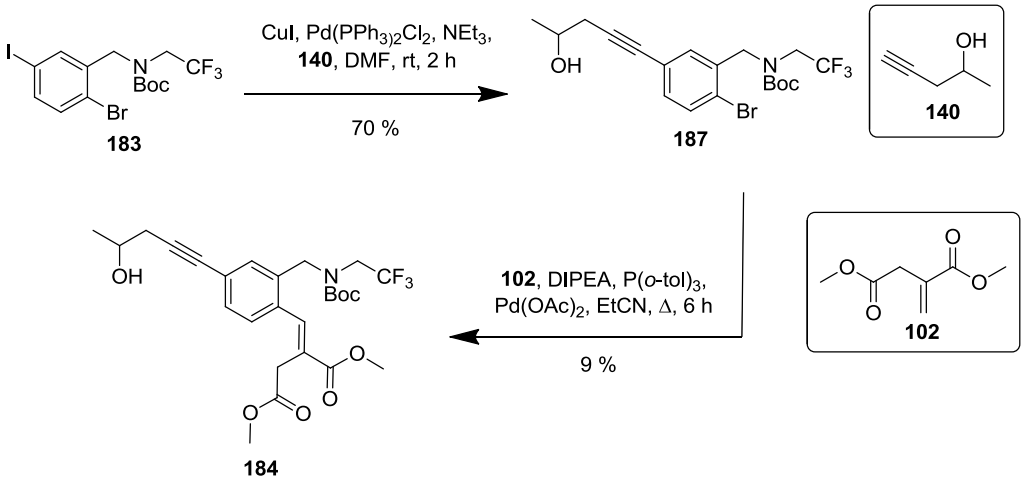

Scheme 72 *The sequential Sonogashira coupling of **183**, followed by Heck reaction with **102**, to give **184***

The same Sonogashira conditions were utilised as had been employed for the synthesis of the thiophene-containing compounds, except that the reaction was carried out at rt, and pleasingly **187** was afforded in good yield with no reaction observed at the bromide position **(Scheme 72)**. Bromide **187** was then subjected to the same Heck coupling conditions as previously. Whist the reaction gave a 29 % yield of product on a small scale, the same protocol unfortunately only gave a disappointing 9 % yield on a larger scale. Nonetheless, sufficient **184** was obtained, and the *E* geometry of the double bond was confirmed by nOe correlation in the same manner as with thiophene **116**.

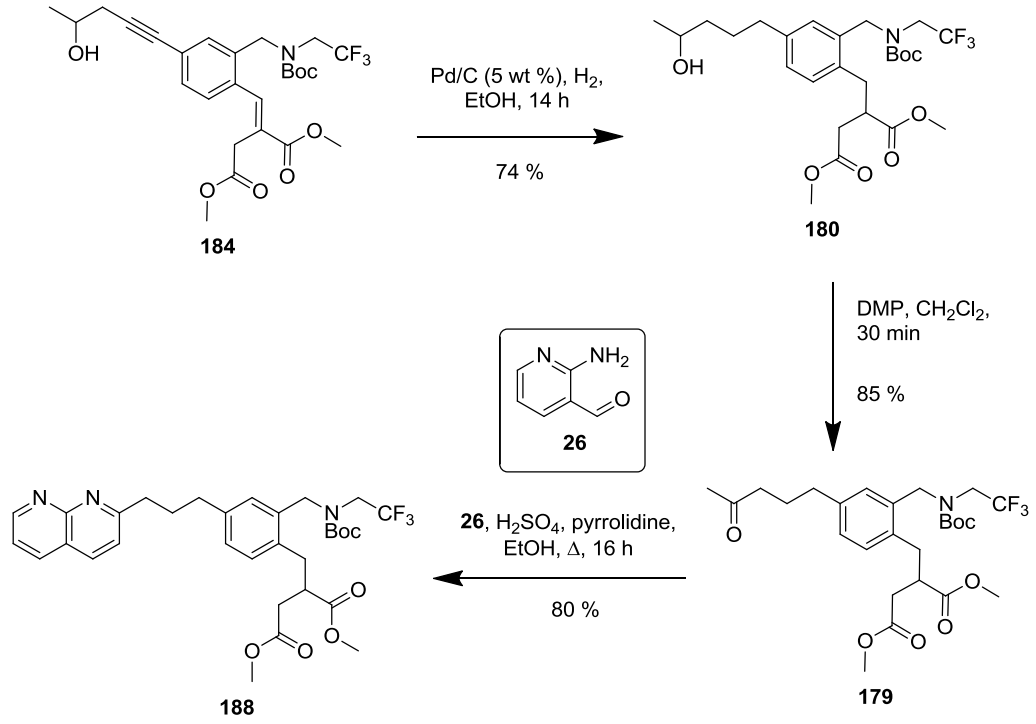

*Scheme 73 The elaboration of **184** to **188** by reduction, oxidation, then Friedländer reaction*

The α_V-binding portion of the molecule could then be elaborated in the familiar fashion **(Scheme 73)**. Reduction of **184** to **180** was carried out under atmospheric pressure, unlike the troublesome reduction of the thiophene analogues. Oxidation gave **179**, followed by Friedländer reaction to give **188**. Although the Friedländer reaction was high yielding, unfortunately some of one of the methyl ester groups on

188 was transesterified to the ethyl ester equivalent during the reaction. This was not a problem for the synthetic route, as eventually the ester groups will both be reacted, but this side product was inseparable from the product (6:1 ratio), and the transesterified ethyl ester side product was carried through the route until the final hydrolysis step.

Compound **188** was then reduced to **178 (Scheme 74)**. Subsequent azepine formation after Boc deprotection to give **189** was much more successful than for the thiophene analogues, because the cyclisation proceeded in PhMe under reflux, and did not require the 200 °C conditions in the microwave that had been used previously. With a significant supply of **189** in hand, hydrolysis to give **174** could be carried out. Although the reaction itself proceeded smoothly, upon neutralisation of the crude product before purification, the solubility of the resulting white solid was extremely low in MeCN:H_2O. The crude product had to be in solution for the purification by HPLC, so only the small proportion of the product that was in solution was purified to give **174**, hence the low yield for the reaction.

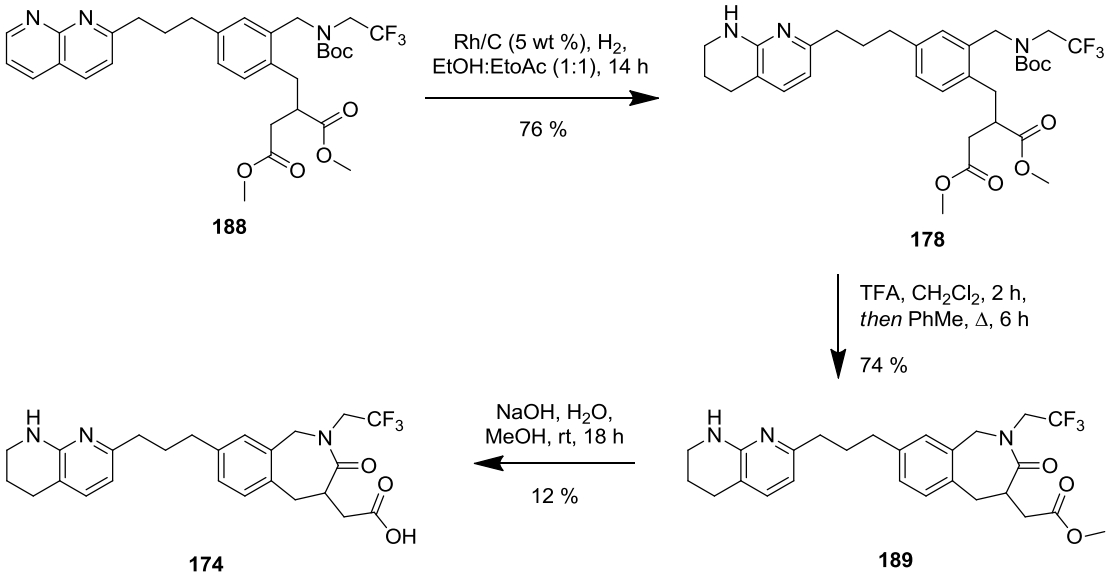

Scheme 74 The completion of the synthesis of 174

Having obtained **174**, the compound was tested in the integrin cell adhesion assays **(Table 29)**. Compared to lead compound **107**, the compound showed no loss in

potency at $\alpha_V\beta_3$ or $\alpha_V\beta_5$, but approximately a log reduction in potency at $\alpha_V\beta_1$ was observed. This was not hugely surprising given that the carbon-linked thiophene **146** (**Table 26**, page 164) had been significantly less potent than the corresponding oxygen linked compound **173** (**Table 28**, page 173). However, this data also allows for comparison with the homology model docking of the compound, to further establish its reliability.

	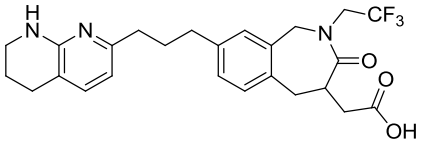 **174**
$\alpha_V\beta_1$ pIC_{50}	7.3 (n = 4)
$\alpha_V\beta_3$ pIC_{50}	8.2 (n = 1)
$\alpha_V\beta_5$ pIC_{50}	8.3 (n = 2)
$\alpha_V\beta_6$ pIC_{50}	5.6* (n = 7)
ChromlogD	2.93

*Table 29 The measured lipophilicity and potency of **174** in the integrin assays. *On one test occasion, measured as < 5*

Figure 94 shows **174** docked into the homology model, overlaid with the oxygen-linked lead **107**. Overall, the positions of the two docked compounds within the active site are similar, although the alkyl chain of **174** is twisted out of the plane of the aromatic core of the compound, compared to in **107**. This is reminiscent of compound **112** (**Figure 81**, page 141), where the chain was twisted out of plane, leading to compound of very similar potency.

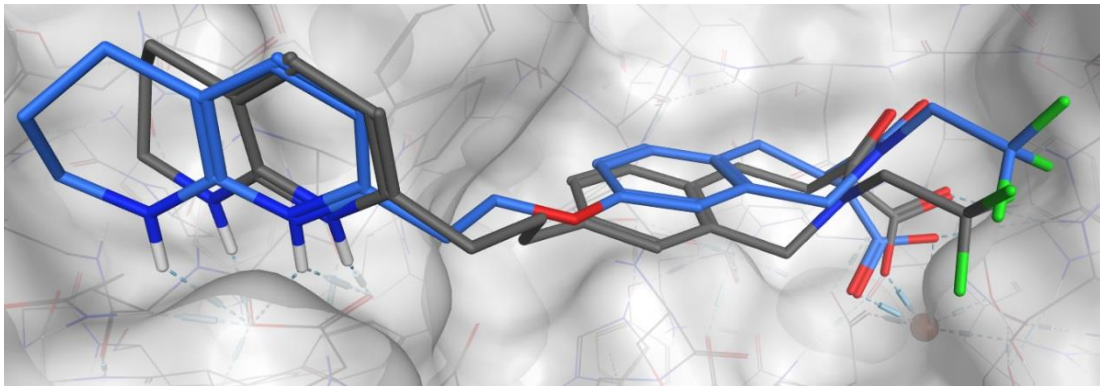

Figure 94 *The docked conformation of **174** in grey, overlaid with the lead compound **107** in blue. Overall, the compounds dock into similar positions in the active site, though the chain conformations differ.*

When the all-carbon chain was assessed using Mogul **(Figure 95)**, the substructure search (inlaid, right, on **Figure 95**) generated the frequency distribution shown. Clearly, though most angles are represented in the database, 90 ° is the preferred angle. The docking studies so far have indicated that a flat conformation is preferred for potency, and so perhaps the measured dihedral angle of 52 ° for compound **174** (**Figure 95**, inlaid left) is a compromise between these two factors.

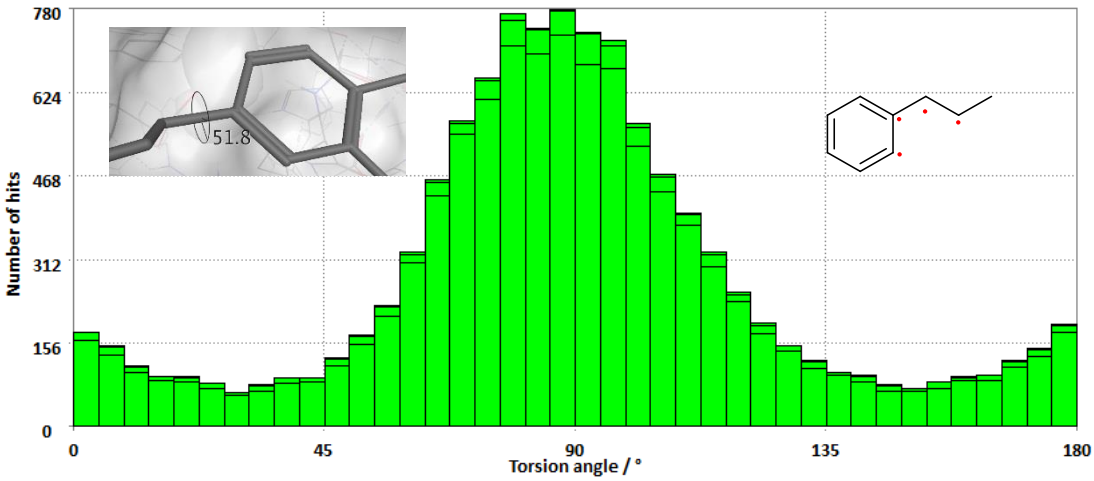

Figure 95 *The Mogul database results for the dihedral angle search for the substructure (inlaid, right). An angle of 90 ° is preferred according to mogul, but the most potent conformation for docking would be 0°. The measured dihedral angle of the docked conformation (inlaid, left) is, perhaps, a compromise between the two.*

On the basis that the homology model appears to provide a good indication of whether the compounds will be potent, attention was then turned to the third possible analogue with a pyridine ring in the core of the compound **(190, Figure 96)**.

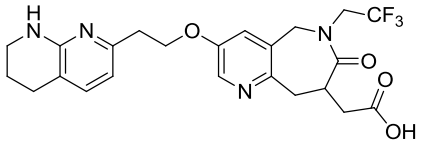

190

Figure 96 *The third possible pyridyl core regioisomer,* ***190***

The reason for the renewed interest in this compound is that when this compound was docked in to the homology model in a predictive sense **(Figure 97)**, the compound was found to occupy an almost identical space to the lead compound **107** in the active site, and was therefore expected to be highly potent. It also has a nitrogen lone pair directed towards the edge of the pocket, which was also thought to confer selectivity over the other integrins.

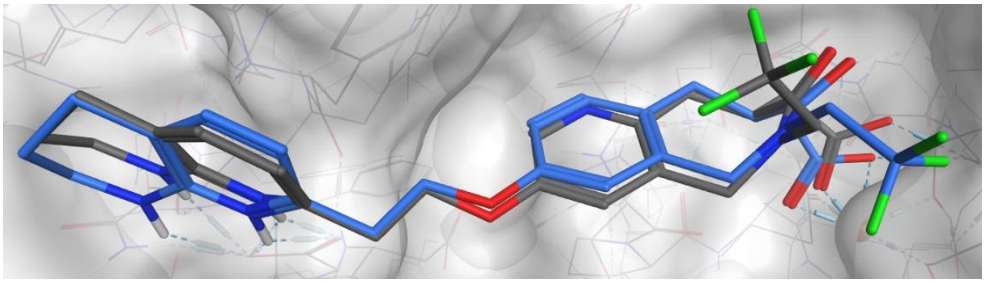

Figure 97 *Compound* ***190*** *in grey, docked into the homology model, overlaid with the lead compound* ***107****, with both compounds appearing to accommodate similar positions within the active site*

This selectivity was anticipated because when the compound was docked into the $\alpha_V\beta_3$ crystal structure **(Figure 98)**, **190** was found to dock much less favourably than into the $\alpha_V\beta_1$ homology model. In particular the aryl ring was puckered downwards. One possible for reason for this is the presence of the carbonyl of a backbone amide bond (circled in red on **Figure 98**), which is situated at the surface of the receptor. This electron rich oxygen may interact unfavourably with the pyridyl nitrogen if it were orientated in the same plane as lead compound **107**, resulting in the docked conformation rotating downwards to avoid this.

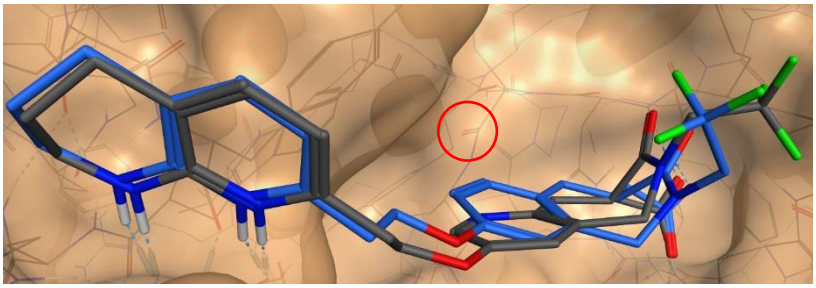

Figure 98 *Compound **190** (grey) docked into the $\alpha_V\beta_3$ crystal structure, overlaid with lead compound **107**. The core of compound **190** is twisted downwards, resulting in a less low-energy chain conformation. This puckering of the ring may be as a result of the presence of the carbonyl of a backbone arginine (circled in red) which may interact unfavourably with the pyridine lone pair.*

In an attempt to begin to use the docking model prospectively, the evidence from the docking into the $\alpha_V\beta_1$ and $\alpha_V\beta_3$ receptors warranted the synthesis of this compound.

The retrosynthetic analysis of **190** is shown in **Scheme 75**. The key fragment union was proposed to be a Mitsunobu reaction of alcohol **67** and azepine **191**. The usual Heck, reduction and cyclisation sequence was proposed to derive azepine **191** from bromide **192**. Work had been begun by co-worker Taylor on this target, but the target molecule had not been obtained. However, this previous work had successfully afforded intermediate **192**, so this work could be repeated.

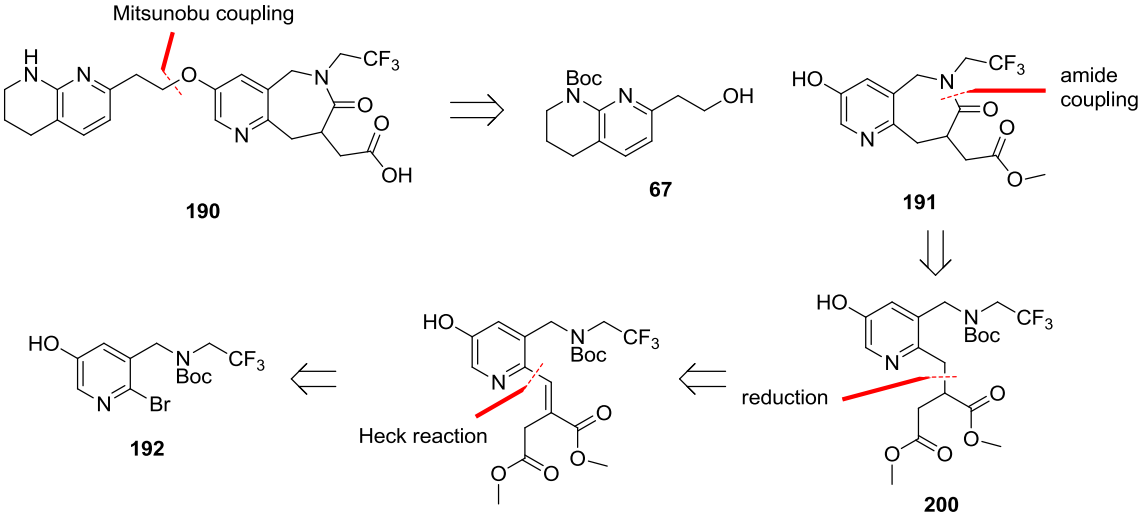

Scheme 75 *The retrosynthesis of **190**, proposed to arise from **191**, originally deriving from bromide **192***

Bromide **192** arose from the *meta*-selective hydroxylation of **193**, using an iridium-catalysed borylation, followed by oxidation to alcohol **192 (Scheme 76)**. Bromide **193**

could be obtained from the same amination and protection as was suitable for the synthesis of **174**, from commercially available aldehyde **194**.

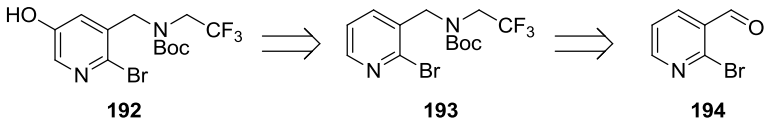

*Scheme 76 The retrosynthesis of **192**, proposed to arise from **193**, originally deriving from bromide **194***

The synthesis began with the reductive amination of **194**. Initially, the reaction was attempted in the same way as for the phenyl analogue **174 (Scheme 71)**, but when the hydrochloride salt of trifluoroethylamine and zinc chloride were used, the product obtained was chloride **195 (Figure 99)**.

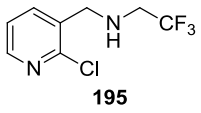

*Figure 99 Unwanted chloride **195***

It was assumed that chloride **195** would not be a competent coupling partner in the Heck reaction during the route, so instead, the reaction was repeated without any chloride sources in the reaction, exactly as had been carried out previously within our laboratories **(Scheme 77)**.[207] Amine **196** was furnished, and then Boc protected to give **193**.

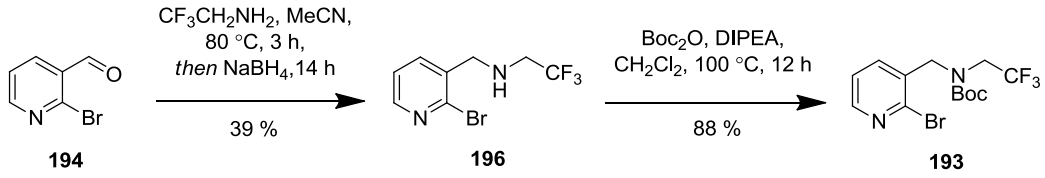

*Scheme 77 The synthesis of bromide **193** from commercially available aldehyde **194***

Bromide **193** was then hydroxylated *via* an iridium-catalysed *meta*-selective borylation (using ligand **197**), followed by oxidation of the resulting boronic ester **(Scheme 78)**. The intermediate borylated species is visible by LCMS, but was not isolated; rather it was oxidised *in situ* after a solvent swap to give **192** in a rather

disappointing yield, although most of the unreacted starting material **193** was recovered (43 %).

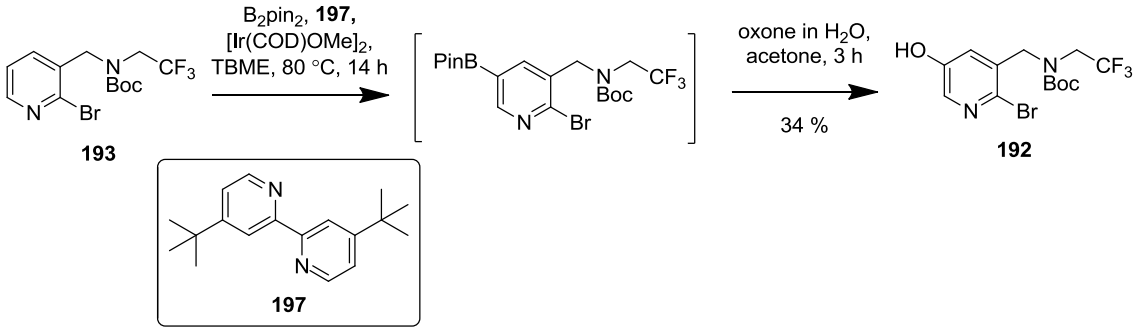

Scheme 78 *The selective hydroxylation of* ***193***

With **192** in hand, the Heck coupling was investigated. A recent publication details the development of conditions for the Heck coupling of 2-bromo-5-hydroxypyridine substrates, where the use of NBu_3 was found to be the most suitable base for the reaction.[230] However, these conditions were unsuccessful **(Scheme 79)**. It is thought that dimethyl itaconate **(102)** represents a more sensitive case than, for example, methyl acrylate (a common substrate in publications on Heck reactions), since the double bond of **102** is able to rearrange into conjugation with the two esters, and so if the temperature is too high or the base is too strong, it is anticipated that this would occur before coupling could take place.

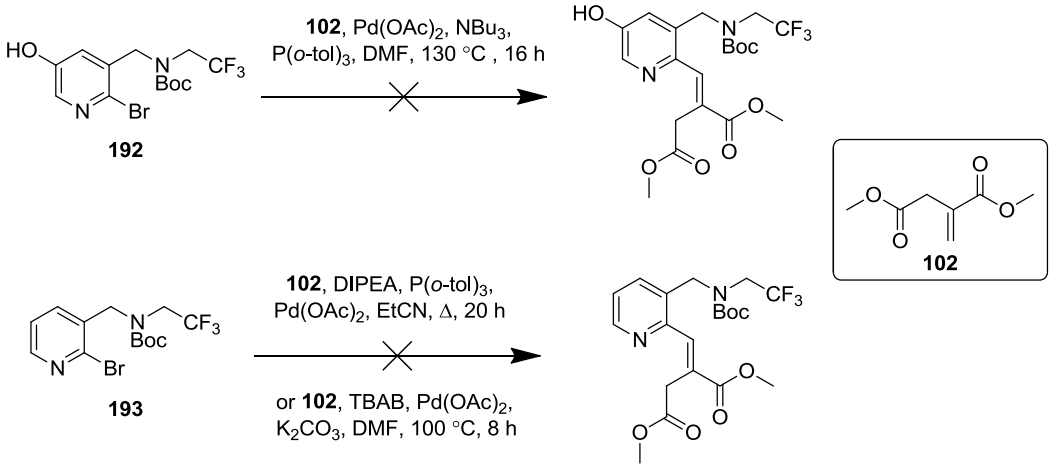

Scheme 79 *Unsuccessful attempts to couple* ***102*** *to* ***193*** *or* ***192*** *via Heck reaction*

As an alternative, the normal Heck reaction conditions were attempted on bromide **193**, but this was also unsuccessful, as were the conditions which had been used for the 2-bromothiophene analogues earlier **(Scheme 79)**. During the synthesis of **97**, the hydroxyl group had been protected as the methyl ether for the Heck coupling step, so it was thought that protection of the free alcohol might be most productive. However, a *para*-methoxybenzyl (PMB) protecting group was preferred to a methyl group, as after the Heck reaction, it was envisaged that it could be reductively cleaved at the same time as the double bond formed in the Heck reaction was reduced, thus saving a step in the overall route. Additionally, PMB protection of substrate **192** had shown some promise in the Heck coupling during the previous work within our laboratories, although the product was never obtained in pure form.[207] Therefore, PMB protection of **192** was carried out **(Scheme 80)**. Pleasingly, this substrate **(198)** was then found to be competent in the Heck reaction, affording **199** in moderate yield. Unfortunately, some protodebromination of the starting material **198** was observed in the reaction, and this was inseparable from the product, leaving **199** as a mixture in a 5:1 ratio with this side product.

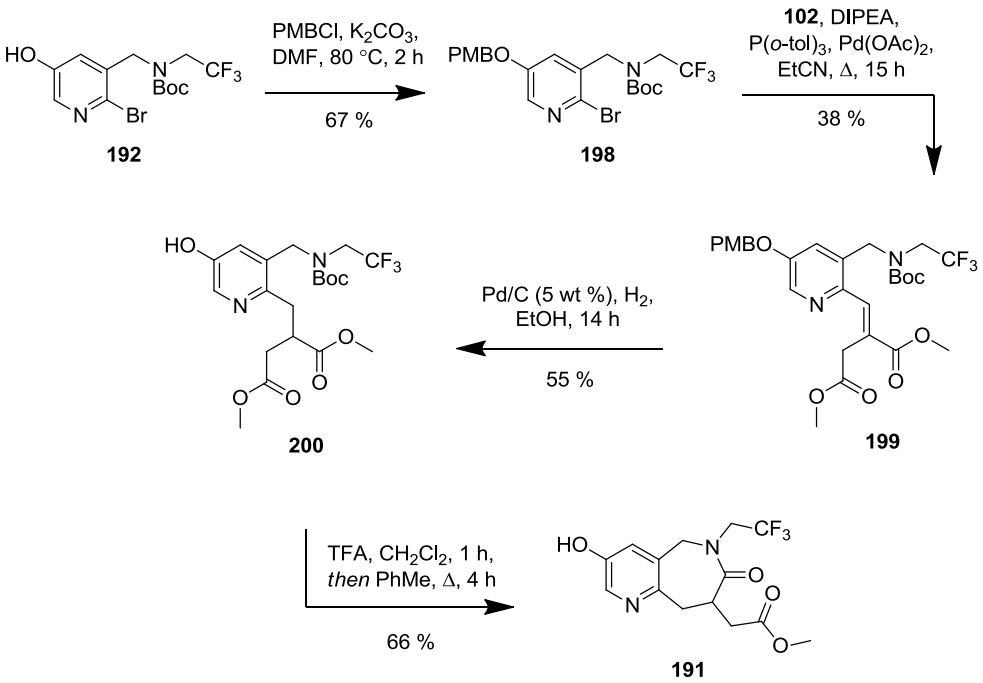

Scheme 80 *The protection and subsequent Heck coupling of* ***192****, followed by elaboration to azepine* ***191***

Heck product **199** was then reductively deprotected to give **200**, which underwent the usual cyclisation conditions to give **191**. After the cyclisation was carried out, the unwanted side product mentioned above could be separated to give **191** as a clean product, it having also been deprotected during the reduction step to form **201 (Figure 100)**.

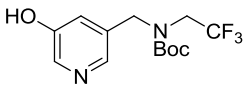

201

Figure 100 *Side product* ***201****, formed from the protodebromination of* ***198*** *during the Heck reaction, followed by reduction to* ***201*** *during the formation of* ***200****. After the cyclisation to give* ***191****, it was separable and could be removed.*

Alcohol **191** then underwent Mitsunobu coupling with alcohol **67** as planned, using (cyanomethylene)tributylphosphorane (CMBP) as the coupling agent**.**[231] This reagent was chosen because it had been used successfully in our laboratories on similar substrates. Alcohol **67** is known to be a challenging substrate for Mitsunobu chemistry, because of its propensity for eliminate to form the vinyl tetrahydronaphthyridine **202 (Figure 101)** once the alcohol is activated as a leaving group.[232] This was indeed found to be the case, with significant quantities of **202** observed by LCMS in the reaction. This resulted in the requirement for several equivalents of **67** and CMBP in the reaction for full conversion to product to be observed. Fortunately, a large supply of **67** was available, so this intermediate was not precious. During formic acid-modified HPLC purification to separate **202** from the product, partial Boc deprotection was observed, so the material was subjected to acidic deprotection to remove the Boc group before further purification, giving **203**.

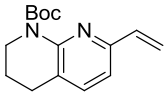

202

Figure 101 *Unwanted elimination product* ***202*** *from Mitsunobu couplings of* ***67***

In spite of these challenges, ether **203** was formed in moderate yield **(Scheme 81)**. This was followed by the facile hydrolysis to give **190**, which was sent for biological testing.

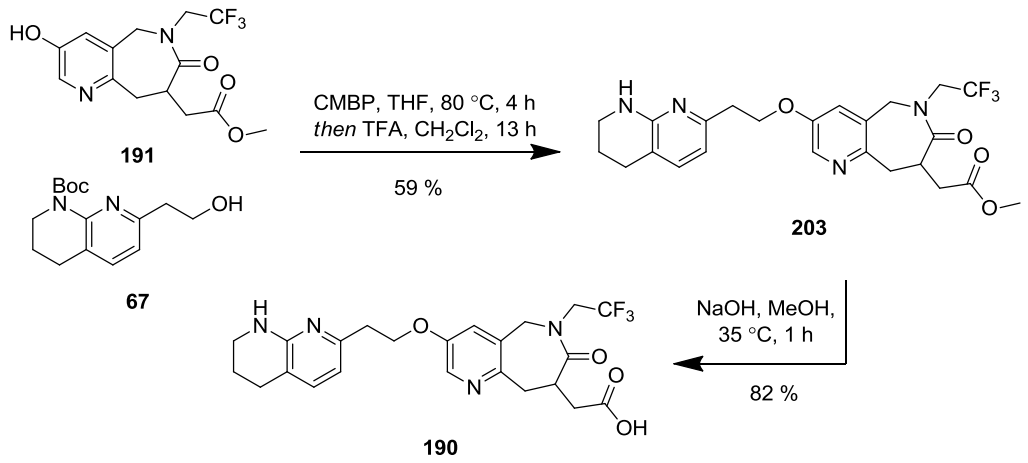

Scheme 81 *The Mitsunobu coupling and subsequent hydrolysis of **203** to give **190***

The resulting assay data for compound **190** are shown in **Table 30**. Disappointingly, **190** had a lower-than-expected potency at $\alpha_V\beta_1$, compared to the way in which the compound had docked into the $\alpha_V\beta_1$ homology model (**Figure 97**, page 182). Furthermore, docking into the $\alpha_V\beta_3$ had indicated that this compound may not be so well accommodated into this receptor, implying that this may lead to selectivity over $\alpha_V\beta_3$ and $\alpha_V\beta_5$ (since compounds usually show similar potency at $\alpha_V\beta_3$ and $\alpha_V\beta_5$).[233] Unfortunately, this predictive use of the model was unsuccessful.

	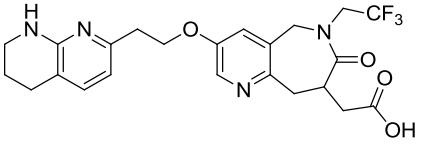 **190**
$\alpha_V\beta_1$ pIC_{50}	6.4 (n = 2)
$\alpha_V\beta_3$ pIC_{50}	8.1 (n = 1)
$\alpha_V\beta_5$ pIC_{50}	8.3 (n = 2)
$\alpha_V\beta_6$ pIC_{50}	5.3 (n = 7*)
ChromlogD	1.96

Table 30 *The measured integrin potency data for compound **190**. *On one test occasion out of 8, the pIC_{50} was measured as < 6, so this has been excluded from the values from which the mean was calculated.*

3.5 Results and discussion: Substitution α to the carboxylic acid

Having considered the core aromatic ring of the compound and assessed the effect of a carbon linker atom to the aryl ring, another vector on **107** was investigated, in order to attempt to gain some selectivity over the other integrins. Although the model was not successful in predicting the potency and selectivity of pyridyl analogue **190**, it was still considered a useful means of generating hypotheses for alternative vectors for investigation.

The first such vector for investigation was close to the β-binding domain of the compounds. **Figure 102**, where lead compound **107** is shown docked into both the homology model (left) and the crystal structure (right), indicates why this is the case.

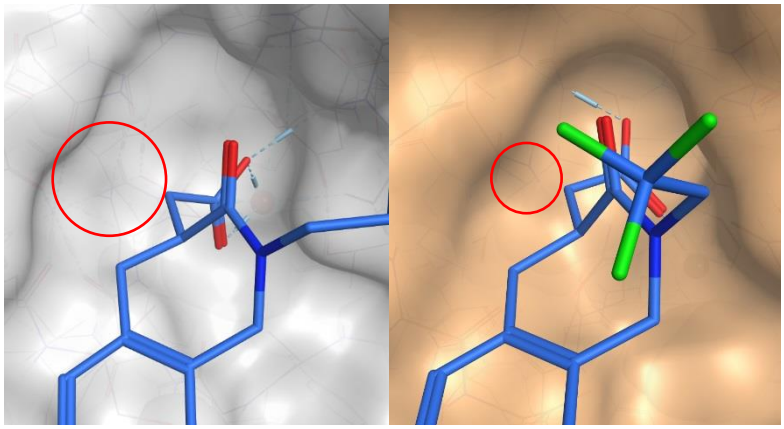

Figure 102 *Compound **107** docked into the $\alpha_V\beta_1$ integrin homology model (left), and the $\alpha_V\beta_3$ crystal structure (right). The pocket in which the carboxylate group binds is noticeably smaller in the $\alpha_V\beta_3$ integrin than in the $\alpha_V\beta_1$ integrin. The space which could be filled by alkylation α to the acid group is indicated by the red circles, and is larger in the $\alpha_V\beta_1$ receptor.*

In the $\alpha_V\beta_1$ active site (left, white surface), the space in the pocket, indicated by the shadowed contour of the surface, appears significantly greater than in the $\alpha_V\beta_3$ active site (right, orange surface).

In order to exploit this proposed difference between the integrins, alkylations α to the acid group were proposed. Clearly, a disadvantage of the work done so far to vary

the core of the compound has been that each has required its own synthetic route, greatly reducing the number of compounds that it is possible to synthesise. For the alkylation work, therefore, it was believed that the alkylation would be possible at a late stage in the synthesis. Specifically, it was envisaged that **97** could be used, since a significant quantity of the compound was available from previous clinical work with the compound.

It was believed that the methyl ester derivative of **97** could be alkylated *via* the lithium enolate, followed by ester hydrolysis to the final compound **(Scheme 82)**. In addition to the abundance of **97** available, this approach was advantageous in that **97** was available as a single enantiomer, and so if both diastereomers could be generated in the alkylation, then they might be separable by achiral chromatography. This would generate the final compounds as single stereoisomers without requiring lengthy chiral separations, and allow for proper assessment of their individual selectivities and potencies.

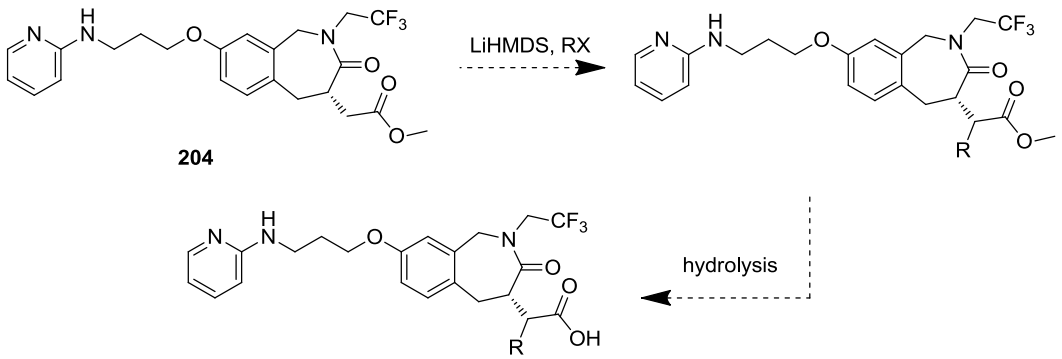

Scheme 82 *The proposed method of alkylation of* ***204*** *to give products alkylated in next to the acid group*

Esterification of **97** proceeded smoothly to afford **204 (Scheme 83)**. Unfortunately, when methylation of **204** was attempted using lithium hexamethyldisilazide (LiHMDS), a complex mixture of products was obtained. This is thought to be a result of the aminopyridyl hydrogen being of similar acidity to the carbon α to the ester, leading to deprotonation at this position and unwanted side reactivity.

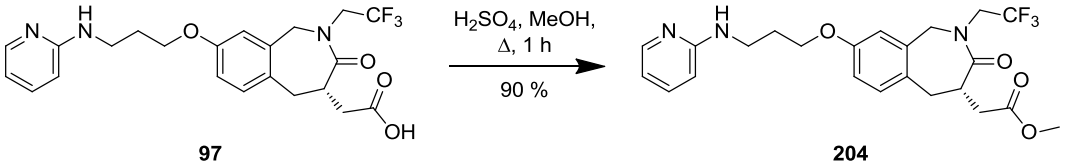

Scheme 83 The acid catalysed esterification of ***97*** to ***204***

Therefore, ester **204** was Boc protected, giving **205** in good yield **(Scheme 84)**. When **205** was subjected to the reaction conditions, methylation occurred in a good yield **(Scheme 85)** to give **206** as an inseparable mixture of diastereomers.

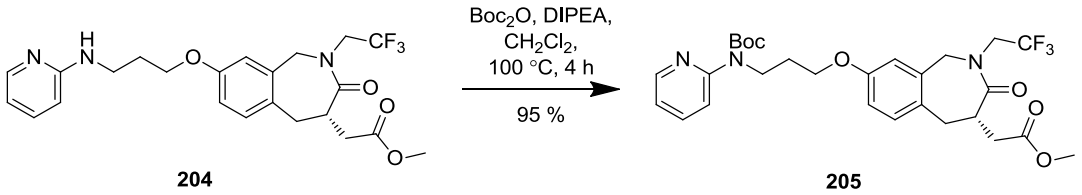

Scheme 84 Boc protection of ***204*** to give ***205***

Pleasingly, after hydrolysis, the two diastereomers were separable by achiral HPLC to yield **207** and **208**. It was not possible to determine which diastereomer is which for **207** and **208**, but for the sake of differentiating the two, the two diastereomers have been arbitrarily assigned as the (*R*) and (*S*) stereoisomers.

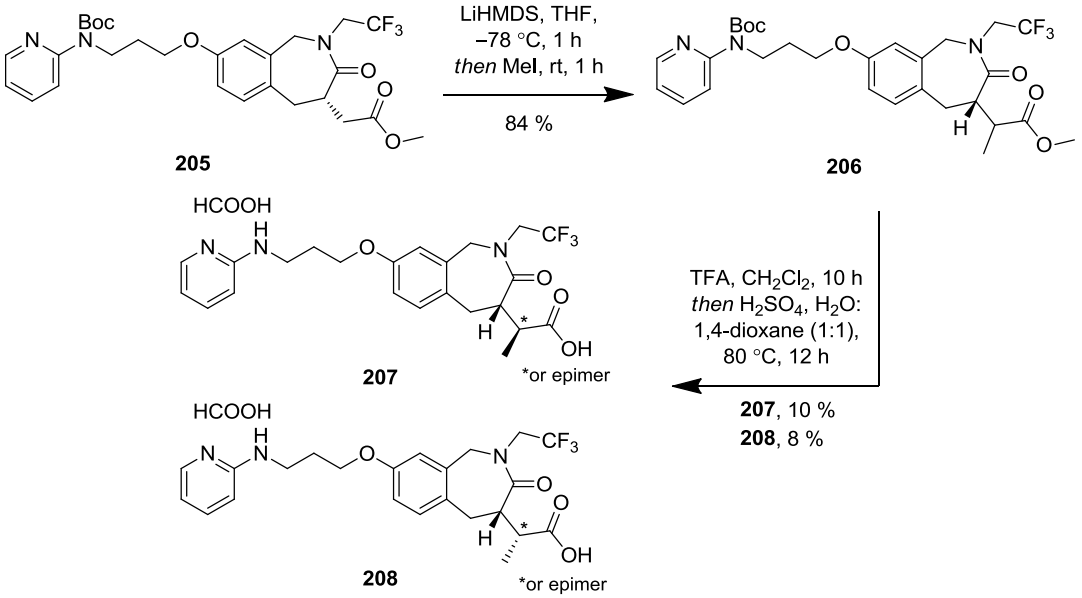

Scheme 85 Methylation of ***205*** to give ***206*** as a mixture of diastereomers, followed by deprotection to give ***207*** and ***208*** as single stereoisomers

These compounds were docked into the $\alpha_V\beta_1$ homology model and the $\alpha_V\beta_3$ crystal structure, and, as had been indicated by the comparison of the β-binding domains in **Figure 102**, the differing amount of space in this part of the receptor led to the prospect of selectivity. **Figure 103** shows one of the possible diastereomers, compound **207**, docked into the homology model and crystal structure. In the $\alpha_V\beta_1$ homology model, the methyl substitution is accommodated in the receptor, resulting in a docked conformation very similar to that of potent *N*-methyl analogue **108**. However, in the $\alpha_V\beta_3$ crystal structure, the methyl substitution is not accommodated, resulting in a twisting of the azepine, and a conformation that appears to be less potent.

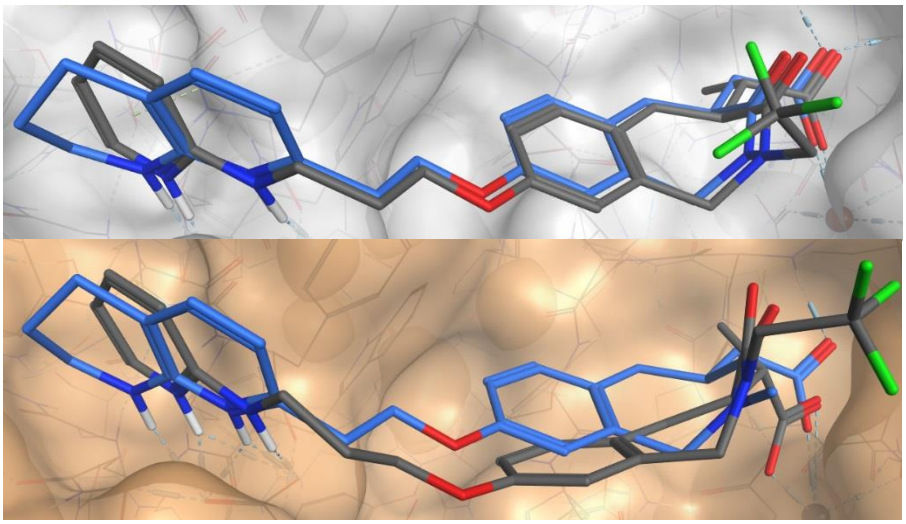

Figure 103 *The docked conformation of **207** (grey) into the $\alpha_V\beta_1$ integrin (top), and the $\alpha_V\beta_3$ crystal structure (bottom), both overlaid with the lead compound **108** (blue). The α-methyl substitution is accommodated into the pocket in $\alpha_V\beta_1$, but is not in $\alpha_V\beta_3$, rotating the compound to avoid a clash with the protein surface.*

When the second diastereomer **(208)** was docked into both models **(Figure 104)**, the compound, similarly, appears to dock better into $\alpha_V\beta_1$ than $\alpha_V\beta_3$, but the methyl substitution does not appear to point towards the pocket in $\alpha_V\beta_1$, rather it points towards solvent-exposed space, so it may not confer any additional potency. However, the binding mode for the compound in the $\alpha_V\beta_1$ homology model is still much better than for the compound in the $\alpha_V\beta_3$ crystal structure, implying that this compound may not be active in the $\alpha_V\beta_3$ integrin assay.

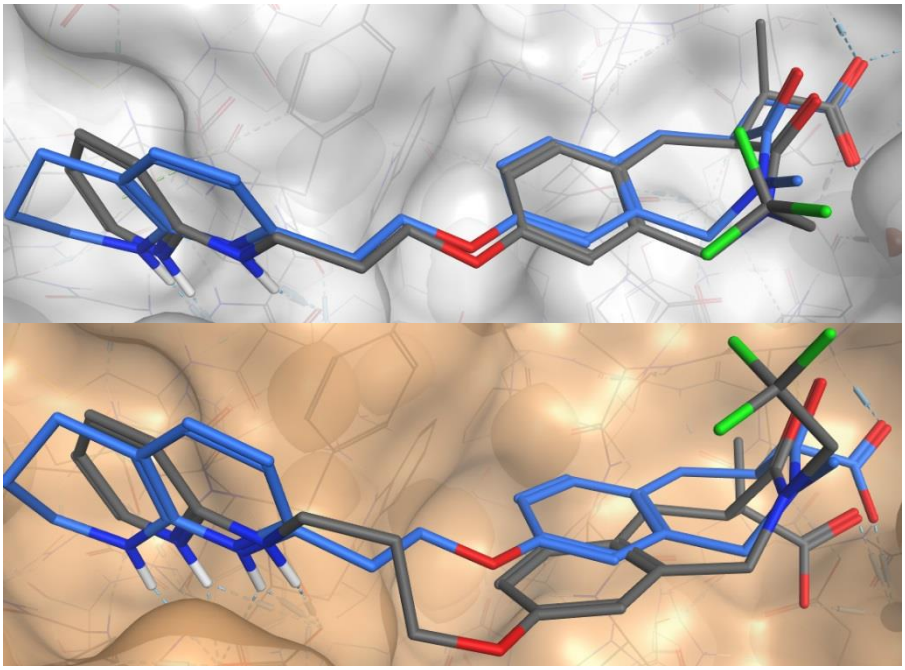

Figure 104 *The docked conformation of* ***208*** *(grey) into the $\alpha_V\beta_1$ integrin (top), and the $\alpha_V\beta_3$ crystal structure (bottom), both overlaid with the lead compound* ***108*** *(blue). In the $\alpha_V\beta_1$ model, the compound docks in the same fashion as* ***108****, but unlike for diastereomer* ***207****, the methyl group does not extend into a pocket, rather out into solvent-exposed space, so this may not confer any additional potency. In contrast, the compound does not appear to be accommodated in the $\alpha_V\beta_3$ crystal structure.*

In order to investigate the extent of the space available in the pocket under examination here, the ethyl-substituted analogues were also prepared **(Scheme 86)**. EtI was used as the electrophile in a similar alkylation to previously, giving **209** and **210** which were separable by normal phase column chromatography. These were then deprotected under acidic conditions to give **211** and **212**.

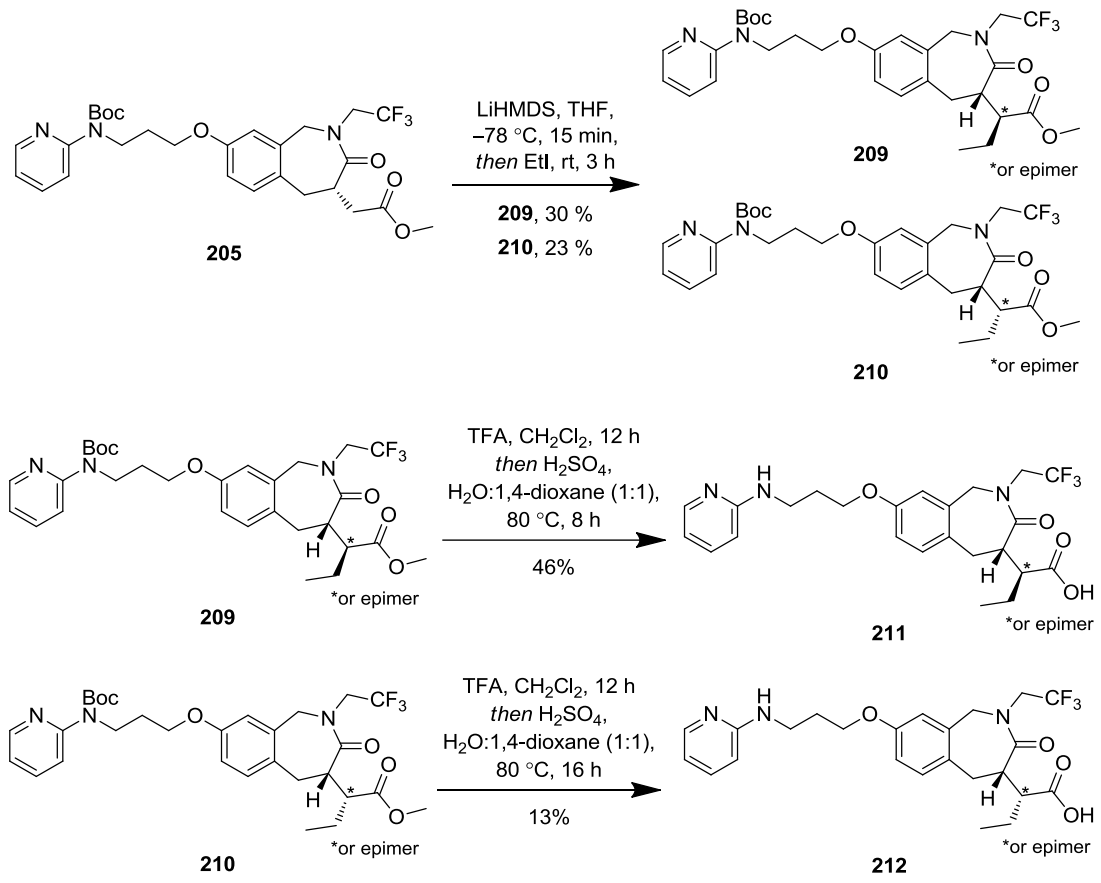

Scheme 86 *The alkylation of **205** with ethyl iodide, followed by acidic deprotection to yield the final compounds*

The potency of the α-methyl and α-ethyl compounds was measured in the integrin cell adhesion assays, and the results are shown in **Table 31**. Unfortunately, these compounds were found to be less active than compound **97**, from which they were derived. The cell assay potency of compound **207** was reduced by 1 log at the $\alpha_V\beta_3$ and $\alpha_V\beta_5$ integrins compared to **97**, but no selectivity was conferred as the $\alpha_V\beta_1$ potency has been reduced by over 1 log unit. Diastereomer **208** was inactive at $\alpha_V\beta_1$. Since the methyl substitution was not tolerated in the receptor, it was no surprise that ethyl-substituted compounds **211** and **212** were also less active.

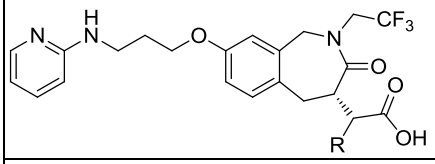	 *or epimer	 *or epimer	 *or epimer	 *or epimer
Compound number	**207**	**208**	**211**	**212**
$\alpha_V\beta_1$ pIC_{50}	5.6* (n = 2)	< 5 (n = 4)	< 5 (n = 2)	5.3 (n = 2)
$\alpha_V\beta_3$ pIC_{50}	7.3 (n = 3)	< 5 (n = 2)	-	-
$\alpha_V\beta_5$ pIC_{50}	7.2 (n = 6)	5.9† (n = 3)	5.4 (n = 2)	6.8 (n = 2)
$\alpha_V\beta_6$ pIC_{50}	< 6** (n = 2)	< 6** (n = 2)	-	-
ChromlogD	2.44	2.35	2.62	2.95

Table 31 *The integrin cell assay data for compounds **207**, **208**, **211**, and **212**. *On one occasion, <5. **For compounds **207** and **208**, the $\alpha_V\beta_6$ potency was measured 3 times, and on two occasions for each, the pIC_{50} was < 6, and on the other occasion it was 7.0 and 6.3, respectively. †On three occasions, <5, but these are excluded*

Having found these alkyl substitutions to be unsuccessful, attention was turned back to the computational model. In **Figure 105**, the protein surface of the $\alpha_V\beta_1$ homology model is coloured by lipophilicity (hydrophobic areas are displayed in green, hydrophilic areas in purple). It is apparent that the part of the receptor occupied by the substitutions α to the carboxylate is hydrophilic in nature. Therefore, it was hoped that a group of analogues with more polar substitutions might be a more productive means of filling this pocket.

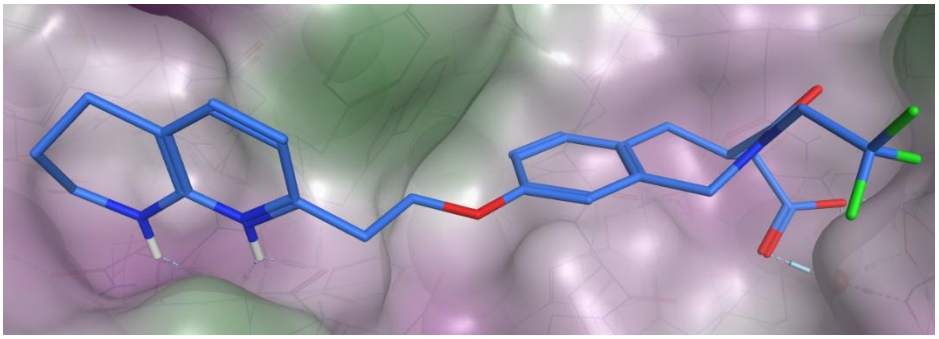

Figure 105 *Compound **107** docked into the homology model, with the surface coloured according to lipophilicity, where hydrophilic areas are coloured in purple, and hydrophobic areas are in green. The pocket next to the carboxylate group is noticeably hydrophilic in nature.*

In light of this, two further functionalisations were carried out on **205 (Scheme 87)**. An α-hydroxylation was carried out using a Davis oxaziridine **213**,[234] yielding separable diastereomeric intermediates **214** and **215**. These diastereomers could not be separated using normal phase chromatography, rather they were separated using achiral reverse phase chromatography, by co-worker Hobbs within our laboratories.[235] Additionally, an aldol reaction was carried out with paraformaldehyde as the electrophile to give **216** as a mixture of diastereomers that was inseparable by normal phase chromatography.

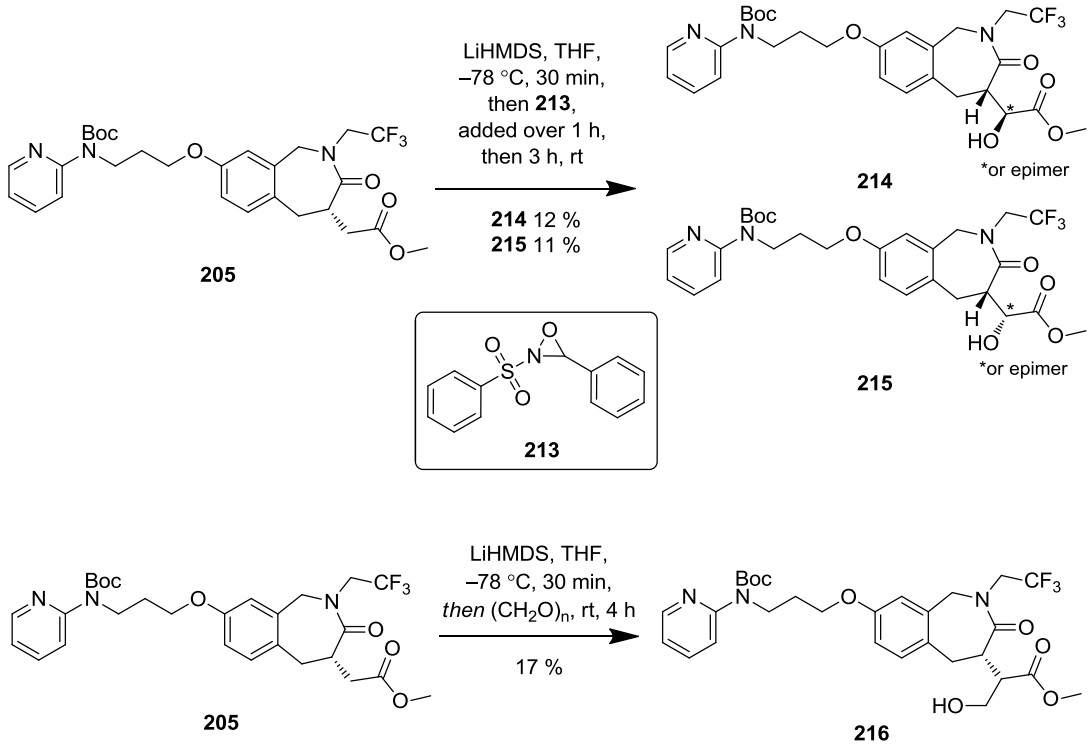

*Scheme 87 The alkylations of **205** with paraformaldehyde and Davis oxaziridine **(213)***

Intermediates **214** and **215** were deprotected using the normal method **(Scheme 88)** to give compounds **217** and **218**, although compound **218** was obtained as an inseparable mixture with an unidentified impurity in an 8:1 ratio. When the deprotection and hydrolysis were carried out on intermediate **216**, the diastereomeric products were separable, but found to be unstable after purification, and so the final compounds deriving from intermediate **216** were not obtained.

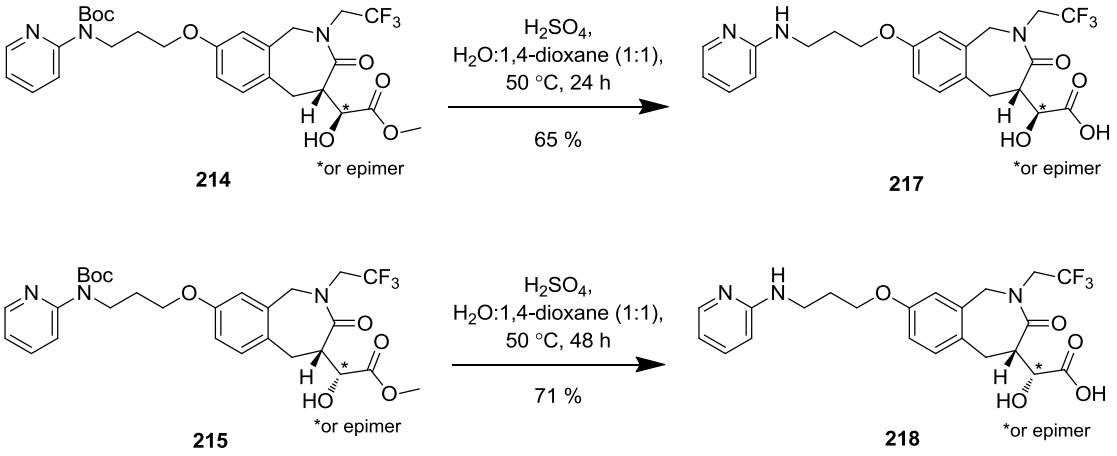

Scheme 88 *The deprotection of compounds **214** and **215** to give **217** and **218***

Having obtained compounds **217** and **218**, they were docked into the homology model **(Figure 106)**. Both diastereomers seem to be accommodated, though **217** in particular the hydroxyl substitution appears to fit into the desired pocket whilst the rest of the compound can overlay closely to current lead **107 (Figure 106, top)**. The hydroxyl makes a polar interaction with an asparagine residue in the protein. For arbitrarily assigned diastereomer **218**, the hydroxyl also appears to make a hydrogen bonding interaction with the edge of the pocket, but the rest of the azepine is more significantly displaced in order to accommodate that interaction. That compound, therefore, is envisaged not to be as active.

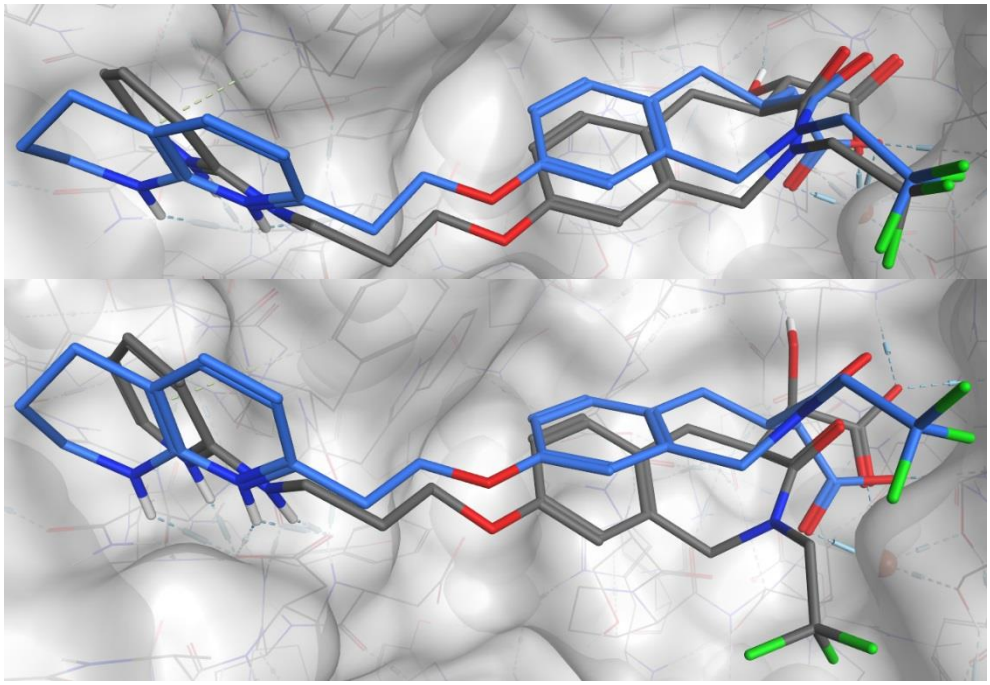

Figure 106 *hydroxyl-substituted analogues* ***217*** *and* ***218*** *(in grey) docked into the homology model, with* ***217*** *(top) showing a particularly good fit into the desired pocket, whilst not disturbing the rest of the compound, in comparison to lead* ***107*** *(in blue), whereas* ***218*** *(bottom) appears to have the hydroxyl group sitting on the ledge of the pocket. In both cases, the hydroxyl group makes a hydrogen bonding interaction to the protein*

The integrin potency of these compounds was measured **(Table 32)**. In spite of the promising docking poses, in particular for diastereomer **217** (though stereochemistry of the two diastereomers has not been identified), these compounds were inactive at $\alpha_V\beta_1$. It appears, therefore, that this vector is not likely to be a means of providing selectivity for this integrin over $\alpha_V\beta_3$ and $\alpha_V\beta_5$. Moreover, it appears again that the $\alpha_V\beta_3$ and $\alpha_V\beta_5$ integrins are more accommodating of changes to this template than the $\alpha_V\beta_1$ integrin.

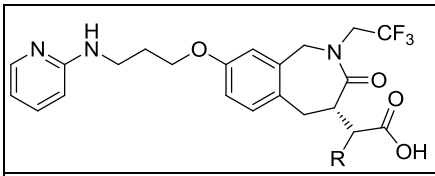	 *or epimer	 *or epimer
Compound number	**217**	**218**
$\alpha_V\beta_1$ pIC_{50}	< 5 (n = 2)	< 5 (n = 2)
$\alpha_V\beta_3$ pIC_{50}	6.4 (n = 1)	6.5 (n = 1)
$\alpha_V\beta_5$ pIC_{50}	6.6 (n = 2)	7.0 (n = 2)
$\alpha_V\beta_6$ pIC_{50}	-	-
ChromlogD	2.12	2.10

Table 32 *The profile of compounds **217** and **218**. These compounds were not active at $\alpha_V\beta_1$*

3.6 Results and discussion: Aryl core substitutions

Having found the pocket adjacent to where the carboxylate binds in the integrin active site to be unproductive as a means of obtaining selectivity for $\alpha_V\beta_1$, another position for substitution was sought. Upon comparison of the $\alpha_V\beta_1$ homology model with the $\alpha_V\beta_3$ crystal structure, it was noted that there was some additional space in the $\alpha_V\beta_1$ receptor next to the aromatic core of the molecule. This is shown in **Figure 107**.

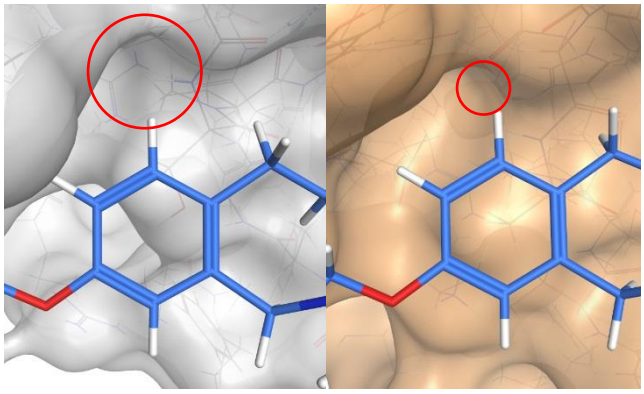

Figure 107 *A comparison of the space in next to the aryl core of lead compound **107** in the $\alpha_V\beta_1$ homology model (left) compared to the $\alpha_V\beta_3$ crystal structure (right). The red circles indicate the increased space in the $\alpha_V\beta_1$ homology model.*

This vector had been unsuccessfully exploited in the case of pyridyl analogue **190**, but it appears that there may be space for substitution from this position, which may result in a clash in $\alpha_v\beta_3$ but not in $\alpha_v\beta_1$. Given the limited success in using the homology model in a predictive fashion, the intention was to make a variety of substitutions at this position, to investigate what groups might be tolerated. Two such compounds are shown docked in **Figure 108**, with methyl-substituted analogue **219 (Figure 108, top)**, and hydroxyl-substituted analogue **220 (Figure 108, bottom)** shown. In both cases, the substitution appears to be tolerated and the docking pose overlays with lead compound **107**. For analogue **220**, a hydrogen bonding interaction with the protein backbone is indicated. In addition to these substitutions, ethyl and chloro substitutions appeared to be tolerated, but methoxy and cyano substitutions resulted in a twisting of the aryl ring when docked (see electronic supporting information for the docking poses for all compounds). Additionally, the hydroxy-substituted analogue **220** appeared to also be tolerated in the $\alpha_v\beta_3$ crystal structure, whereas the others did not, suggesting that selectivity may be obtainable *via* this approach.

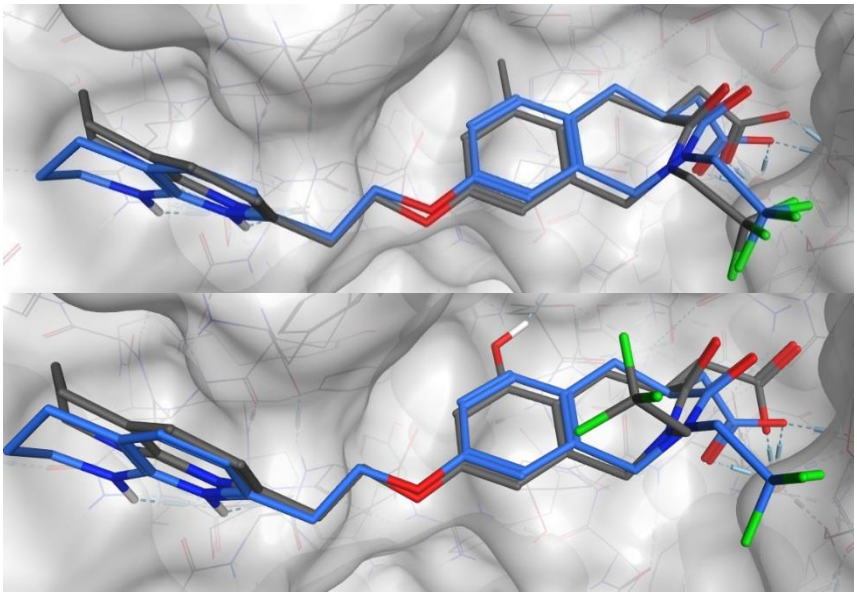

Figure 108 *Lead compound* ***107*** *overlaid with methyl-substituted analogue* ***219*** *(top), and hydroxyl-substituted analogue* ***220*** *(bottom). In both cases, the substitution appears to be accommodated.*

Synthetically, it was envisaged that these compounds might be accessible *via* a late-stage functionalisation of intermediate **105 (Figure 109)**, in order to again capitalise on the supply of **97** available within our laboratories (**Scheme 32**, page 128), and avoid lengthy syntheses for each analogue.

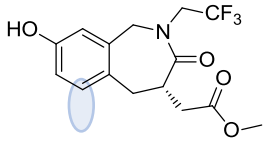

105

Figure 109 *Intermediate **105**, intended for late-stage functionalisation to substitute the aryl ring (in the position shown in blue).*

Given the challenges of the *meta*-selective functionalisation of a phenol, it was envisaged that the most promising means of functionalising this position would be to oxidise the ring, *via* a C-H borylation, making the assumption that the desired position on the ring would be the sterically most accessible position. The great benefit of this approach would be that, should a boronic ester be installed, this could lead to facile derivatisation to a range of analogues.

Unlike the approach taken for α-substitution of the carboxylic acid group of **97**, it was envisaged that the functionalisation would need to take place on intermediate **105** rather than on the fully elaborated compound, because of selectivity concerns relating to the unwanted borylation of the sterically accessible aminopyridine functionality. This did, however, mean that once functionalisation was carried out, the more potent tetrahydronaphthyridine group could be appended to the azepine, furnishing more potent compounds than the corresponding aminopyridine compounds would be. Additionally, it had been shown within our laboratories that **105** could be obtained directly from **97** *via* a BBr_3-induced dealkylation reaction.[207] Therefore, this reaction was repeated to obtain intermediate **105 (Scheme 89)**.

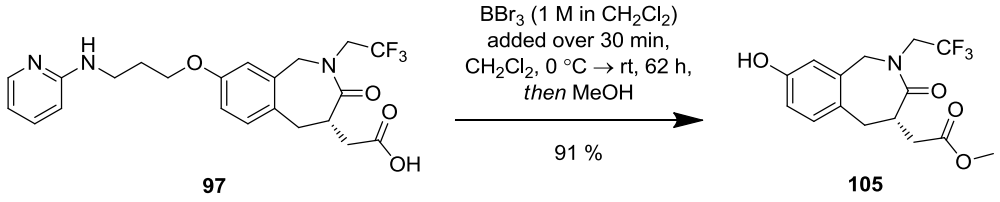

*Scheme 89 The synthesis of intermediate **105***

It was anticipated that the borylation could be directed to the desired position if a bulky protecting group was appended to **105**, so a *tert*-butyldimethylsilyl (TBS) group was added **(Scheme 90)** to give **221**.

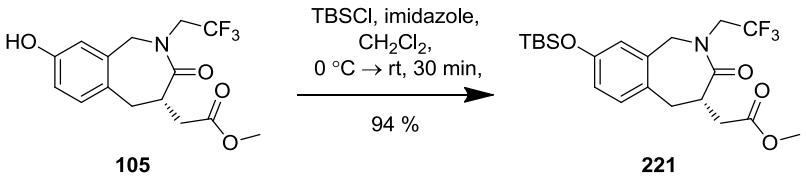

*Scheme 90 The TBS protection of **105***

With **221** in hand, the crucial borylation could be attempted. Beginning with the same conditions used for the borylation of **193** during the synthesis of pyridyl analogue **190** (**Scheme 78**, page 185), no conversion was observed at 80 °C, but a small amount was observed by LCMS at 100 °C. No improvement was observed when the reaction was carried out in a microwave reactor, so it was hypothesised that the phenyl ring may have been too sterically hindered for borylation to take place to a significant extent. Instead, therefore, the borylation was attempted on less hindered substrate **105 (Scheme 91)**.

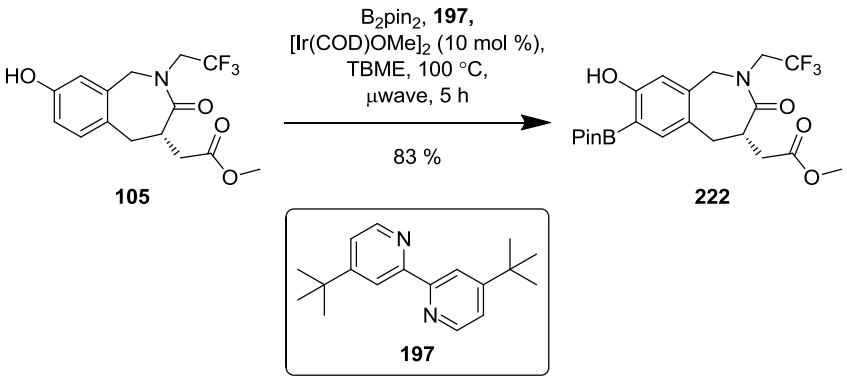

*Scheme 91 The borylation of unprotected substrate **105**, leading to the undesired regioisomer **222**.*

Unfortunately, this led to the borylation occurring *ortho* to the phenol, forming **222**, which was not desired. Instead, therefore, the catalyst loading of iridium was significantly increased, and the reaction was again carried out with TBS-protected substrate **221 (Scheme 92)** to form useable quantities of borylated product **223**. Unfortunately, it was not possible to separate the product from unreacted starting material using normal phase chromatography, and attempts to purify using reverse phase chromatography led to boronic ester hydrolysis, and the resulting boronic acid protodeborylated upon standing. Therefore, the product was obtained as an inseparable mixture with starting material **221**.

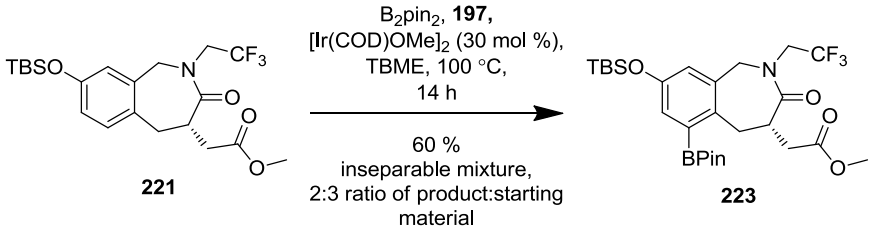

Scheme 92 *The borylation of TBS-protected substrate **221**, giving product **223** as an inseparable mixture with unreacted starting material.*

Due to this inability to separate the starting material from the product, attempts were made to improve the conversion of the reaction. Increasing the temperature to 110 °C led to the formation of the unwanted regioisomer (the corresponding TBS-protected form of **222**), and a solvent swap to cyclopentyl methyl ether also showed no improvement (reactions were carried out at 110 °C and 130 °C). As these attempts were unsuccessful, **223** had to be used in the following reactions as an inseparable mixture with **221**. The ratio of product to starting material varied between the different repeats of the reaction shown in **Scheme 92**, but in each case, the quantity of **223** in the product was determined by NMR, and used to calculated the stoichiometry required for, and yield from, the subsequent reactions.

With **223** in hand, albeit in moderate yield and as a mixture with **221**, functionalisation could take place. Initially, methyl and methoxy substitutions were targeted **(Scheme 93)**. A Suzuki reaction readily afforded the desired methyl substitution, and subsequent TBS deprotection using tetrabutylammonium fluoride (TBAF) afforded **224**. The low yield is attributed to the need for multiple purifications, required to separate the unfunctionalised product **105**. A Chan-Lam reaction, using MeOH as the solvent, followed by deprotection gave methoxy-substituted intermediate **225**, with similar difficulties in removing **105**.

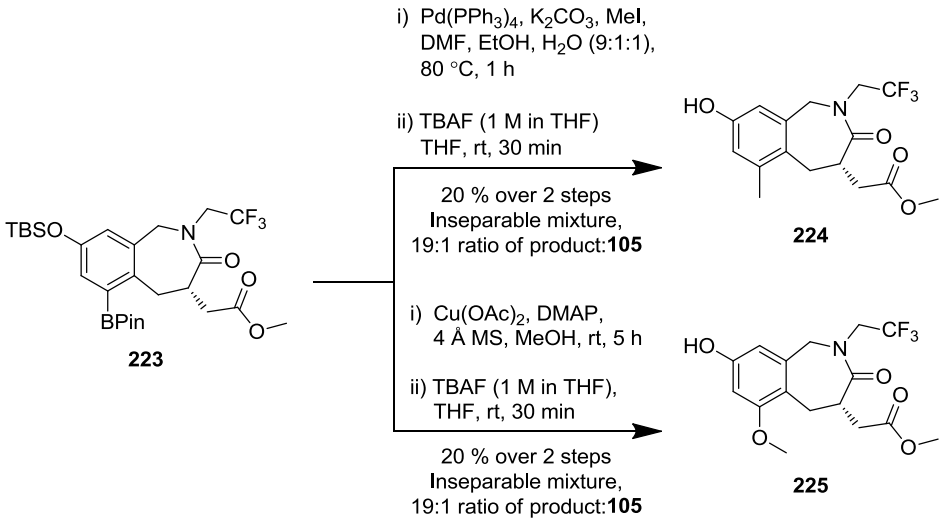

Scheme 93 The functionalisation of 223 to form 224 and 225

With these intermediates in hand, they could be elaborated to the final compounds. Inspiration was again drawn from the appendage of **67** during the synthesis of **190** (**Scheme 81**, page 188) using a Mitsunobu reaction, although, again, further optimisation was sought. It was hypothesised that utilising naphthyridine alcohol **65**, without a Boc group, would both avoid an unnecessary protecting group, but also reduce the unwanted elimination of vinyl naphthyridine, by reducing the acidity of the benzylic position of the naphthyridine alcohol. This approach was used to elaborate the final compounds, **219** and **226**, *via* methyl esters **227** and **228 (Scheme 94)**. Fortunately, after the Mitsunobu step, in both cases the final remaining unfunctionalised material could be separated from the products.

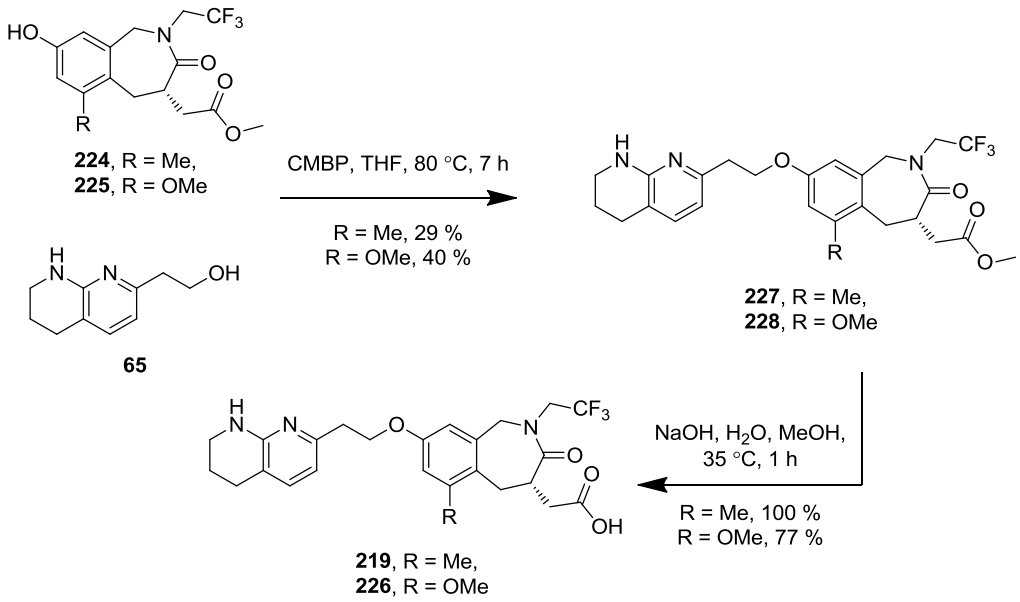

*Scheme 94 The elaboration of **224** and **225** to form **219** and **226***

Encouraged by the success of this approach, attention was turned to ethyl, chloro and cyano substitution of the aryl ring. In the case of the ethyl substitution **(Scheme 95)**, this involved a Suzuki reaction with bromoethene (during which TBS deprotection took place) to form alkene **229**, followed by reduction of the resulting alkene to form **230**.

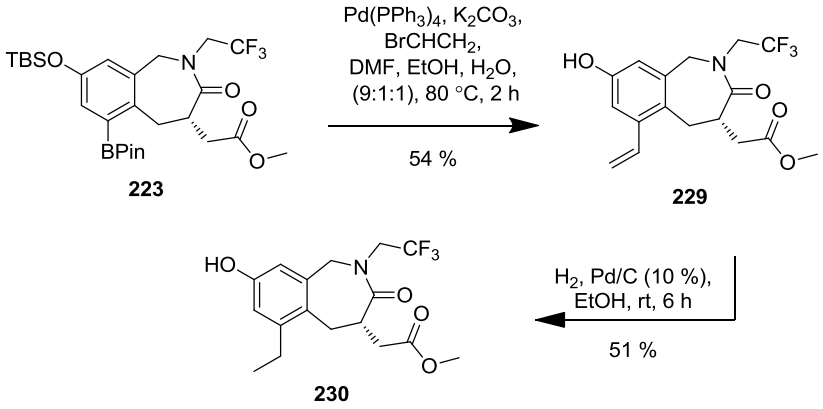

*Scheme 95 The functionalisation of **223** to form **230***

In the case of the chloro substitution, a copper-mediated chlorination was carried out, followed by TBS deprotection to form **231 (Scheme 96)**. A copper-mediated cyanation provided **232** in a very poor, but acceptable yield. This low yield meant that this compound could not be fully purified, and **232** and the following corresponding

intermediates were not fully characterised until the final compound was synthesised, in order to avoid loss of material.

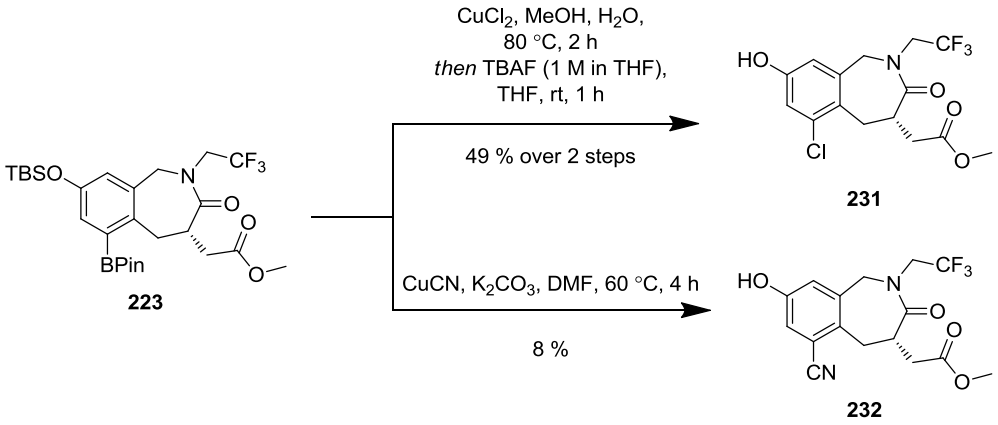

Scheme 96 *The synthesis of* ***231*** *and* ***232***

These compounds were then elaborated to the final compounds using the same approach as previously. Ethyl-substituted analogue **233** was formed *via* **234**, chloro-analogue **235** *via* methyl ester **236**, and cyano-substituted compound **237** *via* **238** **(Scheme 97)**.

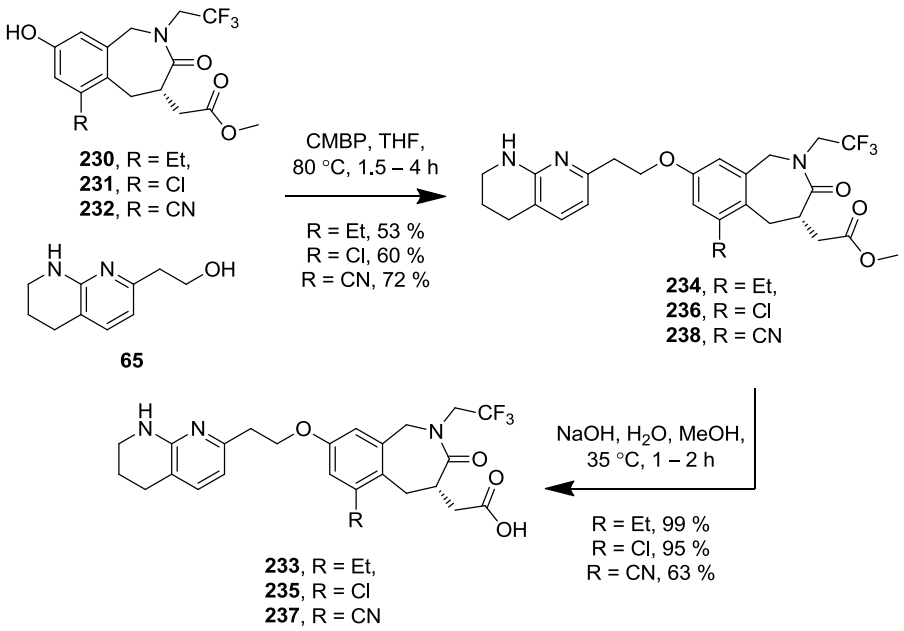

Scheme 97 *The completion of the synthesis of* ***233, 235,*** *and* ***237***

The hydroxyl-substituted target **220** required a more careful approach, as the previous approach had involved Mitsunobu reaction of the phenol to append **65**. However, since another hydroxyl group would be installed onto this arene, an appropriate protecting group strategy would be required to ensure differentiability between the positions. Initially, borylated intermediate **223** was oxidised using oxone, in the same way as had been carried out for the synthesis of pyridyl analogue **190** *via* compound **192** (**Scheme 78**, page 185). This was successful in furnishing the product, but it was not then possible to protect the resulting hydroxyl group with a PMB group in the presence of the other TBS protected phenol, so another approach was sought.

As an alternative, a Chan-Lam reaction was carried out on the borylated product **223** using PMB alcohol **(Scheme 98)**. To the author's knowledge, no such transformation has been previously reported. Whilst conversion to the desired product was observed, separation of the product from the PMB alcohol, which had to be used as the reaction solvent to improve conversion, was very challenging. A combination of triturations and several chromatographic purifications were necessary to obtain **239**. Subsequent TBS deprotection and Mitsunobu reaction with **65** gave straightforward access to **240**, then to **241**. Having performed the Mitsunobu reaction, the newly-installed hydroxyl group could be reductively deprotected to form **242**, followed by hydrolysis to form **220**.

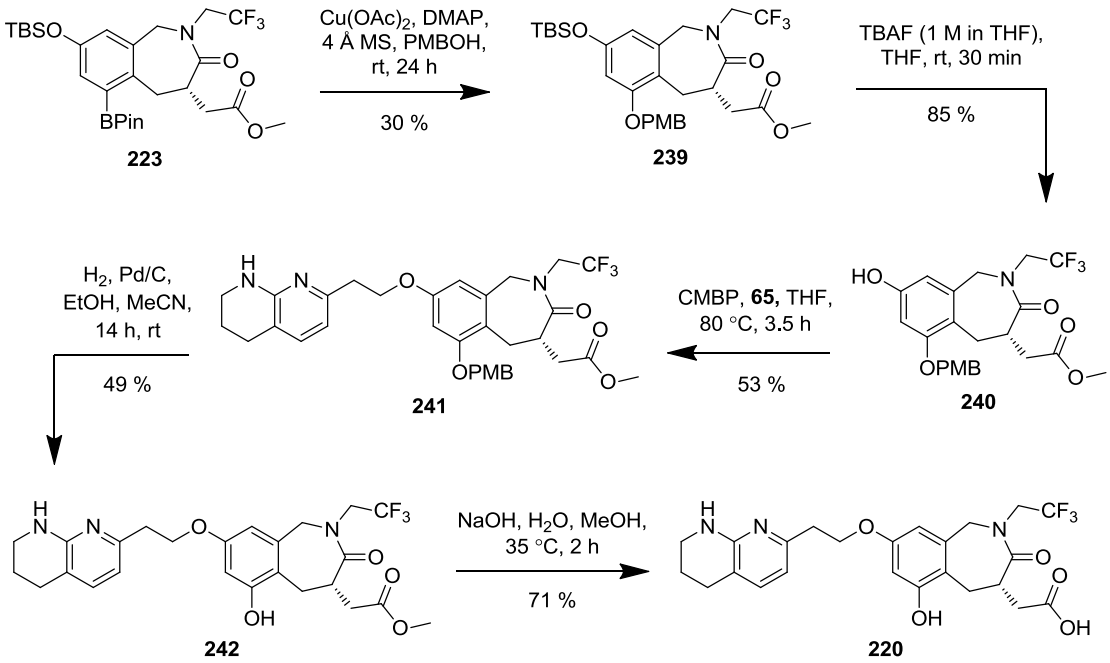

Scheme 98 *The synthesis of hydroxyl-substituted analogue* ***220****, via a Chan-Lam coupling and subsequent orthogonal deprotections*

The principal intention of this approach had been the functionalisation of the ring *meta* to the ether linkage, but, since borylation of unprotected azepine **105** had led to unwanted regioisomer **222** (**Scheme 91**, page 202), this intermediate was also elaborated into a regioisomeric *ortho*-methylated analogue **243 (Scheme 99)**. In fact, the computational modelling had suggested that substitution from this vector would not be accommodated, hence why this vector was not investigated further. The route to **243** proceeded smoothly, via a Suzuki coupling to methylate the ring, followed by the Mitsunobu reaction of **244**, followed by the hydrolysis of **245** to give the final product **243**. Of note, however, was the unexpected isolation of phenyl-substituted side product **246** during the Suzuki reaction.

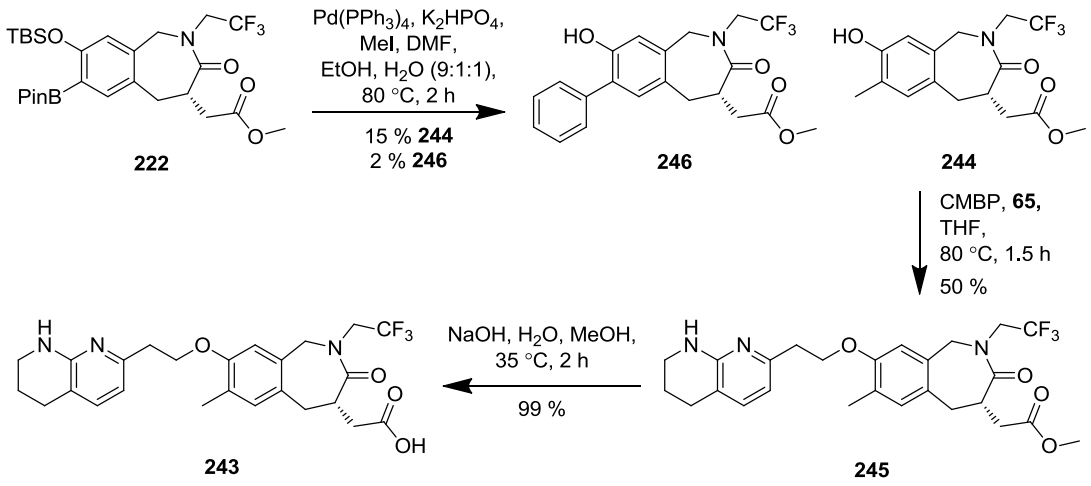

Scheme 99 *The synthesis of ortho-methylated analogue* ***243****, during which phenylated analogue* ***246*** *was unexpectedly isolated.*

The formation of **246** must arise from the cross-coupling of one of the phenyl groups on the triphenylphosphine ligand, *via* C-P bond cleavage. There are many examples of the identification of such side products during palladium-catalysed cross-coupling reactions, but few examples of its use synthetically.[236]

Having prepared these analogues, their potency in the integrin assays was measured **(Table 33)**. Unfortunately, the work on α_V integrins within our laboratories was drawing to an end at this stage of the project, so these assays had a reduced throughput. This meant that *ortho*-substituted analogue **243** was not tested, and only two of this group of analogues had their potency tested in the $\alpha_V\beta_3$ assay. However, since the compounds in this series have all had similar $\alpha_V\beta_3$ and $\alpha_V\beta_5$ potency to one another (exemplified by **235** and **220**), the selectivity can be in inferred from the $\alpha_V\beta_5$ potency.

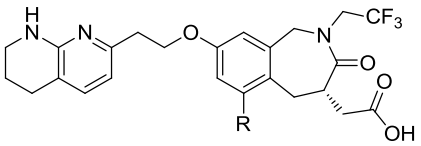	Me	Cl	Et	OH	OMe	CN
Compound number	**219**	**235**	**233**	**220**	**226**	**237**
$\alpha_V\beta_1$ pIC_{50}	6.6 (n = 2)	7.1 (n = 2)	6.4 (n = 2)	7.6 (n = 2)	6.5 (n = 2)	5.4 (n = 2)
$\alpha_V\beta_3$ pIC_{50}	-	8.4 (n = 1)	-	8.7 (n = 1)	-	-
$\alpha_V\beta_5$ pIC_{50}	8.5 (n =2)	8.4 (n = 2)	8.3 (n = 2)	8.7 (n = 2)	8.4 (n = 2)	7.9 (n = 2)
$\alpha_V\beta_6$ pIC_{50}	< 6 (n = 1)	-	-	-	< 6 (n = 1)	-
ChromlogD	2.84	3.09	3.15	2.28	2.82	2.76

Table 33 *The integrin potency data for the analogues substituted meta to the phenol in the aryl core of the compound. This vector was not successful in obtaining selectivity for $\alpha_V\beta_1$*

Unfortunately, this vector was, again, unproductive with regards to gaining selectivity over the other integrins. In all cases the $\alpha_V\beta_1$ integrin potency was lower than the lead compounds **107** and **108**, with hydroxyl-substituted analogue **220** the most potent of the substitutions made. In the homology model, a hydrogen bonding interaction had been indicated between the hydroxyl hydrogen and the protein backbone, which may have formed and may explain the increased potency of **220** compared to the other substitutions, which were not well tolerated sterically but could not form this interaction to compensate. Additionally, of the proposed substitutions, the docking model indicated that the cyano group **(237)** would be the least well tolerated, and this was indeed found to be the case. These results, again, indicate that it appears that the affinity for the $\alpha_V\beta_1$ integrin is more sensitive to changes than the $\alpha_V\beta_3$ and $\alpha_V\beta_5$ integrins. Indeed, compound **220** is one of the most potent inhibitors of $\alpha_V\beta_3$ and $\alpha_V\beta_5$ that has been synthesised within our laboratories.

Therefore, it is possible to rationalise some of the differences in potency between these compounds using the homology model, but again, using this model has not

been successful as a means of prospectively designing compounds with high potency for the $\alpha_V\beta_1$ integrin.

3.7 Conclusions and future work

3.7.1 General conclusions

The aim of this project was to further optimise the lead compounds **107** and **108** to further improve the potency at $\alpha_V\beta_1$ and gain selectivity over the other RGD integrins, in particular $\alpha_V\beta_3$ and $\alpha_V\beta_5$. In the process, it was intended that the compound might be moved into chemical space outside of that previously exemplified in the existing patent literature, whilst retaining enough similarity to the original compounds to maintain the promising PK properties of these compounds, which had profiles approaching that required for an oral drug.

Two main strategies for obtaining chemical originality and seeking improved potency were to explore a carbon atom linker between the alkyl chain linking the two ends of the compound, and to insert heterocyclic aromatics in the core of the molecule.

Initially, both these changes were made at once, with the synthesis of thiophenes **133** and **146 (Figure 110)**. Despite being synthetically demanding to make, these compounds were both significantly less potent than the lead compound at $\alpha_V\beta_1$, although **146** showed improved potency compared with **133**, due to the improved vector offered by the larger sulfur atom being at the specific position shown in the ring. Attempts to improve the potency by increasing the length of the carbon chain (with compound **160**) were unsuccessful. These potency values were rationalised by docking the compounds into the computational model, which was at the time of the

synthesis of these compounds not in use for the prediction of the potency of the compounds.

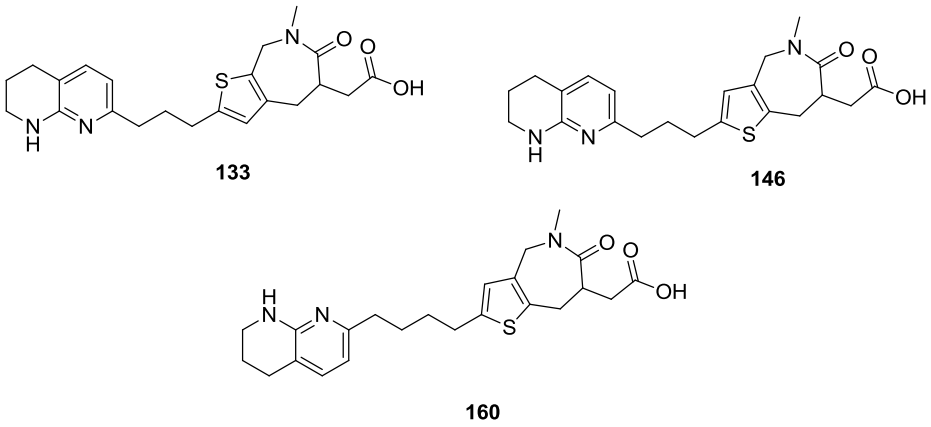

Figure 110 *Carbon linked thiophene analogues, which suffer from significantly reduced potency at* $\alpha_V\beta_1$

In order to delineate whether the loss of potency was as a result of the linker atom or of the heterocycle, compounds **173** and **174 (Figure 111)** were then synthesised. Pleasingly, thiophene **173** was equipotent with the lead compounds **107** and **108**, although subsequent retesting of the compound potency cast doubt over the original potency measurement. This is expected to be the result of compound instability in solution, though this could not be confirmed. As anticipated, **174** had a reduced potency, clarifying the importance of the oxygen atom in the linker, to allow the chain to lie flat with respect to the ring.

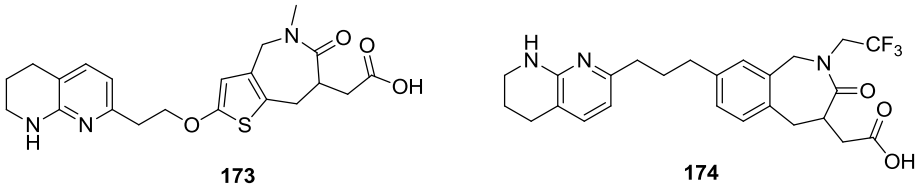

Figure 111 *Oxygen linked thiophene analogue* ***173*** *and all carbon analogue* ***174***

These observations were rationalised by the docking of these compounds into the homology model. During previous work carried out in our laboratories, pyridyl analogues **112** and **113** were synthesised **(Figure 112)**.[207] Compound **113** was found to maintain potency, whereas **112** was found to lose activity. This was also

rationalised using the docking model, where it appears that the presence of the nitrogen atom in this position leads to the preferred conformation of the alkyl chain no longer being flat, raising the energy of this conformation.

In light of the increased confidence in the docking model to explain the observed activity of the compounds, the third pyridyl regioisomer **190** was accessed, on the basis that it appeared to dock consistently with the lead compound in the homology model. Additionally, it appeared that its position of the nitrogen might result in some selectivity over $\alpha_V\beta_3$. Unfortunately, however, this was found not to be the case, and this compound had reduced potency at $\alpha_V\beta_1$, but not at $\alpha_V\beta_3$ or $\alpha_V\beta_5$.

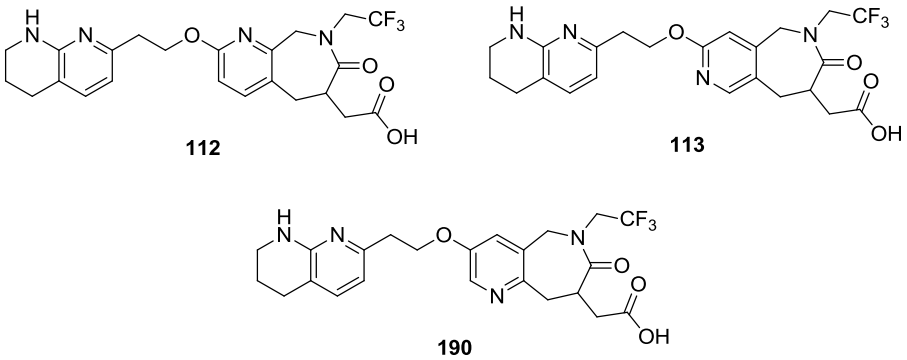

Figure 112 *Three analogues with a pyridine atom in the core of the molecule.* ***113*** *retained the same potency as the lead, whereas* ***112*** *and* ***190*** *lost potency.*

In summary, this part of the work has shown that it is possible to include a heteroatom in the core of the compound whilst still maintaining the potency of the compound (in the cases of compounds **113** and **173**). This means that the series may be taken into chemical space beyond that currently exemplified in the patent literature, although this approach does not appear to be a means of obtaining selectivity for $\alpha_V\beta_1$. It also means that there are several possible starting points for the core of the compound, with varying available vectors and variable lipophilicity of the aromatic cores. It has also been shown that a carbon atom linking the alkyl chain to the aromatic core is not tolerated, as it appears to prevent a flat, all *trans* conformation of the linker chain, relative to the aromatic core.

Seeking, again, to use the homology model in a predictive fashion to generate hypotheses to test in structure-based drug design, the receptor was examined for means to obtain selectivity for $\alpha_V\beta_1$. Firstly, it was hypothesised that a small substitution next to the carboxylate group in the molecule could occupy a pocket that is larger in the $\alpha_V\beta_1$ active site than in the $\alpha_V\beta_3$ active site. In order to test this theory, original candidate **97** was functionalised directly, to avoid lengthy syntheses, leading to a range of analogues shown in **Figure 113, left**.

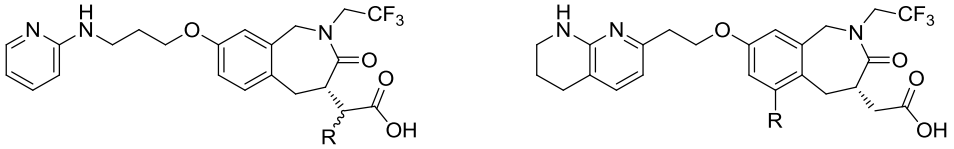

Figure 113 *Left, analogues of compound **97**, functionalised α to the acid group. Right, analogues of **107**, functionalised on the aryl core*

These compounds were prepared *via* the enolate alkylation or hydroxylation of a protected form of **97**, giving access to a group of single enantiomers which had both polar and apolar functionality incorporated in this position. Unfortunately, when these compounds were tested, substitution in this position was not tolerated.

A second group of substitutions were made, as the homology model and crystal structure appeared to reveal additional space in the $\alpha_V\beta_1$ binding pocket, *meta* to the phenol oxygen atom, compared to in the $\alpha_V\beta_3$ crystal structure. As an advancement over the preparation of the substituted analogues described above, which were analogues of aminopyridine-containing **97**, this time the analogues of tetrahydronaphthyridine-containing lead compound **107** were accessed **(Figure 113, right)**.

Synthetically, these were accessed *via* the BBr_3-incuded cleavage of the ether linkage in **97**, followed by hydroxyl group protection and C-H activation of the aryl ring (to the corresponding boronic ester), subsequent functionalisation to add the substituent, then Mitsunobu reaction to reappend the α_V-binding group. This

approach, *via* the versatile boronic ester functionality, allowed for a broad range of substituents to be added in order to investigate the relevant space.

Disappointingly, however, thorough exploration of this vector was also unproductive with regards to obtaining selectivity for $\alpha_V\beta_1$. In fact, these compounds retained their potency at $\alpha_V\beta_3$ and, where measured, $\alpha_V\beta_5$, and showed reduced potency at $\alpha_V\beta_1$. These compounds (especially hydroxyl-substituted analogue **220**) were extremely potent at $\alpha_V\beta_3$ and $\alpha_V\beta_5$ and, therefore, at the very least, represent potentially useful elaborations of the lead compounds **107** and **108**, should this compound be of further interest for targeting $\alpha_V\beta_3$ or $\alpha_V\beta_5$, although that was not the intention within this work.

In overall summary, therefore, of the SAR analysis of the series, a small group of aryl core substitutions were tolerated with regards to $\alpha_V\beta_1$ potency, but the oxygen linker atom was required for potency, and length changes to the linking chain were not tolerated. With regards to obtaining selectivity, changes to the amide alkyl group (investigated prior to this project) did not affect the selectivity of the compounds,[206] whilst substitutions α to the carboxylic acid were more detrimental to $\alpha_V\beta_1$ potency than $\alpha_V\beta_3$, likewise for substitutions made to the aryl ring of the compound.

Although the profiles of the compounds that were synthesised were disappointing, this project has led to the development of synthetic routes to thioazepine cores which are thought to be pharmaceutically valuable, and highly challenging to access.[237] Furthermore, a route to the challenging three carbon linkage between the aryl core and tetrahydronaphthyridine group has been established, which could be significant for other researchers targeting other integrins.

Additionally, late-stage functionalisation of analogues **97** and **107**, using both traditional enolate chemistry and more recently developed C-H borylation methodology, has provided rapid access to a wide range of substitutions on these compounds. This has resulted in the efficient investigation of the effect of these

changes on the profile of the compounds, which were obtained as single stereoisomers without the requirement for chiral separation.

3.7.2 Assessment of the use of the $\alpha_V\beta_1$ homology model

During the synthesis of several analogues with differing aromatic cores and linker atoms to the alkyl chain connecting the α_V-binding group, these compounds were docked into the homology model. Broadly speaking, the potencies of these compounds were rationalised by the similarity of the docked conformations to the binding poses of the lead compounds. As outlined above, this included the improved vector for thiophene isomer **146** (**Figure 88**, page 165) compared to isomer **133** (**Figure 86**, page 160), and rationalisation of the reduced potency of pyridyl analogue **112** and carbon-linked analogue **174** by considering the dihedral angle of the bonds from aromatic core to the alkyl chain (**Figure 82**, page 142 and **Figure 95**, page 181), which were sub-optimally oriented.

Having found the potency of these compounds, broadly speaking, to be rationalised by their docked conformations, it was envisaged that the model could be used prospectively, for the design of new compounds prior to their synthesis. This enabled hypotheses to be generated based on the conformations that the compounds docked with, both into the $\alpha_V\beta_1$ homology model, and into the $\alpha_V\beta_3$ crystal structure. This approach was used in an attempt to design selective compounds, by comparing the active site of the $\alpha_V\beta_1$ homology model and the $\alpha_V\beta_3$ crystal structure. This led to two promising vectors on the compounds for exploration. However, unfortunately, despite the docked conformations indicating that the substitutions on these vectors would be better accommodated in $\alpha_V\beta_1$ than $\alpha_V\beta_3$, these hypotheses were not borne out by experiment, and, more specifically, the compounds lacked the desired selectivity, and had reduced $\alpha_V\beta_1$ potency.

Clearly, whilst this model could be used to rationalise measured potency, a greater robustness is required to allow its use predictively and, in this regard, this model has fallen short. At this point, therefore, it is pertinent to consider the reason for such limitations in applicability.

Clearly, the absence of a crystal structure for $\alpha_V\beta_1$ and, therefore, the requirement for the use of a homology model, demands the assumption that the shape of the individual sides of the integrin binding pocket in different integrins (for example, that the shape of the α_V side in $\alpha_V\beta_1$ and $\alpha_V\beta_3$) is highly conserved. The fact that this approach has been used for other $\alpha_V\beta_1$ small molecule drug discovery programmes does, however, give credibility to this approach.[57]

The drawback to relying on a crystal structure in general is that, clearly, a crystal structure is a single, stationary snapshot of a dynamic system, which is averaged across the unit cells. Additionally, proteins change shape according to the ligand which is bound, so if the crystal structure was generated with, for example, a peptide within the binding site (as was the case for the $\alpha_V\beta_3$ crystal structure),[44] it may not represent the shape of the actual binding site when a non-peptidic small molecule is bound.

These differences between crystal structures is clearly demonstrated by the difference in the $\alpha_V\beta_1$ homology model created using different crystal structures. Another homology model was created by co-worker Pal within our laboratories,[238] using the α_V portion of the $\alpha_V\beta_6$ crystal structure generated with compound **1** bound (**Figure 6**, page 7), and another published crystal structure for the $\alpha_5\beta_1$ integrin (accessed from the Protein Data Bank, ID: 4WK4) to that used in the previous homology model for the β_1 portion.[45] When compound **107** was docked into this homology model **(Figure 114)**, the receptor was slightly shorter than in the previous $\alpha_V\beta_1$ homology model. The alkyl chain is still able to lie flat with respect to the aryl core, but this reduced length is expected to affect how other compounds dock into this model.

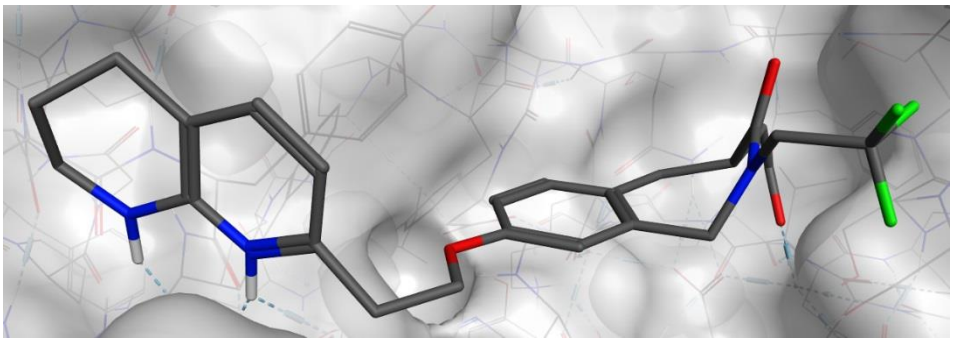

Figure 114 *Compound* ***107*** *docked into the alternative $\alpha_V\beta_1$ homology model, where the receptor is noticeably shorter*

Furthermore, when the pocket of this alternative $\alpha_V\beta_1$ homology model is examined further, it is evident that the additional space previously thought to be available for substitution *meta* to the oxygen on the aryl core is not present in this model, shown by the red circle in the alternative view of the docked conformation of **107 (Figure 115)**.

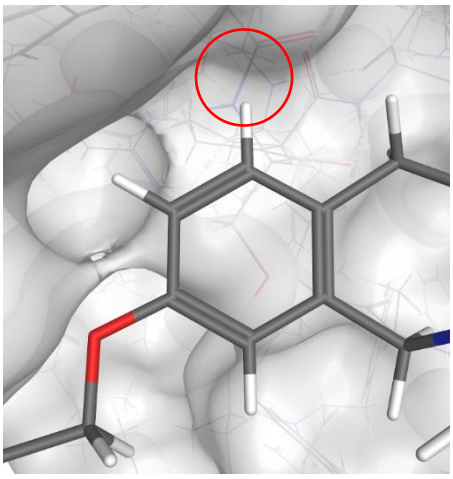

Figure 115 *Compound* ***107*** *docked into the alternative $\alpha_V\beta_1$ homology model (showing only the core), where no space for substitution is apparent meta to the phenolic oxygen, shown by the red circle*

Clearly, this observation sheds light on the disappointing potency values measured for the compounds with substitutions in this position (**Table 33**, page 210), and indeed, had this model been used for the generation of hypotheses in the structure-based design, this vector is unlikely to have been chosen as one by which to obtain selectivity.

This example is a clear demonstration of the disadvantages of using docking studies such as these with the expectation of being led directly to potent or selective compounds. However, the model did broadly indicate which parts of the molecule might be varied as a means of gaining selectivity, by showing which parts of the compound were solvent exposed, and which parts were deep within the pocket. A possible alternative means of determining the stability of the ligands in the receptor would be the use of molecular dynamics simulations, to determine whether the docked poses found were indeed preferred conformations within the binding site.

These simulations have the advantage of considering the receptor as flexible, and are able to indicate, by a real-time visualisation, whether the compound is stable when bound.[239] However, such calculations come at a dramatically increased level of computational complexity and resource-intensity, and so such calculations were beyond the scope of this study.

Throughout this work, whenever the potency of newly synthesised compounds has been compared with lead compounds **107** and **108**, the $\alpha_V\beta_1$ potency of the compounds has always been more markedly reduced in comparison with $\alpha_V\beta_3$ and $\alpha_V\beta_5$. This suggests that the $\alpha_V\beta_1$ integrin may have a more rigid pocket, which is less able to accommodate a range of different ligands, compared with $\alpha_V\beta_3$ and $\alpha_V\beta_5$. Having investigated a range of vectors on the compound to obtain selectivity, it appears that this series of compounds may not lead to a selective $\alpha_V\beta_1$ inhibitor. If this is the case, then clearly the homology model could not have been successful in the achieving the aim for which it was being employed. Accordingly, this does not indicate a short falling of the homology model, rather this provides an indication of the challenge associated with this project.

Since only one highly selective $\alpha_V\beta_1$ selective antagonist has been published (**3**, page 10), clearly developing such compounds is not trivial. Although another series of $\alpha_V\beta_1$ selective compounds has been developed within our laboratories, of which compound **109** (page 135) is a representative, it is noteworthy that both compounds

3 and **109** appear to derive their selectivity from occupation of the SDL (**Figure 76**, page 135, and **Figure 78**, page 136). The series presented herein had the additional challenge of seeking selectivity without use of this part of the receptor, and this work may be an indication that filling the SDL is a requirement for an $\alpha_V\beta_1$ selective compound. The series investigated herein held much promise for leading to the first orally bioavailable, $\alpha_V\beta_1$ selective integrin antagonist but, unfortunately, that prize remains elusive at present.

3.7.3 Future work

As described above it does not seem likely that this series could be used to develop an $\alpha_V\beta_1$ selective compound, but the incorporation of heteroatoms into the core of the compound, in order to move away from cores already described within the patent literature, was more successful. If this series was to be used as an inhibitor of $\alpha_V\beta_1$, $\alpha_V\beta_3$, and $\alpha_V\beta_5$ unselectively (or even still as an $\alpha_V\beta_3$, and $\alpha_V\beta_5$ antagonist) in the future, then these novel cores are still of significant value, even though selectivity was not obtained. Should further investigation of core changes to the compound be of interest, one such compound of interest would be thiazole **247 (Figure 116)**, a final substitution pattern that is of interest because if more polarity in the core is tolerated, it may lead to a reduction in lipophilicity without a loss of potency, which is an attractive starting point for balancing the properties of the final compound, should more lipophilic groups be incorporated elsewhere on the compound.

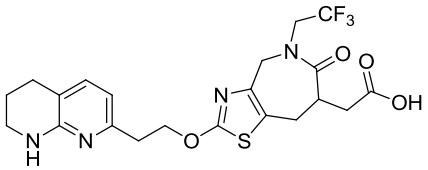

247

*Figure 116 Thiazole analogue **247***

When this compound was docked into the homology model **(Figure 117)**, it was found to overlay well with lead compound **108** (in blue in **Figure 117**), in the same way as potent oxygen-linked thiophene compound **173**. Therefore, this compound is expected to also maintain potency.

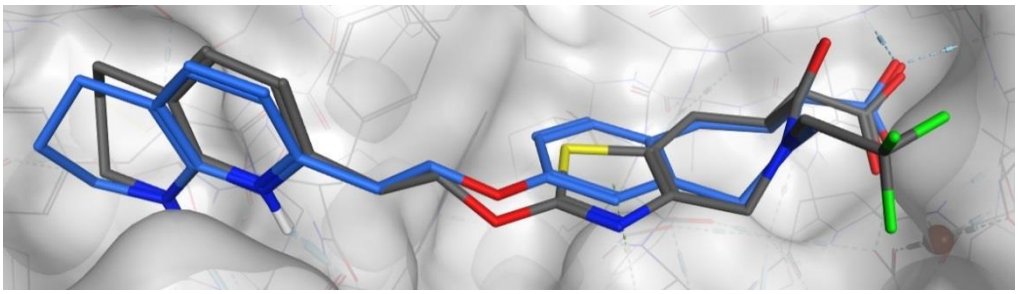

Figure 117 *Thiazole analogue* ***247*** *docked into the homology model (in grey), overlaid with lead compound* ***108*** *(in blue)*

If thiazole **247** was to be accessed, it would first be important to establish whether the variable measured potency of oxygen-linked thiophene **173** was, as anticipated, the result of degradation of the solution before retest. It is important to confirm the potency of thiophene **173** before **247** is synthesised, since the promise of compound **247** is largely based on its similarity to the previously synthesised thiophene **173**. Although the latter part of this project had shown that selectivity for $\alpha_V\beta_1$ could not be designed using the homology model in a prospective sense, the potency of the core changes made earlier in the project had largely matched the docked conformations, hence why the model has been used here to suggest that thiazole **247** may be active.

With regards to future work more broadly, the learnings from this project can be of value to other work towards a selective $\alpha_V\beta_1$ integrin antagonist. Firstly, the limitations of use of the $\alpha_V\beta_1$ homology model are clear, and the requirement for a published crystal structure for $\alpha_V\beta_1$ is plainer than ever. More importantly, perhaps, is the conclusion from this work that filling the SDL part of the active site is crucially important, should selectivity for $\alpha_V\beta_1$ be desired. Future work on this target should, therefore, include significant efforts to fill this part of the receptor efficiently. The

challenge remains to create an antagonist with the appropriate functionality to both bind to the RGD-recognising groups and fill the SDL loop, whilst preserving the balance of lipophilicity required to possess oral bioavailability, thereby maximising the use of the compound *in vivo*.

Chapter 4: Experimental

4.1 General experimental procedures

Unless otherwise stated, all other chemicals were used as received, all solutions used during work-ups were saturated and aqueous, and all reactions were carried out at room temperature (rt). All reactions were followed by LCMS or thin layer chromatography (TLC).

4.2 General analytical procedures

TLC was carried out on Merck Kieselgel 60 F_{254} plates which were visualised using ultraviolet light (254 nm). Flash column chromatography was conducted with Teledyne ISCO Combi*Flash*® R*f+* apparatus with Redi*Sep*® R*f* silica or Biotage KP-C18-HS cartridges, and the solvents are reported as vol:vol mixtures. Fourier transform infrared (IR) spectroscopy was performed using a Perkin-Elmer Spectrum-Two spectrometer. Maximum absorbance wavelengths (ν_{max}) are reported as reciprocal centimetres (cm^{-1}). High resolution mass spectrometry (HRMS) data was recorded using electrospray ionisation (ESI) techniques, and the parent ion is quoted unless otherwise stated. Melting points were measured using a BUCHI Melting Point M-565 machine, and optical rotations were measured using a JASCO P-1030 polarimeter, at ambient temperatures and using a sodium lamp, measuring the rotation of the sodium D line at a wavelength of 589 nm. ^{1}H nuclear magnetic resonance (NMR) spectroscopy was carried out on a Bruker-AV400 MHz, a Brucker AVANCE II 600 MHz, or an AVANCE 111 700 MHz machine at ambient temperature (unless otherwise stated), using an internal deuterium lock. ^{1}H NMR data are presented as: chemical

shift δ (in ppm, relative to the residual solvent peak (δ_H= 7.26 ppm in $CDCl_3$, 2.50 ppm in DMSO-d_6, 3.31 ppm in CD_3OD),[240] proton integration, multiplicity (s = singlet, d = doublet, t = triplet, q = quartet, quint = quintet, m = multiplet, r = broad, app = apparent), coupling constants (*J* in Hz), and assignment to the structure. Signals are assigned according to the numbering scheme presented on the structure itself, which is arbitrarily chosen and is not related to the numbering used in the IUPAC title name given to each compound. Assignments have been made using the 1D data presented, using COSY, HMBC and HSQC experiments, or by analogy with interpreted spectral data for similar compounds. Proton decoupled ^{13}C NMR were also recorded on a Bruker-AV400 (at 101 MHz), a Brucker AVANCE II 600 (at 151 MHz), or an AVANCE 111 700 (at 176 MHz) machine using an internal deuterium lock at ambient temperatures. ^{13}C NMR spectra are presented as a chemical shift in ppm relative to the residual solvent peak (δ_C= 77.16 ppm in $CDCl_3$, 39.52 ppm in DMSO-d_6, 49.00 ppm in CD_3OD),[240] and if necessary, the number of carbon atoms at that shift, the multiplicity and coupling constant. In the case of some broadened peaks, the HSQC or HMBC spectrum was required to identify the carbon shift, and these shifts are indicated by an asterisk (*) after the shift. ^{15}N NMR were measured on a Brucker AVANCE II machine at 60.8 MHz, measured relative to the shift of liquid ammonia. The ^{15}N shifts were obtained from the H-^{15}N HMBC spectra. ^{19}F NMR spectra were measured on a Bruker AV400 machine at 376 MHz, relative to the frequency generation of the machine.

LCMS analysis was conducted using an Acquity UPLC BEH or CSH C18 column (2.1 mm × 50 mm i.d. 1.7 µm packing diameter) using two different systems:

System A: Conducted by eluting with 0.1 % formic acid in H_2O (solvent A), and 0.1 % formic acid in MeCN (solvent B), with the following elution gradient for BEH column: 0.0–1.5 min 1–97 % B, 1.5–1.9 min 97 % B, 1.9–2.0 min 97–1 % B, and for CSH column: 0.0–1.5 min 3–100 % B, 1.5–1.9 min 100 % B, 1.9–2.0 min 100–3 % B, at a flow rate of 1 mL min^{-1} at 40 °C.

System B: Conducted by eluting with 10 mM ammonium bicarbonate in H_2O adjusted to pH 10 using aqueous ammonia (solvent A), and MeCN (solvent B), with the following elution gradient for BEH column: 0.0–1.5 min 1–97 % B, 1.5–1.9 min 97 % B, 1.9–2.0 min 97–1 % B, and for CSH column: 0.0–1.5 min 3–95 % B, 1.5–1.9 min 95 % B, 1.9–2.0 min 95–3 % B, at a flow rate of 1 mL min^{-1} at 40 °C.

For both methods, the UV detection was based on a signal averaged from wavelengths of 210 nm to 350 nm, and mass spectra were recorded on a mass spectrometer with alternate-scan electrospray positive and negative mode ionisation (ES+ve and ES−ve).

Mass-directed auto-preparative HPLC (MDAP) was conducted on an Xbridge Prep RP18 OBD™ column (100 mm × 30 mm i.d. 5 µm packing diameter), eluting with 10 mM ammonium bicarbonate in H_2O adjusted to pH 10 with an ammonium carbonate modifier (solvent A) and MeCN (solvent B), using an appropriate elution gradient over 25 min at a flow rate of 40 mL min^{-1} and detecting at 210–350 nm at rt. The mass spectra were also recorded on a mass spectrometer with alternate-scan electrospray positive and negative mode ionisation (ES+ve and ES−ve).

4.3 Chapter 2 experimental details

4.3.1 Synthetic experimental details

Ethyl 4-(1,8-naphthyridin-2-yl)butanoate (25)

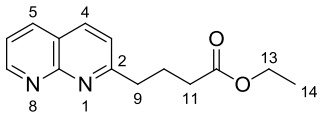

To a solution of ethyl 5-oxohexanoate **(27)** (5.00 mL, 31.3 mmol) in EtOH (150 mL) was added sulfuric acid (0.083 mL, 1.563 mmol), pyrrolidine (2.87 mL, 34.4 mmol)

and 2-aminonicotinaldehyde **(26)** (4.58 g, 37.5 mmol), and the reaction was heated under reflux for 24 h, before the orange coloured solution was cooled to rt and the solvent was removed *in vacuo.* The crude product was purified using a 120 g silica column, eluting with 80 – 95 % EtOAc:cyclohexane, and the desired fractions were combined and concentrated *in vacuo* to furnish ethyl 4-(1,8-naphthyridin-2-yl)butanoate **(25)** (6.30 g, 25.8 mmol, 83 % yield) as a pale yellow coloured solid. Also formed was side-product ethyl 3-(2-methyl-1,8-naphthyridin-3-yl)propanoate **(31)**, which was not isolated on this occasion, but had previously been collected as an orange coloured solid and characterised (an alternative synthesis and characterisation is detailed later).

LCMS t_R = 0.81 min (system B), 97 %, ES+ve *m/z* 245 $(M + H)^+$; **^{1}H NMR** (400 MHz, $CDCl_3$): δ = 9.01 (1H, dd, *J* = 4.2, 2.0 Hz, H_7), 8.09 (1H, dd, *J* = 8.1, 2.0 Hz, H_5), 8.04 (1H, d, *J* = 8.1 Hz, H_4), 7.37 (1H, dd, *J* = 8.1, 4.2 Hz, H_6), 7.33 (1H, d, *J* = 8.3 Hz, H_3), 4.06 (2H, q, *J* = 7.2 Hz, H_{13}), 3.07 – 3.00 (2H, m, H_9), 2.38 (2H, t, *J* = 7.3 Hz, H_{11}), 2.20 (2H, quin, *J* = 7.5 Hz, H_{10}), 1.18 (3H, t, *J* = 7.2 Hz, H_{14}); **^{13}C NMR** (101 MHz, $CDCl_3$): δ = 173.3, 165.6, 156.0, 153.3, 137.1, 136.7, 122.6, 121.5, 121.1, 60.3, 38.2, 33.8, 24.3, 14.2; **IR** (neat, ν_{max} /cm^{-1}): 1725, 1611, 1269, 1180, 1157, 1129, 1034; **mp** 45 – 47 °C; **HRMS** (ESI): calc for $C_{14}H_{17}N_2O_2$ $(M + H)^+$ 245.1290, found 245.1291.

4-(1,8-Naphthyridin-2-yl)butanoic acid, lithium salt

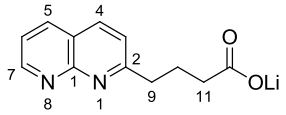

To a stirring solution of ethyl 4-(1,8-naphthyridin-2-yl)butanoate **(25)** (5.04 g, 20.63 mmol) in MeOH (30 mL) was added lithium hydroxide (2 M, 11.4 mL, 22.7 mmol) and the reaction was stirred at rt for 18 h. The solvent was removed *in vacuo* and the crude material was used directly in the preparation of **24** without further purification.

LCMS t_R = 0.41 min (system B), 100 %, ES+ve *m/z* 217 (M – Li + 2H).

N-(2-Fluoroethyl)-4-(1,8-naphthyridin-2-yl)butanamide (24)

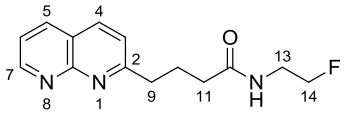

To a stirring solution of 4-(1,8-naphthyridin-2-yl)butanoic acid, lithium salt (3.60 g, 16.2 mmol) in *N*,*N*-dimethylformamide (DMF) (20 mL) was added HATU (6.78 g, 17.8 mmol), DIPEA (3.10 mL, 17.8 mmol) and 2-fluoroethylamine hydrochloride (1.77 g, 17.8 mmol). The yellow coloured reaction mixture was stirred at rt for 15 h, and then the solvent was removed *in vacuo.* The crude product was purified using a 120 g silica column in 0 – 20 % MeOH:EtOAc, and the desired fractions were combined and concentrated *in vacuo* to yield the desired product *N*-(2-fluoroethyl)-4-(1,8-naphthyridin-2-yl)butanamide **(24)** (3.14 g, 12.0 mmol, 74 % yield over 2 steps) as a light grey coloured solid.

LCMS t_R = 0.61 min (system B), 96 %, ES+ve *m/z* 262 $(M + H)^+$; **^{1}H NMR** (400 MHz, $CDCl_3$): δ = 9.09 (1H, dd, *J* = 4.2, 2.0 Hz, H_7), 8.17 (1H, dd, *J* = 8.1, 2.0 Hz, H_5), 8.12 (1H, d, *J* = 8.3 Hz, H_4), 7.46 (1H, dd, *J* = 8.1, 4.4 Hz, H_6), 7.42 (1H, d, *J* = 8.3 Hz, H_3), 6.43 (1H, br s, NH), 4.50 (2H, dt, *J* = 47.4, 4.9 Hz, H_{14}), 3.58 (2H, dq, *J* = 27.4, 5.1 Hz, H_{13}), 3.13 (2H, t, *J* = 7.3 Hz, H_9), 2.43 – 2.32 (2H, m, H_{11}), 2.31 – 2.19 (2H, m, H_{10}); **^{13}C NMR** (101 MHz, $CDCl_3$): δ = 173.3, 165.8, 155.9, 153.5, 137.4, 136.9, 122.9, 121.7, 121.3, 82.8 (d, *J* = 167.3 Hz), 40.0 (d, *J* = 19.8 Hz), 37.9, 35.6, 25.0; **IR** (neat, ν_{max} /cm^{-1}): 3312, 1664, 1524, 1496, 1413, 1241, 1022; **mp:** 104 – 107 °C; **HRMS** (ESI): calc for $C_{14}H_{17}FN_3O$ $(M + H)^+$ 262.1356, found 262.1356.

_N_-(2-Fluoroethyl)-4-(5,6,7,8-tetrahydro-1,8-naphthyridin-2-yl)butanamide (23)

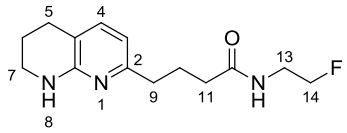

_N_-(2-Fluoroethyl)-4-(1,8-naphthyridin-2-yl)butanamide **(24)** (491 mg, 1.88 mmol) in EtOH (4.00 mL) and EtOAc (4.00 mL) was stirred over rhodium (5 wt %) on carbon (387 mg, 0.188 mmol) in the presence of hydrogen for 24 h. The reaction mixture was filtered through Celite® with EtOH:EtOAc 1:1 (50 mL) and concentrated *in vacuo,* then purified with a 40 g column in 0 – 20 % MeOH:EtOAc for 25 min, and the desired fractions combined and concentrated *in vacuo* to yield the desired product _N_-(2-fluoroethyl)-4-(5,6,7,8-tetrahydro-1,8-naphthyridin-2-yl)butanamide **(23)** (260 mg, 0.980 mmol, 52 % yield) as a white coloured solid.

LCMS t_R = 0.79 min (system B), 100 %, ES+ve *m/z* 266 $(M + H)^+$; **^{1}H NMR** (400 MHz, $CDCl_3$): δ = 7.50 (1H, br s, NH), 7.09 (1H, d, *J* = 7.1 Hz, H_4), 6.35 (1H, d, *J* = 7.3 Hz, H_3), 4.90 (1H, br s, NH), 4.54 (2H, dt, *J* = 47.4, 4.9 Hz, H_{14}), 3.61 (2H, dq, *J* = 29.6, 4.8 Hz, H_{13}), 3.44 – 3.37 (2H, m, H_9), 2.70 (2H, t, *J* = 6.1 Hz, H_7), 2.62 (2H, t, *J* = 6.9 Hz, H_5), 2.23 (2H, t, *J* = 6.9 Hz, H_{11}), 2.02 – 1.94 (2H, m, H_{10}), 1.94 – 1.87 (2H, m, H_6); **^{13}C NMR** (101 MHz, $CDCl_3$): δ = 173.6, 157.4, 155.6, 137.1, 113.7, 111.8, 83.7 (d, *J* = 165.1 Hz), 41.7, 39.8 (d, *J* = 19.8 Hz), 35.8, 35.3, 26.5, 26.4, 21.6; **IR** (neat, ν_{max} /cm^{-1}): 3300, 3264, 1648, 1606, 1550, 1442, 1324, 1039; **mp** 127 – 128 °C; **HRMS** (ESI): calc for $C_{14}H_{21}FN_3O$ $(M + H)^+$ 266.1669, found 266.1671.

2-((4-(5,6,7,8-Tetrahydro-1,8-naphthyridin-2-yl)butyl)amino)ethanol (32)

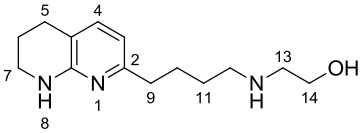

To *N*-(2-fluoroethyl)-4-(5,6,7,8-tetrahydro-1,8-naphthyridin-2-yl)butanamide **(23)** (257 mg, 0.969 mmol) in THF (7.5 mL) under an inert atmosphere at 0 °C was added lithium aluminium hydride in THF (2 M, 0.969 mL, 1.937 mmol) dropwise over 5 min. After stirring for 30 min the reaction was warmed to 60 °C and stirred for 90 min. The mixture was cooled and filtered through Celite®, washed with EtOAc (20 mL), and the filtrate concentrated *in vacuo.* The crude product was purified with a 24 g column in 0 – 50 % MeOH:EtOAc, and the desired fractions were combined and concentrated *in vacuo* to yield 2-((4-(5,6,7,8-tetrahydro-1,8-naphthyridin-2-yl)butyl)amino)ethanol **(32)** (111 mg, 0.445 mmol, 46 % yield) as a yellow coloured oil.

LCMS t_R = 0.76 min (system B), 96 %, ES+ve *m/z* 250 $(M + H)^+$; **^{1}H NMR** (400 MHz, $CDCl_3$): δ = 7.05 (1H, d, *J* = 7.3 Hz, H_4), 6.33 (1H, d, *J* = 7.3 Hz, H_3), 4.80 (1H, br s, NH), 3.62 (2H, t, *J* = 5.3 Hz, H_{14}), 3.39 (2H, t, *J* = 5.3 Hz, H_5), 2.77 – 2.72 (2H, m, H_{13}), 2.71 – 2.58 (4H, m, H_{12}, H_7), 2.56 – 2.51 (2H, m, H_9), 1.93 – 1.85 (2H, m, H_6), 1.74 – 1.65 (2H, m, H_{11}), 1.58 – 1.49 (2H, m, H_{10}), *second amine H and OH signal not observed*; **^{13}C NMR** (101 MHz, $CDCl_3$): δ = 158.4, 155.9, 136.8, 113.4, 111.4, 61.0, 51.1, 49.1, 41.8, 37.7, 29.9, 27.6, 26.5, 21.7.

_N_-(2-Fluoroethyl)-4-(5,6,7,8-tetrahydro-1,8-naphthyridin-2-yl)butan-1-amine (20)

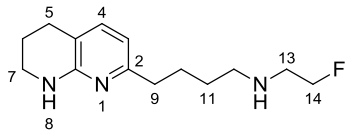

To *N*-(2-fluoroethyl)-4-(5,6,7,8-tetrahydro-1,8-naphthyridin-2-yl)butanamide **(23)** (796 mg, 3.00 mmol) in THF (15 mL) at 0 °C was added borane in THF (1 M, 15.0 mL, 15.0 mmol) dropwise over 5 min, then the solution was warmed to rt and then heated under reflux for 68 h, before cooling to rt. The reaction mixture was quenched with HCl (2 M, 15 mL), then heated to 90 °C for 10 min. The cooled solution was basified to pH 14 with NaOH (2 M) and then a portion of the solvent was removed *in vacuo*. The mixture was extracted three times with EtOAc, dried ($MgSO_4$), and concentrated

in vacuo to yield *N*-(2-fluoroethyl)-4-(5,6,7,8-tetrahydro-1,8-naphthyridin-2-yl)butan-1-amine **(20)** (662 mg, 2.63 mmol, 88 % yield) as a cloudy white coloured oil.

LCMS t_R = 0.92 min (system B), 96 %, ES+ve *m/z* 252 $(M + H)^+$; **^{1}H NMR** (400 MHz, $CDCl_3$): δ = 7.05 (1H, d, *J* = 7.3 Hz, H_4), 6.34 (1H, d, *J* = 7.3 Hz, H_3), 4.85 (1H, br s, NH), 4.52 (2H, dm, *J* = 47.4 Hz, H_{14}), 3.42 – 3.36 (2H, m, H_7), 2.89 (2H, dt, *J* = 28.1, 4.8 Hz, H_{13}), 2.71 – 2.63 (4H, m, H_5, H_9), 2.58 – 2.51 (2H, m, H_{12}), 1.94 – 1.85 (2H, m, H_6), 1.77 – 1.61 (2H, m, H_{10}), 1.59 – 1.50 (2H, m, H_{11}), *second amine H signal not observed*; **^{13}C NMR** (101 MHz, $CDCl_3$): δ = 158.4, 155.9, 136.7, 113.3, 111.5, 83.7 (d, *J* = 165.1 Hz), 49.9 (d, *J* = 19.8 Hz), 49.8, 41.8, 37.8, 30.0, 27.6, 26.5, 21.7; **IR** (neat, ν_{max} /cm^{-1}): 3254, 1599, 1587, 1481, 1462, 1389, 1321, 1120, 1028; **HRMS** (ESI): calc for $C_{14}H_{23}FN_3$ $(M + H)^+$ 252.1876, found 252.1877.

Methyl (*E*)-4-((2-fluoroethyl)(4-(5,6,7,8-tetrahydro-1,8-naphthyridin-2-yl)butyl) amino)but-2-enoate (22)

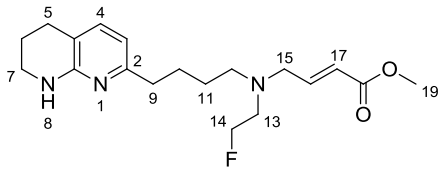

To a solution of *N*-(2-fluoroethyl)-4-(5,6,7,8-tetrahydro-1,8-naphthyridin-2-yl)butan-1-amine **(20)** (159 mg, 0.633 mmol) in CH_2Cl_2 (10 mL) was added methyl (*E*)-4-bromobut-2-enoate **(33)** (0.076 mL, 0.633 mmol) and triethylamine (0.132 mL, 0.949 mmol), and the reaction stirred for 4 h, after which a further portion of methyl (*E*)-4-bromobut-2-enoate **(33)** (0.113 mL, 0.949 mmol) and triethylamine (0.132 mL, 0.949 mmol) were added, followed by stirring for 4 h, after which a further portions of methyl (*E*)-4-bromobut-2-enoate **(33)** (0.076 mL, 0.633 mmol) and triethylamine (0.132 mL, 0.949 mmol) were added, after which the orange coloured solution was stirred for a further 12 h, after which the solution was diluted with H_2O (15 mL) and the layers were separated. The aqueous layer was extracted with CH_2Cl_2 (2 x 15 mL), and the combined organic extracts were dried and concentrated *in vacuo.* The crude

product was purified using a 30 g C18 silica column, eluting with 0 – 100 % MeCN:ammonium carbonate modified H_2O, and the desired fractions were combined and concentrated *in vacuo* to give methyl (*E*)-4-((2-fluoroethyl)(4-(5,6,7,8-tetrahydro-1,8-naphthyridin-2-yl)butyl)amino)but-2-enoate **(22)** (109 mg, 0.312 mmol, 49 % yield) as an orange coloured oil.

LCMS t_R = 1.14 min (system B), 94 %, ES+ve *m/z* 350 $(M + H)^+$; **^{1}H NMR** (400 MHz, $CDCl_3$): δ = 7.04 (1H, d, *J* = 7.1 Hz, H_4), 6.95 (1H, dt, *J* = 15.9, 6.1 Hz, H_{16}), 6.33 (1H, d, *J* = 7.1 Hz, H_3), 6.00 (1H, d, *J* = 15.9 Hz, H_{17}), 4.74 (1H, br s, NH), 4.48 (2H, dt, *J* = 47.4, 5.1 Hz, H_{14}), 3.74 (3H, s, H_{19}), 3.42 – 3.36 (2H, m, H_7), 3.29 (2H, dd, *J* = 6.0, 1.6 Hz, H_{15}), 2.76 (2H, dt, *J* = 25.7, 5.1 Hz, H_{13}), 2.68 (2H, t, *J* = 6.4 Hz, H_5), 2.56-2.49 (4H, m, H_9, H_{12}) 1.94 – 1.85 (2H, m, H_6), 1.70 – 1.60 (2H, m, H_{10}), 1.54 – 1.44 (2H, m, H_{11}); **^{13}C NMR** (101 MHz, $CDCl_3$): δ = 166.9, 158.4, 155.9, 146.6, 136.8, 122.6, 113.3, 111.5, 82.9 (d, *J* = 168.0 Hz), 55.8, 54.8, 53.9 (d, *J* = 20.5 Hz), 51.6, 41.8, 37.9, 27.6, 27.2, 26.5, 21.7; **IR** (neat, ν_{max} /cm^{-1}): 3243, 1721, 1600, 1585, 1461, 1435, 1320, 1270, 1171, 1119, 1011; **HRMS** (ESI): calc for $C_{19}H_{29}FN_3O_2$ $(M + H)^+$ 350.2244, found 350.2243.

Methyl (*S*)-4-((2-fluoroethyl)(4-(5,6,7,8-tetrahydro-1,8-naphthyridin-2-yl)butyl) amino)-3-(3-(2-methoxyethoxy)phenyl)butanoate (21)

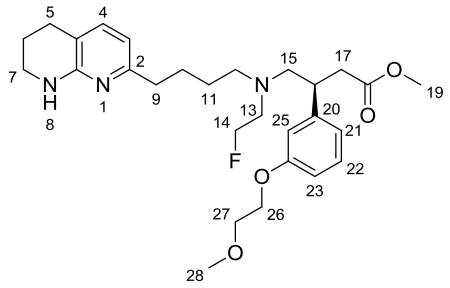

Methyl (*E*)-4-((2-fluoroethyl)(4-(5,6,7,8-tetrahydro-1,8-naphthyridin-2-yl)butyl) amino)but-2-enoate **(22)** (337 mg, 0.964 mmol) in 1,4-dioxane (6 mL) was added to 2-(3-(2-methoxyethoxy)phenyl)-4,4,5,5-tetramethyl-1,3,2-dioxaborolane **(34)** (536

mg, 1.929 mmol), (*R*)-BINAP (72.1 mg, 0.116 mmol), KOH (3.8 M in H_2O, 0.508 mL, 1.929 mmol) and chloro(1,5-cyclooctadiene)rhodium(I) dimer (23.8 mg, 0.048 mmol), and the mixture was degassed and stirred under nitrogen for 3 h at 90 °C, then cooled to rt. The resulting mixture was diluted with HCl (2 M, 10 mL) and TBME (5 mL), and the organic layer separated. The aqueous layer was basified to pH 14 with NaOH and extracted three times with EtOAc, then twice with CH_2Cl_2. The organic extracts were combined, dried ($MgSO_4$), and concentrated *in vacuo*. The crude product was purified using a 30 g C18 column in 55 – 90 % MeCN: ammonium carbonate modified H_2O, and the desired fractions were combined and concentrated *in vacuo* to yield methyl (*S*)-4-((2-fluoroethyl)(4-(5,6,7,8-tetrahydro-1,8-naphthyridin-2-yl)butyl)amino)-3-(3-(2-methoxyethoxy)phenyl)butanoate **(21)** (251 mg, 0.500 mmol, 52 % yield) as a colourless oil.

LCMS t_R = 1.35 min (system B), 100 %, ES+ve *m/z* 502 $(M + H)^+$; **^{1}H NMR** (400 MHz, $CDCl_3$): δ = 7.18 (1H, m, H_{22}), 7.05 (1H, d, *J* = 7.3 Hz, H_4), 6.80 – 6.73 (3H, m, H_{21}, H_{23}, H_{25}), 6.33 (1H, d, *J* = 7.3 Hz, H_3), 4.86 (1H, br s, NH), 4.42 (2H, dtd, *J* = 47.4, 5.4, 2.0 Hz, H_{14}), 4.12 – 4.07 (2H, m, H_{26}), 3.76 – 3.72 (2H, m, H_{27}), 3.56 (3H, s, H_{19}), 3.45 (3H, s, H_{28}), 3.42 – 3.36 (2H, m, H_7), 3.29 – 3.19 (1H, m, H_{16}), 2.91 (1H, dd, *J* = 15.7, 6.1 Hz, H_{17a}), 2.86 – 2.42 (11H, m, H_5, H_9, H_{12}, H_{13}, H_{15}, H_{17b}), 1.94 – 1.86 (2H, m, H_6), 1.61 – 1.54 (2H, m, H_{10}), 1.49 – 1.39 (2H, m, H_{11}); **^{13}C NMR** (101 MHz, $CDCl_3$): δ = 173.4, 159.0, 158.4, 155.8, 144.8, 136.8, 129.5, 120.4, 114.5, 113.3, 112.5, 111.4, 83.0 (d, *J* = 168.0 Hz), 71.2, 67.3, 61.4, 59.3, 55.1, 54.2 (d, *J* = 19.8 Hz), 51.5, 41.8, 41.1, 38.7, 37.8, 27.7, 27.0, 26.5, 21.7; **IR** (neat, ν_{max} /cm^{-1}): 3249, 1733, 1600, 1584, 1462, 1446, 1260, 1163, 1126, 1065, 1028; **HRMS** (ESI): calc for $C_{28}H_{41}FN_3O_4$ $(M + H)^+$ 502.3081, found 502.3079; **analytical chiral HPLC** (20 % EtOH:heptane (0.1 % isopropylamine), f = 1.0 mL/min, detecting at 235 nm; column 25 cm Chiralcel IA, no. OJHOCE-RK007):*ee* = 77 %, t_R = 10.36 min for major enantiomer, t_R = 11.51 min for the undesired enantiomer.

The two enantiomers were subsequently separated by chiral column chromatography, using a GF Prep 1: Agilent™ Preparative 1200 machine, a *Chiralpak IA* 250x30 mm ID column (No. IA00SA-OC001), using 20 % EtOH:heptane (0.2 % isopropylamine) at 40 ml/min, detection at 280 nM and 140 nM bandwidth to yield **21** (210 mg, 0.419 mmol, 43 % yield) as a colourless oil to >99.9 % *ee*.

$[\boldsymbol{\alpha}]_D^{20}$= +35 (*c* 1.0, MeOH).

Methyl 4-((2-fluoroethyl)(4-(5,6,7,8-tetrahydro-1,8-naphthyridin-2-yl)butyl) amino)-3-(3-(2-methoxyethoxy)phenyl)butanoate (*rac*-21)

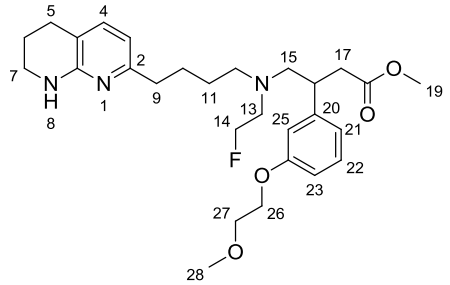

Methyl (*E*)-4-((2-fluoroethyl)(4-(5,6,7,8-tetrahydro-1,8-naphthyridin-2-yl)butyl) amino)but-2-enoate **(22)** (20 mg, 0.057 mmol) in 1,4-dioxane (1 mL) was added to 2-(3-(2-methoxyethoxy)phenyl)-4,4,5,5-tetramethyl-1,3,2-dioxaborolane **(34)** (40 mg, 0.144 mmol), (*rac*)-BINAP (7.6 mg, 0.012 mmol), KOH (3.8 M in H_2O, 0.038 mL, 0.143 mmol) and chloro(1,5-cyclooctadiene) rhodium(I) dimer (2.5 mg, 5.07 µmol), and the mixture was degassed and stirred under nitrogen for 3 at 90 °C, then cooled to rt. The reaction was diluted with HCl (2 M, 2 mL), and TBME (0.5 mL) and the organic layer separated. The aqueous layer was basified with NaOH and extracted three times with CH_2Cl_2. The organic extracts were combined, dried and concentrated *in vacuo*. The crude product was purified using the MDAP and the desired fractions were combined and concentrated *in vacuo* to yield methyl 4-((2-fluoroethyl)(4-(5,6,7,8-tetrahydro-1,8-naphthyridin-2-yl)butyl)amino)-3-(3-(2-methoxyethoxy)phenyl)butanoate **(*rac*-21)** (10.5 mg, 0.021 mmol, 37 % yield) as a yellow coloured oil.

LCMS t_R = 1.35 min (system B), 100 %, ES+ve *m/z* 502 $(M + H)^+$; **^{1}H NMR** (400 MHz, $CDCl_3$): δ =7.18 (1H, t, *J* = 7.8 Hz, H_{22}), 7.05 (1H, d, *J* = 7.3 Hz, H_4), 6.79 – 6.73 (3H, m, H_{21}, H_{23}, H_{25}), 6.33 (1H, d, *J* = 7.3 Hz, H_3), 4.78 (1H, br s, NH), 4.51 – 4.33 (2H, m, H_{14}), 4.12 – 4.07 (2H, m, H_{26}), 3.76 – 3.72 (2H, m, H_{27}), 3.56 (3H, s, H_{19}), 3.45 (3H, s, H_{28}), 3.42 – 3.36 (2H, m, H_7), 3.29 – 3.20 (1H, m, H_{16}), 2.91 (1H, dd, *J* = 15.9, 6.1 Hz, H_{17a}), 2.86 – 2.42 (11H, m, H_5, H_9, H_{12}, H_{13}, H_{15}, H_{17b}), 1.90 (2H, dt, *J* = 11.7, 5.9 Hz, H_6), 1.61 – 1.54 (2H, m, H_{10}), 1.48 – 1.39 (2H, m, H_{11}).

(*S*)-4-((2-Fluoroethyl)(4-(5,6,7,8-tetrahydro-1,8-naphthyridin-2-yl)butyl)amino)-3-(3-(2-methoxyethoxy)phenyl)butanoic acid, formic acid salt (18)

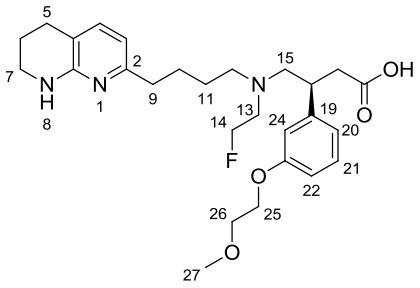

To a stirring solution of methyl (*S*)-4-((2-fluoroethyl)(4-(5,6,7,8-tetrahydro-1,8-naphthyridin-2-yl)butyl)amino)-3-(3-(2-methoxyethoxy)phenyl)butanoate **(21)** (210 mg, 0.419 mmol) in H_2O (1 mL) and 1,4-dioxane (1 mL) was added sulfuric acid (0.112 mL, 2.09 mmol) and the reaction was heated to 60 °C in a sealed tube for 68 h, after which half of the solvent was removed using a flow of nitrogen, and the solution was cooled to rt. The pH of the pale-yellow coloured solution was adjusted to 7 by the dropwise addition of NaOH (2 M). The resulting solution was purified directly using a Sunfire® Prep C18 OBD™ column in 0 – 50 % MeCN:formic acid modified H_2O, and the desired fractions were combined and concentrated *in vacuo* to furnish (*S*)-4-((2-fluoroethyl)(4-(5,6,7,8-tetrahydro-1,8-naphthyridin-2-yl)butyl)amino)-3-(3-(2-methoxyethoxy)phenyl)butanoic acid, formic acid salt **(18)** (209 mg, 0.392 mmol, 94 % yield) as a yellow coloured gum.

LCMS t_R = 0.48 min (system A), 100 %, ES+ve *m/z* 488 $(M + H)^+$; **^{1}H NMR** (400 MHz, $CDCl_3$): δ = 9.66 (1H, br s, COOH), 8.36 (1H, s, HCOOH), 7.28 (1H, m, H_4), 7.18 (1H, t, *J* = 8.1 Hz, H_{21}), 6.84 – 6.79 (2H, m, ArH), 6.79 – 6.75 (1H, m, ArH), 6.30 (1H, d, *J* = 7.3 Hz, H_3), 4.66 (1H, t, *J* = 47.4, 4.4 Hz, H_{14}), 4.10 (2H, dd, *J* = 5.4, 3.9 Hz, H_{25}), 3.72 (2H, dd, *J* = 5.4, 3.9 Hz, H_{26}), 3.47 – 3.38 (6H, m, H_7, H_{16}, H_{27}), 3.21 – 2.95 (5H, m, H_{12a}, H_{13}, H_{15}), 2.90 (1H, dd, *J* = 16.3, 9.2 Hz, H_{17a}), 2.85 – 2.76 (1H, m, H_{12b}), 2.75 – 2.62 (5H, m, H_5, H_9, H_{17b}), 1.94 – 1.84 (2H, m, H_6), 1.83 – 1.60 (4H, m, H_{10}, H_{11}), *formic acid H signal and amine H not observed*; **^{13}C NMR** (101 MHz, $CDCl_3$): δ = 175.1, 165.0, 159.3, 152.1, 149.4, 144.3, 140.3, 130.0, 120.0, 118.5, 114.1, 113.2, 109.4, 81.1 (d, *J* = 168.0 Hz, 1C), 71.2, 67.4, 61.3, 59.3, 54.0 (d, *J* = 16.2 Hz), 53.4, 42.1, 41.0, 39.1, 32.3, 26.8, 26.0, 24.8, 19.6; **IR** (neat, ν_{max} /cm^{-1}): 3238, 1657, 1122, 1087, 1057, 1033, 701, 606; **HRMS** (ESI): calc for $C_{27}H_{39}FN_3O_4$ $(M + H)^+$ 488.2925, measured 488.2927; $[\boldsymbol{\alpha}]_D^{20}$= +29 (*c* 0.5, MeCN).

In order to obtain the free base of **18** for ^{15}N NMR studies, a small portion of the formic acid salt was purified using an Xterra® Prep RP18 OBD™ column, eluting with 0 – 100 % MeCN:ammonium carbonate modified H_2O, and the desired fractions were combined and concentrated *in vacuo* to yield (*S*)-4-((2-fluoroethyl)(4-(5,6,7,8-tetrahydro-1,8-naphthyridin-2-yl)butyl)amino)-3-(3-(2-methoxyethoxy)phenyl) butanoic acid (8.3 mg, 17.0 µmol) as a colourless gum.

^{15}N NMR (60.8 MHz, $CDCl_3$): δ = 195, 83, 37.

Ethyl 4-(5,6,7,8-tetrahydro-1,8-naphthyridin-2-yl)butanoate (30)[241]

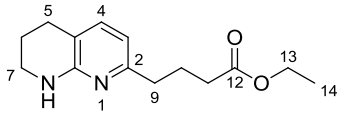

Ethyl 4-(1,8-naphthyridin-2-yl)butanoate **(25)** (0.249 g, 1.02 mmol) in MeOH (34 mL) was passed through the H-Cube® (flow H_2 generation) using a Pd/C (10 %) catalyst, at

35 °C and 5 bar H_2 pressure, at 1 mL / min, and the resulting solution was concentrated *in vacuo* to yield 4-(5,6,7,8-tetrahydro-1,8-naphthyridin-2-yl)butanoate **(30)** (247 mg, 0.995 mmol, 98 % yield) as a colourless oil.

LCMS t_R = 1.03 min (system B), 84 %, ES+ve *m/z* 249 $(M + H)^+$; **^{1}H NMR** (400 MHz, $CDCl_3$): δ = 7.04 (1H, d, *J* = 7.1 Hz, H_4), 6.34 (1H, d, *J* = 7.3 Hz, H_3), 4.89 (1H, br s, NH), 4.11 (2H, q, *J* = 7.2 Hz, H_{13}), 3.42 – 3.34 (2H, m, H_7), 2.68 (2H, t, *J* = 6.4 Hz, H_5), 2.57 (2H, t, *J* = 7.6 Hz, H_9), 2.33 (2H, t, *J* = 7.6 Hz, H_{11}), 1.99 (2H, quin, *J* = 7.5 Hz, H_{10}), 1.89 (2H, quin, *J* = 6.0 Hz, H_6), 1.24 (3H, t, *J* = 7.1 Hz, H_{14}); **^{13}C NMR** (101 MHz, $CDCl_3$): δ = 173.6, 157.3, 155.8, 136.6, 113.3, 111.4, 60.1, 41.6, 37.0, 33.9, 26.4, 24.9, 21.5, 14.2; **IR** (neat, ν_{max} /cm^{-1}): 3249, 1730, 1599, 1585, 1461, 1182, 1144; **HRMS** (ESI): calc for $C_{14}H_{21}N_2O_2$ $(M + H)^+$ 249.1603, found 249.1596.

tert-Butyl 7-(4-ethoxy-4-oxobutyl)-3,4-dihydro-1,8-naphthyridine-1(2H)-carboxylate (35)

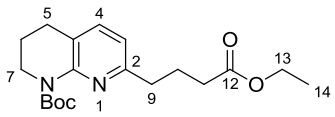

To di-*tert*-butyl dicarbonate (4.03 mL, 17.6 mmol) was added ethyl 4-(5,6,7,8-tetrahydro-1,8-naphthyridin-2-yl)butanoate **(30)** (2.18 g, 8.78 mmol) in CH_2Cl_2 (3 mL) whilst stirring, and the reaction was heated at 60 °C until the solvent had evaporated, then at 80 °C for 15 h before cooling, upon which time the mixture had turned a dark brown colour. The cooled reaction mixture was purified directly with an 80 g silica column in 0 – 50 % EtOAc:cyclohexane, and the desired fractions were combined and concentrated *in vacuo*. Mixed fractions were repurified using a 40 g silica column, eluting with 0 – 50 % EtOAc:cyclohexane, and the desired fractions were concentrated *in vacuo*, then combined with the product obtained from the first purification, to yield *tert*-butyl 7-(4-ethoxy-4-oxobutyl)-3,4-dihydro-1,8-

naphthyridine-1(2H)-carboxylate **(35)** (2.76 g, 7.92 mmol, 90 % yield) as an orange coloured oil.

LCMS t_R = 1.23 min (system B), 93 %, ES+ve *m/z* 349 $(M + H)^+$; **^{1}H NMR** (400 MHz, $CDCl_3$): δ = 7.28 (1H, d, *J* = 7.6 Hz, H_4), 6.80 (1H, d, *J* = 7.6 Hz, H_3), 4.12 (2H, q, *J* = 7.2 Hz, H_{13}), 3.77 – 3.73 (2H, m, H_7), 2.77 – 2.69 (4H, m, H_5, H_9), 2.37 (2H, t, *J* = 7.6 Hz, H_{11}), 2.07 (2H, t, *J* = 7.6 Hz, H_{10}), 1.95 – 1.88 (2H, m, H_6), 1.51 (9H, s, ^{t}Bu-H), 1.25 (3H, t, *J* = 7.1 Hz, H_{14}); **^{13}C NMR** (101 MHz, $CDCl_3$): δ = 173.7, 157.5, 154.3, 151.4, 137.3, 122.1, 118.4, 80.9, 60.3, 44.9, 37.3, 34.1, 28.6, 26.5, 24.9, 23.5, 14.4; **IR** (neat, ν_{max} /cm^{-1}): 3249 1731, 1691, 1365, 1334, 1145; **HRMS** (ESI): *molecular ion not observed*, calc for $C_{15}H_{21}N_2O_4$ $(M - {}^tBu + 2H)^+$ 293.1501, found 293.1497.

tert-Butyl 7-(4-hydroxybutyl)-3,4-dihydro-1,8-naphthyridine-1(2H)-carboxylate (36)

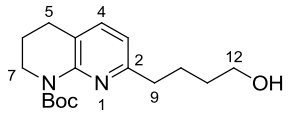

Method A: A mixture of sodium borohydride (1.71 g, 45.1 mmol) and calcium chloride (2.5 g, 22.5 mmol) in THF (50 mL) was stirred under nitrogen for 2 h. The mixture was cooled to 0 °C and *tert*-butyl 7-(4-ethoxy-4-oxobutyl)-3,4-dihydro-1,8-naphthyridine-1(2H)-carboxylate **(35)** (3.74 g, 10.7 mmol) in THF (50 mL) was added to the mixture over 5 min. The mixture was allowed to warm to rt and stirred for 24 h, before heating under reflux for a further 7 h, after which the reaction mixture was cooled to 0 °C and H_2O (150 mL) was added, followed by EtOAc (150 mL). The phases were separated, and the aqueous phase was extracted with EtOAc (150 mL). The combined organic extracts were filtered through a hydrophobic frit and were concentrated *in vacuo* to yield *tert*-butyl 7-(4-hydroxybutyl)-3,4-dihydro-1,8-naphthyridine-1(2H)-carboxylate **(36)** (3.30 g, 10.77 mmol, 100 % yield) as a pale yellow coloured oil, which was used without further purification.

LCMS t_R = 0.98 min (system B), 85 %, ES+ve *m/z* 307 $(M + H)^+$

Method B: A mixture of sodium borohydride (1.25 g, 33.1 mmol) and calcium chloride (1.84 g, 16.6 mmol) in THF (100 mL) was stirred under nitrogen for 1 h. The mixture was cooled to 0 °C and *tert*-butyl 7-(4-ethoxy-4-oxobutyl)-3,4-dihydro-1,8-naphthyridine-1(2H)-carboxylate **(35)** (2.75 g, 7.89 mmol) in THF (20 mL) was added dropwise to the mixture. The mixture was allowed to warm to rt and stirred for 16 h before heating under reflux for a further 2 h, after which the reaction mixture was cooled to 0 °C and H_2O (70 mL) was added, followed by EtOAc (100 mL). The phases were separated, and the aqueous phase was extracted with EtOAc (3 x 100 mL). The combined organic extracts were filtered through a hydrophobic frit and were concentrated *in vacuo*. The crude product was purified using a 120 g column, eluting with 0 – 100 % EtOAc-cyclohexane, and the desired fractions were combined and concentrated in vacuo to yield *tert*-butyl 7-(4-hydroxybutyl)-3,4-dihydro-1,8-naphthyridine-1(2H)-carboxylate **(36)** (1.59 g, 5.19 mmol, 66 % yield) as a pale yellow coloured oil.

LCMS t_R = 1.00 min (system B), 99 %, ES+ve *m/z* 307 $(M + H)^+$; **^{1}H NMR** (400 MHz, $CDCl_3$): δ 7.29 (1H, d, *J* = 7.6 Hz, H_4), 6.81 (1H, d, *J* = 7.6 Hz, H_3), 3.78 – 3.72 (2H, m, H_7), 3.64 (2H, t, *J* = 6.2 Hz, H_{12}), 2.77 (2H, t, *J* = 7.3 Hz, H_9), 2.72 (2H, t, *J* = 6.6 Hz, H_5), 2.20 (1H, br s, OH), 1.95 – 1.88 (2H, m, H_6), 1.88 – 1.81 (2H, m, H_{10}), 1.68 – 1.62 (2H, m, H_{11}), 1.52 (9H, s, ^{t}Bu-H); **^{13}C NMR** (101 MHz, $CDCl_3$): *δ* 158.4, 154.1, 151.2, 137.4, 122.0, 118.5, 81.1, 62.5, 45.1, 37.2, 32.3, 28.5, 26.5, 25.4, 23.4; **IR** (neat, ν_{max} /cm^{-1}): 3385 (br), 1692, 1365, 1334, 1146; **HRMS** (ESI): *molecular ion not observed*, calc for $C_{13}H_{19}N_2O_3$ $(M - {}^tBu + 2H)^+$ 251.1396, found 251.1392.

tert-Butyl 7-(4-oxobutyl)-3,4-dihydro-1,8-naphthyridine-1(2H)-carboxylate (29)

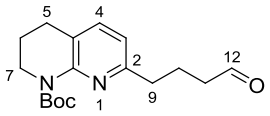

To a stirring mixture of *tert*-butyl 7-(4-hydroxybutyl)-3,4-dihydro-1,8-naphthyridine-1(2H)-carboxylate **(36)** (1.21 g, 3.95 mmol) and sodium hydrogen carbonate (1.99 g, 23.7 mmol) in CH_2Cl_2 (20 mL) and a drop of H_2O at 0 °C was added DMP (3.10 g, 7.90 mmol) in five portions, and the reaction was warmed to rt. After 1 h, the mixture was triturated with CH_2Cl_2 (50 mL) and the filtrate was concentrated *in vacuo*. The crude product was purified directly using an 80 g silica column, eluting with 0 – 100 % EtOAc:cyclohexane, and the desired fractions were combined and concentrated *in vacuo* to yield *tert*-butyl 7-(4-oxobutyl)-3,4-dihydro-1,8-naphthyridine-1(2H)-carboxylate **(29)** (1.00 g, 3.29 mmol, 83 % yield) as a yellow coloured oil.

LCMS t_R = 1.10 min (system B), 81 %, ES+ve *m/z* 305 $(M + H)^+$; **^{1}H NMR** (400 MHz, $CDCl_3$): δ = 9.78 (1H, t, *J* = 1.7 Hz, H_{12}), 7.29 (1H, d, *J* = 7.6 Hz, H_4), 6.80 (1H, d, *J* = 7.6 Hz, H_3), 3.78 – 3.72 (2H, m, H_7), 2.79 – 2.68 (4H, m, H_9, H_5), 2.52 (2H, td, *J* = 7.3, 1.6 Hz, H_{11}), 2.09 (2H, t, *J* = 7.5 Hz, H_{10}), 1.95 – 1.87 (2H, m, H_6), 1.51 (9H, s, ^{t}Bu-H); **^{13}C NMR** (101 MHz, $CDCl_3$): δ = 202.7, 157.3, 154.1, 151.3, 137.5, 122.4, 118.5, 81.0, 45.0, 43.4, 36.9, 28.5, 26.5, 23.4, 20.7; **IR** (neat, ν_{max} /cm^{-1}): 1720, 1689, 1365, 1334, 1318, 1146; **HRMS** (ESI): *molecular ion not observed*, calc for $C_{13}H_{17}N_2O_3$ $(M - {}^t\text{Bu} + 2H)^+$ 249.1239, found 249.1233.

(*R*)-*tert*-Butyl 7-(4-(benzyl(ethyl)amino)-3-fluorobutyl)-3,4-dihydro-1,8-naphthyridine-1(2H)-carboxylate (39)

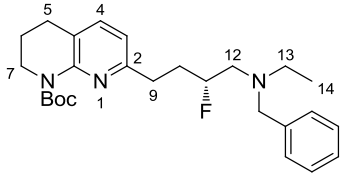

A solution of (*R*)-5-benzyl-2,2,3-trimethylimidazolidin-4-one 2,2-dichloroacetate **(37)** (0.242 g, 0.696 mmol) and *N*-fluoro-*N*-(phenylsulfonyl)benzenesulfonamide (1.318 g, 4.18 mmol) in 10 % ^{i}PrOH/THF (12 mL) was stirred at rt before cooling to − 20 °C, and then was added to *tert*-butyl 7-(4-oxobutyl)-3,4-dihydro-1,8-naphthyridine-1(2H)-carboxylate **(29)** (1.06 g, 3.48 mmol) at –20 °C and the reaction was stirred for 3 h, before the addition of *N*-benzylethanamine (0.518 ml, 3.48 mmol) and sodium triacetoxyborohydride (1.624 g, 7.66 mmol) and warming to rt. The reaction was stirred at rt for a further 22 h, before diluting with H_2O (50 mL) and EtOAc (50 mL). The layers were separated, and the aqueous layer was extracted with EtOAc (2 x 50 mL). The combined organic extracts were filtered through a hydrophobic frit and concentrated *in vacuo*. The crude product was purified using a 60 g C18 silica column using 50 – 100 % MeCN:ammonium carbonate modified H_2O, and the desired fractions were combined and concentrated *in vacuo* to yield *tert*-butyl (*R*)-7-(4-(benzyl(ethyl)amino)-3-fluorobutyl)-3,4-dihydro-1,8-naphthyridine-1(2H)-carboxylate **(39)** (319 mg, 0.722 mmol, 21 % yield) as a yellow coloured oil.

LCMS t_R = 1.56 min (system B), 79 %, ES+ve *m/z* 442 $(M + H)^+$; **^{1}H NMR** (400 MHz, $CDCl_3$): δ = 7.38 – 7.19 (6H, m, H_4, PhH), 6.78 (1H, d, *J* = 7.6 Hz, H_3), 4.68 (1H, dm, *J* = 49.2 Hz, H_{11}), 3.80 – 3.68 (2H, m, H_7), 3.65 (2H, s, Bn-H), 2.89 – 2.64 (6H, m, H_5, H_9, H_{12}), 2.64 – 2.47 (2H, m, H_{13}), 2.15 – 1.96 (2H, m, H_{10}), 1.95 – 1.87 (2H, t, *J* = 6.2 Hz, H_6), 1.50 (9H, s, ^{t}Bu-H) 1.03 (3H, t, *J* = 7.1 Hz, H_{14}); **^{13}C NMR** (101 MHz, $CDCl_3$): δ = 157.5, 154.3, 151.4, 139.8, 137.3, 129.0, 128.3, 127.0, 122.0, 118.4, 93.0 (d, *J* = 169.5 Hz), 80.9, 58.9, 57.3 (d, *J* = 21.3 Hz), 48.3, 44.9, 33.4, 33.3 (d, *J* = 20.5 Hz), 28.6, 26.5, 23.4, 12.0; **IR** (neat, ν_{max} /cm^{-1}): 1693, 1465, 1365, 1335, 1148; **HRMS** (ESI): calc for $C_{26}H_{37}FN_3O_2$ $(M + H)^+$ 442.2870, found 442.2868; **analytical chiral HPLC:** (10 %EtOH/Heptane, f = 1.0 mL/min, detecting at 215 nm; column 25 cm Chiralcel IA, no. OJHOCE-RK007): *ee* = 79 %, t_R = 8.79 min.

tert-Butyl 7-(4-(benzyl(ethyl)amino)-3-fluorobutyl)-3,4-dihydro-1,8-naphthyridine-1(2H)-carboxylate (_rac_-39)

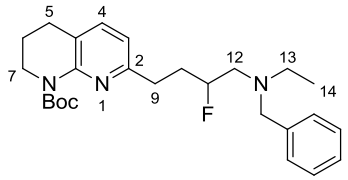

A solution of pyrrolidine (1.66 µl, 0.020 mmol) and *N*-fluoro-*N*-(phenylsulfonyl)benzenesulfonamide (37.5 mg, 0.119 mmol) in 10 % ^{i}PrOH/THF (0.30 mL) was stirred at rt before cooling to –20 °C, and then was added to *tert*-butyl 7-(4-oxobutyl)-3,4-dihydro-1,8-naphthyridine-1(2H)-carboxylate **(29)** (30.2 mg, 0.099 mmol) and the reaction was stirred for 2 h before *N*-benzylethylamine (20 µl, 0.134 mmol) and sodium acetoxyborohydride (46.3 mg, 0.218 mmol) were added, followed by warming to rt. The reaction was stirred at rt for a further 22 h, before diluting with H_2O (2 mL) and EtOAc (2 mL). The layers were separated, and the aqueous layer was extracted with EtOAc (2 x 2 mL). The combined organic extracts were filtered through a hydrophobic frit and concentrated *in vacuo*. The crude product was purified using by MDAP, using 50 – 100 % MeCN:ammonium carbonate modified H_2O, and the desired fractions were combined and concentrated *in vacuo* to yield *tert*-butyl 7-(4-(benzyl(ethyl)amino)-3-fluorobutyl)-3,4-dihydro-1,8-naphthyridine-1(2H)-carboxylate **(_rac_-39)** (3.5 mg, 7.93 µmol, 8 % yield) as a pale yellow coloured oil.

LCMS t_R = 1.56 min (system B), 93 %, ES+ve *m/z* 442 $(M + H)^+$.

(_R_)-_N_-Ethyl-2-fluoro-4-(5,6,7,8-tetrahydro-1,8-naphthyridin-2-yl)butan-1-amine (42)

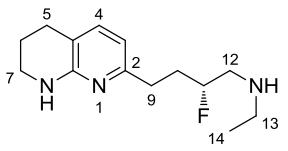

To a stirring solution of *tert*-butyl (*R*)-7-(4-(benzyl(ethyl)amino)-3-fluorobutyl)-3,4-dihydro-1,8-naphthyridine-1(2H)-carboxylate **(39)** (58.9 mg, 0.133 mmol) in CH_2Cl_2 (1 mL) was added 1-chloroethyl chloroformate **(41)** (0.022 mL, 0.200 mmol) at 0 °C and the pale yellow solution was stirred for 2 h before warming to rt and the addition of a further portion of 1-chloroethyl chloroformate **(41)** (3 µl, 0.027 mmol) and the reaction was stirred for 30 min, after which time the solvent was removed using a flow of nitrogen gas, and MeOH (1 mL) was added, and the reaction was stirred at rt for 68 h after which the reaction solution was purified directly using an Xterra® Prep RP18 OBD™ column in 0 – 100 % MeCN:ammonium carbonate modified H_2O, and the desired fractions were combined and concentrated *in vacuo* to yield (*R*)-*N*-ethyl-2-fluoro-4-(5,6,7,8-tetrahydro-1,8-naphthyridin-2-yl)butan-1-amine **(42)** (26.4 mg, 0.105 mmol, 79 % yield) as a brown coloured gum.

LCMS t_R = 0.96 min (system B), 98 %, ES+ve *m/z* 252 $(M + H)^+$; **^{1}H NMR** (400 MHz, $CDCl_3$): δ = 7.05 (1H, d, *J* = 7.3 Hz, H_4), 6.36 (1H, d, *J* = 7.3 Hz, H_3), 4.80 (1H, br s, NH), 4.74 – 4.65 (1H, dm, *J* = 50.4 Hz, H_{11}), 3.42 – 3.36 (2H, m, H_7), 2.90 – 2.72 (2H, m, H_{12}), 2.72 – 2.57 (6H, m, H_5, H_9, H_{13}), 2.09 – 1.93 (2H, m, H_{10}), 1.92 – 1.86 (2H, m, H_6), 1.10 (3H, t, *J* = 7.1 Hz, H_{14}), *second amine H signal not observed*; **^{13}C NMR** (101 MHz, $CDCl_3$): δ = 157.1, 155.9, 136.9, 113.7, 111.6, 93.5 (d, *J* = 167.3 Hz), 53.8 (d, *J* = 20.5 Hz), 44.2, 41.8, 33.3, 33.1 (d, *J* = 15.4 Hz), 26.5, 21.7, 15.4; **IR** (neat, ν_{max} /cm^{-1}): 3242, 1600, 1586, 1461, 1321, 789; **HRMS** (ESI): calc for $C_{14}H_{23}FN_3$ $(M + H)^+$ 252.1876, found 252.1883.

(*R,E*)-Methyl 4-(ethyl(2-fluoro-4-(5,6,7,8-tetrahydro-1,8-naphthyridin-2-yl)butyl) amino) but-2-enoate (44)

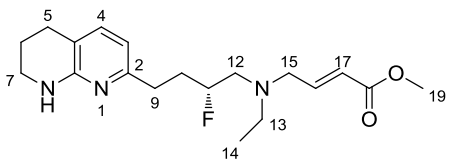

To a stirring solution of (*R*)-*N*-ethyl-2-fluoro-4-(5,6,7,8-tetrahydro-1,8-naphthyridin-2-yl)butan-1-amine **(42)** (37.9 mg, 0.151 mmol) in CH_2Cl_2 (2 mL) was added methyl (*E*)-4-bromobut-2-enoate **(33)** (0.018 mL, 0.151 mmol) and triethylamine (0.032 mL, 0.226 mmol). After 16 h, further portions of methyl (*E*)-4-bromobut-2-enoate **(33)** (0.018 mL, 0.151 mmol) and triethylamine (0.032 mL, 0.226 mmol) were added and the reaction was stirred for 8 h, before a further portion of methyl (*E*)-4-bromobut-2-enoate **(33)** (0.018 mL, 0.151 mmol) was added, and the reaction stirred for a further 15 h before the addition of a final portion of methyl (*E*)-4-bromobut-2-enoate **(33)** (9.0 µl, 0.075 mmol), and a further 2 h of stirring. H_2O (2 mL) was added and the layers were separated. The aqueous layer was extracted with CH_2Cl_2 (2 x 2 mL) and the organic extracts were combined, filtered through a hydrophobic frit, and concentrated *in vacuo*. The crude product was purified using an Xterra® Prep RP18 OBD™ column, eluting with 0 – 100 % MeCN:ammonium carbonate modified H_2O, and the desired fractions were combined and concentrated *in vacuo* to yield methyl (*R,E*)-4-(ethyl(2-fluoro-4-(5,6,7,8-tetrahydro-1,8-naphthyridin-2-yl)butyl)amino)but-2-enoate **(44)** (34.5 mg, 0.099 mmol, 66 % yield) as an orange coloured gum.

LCMS t_R = 1.17 min (system B), 100 %, ES+ve *m/z* 350 $(M + H)^+$; **^{1}H NMR** (400 MHz, $CDCl_3$): δ = 7.05 (1H, d, *J* = 7.3 Hz, H_4), 6.96 (1H, dt, *J* = 15.6, 6.0 Hz, H_{16}), 6.36 (1H, d, *J* = 7.3 Hz, H_3), 6.00 (1H, dt, *J* = 15.6, 1.6 Hz, H_{17}), 4.77 (1H, br s, NH), 3.74 (3H, s, H_{19}), 4.63 (1H, dm, *J* = 49.9 Hz, H_{11}), 3.39 (2H, td, *J* = 5.5, 2.5 Hz, H_7), 3.30 (2H, dd, *J* = 6.0, 1.5 Hz, H_{15}), 2.76 – 2.54 (8H, m, H_5, H_9, H_{12}, H_{13}), 2.05 – 1.92 (2H, m, H_{10}), 1.92 – 1.86 (2H, m, H_6), 1.02 (3H t, *J* = 7.1 Hz, H_{14}); **^{13}C NMR** (101 MHz, $CDCl_3$): δ = 166.9, 157.3, 155.9, 146.7, 136.8, 122.5, 113.6, 111.6, 93.0 (d, *J* = 169.8 Hz), 57.6 (d, *J* = 21.6 Hz), 55.5, 51.6, 48.7, 41.8, 33.5 (d, *J* = 26.4 Hz), 33.4, 26.5, 21.7, 12.3; **IR** (neat, ν_{max} /cm^{-1}): 3251, 1721, 1586, 1462, 1272, 1168, 1041; **HRMS** (ESI): calc for $C_{19}H_{29}FN_3O_2$ $(M + H)^+$ 350.2244, found 350.2243.

(*S*)-Methyl 4-(ethyl((*R*)-2-fluoro-4-(5,6,7,8-tetrahydro-1,8-naphthyridin-2-yl)butyl) amino)-3-(3-(2-methoxyethoxy)phenyl)butanoate (45)

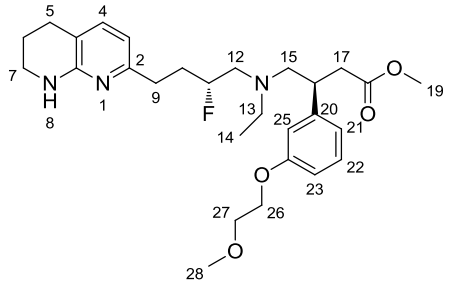

Methyl (*R,E*)-4-(ethyl(2-fluoro-4-(5,6,7,8-tetrahydro-1,8-naphthyridin-2-yl)butyl) amino)but-2-enoate **(44)** (101 mg, 0.289 mmol) in 1,4-dioxane (3 mL) was added to 2-(3-(2-methoxyethoxy)phenyl)-4,4,5,5-tetramethyl-1,3,2-dioxaborolane **(34)** (161 mg, 0.578 mmol), (*R*)-BINAP (21.6 mg, 0.035 mmol), KOH (3.8 M in H_2O, 0.152 mL, 0.578 mmol), and chloro(1,5-cyclooctadiene)rhodium(1) dimer (7.1 mg, 0.014 mmol), and the mixture was degassed and stirred under nitrogen for 3 h at 90 °C, then cooled to rt. The reaction mixture was diluted with HCl (2M, 5 mL), TBME (10 mL) added, and the organic layer separated. The aqueous layer was basified with NaOH (2 M, 10 mL) and extracted with CH_2Cl_2 (3 x 15 mL). The organic extracts were combined, dried ($MgSO_4$), and concentrated *in vacuo*. The crude product was purified using a Xterra® Prep RP18 OBD™ column, eluting with 0 – 100 % MeCN:ammonium carbonate modified H_2O, and the desired fractions were combined and concentrated *in vacuo* to yield methyl (*S*)-4-(ethyl((*R*)-2-fluoro-4-(5,6,7,8-tetrahydro-1,8-naphthyridin-2-yl)butyl)amino)-3-(3-(2-methoxyethoxy)phenyl)butanoate **(45)** (79.7 mg, 0.159 mmol, 55 % yield) as a yellow coloured oil.

LCMS t_R = 1.38 min (system B), 99 %, ES+ve *m/z* 502 $(M + H)^+$; **^{1}H NMR** (400 MHz, $CDCl_3$): δ = 7.20 – 7.15 (1H, m, H_{22}), 7.06 (1H, d, *J* = 7.1 Hz, H_4), 6.79 – 6.73 (3H, m, H_{21}, H_{23}, H_{25}), 6.38 – 6.33 (1H, m, H_3), 4.79 (1H, br s, NH), 4.58 (1H, dm, *J* = 49.8 Hz, H_{11}), 4.10 (2H, dd, *J* = 5.4, 4.2 Hz, H_{26}), 3.76 – 3.72 (2H, m, H_{27}), 3.55 (3H, s, H_{19}), 3.45 (3H, s, H_{28}), 3.41 – 3.37 (2H, m, H_7), 3.25 (1H, tt, *J* = 9.1, 5.8 Hz, H_{16}), 2.99 – 2.89 (1H, m, H_{17a}), 2.75 – 2.45 (11H, m, H_5, H_9, H_{12}, H_{13}, H_{15}, H_{17b}), 2.05 – 1.79 (4H, m, H_6, H_{10}),

0.99 – 0.93 (3H, m, H_{14}); **^{13}C NMR** (101 MHz, $CDCl_3$): δ = 173.5, 159.0, 157.5, 155.9, 144.8, 136.8, 129.5, 120.3, 114.5, 113.5, 112.5, 111.6, 93.5 (d, *J* = 169.5 Hz), 71.2, 67.3, 61.1, 59.3, 58.1 (d, *J* = 21.3 Hz), 51.5, 48.7, 41.8, 41.0, 38.7, 33.6 (d, *J* = 20.54 Hz), 33.4 (d, *J* = 4.4 Hz), 26.5, 21.7, 11.8; **IR** (neat, ν_{max} /cm^{-1}): 3411, 3249, 1733, 1599, 1584, 1562, 1446, 1260, 1161, 1127; **HRMS** (ESI): calc for $C_{28}H_{41}FN_3O_4$ $(M + H)^+$ 502.3081, found 502.3080; $[\alpha]_D^{20}$= +44 (*c* 1.0, MeOH); **analytical chiral HPLC** (40 % EtOH:heptane), f = 1.0 mL/min, detecting at 215 nm; column 25 cm Chiralcel OD-H, no. ODHOCE-IF029): t_R = 9.56 min for one undesired diastereomer (10 % area), t_R = 12.63 min for the desired enantiomer (82 % area), t_R = 18.09 min for the second undesired diastereomer (7.9 % area).

The desired enantiomer was subsequently separated from the other stereoisomers by chiral column chromatography, using a GF Prep 1: Agilent™ Preparative 1200 machine, a *Chiralcel OD-H* column 250x30 mm ID column, using 40 % EtOH:heptane at f = 30 ml/min, detection at 280 nM and 140 nM bandwidth to yield **(45)** (45 mg, 0.090 mmol, 31 % yield) as a pale yellow oil.

$[\alpha]_D^{20}$= +47 (*c* 2.0, MeOH).

(*S*)-4-(Ethyl((*R*)-2-fluoro-4-(5,6,7,8-tetrahydro-1,8-naphthyridin-2-yl)butyl)amino)-3-(3-(2-methoxyethoxy)phenyl)butanoic acid, formic acid salt (19)

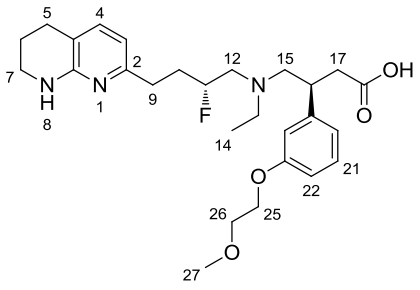

To a stirring solution of methyl (*S*)-4-(ethyl((*R*)-2-fluoro-4-(5,6,7,8-tetrahydro-1,8-naphthyridin-2-yl)butyl)amino)-3-(3-(2-methoxyethoxy)phenyl)butanoate **(45)** (45

mg, 0.090 mmol) in H_2O (1 mL) and 1,4-dioxane (1 mL) was added sulfuric acid (0.024 mL, 0.449 mmol) and the reaction was heated to 60 °C in a sealed tube for 40 h, after which time the cooled reaction mixture was neutralised with NaOH (2 M) and purified using a Sunfire® Prep C18 OBD™ column, eluting with 0 – 50 % MeCN:formic acid modified H_2O, and the desired fractions were combined and concentrated *in vacuo,* but separation from the salts was not obtained, so the material was repurified using the same method, and the desired fractions were combined and concentrated *in vacuo* to furnish (*S*)-4-(ethyl((*R*)-2-fluoro-4-(5,6,7,8-tetrahydro-1,8-naphthyridin-2-yl)butyl)amino)-3-(3-(2-methoxyethoxy)phenyl)butanoic acid, formic acid salt **(19)** (34 mg, 0.064 mmol, 71 % yield) as a yellow coloured gum.

LCMS t_R = 0.44 min (system A), 97 %, ES+ve *m/z* 488 $(M + H)^+$; **^{1}H NMR** (400 MHz, $CDCl_3$): δ = 8.47 (1H, s, HCOOH), 7.28 (1H, d, *J* = 7.3 Hz, H_4), 7.22 – 7.17 (1H, m, H_{21}), 6.80 – 6.75 (3H, m, H_{20}, H_{22}, H_{24}), 6.34 (1H, d, *J* = 7.3 Hz, H_3), 4.82 (d, *J* = 50.4 Hz, H_{11}), 4.11 (2H, dd, *J* = 5.3, 4.0 Hz, H_{25}), 3.74 (2H, dd, *J* = 5.4, 3.9 Hz, H_{26}), 3.50 – 3.45 (2H, m, H_7), 3.44 (3H, s, H_{27}), 3.38 – 3.29 (1H, m, H_{16}), 2.94 – 2.65 (12H, m, H_5, H_9, H_{12}, H_{13}, H_{15}, H_{17}), 2.32 – 2.13 (1H, m, H_{10a}), 1.98 – 1.82 (3H, m, H_6, H_{10b}), 1.09 (3H, t, *J* = 7.1 Hz, H_{14}), *acid H signals and amine H not observed*; **^{13}C NMR** (101 MHz, $CDCl_3$): δ = 175.7, 167.6, 159.2, 152.8, 148.6, 144.9, 140.2, 129.9, 119.8, 118.7, 114.1, 112.7, 109.8, 91.7 (d, *J* = 170.9 Hz), 71.2, 67.4, 62.1, 59.3, 56.9 (d, *J* = 22.0 Hz), 48.9, 42.8, 40.9, 39.3, 33.6 (d, *J* = 21.3 Hz), 28.8 (d, *J* = 4.4 Hz), 26.0, 19.6, 10.5; **IR** (neat, ν_{max} /cm^{-1}): 1662, 1264, 1196, 1128, 1059, 1033, 730, 700, 609; **HRMS** (ESI): $C_{27}H_{39}FN_3O_4$ $(M + H)^+$ 488.2924, found 488.2927; $[\boldsymbol{\alpha}]_D^{20}$= +60 (*c* 0.5, MeCN).

In order to obtain the free base of compound **19** for ^{15}N NMR studies, a small portion of the formic acid salt was purified using an Xterra® Prep RP18 OBD™ column, eluting with 0 – 60 % MeCN:ammonium carbonate modified H_2O, and the desired fractions were combined and concentrated *in vacuo* to yield (*S*)-4-(ethyl((*R*)-2-fluoro-4-(5,6,7,8-tetrahydro-1,8-naphthyridin-2-yl)butyl)amino)-3-(3-(2-methoxyethoxy) phenyl)butanoic acid (2.9 mg, 5.95 µmol) as an orange coloured gum.

^{15}N NMR (60.8 MHz, $CDCl_3$): δ = 207, 82, 42.

(*R*)-7-(2-(3-Fluoropyrrolidin-3-yl)ethyl)-1,2,3,4-tetrahydro-1,8-naphthyridine (49)

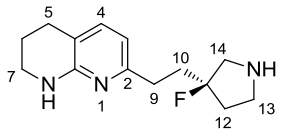

To a stirring solution of *tert*-butyl (*R*)-3-fluoro-3-(2-(5,6,7,8-tetrahydro-1,8-naphthyridin-2-yl)ethyl)pyrrolidine-1-carboxylate **(48)** (1.30 g, 3.72 mmol) in CH_2Cl_2 (30 mL) at rt was added hydrochloric acid in 1,4-dioxane (4 M, 5.58 mL, 22.3 mmol) and the solution was stirred for 6 h before H_2O (30 mL) was added and the layers were separated. The aqueous phase was basified with NaOH (2 M, 25 mL) and extracted with CH_2Cl_2 (3 x 40 mL). The combined organic extracts were combined, filtered through a hydrophobic frit, and concentrated *in vacuo* to yield (*R*)-7-(2-(3-fluoropyrrolidin-3-yl)ethyl)-1,2,3,4-tetrahydro-1,8-naphthyridine **(49)** (0.497 g, 1.99 mmol, 54 % yield) as a pale yellow coloured oil.

LCMS t_R = 0.87 min (system B), 100 %, ES+ve *m/z* 250 $(M + H)^+$; **^{1}H NMR** (400 MHz, $CDCl_3$): δ = 7.06 (1H, d, *J* = 7.3 Hz, H_4), 6.36 (1H, d, *J* = 7.3 Hz, H_3), 4.86 (1H, br s, NH), 3.39 (2H, t, *J* = 4.8 Hz, H_7), 3.22 – 3.10 (2H, m, H_{13a}, H_{14a}), 2.98 – 2.87 (1H, m, H_{13b}), 2.81 – 2.62 (5H, m, H_5, H_9, H_{14b}), 2.21 – 1.91 (3H, m, H_{10}, H_{12a}), 1.94 – 1.72 (3H, m, H_6, H_{12b}), *second amine H signal not observed*; **^{13}C NMR** (101 MHz, $CDCl_3$): δ = 157.4, 155.8, 136.8, 113.5, 111.2, 105.8 (d, *J* = 174.6 Hz), 57.9 (d, *J* = 25.7 Hz), 46.1, 41.6, 38.1 (d, *J* = 22.7 Hz), 36.6 (d, *J* = 24.2 Hz), 32.7 (d, *J* = 3.7 Hz), 26.4, 21.5; **IR** (neat, ν_{max} /cm^{-1}): 3247, 1599, 1586, 1480, 1462, 1391, 1321; **HRMS** (ESI): calc for $C_{14}H_{21}FN_3$ $(M + H)^+$ 250.1720, found 250.1721; $[\alpha]_D^{20}$= +12 (*c* 1.0, MeOH).

(*R,E*)-Methyl 4-(3-fluoro-3-(2-(5,6,7,8-tetrahydro-1,8-naphthyridin-2-yl)ethyl) pyrrolidin-1-yl)but-2-enoate (50)

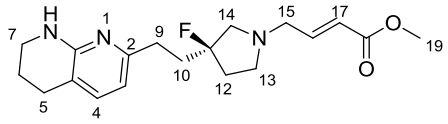

To a stirring solution of (*R*)-7-(2-(3-fluoropyrrolidin-3-yl)ethyl)-1,2,3,4-tetrahydro-1,8-naphthyridine **(49)** (477 mg, 1.913 mmol) and DIPEA (0.666 mL, 3.83 mmol) in CH_2Cl_2 (20 mL) at 0 °C was added methyl (*E*)-4-bromobut-2-enoate **(33)** (0.217 mL, 1.817 mmol). The reaction was stirred whilst warming to rt for 5 h, after which H_2O (20 mL) was added and the layers were separated. The aqueous layer was extracted with CH_2Cl_2 (2 x 20 mL) and the organic extracts were combined, filtered through a hydrophobic frit, and concentrated *in vacuo*. The crude product was purified in two portions using an Xterra® Prep RP18 OBD™ column, eluting with 0 – 100 % MeCN:ammonium carbonate modified H_2O, and the desired fractions were combined and concentrated *in vacuo* to yield methyl (*R,E*)-4-(3-fluoro-3-(2-(5,6,7,8-tetrahydro-1,8-naphthyridin-2-yl)ethyl)pyrrolidin-1-yl)but-2-enoate **(50)** (522 mg, 1.502 mmol, 79 % yield) as a pale yellow coloured oil.

LCMS t_R = 1.07 min (system B), 100 %, ES+ve *m/z* 348 $(M + H)^+$; **^{1}H NMR** (400 MHz, $CDCl_3$): δ = 7.05 (1H, d, *J* = 7.3 Hz, H_4), 6.97 (1H, dt, *J* = 15.7, 6.0 Hz, H_{16}), 6.36 (1H, d, *J* = 7.1 Hz, H_3), 6.00 (1H, dt, *J* = 15.8, 1.5 Hz, H_{17}), 4.75 (1H, br s, NH), 3.74 (3H, s, H_{19}), 3.39 (2H, td, *J* = 5.6, 2.6 Hz, H_7), 3.27 (2H, dd, *J* = 6.0, 1.6 Hz, H_{15}), 2.95 – 2.88 (1H, m, H_{14a}), 2.88 – 2.83 (1H, m, H_{13a}), 2.75 – 2.53 (6H, m, H_5, H_9, H_{13b}, H_{14b}), 2.22 – 1.93 (4H, m, H_{10}, H_{12}), 1.92 – 1.86 (2H, m, H_6); **^{13}C NMR** (101 MHz, $CDCl_3$): δ = 166.8, 157.6, 155.9, 145.6, 136.8, 122.5, 113.5, 111.4, 103.8 (d, *J* = 177.5 Hz), 64.4 (d, *J* = 24.9 Hz), 56.7, 53.1, 51.6, 41.8, 38.3 (d, *J* = 24.9 Hz), 37.3 (d, *J* = 23.5 Hz), 32.4 (d, *J* = 3.7 Hz), 26.5, 21.7; **IR** (neat, ν_{max} /cm^{-1}): 3251, 1721, 1599, 1585, 1461, 1435, 1321, 1269, 1172; **HRMS** (ESI): calc for $C_{19}H_{27}FN_3O_2$ $(M + H)^+$ 348.2087, found 348.2088; $[\alpha]_D^{20}$= +39 (*c* 1.0, MeOH).

(*S*)-Methyl 4-((*R*)-3-fluoro-3-(2-(5,6,7,8-tetrahydro-1,8-naphthyridin-2-yl)ethyl) pyrrolidin-1-yl)-3-phenylbutanoate (51)

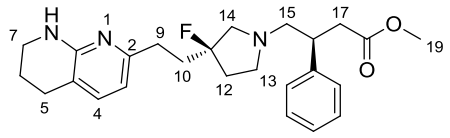

Methyl (*R,E*)-4-(3-fluoro-3-(2-(5,6,7,8-tetrahydro-1,8-naphthyridin-2-yl)ethyl) pyrrolidin-1-yl) but-2-enoate **(50)** (88.2 mg, 0.254 mmol) in 1,4-dioxane (3 mL) was added to phenylboronic acid (61.9 mg, 0.508 mmol), (*R*)-BINAP (18.97 mg, 0.030 mmol), KOH (3.8 M in H_2O, 0.134 mL, 0.508 mmol), and chloro(1,5-cyclooctadiene)rhodium(I) dimer (6.3 mg, 0.013 mmol), and the mixture was degassed and stirred under nitrogen for 3 h at 80 °C, then cooled to rt. The reaction was diluted with HCl (2M, 5 mL) and TBME (10 mL), and the organic layer separated. The aqueous layer was basified with NaOH (2 M, 10 mL) and extracted with CH_2Cl_2 (2 x 15 mL). The organic extracts were combined, dried ($MgSO_4$), and concentrated *in vacuo*. The crude product was purified using a Xterra® Prep RP18 OBD™ column, eluting with 0 – 100 % MeCN:ammonium carbonate modified H_2O, and the desired fractions were combined and concentrated *in vacuo* to yield methyl (*S*)-4-((*R*)-3-fluoro-3-(2-(5,6,7,8-tetrahydro-1,8-naphthyridin-2-yl)ethyl)pyrrolidin-1-yl)-3-phenylbutanoate **(51)** (77.9 mg, 0.183 mmol, 72 % yield, *de* = 78 %, determined by ^{19}F NMR) as a brown coloured oil.

LCMS t_R = 1.32 min (system B), 100 %, ES+ve *m/z* 426 $(M + H)^+$; **^{1}H NMR** (400 MHz, $CDCl_3$): δ = 7.31 – 7.26 (2H, m, ArH), 7.23 – 7.16 (3H, m, ArH), 7.05 (1H, d, *J* = 7.3 Hz, H_4), 6.35 (1H, d, *J* = 7.3 Hz, H_3), 4.72 (1H, br s, NH), 3.57 (3H, s, H_{19}) 3.39 (2H, td, *J* = 5.4, 2.6 Hz, H_7), 3.35 – 3.24 (1H, m, H_{16}), 3.01 – 2.82 (2H, m, H_{14a}, H_{17a}), 2.79 – 2.60 (8H, m, H_5, H_9, H_{13}, H_{14b}, H_{15a}), 2.58 – 2.48 (2H, m, H_{15b}, H_{17b}), 2.16 – 2.00 (2H, m, H_{10}), 1.96 – 1.79 (4H, m, H_6, H_{12}); **^{13}C NMR** (101 MHz, $CDCl_3$): δ (major diasteromer) = 173.2, 157.8, 155.9, 143.0, 136.8, 128.6, 127.5, 126.8, 113.5, 111.4, 103.8 (d, *J* = 176.8 Hz), 64.7 (d, *J* = 24.9 Hz), 62.4, 53.3, 51.6, 41.8, 41.5, 39.3, 38.7 (d, *J* = 24.9 Hz), 37.1 (d, *J* = 24.2 Hz), 32.4 (d, *J* = 3.7 Hz), 26.5, 21.7; **^{19}F NMR {^{1}H}** (376 MHz, $CDCl_3$): δ = –139.91

(0.89F, s), –140.30 (0.11F, s); **IR** (neat, ν_{max} /cm^{-1}): 3422, 3248, 1732, 1600, 1585, 1462, 1435, 1163, 1116, 762, 700; **HRMS** (ESI): calc for $C_{25}H_{33}FN_3O_2$ $(M + H)^+$ 426.2557, found 426.2555; $[\boldsymbol{\alpha}]_D^{20}$ = +48 (*c* = 0.5, MeOH).

(*R*)-Methyl 4-((*R*)-3-fluoro-3-(2-(5,6,7,8-tetrahydro-1,8-naphthyridin-2-yl)ethyl) pyrrolidin-1-yl)-3-phenylbutanoate (52)

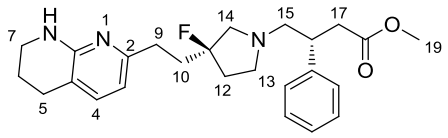

Methyl (*R,E*)-4-(3-fluoro-3-(2-(5,6,7,8-tetrahydro-1,8-naphthyridin-2-yl)ethyl)pyrrolidin-1-yl) but-2-enoate **(50)** (93.1 mg, 0.268 mmol) in 1,4-dioxane (3 mL) was added to phenylboronic acid (65.3 mg, 0.536 mmol), (*S*)-BINAP (20.0 mg, 0.032 mmol), KOH (3.8 M in H_2O, 0.141 mL, 0.536 mmol), and chloro(1,5-cyclooctadiene)rhodium(I) dimer (6.6 mg, 0.013 mmol), and the mixture was degassed and stirred under nitrogen for 3 h at 80 °C, then cooled to rt. The reaction was diluted with HCl (2M, 5 mL) and TBME (10 mL), and the organic layer separated. The aqueous layer was basified with NaOH (2 M, 10 mL) and extracted with CH_2Cl_2 (2 x 15 mL). The organic extracts were combined, dried ($MgSO_4$), and concentrated *in vacuo*. The crude product was purified using a Xterra® Prep RP18 OBD™ column, eluting with 0 – 100 % MeCN:ammonium carbonate modified H_2O:MeCN, and the desired fractions were combined and concentrated *in vacuo* to yield methyl (*R*)-4-((*R*)-3-fluoro-3-(2-(5,6,7,8-tetrahydro-1,8-naphthyridin-2-yl)ethyl)pyrrolidin-1-yl)-3-phenylbutanoate **(52)** (70.0 mg, 0.164 mmol, 61 % yield, *de* = 74 %, determined by ^{19}F NMR) as a brown coloured oil.

LCMS t_R = 1.32 min (system B), 99 %, ES+ve *m/z* 426 $(M + H)^+$; **^{1}H NMR** (400 MHz, $CDCl_3$): δ = 7.32 – 7.26 (2H, m, ArH), 7.23 – 7.15 (3H, m, ArH), 7.05 (1H, d, *J* = 7.3 Hz,

H_4), 6.35 (1H, d, *J* = 7.3 Hz, H_3), 4.71 (1H, br s, NH), 3.57 (3H, s, H_{19}), 3.42 – 3.36 (2H, m, H_7), 3.34 – 3.25 (1H, m, H_{16}), 2.94 – 2.59 (9H, m, H_5, H_9, H_{13a}, H_{14}, H_{15a}, H_{17a}), 2.58 – 2.43 (3H, m, H_{13b}, H_{15b}, H_{17b}), 2.13 – 1.81 (6H, m, H_6, $H_{10,}$ H_{12}); **^{13}C NMR** (101 MHz, $CDCl_3$): *δ* (major diasteromer) = 173.2, 157.8, 155.9, 143.1, 136.9, 128.7, 127.5, 126.8, 113.5, 111.4, 103.7 (d, *J* = 176.8 Hz), 64.9 (d, *J* = 24.9 Hz), 62.4, 53.1, 51.6, 41.6, 41.8, 39.4, 38.4 (d, *J* = 24.9 Hz), 37.3 (d, *J* = 23.5 Hz), 32.4 (d, *J* = 3.7 Hz), 26.5, 21.7; **^{19}F NMR {^{1}H}** (376 MHz, $CDCl_3$): *δ* = –139.92 (0.13F, s), –140.30 (0.87F, s); **IR** (neat, ν_{max} /cm^{-1}): 3422, 3248, 1732, 1600, 1586, 1462, 1435, 1165, 1117, 763, 700; **HRMS** (ESI): calc for $C_{25}H_{33}FN_3O_2$ $(M + H)^+$ 426.2557, found 426.2555; $[\alpha]_D^{20}$= +20 (*c* = 0.5, MeOH).

(*R*)-4-((*R*)-3-Fluoro-3-(2-(5,6,7,8-tetrahydro-1,8-naphthyridin-2-yl)ethyl)pyrrolidin-1-yl)-3-phenylbutanoic acid, formic acid salt (47)

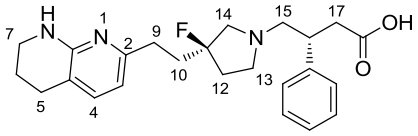

To a stirring solution of methyl (*R*)-4-((*R*)-3-fluoro-3-(2-(5,6,7,8-tetrahydro-1,8-naphthyridin-2-yl)ethyl)pyrrolidin-1-yl)-3-phenylbutanoate **(52)** (66.5 mg, 0.156 mmol) in H_2O (1 mL) and 1,4-dioxane (1 mL) was added sulfuric acid (0.042 mL, 0.78 mmol) and the reaction was heated to 60 °C in a sealed tube for 24 h, after which time half of the solvent was removed using a flow of nitrogen, and the solution was cooled to rt. The resulting solution was purified directly using a Sunfire® Prep C18 OBD™ column, eluting with 0 – 50 % MeCN:formic acid modified H_2O, and the desired fractions were combined and concentrated *in vacuo* to furnish (*R*)-4-((*R*)-3-fluoro-3-(2-(5,6,7,8-tetrahydro-1,8-naphthyridin-2-yl)ethyl)pyrrolidin-1-yl)-3-phenylbutanoic acid, formic acid salt **(47)** (49.2 mg, 0.109 mmol, 69 % yield, 74 % *de* as determined by ^{19}F NMR) as an off-white coloured powder.

LCMS t_R = 0.38 min (system A), 99 %, ES+ve *m/z* 412 $(M + H)^+$; **^{1}H NMR** (400 MHz, CD_3OD): δ = 8.15 (1H, s, HCOOH), 7.47 (1H, d, *J* = 7.3 Hz, H_4), 7.41 – 7.34 (4H, m, H_{20}, H_{21}), 7.33 – 7.27 (1H, m, H_{22}), 6.53 (1H, d, *J* = 7.3 Hz, H_3), 3.91 – 3.75 (1H, m, H_{14a}) 3.69 – 3.40 (8H, m, H_7, H_{13}, H_{14b}, H_{15}, H_{16}), 2.92 – 2.72 (5H, m, H_5, H_9, H_{17a}), 2.72 – 2.59 (1H, m, H_{17b}), 2.48 – 2.21 (4H, m, H_{10}, H_{12}), 1.96 – 1.87 (2H, m, H_6), *acid H signals not observed*; **^{13}C NMR** (101 MHz, CD_3OD): δ (major diasteromer) = 176.3, 163.9, 154.0, 148.8, 142.0, 141.8, 130.3, 128.9, 128.8, 120.7, 111.3, 103.0 (d, *J* = 179.7 Hz), 63.5 (d, *J* = 25.7 Hz), 62.3, 54.5, 42.1, 41.9, 40.5, 36.5 (d, *J* = 26.4 Hz), 36.2 (d, *J* = 24.2 Hz), 28.7 (d, *J* = 4.4 Hz), 26.6, 20.6; **^{19}F NMR {^{1}H}** (376 MHz, CD_3OD): δ = –145.14 (0.13F, s), –146.35 (0.87F, s); **IR** (neat, ν_{max} /cm^{-1}): 1718, 1658, 1317, 1321, 1048, 1011, 764, 702, 600; **mp**: 108 − 113 °C; **HRMS** (ESI): calc for $C_{24}H_{31}FN_3O_2$ $(M + H)^+$ 412.2400, found 412.2400; $[\alpha]_D^{20}$= +20 (*c* = 1.0, MeOH).

(*S*)-4-((*R*)-3-Fluoro-3-(2-(5,6,7,8-tetrahydro-1,8-naphthyridin-2-yl)ethyl)pyrrolidin-1-yl)-3-phenylbutanoic acid, formic acid salt (46)

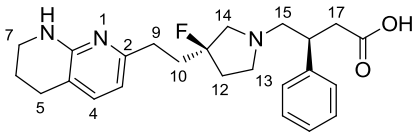

To a stirring solution of methyl (*S*)-4-((*R*)-3-fluoro-3-(2-(5,6,7,8-tetrahydro-1,8-naphthyridin-2-yl)ethyl)pyrrolidin-1-yl)-3-phenylbutanoate **(51)** (66 mg, 0.155 mmol) in H_2O (1 mL) and 1,4-dioxane (1 mL) was added sulfuric acid (0.041 mL, 0.78 mmol) and the reaction was heated to 60 °C in a sealed tube for 24 h, after which time half of the solvent was removed using a flow of nitrogen, and the solution was cooled to rt. The resulting solution was purified using a Sunfire® Prep C18 OBD™ column in formic acid modified H_2O:MeCN 0 – 50 %, and the desired fractions were combined and concentrated *in vacuo* to furnish (*S*)-4-((*R*)-3-fluoro-3-(2-(5,6,7,8-tetrahydro-1,8-naphthyridin-2-yl)ethyl)pyrrolidin-1-yl)-3-phenylbutanoic acid, formic acid salt **(46)**

(62.2 mg, 0.136 mmol, 88 % yield, 78 % *de* as determined by ^{19}F NMR) as an off-white coloured powder.

LCMS t_R = 0.38 min (system A), 96 %, ES+ve *m/z* 412 $(M + H)^+$; **^{1}H NMR** (400 MHz, CD_3OD): δ = 8.16 (1H, s, HCOOH), 7.47 (1H, d, *J* = 7.3 Hz, H_4), 7.42 – 7.34 (4H, m, H_{20}, H_{21}), 7.29 (1H, m, H_{22}), 6.53 (1H, d, *J* = 7.1 Hz, H_3), 3.88 – 3.74 (1H, m, H_{14a}), 3.73 – 3.40 (8H, m, H_7, H_{13}, H_{14b}, H_{15}, H_{16}), 2.92 – 2.73 (5H, m, H_5, H_9, H_{17a}), 2.67 (1H, dd, *J* = 16.3, 6.2 Hz, H_{17b}), 2.47 – 2.21 (4H, m, H_{10}, H_{12}), 1.91 (2H, quin, *J* = 5.9 Hz, H_6), *acid H signals and amine H not observed*; **^{13}C NMR** (101 MHz, CD_3OD): δ (major diasteromer) = 176.2, 165.6, 153.3, 148.9, 142.0, 140.2, 130.3, 130.2, 128.8, 120.6, 111.3, 103.1 (d, *J* = 180.5 Hz), 63.8 (d, *J* = 27.9 Hz), 62.5, 54.8, 42.0, 41.7, 40.6, 36.7 (d, *J* = 22.0 Hz), 36.4 (d, *J* = 24.2 Hz), 28.7 (d, *J* = 3.7 Hz), 26.6, 20.6; **^{19}F NMR {^{1}H}** (376 MHz, CD_3OD): δ = −145.15 (0.89F, s), −146.43 (0.11F, s); **IR** (neat, ν_{max} /cm^{-1}): 1714, 1656, 1371, 1320, 1291, 1043, 765, 731, 702, 602; **mp**: 65 − 70 °C; **HRMS** (ESI): calc for $C_{24}H_{31}FN_3O_2$ $(M + H)^+$ 412.2400, found 412.2400; $[\alpha]_D^{20}$= +11 (*c* = 1.0, MeOH).

Benzyltriphenylphosphonium bromide (56)[242]

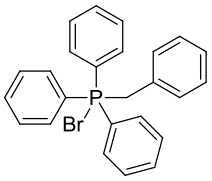

To a stirring solution of benzyl bromide (1.391 mL, 11.69 mmol) in PhMe (100 mL) was added triphenylphosphine (3.07 g, 11.69 mmol) and the solution was heated under reflux for 21 h before the white mixture was cooled to rt. The mixture was filtered under reduced pressure and the residue was washed with cyclohexane (50 mL) and collected to yield benzyltriphenylphosphonium bromide **(56)** (4.58 g, 10.57 mmol, 90 % yield) as a white coloured solid.

LCMS t_R = 1.34 min (system B), 100 %, ES+ve *m/z* 353 $(M - Br)^+$; **^{1}H NMR** (400 MHz, $CDCl_3$): δ = 7.81 – 7.70 (9H, m, ArH), 7.67 – 7.60 (6H, m, ArH), 7.25 – 7.19 (1H, m, ArH), 7.17 – 7.07 (4H, m, ArH), 5.45 (2H, d, *J* = 14.4 Hz, $ArCH_2$).

(*S*)-Benzyl 3-fluoro-3-styrylpyrrolidine-1-carboxylate (57)

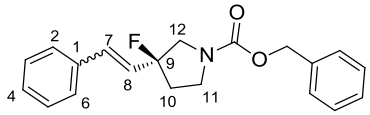

To a stirring solution of benzyl (*R*)-3-fluoro-3-(hydroxymethyl)pyrrolidine-1-carboxylate **(55)** (500 mg, 1.974 mmol) and sodium hydrogen carbonate (995 mg, 11.84 mmol) in CH_2Cl_2 (15 mL) at 0 °C was added DMP (1.68 g, 3.95 mmol) in three portions, and the reaction was warmed to rt and stirred for 2 h, after which time the mixture was filtered, and the residue was washed with CH_2Cl_2 (15 mL). The resulting suspension was concentrated *in vacuo* and purified using a 40 g silica column, eluting with 0 – 100 % EtOAc:cyclohexane. The desired fractions were combined and concentrated *in vacuo* to yield the desired aldehyde. In the meantime, to a stirring solution of benzyltriphenylphosphonium bromide **(56)** (855 mg, 1.974 mmol) in CH_2Cl_2 (15 mL) under nitrogen was added potassium *tert*-butoxide (244 mg, 2.172 mmol) over 5 min to yield an orange coloured solution. After 10 min, the freshly prepared aldehyde in CH_2Cl_2 (15 mL) was added, and the mixture was stirred at rt for 72 h, before being diluted with H_2O (30 mL). The layers were separated, and the aqueous layer was extracted with CH_2Cl_2 (3 x 30 mL). The combined organic extracts were filtered through a hydrophobic frit and concentrated *in vacuo*. The crude product was purified using a 40 g silica column, eluting with 0 – 100 % EtOAc:cyclohexane. The desired fractions were combined and concentrated *in vacuo*, followed by further purification using a Xterra® Prep RP18 OBD™ column, eluting with 0 – 100 % MeCN: ammonium carbonate modified H_2O, and the desired fractions were combined and concentrated *in vacuo* to furnish benzyl (*S*)-3-fluoro-3-

styrylpyrrolidine-1-carboxylate **(57)** (157 mg, 0.483 mmol, 24 % yield) as a pale brown coloured oil, as a mix of geometric isomers, which were not separated.

Isomer 1: **LCMS** t_R = 1.31 min (system B), 74 %, ES+ve *m/z* 326 $(M + H)^+$; **^{1}H NMR** (400 MHz, $CDCl_3$): δ = 7.42 – 7.21 (10H, m, ArH), 6.86 – 6.75, (1H, m, H_7), 5.85 – 5.72 (1H, m, H_8) 5.22 – 5.08 (2H, m, BnH), 4.00 – 3.45 (4H, m, H_{11}, H_{12}), 2.32 (1H, td, *J* = 14.1, 6.5 Hz, H_{10a}), 2.23 – 1.90 (1H, m, H_{10b}).

Isomer 2: **LCMS** t_R = 1.34 min (system B), 22 %, ES+ve *m/z* 326 $(M + H)^+$ **^{1}H NMR** (400 MHz, $CDCl_3$): δ = 7.42 – 7.21 (10H, m, ArH), 6.86 – 6.75, (1H, m, H_7), 6.34 – 6.21 (1H, td, *J* = 16.4, 11.0 Hz, H_8), 5.22 – 5.08 (2H, m, BnH), 4.00 – 3.45 (4H, m, H_{11}, H_{12}), 2.32 (1H, td, *J* = 14.1, 6.5 Hz, H_{10a}), 2.23 – 1.90 (1H, m, H_{10b}).

Benzyl (*R*)-3-fluoro-3-phenethylpyrrolidine-1-carboxylate (58)

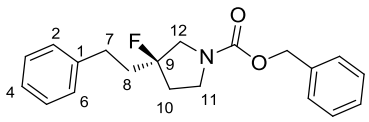

To a stirring solution of benzyl (*S*)-3-fluoro-3-styrylpyrrolidine-1-carboxylate **(57)** (144 mg, 0.443 mmol) and potassium carbonate (245 mg, 1.77 mmol) in DMF (4 mL) at 100 °C was added benzenesulfonyl hydrazide (191 mg, 1.11 mmol) portion-wise over 10 min, and the reaction was stirred for 16 h, after which a further portion of benzenesulfonyl hydrazide (191 mg, 1.11 mmol) was added portion-wise over 5 mins. After a further 2 h of stirring a final portion of benzenesulfonyl hydrazide (191 mg, 1.106 mmol) was added and the reaction was stirred for 2 h. The reaction was cooled and diluted with H_2O (4 mL), followed by extraction with CH_2Cl_2 (3 x 10 mL). The combined organic extracts were filtered through a hydrophobic frit and were concentrated *in vacuo*. The crude product was purified using an Xterra® Prep RP18 OBD™ column, eluting with 0 – 100 % MeCN:ammonium carbonate modified H_2O,

and the desired fractions were combined and concentrated *in vacuo.* However, separation from side products was not attained, so the product was repurified using a Sunfire® Prep C18 OBD™ column, eluting with 0 – 50 % MeCN:formic acid modified H_2O, and the desired fractions were combined and concentrated *in vacuo* to furnish benzyl (*R*)-3-fluoro-3-phenethylpyrrolidine-1-carboxylate **(58)** (110 mg, 0.336 mmol, 76 % yield) as a colourless oil.

LCMS t_R = 1.34 min (system A), 99 %, ES+ve *m/z* 328 $(M + H)^+$; **^{1}H NMR** (400 MHz, $CDCl_3$): δ = 7.41 – 7.25 (7H, m, ArH), 7.23 – 7.16 (3H, m, ArH), 5.20 – 5.10 (2H, m, BnH), 3.85 – 3.53 (3H, m, H_{12a}, H_{11}), 3.49 – 3.28 (1H, m, H_{12b}), 2.88 – 2.70 (2H, m, H_7), 2.27 – 2.16 (1H, m, H_{10a}), 2.15 – 2.01 (2H, m, H_8), 2.00 – 1.77 (1H, m, H_{10b}); **^{13}C NMR** (101 MHz, $CDCl_3$): δ = 153.5, 140.7, 136.6, 127.6, 127.6, 127.5, 127.0, 126.7, 125.2, 103.8 (d, *J* = 165.0 Hz), 65.4, 54.9 (d, *J* = 24.9 Hz), 43.8, 36.0 (d, *J* = 22.7 Hz), 34.5 (d, *J* = 23.5 Hz), 29.0 (d, *J* = 3.7 Hz); **IR** (neat, ν_{max} /cm^{-1}): 1700, 1417, 1353, 1112, 1090, 734, 697; **HRMS** (ESI): calc for $C_{20}H_{23}FNO_2$ $(M + H)^+$ 328.1713, found 328.1715; $[\alpha]_D^{20}$= –13 (*c* 1.0, MeOH).

(*R*)-3-Fluoro-3-phenethylpyrrolidine, formic acid salt (59)

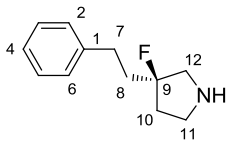

Benzyl (*R*)-3-fluoro-3-phenethylpyrrolidine-1-carboxylate **(58)** (422 mg, 1.289 mmol) in MeOH (24 mL) was passed through the H-Cube® (flow H_2 generation) using a $Pd(OH)_2$/C (20 %) catalyst, at 50 °C and 10 bar pressure, at 1 mL/min, and the resulting solution was concentrated *in vacuo*. The crude product was purified using a Sunfire® Prep C18 OBD™ column, eluting with 0 – 50 % MeCN:formic acid modified H_2O, and the desired fractions were combined and concentrated *in vacuo* to furnish (*R*)-3-

fluoro-3-phenethylpyrrolidine, formic acid salt **(59)** (301 mg, 1.258 mmol, 98 % yield) as a white coloured solid.

LCMS t_R = 0.45 min (system A), 97 %, ES+ve *m/z* 194 $(M + H)^+$; **^{1}H NMR** (400 MHz, $CDCl_3$): δ = 8.45 (1H, s, HCOOH), 7.31 – 7.27 (2H, m, ArH), 7.24 – 7.16 (3H, m, ArH), 3.50 – 3.35 (3H, m, H_{11}, H_{12a}), 3.21 (1H, dd, *J* = 33.3, 13.0 Hz, H_{12b}), 2.88 – 2.73 (2H, m, H_7), 2.36 – 2.24 (1H, m, H_{10a}), 2.23 – 2.10 (2H, m, H_8), 2.10 – 1.93 (1H, m, H_{10b}), *NH and second formic acid proton not observed*; **^{13}C NMR** (101 MHz, $CDCl_3$): δ = 168.7, 140.6, 128.8, 128.4, 126.5, 102.8 (d, *J* = 178.3 Hz), 53.7 (d, *J* = 26.4 Hz), 43.9, 37.2 (d, *J* = 23.5 Hz), 36.1 (d, *J* = 23.5 Hz), 30.4; **IR** (neat, ν_{max} /cm^{-1}): 2357 (br), 1580, 1450, 1366, 1347, 903, 765, 749, 705; **HRMS** (ESI): calc for $C_{12}H_{17}FN$ $(M + H)^+$ 194.1345, found 194.1349; **mp** 125 – 127 °C; $[\alpha]_D^{20}$= +3 (*c* 1.0, MeOH).

(*R,E*)-Methyl 4-(3-fluoro-3-phenethylpyrrolidin-1-yl)but-2-enoate (60)

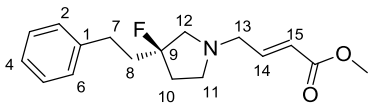

To a stirring solution of (*R*)-3-fluoro-3-phenethylpyrrolidine **(59)** (272 mg, 1.407 mmol) and DIPEA (735 µl, 4.22 mmol) in CH_2Cl_2 (14 mL) was added methyl (*E*)-4-bromobut-2-enoate **(33)** (168 µl, 1.407 mmol). The reaction was stirred for 15 h, after which H_2O (10 mL) was added and the layers were separated. The aqueous layer was extracted with CH_2Cl_2 (2 x 15 mL) and the organic extracts were combined, filtered through a hydrophobic frit, and concentrated *in vacuo*. The crude product was purified using an Xterra® Prep RP18 OBD™ column, eluting with 0 – 100 % MeCN:ammonium carbonate modified H_2O, and the desired fractions were combined and concentrated *in vacuo* to furnish methyl (*R,E*)-4-(3-fluoro-3-phenethylpyrrolidin-1-yl)but-2-enoate **(60)** (226 mg, 0.776 mmol, 55 % yield) as a very pale yellow coloured oil.

LCMS t_R = 1.19 min (system B), 100 %, ES+ve *m/z* 292 $(M + H)^+$; **^{1}H NMR** (400 MHz, $CDCl_3$): δ = 7.31 – 7.26 (2H, m, ArH), 7.22 – 7.16 (3H, m, ArH), 6.97 (1H, dt, *J* = 15.7, 6.1 Hz, H_{14}), 6.01 (1H, dt, *J* = 15.7, 1.7 Hz, H_{15}), 3.74 (3H, s, OMe), 3.28 (2H, dd, *J* = 6.0, 1.6 Hz, H_{13}), 2.96 – 2.57 (6H, m, H_7, H_{11}, H_{12}), 2.24 – 2.11 (1H, m, H_{10a}), 2.11 – 2.00 (2H, m, H_8), 2.00 – 1.87 (1H, m, H_{10b}); **^{13}C NMR** (101 MHz, $CDCl_3$): δ = 166.8, 145.5, 141.7, 128.6, 128.4, 126.1, 122.6, 103.6 (d, *J* = 177.5 Hz), 64.5 (d, *J* = 25.7 Hz), 56.7, 53.1, 51.7, 40.4 (d, *J* = 24.9 Hz), 37.4 (d, *J* = 24.2 Hz), 30.4 (d, *J* = 3.7 Hz); **IR** (neat, ν_{max} /cm^{-1}): 1732, 1435, 1269, 1194, 1171, 1029, 747, 699; **HRMS** (ESI): calc for $C_{17}H_{23}FNO_2$ $(M + H)^+$ 292.1713, found 292.2718; $[\alpha]_D^{20}$= +11 (*c* 1.0, MeOH).

(*R*)-Methyl 4-((*R*)-3-fluoro-3-phenethylpyrrolidin-1-yl)-3-(3-(2-methoxyethoxy) phenyl) butanoate (61)

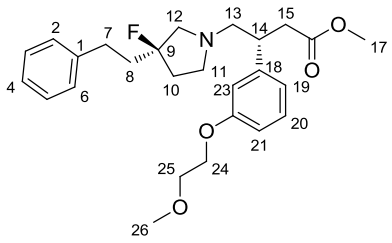

Methyl (*R,E*)-4-(3-fluoro-3-phenethylpyrrolidin-1-yl)but-2-enoate **(60)** (80.0 mg, 0.275 mmol) in 1,4-dioxane (3 mL) was added to 2-(3-(2-methoxyethoxy)phenyl)-4,4,5,5-tetramethyl-1,3,2-dioxaborolane **(34)** (153 mg, 0.549 mmol), (*S*)-BINAP (20.52 mg, 0.033 mmol), potassium hydroxide (0.145 mL, 0.549 mmol) and chloro(1,5-cyclooctadiene) rhodium(I) dimer (6.8 mg, 0.014 mmol), and the mixture was degassed and stirred under nitrogen for 3 hours at 80 °C, then cooled to rt. The reaction was diluted with HCl (2 M, 2 mL) and TBME (5 mL), and the organic layer was separated. The aqueous layer was basified with NaOH (2 M, 5 mL) and extracted with CH_2Cl_2 (2 x 15 mL). The organic extracts were combined, filtered through a hydrophobic frit and concentrated *in vacuo*. The crude product was purified using a Sunfire® Prep C18 OBD™ column, eluting 0 – 100 % MeCN: formic acid modified H_2O, and the desired fractions were combined and concentrated *in vacuo* to furnish

methyl (*R*)-4-((*R*)-3-fluoro-3-phenethylpyrrolidin-1-yl)-3-(3-(2-methoxyethoxy) phenyl) butanoate **(61)** (111 mg, 0.250 mmol, 91 % yield, 70 % *de*, determined by ^{19}F NMR) as a pale yellow coloured oil.

LCMS t_R = 1.41 min (system B), 98 %, ES+ve *m/z* 444 $(M + H)^+$; **^{1}H NMR** (400 MHz, $CDCl_3$): δ = 7.31 – 7.27 (2H, m, ArH), 7.23 – 7.16 (4H, ArH), 6.82 – 6.76 (3H, m, H_{19}, H_{21}, H_{23}), 4.11 (2H, dd, *J* = 5.5, 4.0 Hz, H_{24}), 3.74 (2H, dd, *J* = 5.5, 4.0 Hz, H_{25}), 3.59 (3H, s, H_{17}), 3.45 (3H, s, H_{26}), 3.38 – 3.29 (1H, m, H_{14}), 2.94 – 2.63 (9H, m, H_7, H_{11}, H_{12}, H_{13}, H_{15a}), 2.55 (1H, dd, *J* = 15.7, 7.8, Hz, H_{15b}), 2.17 – 1.82 (4H, m, H_8, H_{10}); **^{13}C NMR** (101 MHz, $CDCl_3$): δ (major diasteromer) = 172.9, 159.1, 144.1, 141.7, 129.8, 128.6, 128.4, 126.1, 120.2, 114.3, 112.9, 103.6 (d, *J* = 177.5 Hz), 71.2, 67.4, 64.1 (d, *J* = 24.9 Hz), 62.1, 59.4, 53.3, 51.7, 41.2, 39.9 (d, *J* = 24.9 Hz), 39.4, 37.0 (d, *J* = 23.5 Hz), 30.4 (d, *J* = 2.7 Hz); **^{19}F NMR {^{1}H}** (376 MHz, $CDCl_3$): δ = –141.17 (0.15F, s), –141.46 (0.85F, s); **IR** (neat, ν_{max} /cm^{-1}): 1732, 1584, 1259, 1196, 1161, 1127, 1064, 788, 751, 700; **HRMS** (ESI): calc for $C_{26}H_{34}FNO_4$ $(M + H)^+$ 444.2550, found 444.2551; $[\alpha]_D^{20}$= +6 (*c* 1.0, MeOH).

(*S*)-Methyl 4-((*R*)-3-fluoro-3-phenethylpyrrolidin-1-yl)-3-(3-(2-methoxyethoxy) phenyl) butanoate, formic acid salt (62)

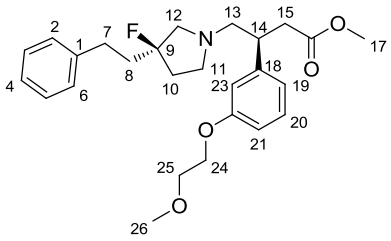

Methyl (*R,E*)-4-(3-fluoro-3-phenethylpyrrolidin-1-yl)but-2-enoate **(60)** (78.3 mg, 0.269 mmol) in 1,4-dioxane (3 mL) was added to 2-(3-(2-methoxyethoxy)phenyl)-4,4,5,5-tetramethyl-1,3,2-dioxaborolane **(34)** (149 mg, 0.537 mmol), (*R*)-BINAP (20.08 mg, 0.032 mmol), potassium hydroxide (0.141 mL, 0.537 mmol) and

chloro(1,5-cyclooctadiene) rhodium(I) dimer (6.6 mg, 0.013 mmol), and the mixture was degassed and stirred under nitrogen for 3 hours at 80 °C, then cooled to rt. The reaction was diluted with HCl (2M, 2 mL) and TBME (5 mL), and the organic layer separated. The aqueous layer was basified with NaOH (2 M, 5 mL) and extracted with CH_2Cl_2 (2 x 15 mL). The organic extracts were combined, filtered through a hydrophobic frit and concentrated *in vacuo*. The crude product was purified using a Sunfire® Prep C18 OBD™ column, eluting with 0 – 100 % MeCN:formic acid modified H_2O, and the desired fractions were combined and concentrated *in vacuo* to furnish methyl (*S*)-4-((*R*)-3-fluoro-3-phenethylpyrrolidin-1-yl)-3-(3-(2-methoxyethoxy) phenyl)butanoate, formic acid salt **(62)** (104 mg, 0.212 mmol, 79 % yield, 78 % *de*, determined by ^{19}F NMR) as a yellow coloured oil.

LCMS t_R = 1.41 min (system B), 95 %, ES+ve *m/z* 444 $(M + H)^+$; **^{1}H NMR** (400 MHz, $CDCl_3$): δ = 8.21 (1H, s, HCOOH), 7.31 – 7.26 (2H, m, ArH), 7.24 – 7.14 (4H, m, ArH), 6.89 – 6.65 (3H, m, H_{19}, H_{21}, H_{23}), 4.11 (2H, dd, *J* = 5.5, 4.0 Hz, H_{24}), 3.74 (2H, dd, *J* = 5.5, 4.0 Hz, H_{25}), 3.59 (3H, s, H_{17}), 3.45 (3H, s, H_{26}), 3.41 – 3.31 (1H, m, H_{14}), 3.03 – 2.67 (9H, m, H_7, H_{11}, H_{12}, H_{13}, H_{15a}), 2.56 (1H, dd, *J* = 15.7, 7.8, Hz, H_{15b}), 2.16 – 1.93 (4H, m, H_8, H_{10}), *second formic acid proton not observed*; **^{13}C NMR** (101 MHz, $CDCl_3$): δ (major diasteromer) = 172.7, 165.3, 159.2, 143.9, 141.6, 129.8, 128.6, 128.4, 126.2, 120.2, 114.4, 112.9, 103.4 (d, *J* = 177.5 Hz), 71.2, 67.4, 64.3 (d, *J* = 24.9 Hz), 62.0, 59.4, 53.2, 51.7, 41.0, 39.8 (d, *J* = 24.9 Hz), 39.3, 37.1 (d, *J* = 24.2 Hz), 30.3 (d, *J* = 4.4 Hz); **^{19}F NMR {^{1}H}** (376 MHz, $CDCl_3$): δ = −141.37 (0.89F, s), −141.64 (0.11F, s); **IR** (neat, ν_{max} /cm^{-1}): 1732, 1584, 1447, 1259, 1161, 1126, 1063, 748, 700; **HRMS** (ESI): calc for $C_{26}H_{34}FNO_4$ $(M + H)^+$ 444.2550, found 444.2552; $[\alpha]_D^{20}$= +20 (*c* 1.0, MeOH).

(*R*)-4-((*R*)-3-Fluoro-3-phenethylpyrrolidin-1-yl)-3-(3-(2-methoxyethoxy)phenyl) butanoic acid, formic acid salt (53)

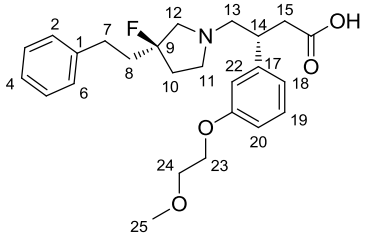

To a stirring solution of methyl (*R*)-4-((*R*)-3-fluoro-3-phenethylpyrrolidin-1-yl)-3-(3-(2-methoxyethoxy)phenyl)butanoate **(61)** (93 mg, 0.210 mmol) in H_2O (1.5 mL) and 1,4-dioxane (1.5 mL) was added sulfuric acid (0.056 mL, 1.048 mmol) and the reaction was heated to 60 °C in a sealed tube for 18 h, after which time the cooled reaction mixture was neutralised with NaOH (2 M), and concentrated *in vacuo*. The crude product was purified using a Sunfire® Prep C18 OBD™ column, eluting with 0 – 50 % MeCN:formic acid modified H_2O, and the desired fractions were combined and concentrated *in vacuo* to furnish (*R*)-4-((*R*)-3-fluoro-3-phenethylpyrrolidin-1-yl)-3-(3-(2-methoxyethoxy)phenyl)butanoic acid, formic acid salt **(53)** (72.5 mg, 0.152 mmol, 73 % yield, 78 % *de* according to ^{19}F NMR) as a colourless gum.

LCMS t_R = 0.71 min (system A), 99 %, ES+ve *m/z* 430 $(M + H)^+$; **^{1}H NMR** (400 MHz, $CDCl_3$): δ = 8.21 (1H, s, HCOOH), 7.31 – 7.14 (6H, m, ArH), 6.83 – 6.74 (3H, m, H_{18}, H_{20}, H_{22}), 4.10 (2H, m, H_{23}), 3.78 – 3.70 (2H, m, H_{24}), 3.54 – 3.25 (7H, m, H_{11a}, H_{12a}, H_{13a}, $H_{14,}$ H_{25}), 3.19 – 3.10 (1H, m, H_{11b}), 3.09 – 2.95 (2H, m, H_{12b}, H_{13b}), 2.91 – 2.83 (1H, m, H_{15a}), 2.83 – 2.62 (3H, m, H_7, H_{15b}), 2.29 – 2.16 (1H, m, H_{10a}), 2.16 – 1.97 (3H, m, $H_{8,}$ H_{10b}), *acid H signals not observed*; **^{13}C NMR** (101 MHz, $CDCl_3$): δ (major diasteromer) = 175.0, 164.8, 159.4, 143.4, 140.7, 130.3, 128.7, 128.4, 126.5, 119.6, 114.0, 113.3, 103.0 (d, *J* = 178.3 Hz), 71.2, 67.4, 63.5, 62.6 (d, *J* = 26.3 Hz), 59.3, 53.8, 43.2, 39.7, 38.0 (d, *J* = 22.7 Hz), 36.1 (d, *J* = 22.7 Hz), 30.2 (d, *J* = 3.7 Hz); **^{19}F NMR {^{1}H}** (376 MHz, $CDCl_3$): δ = −143.79 (0.11F, s), −144.28 (0.89F, s); **IR** (neat, ν_{max} /cm^{-1}): 1712, 1600, 1584, 1447, 1260, 1124, 1061, 700; **HRMS** (ESI): calc for $C_{25}H_{33}FNO_4$ $(M + H)^+$ 430.2394, found 430.2397; $[\alpha]_D^{20}$= +9 (*c* 1.0, MeCN).

(*S*)-4-((*R*)-3-Fluoro-3-phenethylpyrrolidin-1-yl)-3-(3-(2-methoxyethoxy)phenyl) butanoic acid (54)

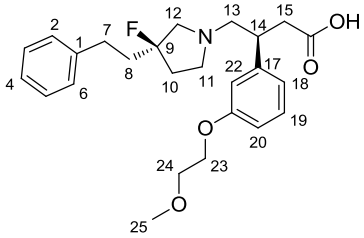

To a stirring solution of methyl (*S*)-4-((*R*)-3-fluoro-3-phenethylpyrrolidin-1-yl)-3-(3-(2-methoxyethoxy)phenyl)butanoate **(62)** (90 mg, 0.203 mmol) in H_2O (2 mL) and 1,4-dioxane (2 mL) was added sulfuric acid (0.054 mL, 1.015 mmol) and the reaction was heated to 60 °C in a sealed tube for 40 h, after which time the cooled reaction mixture was neutralised with NaOH (2 M), and concentrated *in vacuo*. The crude product was purified using a Sunfire® Prep C18 OBD™ column, eluting with 0 – 50 % MeCN:formic acid modified H_2O, and the desired fractions were combined and concentrated *in vacuo* to furnish (*S*)-4-((*R*)-3-fluoro-3-phenethylpyrrolidin-1-yl)-3-(3-(2-methoxyethoxy)phenyl)butanoic acid **(54)** (63 mg, 0.147 mmol, 72 % yield, 74 % *de* based on ^{19}F NMR) as a colourless gum.

LCMS t_R = 0.75 min (system A), 100 %, ES+ve *m/z* 430 $(M + H)^+$; **^{1}H NMR** (400 MHz, $CDCl_3$): δ = 7.32 – 7.14 (6H, m, ArH), 6.84 – 6.74 (3H, m, H_{18}, H_{20}, H_{22}), 4.13 – 4.08 (2H, m, H_{23}), 3.77 – 3.71 (2H, m, H_{24}), 3.44 (3H, s, H_{25}), 3.43 – 3.26 (4H, m, H_{11a}, H_{12a}, H_{13a}, H_{14}), 3.16 – 2.99 (2H, m, H_{12b}, H_{13b}), 2.99 – 2.82 (3H, m, H_{11b}, H_{15}), 2.81 – 2.69 (2H, m, H_7), 2.29 – 2.16 (1H, m, H_{10a}), 2.16 – 1.96 (3H, m, $H_{8,}$ H_{10b}), *acid H not observed*; **^{13}C NMR** (101 MHz, $CDCl_3$): δ (major diasteromer) = 174.3, 159.4, 143.7, 140.8, 130.3, 128.7, 128.4, 126.4, 119.6, 114.1, 113.1, 102.7 (d, *J* = 178.3 Hz), 71.2, 67.4, 64.3 (d, *J* = 25.7 Hz), 63.7, 59.4, 52.9, 43.4, 39.7, 38.5 (d, *J* = 22.7 Hz), 36.6 (d, *J* = 23.5 Hz), 30.2 (d, *J* = 3.7 Hz); **^{19}F NMR {^{1}H}** (376 MHz, $CDCl_3$): δ = –143.34 (0.87F, s), –143.82 (0.13F, s); **IR** (neat, ν_{max} /cm^{-1}): 2925, 1601, 1584, 1447, 1259, 1128, 1060, 1034, 700; **HRMS** (ESI): calc for $C_{25}H_{33}FNO_4$ $(M + H)^+$ 430.2394, found 430.2391; $[\alpha]_D^{20}$= +34 (*c* 0.5, MeCN).

(*S*)-4-((*S*)-3-Fluoro-3-(2-(5,6,7,8-tetrahydro-1,8-naphthyridin-2-yl)ethyl)pyrrolidin-1-yl)-3-(3-(2-methoxyethoxy)phenyl)butanoic acid (1)[86]

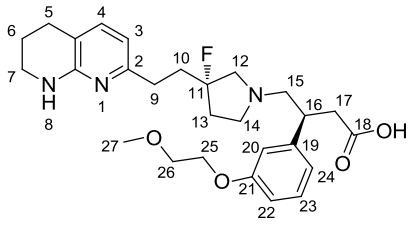

A sample of (*S*)-4-((*S*)-3-fluoro-3-(2-(5,6,7,8-tetrahydro-1,8-naphthyridin-2-yl)ethyl)pyrrolidin-1-yl)-3-(3-(2-methoxyethoxy)phenyl)butanoic acid, maleate salt **(1)** was converted to the free base form using a Xterra® Prep RP18 OBD™ column, eluting with 0 – 100 % MeCN:ammonium carbonate modified H_2O, and the desired fractions were combined and concentrated *in vacuo* to furnish (*S*)-4-((*S*)-3-fluoro-3-(2-(5,6,7,8-tetrahydro-1,8-naphthyridin-2-yl)ethyl)pyrrolidin-1-yl)-3-(3-(2-methoxyethoxy)phenyl)butanoic acid **(1)** as a pale yellow coloured oil.

LCMS t_R = 0.81 min (system B), 100 %, ES+ve *m/z* 486 $(M + H)^+$; **^{1}H NMR** (600 MHz, $CDCl_3$): δ = 8.37 (1H, br s, COOH), 7.21 (1H, t, *J* = 7.7 Hz, H_{23}), 7.16 (1H, d, *J* = 7.3 Hz, H_4), 6.83 – 6.75 (3H, m, H_{20}, H_{22}, H_{24}), 6.32 (1H, d, *J* = 7.0 Hz, H_3), 4.13 – 4.10 (2H, m, H_{25}), 4.08 (1H, br s, H_{12a}), 3.75 (2H, dd, *J* = 5.5, 4.0 Hz, H_{26}), 3.50 – 3.40 (5H, m, H_7, H_{27}), 2.96 – 2.88 (2H, m, H_{9a}, H_{14a}), 2.79 (1H, app br t, *J* = 11.6 Hz, H_{15a}), 2.73 – 2.62 (4H, m, H_5, H_{9b}, H_{17a}), 2.62 – 2.56 (1H, m, H_{17b}), 2.50 (1H, br d, *J* = 7.7 Hz, H_{14b}), 2.45 (1H, br dd, *J* = 2.6, 11.7 Hz, H_{15b}), 2.21 – 1.98 (4H, m, H_{10}, H_{13a}, H_{12b}), 1.96 – 1.80 (3H, m, H_6, H_{13b}), *amine H not observed*; **^{15}N NMR** (60.8 MHz, $CDCl_3$): δ = 197, 82, 50.

Quantitative nOe value, with distances measured relative to the known distance between methylene protons H_{9a} and H_{9b}:

Hydrogen atoms	Relative magnitude	Distance / Å
H_{9a} – H_{9b}	100.00	1.75
H_{15a} – H_{16}	10.10	2.56
H_{17b} – H_{15a}	8.31	2.65

H_{15b}– H_{12b}	7.37	2.70
H_{15b} – H_{12a}	1.88	3.39
H_{16} – H_{12a}	16.85	2.35
H_{16}– H_{12b}	0.98	3.78
H_{16} – H_{20}/H_{24}	16.35	2.37
H_{15a} – H_{20}/H_{24}	7.70	2.68
H_{17a} – H_{20}/H_{24}	6.50	2.76
H_{15b} – H_{20}/H_{24}	3.40	3.07

This nOe experiment was carried out by co-worker Upton within our laboratories.[141]

Methyl (*S*)-4-((*S*)-3-fluoro-3-(2-(5,6,7,8-tetrahydro-1,8-naphthyridin-2-yl)ethyl) pyrrolidin-1-yl)-3-(3-(2-methoxyethoxy)phenyl)butanoate (63)

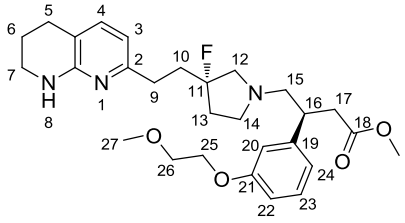

To a stirring solution of (*S*)-4-((*S*)-3-fluoro-3-(2-(5,6,7,8-tetrahydro-1,8-naphthyridin-2-yl)ethyl)pyrrolidin-1-yl)-3-(3-(2-methoxyethoxy)phenyl)butanoic acid **(1)** (10.1 mg, 0.021 mmol) in MeOH (1 mL) was added sulfuric acid (5 µl, 0.094 mmol), and the colourless solution was stirred for 20 h, followed by removal of the solvent *in vacuo*. The resulting solid was diluted with saturated aqueous sodium hydrogen carbonate solution (2 mL), followed by the addition of CH_2Cl_2 (2 mL). The layers were separated, and the aqueous layer was extracted with CH_2Cl_2 (2 x 2 mL), and the combined organic layers were filtered through a hydrophobic frit and concentrated *in vacuo*. The resulting oil was filtered through a 500 mg aminopropyl column, eluting with MeOH (5 mL), and the filtrate was concentrated *in vacuo* to furnish methyl (*S*)-4-((*S*)-3-fluoro-3-(2-(5,6,7,8-tetrahydro-1,8-naphthyridin-2-yl)ethyl)pyrrolidin-1-yl)-3-(3-(2-

methoxyethoxy)phenyl)butanoate **(63)** (7.7 mg, 0.015 mmol, 74 % yield) as a pale yellow coloured gum.

LCMS t_R = 1.29 min (system B), 100 %, ES+ve *m/z* 500 $(M + H)^+$; **^{1}H NMR** (600 MHz, $CDCl_3$): δ = 7.19 (1H, t, *J* = 7.9 Hz, H_4), 7.05 (1H, d, *J* = 7.3 Hz, H_{23}), 6.81 – 6.75 (3H, m, H_{20}, H_{22}, H_{24}), 6.35 (1H, d, *J* = 7.3 Hz, H_3), 4.85 (1H, br s, NH), 4.12 – 4.09 (2H, m, H_{25}), 3.74 (2H, dd, *J* = 3.9, 5.3 Hz, H_{26}), 3.58 (3H, s, OMe), 3.45 (3H, s, H_{27}), 3.41 – 3.37 (2H, m, H_7), 3.29 – 3.23 (1H, m, H_{16}), 2.93 – 2.88 (1H, m, H_{14a}), 2.87 – 2.60 (8H, m, H_5, H_9, H_{12}, H_{15a}, H_{17a}), 2.54 – 2.44 (3H, m, H_{14b}, H_{15b}, H_{17b}), 2.12 – 1.99 (4H, m, H_{10}, H_{13}), 1.96 – 1.82 (2H, m, H_6); **^{13}C NMR** (150 MHz, $CDCl_3$): δ = 173.2, 159.0, 157.6, 155.8, 144.7, 136.9, 129.6, 120.2, 114.3, 113.6, 112.6, 111.4, 103.8 (d, *J* = 176.9 Hz), 71.2, 67.3, 64.8 (d, *J* = 24.9 Hz), 62.4, 59.4, 53.1, 51.6, 41.8, 41.6, 39.3, 38.4 (d, *J* = 24.9 Hz), 37.3 (d, *J* = 23.8 Hz), 32.3 (d, *J* = 3.9 Hz), 26.5, 21.7; **^{15}N NMR** (60.8 MHz, $CDCl_3$): δ = 260, 74, 47; **IR** (thin film, ν_{max} /cm^{-1}): 3421 (br), 3263 (br), 1733, 1600, 1586, 1463, 1446, 1322, 1263, 1162, 1126, 868, 785, 701; **HRMS** (ESI): calc for $C_{28}H_{39}FN_3O_4$ $(M + H)^+$ 500.2925, found 500.2925; $[\boldsymbol{\alpha}]_D^{20}$= –15 (*c* 0.33, MeOH).

(*R*)-4-((*S*)-3-Fluoro-3-(2-(5,6,7,8-tetrahydro-1,8-naphthyridin-2-yl)ethyl)pyrrolidin-1-yl)-3-(3-(2-methoxyethoxy)phenyl)butanoic acid (16)

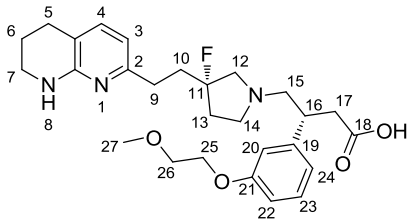

To a stirring solution of methyl (*R*)-4-((*S*)-3-fluoro-3-(2-(5,6,7,8-tetrahydro-1,8-naphthyridin-2-yl)ethyl)pyrrolidin-1-yl)-3-(3-(2-methoxyethoxy)phenyl)butanoate **(64)** (928 mg, 1.857 mmol) in H_2O (15 mL) and 1,4-dioxane (15 mL) was added sulfuric acid (0.495 mL, 9.29 mmol) and the reaction was heated to 60 °C in a sealed tube for 40 h, after which the cooled reaction mixture was neutralised with aqueous NaOH

solution (2 M), and concentrated *in vacuo*. The crude product was purified using an Xterra® Prep RP18 OBD™ column, eluting with 0 – 100 % MeCN:ammonium carbonate modified H_2O, and the desired fractions were combined and concentrated *in vacuo* to furnish (*R*)-4-((*S*)-3-fluoro-3-(2-(5,6,7,8-tetrahydro-1,8-naphthyridin-2-yl)ethyl)pyrrolidin-1-yl)-3-(3-(2-methoxyethoxy)phenyl)butanoic acid **(16)** (662 mg, 1.363 mmol, 73 % yield) as a light brown coloured gum.

LCMS t_R = 0.41 min (system A), 100 %, ES+ve *m/z* 486 $(M + H)^+$; **^{1}H NMR** (400 MHz, $CDCl_3$): δ = 7.76 (1H, br s, COOH), 7.22 – 7.14 (1H, m, H_{23}), 7.10 (1H, d, *J* = 7.1 Hz, H_4), 6.87 – 6.71 (3H, m, H_{20}, H_{22}, H_{24}), 6.28 (1H, d, *J* = 7.3 Hz, H_3), 4.08 (2H, m, H_{25}), 3.72 (2H, m, H_{26}), 3.43 (3H, s, H_{27}), 3.39 (2H, t, *J* = 5.5 Hz, H_7), 3.36 – 3.28 (1H, m, H_{16}), 3.18 – 3.05 (1H, m, H_{14a}), 3.00 (1H, td, *J* = 8.3, 3.7 Hz, H_{13a}), 2.92 (1H, dd, *J* = 12.2, 10.3 Hz, H_{15a}), 2.89 – 2.78 (1H, m, H_{14b}), 2.78 – 2.56 (8H, m, H_5, H_9, H_{13b}, H_{15b}, H_{17}), 2.20 – 1.93 (4H, m, H_{10}, H_{12}), 1.91 – 1.82 (2H, m, H_6), *amine H not observed*; **^{13}C NMR** (101 MHz, $CDCl_3$): δ = 178.2, 159.0, 155.0, 154.0, 145.6, 138.2, 129.6, 120.1, 115.7, 114.1, 112.5, 110.3, 103.1 (d, *J* = 178.3 Hz), 71.2, 67.3, 63.9 (d, *J* = 26.4 Hz), 62.8, 59.3, 52.4, 43.1, 41.7, 41.2, 38.5 (d, *J* = 23.5 Hz), 37.0 (d, *J* = 22.7 Hz), 30.0 (d, *J* = 4.4 Hz), 26.3, 20.7; **^{15}N NMR** (60.8 MHz, $CDCl_3$): δ = 216, 81, 48; (60.8 MHz, DMSO-d_6): δ = 265, 76, 48; **IR** (neat, ν_{max} /cm^{-1}): 1605, 1584, 1448, 1264, 1128, 699; **HRMS** (ESI): calc for $C_{27}H_{36}FN_3O_4$ $(M + H)^+$ 486.2768, found 486.2767; $[\alpha]_D^{20}$= –28 (*c* 0.5, MeCN).

Methyl (*R*)-4-((*S*)-3-fluoro-3-(2-(5,6,7,8-tetrahydro-1,8-naphthyridin-2-yl)ethyl) pyrrolidin-1-yl)-3-(3-(2-methoxyethoxy)phenyl)butanoate (64)

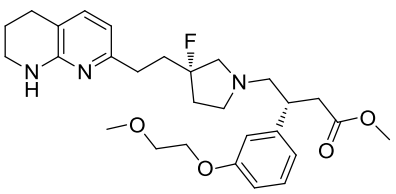

Compound used as received.[243]

^{15}N NMR (60.8 MHz, $CDCl_3$): δ = 258, 75, 47; (60.8 MHz, DMSO-d_6): δ = 263, 76, 48.

2-(5,6,7,8-Tetrahydro-1,8-naphthyridin-2-yl)ethanol (65) [244]

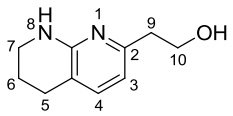

To a solution of *tert*-butyl 7-(2-hydroxyethyl)-3,4-dihydro-1,8-naphthyridine-1(2H)-carboxylate (0.508 g, 1.825 mmol) **(67)** and CH_2Cl_2 (10 mL) was added TFA (1.5 mL, 19.59 mmol), and the yellow coloured solution stood for 64 h during which the volatiles evaporated. The crude product was purified using a 40 g silica column, eluting with 0 – 25 % (EtOH + 1 % NEt_3):EtOAc, and the desired fractions were combined and concentrated *in vacuo*, followed by filtration of the resulting oil through a 2 g aminopropyl column, eluting with MeOH (50 mL). The filtrate was concentrated *in vacuo* to yield 2-(5,6,7,8-tetrahydro-1,8-naphthyridin-2-yl)ethan-1-ol **(65)** (290 mg, 1.627 mmol, 89 % yield) as a yellow coloured oil.

LCMS t_R = 0.69 min (system B), 97 %, ES+ve *m/z* 179 $(M + H)^+$; **^{1}H NMR** (400 MHz, $CDCl_3$): δ = 7.07 (1H, d, *J* = 7.3 Hz, H_4), 6.34 – 6.29 (1H, d, *J* = 7.3 Hz, H_3), 4.75 (1H, br s, NH), 3.91 (2H, t, *J* = 5.9 Hz, H_{10}), 3.42 – 3.35 (2H, m, H_7), 2.76 (2H, t, *J* = 5.9 Hz, H_9), 2.72 – 2.65 (2H, t, *J* = 6.4 Hz, H_5), 1.95 – 1.86 (2H, m, H_6), *OH not observed*; **^{13}C NMR** (151 MHz, $CDCl_3$): δ = 157.1, 155.5, 137.0, 113.9, 111.8, 62.4, 41.7, 38.3, 26.4, 21.5; **^{15}N NMR** (60.8 MHz, $CDCl_3$): δ = 254, 75; **IR** (neat, ν_{max} /cm^{-1}): 3251 (br), 1587, 1509, 1481, 1461, 1445, 1387, 1352, 1321, 1276, 1183, 1118, 1039, 1011, 802, 700, 656; **HRMS** (ESI): calc for $C_{10}H_{15}N_2O$ $(M + H)^+$ 179.1184, found 179.1186.

For the acidified ^{15}N NMR spectrum, to the NMR sample was added one drop of aqueous DCl (11 M), and the resulting mixture was dried (Na_2SO_4), filtered, and the spectrum rerun.

^{15}N NMR (60.8 MHz, $CDCl_3$): δ = 165, 86.

tert-Butyl 2-(2-methoxyethyl)-5,6-dihydro-1,8-naphthyridine-1(2H)-carboxylate (68)

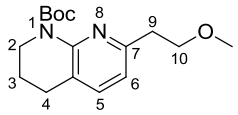

To a stirring solution of *tert*-butyl 7-(2-hydroxyethyl)-3,4-dihydro-1,8-naphthyridine-1(2H)-carboxylate **(67)** (0.487 g, 1.75 mmol) in THF (20 mL) at 0 °C under nitrogen was added sodium hydride (60 wt % dispersion in mineral oil, 0.084 g, 2.099 mmol) and the suspension was stirred for 10 min, followed by the dropwise addition of iodomethane (0.195 mL, 2.10 mmol), and warming to rt. After stirring for a 1 h, the suspension was cooled to 0 °C followed by the careful addition of H_2O (10 mL). The resulting solution was diluted with CH_2Cl_2 (20 mL), and the layers were separated. The aqueous layer was extracted with CH_2Cl_2 (3 x 20 mL), and the combined organic phases were filtered through a hydrophobic frit and concentrated *in vacuo.* The crude product was purified using a 40 g silica column, eluting with 0 – 100 % EtOAc:cyclohexane, and the desired fractions were combined and concentrated *in vacuo* to furnish *tert*-butyl 7-(2-methoxyethyl)-3,4-dihydro-1,8-naphthyridine-1(2H)-carboxylate **(68)** (445 mg, 1.52 mmol, 87 % yield) as a yellow coloured oil.

LCMS t_R = 1.09 min (system B), 100 %, ES+ve *m/z* 293 $(M + H)^+$; **^{1}H NMR** (400 MHz, $CDCl_3$): δ = 7.31 – 7.27 (1H, m, H_5), 6.88 – 6.83 (1H, m, H_6), 3.79 – 3.72 (4H, m, H_2, H_{10}), 3.36 (3H, s, OMe), 2.98 (3H, t, J = 6.8 Hz, H_9), 2.75 – 2.69 (2H, m, H_4), 1.95 – 1.87 (2H, m, H_3), 1.52 (9H, s, ^{t}BuH); **^{13}C NMR** (101 MHz, $CDCl_3$): δ = 155.4, 154.3, 151.4, 137.3, 122.3, 119.0, 80.9, 72.2, 58.8, 44.9, 38.3, 28.6, 26.5, 23.4; **IR** (thin film, ν_{max} /cm^{-1}): 1691, 1571, 1464, 1416, 1364, 1334, 1317, 1252, 1279, 1079, 858, 763; **HRMS** (ESI): calc for $C_{16}H_{25}N_2O_3$ $(M + H)^+$ 293.1865, found 293.1871.

7-(2-Methoxyethyl)-1,2,3,4-tetrahydro-1,8-naphthyridine (66)

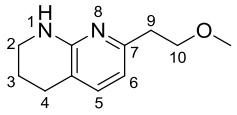

To a solution of *tert*-butyl 7-(2-methoxyethyl)-3,4-dihydro-1,8-naphthyridine-1(2H)-carboxylate **(68)** (0.445 g, 1.52 mmol) and CH_2Cl_2 (5 mL) was added TFA (1.5 mL, 19.6 mmol), and the yellow coloured solution was left to stand for 20 h, during which time the volatiles evaporated. A further portion of TFA (1 mL, 13.1 mmol) was added, and the solution was stirred for a further 1 h, after which the yellow coloured solution was filtered through 2 x 2 g isopropyl columns, eluting with MeOH (40 mL). The filtrate was concentrated *in vacuo* to yield 7-(2-methoxyethyl)-1,2,3,4-tetrahydro-1,8-naphthyridine **(66)** (294 mg, 1.53 mmol, 100 %) as an off-white coloured solid.

LCMS t_R = 0.83 min (system B), 97 %, ES+ve *m/z* 193 $(M + H)^+$; **^{1}H NMR** (600 MHz, $CDCl_3$): δ = 7.06 (1H, d, *J* = 7.3 Hz, H_5), 6.40 (1H, d, *J* = 7.3 Hz, H_6), 4.76 (1H, br s, NH), 3.68 (2H, t, *J* = 7.0 Hz, H_{10}), 3.39 (1H, dt, *J* = 5.6, 2.4 Hz, H_2), 3.34 (3H, s, OMe), 2.81 (2H, t, *J* = 7.0 Hz, H_9), 2.68 (2H, t, *J* = 6.4 Hz, H_4), 1.95 – 1.85 (2H, m, H_3); **^{13}C NMR** (151 MHz, $CDCl_3$): δ = 156.0, 155.3, 136.8, 113.8, 112.2, 72.5, 58.8, 41.8, 38.3, 26.5, 21.7; **^{15}N NMR** (60.8 MHz, $CDCl_3$): δ = 262, 74; **IR** (neat, ν_{max} /cm^{-1}): 3251, 1599, 1587, 1531, 1475, 1442, 1393, 1366, 1324, 1289, 1191, 1106, 1076, 969, 811, 637; **HRMS** (ESI): calc for $C_{11}H_{17}N_2O$ $(M + H)^+$ 193.1341, found 193.1349; **mp** 66-68 °C.

Ethyl 2-(5,6,7,8-tetrahydro-1,8-naphthyridin-2-yl)acetate (69)[245]

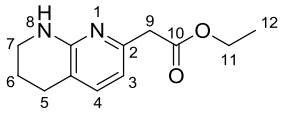

To a solution of 2-methyl-1,8-naphthyridine **(71)** (510 mg, 3.54 mmol) in THF (30 mL) at −78 °C under nitrogen was added lithium bis(trimethylsilyl)amide in THF (1.5 M, 4.72 mL, 7.07 mmol) and the solution was stirred for 20 min, followed by dropwise the addition of diethyl carbonate (0.471 mL, 3.89 mmol). After 10 min, the solution

was warmed to 0 °C and stirred for a further 1 h, after which acetic acid (0.405 mL, 7.07 mmol) was added dropwise to the black coloured mixture. The mixture was diluted with H_2O (20 mL) and EtOAc (20 mL), and the layers were separated. The aqueous layer was extracted with EtOAc (20 mL), and the combined organic layers were filtered through a hydrophobic frit and concentrated *in vacuo*. The crude product was purified using a 40 g silica column, eluting with 0 – 100 % EtOAc:cyclohexane, and the desired fractions were combined and concentrated *in vacuo*, followed by further purification using a Sunfire® Prep C18 OBD™ column, eluting with 0 – 100 % MeCN:ammonium carbonate modified H_2O, and the desired fractions were combined and concentrated *in vacuo*. The resulting oil was dissolved in EtOAc (10 mL) and EtOH (10 mL), followed by the addition of rhodium on carbon (5 wt %) (238 mg, 0.116 mmol). The mixture was stirred in presence of hydrogen gas for 14 h, after which the mixture was filtered through Celite®, washing the filter with EtOH (100 mL). The solution was concentrated *in vacuo,* followed by purification using a 40 g silica column chromatography, eluting with 0 – 100 % EtOAc:cyclohexane, and the desired fractions were combined and concentrated *in vacuo* to furnish ethyl 2-(5,6,7,8-tetrahydro-1,8-naphthyridin-2-yl)acetate **(69)** (199 mg, 0.903 mmol, 26 % yield) as a bright orange coloured oil.

LCMS t_R = 0.91 min (system B), 100 %, ES+ve *m/z* 221 $(M + H)^+$; **^{1}H NMR** (400 MHz, $CDCl_3$): δ = 7.11 – 7.07 (1H, m, H_4), 6.45 (1H, d, J = 7.3 Hz, H_3), 4.87 – 4.73 (1H, m, NH), 4.16 (2H, q, J = 7.3 Hz, H_{11}), 3.57 (2H, s, H_9), 3.39 (2H, dt, J = 5.5, 2.7 Hz, H_7), 2.70 (2H, t, J = 6.4 Hz, H_5), 1.94 – 1.86 (2H, m, H_6), 1.28 – 1.23 (3H, t, H_{12}); **^{13}C NMR** (101 MHz, $CDCl_3$): δ = 171.3, 156.1, 150.7, 136.9, 114.6, 112.4, 60.9, 43.8, 41.7, 26.6, 21.5, 14.4; **^{15}N NMR** (60.8 MHz, $CDCl_3$): δ = 263, 75; **IR** (neat, ν_{max} /cm^{-1}): 3421 (br), 3274 (br), 1731, 1600, 1586, 1480, 1461, 1366, 1321, 1298, 1252, 1187, 1148, 1116, 1030, 1012, 732; **HRMS** (ESI): calc for $C_{12}H_{17}N_2O_2$ $(M + H)^+$ 221.1290, found 221.1296.

2-(5,6,7,8-Tetrahydro-1,8-naphthyridin-2-yl)acetic acid (70)[246]

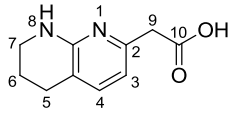

To a stirring solution of ethyl 2-(5,6,7,8-tetrahydro-1,8-naphthyridin-2-yl)acetate **(69)** (93 mg, 0.422 mmol) in 1,4-dioxane (2 mL) and H_2O (2 mL) was added sulfuric acid (100 µl, 1.876 mmol), and the yellow coloured solution was stirred for 14 h, after which the solution was heated to 80 °C and stirred for a further 6 h. The solution was neutralised by the dropwise addition of NaOH solution (2 M), and the solvent was partially removed *in vacuo.* The crude product was purified using an Xbridge Prep RP18 OBD^{TM} column, eluting with 0 – 30 % MeCN: ammonium carbonate modified H_2O, and the desired fractions were combined and concentrated *in vacuo* to furnish 2-(5,6,7,8-tetrahydro-1,8-naphthyridin-2-yl)acetic acid **(70)** (28 mg, 0.146 mmol, 35 % yield) as a yellow coloured gum.

LCMS t_R = 0.43 min (system B), 92 %, ES+ve *m/z* 193 $(M + H)^+$; **^{1}H NMR** (600 MHz, $CDCl_3$): δ = 10.41 (1H, br s, COOH), 7.22 (1H, d, *J* = 7.0 Hz, H_4), 6.30 (1H, d, *J* = 7.3 Hz, H_3), 3.61 (2H, s, H_9), 3.48 (2H, br t, *J* = 5.7 Hz, H_7), 2.70 (2H, br t, *J* = 5.9 Hz, H_5), 1.92 – 1.86 (2H, m, H_6), *amine H not observed*; **^{13}C NMR** (151 MHz, $CDCl_3$): δ = 173.9, 152.4, 145.8, 139.6, 117.9, 110.2, 41.2, 40.9, 26.1, 19.8; **^{15}N NMR** (60.8 MHz, $CDCl_3$): δ = 169, 90; **IR** (neat, ν_{max} /cm^{-1}): 3249, 1980, 1665, 1625, 1561, 1433, 1357, 1318, 1287, 1177, 1110, 1011, 908, 867, 787, 710, 607, 495; **HRMS** (ESI): calc for $C_{10}H_{13}N_2O_2$ $(M + H)^+$ 193.0977, found 193.0982.

Ethyl 3-(2-methyl-1,8-naphthyridin-3-yl)propanoate (31)

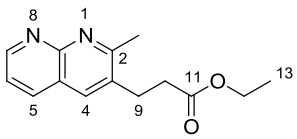

To a solution of 2-aminonicotinaldehyde **(26)** (0.490 g, 4.01 mmol) in EtOH (20 mL) was added ethyl 5-oxohexanoate **(27)** (0.635 g, 4.01 mmol) and NaOH (0.175 g, 4.38 mmol), and the reaction was heated under reflux for 2 h, before acetic acid (0.5 mL, 8.73 mmol) was added and the solvent was removed *in vacuo*. Th crude product was purified using a 40 g silica column, eluting with 90 – 100 % EtOAc:cyclohexane, then 10 – 30 % MeOH:EtOAc, and the desired fractions were combined and concentrated *in vacuo*, followed by the addition of sulfuric acid (0.214 mL, 4.01 mmol) and EtOH (20 mL). After stirring for 2 h, the solvent was removed *in vacuo,* and the product was purified using a 40 g silica column, eluting with NEt_3 (2 mL) followed by 80 – 100 % EtOAc:cyclohexane, and the desired fractions were combined and concentrated *in vacuo* to furnish ethyl 3-(2-methyl-1,8-naphthyridin-3-yl)propanoate **(31)** (333 mg, 1.363 mmol, 34 % yield) as a white coloured solid.

LCMS t_R = 0.79 min (system B), 96 %, ES+ve *m/z* 245 $(M + H)^+$; **^{1}H NMR** (400 MHz, $CDCl_3$): δ = 9.03 (1H, dd, *J* = 4.2, 2.0 Hz, H_7), 8.10 (1H, dd, *J* = 8.1, 2.0 Hz, H_5), 7.90 (1H, br s, H_4), 7.41 (1H, dd, *J* = 8.1, 4.4 Hz, H_6), 4.15 (2H, q, *J* = 7.1 Hz, H_{12}), 3.16 (2H, t, *J* = 7.6 Hz, H_9), 2.82 (3H, s, Me_2), 2.73 (2H, t, *J* = 7.8 Hz, H_{10}), 1.24 (3H, t, *J* = 7.1 Hz, H_{13}); **^{13}C NMR** (101 MHz, $CDCl_3$): δ = 172.4, 162.3, 154.9, 152.8, 136.2, 135.2, 133.8, 121.6, 121.5, 60.8, 33.8, 27.9, 23.7, 14.3; **IR** (neat, ν_{max} /cm^{-1}): 1740, 1474, 1454, 1428, 1381, 1291, 1169, 1160, 1146, 1031, 917, 784, 759; **mp** 63 – 65 °C; **HRMS** (ESI): calc for $C_{14}H_{17}N_2O_2$ $(M + H)^+$ 245.1290, found 245.1301.

Ethyl 3-(2-methyl-5,6,7,8-tetrahydro-1,8-naphthyridin-3-yl)propanoate (72)

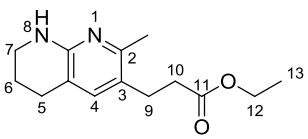

A mixture of rhodium on carbon (5 wt %) (79 mg, 0.038 mmol) and ethyl 3-(2-methyl-1,8-naphthyridin-3-yl)propanoate **(31)** (47 mg, 0.192 mmol) in EtOAc (3 mL) and EtOH (3 mL) was stirred in presence of hydrogen gas for 20 h, after which time the solution was filtered through Celite®, washing the filter with EtOH (100 mL). The solution was concentrated *in vacuo* to furnish ethyl 3-(2-methyl-5,6,7,8-tetrahydro-1,8-naphthyridin-3-yl)propanoate **(72)** (48 mg, 0.193 mmol, 100 % yield) as a yellow coloured viscous oil.

LCMS t_R = 0.99 min (system B), 86 %, ES+ve *m/z* 249 $(M + H)^+$; **^{1}H NMR** (400 MHz, $CDCl_3$): δ = 6.92 (1H, s, H_4), 4.65 (1H, br s, NH), 4.13 (2H, q, *J* = 7.0 Hz, H_{12}), 3.37 (2H, dt, *J* = 2.4, 5.4 Hz, H_7), 2.80 – 2.74 (2H, m, H_{10}), 2.66 (2H, t, *J* = 6.4 Hz, H_5), 2.55 – 2.44 (2H, m, H_9), 2.31 (3H, s, Me_2), 1.92 – 1.83 (2H, m, H_6), 1.24 (3H, t, *J* = 7.1 Hz, H_{13}); **^{13}C NMR** (151 MHz, $CDCl_3$): δ = 173.0, 154.0, 151.0, 138.2, 122.0, 114.2, 60.6, 41.7, 35.2, 27.1, 26.2, 21.6, 20.9, 14.4; ; **^{15}N NMR** (60.8 MHz, $CDCl_3$): δ = 264, 73; **IR** (neat, ν_{max} /cm^{-1}): 3415 (br), 3242 (br), 1731, 1613, 1512, 1449, 1371, 1343, 1317, 1273, 1182; **HRMS** (ESI): calc for $C_{14}H_{21}N_2O_2$ $(M + H)^+$ 249.1603, found 249.1612.

3-(2-Methyl-5,6,7,8-tetrahydro-1,8-naphthyridin-3-yl)propanoic acid (73)

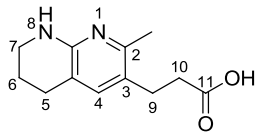

To a stirring solution of ethyl 3-(2-methyl-5,6,7,8-tetrahydro-1,8-naphthyridin-3-yl)propanoate (290 mg, 1.168 mmol) **(72)** in 1,4-dioxane (1 mL) and H_2O (2 mL) was added sulfuric acid (0.250 ml, 4.69 mmol), and the colourless solution was stirred at 80 °C for 3 h, followed by cooling to rt and neutralisation of the resulting yellow coloured solution by dropwise addition of NaOH solution (2 M). The solvent was partially removed *in vacuo,* followed by the purification of a small sample of the crude using an Xbridge Prep RP18 OBD™ column, eluting with 0 – 10 % MeCN:ammonium

bicarbonate modified H_2O, and the desired fractions were combined and concentrated *in vacuo* to furnish 3-(2-methyl-5,6,7,8-tetrahydro-1,8-naphthyridin-3-yl)propanoic acid **(73)** (14.6 mg, 0.066 mmol, 6 % yield) as a white coloured solid.

LCMS t_R = 0.44 min (system B), 97 %, ES+ve *m/z* 221 $(M + H)^+$; **^{1}H NMR** (600 MHz, $CDCl_3$): δ = 10.83 (1H, m, COOH), 7.21 (1H, s, H_4), 3.36 (2H, t, *J* = 5.7 Hz, H_7), 2.74 (2H, t, *J* = 6.6 Hz, H_9), 2.65 (2H, br t, *J* = 6.2 Hz, H_5), 2.51 (2H, t, *J* = 6.8 Hz, H_{10}), 2.47 (3H, s, Me_2), 1.83 (2H, quin, *J* = 5.9 Hz, H_6), *amine H not observed*; **^{13}C NMR** (151 MHz, $CDCl_3$): δ = 180.2, 151.6, 143.2, 141.3, 122.2, 117.4, 40.7, 38.0, 26.4, 25.9, 20.1, 16.3; **^{15}N NMR** (60.8 MHz, $CDCl_3$): δ = 173, 85; **IR** (neat, ν_{max} /cm^{-1}): 3431 (br), 3253 (br), 1678, 1571, 1404, 1385, 1353, 1292, 1238, 1054, 740, 713, 676, 613, 545, 526, 495; **HRMS** (ESI): calc for $C_{12}H_{17}N_2O_2$ $(M + H)^+$ 221.1290, found 221.1299; **mp** 132 – 142 °C.

(*S*)-4-(3-(1,1-Difluoro-3-(5,6,7,8-tetrahydro-1,8-naphthyridin-2-yl)propyl)azetidin-1-yl)-3-(3-(2-methoxyethoxy)phenyl)butanoic acid (74)

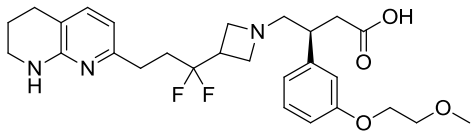

Compound used as received.[151]

^{15}N NMR (60.8 MHz, $CDCl_3$): δ = 230, 78, 35.

Methyl (*R*)-4-(3-(1,1-difluoro-3-(5,6,7,8-tetrahydro-1,8-naphthyridin-2-yl)propyl)azetidin-1-yl)-3-(3-(2-methoxyethoxy)phenyl)butanoate (75)

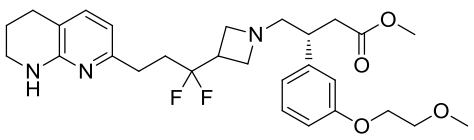

Compound used as received.[247]

^{15}N NMR (60.8 MHz, $CDCl_3$): δ = 260, 75, 31.

(*S*)-3-(3-(2-Methoxyethoxy)phenyl)-4-(3-((2-(5,6,7,8-tetrahydro-1,8-naphthyridin-2-yl)ethyl)thio)azetidin-1-yl)butanoic acid (76)

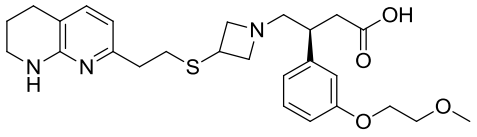

The compound was received in an impure form,[152] so it was dissolved in MeCN (1 mL) and H_2O (1 mL), and purified using an Xbridge^{TM} Prep C18 column, eluting with 0 – 100 % MeCN:ammonium carbonate modified H_2O, and the desired fractions were combined and concentrated *in vacuo* to furnish (*S*)-3-(3-(2-methoxyethoxy)phenyl)-4-(3-((2-(5,6,7,8-tetrahydro-1,8-naphthyridin-2-yl)ethyl)thio)azetidin-1-yl)butanoic acid **(76)** (15.2 mg, 0.0313 mmol) as a yellow coloured oil.

LCMS t_R = 0.78 min (system B), 100 %, ES+ve *m/z* 486 $(M + H)^+$; **^{15}N NMR** (60.8 MHz, $CDCl_3$): δ = 200, 85, 34.

(*S*)-3-(3-(2-Methoxyethoxy)phenyl)-4-(3-(2-(5,6,7,8-tetrahydro-1,8-naphthyridin-2-yl)ethoxy)azetidin-1-yl)butanoic acid (77)

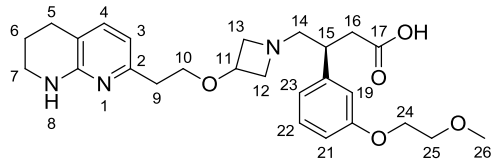

A solution of methyl (*E*)-4-(3-(2-(5,6,7,8-tetrahydro-1,8-naphthyridin-2-yl)ethoxy) azetidin-1-yl)but-2-enoate (19.1 mg, 0.058 mmol), 2-(3-(2-methoxyethoxy)phenyl)-4,4,5,5-tetramethyl-1,3,2-dioxaborolane **(34)** (80 mg, 0.288 mmol), (*R*)-BINAP (19.7 mg, 0.032 mmol), $[Rh(COD)Cl]_2$ (7.8 mg, 0.016 mmol) and potassium hydroxide (3.8 M in H_2O, 0.045 mL, 0.173 mmol) in 1,4-dioxane (1 mL) under nitrogen was heated in a microwave reactor at 100 °C for 1 h. The cooled reaction mixture was concentrated *in vacuo* then redissolved in MeOH (1 mL) and sodium hydroxide (1 M in H_2O, 0.3 mL, 0.300 mmol) was added. The resulting mixture was stirred for 1 h at 35 °C. The reaction mixture was concentrated *in vacuo*, then redissolved in H_2O (1 mL) and MeCN (1 mL) The resulting brown coloured mixture was acidified to pH 5 by the dropwise addition of 2 M aqueous hydrochloric acid solution, and then purified using an Xbridge™ Prep C18 column, eluting with 0 – 100 % MeCN:ammonium carbonate modified H_2O, and the desired fractions were combined and concentrated *in vacuo* to yield (*S*)-3-(3-(2-methoxyethoxy)phenyl)-4-(3-(2-(5,6,7,8-tetrahydro-1,8-naphthyridin-2-yl)ethoxy) azetidin-1-yl)butanoic acid **(77)** (5.6 mg, 0.012 mmol, 21 % yield) as a yellow coloured gum, as an unequal mixture of enantiomers, in an unknown ratio.

LCMS t_R = 0.73 min (system B), 99 %, ES+ve *m/z* 470 $(M + H)^+$; **^{1}H NMR** (600 MHz, $CDCl_3$): δ = 7.19 (1H, t, *J* = 8.1 Hz, H_{22}), 7.08 (1H, d, *J* = 7.3 Hz, H_4), 6.79 – 6.75 (3H, m, H_{19}, H_{21}, H_{23}), 6.30 (1H, d, *J* = 7.3 Hz, H_3), 4.16 (1H, quin, *J* = 5.9 Hz, H_{11}), 4.11 – 4.08 (2H, m, H_{24}), 3.80 – 3.71 (4H, m, H_{12a}, H_{13a}, H_{25}), 3.67 – 3.61 (2H, m, H_{10}), 3.44 (3H, s, H_{26}), 3.40 – 3.36 (2H, m, H_7), 3.16 – 3.08 (2H, m, H_{12b}, H_{15}), 3.01 (1H, br dd, *J* = 8.4, 6.2

Hz, H_{13b}), 2.97 (1H, br dd, *J* = 11.9, 8.6 Hz, H_{14a}), 2.82 (1H, dd, *J* = 12.1, 5.5 Hz, H_{14b}), 2.77 (2H, t, *J* = 7.0 Hz, H_9), 2.73 – 2.59 (4H, m, H_5, H_{16}), 1.87 (2H, quin, *J* = 5.9 Hz, H_6); **^{13}C NMR** (151 MHz, $CDCl_3$): δ = 176.8, 159.1, 155.3, 152.1, 144.9, 137.7, 129.8, 120.0, 115.4, 114.0, 112.8, 111.4, 71.2, 68.3, 68.1, 67.4, 65.8, 62.1, 61.6, 59.4, 43.5, 41.4, 40.4, 36.7, 26.4, 21.0; **^{15}N NMR** (60.8 MHz, $CDCl_3$): δ = 232, 79, 32; **IR** (neat, ν_{max} /cm^{-1}): 3258 (br), 1598, 1584, 1462, 1446, 1389, 1361, 1320, 1259, 1182, 1119, 1062, 1031, 785, 727, 701; **HRMS** (ESI): calc for $C_{26}H_{36}N_3O_5$ $(M + H)^+$ 470.2655, found 470.2656.

(*S*)-2-(3,5-Dimethylisoxazole-4-carboxamido)-3-(4-(4-(5,6,7,8-tetrahydro-1,8-naphthyridin-2-yl)butoxy)phenyl)propanoic acid (85)

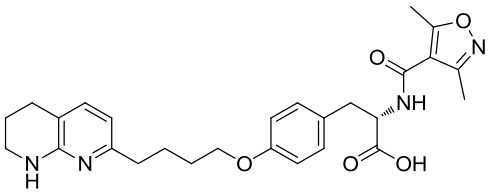

Compound was used as received.[205]

^{15}N NMR (60.8 MHz, $CDCl_3$): δ = 357, 168, 122, 88.

(*S*)-2-(3-Chloroisonicotinamido)-3-(4-(4-(5,6,7,8-tetrahydro-1,8-naphthyridin-2-yl)butoxy)phenyl)propanoic acid (86)

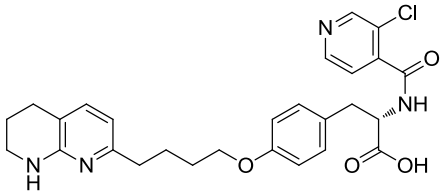

Compound was used as received.[248]

^{15}N NMR (60.8 MHz, $CDCl_3$): δ = 321, 167, 126, 88.

(*S*)-3-(3-Morpholinophenyl)-4-((*R*)-2-(2-(5,6,7,8-tetrahydro-1,8-naphthyridin-2-yl)ethyl)morpholino)butanoic acid (82)

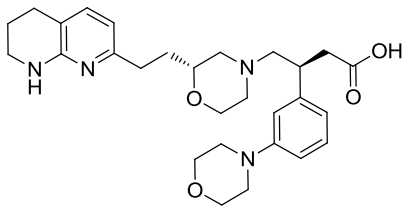

Compound was used as received.[249]

^{15}N NMR (60.8 MHz, $CDCl_3$): δ = 190, 86, 64, 45.

3-(3-Cyclopropyl-4-methoxyphenyl)-4-(4-(((5,6,7,8-tetrahydro-1,8-naphthyridin-2-yl)methoxy)methyl)piperidin-1-yl)butanoic acid (83)

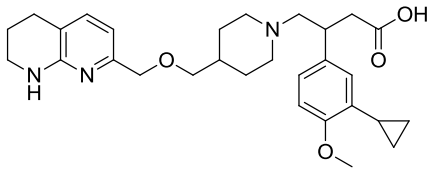

Compound was used as received.[250]

^{15}N NMR (60.8 MHz, $CDCl_3$): δ = 255, 74, 51.

(*S*)-2-(3-Oxo-8-((5,6,7,8-tetrahydro-1,8-naphthyridin-2-yl)methoxy)-2-(2,2,2-trifluoroethyl)-2,3,4,5-tetrahydro-1H-benzo[c]azepin-4-yl)acetic acid (91)

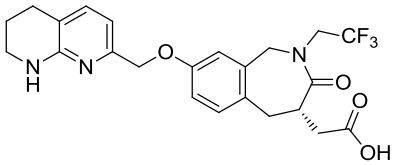

Compound was used as received.[191]

^{15}N NMR (60.8 MHz, $CDCl_3$): δ = 205, 110, 82.

(*S*)-2-(2-Chlorobenzamido)-4-(4-(5,6,7,8-tetrahydro-1,8-naphthyridin-2-yl)butanamido)butanoic acid (90)

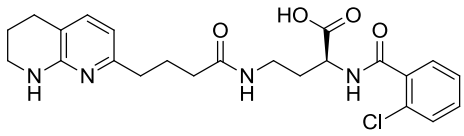

Compound was used as received.[251]

^{15}N NMR (60.8 MHz, $CDCl_3$): δ = 171, 125, 117, 85.

(*S*)-3-(3-Cyclopropylphenyl)-4-(2-((5,6,7,8-tetrahydro-1,8-naphthyridin-2-yl)methyl)-4,5-dihydrothieno[2,3-c]pyridin-6(7H)-yl)butanoic acid (87)

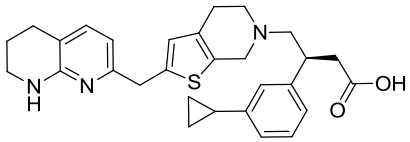

Compound was impure when it was received,[252] so it was repurified using an Xbridge™ C18 Prep column, eluting with 0 – 100 % MeCN:ammonium carbonate modified H_2O, and the desired fractions were combined and concentrated to yield (*S*)-3-(3-cyclopropylphenyl)-4-(2-((5,6,7,8-tetrahydro-1,8-naphthyridin-2-yl)methyl)-4,5-dihydrothieno[2,3-c]pyridin-6(7H)-yl)butanoic acid **(87)** as a yellow-coloured oil

^{15}N NMR (60.8 MHz, $CDCl_3$): δ = 235, 78, 43.

3-(3-Chlorophenyl)-4-(2-((5,6,7,8-tetrahydro-1,8-naphthyridin-2-yl)methyl)-6,7-dihydro-2H-pyrazolo[4,3-c]pyridin-5(4H)-yl)butanoic acid (88)

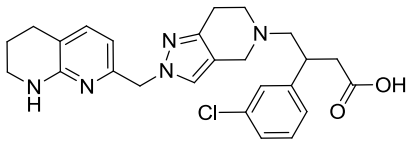

Compound was used as received.[253]

^{15}N NMR (60.8 MHz, $CDCl_3$): δ = 296, 234, 205, 78, 41.

(*S*)-3-(3-Morpholinophenyl)-4-(4-(3-(5,6,7,8-tetrahydro-1,8-naphthyridin-2-yl)propyl)piperidin-1-yl)butanoic acid (89)

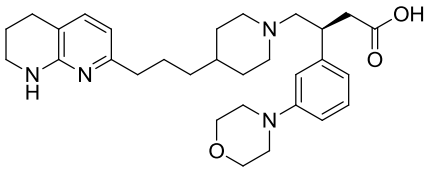

Compound was used as received.[254]

^{15}N NMR (60.8 MHz, $CDCl_3$): δ = 251, 75, 64, 51.

3-(3-Ethylphenyl)-4-(4-(3-(5,6,7,8-tetrahydro-1,8-naphthyridin-2-yl)propanoyl) piperazin-1-yl)butanoic acid (92)

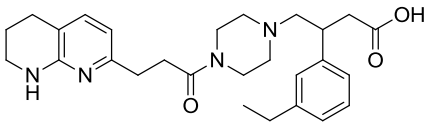

Compound was used as received.[255]

^{15}N NMR (60.8 MHz, $CDCl_3$): δ = 201, 117, 83, 45.

3-(3-Cyclopropylphenyl)-4-(4-(((5,6,7,8-tetrahydro-1,8-naphthyridin-2-yl)methyl)thio)piperidin-1-yl)butanoic acid (93)

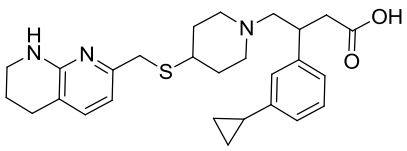

Compound was used as received.[256]

^{15}N NMR (60.8 MHz, $CDCl_3$): δ = 249, 76, *piperidyl N not observed*.

(*S*)-3-(2-Fluoro-5-morpholinophenyl)-4-((*R*)-2-(2-(5,6,7,8-tetrahydro-1,8-naphthyridin-2-yl)ethyl)morpholino)butanoic acid (94)

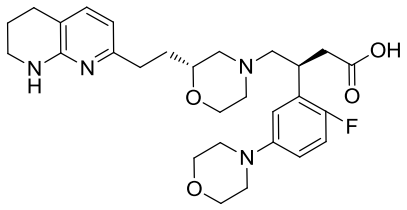

Compound was used as received.[257]

^{15}N NMR (60.8 MHz, $CDCl_3$): δ = 187, 86, 61, 44.

(*S*)-3-(3-(5-Methyl-1H-pyrazol-1-yl)phenyl)-4-((*S*)-2-(2-(5,6,7,8-tetrahydro-1,8-naphthyridin-2-yl)ethyl)-1,4-oxazepan-4-yl)butanoic acid (95)

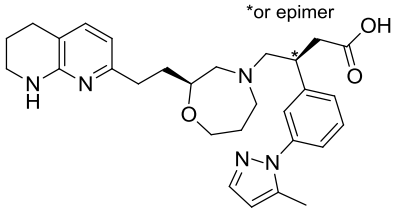

Compound was used as received.[258]

^{15}N NMR (60.8 MHz, $CDCl_3$): δ = 304, 218, 199, 83, 44.

(*R*)-3-(3-(5-Methyl-1H-pyrazol-1-yl)phenyl)-4-((*S*)-2-(2-(5,6,7,8-tetrahydro-1,8-naphthyridin-2-yl)ethyl)-1,4-oxazepan-4-yl)butanoic acid (96)

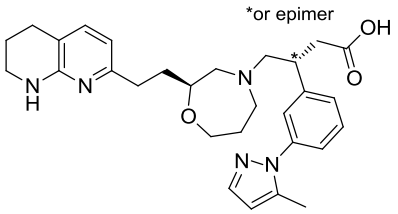

Compound was used as received.[258]

^{15}N NMR (60.8 MHz, $CDCl_3$): δ = 304, 218, 190, 84, 47.

4.3.2 Determination of enantiomeric excess

Chiral HPLC was carried out by co-workers Hindley and Hortense within our laboratories.[129]

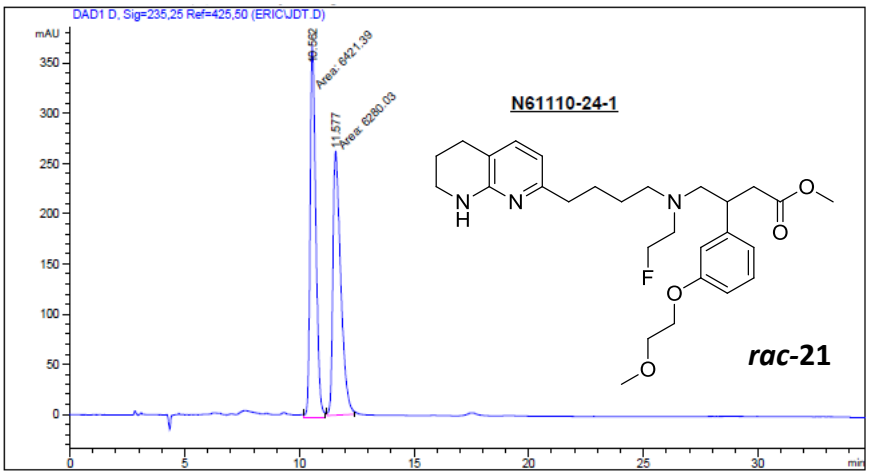


```
================================================================================
                          Area Percent Report
================================================================================

Sorted By             :      Signal
Multiplier            :      1.0000
Dilution              :      1.0000
Do not use Multiplier & Dilution Factor with ISTDs


Signal 1: DAD1 D, Sig=235,25 Ref=425,50

Peak RetTime Type  Width     Area      Height     Area
  #   [min]        [min]   [mAU*s]     [mAU]       %
----|-------|----|-------|----------|----------|--------
   1  10.562 MM    0.2896 6421.38965  369.51968  50.5565
   2  11.577 MM    0.3983 6280.02588  262.76901  49.4435
```

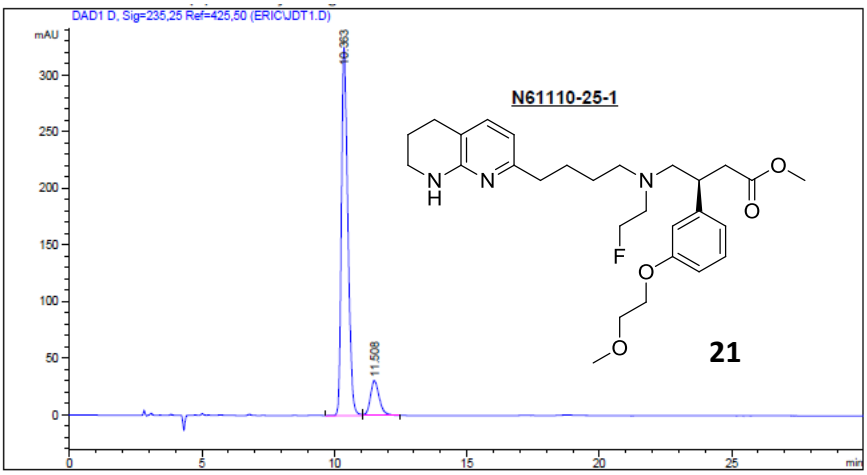


```
================================================================================
                          Area Percent Report
================================================================================

Sorted By             :      Signal
Multiplier            :      1.0000
Dilution              :      1.0000
Do not use Multiplier & Dilution Factor with ISTDs


Signal 1: DAD1 D, Sig=235,25 Ref=425,50

Peak RetTime Type  Width     Area      Height     Area
  #   [min]        [min]   [mAU*s]     [mAU]       %
----|-------|----|-------|----------|----------|-------
   1  10.363 VV    0.2620 5506.78467  324.52063  88.3392
   2  11.508 VB    0.3584  726.89563   30.91065  11.6608
```

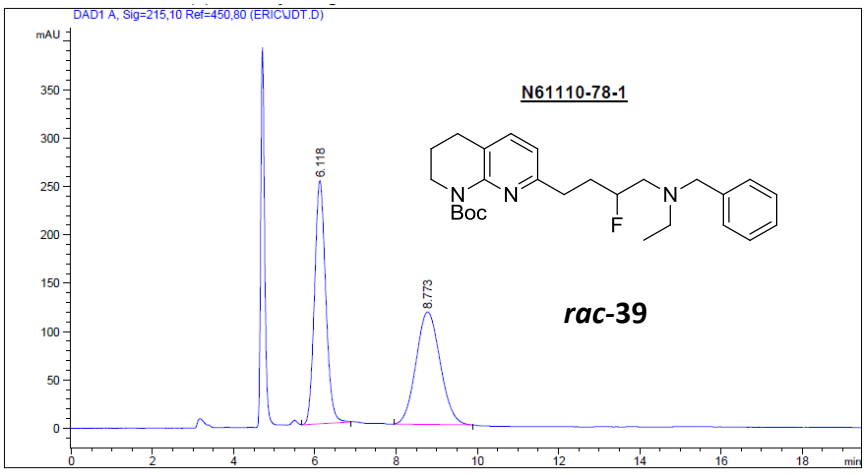


```
================================================================================
                          Area Percent Report
================================================================================

Sorted By             :      Signal
Multiplier            :      1.0000
Dilution              :      1.0000
Do not use Multiplier & Dilution Factor with ISTDs


Signal 1: DAD1 A, Sig=215,10 Ref=450,80

Peak RetTime Type  Width     Area      Height     Area
  #   [min]        [min]   [mAU*s]     [mAU]       %
----|-------|----|-------|----------|----------|-------
   1   6.118 VB    0.2958 4816.37939  251.04546  49.9921
   2   8.773 BB    0.6431 4817.90869  116.35938  50.0079
```

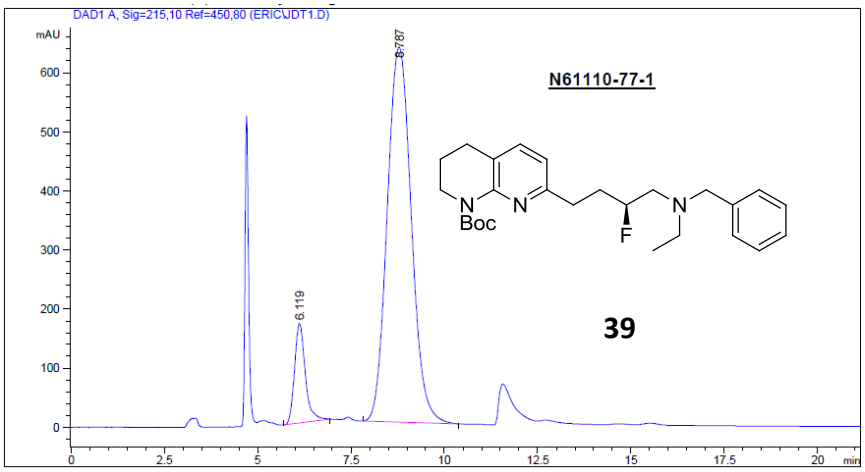


```
================================================================================
                          Area Percent Report
================================================================================

Sorted By             :      Signal
Multiplier            :      1.0000
Dilution              :      1.0000
Do not use Multiplier & Dilution Factor with ISTDs


Signal 1: DAD1 A, Sig=215,10 Ref=450,80

Peak RetTime Type  Width     Area      Height     Area
  #   [min]        [min]   [mAU*s]     [mAU]       %
----|-------|----|-------|----------|----------|-------
   1   6.119 VB    0.3057 3375.10620  168.46721  10.6094
   2   8.787 BB    0.7070 2.84374e4   634.37677  89.3906
```

4.3.3 Computational details

After importing the structures of the compounds for which the minimum energy conformation was desired into Maestro, an initial energy minimisation was performed on a random conformation using LigPrep.[259] This was followed by a conformational search of the neutral tautomer using low-mode sampling in MacroModel,[163] with the OPLS3 forcefield and the GB/SA solvation model using $CHCl_3$ to sample the conformational space.[260,261] Redundant conformations were removed by only considering two structures as different if the maximum atom deviation of any pair of corresponding atoms was greater than 0.5 Å.

The 200 – 400 conformations which resulted from this search were then clustered according to the root mean-squared deviation (RMSD) of the heavy atoms, and either the optimal number of clusters was calculated by minimising the Kelley index, or the number of clusters was set to 25.[262] The resulting clusters were then represented by

the conformation closest to the centroid of each cluster. These conformers were then optimised with density functional theory (DFT) using Jaguar,[164,263] using the B3LYP-D3/6-31G** level of theory,[160,161,162,264] using the PBF solvation model with $CHCl_3$ as the solvent.[265]

The vibrational frequencies for the resulting conformations were also calculated. If any negative frequencies were identified for the low energy conformations (indicating that the structure occupies a saddle point on the potential energy surface), these conformations were perturbed by a small amount at the dihedral angles involved in the negative frequency and then the resulting structure was reoptimized. This process was repeated if necessary until the lowest-energy conformation contained no negative frequencies (except for the cases where the ether chain of the analogues of **1** was not minimised).

The results of the optimisation and the frequency calculations gave a total free energy value at 298 K for each conformer, and the conformation with the lowest total free energy was used. These conformations were then exported to MOE 2016 to create the visualisation presented herein.

The lowest energy conformations of all compounds calculated are included as SD files in the electronic supporting information.

The accessible surface area calculations were then carried out in MOE using the QuaSAR calculation software, by calculating the partial charges of the atoms using an AMBER forcefield. Then, the H_2O-accessible surface areas were calculated using a probe radius of 1.4 Å. ASA_H is the H_2O-accessible surface area of all hydrophobic atoms (where the modulus of partial charge on the atom is < 0.2), and ASA_P the area of all hydrophilic atoms (modulus of partial charge > 0.2). FASA_P is ASA_P / ASA (ASA is the total H_2O-accessible surface area regardless of partial charge).[165]

4.4 Chapter 3 experimental details

4.4.1 Synthetic experimental details

3-Bromo-*N*-methoxy-*N*-methylthiophene-2-carboxamide (119)[266]

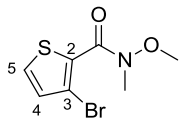

To a stirring suspension of *N*,*O*-dimethylhydroxylamine hydrochloride (1.23 g, 12.6 mmol), HATU (4.77 g, 12.6 mmol), and 3-bromothiophene-2-carboxylic acid **(118)** (2.00 g, 9.66 mmol) in CH_2Cl_2 (100 mL) was added DIPEA (4.21 ml, 24.2 mmol) and the reaction was stirred for 16 h, after which the yellow coloured solution was diluted with H_2O (100 mL), and the layers were separated. The aqueous layer was extracted with CH_2Cl_2 (100 mL), and the combined organic extracts were filtered through a hydrophobic frit and concentrated *in vacuo.* The crude product was purified using an 80 g silica column, eluting with 0 – 100 % EtOAc:cyclohexane, and the desired fractions were combined and concentrated *in vacuo* to yield **(119)** 3-bromo-*N*-methoxy-*N*-methylthiophene-2-carboxamide (2.27 g, 9.08 mmol, 94 % yield) as a colourless oil.

LCMS t_R = 0.83 min (system B), 99 %, ES+ve *m/z* 252/250 $(M + H)^+$; **^{1}H NMR** (400 MHz, $CDCl_3$): δ = 7.42 (1H, d, *J* = 5.4 Hz, ArH), 7.06 (1H, d, *J* = 5.1 Hz, ArH), 3.69 (3H, s, OMe), 3.35 (3H, s, NMe); **^{13}C NMR** (101 MHz, $CDCl_3$): δ = 161.8, 131.6, 129.5, 127.2, 115.7, 61.8, 33.6; **IR** (neat, ν_{max} /cm^{-1}): 1635, 1418, 1369, 978, 871, 748; **HRMS** (ESI): calc for $C_7H_9BrNO_2S$ $(M + H)^+$ 249.9537, found 249.9541.

3-Bromothiophene-2-carbaldehyde (120)[267]

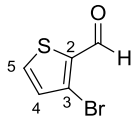

A stirring solution of 3-bromo-*N*-methoxy-*N*-methylthiophene-2-carboxamide **(119)** (10.8 g, 43.2 mmol) in THF (200 mL) under nitrogen was cooled to –78 °C, followed by the careful addition of $LiAlH_4$ in Et_2O (1 M, 43.2 ml, 43.2 mmol). The reaction was stirred for 25 min, after which it was quenched by the careful addition of ammonium chloride solution (80 mL). The mixture was left to warm up to rt, before the THF was removed *in vacuo.* Dilution with EtOAc (200 mL) and H_2O (150 mL) followed, and the layers were separated. The aqueous layer was extracted with EtOAc (3 x 150 mL), then the combined organic layers were filtered through a hydrophobic frit and concentrated *in vacuo* to furnish **(120)** 3-bromothiophene-2-carbaldehyde a pale yellow coloured oil which was used without further purification.

LCMS t_R = 0.90 min (system B), 80 %, ES+ve *m/z* 191/189 $(M - H)^+$.

1-(3-Bromothiophen-2-yl)-*N*-methylmethanamine (121)

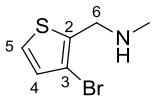

To a stirring solution of 3-bromothiophene-2-carbaldehyde **(120)** (7.66 g, 40.1 mmol) in MeCN (200 mL) under nitrogen was added methylamine in THF (2 M, 75 mL, 150 mmol). After 90 min, sodium triacetoxyhydroborate (9.76 g, 46.1 mmol) was added and the reaction was stirred for 4 h, after which the mixture was cooled to 0 °C and sodium borohydride (1.67 g, 44.1 mmol) was added, then the ice bath was removed. The cloudy suspension was stirred for 16 h, after which further portions of MeCN

(200 mL) and sodium borohydride (1.55 g, 41.0 mmol) were added, followed by stirring for a further 3 h. The suspension was cooled back to 0 °C, followed by the careful addition of H_2O (80 mL) and HCl (2 M, 150 mL). The MeCN was removed *in vacuo*, followed by the addition of MeOH (200 mL) and HCl (100 mL) and heating under reflux for 1 h. The solution was cooled to rt and concentrated *in vacuo,* followed by the addition of aqueous NaOH (2 M, 250 mL) and EtOAc (300 mL). The layers were separated, and the aqueous layer was extracted with EtOAc (300 mL). The combined organic phases were filtered through a hydrophobic frit and concentrated *in vacuo* to furnish 1-(3-bromothiophen-2-yl)-*N*-methylmethanamine **(121)** (8.25 g, 40.0 mmol, 100 % yield) as a yellow coloured oil.

LCMS t_R = 0.89 min (system B), 95 %, ES+ve *m/z* 206/208 $(M + H)^+$; **^{1}H NMR** (400 MHz, $CDCl_3$): δ = 7.20 (1H, d, *J* = 5.4 Hz, ArH), 6.93 (1H, d, *J* = 5.4 Hz, ArH), 3.90 (2H, s, H_6), 2.48 (3H, s, NMe), *amine H not observed*; **^{13}C NMR** (101 MHz, $CDCl_3$): δ =138.4, 130.1, 124.6, 108.7, 49.5, 36.0; **IR** (neat, ν_{max} /cm^{-1}): 1526, 1447, 1349, 1332, 1152, 1127, 857, 765, 699, 583; **HRMS** (ESI): calc for C_6H_9BrNS $(M+H)^+$ 205.9639, found 205.9645

tert-Butyl ((3-bromothiophen-2-yl)methyl)(methyl)carbamate (117)

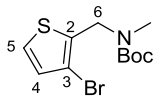

To a stirring solution of DIPEA (6.97 mL, 40.0 mmol) and 1-(3-bromothiophen-2-yl)-*N*-methylmethanamine **(121)** (8.25 g, 40.0 mmol) was added di-*tert*-butyl dicarbonate (10.12 mL, 44.0 mmol), and the reaction was stirred for 1 min, after which time imidazole (0.818 g, 12.01 mmol) and CH_2Cl_2 (10 mL) were added and the reaction was stirred for 20 min. The solution was diluted with EtOAc (150 mL) and HCl (0.2 M, 100 mL), and the layers were separated. The organic phase was washed

with HCl (0.2 M, 2 x 100 mL), then filtered through a hydrophobic frit and concentrated *in vacuo* to furnish *tert*-butyl ((3-bromothiophen-2-yl)methyl)(methyl)carbamate **(117)** (10.09 g, 33.0 mmol, 82 % yield) as a yellow coloured oil.

LCMS t_R = 1.36 min (system B), 98 %, *no mass ion observed*; **^{1}H NMR** (400 MHz, $CDCl_3$): δ = 7.23 (1H, d, *J* = 5.4 Hz, ArH), 6.91 (1H, d, *J* = 5.4 Hz, ArH), 4.56 (2H, br. s., H_6), 2.87 (3H, br. s., NMe), 1.50 (9H, s, ^{t}BuH); **^{13}C NMR** (101 MHz, $CDCl_3$): δ = 146.9, 136.1, 129.7, 125.4, 109.9, 85.3, 46.8, 34.2, 27.6; **IR** (neat, ν_{max} /cm^{-1}): 1693, 1390, 1366, 1151, 1115, 1066, 872; **HRMS** (ESI): *no mass ion observed*.

Dimethyl (*E*)-2-((2-(((*tert*-butoxycarbonyl)(methyl)amino)methyl)thiophen-3-yl) methylene) succinate (116)

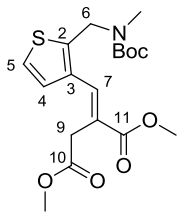

A flask containing *tert*-butyl ((3-bromothiophen-2-yl)methyl)(methyl)carbamate **(117)** (10.09 g, 33.0 mmol), DIPEA (23.0 mL, 132 mmol), tri-*ortho*-tolylphosphine (1.61 g, 5.27 mmol), diacetoxypalladium (0.96 g, 4.28 mmol) and dimethyl 2-methylenesuccinate **(102)** (4.87 mL, 34.6 mmol) in propionitrile (132 mL) was purged with nitrogen and heated under reflux for 3 h, after which time a further portion of dimethyl 2-methylenesuccinate **(102)** (1.39 mL, 9.89 mmol) was added, and the reaction stirred for a further 15 h, after which a final portion of dimethyl 2-methylenesuccinate **(102)** (1.39 mL, 9.89 mmol) was added, and the reaction was stirred for 2 h before the mixture was cooled to rt and filtered through Celite®, washing the filter with EtOAc (100 mL). The filtrate was concentrated *in vacuo,* followed by purification using a 330 g silica column, eluting with 0 – 25 %

EtOAc:cyclohexane. The desired fractions were combined and concentrated *in vacuo* to furnish dimethyl (*E*)-2-((2-(((*tert*-butoxycarbonyl)(methyl)amino)methyl)thiophen-3-yl)methylene)succinate **(116)** (5.16 g, 13.46 mmol, 41 % yield) as an orange coloured oil.

LCMS t_R = 1.25 min (system B), 95 %, ES+ve *m/z* 284 $(M + H - CO_2{}^tBu)^+$; **^{1}H NMR** (400 MHz, $CDCl_3$): δ = 7.81 (1H, s, H_7), 7.24 (1H, d, *J* = 5.1 Hz, ArH), 7.02 (1H, d, *J* = 5.4 Hz, ArH), 4.59 (2H, br s, H_6), 3.82 (3H, s, OMe), 3.72 (3H, s, OMe), 3.52 (2H, s, H_9), 2.83 (3H, br s, NMe), 1.49 (9H, s, ^{t}BuH), *NOE observed between 3.52 and 7.02, confirming (E) geometry*; **^{13}C NMR** (101 MHz, $CDCl_3$): δ = 171.3, 167.7, 155.3, 142.6, 134.2, 132.9, 127.4, 125.6, 124.6, 80.2, 52.3, 52.2, 45.7, 33.9, 33.7, 28.4; **IR** (neat, ν_{max} /cm^{-1}): 1738, 1693, 1435, 1390, 1366, 1271, 1247, 1196, 1153, 1094; **HRMS** (ESI): calc for $C_{18}H_{25}NNaO_6S$ $(M + Na)^+$ 406.1300, found 406.1301.

Dimethyl 2-((2-(((*tert*-butoxycarbonyl)(methyl)amino)methyl)thiophen-3-yl) methyl)succinate (122)

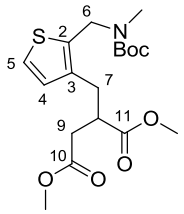

Method A:

A yellow coloured solution of dimethyl (*E*)-2-((2-(((*tert*-butoxycarbonyl)(methyl) amino)methyl)thiophen-3-yl)methylene)succinate **(116)** (55 mg, 0.143 mmol) in MeOH (10 mL) was passed through the H-Cube® (flow H_2 generation) at using a Pd/C (10 %) cartridge, at 1 mL/min and 50 bar H_2 pressure at 50 °C for 12 h, recycling the product through the machine for 3 h (a total of 18 cycles through the catalyst cell),

after which the colourless solution was concentrated *in vacuo* to yield dimethyl 2-((2-(((*tert*-butoxycarbonyl)(methyl)amino)methyl)thiophen-3-yl)methyl)succinate **(122)** (32 mg, 0.083 mmol, 58 % yield) as a colourless oil.

Method B:

A yellow coloured solution of dimethyl (*E*)-2-((2-(((*tert*-butoxycarbonyl)(methyl) amino)methyl)thiophen-3-yl)methylene)succinate **(116)** (1.32 g, 3.44 mmol) in MeOH (40 mL) was passed through the H-Cube® (flow H_2 generation) using a Pd/C (10 %) cartridge, at 1 mL/min and 50 bar H_2 pressure at 50 °C, recycling the product through the machine for 5 h, after which the colourless solution was concentrated *in vacuo.* The reaction was not complete, so the pale-yellow coloured oil was redissolved in MeOH (40 mL), and exposed to the same hydrogenation conditions for a further 6 h (a total of 15 cycles through the catalyst cell). However, the reaction was still not complete, so to the resulting oil was added potassium carbonate (1.62 g, 11.68 mmol) and DMF (30 mL), followed by heating to100 °C. To the stirring mixturewas added benzenesulfonyl hydrazide (1.26 g, 7.33 mmol) portionwise over 1 h, and the reaction was stirred for 4 h, after which another portion of benzenesulfonyl hydrazide (1.26 g, 7.30 mmol) was added portionwise over 1 h and the reaction was stirred for 3 h, after which a final portion of benzenesulfonyl hydrazide (1.26 g, 7.33 mmol) was added over 1 h. After a further 2 h, H_2O (30 mL) was added and the reaction mixture was cooled to rt. CH_2Cl_2 (50 mL) was added and the layers were separated. The aqueous layer as extracted with CH_2Cl_2 (50 mL) and the organic layers were combined. The combined organic layers were washed with 5 % aqueous lithium chloride solution, filtered through a hydrophobic frit, and concentrated *in vacuo*. The crude product was purified using a 120 g silica column, eluting with 0:100 % EtOAc:cyclohexane, and the desired fractions were combined and concentrated *in vacuo* to furnish dimethyl 2-((2-(((*tert*-butoxycarbonyl)(methyl)amino)methyl)thiophen-3-yl)methyl)succinate **(122)** (887 mg, 2.301 mmol, 67 % yield) as a colourless oil.

LCMS t_R = 1.23 min (system B), 99 %, ES+ve *m/z* 286 $(M + H - CO_2{}^tBu)^+$; **^{1}H NMR** (400 MHz, $CDCl_3$): δ = 7.15 (1H, d, *J* = 5.1 Hz, ArH), 6.80 (1H, d, *J* = 5.1 Hz, ArH), 4.66 – 4.44 (2H, m, H_6), 3.67 (3H, s, OMe), 3.65 (3H, s, OMe), 3.13 – 3.04 (1H, m, H_8), 3.03 – 2.96 (1H, m, H_{7a}), 2.87 – 2.78 (4H, m, H_{7b}, NMe), 2.67 (1H, dd, *J* = 16.6, 8.8 Hz, H_{9a}), 2.41 (1H, dd, *J* = 16.8, 5.3 Hz, H_{9b}), 1.49 (9H, s, ^{t}BuH); **^{13}C NMR** (101 MHz, $CDCl_3$): δ = 174.6, 172.2, 155.4, 136.9, 135.2, 128.7, 124.1, 80.2, 52.1, 51.9, 45.1, 42.5, 35.3, 33.8, 30.0, 28.5; **IR** (neat, ν_{max} /cm^{-1}): 1733, 1689, 1437, 1391, 1366, 1247, 1147, 874; **HRMS** (ESI): calc for $C_{18}H_{27}NO_6SNa$ $(M + Na)^+$ 408.1457, found 408.1453.

Dimethyl 2-((4,4,5,5-tetramethyl-1,3,2-dioxaborolan-2-yl)methyl)succinate (123)

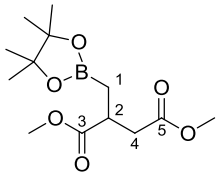

A flask was charged with triphenylphosphine (0.332 g, 1.27 mmol) and copper(II) carbonate (0.156 g, 1.27 mmol), and the flask was purged with nitrogen gas. H_2O (40 mL) was added and the solution was stirred vigorously for 15 min, after which time 4,4,4',4',5,5,5',5'-octamethyl-2,2'-bi(1,3,2-dioxaborolane) (3.53 g, 13.91 mmol) was added and the stirring continued for 15 min, after which time dimethyl 2-methylenesuccinate **(102)** (1.78 mL, 12.65 mmol) was added and the reaction was stirred vigorously for 65 h, after which time the turquoise coloured solution was diluted with H_2O (20 mL) and EtOAc (60 mL), and the layers were separated. The aqueous layer was extracted with EtOAc (3 x 60 mL) and the combined organic extracts were filtered through a hydrophobic frit and concentrated *in vacuo*. The crude product was purified using a 40 g silica column, eluting with 0 – 50 % EtOAc:cyclohexane, and the desired fractions were combined and concentrated i*n vacuo,* before further purification using an 80 g silica column, eluting with 0 – 50 % EtOAc:cyclohexane, and the desired fractions were combined and concentrated *in*

vacuo to yield dimethyl 2-((4,4,5,5-tetramethyl-1,3,2-dioxaborolan-2-yl)methyl)succinate **(123)** (2.77 g, 9.68 mmol, 77 % yield) as a colourless oil.

^{1}H NMR (400 MHz, $CDCl_3$): δ = 3.67 (6H, m, OMe, OMe), 3.11 – 3.01 (1H, m, H_2), 2.74 (1H, dd, *J* = 16.5, 8.3 Hz, H_{4a}), 2.53 (1H, dd, *J*= 16.4, 5.9 Hz, H_{4b}), 1.23 (12H, d, *J* = 2.5 Hz, 4 x Me) 1.14 (1H, dd, *J* = 15.9, 7.6 Hz, H_{1a}), 1.00 (1H, dd, *J* = 15.9, 7.3 Hz, H_{1b}), **^{13}C NMR** (101 MHz, $CDCl_3$): δ = 175.8, 172.5, 83.4, 51.9, 51.7, 37.7, 37.2, 24.9, 24.8; **IR** (neat, ν_{max} /cm^{-1}): 1734, 1437, 1371, 1320, 1269, 1202, 1165, 1140, 968, 845.

Potassium trifluoro(4-methoxy-2-(methoxycarbonyl)-4-oxobutyl)borate (124)

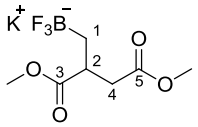

A solution of potassium fluoride (10 M, 0.419 mL, 4.19 mmol) was added to a stirring solution of dimethyl 2-((4,4,5,5-tetramethyl-1,3,2-dioxaborolan-2-yl)methyl)succinate **(123)** (300 mg, 1.05 mmol) in MeOH (5 mL) and MeCN (5 mL). After 1 min, (2*R*,3*R*)-2,3-dihydroxysuccinic acid in THF (2 M, 1.08 mL, 2.15 mmol) was and the white coloured slurry was filtered, washing the filter with MeCN (20 mL). The filtrate was concentrated *in vacuo* using a trolley pump to furnish potassium trifluoro(4-methoxy-2-(methoxycarbonyl)-4-oxobutyl)borate **(124**) (287 mg, 1.08 mmol, 103 % crude yield) as a translucent gum containing 10 % unreacted starting material, that was used without further purification.

^{1}H NMR (400 MHz, $CDCl_3$): δ = 3.62 (6H, s, OMe, OMe), 2.87 – 2.74 (1H, m, H_2), 2.66 (1H, dd, *J* = 16.8, 8.7 Hz, H_{4a}), 2.48 (1H, dd, *J* = 16.6, 5.6 Hz, $H4_b$), 0.64 – 0.51 (1H, m, H_{1a}), 0.50 – 0.35 (1H, m, H_{1b}).

Dimethyl 2-((5-bromo-2-(((*tert*-butoxycarbonyl)(methyl)amino)methyl)thiophen-3-yl)methyl)succinate (115)

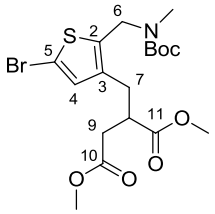

To a stirring solution of dimethyl 2-((2-(((*tert*-butoxycarbonyl)(methyl)amino)-methyl)thiophen-3-yl)methyl)succinate **(122)** (24.9 mg, 0.065 mmol) in $CHCl_3$ (650 µl) and acetic acid (7.40 µl, 0.129 mmol) was added *N*-bromosuccinimide (16.6 mg, 0.093 mmol), and the reaction was stirred for 2 h, after which H_2O (2 mL) was added. The layers were separated, and the aqueous layer was extracted with CH_2Cl_2 (2 mL). The combined organic layers were filtered through a hydrophobic frit and concentrated *in vacuo*. The crude product was purified using an Xterra® Prep RP18 OBD™ column, eluting with MeCN:ammonium carbonate modified H_2O 0 – 100 %, and the desired fractions were combined and concentrated *in vacuo* to yield dimethyl 2-((5-bromo-2-(((*tert*-butoxycarbonyl)(methyl)amino)methyl) thiophen-3-yl)methyl)succinate **(115)** (11.9 mg, 0.026 mmol, 40 % yield) as a yellow coloured oil.

LCMS t_R = 1.37 min (system B), 100 %, ES+ve *m/z* 364/366 $(M + H - CO_2{}^tBu)^+$; **^{1}H NMR** (400 MHz, $CDCl_3$): δ = 6.76 (1H, s, H_4), 4.55 – 4.36 (2H, m, H_6), 3.68 (3H, s, OMe), 3.66 (3H, s, OMe), 3.07 – 2.99 (1H, m, H_8), 2.97 – 2.89 (1H, m, H_{7a}), 2.82 (3H, s, NMe), 2.79 – 2.71 (1H, m, H_{7b}), 2.67 (1H, dd, *J* = 16.6, 8.3 Hz, H_{9a}), 2.42 (1H, dd, *J* = 16.6, 5.6 Hz, H_{9b}), 1.49 (9H, s, ^{t}BuH).

Dimethyl 2-((2-(((*tert*-butoxycarbonyl)(methyl)amino)methyl)-5-iodothiophen-3-yl)methyl)succinate (127)

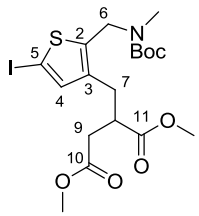

To a stirring solution of dimethyl 2-((2-(((*tert*-butoxycarbonyl)(methyl)amino)methyl) thiophen-3-yl)methyl)succinate **(122)** (49 mg, 0.127 mmol) in $CHCl_3$ (1.5 mL) and acetic acid (0.015 mL, 0.254 mmol) was added *N*-iodosuccinimide (28.6 mg, 0.127 mmol), and the pink coloured solution was stirred for 8 h, after which a further portion of *N*-iodosuccinimide (28.6 mg, 0.127 mmol) was added and the dark pink coloured solution was stirred for a further 16 h. H_2O (2 mL) was added and the layers were separated. The aqueous phase was extracted with CH_2Cl_2 (2 x 2 mL), and the combined organic phases were concentrated using a flow of nitrogen gas. The crude product was purified using an Xterra® Prep RP18 OBD™ column, eluting with MeCN:ammonium carbonate modified H_2O 0 – 100 %, and the desired fractions were combined and concentrated *in vacuo* to yield dimethyl 2-((2-(((*tert*-butoxycarbonyl)(methyl)amino)methyl)-5-iodothiophen-3-yl)methyl)succinate **(127)** (55 mg, 0.108 mmol, 85 % yield) as a pale yellow coloured oil.

LCMS t_R = 1.38 min (system B), 100 %, ES+ve *m/z* 412 $(M + H - CO_2{}^tBu)^+$; **^{1}H NMR** (400 MHz, $CDCl_3$): δ = 6.94 (1H, s, ArH), 4.59 – 4.39 (2H, m, H_6), 3.67 (3H, s, OMe), 3.66 (3H, s, OMe), 3.07 – 2.98 (1H, m, H_8), 2.98 – 2.91 (1H, m, H_{7a}), 2.82 (3H, s, NMe), 2.80 – 2.71 (1H, m, H_{7b}), 2.67 (1H, dd, *J* = 16.6, 8.3 Hz, H_{9a}), 2.42 (1H, dd, *J* = 16.6, 5.6 Hz, H_{9b}), 1.49 (9H, s, ^{t}BuH).

2-(2-Methyl-1,3-dioxolan-2-yl)ethan-1-ol (129)[268]

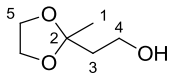

Ethylene glycol (6.33 ml, 113 mmol), 4-hydroxybutan-2-one **(128)** (4.89 ml, 56.7 mmol), $MgSO_4$ (2.05 g, 17.0 mmol), EtOAc (200 mL), and (2*S*,3*S*)-2,3-dihydroxysuccinic acid (0.426 g, 2.84 mmol) were combined in a flask, and the flask fitted with a Dean Stark apparatus and flushed with nitrogen gas. The stirring suspension was then heated under reflux for 23 h, after which time it was cooled to rt. The suspension was filtered and then saturated aqueous $NaHCO_3$ (120 mL) was added and the layers were separated. The aqueous layer was extracted with EtOAc (150 mL), and the combined organic phases were filtered through a hydrophobic frit and concentrated *in vacuo.* The crude product was purified using a 120 g silica column, eluting with 0 – 100 % EtOAc:cyclohexane, and the desired fractions were combined and concentrated *in vacuo* to furnish 2-(2-methyl-1,3-dioxolan-2-yl)ethan-1-ol **(129)** (3.29 g, 24.89 mmol, 44 % yield).

^{1}H NMR (400 MHz, $CDCl_3$): δ = 3.99 (4H, s, H_5), 3.80 – 3.73 (2H, m, H_4), 2.73 (1H, br s, OH), 1.98 – 1.92 (2H, m, H_3), 1.37 (3H, s, H_1).

Methyl 2-(7-methyl-6-oxo-5,6,7,8-tetrahydro-4H-thieno[2,3-c]azepin-5-yl)acetate (131)

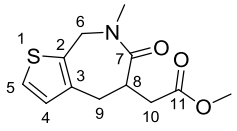

To a stirring solution of dimethyl 2-((2-(((*tert*-butoxycarbonyl)(methyl)amino) methyl)thiophen-3-yl)methyl)succinate **(122)** (150 mg, 0.389 mmol) in CH_2Cl_2 (5 mL) was added TFA (0.5 mL, 6.57 mmol), and the reaction was stirred for 1.5 h, after which the solvent was concentrated using a flow of nitrogen gas, followed by the addition of PhMe (5 mL). The sealed tube was purged with nitrogen gas, and the solution was

heated to 200 °C for 40 min in a microwave reactor, then cooled to rt, followed by a further 1 h at 200 °C in a microwave reactor. The brown coloured solution was cooled to rt, then concentrated *in vacuo*. The crude product was purified using an Xterra® Prep RP18 OBD™ column, eluting with MeCN:ammonium carbonate modified H_2O 0 – 100 %, and the desired fractions were combined and concentrated *in vacuo* to furnish methyl 2-(7-methyl-6-oxo-5,6,7,8-tetrahydro-4H-thieno[2,3-c]azepin-5-yl)acetate **(131)** (43 mg, 0.170 mmol, 44 % yield) as a while coloured solid.

LCMS t_R = 0.83 min (system B), 97 %, ES+ve *m/z* 254 $(M + H)^+$; **^{1}H NMR** (400 MHz, $CDCl_3$): δ = 7.07 (1H, d, *J* = 5.1 Hz, ArH), 6.76 (1H, d, *J* = 5.1 Hz, ArH), 5.22 (1H, td, *J* = 17.1, 2.0 Hz, H_{6a}), 3.95 (1H, d, *J* = 17.1 Hz, H_{6b}), 3.84 – 3.72 (1H, m, H_8), 3.70 (3H, s, OMe), 3.10 – 3.01 (4H, m, NMe, H_{10a}), 2.96 – 2.87 (1H, m, H_{9a}), 2.83 – 2.70 (1H, m, H_{9b}), 2.42 (1H, dd, *J* = 16.8, 5.3 Hz, H_{10b}); **^{13}C NMR** (101 MHz, $CDCl_3$): δ = 174.2, 173.1, 136.2, 131.1, 129.8, 122.5, 51.9, 47.4, 37.2, 36.6, 35.9, 31.9; **IR** (neat, ν_{max} /cm^{-1}): 1736, 1638, 1358, 1199, 1165, 997, 745, 720, 589; **HRMS** (ESI): calc for $C_{12}H_{16}NO_3S$ $(M + H)^+$ 254.0851, found 254.0848.

Methyl 2-(2-iodo-7-methyl-6-oxo-5,6,7,8-tetrahydro-4H-thieno[2,3-c]azepin-5-yl)acetate (132)

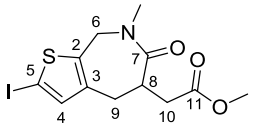

To a stirring solution of methyl 2-(7-methyl-6-oxo-5,6,7,8-tetrahydro-4H-thieno[2,3-c]azepin-5-yl)acetate **(131)** (45 mg, 0.178 mmol) in $CHCl_3$ (2 mL) and acetic acid (10 µl, 0.178 mmol) at 0 °C was added *N*-iodosuccinimide (40.0 mg, 0.178 mmol), and the pink coloured solution was warmed to rt, followed by stirring for 16 h, after which the solution was heated to 40 °C and stirred for 24 h, after which time H_2O (2 mL) was added and the layers were separated. The aqueous phase was extracted with CH_2Cl_2

(2 x 2 mL), and the combined organic phases were concentrated using a flow of nitrogen gas. The crude product was purified using an Xterra® Prep RP18 OBD™ column, eluting with 0 – 100 % MeCN:ammonium carbonate modified H_2O, and the desired fractions were combined and concentrated *in vacuo* to yield methyl 2-(2-iodo-7-methyl-6-oxo-5,6,7,8-tetrahydro-4H-thieno[2,3-c]azepin-5-yl)acetate **(132)** (45 mg, 0.119 mmol, 67 % yield) as a pale yellow coloured oil.

LCMS t_R = 1.04 min (system B), 71 %, ES+ve *m/z* 380 $(M + H)^+$; **^{1}H NMR** (400 MHz, $CDCl_3$): δ = 6.91 (1H, s, H_4), 5.15 (1H, td, *J* = 17.1, 2.0 Hz, H_{6a}), 3.89 (1H, d, *J* = 17.1 Hz, H_{6b}), 3.78 – 3.70 (1H, m, H_8), 3.70 – 3.65 (3H, s, OMe), 3.07 – 2.98 (4H, m, NMe, H_{10a}), 2.92 – 2.82 (1H, m, H_{9a}), 2.75 – 2.64 (1H, m, H_{9b}), 2.40 (1H, dd, *J* = 16.8, 5.3 Hz, H_{10b}); **^{13}C NMR** (101 MHz, $CDCl_3$): δ = 174.0, 172.9, 139.4, 138.2, 137.2, 70.3, 51.9, 47.0, 37.1, 36.5, 35.9, 31.3; **IR** (neat, ν_{max} /cm^{-1}): 1725, 1628, 1437, 1358, 1161, 489; **HRMS** (ESI): calc for $C_{12}H_{15}INO_3S$ $(M + H)^+$ 379.9817, found 379.9815.

(*E*)-Dimethyl 2-((2-(((*tert*-butoxycarbonyl)(methyl)amino)methyl)-5-iodothiophen-3-yl)methylene)succinate (136)

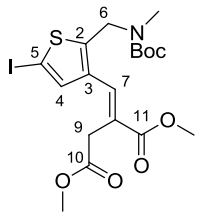

To a stirring solution of dimethyl (*E*)-2-((2-(((*tert*-butoxycarbonyl)(methyl) amino)methyl)thiophen-3-yl)methylene)succinate **(116)** (4.79 g, 12.49 mmol) in $CHCl_3$ (100 mL) and acetic acid (0.715 ml, 12.49 mmol) was added *N*-iodisuccinimide (2.90 g, 12.87 mmol), and the pink coloured solution was heated under reflux and stirred for 5 h, after which a further portion of *N*-iodisuccinimide (0.843 g, 3.75 mmol) was added and the reaction was stirred for a further 6 h, after which the dark purple

coloured solution was cooled to rt and diluted with H_2O (100 mL) and the layers were separated. The aqueous phase was extracted with CH_2Cl_2 (2 x 100 mL), and the combined organic extracts were filtered through a hydrophobic frit and concentrated *in vacuo*, before purification with a 120 g silica column, eluting with 0 – 40 % EtOAc:cyclohexane. The desired fractions were combined and concentrated *in vacuo* to yield dimethyl (*E*)-2-((2-(((*tert*-butoxycarbonyl)(methyl)amino)methyl)-5-iodothiophen-3-yl)methylene)succinate **(136)** (5.78 g, 11.35 mmol, 91 % yield) as a pale yellow coloured oil.

LCMS t_R = 1.40 min (system B), 94 %, ES+ve *m/z* 410 $(M + H - CO_2{}^tBu)^+$; **^{1}H NMR** (400 MHz, $CDCl_3$): δ = 7.68 (1H, s, H_7), 7.13 (1H, s, H_4), 4.53 (2H, br s, H_6), 3.83 – 3.77 (3H, s, OMe), 3.73 (3H, s, OMe), 3.47 (2H, s, H_9), 2.82 (3H, s, NMe), 1.49 (9H, s, ^{t}BuH); **^{13}C NMR** (101 MHz, $CDCl_3$): δ = 171.0, 167.3, 155.4, 148.2, 136.7, 134.7, 133.0, 126.8, 80.5, 73.0, 52.4, 52.2, 45.7, 34.1, 33.7, 28.4; **IR** (neat, ν_{max} /cm^{-1}): 1693, 1435, 1390, 1366, 1267, 1195, 1152, 1094, 872, 774; **HRMS** (ESI): calc for $C_{18}H_{24}INO_6SNa$ $(M + Na)^+$ 532.0267, found 532.0265.

(*E*)-Dimethyl 2-((2-(((*tert*-butoxycarbonyl)(methyl)amino)methyl)-5-(4-hydroxy pent-1-yn-1-yl)thiophen-3-yl)methylene)succinate (141)

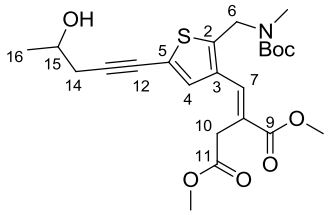

A solution of triethylamine (0.325 ml, 2.332 mmol), $Pd(PPh_3)Cl_2$ (0.055 g, 0.078 mmol), copper(I) iodide (0.018 g, 0.093 mmol), pent-4-yn-2-ol **(140)** (0.088 ml, 0.933 mmol) and dimethyl (*E*)-2-((2-(((*tert*-butoxycarbonyl)(methyl)amino)methyl)-5-iodothiophen-3-yl)methylene)succinate **(136)** (0.396 g, 0.777 mmol) in DMF (8 mL) under nitrogen was heated to 80 °C for 16 h, followed by cooling to rt. The brown

coloured solution was filtered through Celite®, washing with EtOAc (20 mL), and the resulting orange coloured solution was washed with 5 % aqueous lithium chloride solution (2 x 20 mL), then filtered through a hydrophobic frit and concentrated *in vacuo.* The crude product was purified using a 40 g silica column, eluting with 0 – 100 % EtOAc:cyclohexane, and the desired fractions were combined and concentrated *in vacuo* to furnish dimethyl (*E*)-2-((2-(((*tert*-butoxycarbonyl)(methyl)amino)methyl)-5-(4-hydroxypent-1-yn-1-yl)thiophen-3-yl)methylene)succinate **(141)** (355 mg, 0.763 mmol, 98 % yield) as a yellow coloured oil.

LCMS t_R = 1.22 min (system B), 93 %, *molecular mass ion not observed,* ES+ve *m/z* 366 $(M + H - CO_2{}^tBu)^+$; **^{1}H NMR** (400 MHz, $CDCl_3$): δ = 7.70 (1H, s, H_7), 7.04 (1H, s, H_4), 4.53 (2H, s, H_6), 4.05 (1H, s, H_{15}), 3.81 (3H, s, OMe), 3.72 (3H, s, OMe), 3.48 (2H, s, H_{10}), 2.83 (3H, s, NMe), 2.68 – 2.52 (2H, m, H_{14}), 1.97 (1H, d, *J* = 3.4 Hz, OH), 1.49 (9H, s, ^{t}BuH), 1.31 (3H, d, *J* = 6.1 Hz, H_{16}); **^{13}C NMR** (101 MHz, $CDCl_3$): δ = 171.2, 167.5, 155.1, 143.3, 133.8, 132.6, 131.5, 126.7, 122.9, 91.7, 80.5, 75.6, 66.6, 52.5, 52.4, 45.9, 34.2, 33.8, 30.4, 28.5, 22.7; **IR** (neat, ν_{max} /cm^{-1}): 3444 (br), 1694, 1435, 1391, 1367, 1268, 1194, 1155, 1094, 732; **HRMS** (ESI): calc for $C_{23}H_{31}NNaO_7S$ $(M + Na)^+$ 488.1719, found 488.1718.

Dimethyl 2-((2-(((*tert*-butoxycarbonyl)(methyl)amino)methyl)-5-(4-hydroxypentyl) thiophen-3-yl)methyl)succinate (142)

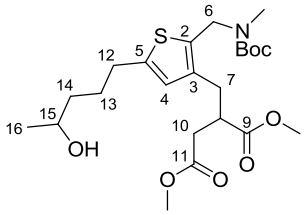

A solution of dimethyl (*E*)-2-((2-(((*tert*-butoxycarbonyl)(methyl)amino)methyl)-5-(4-hydroxypent-1-yn-1-yl)thiophen-3-yl)methylene)succinate **(141)** (4.21 g, 9.04 mmol) in DMF (100 mL) was heated to 100 °C, after which potassium carbonate (6.25 g, 45.2

mmol) was added, followed by the portionwise addition of benzenesulfonyl hydrazide (7.79 g, 45.2 mmol) over 1 h, and the reaction was stirred for a further 1 h before the addition of a further portion of benzenesulfonyl hydrazide (7.79 g, 45.2 mmol) over 1 h. After a further 3 h, a further portion of benzenesulfonyl hydrazide (7.79 g, 45.2 mmol) was added and the reaction stirred for 4 h. After, further portions of potassium carbonate (6.25 g, 45.2 mmol) and benzenesulfonyl hydrazide (7.79 g, 45.2 mmol) were added and the reaction was stirred for a further 3 h before being cooled to rt and diluted with H_2O (100 mL) and CH_2Cl_2 (100 mL). The layers were separated, and the aqueous phase was extracted with CH_2Cl_2 (2 x 100 mL), before the combined organic phases were washed with 10 % aqueous lithium chloride (3 x 100 mL) and filtered through a hydrophobic frit. The crude product was purified using a 120 g silica column, eluting with 0 – 100 % EtOAc:cyclohexane, and the desired fractions were combined and concentrated *in vacuo,* before being dissolved in EtOAc (30 mL), washed with 10 % aqueous lithium chloride (3 x 50 mL), filtered through a hydrophobic frit, and concentrated *in vacuo* to yield dimethyl 2-((2-(((*tert*-butoxycarbonyl)(methyl)amino)methyl)-5-(4-hydroxypentyl)thiophen-3-yl)methyl)succinate **(142)** (3.18 g, 6.74 mmol, 75 % yield) as an orange coloured oil, as an inseparable mixture with the corresponding compound without C_7-C_8 alkene reduction (4:1 ratio).

LCMS t_R = 1.22 min (system B), 79 %, *molecular ion not observed* ES+ve *m/z* 472 (M + H – $CO_2{}^t$Bu)$^+$; **^{1}H NMR** (400 MHz, $CDCl_3$): δ = 6.48 (1H, s, H_4), 4.50 – 4.38 (2H, m, H_6), 3.87 – 3.79 (1H, m, H_{15}), 3.68 (3H, s, OMe), 3.65 (3H, s, OMe), 3.11 – 3.00 (1H, m, H_8), 2.96 – 2.89 (1H, dd, *J* = 14.2, 6.6 Hz, H_{7a}), 2.81 (3H, s, NMe), 2.74 (3H, m, H_{7b}, H_{12}), 2.66 (1H, dd, *J* = 16.6, 9.0 Hz, H_{10a}), 2.41 (1H, dd, *J* = 16.6, 5.1 Hz, H_{10b}), 1.83 – 1.61 (2H, m, H_{13}), 1.53 – 1.45 (11H, m, ^{t}BuH, H_{14}), 1.23 – 1.18 (3H, d, *J* = 6.1 Hz, H_{16}), *OH not observed*; **^{13}C NMR** (101 MHz, $CDCl_3$): δ = 174.7, 172.3, 155.3, 143.9, 135.0, 134.1, 125.7, 80.0, 67.9, 52.1, 51.9, 44.9, 42.5, 38.7, 35.2, 33.6, 30.1 (2C), 28.6, 27.7, 23.7;

IR (neat, ν_{max} /cm^{-1}): 3444 (br), 1735, 1690, 1437, 1391, 1366, 1250, 1197, 1155; **HRMS** (ESI): calc for $C_{23}H_{37}NNaO_7S$ $(M + Na)^+$ 494.2188, found 494.2187.

Dimethyl 2-((2-(((*tert*-butoxycarbonyl)(methyl)amino)methyl)-5-(4-oxopentyl) thiophen-3-yl) methyl)succinate (143)

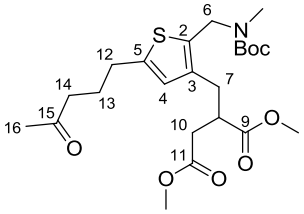

To a stirring solution of dimethyl 2-((2-(((*tert*-butoxycarbonyl)(methyl)amino) methyl)-5-(4-hydroxypentyl)thiophen-3-yl)methyl)succinate **(142)** (1.34 g, 2.84 mmol) in CH_2Cl_2 (30 mL) was added DMP (1.45 g, 3.42 mmol) and the reaction was stirred for 20 min, after which time the solution was filtered, and the filter was washed with CH_2Cl_2 (10 mL). The filtrate was concentrated *in vacuo,* then purified using a 24 g silica column, eluting with 0 – 100 % EtOAc:cyclohexane, and the desired fractions were combined and concentrated *in vacuo* to furnish dimethyl 2-((2-(((*tert*-butoxycarbonyl)(methyl)amino)methyl)-5-(4-oxopentyl)thiophen-3-yl)methyl)succinate **(143)** (1.00 g, 2.13 mmol, 75 % yield) as an orange coloured oil, as an inseparable mixture with the corresponding compound without C_7-C_8 alkene reduction (13:1 ratio).

LCMS t_R = 1.26 min (system B), 93 %, *molecular ion not observed* ES+ve *m/z* 470 $(M + H - CO_2{}^tBu)^+$; **^{1}H NMR** (600 MHz, $CDCl_3$): δ = 6.47 (1H, s, H_4), 4.52 – 4.36 (2H, m, H_6), 3.67 (3H, s, OMe), 3.65 (3H, s, OMe), 3.08 – 3.01 (1H, m, H_8), 2.91 (1H, dd, *J* = 14.1, 6.8 Hz, H_{7a}), 2.81 (3H, s, NMe), 2.72 – 2.69 (3H, m, H_{7b}, H_{12}), 2.66 (1H, dd, *J* = 16.7, 9.0 Hz, H_{10a}), 2.47 (2H, t, *J* = 7.3 Hz, H_{14}), 2.41 (1H, dd, *J* = 16.9, 5.1 Hz, H_{10b}), 2.13 (3H, s, H_{16}), 1.90 (2H, quin, *J* = 7.3 Hz, H_{13}), 1.49 (9H, s, ^{t}BuH); **^{13}C NMR** (151 MHz, $CDCl_3$): δ = 174.7, 172.3, 155.3, 143.9, 135.0, 134.1, 125.7, 80.0, 67.9, 52.1, 51.9, 44.9, 42.5,

38.7, 35.2, 33.6, 30.1 (2C), 28.6, 27.7, 23.7; **IR** (neat, ν_{max} /cm^{-1}): 1735, 1714, 1691, 1437, 1390, 1365, 1249, 1152; **HRMS** (ESI): calc for $C_{23}H_{35}NO_7SNa$ $(M + Na)^+$ 492.2032, found 492.2030.

Dimethyl 2-((5-(3-(1,8-naphthyridin-2-yl)propyl)-2-(((*tert*-butoxycarbonyl)(methyl) amino)methyl) thiophen-3-yl)methyl)succinate (144)

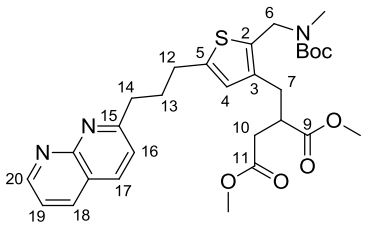

To a solution of dimethyl 2-((2-(((*tert*-butoxycarbonyl)(methyl)amino)methyl)-5-(4-oxopentyl)thiophen-3-yl)methyl)succinate **(143)** (926 mg, 1.972 mmol) in EtOH (20 mL) was added sulfuric acid (10 µl, 0.188 mmol), pyrrolidine (181 µl, 2.169 mmol) and 2-aminonicotinaldehyde **(26)** (313 mg, 2.56 mmol), and the reaction was heated under reflux for 4 h, before the orange coloured solution was cooled to rt and the solvent was removed *in vacuo.* The crude product was purified using an 80 g silica column, eluting with 20 – 100 % EtOAc:cyclohexane, and the desired fractions were combined and concentrated *in vacuo* to yield dimethyl 2-((5-(3-(1,8-naphthyridin-2-yl)propyl)-2-(((*tert*-butoxycarbonyl)(methyl)amino)methyl)thiophen-3-yl)methyl)succinate **(144)** (679 mg, 1.22 mmol, 62 % yield) as an orange coloured oil, as an inseparable mixture with the corresponding compound without C_7-C_8 alkene reduction (13:1 ratio).

LCMS t_R = 1.25 min (system B), 95 %, ES+ve *m/z* 556 $(M + H)^+$; **^{1}H NMR** (400 MHz, $CDCl_3$): δ = 9.09 (1H, dd, *J* = 4.4, 2.0 Hz, H_{20}), 8.16 (1H, dd, *J* = 8.1, 2.0 Hz, H_{18}), 8.10 (1H, d, *J* = 8.3 Hz, H_{17}), 7.45 (1H, dd, *J* = 8.1, 4.4 Hz, H_{19}), 7.38 (1H, d, *J* = 8.3 Hz, H_{16}), 6.50 (1H, s, H_4), 4.59 – 4.35 (2H, m, H_6), 3.66 (3H, s, OMe), 3.64 (3H, s, OMe), 3.14 – 3.00 (3H, m, H_8, H_{14}), 2.94 – 2.88 (1H, m, H_{7a}), 2.85 (2H, t, *J* = 7.5 Hz, H_{12}), 2.80 (3H, s,

NMe), 2.76 – 2.70 (1H, m, H_{7b}), 2.65 (1H, dd, *J* = 16.6, 9.0 Hz, H_{10a}), 2.40 (1H, dd, *J* = 16.6, 5.1 Hz, H_{10b}), 2.26 (2H, quin, *J* = 7.6 Hz, H_{13}), 1.49 (9H, s, ^{t}BuH); **^{13}C NMR** (101 MHz, $CDCl_3$): δ = 174.6, 172.2, 166.0, 156.1, 155.4, 153.4, 143.5, 137.1, 136.8, 135.0, 134.2, 125.9, 122.7, 121.5, 121.2, 80.1, 52.1, 51.8, 44.8, 42.5, 38.5, 35.2, 33.6, 30.8, 30.0, 29.8, 28.5; **IR** (neat, ν_{max} /cm^{-1}): 1734, 1689, 1608, 1437, 1390, 1366, 1250, 1156; **HRMS** (ESI): calc for $C_{29}H_{38}N_3O_6S$ $(M + H)^+$ 556.2481, found 556.2486

Dimethyl 2-((2-(((*tert*-butoxycarbonyl)(methyl)amino)methyl)-5-(3-(5,6,7,8-tetrahydro-1,8-naphthyridin-2-yl)propyl)thiophen-3-yl)methyl)succinate (134)

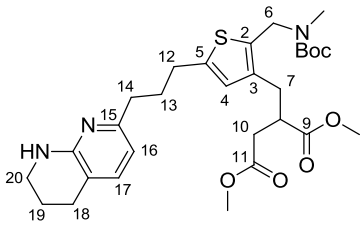

A pale yellow coloured solution of dimethyl 2-((5-(3-(1,8-naphthyridin-2-yl)propyl)-2-(((*tert*-butoxycarbonyl)(methyl)amino)methyl)thiophen-3-yl)methyl)succinate **(144)** (70 mg, 0.126 mmol) in MeOH (10 mL) was passed through the H-Cube® (flow H_2 generation), using a Pd/C (10 %) catalyst cartridge, at 1 mL/min, at 40 °C, 5 bar H_2 pressure, and the resulting colourless solution was concentrated *in vacuo* to yield dimethyl 2-((2-(((*tert*-butoxycarbonyl)(methyl)amino)methyl)-5-(3-(5,6,7,8-tetra hydro-1,8-naphthyridin-2-yl)propyl)thiophen-3-yl)methyl)succinate **(134)** (48.2 mg, 0.086 mmol, 68 % yield) as a colourless oil.

LCMS t_R = 1.40 min (system B), 90 %, ES+ve *m/z* 560 $(M + H)^+$; **^{1}H NMR** (400 MHz, $CDCl_3$): δ = 7.06 (1H, d, *J* = 7.1 Hz, H_{17}), 6.47 (1H, s, H_4), 6.33 (1H, d, *J* = 7.3 Hz, H_{16}), 4.61 – 4.35 (2H, m, H_6), 3.66 (3H, s, OMe), 3.64 (3H, s, OMe), 3.40 (2H, t, *J* = 4.5 Hz, H_{20}), 3.09 – 3.00 (1H, m, H_8), 2.94 – 2.87 (1H, m, H_{7a}), 2.82 – 2.79 (3H, s, NMe), 2.77 – 2.55 (8H, m, H_{7b}, H_{10a}, H_{12}, H_{14}, H_{18}), 2.40 (1H, dd, *J* = 16.6, 5.1 Hz, H_{10b}), 2.06 – 1.95 (2H, m, H_{13}), 1.94 – 1.86 (2H, m, H_{19}), 1.49 (9H, s, ^{t}BuH), *amine H not observed*; **^{13}C**

NMR (101 MHz, $CDCl_3$): δ = 174.8, 172.4, 157.9, 156.0, 155.5, 144.2, 136.9, 135.1, 134.1, 125.8, 113.5, 111.7, 80.2, 52.2, 52.0, 45.0, 42.6, 41.9, 37.4, 35.3, 33.7, 31.7, 30.2, 29.9, 28.7, 26.6, 21.8; **IR** (neat, ν_{max} /cm^{-1}): 1735, 1690, 1459, 1436, 1389, 1365, 1248, 1153, 731; **HRMS** (ESI): calc for $C_{29}H_{42}N_3O_6S$ $(M + H)^+$ 560.2794, found 560.2795.

Methyl 2-(7-methyl-6-oxo-2-(3-(5,6,7,8-tetrahydro-1,8-naphthyridin-2-yl)propyl)-5,6,7,8-tetrahydro-4H-thieno[2,3-c]azepin-5-yl)acetate (145)

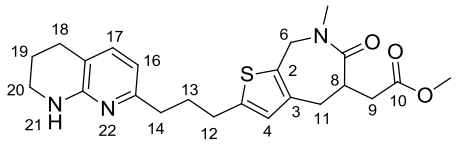

To a stirring solution of dimethyl 2-((2-(((*tert*-butoxycarbonyl)(methyl)amino) methyl)-5-(3-(5,6,7,8-tetrahydro-1,8-naphthyridin-2-yl)propyl)thiophen-3-yl)methyl) succinate **(134)** (45 mg, 0.080 mmol) in CH_2Cl_2 (1 mL) was added TFA (0.184 mL, 2.412 mmol), and the reaction was stirred for 1 h, after which time the solvent was concentrated using a flow of nitrogen gas, followed by the addition of PhMe (1 mL). Nitrogen gas was bubbled through the solution for 30 min, before the vial was sealed and purged with nitrogen gas. The yellow coloured solution was heated in a microwave reactor at 200 °C for 40 min, followed by cooling to rt and removal of the solvent under a flow of nitrogen gas. The crude product was purified using an Xterra® Prep RP18 OBD™ column, eluting with 0 – 100 % MeCN:ammonium carbonate modified H_2O, and the desired fractions were combined and concentrated *in vacuo* to furnish methyl 2-(7-methyl-6-oxo-2-(3-(5,6,7,8-tetrahydro-1,8-naphthyridin-2-yl)propyl)-5,6,7,8-tetrahydro-4H-thieno[2,3-c]azepin-5-yl)acetate **(145)** (6.8 mg, 0.016 mmol, 20 % yield) as a brown coloured oil.

LCMS t_R = 0.60 min (system A), 75 %, ES+ve *m/z* 428 $(M + H)^+$; **^{1}H NMR** (400 MHz, $CDCl_3$): δ = = 7.05 (1H, d, *J* = 7.3 Hz, H_{17}), 6.45 (1H, s, H_4), 6.33 (1H, d, *J* = 7.3 Hz, H_{16}),

5.16 (1H, d, *J* = 17.1 Hz, H_{6a}), 4.75 (1H, br s, NH), 3.88 – 3.62 (5H, m, OMe, H_{6b}, H_8), 3.44 – 3.36 (2H, m, H_{20}), 3.09 – 2.99 (4H, m, NMe, H_{9a}), 2.95 – 2.87 (1H, m, H_{11a}), 2.83 – 2.62 (5H, H_{11b}, H_{12}, H_{18}), 2.58 (2H, t, *J* = 7.7 Hz, H_{14}), 2.43 – 2.35 (1H, m, H_{9b}), 2.04 – 1.95 (2H, m, H_{13}), 1.95 – 1.86 (2H, m, H_{19}); **^{13}C NMR** (101 MHz, $CDCl_3$): δ = 174.3, 173.1, 157.7, 155.9, 142.5, 136.7, 135.6, 128.3, 127.0, 113.5, 111.5, 51.9, 47.4, 41.8, 37.3, 37.2, 36.6, 35.8, 31.9, 31.6, 29.5, 26.5, 21.7; **IR** (neat, ν_{max} /cm^{-1}): 1732, 1649, 1598, 1585, 1460, 1435, 1355, 1196, 1162, 1117, 730; **HRMS** (ESI): calc for $C_{23}H_{30}N_3O_3S$ $(M + H)^+$ 428.2008, found 428.2001.

2-(7-Methyl-6-oxo-2-(3-(5,6,7,8-tetrahydro-1,8-naphthyridin-2-yl)propyl)-5,6,7,8-tetrahydro-4H-thieno[2,3-c]azepin-5-yl)acetic acid, formic acid salt (133)

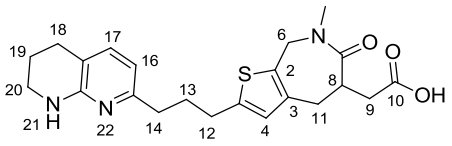

To a stirring solution of methyl 2-(7-methyl-6-oxo-2-(3-(5,6,7,8-tetrahydro-1,8-naphthyridin-2-yl)propyl)-5,6,7,8-tetrahydro-4H-thieno[2,3-c]azepin-5-yl)acetate **(145)** (16.3 mg, 0.038 mmol) in MeOH (1 mL) was added NaOH (1 M, 0.7 mL, 0.700 mmol), and the reaction stirred for 18 h. The solution was concentrated using a flow of nitrogen gas, and redissolved in H_2O (2 mL) and MeCN (1 mL), before neutralisation with the dropwise addition of HCl (2 M). The solvent was partially removed under a flow of nitrogen gas and the crude product was purified using an Xbridge Prep RP18 OBD™ column, eluting with 0 – 100 % MeCN:ammonium carbonate modified H_2O, and the desired fractions were combined and concentrated *in vacuo*, followed by further purification using a Sunfire® Prep C18 OBD™ column, eluting with 0 – 100 % MeCN:formic acid modified H_2O, and the desired fractions were combined and concentrated *in vacuo* to furnish 2-(7-methyl-6-oxo-2-(3-(5,6,7,8-tetrahydro-1,8-naphthyridin-2-yl)propyl)-5,6,7,8-tetrahydro-4H-thieno[2,3-c]azepin-5-yl)acetic acid, formic acid salt **(133)** (9.2 mg, 0.020 mmol, 53 % yield) as a pale yellow coloured gum.

LCMS t_R = 0.76 min (system B), 97 %, ES+ve *m/z* 414 $(M + H)^+$; **^{1}H NMR** (600 MHz, $CDCl_3$): δ = 10.23 (1H, br s, COO<u>H</u>), 8.61 (1H, br s, <u>H</u>COOH), 7.21 (1H, d, *J* = 7.3 Hz, H_{17}), 6.41 (1H, s, H_4), 6.25 (1H, d, *J* = 7.3 Hz, H_{16}), 5.09 (1H, d, *J* = 16.9 Hz, H_{6a}), 3.81 (1H, d, *J* = 17.2 Hz, H_{6b}), 3.77 – 3.66 (1H, m, H_8), 3.46 (2H, t, *J* = 5.5 Hz, H_{20}), 3.05 (3H, s, NMe), 2.97 – 2.87 (2H, m, H_{9a}, H_{11a}), 2.76 – 2.65 (7H, m, H_{11b}, H_{12}, H_{14}, H_{18}), 2.54 (1H, dd, *J* = 16.0, 6.1 Hz, H_{9b}), 1.99 (2H, quin, *J* = 7.6 Hz, H_{13}), 1.89 (2H, quin, *J* = 5.9 Hz, H_{19}) *formic acid carboxylic acid and amine H not observed*; **^{13}C NMR** (151 MHz, $CDCl_3$): δ = 176.8, 175.7, 169.9, 153.5, 150.2, 141.3, 139.5, 136.3, 128.3, 127.5, 117.8, 109.3, 47.6, 40.9, 38.5, 37.8, 36.0, 32.6, 31.7, 31.0, 29.2, 26.0, 19.9; **IR** (neat, ν_{max} /cm^{-1}): 1638, 1396, 1319, 1226, 1195, 1114, 908, 724, 644; **HRMS** (ESI): calc for $C_{22}H_{28}N_3O_3S$ $(M + H)^+$ 414.1851, found 414.1854.

2-Bromo-*N*-methoxy-*N*-methylthiophene-3-carboxamide (148)

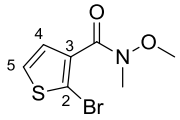

To a stirring suspension of *N,O*-dimethylhydroxylamine hydrochloride (2.93 g, 30.0 mmol) HATU (11.02 g, 29.0 mmol), and 2-bromothiophene-3-carboxylic acid **(149)** (5.0 g, 24.15 mmol) in CH_2Cl_2 (250 mL) was added DIPEA (10.52 ml, 60.4 mmol) and the reaction was stirred for 4 h, after which time the yellow coloured solution was diluted with H_2O (100 mL), and the layers were separated. The aqueous layer was extracted with CH_2Cl_2 (100 mL), and the combined organic extracts were filtered through a hydrophobic frit and concentrated *in vacuo.* The crude product was purified using an 120 g silica column, eluting with 0 – 100 % EtOAc:cyclohexane, and the desired fractions were combined and concentrated *in vacuo* to yield 2-bromo-*N*-methoxy-*N*-methylthiophene-3-carboxamide (5.61 g, 22.43 mmol, 93 % yield) **(148)** as a colourless oil.

LCMS t_R = 0.79 min (system B), 88 %, ES+ve *m/z* 250/252 $(M + H)^+$; **^{1}H NMR** (400 MHz, $CDCl_3$): δ = 7.25 (1H, d, *J* = 5.6 Hz, ArH), 7.04 (1H, d, *J* = 5.6 Hz, ArH), 3.60 (3H, br s, OMe), 3.33 (3H, s, NMe); **^{13}C NMR** (101 MHz, $CDCl_3$): δ = 164.5, 135.5, 127.5, 126.5, 113.2, 61.6, 33.6; **IR** (neat, ν_{max} /cm^{-1}): 1644, 1421, 1380, 1220, 990, 846, 712; **HRMS** (ESI): calc for $C_7H_9BrNO_2S$ $(M+H)^+$ 249.9537, found 249.9542.

2-Bromothiophene-3-carbaldehyde (150)[269]

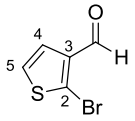

A stirring solution of 2-bromo-*N*-methoxy-*N*-methylthiophene-3-carboxamide **(148)** (4.88 g, 19.51 mmol) in THF (100 mL) under nitrogen was cooled to –78 °C, followed by the careful addition of $LiAlH_4$ in THF (2.0 M, 11.71 ml, 23.41 mmol). The reaction was stirred for 15 min, after which time it was quenched by the careful addition of ammonium chloride solution (40 mL). The mixture was left to warm to rt, before the THF was removed *in vacuo.* Dilution with EtOAc (100 mL) and H_2O (50 mL) followed, and the layers were separated. The aqueous layer was extracted with EtOAc (3 x 150 mL), then the combined organic layers were washed with H_2O (200 mL), filtered through a hydrophobic frit, and concentrated *in vacuo.* The crude product was purified using a 120 g silica column, eluting with 0 – 30 % EtOAc:cyclohexane, and the desired fractions were combined and concentrated *in vacuo* to yield 2-bromothiophene-3-carbaldehyde (2.49 g, 13.03 mmol, 67 % yield) **(150)** as a colourless oil.

LCMS t_R = 0.92 min (system B), 98 %, *no mass ion observed* **^{1}H NMR** (400 MHz, $CDCl_3$): δ = 9.94 (1H, s, CHO), 7.36 (1H, dd, *J* = 1.7, 5.9 Hz, ArH), 7.28 (1H, d, *J* = 5.9 Hz, ArH); **^{13}C NMR** (101 MHz, $CDCl_3$): δ = 184.8, 138.7, 127.1, 126.4, 125.4; **IR** (neat, ν_{max} /cm^{-}

[1]): 1684, 1664, 1515, 1378, 1228, 1005, 818, 732; **HRMS** (ESI): calc for C_5H_4BrOS $(M + H)^+$ 190.9166, found 190.9163.

1-(2-Bromothiophen-3-yl)-*N*-methylmethanamine (151)[270]

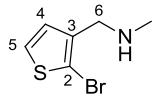

To a solution of 2-bromothiophene-3-carbaldehyde **(150)** (2.49 g, 13.03 mmol) and $MeNH_2$ in THF (2.0 M, 30 ml, 60.0 mmol) in MeCN (160 mL) was stirred for 90 min, followed by the addition of sodium triacetoxyhydroborate (5.52 g, 26.1 mmol). After stirring for 62 h, the white coloured slurry was cooled to 0 °C and sodium borohydride (0.429 g, 11.34 mmol) was added, and the reaction was stirred for a further 22 h whilst warming to rt. The solution was cooled to 0 °C, followed by the careful addition of H_2O (20 mL), and HCl (2M, 30 mL), and then the MeCN was removed *in vacuo*. To the resulting solution was added MeOH (40 mL) and HCl (2 M, 40 mL), then the colourless solution was heated under reflux for 2 h, followed by cooling to rt and removal of the MeOH *in vacuo*. The resulting solution was basified with the addition of NaOH (2 M, 50 mL), and diluted with EtOAc (150 mL). The layers were separated, and the aqueous layer was extracted with EtOAc (150 mL). The combined organic layers were filtered through a hydrophobic frit and concentrated *in vacuo* to yield 1-(2-bromothiophen-3-yl)-N-methylmethanamine **(151)** (2.02 g, 9.80 mmol, 75 % yield) as a yellow coloured oil.

LCMS t_R = 0.87 min (system B), 96 %, ES+ve *m/z* 206/208 $(M + H)^+$; **^{1}H NMR** (400 MHz, $CDCl_3$): δ = 7.23 (1H, d, *J* = 5.6 Hz, ArH), 6.94 (d, *J* = 5.6 Hz, ArH), 3.71 (2H, s, H_6), 2.44 (3H, s, NMe), *amine H not observed*; **^{13}C NMR** (101 MHz, $CDCl_3$): δ = 140.0, 128.4, 125.8, 110.5, 49.6, 36.0; **IR** (neat, ν_{max} /cm^{-1}): 1639, 1455, 1410, 1223, 1033, 990, 825, 693; **HRMS** (ESI): calc for C_6H_9BrNS $(M+H)^+$ 205.9639, found 205.0937.

tert-Butyl ((2-bromothiophen-3-yl)methyl)(methyl)carbamate (147)

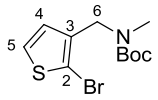

To DIPEA (1.69 mL, 9.70 mmol) was added 1-(2-bromothiophen-3-yl)-*N*-methylmethanamine **(151)** (2.00 g, 9.70 mmol), followed by di-*tert*-butyl dicarbonate (2.33 g, 10.68 mmol) and CH_2Cl_2 (20 mL) whilst stirring. After effervescence was observed, and the reaction was stirred for 5 min, imidazole (366 mg, 5.38 mmol) was added, and reaction was left to stand for 16 h, then washed with HCl (0.2 M, 3 x 20 mL), followed by filtration through a hydrophobic frit, and concentrated *in vacuo* to yield *tert*-butyl ((2-bromothiophen-3-yl)methyl)(methyl)carbamate **(147)** (2.70 g, 8.82 mmol, 91 % yield) as a pale yellow coloured oil.

LCMS t_R = 1.37 min (system B), 94 %, *no mass ion observed*; **^{1}H NMR** (400 MHz, $CDCl_3$): δ = 7.23 (1H, d, *J* = 5.6 Hz, ArH), 6.88 (1H, br s, ArH), 4.37 (2H, br s, H_6), 2.81 (3H, br s, NMe), 1.48 (9H, s, ^{t}BuH); **^{13}C NMR** (101 MHz, $CDCl_3$): 138.0, 128.3, 127.6, 126.2, 110.3, 80.0, 46.6, 34.1, 28.6; **IR** (neat, ν_{max} /cm^{-1}): : 1690, 1390, 1365, 1248, 1170, 1139, 872, 688; **HRMS** (ESI): calc for $C_{11}H_{16}BrNNaO_2S$ $(M + Na)^+$ 329.9983, found 329.9973.

(*E*)-Dimethyl 2-((3-(((*tert*-butoxycarbonyl)(methyl)amino)methyl)thiophen-2-yl) methylene)succinate (152)

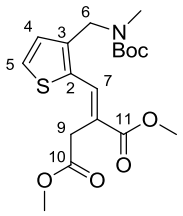

To a stirring solution of *tert*-butyl ((2-bromothiophen-3-yl)methyl)(methyl) carbamate **(147)** (9.81 g, 32.0 mmol) in DMF (150 mL) was added potassium carbonate (4.87 g, 35.2 mmol), tetrabutylammonium bromide (3.61 g, 11.21 mmol),

palladium acetate (0.719 g, 3.20 mmol), and dimethyl 2-methylenesuccinate **(102)** (13.5 ml, 96 mmol), and the reaction was heated to 100 °C for 12 h. The cooled solution was filtered through Celite®, washing with EtOAc (150 mL), and the filtrate was then filtered through a 50 g strong cation exchange column, washing with EtOAc (100 mL). The resulting solution was washed with 10 % lithium chloride solution (3 x 200 mL), and then dried ($MgSO_4$), filtered, and concentrated *in vacuo*. The crude product was purified using a 120 g silica column, eluting with 0 – 50 % EtOAc:cyclohexane, and the desired fractions were combined and concentrated *in vacuo* to yield dimethyl (*E*)-2-((3-(((*tert*-butoxycarbonyl)(methyl)amino) methyl)thiophen-2-yl)methylene)succinate **(152)** (3.79 g, 9.88 mmol, 31 % yield) as a yellow coloured oil.

LCMS t_R = 1.24 min (system B), 95 %, ES+ve *m/z* 284 $(M + H)^+$; **^{1}H NMR** (400 MHz, $CDCl_3$): δ = 8.06 (1H, br s, H_7), 7.43 (1H, d, *J* = 5.1 Hz, ArH), 7.03 (1H, d, *J* = 4.6 Hz, ArH), 4.53 (2H, br s, H_6), 3.82 (3H, s, OMe), 3.79 (2H, s, H_9), 3.72 (3H, s, OMe), 2.91 – 2.68 (3H, br s, NMe), 1.47 (9H, s, ^{t}BuH), *E geometry tentatively assigned by analogy with compounds **85** and **154***; **^{13}C NMR** (101 MHz, $CDCl_3$): δ = 170.8, 168.0, 155.8, 142.6, 132.5, 131.6, 129.3, 128.5, 122.8, 80.1, 52.5, 52.3, 46.0, 34.1, 33.9, 28.5; **IR** (neat, ν_{max} /cm^{-1}): 1740, 1689, 1435, 1390, 1365, 1264, 1247, 1194, 1163, 1139, 1103, 872; **HRMS** (ESI): calc for $C_{18}H_{25}NNaO_6S$ $(M + Na)^+$ 406.1300, found 406.1296.

(*E*)-Dimethyl 2-((3-(((*tert*-butoxycarbonyl)(methyl)amino)methyl)-5-iodothiophen-2-yl)methylene)succinate (153)

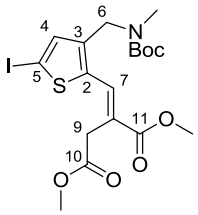

To a stirring solution of dimethyl (*E*)-2-((3-(((*tert*-butoxycarbonyl)(methyl)amino)methyl)thiophen-2-yl)methylene)succinate **(152)** (560 mg, 1.460 mmol) in $CHCl_3$ (15 mL) and acetic acid (0.088 mL, 1.533 mmol) was added *N*-iodisuccinimide (493 mg, 2.191 mmol), and the pink coloured solution was heated under reflux for 20 h, followed by the addition of a further portion of *N*-iodosuccinimide (329 mg, 1.460 mmol). After stirring for a further 8 h, the dark purple coloured reaction mixture was cooled to rt and diluted with H_2O (20 mL) and the layers were separated. The aqueous phase was extracted with CH_2Cl_2 (2 x 20 mL), and the combined organic extracts were filtered through a hydrophobic frit and concentrated *in vacuo*, before purification with an 80 g silica column, eluting with 0 – 20 % EtOAc:cyclohexane. The desired fractions were combined and concentrated *in vacuo* to yield dimethyl (*E*)-2-((3-(((*tert*-butoxycarbonyl)(methyl)amino)methyl)-5-iodothiophen-2-yl)methylene)succinate **(153)** (483 mg, 0.948 mmol, 65 % yield) as a yellow coloured oil.

LCMS t_R = 1.36 min (system B), 100 %, ES+ve *m/z* 410 $(M + H)^+$; **^{1}H NMR** (400 MHz, $CDCl_3$): δ = 7.96 (1H, br s, H_7), 7.17 (1H, br s, H_4), 4.47 (2H, br s, H_6), 3.85 – 3.78 (3H, m, OMe), 3.73 (3H, s, OMe), 3.71 (2H, s, H_9), 2.80 (3H, br s, NMe), 1.57 – 1.40 (9H, s, ^{t}BuH); **^{13}C NMR** (101 MHz, $CDCl_3$): δ = 170.5, 167.7, 155.6, 143.9, 139.3-138.0 (2C, br s), 130.6, 123.7, 80.3, 78.3, 52.6, 52.4, 45.0, 34.2, 34.0, 28.5; **IR** (neat, ν_{max} /cm^{-1}): 1740, 1690, 1435, 1390, 1366, 1264, 1195, 1162, 1095, 872, 776, 731; **HRMS** (ESI): calc for $C_{18}H_{24}INNaO_6S$ $(M + Na)^+$ 532.0267, found 532.0269.

(*E*)-Dimethyl 2-((3-(((*tert*-butoxycarbonyl)(methyl)amino)methyl)-5-(4-hydroxy pent-1-yn-1-yl)thiophen-2-yl)methylene)succinate (154)

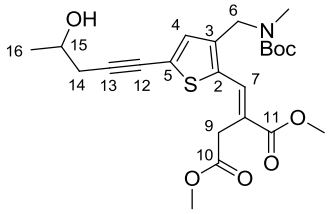

A stirring solution of triethylamine (2.093 ml, 15.02 mmol), $Pd(PPh_3)_2Cl_2$ (0.351 g, 0.501 mmol), copper(I) iodide (0.114 g, 0.601 mmol), pent-4-yn-2-ol **(140)** (0.567 ml, 6.01 mmol) and dimethyl (*E*)-2-((3-(((*tert*-butoxycarbonyl)(methyl)amino)methyl)-5-iodothiophen-2-yl)methylene)succinate **(153)** (2.55 g, 5.01 mmol) in DMF (50 mL) under nitrogen was heated to 80 °C for 17 h, followed by cooling to rt. The brown coloured solution was filtered through Celite®, washing with EtOAc (100 mL), and the resulting orange coloured solution was washed with 10 % lithium chloride solution (3 x 100 mL), then filtered through a hydrophobic frit and concentrated *in vacuo.* The crude product was purified using a 120 g silica column, eluting with 0 – 100 % EtOAc:cyclohexane, and the desired fractions were combined and concentrated *in vacuo,* followed by repurification using a 120 g silica column, eluting with 0 – 50 % EtOAc:cyclohexane, and the desired fractions were combined and concentrated *in vacuo* to furnish dimethyl (*E*)-2-((3-(((*tert*-butoxycarbonyl)(methyl)amino)methyl)-5-(4-hydroxypent-1-yn-1-yl)thiophen-2-yl)methylene)succinate **(154)** (0.728 g, 1.564 mmol, 31 % yield) as a yellow coloured oil.

LCMS t_R = 1.22 min (system B), 97 %, ES+ve *m/z* 366 $(M + H)^+$; **^{1}H NMR** (400 MHz, $CDCl_3$): δ = 7.98 (1H, br s, H_7), 7.03 (1H, br s, H_4), 4.47 (2H, br s, H_6), 4.11 – 4.00 (1H, m, H_{15}), 3.85 – 3.80 (3H, m, OMe), 3.75 (2H, s, H_9), 3.73 (3H, s, OMe), 2.80 (3H, br s, NMe), 2.69 – 2.56 (2H, m, H_{14}), 1.95 (1H, br s, OH), 1.51 – 1.45 (9H, s, ^{t}BuH), 1.32 (3H, d, *J* = 6.4 Hz, H_{16}); **^{13}C NMR** (101 MHz, $CDCl_3$): δ =170.6, 167.8, 155.9, 142.5, 133.3, 132.7, 131.0, 126.5, 123.3, 94.2, 80.3, 75.6, 66.5, 52.6, 52.4, 45.8, 34.1, 34.0, 30.5, 28.5, 22.7; **IR** (neat, ν_{max} /cm^{-1}): 3443 (br), 2223, 1740, 1692, 1434, 1392, 1367, 1269,

1195, 1165, 1096, 732; **HRMS** (ESI): calc for $C_{23}H_{31}NNaO_7S$ $(M+Na)^+$ 488.1720, found 488.1718.

Dimethyl 2-((3-(((*tert*-butoxycarbonyl)(methyl)amino)methyl)-5-(4-hydroxypentyl) thiophen-2-yl)methyl)succinate (155)

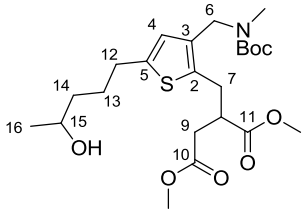

A solution of dimethyl (*E*)-2-((3-(((*tert*-butoxycarbonyl)(methyl)amino)methyl)-5-(4-hydroxypent-1-yn-1-yl)thiophen-2-yl)methylene)succinate **(154)** (1.57 g, 3.37 mmol) in DMF (30 mL) was heated to 100 °C, after which potassium carbonate (2.50 g, 18.09 mmol) was added, followed by the portionwise addition of benzenesulfonyl hydrazide (2.50 g, 14.52 mmol) over 1 h, and the reaction was stirred for 1 h, after which a further portion of potassium carbonate (2.50 g, 18.09 mmol) was added, followed by benzenesulfonyl hydrazide (2.50 g, 14.52 mmol) over 30 min. After a further 1 h of stirring, a further portion of potassium carbonate (2.50 g, 18.09 mmol) was added, followed by benzenesulfonyl hydrazide (2.50 g, 14.52 mmol) over 30 min. After a further 1 h of stirring, the dark coloured slurry was cooled to rt and diluted with H_2O (50 mL) and EtOAc (100 mL). The layers were separated, and the organic phase was washed with 10 % aqueous lithium chloride (2 x 60 mL) and filtered through a hydrophobic frit, then concentrated *in vacuo*. The resulting brown coloured oil was redissolved in DMF (30 mL) and heated to 100 °C whilst stirring. To this solution was added potassium carbonate (2.50 g, 18.09 mmol), followed by benzenesulfonyl hydrazide (2.50 g, 14.52 mmol) portionwise over 30 min, and the mixture was stirred for 1 h. A further portion of potassium carbonate (2.50 g, 18.09 mmol) was added, followed by benzenesulfonyl hydrazide (2.50 g, 14.52 mmol) portionwise over 30 min. After a further 1 h of stirring, a further portion of potassium

carbonate (2.50 g, 18.09 mmol) was added, followed by benzenesulfonyl hydrazide (2.50 g, 14.52 mmol) portionwise over 30 min. A further portion of potassium carbonate (2.50 g, 18.09 mmol) was added, followed by benzenesulfonyl hydrazide (2.50 g, 14.52 mmol) portionwise over 30 min. After stirring for 3 h, a final portion of potassium carbonate (2.50 g, 18.09 mmol) was added, followed by benzenesulfonyl hydrazide (2.50 g, 14.52 mmol) portionwise over 30 min. After stirring for a final 3 h, the mixture was cooled to rt, and diluted with EtOAc (50 mL) and H_2O (50 mL). The layers were separated, and the organic layer was washed with 10 % aqueous lithium chloride solution (2 x 50 mL), before being filtered through a hydrophobic frit and concentrated *in vacuo.* The crude product was purified using an 80 g silica column, eluting with 0 – 100 % EtOAc:cyclohexane, and the desired fractions were combined and concentrated *in vacuo* to furnish dimethyl 2-((3-(((*tert*-butoxycarbonyl)(methyl)amino)methyl)-5-(4-hydroxypentyl)thiophen-2-yl)methyl) succinate **(155)** (195 mg, 0.413 mmol, 12 % yield) as a yellow coloured gum.

LCMS t_R = 1.22 min (system B), 100 %, ES+ve *m/z* 372 $(M + H)^+$; **^{1}H NMR** (400 MHz, $CDCl_3$): δ = 6.51 (1H, s, H_4), 4.29 – 4.17 (2H, m, H_6), 3.87 – 3.78 (1H, m, H_{15}), 3.69 (3H, s, OMe), 3.66 (3H, s, OMe), 3.19 – 3.03 (2H, m, H_{7a}, H_8), 3.02 – 2.92 (1H, m, H_{7b}), 2.79 – 2.64 (6H, m, NMe, H_{9a}, H_{12}), 2.54 – 2.44 (1H, m, H_{9b}), 1.80 – 1.53 (2H, m, H_{13}), 1.53 – 1.45 (11H, m, H_{14}, ^{t}BuH), 1.19 (3H, d, *J* = 6.1 Hz, H_{16}), *OH not observed*; **^{13}C NMR** (101 MHz, $CDCl_3$): δ = 174.2, 172.2, 155.8, 143.3, 135.4, 134.0, 125.4, 79.8, 67.9, 52.2, 51.9, 45.4, 43.4, 38.7, 35.0, 33.7, 30.1, 29.5, 28.6, 27.7, 23.7; **IR** (neat, ν_{max} /cm^{-1}): 3450 (br), 1736, 1686, 1436, 1392, 1366, 1248, 1197, 1157, 873; **HRMS** (ESI): calc for $C_{23}H_{37}NNaO_7S$ $(M + Na)^+$ 494.2189, found 494.2189.

Dimethyl 2-((3-(((*tert*-butoxycarbonyl)(methyl)amino)methyl)-5-(4-oxopentyl) thiophen-2-yl)methyl)succinate (156)

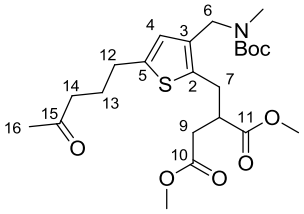

To a stirring solution of dimethyl 2-((3-(((*tert*-butoxycarbonyl)(methyl)amino) methyl)-5-(4-hydroxypentyl)thiophen-2-yl)methyl)succinate **(155)** (171 mg, 0.363 mmol) in CH_2Cl_2 (3 mL) was added DMP (185 mg, 0.435 mmol) and the reaction was stirred for 20 min, after which time half of the solvent was removed using a flow of nitrogen gas, followed by purification using a 24 g silica column, eluting with 0 – 100 % EtOAc:cyclohexane, and the desired fractions were combined and concentrated *in vacuo* to furnish dimethyl 2-((3-(((*tert*-butoxycarbonyl)(methyl)amino)methyl)-5-(4-oxopentyl)thiophen-2-yl)methyl)succinate **(156)** (139 mg, 0.296 mmol, 82 % yield) as a yellow coloured oil.

LCMS t_R = 1.26 min (system B), 72 %, ES+ve *m/z* 370 $(M + H)^+$; **^{1}H NMR** (400 MHz, $CDCl_3$): δ = 6.51 (1H, s, H_4), 4.35 – 4.17 (2H, m, H_6), 3.69 (3H, s, OMe), 3.66 (3H, s, OMe), 3.18 – 3.11 (1H m, H_{7a}), 3.11 – 3.02 (1H, m, H_8), 3.01 – 2.93 (1H, m, H_{7b}), 2.78 – 2.65 (6H, m, NMe, H_{9a}, H_{12}), 2.52 – 2.43 (3H, m, H_{9b}, H_{14}), 2.13 (3H, s, H_{16}), 1.89 (2H, quin, J = 7.3 Hz, H_{13}), 1.48 (9H, s, ^{t}BuH); **^{13}C NMR** (101 MHz, $CDCl_3$): δ = 208.3, 174.2, 172.1, 155.8, 142.4, 135.5, 133.9, 125.5, 79.9, 52.2, 51.9, 45.4, 43.4, 42.7, 35.0, 33.7, 30.1, 29.5, 29.3, 28.6, 25.4; **IR** (neat, ν_{max} /cm^{-1}): 1736, 1714, 1689, 1437, 1392, 1365, 1247, 1157; **HRMS** (ESI): calc for $C_{23}H_{35}NNaO_7S$ $(M + Na)^+$ 492.2032, found 492.2033.

Dimethyl 2-((5-(3-(1,8-naphthyridin-2-yl)propyl)-3-(((*tert*-butoxycarbonyl)(methyl) amino) methyl)thiophen-2-yl)methyl)succinate (157)

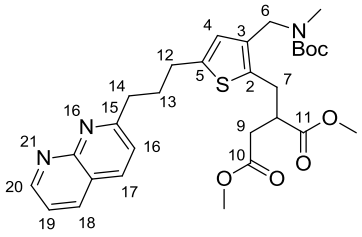

To a solution of dimethyl 2-((3-(((*tert*-butoxycarbonyl)(methyl)amino)methyl)-5-(4-oxopentyl)thiophen-2-yl)methyl)succinate (130 mg, 0.277 mmol) **(156)** in EtOH (6 mL) was added sulfuric acid (1.476 µl, 0.028 mmol), pyrrolidine (0.025 mL, 0.305 mmol) and 2-aminonicotinaldehyde **(26)** (44.0 mg, 0.360 mmol), and the reaction was heated under reflux for 16 h, before the orange coloured solution was cooled to rt and the solvent was removed *in vacuo.* The crude product was purified using a 24 g silica column, eluting with 0 – 100 % EtOAc:cyclohexane, and the desired fractions were combined and concentrated *in vacuo* to yield dimethyl 2-((5-(3-(1,8-naphthyridin-2-yl)propyl)-3-(((*tert*-butoxycarbonyl)(methyl)amino)methyl)thiophen-2-yl)methyl)succinate **(157)** (83 mg, 0.149 mmol, 54 % yield) as an orange coloured oil.

LCMS t_R = 1.24 min (system B), 84 %, ES+ve *m/z* 556 $(M + H)^+$; **^{1}H NMR** (400 MHz, $CDCl_3$): δ = = 9.08 (1H, dd, *J* = 4.2, 2.0 Hz, H_{20}), 8.16 (1H, dd, *J* = 8.1, 2.0 Hz, H_{18}), 8.10 (1H, d, *J* = 8.3 Hz, H_{17}), 7.44 (1H, dd, *J* = 8.1, 4.2 Hz, H_{19}), 7.37 (1H, d, *J* = 8.3 Hz, H_{16}), 6.54 (1H, s, H_4), 4.36 – 4.18 (2H, m, H_6), 3.69 (3H, s, OMe), 3.66 (3H, s, OMe), 3.18 – 3.02 (4H, m, H_{7a}, H_8, H_{14}), 3.02 – 2.92 (1H, m, H_{7b}), 2.84 (2H, t, *J* = 7.5 Hz, H_{12}), 2.75 (3H, s, NMe), 2.68 (dd, *J* = 16.8, 8.4 Hz, H_{9a}), 2.49 (1H, dd, *J* = 16.8, 5.0 Hz, H_{9b}), 2.25 (2H, quin, *J* = 7.6 Hz, H_{13}), 1.47 (9H, s, ^{t}BuH); **^{13}C NMR** (101 MHz, $CDCl_3$): δ = 174.2, 172.2, 166.1, 156.2, 155.8, 153.5, 142.9, 137.1, 136.8, 135.4, 134.2, 125.7, 122.7, 121.6, 121.2, 79.8, 52.2, 51.9, 45.0, 43.4, 38.6, 35.0, 33.6, 30.9, 29.8, 29.5, 28.6; **IR**

(neat, ν_{max} /cm^{-1}): 1734, 1687, 1607, 1437, 1392, 1365, 1247, 1156, 843; **HRMS** (ESI): calc for $C_{29}H_{38}N_3O_6S$ $(M + H)^+$ 556.2481, found 556.2486.

Dimethyl 2-((3-(((*tert*-butoxycarbonyl)(methyl)amino)methyl)-5-(3-(5,6,7,8-tetra hydro-1,8-naphthyridin-2-yl)propyl)thiophen-2-yl)methyl)succinate (158)

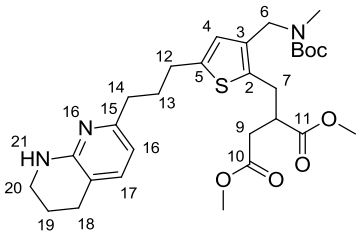

A pale yellow coloured solution of dimethyl 2-((5-(3-(1,8-naphthyridin-2-yl)propyl)-3-(((*tert*-butoxycarbonyl)(methyl)amino)methyl)thiophen-2-yl)methyl)succinate **(157)** (80 mg, 0.144 mmol) in MeOH (15 mL) was passed through the H-Cube® (flow H_2 generation), using a Pd/C (10 %) catalyst cartridge, at 1 mL/min, at 40 °C, 10 bar H_2 pressure, after which it was concentrated *in vacuo.* The crude product was purified using a 80 g silica column, eluting with 0 – 100 % EtOAc:cyclohexane then 0 – 25 % EtOH:EtOAc, but separation was not attained so the relevant fractions were combined and concentrated *in vacuo,* and the crude product was repurified using an Xbridge Prep RP18 OBD™ column, eluting with 0 – 100 % MeCN:ammonium carbonate modified H_2O, and the desired fractions were combined and concentrated *in vacuo* to yield dimethyl 2-((3-(((*tert*-butoxycarbonyl)(methyl)amino)methyl)-5-(3-(5,6,7,8-tetrahydro-1,8-naphthyridin-2-yl)propyl)thiophen-2-yl)methyl)succinate **(158)** (30 mg, 0.054 mmol, 37 % yield) as a brown coloured oil.

LCMS t_R = 0.86 min (system B), 100 %, ES+ve *m/z* 560 $(M + H)^+$; **^{1}H NMR** (400 MHz, $CDCl_3$): δ = = 7.05 (1H, d, *J* = 7.3 Hz, H_{17}), 6.52 (1H, s, H_4), 6.33 (1H, d, *J* = 7.3 Hz, H_{16}), 4.76 (1H, br s, NH), 4.24 (2H, br s, H_6), 3.74 – 3.67 (3H, s, OMe), 3.67 – 3.59 (3H, m, OMe), 3.43 – 3.34 (2H, m, H_{20}), 3.19 – 3.02 (2H, m, H_{7a}, H_8), 3.02 – 2.91 (1H, m, H_{7b}), 2.81 – 2.64 (8H, H_{9a}, NMe, H_{12}, H_{18}), 2.58 (2H, t, *J* = 7.7 Hz, H_{14}), 2.53 – 2.43 (1H, m,

H_{9b}), 2.06 – 1.95 (2H, m, H_{13}), 1.95 – 1.85 (2H, m, H_{19}), 1.47 (9H, s, ^{t}BuH); **^{13}C NMR** (101 MHz, $CDCl_3$): δ = 174.2, 172.1, 157.8, 155.9, 155.7, 143.4, 136.7, 135.3, 133.8, 125.3, 113.3, 111.5, 79.8, 52.2, 51.9, 45.2, 43.4, 41.7, 37.3, 35.0, 33.6, 31.6, 29.8, 29.4, 28.6, 26.5, 21.7; **IR** (neat, ν_{max} /cm^{-1}): 1736, 1689, 1599, 1481, 1465, 1737, 1391, 1366, 1248, 1160; **HRMS** (ESI): calc for $C_{29}H_{42}N_3O_6S$ $(M + H)^+$ 560.2794, found 560.2795.

Methyl 2-(5-methyl-6-oxo-2-(3-(5,6,7,8-tetrahydro-1,8-naphthyridin-2-yl)propyl)-5,6,7,8-tetrahydro-4H-thieno[3,2-c]azepin-7-yl)acetate, formic acid salt (159)

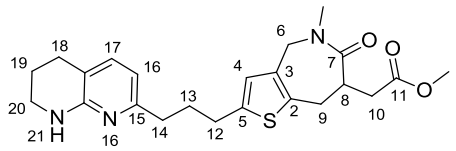

To a stirring solution of dimethyl 2-((3-(((*tert*-butoxycarbonyl)(methyl) amino)methyl)-5-(3-(5,6,7,8-tetrahydro-1,8-naphthyridin-2-yl)propyl)thiophen-2-yl)methyl)succinate **(158)** (30 mg, 0.054 mmol) in CH_2Cl_2 (0.5 mL) was added TFA (0.1 mL, 1.307 mmol), and the reaction was stirred for 30 min, after which time the solvent was concentrated using a flow of nitrogen gas, followed by the addition of PhMe (0.5 mL). Nitrogen gas was bubbled through the solution for 30 min, before the vial was sealed and purged with nitrogen gas. The yellow coloured solution was heated in a microwave reactor at 200 °C for 35 min, followed by cooling to rt and removal of the solvent under a flow of nitrogen gas. The crude product was purified using an Xbridge Prep RP18 OBD™ column, eluting with 0 – 100 % MeCN:ammonium carbonate modified H_2O, and the desired fractions were combined and concentrated *in vacuo*, followed by further purification using a Sunfire® Prep C18 OBD™ column, eluting with 0 – 40 % MeCN:formic acid modified H_2O, and the desired fractions were combined and concentrated *in vacuo* to furnish methyl 2-(5-methyl-6-oxo-2-(3-(5,6,7,8-tetrahydro-1,8-naphthyridin-2-yl)propyl)-5,6,7,8-tetrahydro-4H-thieno[3,2-c]azepin-7-yl)acetate, formic acid salt **(159)** (4.6 mg, 9.71 µmol, 18 % yield) as a colourless gum.

LCMS t_R = 0.61 min (system A), 92 %, ES+ve *m/z* 428 $(M + H)^+$; **^{1}H NMR** (600 MHz, $CDCl_3$): δ = 10.35 (1H, br s, HCOOH), 8.61 (1H, s, HCOOH), 7.24 (1H, d, *J* = 7.3 Hz, H_{17}), 6.47 (1H, s, H_4), 6.28 (1H, d, *J* = 7.3 Hz, H_{16}), 4.95 (1H, d, *J* = 16.9 Hz, H_{6a}), 3.85 (1H, d, *J* = 16.5 Hz, H_{6b}), 3.76 – 3.65 (4H, m, OMe, H_8), 3.48 (2H, t, *J* = 5.5 Hz, H_{20}), 3.07 – 3.01 (4H, m, NMe, H_{9a}), 2.96 – 2.91 (1H, m, H_{10a}), 2.89 – 2.70 (7H, m, H_{10b}, H_{12}, H_{14}, H_{18}), 2.40 (1H, dd, *J* = 16.7, 5.3 Hz, H_{9b}), 2.02 (2H, quin, *J* = 7.6 Hz, H_{13}), 1.91 (2H, quin, *J* = 6.0 Hz, H_{19}), *amine H not observed*; **^{13}C NMR** (151 MHz, $CDCl_3$): δ = 173.9, 173.0, 169.7, 153.4, 150.0, 140.9, 139.7, 134.8, 132.8, 125.4, 118.0, 109.3, 51.9, 48.7, 41.0, 37.7, 36.4, 36.2, 32.4, 30.9, 30.8, 29.1, 26.0, 19.8; **IR** (thin film, ν_{max} /cm^{-1}): 1732, 1647, 1573, 1438, 1372, 1349, 1320, 1200, 1166, 1127, 721; **HRMS** (ESI): calc for $C_{23}H_{30}N_3O_3S$ $(M + H)^+$ 428.2008, found 428.2014.

2-(5-Methyl-6-oxo-2-(3-(5,6,7,8-tetrahydro-1,8-naphthyridin-2-yl)propyl)-5,6,7,8-tetrahydro-4H-thieno[3,2-c]azepin-7-yl)acetic acid (146)

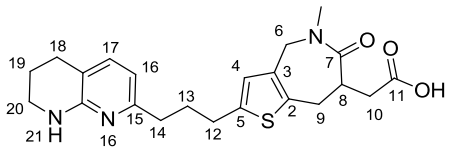

To a stirring solution of methyl 2-(5-methyl-6-oxo-2-(3-(5,6,7,8-tetrahydro-1,8-naphthyridin-2-yl)propyl)-5,6,7,8-tetrahydro-4H-thieno[3,2-c]azepin-7-yl)acetate **(159)** (4.2 mg, 9.82 µmol) in MeOH (1 mL) was added sodium hydroxide (1 M, 0.05 mL, 0.050 mmol), and the reaction stirred for 18 h. The solution was concentrated using a flow of nitrogen gas, and redissolved in H_2O (2 mL) and MeCN (1 mL), before neutralisation by dropwise addition of HCl (2 M). The solvent was partially removed under a flow of nitrogen gas and the crude product was purified using an Xbridge Prep RP18 OBD™ column, eluting with 0 – 100 % MeCN:ammonium carbonate modified H_2O, and the desired fractions were combined and concentrated *in vacuo* to furnish 2-(5-methyl-6-oxo-2-(3-(5,6,7,8-tetrahydro-1,8-naphthyridin-2-yl)propyl)-

5,6,7,8-tetrahydro-4H-thieno[3,2-c]azepin-7-yl)acetic acid **(146)** (3.3 mg, 7.98 µmol, 81 % yield) as a pale yellow coloured gum.

LCMS t_R = 0.75 min (system B), 99 %, ES+ve *m/z* 414 $(M + H)^+$; **^{1}H NMR** (600 MHz, $CDCl_3$): δ = 7.16 (1H, d, *J* = 7.0 Hz, H_{17}), 6.38 (1H, s, H_4), 6.23 (1H, d, *J* = 7.3 Hz, H_{16}), 4.88 (1H, d, *J* = 16.5 Hz, H_{6a}), 3.79 – 3.67 (2H, m, H_{6b}, H_8), 3.44 (2H, t, *J* = 5.5 Hz, H_{20}), 3.15 (1H, d, *J* = 17.2 Hz, H_{10a}), 3.07 – 2.99 (3H, s, NMe), 2.92 (1H, dd, *J* = 15.8, 4.8 Hz, H_{9a}), 2.82 (1H, t, *J* = 14.5 Hz, H_{10b}), 2.75 – 2.59 (6H, m, H_{12}, H_{14}, H_{18}), 2.48 (1H, dd, *J* = 15.8, 8.4 Hz, H_{9b}), 2.00 – 1.91 (2H, m, H_{13}), 1.91 – 1.83 (2H, m, H_{19}), *acid and amine H not observed*; **^{13}C NMR** (151 MHz, $CDCl_3$): δ = 179.7, 175.4, 154.1, 151.3, 141.0, 139.0, 135.7, 132.5, 124.7, 117.2, 109.4, 48.8, 41.0, 39.6, 38.9, 36.1, 33.7, 31.6, 31.1, 29.6, 26.2, 20.1; **IR** (neat, ν_{max} /cm^{-1}): 1645, 1563, 1481, 1461, 1440, 1396, 1319, 1293, 1232, 1197, 1120, 912, 725; **HRMS** (ESI): calc for $C_{22}H_{28}N_3O_3S$ $(M + H)^+$ 414.1851, found 414.1858.

Methyl 3-(1,8-naphthyridin-2-yl)propanoate (165)

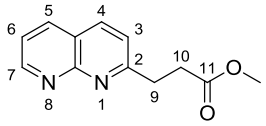

To a solution of methyl 4-oxopentanoate (9.51 mL, 77 mmol) in EtOH (350 mL) was added sulfuric acid (0.205 mL, 3.84 mmol), pyrrolidine (7.06 mL, 85 mmol) and 2-aminonicotinaldehyde **(26)** (11.26 g, 92 mmol), and the reaction was heated under reflux for 4 h, before the orange coloured solution was cooled to rt and the solvent was removed *in vacuo.* The crude product was purified using a 120 g silica column, eluting with 80 – 100 % EtOAc:cyclohexane, and the desired fractions were combined into two portions, which were both separately repurified using 120 g silica columns, eluting with 85 – 95 % EtOAc:cyclohexane, and the desired fractions from both columns were combined and concentrated *in vacuo* to furnish methyl 3-(1,8-

naphthyridin-2-yl)propanoate (9.56 g, 44.2 mmol, 58 % yield) **(165)** as a white coloured solid.

LCMS t_R = 0.68 min (system B), 100 %, ES+ve *m/z* 217 $(M + H)^+$; **^{1}H NMR** (400 MHz, $CDCl_3$): δ = 9.08 (1H, dd, *J* = 4.2, 2.0 Hz, H_7), 8.16 (1H, dd, *J* = 8.1, 2.0 Hz, H_5), 8.10 (1H, d, *J* = 8.3 Hz, H_4), 7.48 – 7.41 (2H, m, H_3, H_6), 3.67 (3H, s, OMe), 3.37 (2H, t, *J* = 7.3 Hz, H_9), 3.08 (2H, t, *J* = 7.3 Hz, H_{10}); **^{13}C NMR** (101 MHz, $CDCl_3$): δ = 173.8, 164.6, 156.1, 153.5, 137.2, 136.9, 123.0, 121.7, 121.4, 51.8, 33.6, 32.4; **IR** (neat, ν_{max} /cm^{-1}): 1609, 1726, 1598, 1554, 1443, 1418, 1304, 1292, 1196, 1173, 1158, 1134, 1119, 989, 849, 817, 776; **HRMS** (ESI): calc for $C_{12}H_{13}N_2O_2$ $(M + H)^+$ 217.0977, found 217.0975; **mp** 123-125 °C.

Methyl 3-(5,6,7,8-tetrahydro-1,8-naphthyridin-2-yl)propanoate (166)

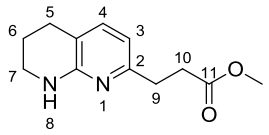

A mixture of rhodium on carbon (5 wt %) (9.08 g, 4.41 mmol) and methyl 3-(1,8-naphthyridin-2-yl)propanoate **(165)** (9.54 g, 44.1 mmol) in EtOAc (150 mL) and EtOH (200 mL) were stirred in presence of hydrogen gas for 62 h, after which the solution was filtered through Celite®, washing the filter with EtOH (300 mL). The solution was concentrated *in vacuo* to furnish methyl 3-(1,8-naphthyridin-2-yl)propanoate **(166)** (9.54 g, 44.1 mmol, 95 %) as an off-white coloured solid.

LCMS t_R = 0.91 min (system B), 96 %, ES+ve *m/z* 221 $(M + H)^+$; **^{1}H NMR** (400 MHz, $CDCl_3$): δ = 7.04 (1H, d, *J* = 7.3 Hz, H_4), 6.36 (1H, d, *J* = 7.3 Hz, H_3), 4.75 (1H, br s, NH), 3.66 (3H, s, OMe), 3.39 (2H, dt, *J* = 5.5, 2.4 Hz, H_7), 2.89 – 2.83 (2H, m, H_9), 2.73 – 2.65 (4H, m, H_5, H_{10}), 1.89 (1H, m, H_6); **^{13}C NMR** (101 MHz, $CDCl_3$): δ = 173.9, 156.4, 155.9, 136.8, 113.7, 111.4, 51.6, 41.7, 33.8, 32.8, 26.5, 21.7; **IR** (neat, ν_{max} /cm^{-1}): 3258 (br),

1721, 1600, 1589, 1458, 1446, 1433, 1357, 1316, 1287, 1197, 1144, 1114, 1009, 806, 790; **HRMS** (ESI): calc for $C_{12}H_{17}N_2O_2$ $(M + H)^+$ 221.1290, found 221.1291; **mp** 63-65 °C.

tert-Butyl 7-(3-methoxy-3-oxopropyl)-3,4-dihydro-1,8-naphthyridine-1(2H)-carboxylate (167)

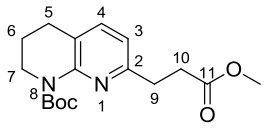

To a stirring solution of DIPEA (7.25 mL, 41.6 mmol) and methyl 3-(5,6,7,8-tetrahydro-1,8-naphthyridin-2-yl)propanoate **(166)** (9.17 g, 41.6 mmol) in CH_2Cl_2 (10 mL) was added di-*tert*-butyl dicarbonate (15 mL, 65.3 mmol), and the reaction was stirred at 100 °C for 30 min, during which time the CH_2Cl_2 evaporated, after which a Findenser^{TM} was placed on the flask and the flask was heated for a further 14 h, after which a further portion of di-*tert*-butyl dicarbonate (15 mL, 65.3 mmol) was added and the brown coloured solution stirred for a further 5 h, after which a final portion of di-*tert*-butyl dicarbonate (4 mL, 17.41 mmol) was added and the reaction was stirred for 1 h, after which time it was cooled to rt, followed by dilution with CH_2Cl_2 (20 mL) and the addition of imidazole (5.67 g, 83 mmol). The brown coloured solution was stirred for 4 h, before dilution with EtOAc (100 mL). The brown coloured solution was washed with HCl (0.2 M, 2 x 100 mL), followed by H_2O (100 mL), and the organic extracts were filtered through ah hydrophobic frit and concentrated *in vacuo.* The crude product was purified using a 120 g silica column, eluting with 0 – 100 % EtOAc:cyclohexane, and the desired fractions were combined and concentrated *in vacuo* to furnish *tert*-butyl 7-(3-methoxy-3-oxopropyl)-3,4-dihydro-1,8-naphthyridine-1(2H)-carboxylate **(167)** (11.02 g, 34.4 mmol, 83 % yield) as a white coloured solid.

LCMS t_R = 1.13 min (system B), 100 %, ES+ve *m/z* 321 $(M + H)^+$; **^{1}H NMR** (400 MHz, $CDCl_3$): δ = 7.28 (1H, d, *J* = 7.6 Hz, H_4), 6.83 (1H, d, *J* = 7.6 Hz, H_3), 3.79 – 3.71 (2H, m, H_7), 3.67 (3H, s, OMe), 3.03 (1H, t, *J* = 7.6 Hz, H_9), 2.81 (2H, t, *J* = 7.7 Hz, H_{10}), 2.72 (2H, t, *J* = 6.6 Hz, H_5), 1.91 (2H, quin, *J* = 6.3 Hz, H_6), 1.52 (9H, s, ^{t}BuH); **^{13}C NMR** (101 MHz, $CDCl_3$): δ = 173.9, 156.3, 154.2, 151.3, 137.4, 122.3, 118.4, 80.9, 51.7, 44.9, 33.4, 32.7, 28.5, 26.5, 23.4; **IR** (neat, ν_{max} /cm^{-1}): 1736, 1689, 1453, 1417, 1364, 1335, 1277, 1253, 1151, 866; **HRMS** (ESI): calc for $C_{17}H_{25}N_2O_4$ $(M + H)^+$ 321.1814, found 321.1806; **mp** 86 – 87 °C.

tert-Butyl 7-(3-hydroxypropyl)-3,4-dihydro-1,8-naphthyridine-1(2H)-carboxylate (168)[271]

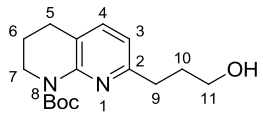

A mixture of sodium borohydride (5.46 g, 144 mmol) and calcium chloride (8.00 g, 72.1 mmol) in THF (100 mL) was stirred under nitrogen for 2 h. The mixture was cooled to 0 °C and *tert*-butyl 7-(3-methoxy-3-oxopropyl)-3,4-dihydro-1,8-naphthyridine-1(2H)-carboxylate **(167)** (11.0 g, 34.3 mmol) in THF (200 mL) was added to the mixture over 5 mins. The mixture was allowed to warm to rt and stirred for 15 h, followed by heating at 65 °C for a further 36 h, after which time the reaction mixture was cooled to 0 °C and H_2O (150 mL) was added, followed by removal of the THF *in vacuo*. The white coloured slurry was diluted with EtOAc (200 mL). The phases were separated, and the aqueous phase was extracted with EtOAc (2 x 200 mL). The combined organic extracts were filtered through a hydrophobic frit and were concentrated *in vacuo*. The crude product was purified using a 120 g silica column, eluting with 0 – 100 % EtOAc:cyclohexane, and the desired fractions were combined and concentrated *in vacuo* to yield *tert*-butyl 7-(3-hydroxypropyl)-3,4-dihydro-1,8-

naphthyridine-1(2H)-carboxylate **(168)** (4.99 g, 17.07 mmol, 50 % yield) as a pale yellow coloured oil.

LCMS t_R = 0.95 min (system B), 94 %, ES+ve *m/z* 293 $(M + H)^+$; **^{1}H NMR** (400 MHz, $CDCl_3$): δ = 7.31 (1H, d, *J* = 7.6 Hz, H_4), 6.82 (1H, d, *J* = 7.6 Hz, H_3), 4.10 (1H, br s, OH), 3.80 – 3.72 (2H, m, H_7), 3.68 (2H, t, *J* = 5.7 Hz, H_{11}), 2.98 – 2.79 (2H, m, H_9), 2.72 (2H, t, *J* = 6.6 Hz, H_5), 1.93 (4H, m, H_6, H_{10}), 1.52 (9H, s, ^{t}BuH); **^{13}C NMR** (101 MHz, $CDCl_3$): δ = 157.9, 153.7, 150.9, 137.8, 122.0, 118.5, 81.3, 62.0, 45.1, 35.0, 31.5, 28.5, 26.6, 23.3; **IR** (neat, ν_{max} /cm^{-1}): 3325 (br), 1690, 1468, 1412, 1365, 1333, 1316, 1278, 1252, 1146, 1078, 1063, 938, 852, 766; **HRMS** (ESI): calc for $C_{16}H_{25}N_2O_3$ $(M + H)^+$ 293.1865, found 293.1861.

***tert*-Butyl 7-(but-3-yn-1-yl)-3,4-dihydro-1,8-naphthyridine-1(2H)-carboxylate (163)**

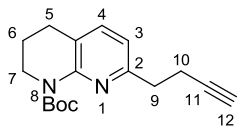

To a stirring solution of *tert*-butyl 7-(3-hydroxypropyl)-3,4-dihydro-1,8-naphthyridine-1(2H)-carboxylate **(168)** (250 mg, 0.855 mmol) in CH_2Cl_2 (10 mL) was added DMP (544 mg, 1.283 mmol) in 3 portions, and the reaction was stirred for 20 min, after which time 28 % aqueous sodium thiosulfate solution (15 mL) and saturated aqueous sodium thiosulfate solution (15 mL) were added, followed by vigorous stirring for 1 h. The layers were separated, and the aqueous layer was extracted with CH_2Cl_2 (10 mL), followed by filtration of the combined organic layers through a hydrophobic frit and concentration of the filtrate *in vacuo.* The residue was redissolved in MeOH (10 mL) and potassium carbonate (210 mg, 1.519 mmol) was added, followed by dimethyl (1-diazo-2-oxopropyl)phosphonate **(171)** (10 % solution in MeCN, 2.87 mL, 1.197 mmol). The flask was purged with nitrogen gas and stirred

for 5 h, after which time the orange coloured mixture was concentrated *in vacuo*, followed by dissolution of the resulting solid in H_2O (10 mL) and EtOAc (10 mL). The layers were separated, and the aqueous layer was extracted with EtOAc (10 mL), before the combined organic phases were filtered through a hydrophobic frit and concentrated *in vacuo.* The crude product was purified using a 40 g silica column, eluting with 0 – 50 % EtOAc:cyclohexane, and the desired fractions were combined and concentrated *in vacuo* to furnish *tert*-butyl 7-(but-3-yn-1-yl)-3,4-dihydro-1,8-naphthyridine-1(2H)-carboxylate **(163)** (200 mg, 0.698 mmol, 82 % yield) as a white coloured solid.

LCMS t_R = 1.19 min (system B), 100 %, ES+ve *m/z* 287 $(M + H)^+$; **^{1}H NMR** (400 MHz, $CDCl_3$): δ = 7.30 (1H, d, *J* = 7.6 Hz, H_4), 6.86 (1H, d, *J* = 7.6 Hz, H_3), 3.78 – 3.72 (2H, m, H_7), 2.97 – 2.89 (2H, m, H_9), 2.73 (2H, t, *J* = 6.6 Hz, H_5), 2.64 (2H, dt, *J* = 7.5, 2.6 Hz, H_{10}), 1.98 – 1.86 (3H, m, H_6, H_{12}), 1.54 – 1.48 (9H, m, ^{t}BuH); **^{13}C NMR** (101 MHz, $CDCl_3$): δ = 156.1, 154.2, 151.4, 137.3, 122.5, 118.5, 84.3, 81.0, 68.7, 44.9, 36.9, 28.6, 26.6, 23.4, 18.6; **IR** (neat, ν_{max} /cm^{-1}): 3245, 1682, 1469, 1416, 1367, 1338, 1286, 127; **HRMS** (ESI): calc for $C_{17}H_{23}N_2O_2$ $(M + H)^+$ 287.1760, found 287.1757; **mp** 77 – 78 °C.

Dimethyl 2-((3-(((*tert*-butoxycarbonyl)(methyl)amino)methyl)thiophen-2-yl)methyl)succinate (172)

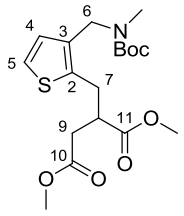

A mixture of dimethyl (*E*)-2-((3-(((*tert*-butoxycarbonyl)(methyl)amino)methyl) thiophen-2-yl)methylene)succinate **(152)** (323 mg, 0.842 mmol) and Pd / C (5 wt %) (179 mg, 0.084 mmol) in MeOH (9 mL), split equally between 3 vials, was stirred in the presence of hydrogen gas at 5 bar, at 50 °C for 12 h using a Biotage® Endeavor™

hydrogenation apparatus. The mixtures were cooled to rt before being filtered through Celite®, washing the filter with EtOH (100 mL), and concentrating the filtrate *in vacuo* to yield dimethyl 2-((3-(((*tert*-butoxycarbonyl)(methyl)amino) methyl)thiophen-2-yl)methyl)succinate **(172)** (297 mg, 0.770 mmol, 91 % yield) as a pale yellow coloured oil.

LCMS t_R = 1.24 min (system B), 95 %, ES+ve *m/z* 286 $(M + H)^+$; **^{1}H NMR** (400 MHz, $CDCl_3$): δ = 7.11 (1H, d, *J* = 5.1 Hz, ArH), 6.85 (1H, d, *J* = 5.4 Hz, ArH), 4.42 – 4.28 (2H, s, H_6), 3.69 (3H, s, OMe), 3.66 (3H, s, OMe), 3.26 – 3.16 (1H, m, H_{7a}), 3.15 – 3.00 (2H, m, H_{7b}, H_8), 2.76 (3H, s, NMe), 2.70 (1H, dd, *J* = 16.9, 8.3 Hz, H_{9a}), 2.49 (1H, dd, *J* = 16.8, 5.0 Hz, H_{9b}), 1.52 – 1.45 (9H, s, ^{t}BuH); **^{13}C NMR** (101 MHz, $CDCl_3$): δ = 174.2, 172.1, 155.9, 135.9, 135.0*, 128.4, 123.5, 79.9, 52.3, 52.0, 45.4, 43.5, 35.1, 33.7, 29.4, 28.6; **IR** (neat, ν_{max} /cm^{-1}): 1734, 1690, 1417, 1392, 1366, 1249, 1157, 874; **HRMS** (ESI): calc for $C_{18}H_{27}NNaO_6S$ $(M + Na)^+$ 408.1451, found 408.1457.

Dimethyl 2-((3-(((*tert*-butoxycarbonyl)(methyl)amino)methyl)-5-iodothiophen-2-yl)methyl)succinate (164)

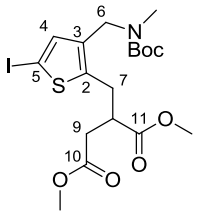

To a stirring solution of dimethyl 2-((3-(((*tert*-butoxycarbonyl)(methyl)amino) methyl)thiophen-2-yl)methyl)succinate **(172)** (1.31 g, 3.40 mmol) in $CHCl_3$ (35 mL) and acetic acid (0.195 ml, 3.40 mmol) was added *N*-iodosuccinimide (1.147 g, 5.10 mmol), and the pink coloured solution was heated under reflux for 6 h, after which time the mixture was diluted with H_2O (50 mL). The layers were separated, the aqueous layer was extracted with CH_2Cl_2 (2 x 50 mL), and the combined organic phases were filtered through a hydrophobic frit and concentrated *in vacuo.* The crude product was purified using a 120 g silica column, eluting with 0 – 30 %

EtOAc:cyclohexane, and the desired fractions were combined and concentrated *in vacuo* to furnish dimethyl 2-((3-(((*tert*-butoxycarbonyl)(methyl)amino)methyl)-5-iodothiophen-2-yl)methyl) succinate **(164)** (1.29 g, 2.52 mmol, 74 % yield) as a yellow coloured oil.

LCMS t_R = 1.36 min (system B), 97 %, ES+ve *m/z* 412 $(M + H)^+$; **^{1}H NMR** (400 MHz, $CDCl_3$): δ = 6.99 (1H, s, H_4), 4.35 – 4.21 (2H, s, H_6), 3.70 (3H, s, OMe), 3.67 (3H, s, OMe), 3.23 – 3.12 (1H, m, H_8), 3.09 – 2.98 (2H, m, H_7), 2.76 (3H, s, NMe), 2.69 (1H, dd, *J* = 16.8, 7.9 Hz, H_{9a}), 2.49 (1H, dd, *J* = 16.6, 5.4 Hz, H_{9b}), 1.48 (9H, s, ^{t}BuH); **^{13}C NMR** (101 MHz, $CDCl_3$): δ = 173.8, 171.9, 155.7, 142.2, 138.1, 137.4*, 80.1, 71.0, 52.4, 52.0, 45.3*, 43.2, 35.1, 33.9, 29.4, 28.6; **IR** (neat, ν_{max} /cm^{-1}): 1737, 1691, 1481, 1436, 1392, 1366, 1247, 1155, 874; **HRMS** (ESI): calc for $C_{18}H_{26}INNaO_6S$ $(M + Na)^+$ 534.0424, found 534.0427.

Dimethyl 2-((3-(((*tert*-butoxycarbonyl)(methyl)amino)methyl)-5-(4-(8-(*tert*-butoxy carbonyl)-5,6,7,8-tetrahydro-1,8-naphthyridin-2-yl)but-1-yn-1-yl)thiophen-2-yl)methyl)succinate (162)

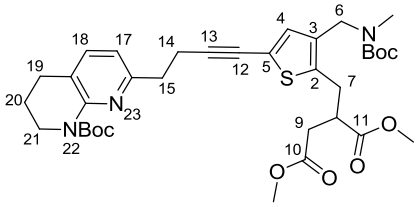

A stirring solution of triethylamine (0.139 mL, 0.997 mmol), $Pd(PPh_3)_2Cl_2$ (23.3 mg, 0.033 mmol), copper(I) iodide (7.6 mg, 0.040 mmol), *tert*-butyl 7-(but-3-yn-1-yl)-3,4-dihydro-1,8-naphthyridine-1(2H)-carboxylate **(163)** (105 mg, 0.366 mmol) and dimethyl 2-((3-(((*tert*-butoxycarbonyl)(methyl)amino)methyl)-5-iodothiophen-2-yl)methyl)succinate **(164)** (170 mg, 0.332 mmol) in DMF (3.5 mL) under nitrogen was heated to 80 °C for 16 h, followed by cooling to rt. The brown coloured solution was filtered through Celite®, washing with EtOAc (20 mL), and the resulting orange

coloured solution was washed with 10 % lithium chloride solution (20 mL), then filtered through a hydrophobic frit and concentrated *in vacuo.* The crude product was purified using a 40 g silica column, eluting with 0 – 100 % EtOAc:cyclohexane, and the desired fractions were combined and concentrated *in vacuo,* followed by repurification using a Sunfire® Prep C18 OBD™ column, eluting with 0 – 100 % MeCN:formic acid modified H_2O, and the desired fractions were combined and concentrated *in vacuo* to furnish dimethyl 2-((3-(((*tert*-butoxycarbonyl)(methyl)amino)methyl)-5-(4-(8-(*tert*-butoxycarbonyl)-5,6,7,8-tetrahydro-1,8-naphthyridin-2-yl)but-1-yn-1-yl)thiophen-2-yl)methyl)succinate **(162)** (68 mg, 0.102 mmol, 31 % yield) as a brown coloured oil, as an inseparable mixture with an unidentified impurity (5:1).

LCMS t_R = 1.53 min (system B), 96 %, ES+ve *m/z* 670 $(M + H)^+$; **^{1}H NMR** (400 MHz, $CDCl_3$): δ = 7.31 (1H, d, *J* = 7.6 Hz, H_{18}), 6.88 (1H, d, *J* = 7.6 Hz, H_{17}), 6.84 (1H, s, H_4), 4.25 (2H, s, H_6), 3.79 – 3.74 (2H, m, H_{21}), 3.69 (3H, s, OMe), 3.66 (3H, s, OMe), 3.19 – 3.11 (1H, m, H_{7a}), 3.09 – 3.03 (1H, m, H_8), 3.04 – 2.87 (3H, m, $H_{7b,}$ H_{15}), 2.86 – 2.81 (2H, m, H_{14}), 2.79 – 2.71 (5H, m, NMe, H_{19}), 2.68 (1H, dd, *J* = 16.7, 8.3 Hz, H_{9a}), 2.48 (1H, dd, *J* = 16.7, 5.3 Hz, H_{9b}), 1.92 (2H, quin, *J* = 6.3 Hz, H_{20}), 1.52 (9H, s, ^{t}BuH), 1.47 (9H, s, ^{t}BuH); **^{13}C NMR** (151 MHz, $CDCl_3$): δ = 174.0, 172.0, 156.1, 155.7, 154.2, 151.4, 137.4, 135.9, 135.8, 132.3, 122.6, 122.1, 118.6, 94.3, 81.0, 80.0, 74.1, 52.3, 52.0, 45.7, 44.9, 43.3, 36.9, 35.0, 33.7, 29.4, 28.6, 28.6, 26.5, 23.4, 19.9; **IR** (neat, ν_{max} /cm^{-1}): 1735, 1688, 1463, 1437, 1417, 1390, 1365, 1335, 1279, 1248, 1148, 874, 766, 670; **HRMS** (ESI): calc for $C_{35}H_{48}N_3O_8S$ $(M + H)^+$ 670.3162, found 670.3160.

Dimethyl 2-((3-(((*tert*-butoxycarbonyl)(methyl)amino)methyl)-5-(4-(8-(*tert*-butoxycarbonyl)-5,6,7,8-tetrahydro-1,8-naphthyridin-2-yl)butyl)thiophen-2-yl)methyl) succinate (161)

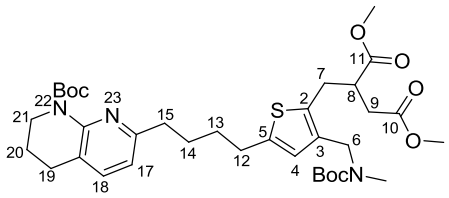

A solution of dimethyl 2-((3-(((*tert*-butoxycarbonyl)(methyl)amino)methyl)-5-(4-(8-(*tert*-butoxycarbonyl)-5,6,7,8-tetrahydro-1,8-naphthyridin-2-yl)but-1-yn-1-yl)thiophen-2-yl)methyl)succinate **(162)** (68 mg, 0.102 mmol) in MeOH (10 mL) was passed through the H-Cube® (flow H_2 generation) using a 10 % Pd/C catalyst, at 1 mL/min, under 8 bar H_2 pressure and at 30 °C, and then concentrated *in vacuo* to yield dimethyl 2-((3-(((*tert*-butoxycarbonyl)(methyl)amino)methyl)-5-(4-(8-(*tert*-butoxycarbonyl)-5,6,7,8-tetrahydro-1,8-naphthyridin-2-yl)butyl)thiophen-2-yl)methyl)succinate **(161)** (39.0 mg, 0.058 mmol, 57 % yield) as a colourless oil.

LCMS t_R = 1.57 min (system B), 100 %, ES+ve *m/z* 674 $(M + H)^+$; **^{1}H NMR** (600 MHz, $CDCl_3$): δ = 7.28 (1H, d, *J* = 7.7 Hz, H_{18}), 6.79 (1H, d, *J* = 7.7 Hz, H_{17}), 6.50 (1H, s, H_4), 4.36 – 4.19 (2H, m, H_6), 3.77 – 3.72 (2H, m, H_{21}), 3.69 (3H, s, OMe), 3.66 (3H, s, OMe), 3.16 – 3.10 (1H, m, H_{7a}), 3.09 – 3.03 (1H, m, H_8), 2.97 (1H, m, H_{7b}), 2.78 – 2.65 (10H, m, H_{9a}, NMe, H_{12}, H_{15}, H_{19}), 2.49 (1H, dd, *J* = 16.7, 5.0 Hz, H_{9b}), 1.91 (2H, quin, *J* = 6.3 Hz, H_{20}), 1.79 (2H, quin, *J* = 7.7 Hz, H_{14}), 1.69 (2H, dt, *J* = 15.1, 7.7 Hz, H_{13}), 1.51 (9H, s, ^{t}BuH), (9H, s, ^{t}BuH); **^{13}C NMR** (151 MHz, $CDCl_3$): δ = 174.3, 172.2, 158.3, 155.9, 154.3, 151.3, 143.6, 137.3, 135.3, 133.7, 125.3, 122.0, 118.3, 80.9, 79.8, 52.2, 52.0, 45.7, 44.9, 43.4, 37.8, 35.0, 33.7, 31.4, 30.1, 29.5, 29.2, 28.6, 28.6, 26.5, 23.5; **IR** (neat, ν_{max} /cm^{-1}): 1736, 1689, 1463, 1436, 1416, 1390, 1365, 1335, 1318, 1278, 1249, 1154, 877, 766; **HRMS** (ESI): calc for $C_{35}H_{52}N_3O_8S$ $(M + H)^+$ 674.3475, found 674.3472.

2-(5-Methyl-6-oxo-2-(4-(5,6,7,8-tetrahydro-1,8-naphthyridin-2-yl)butyl)-5,6,7,8-tetrahydro-4H-thieno[3,2-c]azepin-7-yl)acetic acid (160)

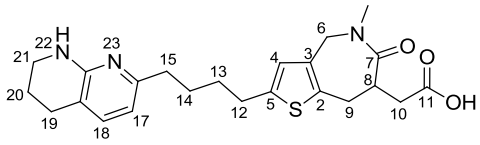

To a stirring solution of dimethyl 2-((3-(((*tert*-butoxycarbonyl)(methyl) amino)methyl)-5-(4-(8-(*tert*-butoxycarbonyl)-5,6,7,8-tetrahydro-1,8-naphthyridin-2-yl)butyl)thiophen-2-yl)methyl)succinate **(161)** (36 mg, 0.053 mmol) in CH_2Cl_2 (0.5 mL) was added TFA (0.102 mL, 1.336 mmol), and the reaction was stirred for 30 min, after which a further portion of TFA (0.2 mL, 2.61 mmol) was added and the reaction was left to stand for 13 h. The solvent was concentrated using a flow of nitrogen gas, followed by the addition of anhydrous PhMe (0.5 mL). Nitrogen gas was bubbled through the solution for 30 min, before the vial was sealed and purged with nitrogen gas. The yellow coloured solution was heated in a microwave reactor at 200 °C for 40 min, followed by cooling to rt and removal of the solvent under a flow of nitrogen gas. The brown coloured gum was redissolved in MeOH (1 mL) and to this solution was added sodium hydroxide (1 M, 0.534 mL, 0.534 mmol), and the solution was stirred for 5 h while warming to 40 °C. The solution was concentrated using a flow of nitrogen gas, and redissolved in H_2O (2 mL) and MeCN (1 mL), before neutralisation with the dropwise addition of HCl (2 M). The solvent was partially removed under a flow of nitrogen gas and the crude product was purified using an Xbridge Prep RP18 OBD™ column, eluting with 0 – 100 % MeCN:ammonium carbonate modified H_2O, and the desired fractions were combined and concentrated *in vacuo* to furnish 2-(5-methyl-6-oxo-2-(4-(5,6,7,8-tetrahydro-1,8-naphthyridin-2-yl)butyl)-5,6,7,8-tetrahydro-4H-thieno[3,2-c]azepin-7-yl)acetic acid **(160)** (9.4 mg, 0.022 mmol, 41 % yield) as a translucent white coloured gum.

LCMS t_R = 0.79 min (system B), 99 %, ES+ve *m/z* 428 $(M + H)^+$; **^{1}H NMR** (400 MHz, $CDCl_3$): δ = 10.45 (1H, br s, COOH), 7.16 (1H, d, *J* = 7.3 Hz, H_{18}), 6.29 (1H, s, H_4), 6.21

(1H, d, *J* = 7.1 Hz, H_{17}), 4.91 (1H, d, *J* = 16.6 Hz, H_{6a}), 3.84 – 3.69 (2H, m, H_{6b}, H_8), 3.43 (2H, t, *J* = 5.4 Hz, H_{21}), 3.14 (1H, d, *J* = 16.4 Hz, H_{10a}), 3.03 (3H, s, NMe), 2.95 (1H, dd, *J* = 15.4, 5.4 Hz, H_{9a}), 2.89 – 2.76 (1H, m, H_{10b}), 2.73 – 2.53 (6H, m, H_{12}, H_{15}, H_{19}), 2.45 (1H, dd, *J* = 15.8, 7.0 Hz, H_{9b}), 1.94 – 1.83 (2H, m, H_{20}), 1.77 – 1.55 (4H, m H_{13}, H_{14}), *amine H not observed*; **^{13}C NMR** (151 MHz $CDCl_3$): δ = 179.9, 175.5, 153.9, 151.5, 141.5, 139.2, 135.6, 132.5, 124.7, 117.1, 108.9, 48.9, 40.9, 39.6, 38.9, 36.1, 33.2, 31.2, 31.1, 29.5, 29.4, 26.2, 20.1; **IR** (neat, ν_{max} /cm^{-1}): 3266 (br), 1630, 1598, 1460, 1437, 1395, 1320, 1227, 1195, 1115, 739, 676, 600, 493; **HRMS** (ESI): calc for $C_{23}H_{30}N_3O_3S$ $(M+H)^+$ 428.2008, found 428.2004.

(*E*)-Dimethyl 2-((3-(((*tert*-butoxycarbonyl)(methyl)amino)methyl)-5-(2-(8-(*tert*-butoxy carbonyl)-5,6,7,8-tetrahydro-1,8-naphthyridin-2-yl)ethoxy)thiophen-2-yl)methylene)succinate (176)

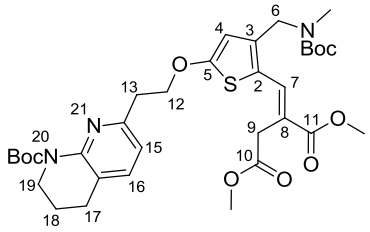

To a solution of dimethyl (*E*)-2-((3-(((*tert*-butoxycarbonyl)(methyl)amino)methyl)-5-iodothiophen-2-yl)methylene)succinate **(153)** (254 mg, 0.499 mmol) in PhMe (4 mL) was added cesium carbonate (325 mg, 0.997 mmol), PdG3RockPhos (32 mg, 0.038 mmol) and *tert*-butyl 7-(2-hydroxyethyl)-3,4-dihydro-1,8-naphthyridine-1(2H)-carboxylate **(67)** (2.25 g, 8.08 mmol). The flask was purged with nitrogen gas and nitrogen gas was bubbled through the mixture for 30 min. The mixture was heated in the microwave at 100 °C for 1 h, before cooling to rt. The mixture was filtered through Celite®, washing the filter with EtOAc (75 mL). The filtrate was concentrated *in vacuo.* The crude product was purified using a 60 g C18 silica column, eluting with 0 – 100 % MeCN:ammonium carbonate modified H_2O, and the desired fractions were combined and concentrated *in vacuo* to furnish dimethyl (*E*)-2-((3-(((*tert*-

butoxycarbonyl)(methyl)amino)methyl)-5-(2-(8-(*tert*-butoxycarbonyl)-5,6,7,8-tetrahydro-1,8-naphthyridin-2-yl)ethoxy)thiophen-2-yl)methylene)succinate **(176)** (235 mg, 0.356 mmol, 71 % yield) as a yellow coloured oil.

LCMS t_R = 1.47 min (system B), 100 %, ES+ve *m/z* 660 $(M + H)^+$; **^{1}H NMR** (400 MHz, $CDCl_3$): δ = 7.99 (1H, br s, H_7), 7.32 (1H, d, *J* = 7.3 Hz, H_{16}), 6.88 (1H, d, *J* = 7.8 Hz, H_{15}), 6.17 (1H, br s, H_4), 4.53 – 4.35 (4H, m, H_6, H_{12}), 3.79 (3H, s, OMe), 3.77 – 3.74 (2H, m, H_{19}), 3.70 (3H, s, OMe), 3.70 (2H, s, H_9), 3.18 (2H, t, *J* = 6.6 Hz, H_{13}), 2.84 – 2.71 (5H, m, NMe, H_{17}), 1.97 – 1.89 (2H, m, H_{18}), 1.50 (9H, s, ^{t}BuH), 1.47 (9H, s, ^{t}BuH); **^{13}C NMR** ^{13}C NMR (151 MHz, $CDCl_3$): δ = 171.1, 168.5 (2C, s), 156.0, 154.1, 153.6, 151.6, 142.6, 137.5, 131.8, 122.9, 120.0, 119.1, 118.1, 106.8 (1C, br d, *J* = 106.1 Hz (due to the presence of rotamers)), 81.0, 80.1, 77.4, 72.9, 52.4, 52.3, 46.0 (1C, br d, *J* = 150.4 Hz (due to the presence of rotamers)), 45.0, 37.5, 34.0, 33.7, 28.6, 28.6, 26.6, 23.3; **IR** (neat, ν_{max} /cm^{-1}): 1690, 1458, 1267, 1252, 1195, 1150, 1094, 730; **HRMS** (ESI): calc for $C_{33}H_{46}N_3O_9S$ $(M + H)^+$ 660.2955, found 660.2955.

Dimethyl 2-((3-((methylamino)methyl)-5-(2-(5,6,7,8-tetrahydro-1,8-naphthyridin-2-yl)ethoxy)thiophen-2-yl)methyl)succinate (177)

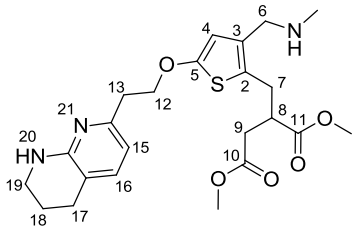

A mixture of dimethyl (*E*)-2-((3-(((*tert*-butoxycarbonyl)(methyl)amino)methyl)-5-(2-(8-(*tert*-butoxycarbonyl)-5,6,7,8-tetrahydro-1,8-naphthyridin-2-yl)ethoxy)thiophen-2-yl)methylene)succinate **(176)** (214 mg, 0.324 mmol) and Pd / C (5 wt %) (138 mg, 0.065 mmol) in MeOH (5 mL) was split across 5 vials and was stirred in the presence of hydrogen gas at 5 bar, at 60 °C for 10 h using the CAT96 apparatus. The solutions were filtered through a Celite® plug to remove the catalyst, washing with MeOH (0.2

mL) for each vial, after which a further portion of Pd / C (5 wt %) (138 mg, 0.065 mmol) was added to the filtrate, and the mixture split across 6 vials was stirred in the presence of hydrogen gas at 5 bar, at 60 °C for 10 h using the CAT96 apparatus. The mixture from each vial was combined and filtered through Celite®, washing the filter with MeOH (5 mL), and the filtrate was concentrated *in vacuo.* The resulting oil was dissolved in CH_2Cl_2 (2 mL) and to this colourless solution was added TFA (1.25 mL, 16.2 mmol), and the solution was stirred for 18 h, after which the volatiles were removed under a flow of nitrogen gas, followed by purification of the resulting brown coloured oil using a 12 g C18 column, eluting with 0 – 100 % MeCN:ammonium carbonate modified H_2O, and the desired fractions were combined and concentrated *in vacuo* to furnish dimethyl 2-((3-((methylamino)methyl)-5-(2-(5,6,7,8-tetrahydro-1,8-naphthyridin-2-yl)ethoxy)thiophen-2-yl)methyl)succinate **(177)** (75.4 mg, 0.163 mmol, 50 % yield) as a yellow coloured oil.

LCMS t_R = 1.15 min (system B), 96 %, ES+ve *m/z* 462 $(M + H)^+$; **^{1}H NMR** (400 MHz, $CDCl_3$): δ = 7.06 (1H, d, *J* = 7.3 Hz, H_{16}), 6.40 (1H, d, *J* = 7.3 Hz, H_{15}), 6.06 (1H, s, H_4), 4.86 (1H, br s, NH), 4.27 (2H, t, *J* = 6.8 Hz, H_{12}), 3.69 (3H, m, OMe), 3.65 (3H, s, OMe), 3.50 (2H, s, H_6), 3.39 (2H, br t, *J* = 4.2 Hz, H_{19}), 3.10 – 2.84 (5H, m, H_7, H_8, H_{13}), 2.72 – 2.63 (3H, m, H_{9a}, H_{17}), 2.50 (1H, dd, *J* = 16.9, 5.1 Hz, H_{9b}), 2.41 (3H, s, NMe), 1.93 – 1.86 (2H, m, H_{18}), *second amine H not observed*; **^{13}C NMR** (101 MHz, $CDCl_3$): δ = 174.4, 172.3, 162.8, 156.0, 153.9, 136.8, 135.3, 122.0, 114.2, 112.3, 106.1, 72.9, 52.2, 51.9, 49.0, 43.5, 41.7, 37.5, 36.3, 34.9, 29.3, 26.5, 21.6; **IR** (neat, ν_{max} /cm^{-1}): 3404 (br), 3332 (br), 3260 (br), 1731, 1587, 1508, 1462, 1437, 1278, 1214, 1163, 1119, 1008, 910, 798, 728, 646; **HRMS** (ESI): Calc for $C_{23}H_{32}N_3O_5S$ $(M + H)^+$ 462.2063, found 462.2061.

2-(5-Methyl-6-oxo-2-(2-(5,6,7,8-tetrahydro-1,8-naphthyridin-2-yl)ethoxy)-5,6,7,8-tetrahydro-4H-thieno[3,2-c]azepin-7-yl)acetic acid, formic acid salt (173)

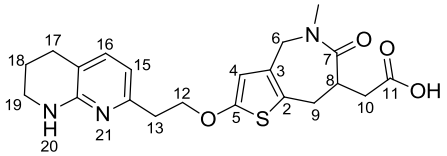

A solution of dimethyl 2-((3-((methylamino)methyl)-5-(2-(5,6,7,8-tetrahydro-1,8-naphthyridin-2-yl)ethoxy)thiophen-2-yl)methyl)succinate **(177)** (35 mg, 0.076 mmol) and TFA (0.012 mL, 0.152 mmol) in anhydrous PhMe (2 mL) was degassed by bubbling nitrogen gas through the solution for 1 h, after which time the solution was heated to 200 °C in a microwave reactor for 45 min, followed by cooling to room temp and removal of the solvent *in vacuo.* The crude product was purified using an Xterra® Prep RP18 OBD™ column, eluting with 0 – 100 % MeCN:ammonium carbonate modified H_2O, and the desired fractions were combined and concentrated *in vacuo,* after which the resulting oil was dissolved in MeOH (1 mL), and sodium hydroxide (0.379 mL, 0.758 mmol) was added. The pale-yellow coloured solution was heated to 40 °C whilst stirring for 5 h, after which the solution was cooled, and neutralised with the dropwise addition of HCl (2 M). The crude material was purified using an Xterra® Prep RP18 OBD™ column, eluting with 0 – 100 % MeCN:ammonium carbonate modified H_2O, and the desired fractions were combined and concentrated *in vacuo*, followed by further purification using a Sunfire® Prep C18 OBD™ column, eluting with 0 – 100 % MeCN:formic acid modified H_2O, and the desired fractions were combined and concentrated *in vacuo* to yield 2-(5-methyl-6-oxo-2-(2-(5,6,7,8-tetrahydro-1,8-naphthyridin-2-yl)ethoxy)-5,6,7,8-tetrahydro-4H-thieno[3,2-c]azepin-7-yl)acetic acid, formic acid salt **(173)** (2.9 mg, 6.28 µmol, 8 % yield) as a colourless gum.

LCMS t_R = 0.71 min (system B), 100 %, ES+ve *m/z* 416 $(M + H)^+$; **^{1}H NMR** (600 MHz, $CDCl_3$): δ = 8.55 (1H, s, HCOOH), 7.21 (1H, d, *J* = 7.0 Hz, H_{16}), 6.36 (1H, d, *J* = 7.3 Hz, H_{15}), 5.87 (1H, s, H_4), 4.82 (1H, br d, *J* = 16.5 Hz, H_{6a}), 4.28 – 4.21 (2H, m, H_{12}), 3.72 – 3.65 (2H, m, H_8, H_{6b}), 3.47 – 3.43 (2H, m, H_{19}), 3.09 – 3.04 (5H, m, H_{13}, NMe), 2.94 –

2.86 (2H, m, H_{9a}, H_{10a}), 2.81 – 2.75 (1H, m, H_{10b}), 2.71 (2H, t, *J* = 6.2 Hz, H_{17}), 2.55 (1H, dd, *J* = 5.5, 15.8 Hz, H_{9b}), 1.93 – 1.87 (2H, m, H_{18}), *carboxylic acid H shifts and amine H not observed*; **^{13}C NMR** (151 MHz, $CDCl_3$): δ = 176.4, 175.4, 169.5, 161.5, 154.1, 147.1, 139.1, 129.8, 123.5, 118.2, 110.9, 105.7, 71.8, 49.1, 41.0, 38.4, 38.3, 36.3, 33.8, 30.2, 26.2, 20.0; **IR** (neat, ν_{max} /cm^{-1}): 1633, 1514, 1375, 1323, 1215, 1015, 908, 725; **HRMS** (ESI): calc for $C_{21}H_{26}N_3O_4S$ $(M + H)^+$ 416.1644, found 416.1642.

2-Bromo-5-iodo-*N*-methoxy-*N*-methylbenzamide (185)

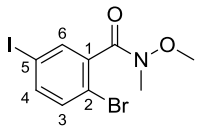

To a stirring suspension of *N,O*-dimethylhydroxylamine hydrochloride (1.611 g, 16.52 mmol), HATU (5.23 g, 13.77 mmol), and 2-bromo-5-iodobenzoic acid **(181)** (4.50 g, 13.77 mmol) in CH_2Cl_2 (50 mL) was added DIPEA (5.99 mL, 34.4 mmol) and the reaction was stirred for 20 min, after which time the yellow coloured solution was diluted with 5 % citric acid solution (50 mL), and the layers were separated, and the organic extracts were filtered through a hydrophobic frit and concentrated *in vacuo.* The crude product was purified using an 80 g silica column in 0 – 100 % EtOAc:cyclohexane, and the desired fractions were combined and concentrated *in vacuo* to yield 2-bromo-5-iodo-*N*-methoxy-*N*-methylbenzamide **(185)** (4.79 g, 12.95 mmol, 94 % yield) as a white coloured solid.

LCMS t_R = 1.03 min (system B), 99 %, ES+ve *m/z* 370/372 $(M + H)^+$; **^{1}H NMR** (400 MHz, $CDCl_3$): δ = 7.63 (1H, d, *J* = 2.4 Hz, H_6), 7.58 (1H, dd, *J* = 8.3, 2.0 Hz, H_4), 7.32 (1H, d, *J* = 8.3 Hz, H_3), 3.51 (3H, br s, OMe), 3.38 (3H, br s, NMe); **^{13}C NMR** (101 MHz, $CDCl_3$): δ = 167.6, 139.5, 139.4, 136.4, 134.4, 119.4, 91.8, 61.7, 32.5; **IR** (neat, ν_{max} /cm^{-1}): 1636, 1574, 1431, 1385, 1359, 1210, 1080, 1026, 987, 877, 803, 761, 739; **HRMS** (ESI): calc for $C_9H_{10}BrINO_2$ $(M + H)^+$ 369.8940, found 369.8937; **mp** 86-89 °C.

2-Bromo-5-iodobenzaldehyde (182)[272]

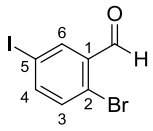

To a stirring solution of 2-bromo-5-iodo-*N*-methoxy-*N*-methylbenzamide **(185)** (8.72 g, 23.57 mmol) in THF) (100 mL) at –78 °C was added lithium aluminium hydride (1 M in Et_2O) (23.6 mL, 23.6 mmol) dropwise and the solution was stirred for 1 h, after which ammonium chloride solution (50 mL) was added carefully and the mixture was warmed to rt. The mixture was diluted with H_2O (200 mL) and EtOAc (200 mL) and the layers were separated. The aqueous layer was extracted with EtOAc (200 mL) and the combined organic layers were filtered through a hydrophobic frit and concentrated *in vacuo.* The crude product was purified using a 120 g silica column, eluting with 0 – 20 % EtOAc:cyclohexane, and the desired fractions were combined and concentrated *in vacuo* to furnish 2-bromo-5-iodobenzaldehyde **(182)** (6.44 g, 20.71 mmol, 88 % yield) as a white coloured solid.

LCMS t_R = 1.22 min (system B), 100 %, *no parent mass ion observed*; **^{1}H NMR** (400 MHz, $CDCl_3$): δ = 10.27 (1H, s, CHO), 8.22 (1H, d, *J* = 2.2 Hz, H_6), 7.76 (1H, dd, *J* = 8.4, 2.3 Hz, H_4), 7.41 (1H, d, *J* = 8.3 Hz, H_3); **^{13}C NMR** (101 MHz, $CDCl_3$): δ = 190.3, 143.8, 138.7, 135.4, 134.8, 126.6, 92.8; **IR** (neat, ν_{max} /cm^{-1}): 1670, 1563, 1450, 1374, 1249, 1188, 1073, 1029, 1016, 890, 870, 822, 699, 633, 512; **HRMS** (ESI): *no parent mass ion observed*; **mp** 104 – 106 °C.

***N*-(2-Bromo-5-iodobenzyl)-2,2,2-trifluoroethanamine (186)**

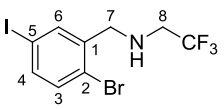

A solution of 2-bromo-5-iodobenzaldehyde **(182)** (6.44 g, 20.71 mmol), 2,2,2-trifluoroethan-1-amine hydrochloride (6.18 g, 45.6 mmol) and zinc(II) chloride (4.14 mL, 2.071 mmol) were combined in MeCN (50 mL) and *N,N*-dimethylacetamide (DMA) (20 mL) and stirred for 6 h at 80 °C, followed by the addition of a further portion of 2,2,2-trifluoroethan-1-amine hydrochloride (6.18 g, 45.6 mmol) and zinc(II) chloride (4.14 mL, 2.071 mmol), and heating for a further 24 h, after which the yellow coloured solution was cooled to rt and the MeCN was removed *in vacuo.* To the resulting yellow coloured solution was added further portions of zinc(II) chloride (4.14 mL, 2.071 mmol) and 2,2,2-trifluoroethan-1-amine hydrochloride (6.18 g, 45.6 mmol), and the flask was purged with nitrogen gas. To the yellow coloured solution was added activated 4 Å molecular sieves, and the solution was stirred for 3 h, followed by the addition of sodium triacetoxyborohydride (6.58 g, 31.1 mmol) and stirring for 2 h, followed by the addition of sodium borohydride (0.940 g, 24.86 mmol), and stirring for a further 4 h, followed by the addition of a further portion of sodium borohydride (0.392 g, 10.36 mmol) and stirring for 3 h. The brown coloured slurry was cooled to rt and diluted with NaOH (2 M, 100 mL), H_2O (100 mL) and EtOAc (200 mL). The layers were separated, and the aqueous layer was extracted with EtOAc (200 mL). The organic layers were combined and washed with 10 % lithium chloride solution (2 x 150 mL), filtered through a hydrophobic frit and concentrated *in vacuo.* The crude product was purified using a 120 g silica column, eluting with 0 – 20 % EtOAc:cyclohexane, and the desired fractions were combined and concentrated *in vacuo* to furnish *N*-(2-bromo-5-iodobenzyl)-2,2,2-trifluoroethan-1-amine **(186)** (7.61 g, 19.32 mmol, 93 % yield) as a pale yellow coloured oil.

LCMS t_R = 1.39 min (system B), 95 %, ES+ve *m/z* 394/396 $(M + H)^+$; **^{1}H NMR** (400 MHz, $CDCl_3$): δ = 7.75 (1H, d, *J* = 2.2 Hz, H_6), 7.46 (1H, dd, *J* = 8.3, 2.2 Hz, H_4), 7.27 (1H, d, *J* = 8.8 Hz, H_3), 3.93 (2H, d, *J* = 6.6 Hz, H_7), 3.20 (2H, dq, *J* = 9.3, 7.2 Hz, H_8), 1.84 – 1.72 (1H, m, NH); **^{13}C NMR** (101 MHz, $CDCl_3$): δ = 140.7, 138.8, 138.0, 134.6, 123.7, 125.6 (1C, q, *J* = 279.2 Hz), 92.9, 52.6, 49.9 (1C, q, *J* = 31.5 Hz); **IR** (neat, ν_{max} /cm^{-1}): 3361,

1458, 1263, 1140, 1077, 1018, 945, 807, 732, 547, 464; **HRMS** (ESI): calc for C_9H_9BrIN $(M + H)^+$ 393.8915, found 393.8919.

tert-Butyl 2-bromo-5-iodobenzyl(2,2,2-trifluoroethyl)carbamate (183)

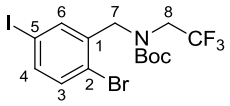

To a stirring solution of *N*-(2-bromo-5-iodobenzyl)-2,2,2-trifluoroethan-1-amine **(186)** (7.61 g, 19.32 mmol) and DIPEA (3.36 mL, 19.32 mmol) was added di-*tert*-butyl dicarbonate (13.31 mL, 57.9 mmol), and the reaction was heated at 100 °C for 4 h, after which the colourless solution was dissolved in CH_2Cl_2 (100 mL) and imidazole (5.26 g, 77 mmol) was added to the stirring solution. After stirring for 1 h, the colourless solution was diluted with aqueous hydrochloric acid (0.2 M, 100 mL), and the layers were separated. The organic layer was washed with aqueous hydrochloric acid (0.2 M, 150 mL), then filtered through a hydrophobic frit and concentrated *in vacuo.* The crude product was purified using a 120 g silica column, eluting with 0 – 20 % EtOAc:cyclohexane, and the desired fractions were combined and concentrated *in vacuo* to furnish *tert*-butyl (2-bromo-5-iodobenzyl)(2,2,2-trifluoroethyl)carbamate **(183)** (9.06 g, 18.34 mmol, 95 % yield) as a pale yellow coloured oil.

LCMS t_R = 1.56 min (system B), 96 %, ES+ve *m/z* 394/396 $(M + H)^+$; **^{1}H NMR** (400 MHz, DMSO-d_6, 120 °C): δ = 7.59 – 7.55 (1H, m, H_4), 7.53 (1H, d, *J* = 2.2 Hz, H_6), 7.39 (1H, d, *J* = 8.3 Hz, H_3), 4.53 (2H, s, H_7), 4.12 (2H, q, *J* = 9.3 Hz, H_8), 1.41 (9H, s, ^{t}BuH); **^{13}C NMR** (101 MHz, $CDCl_3$): δ = 155.0 (1C, br d, *J* = 35.1 Hz), 138.5 (1C, d, *J* = 42.7 Hz), 138.1 (1C, d, *J* = 13.7 Hz), 137.4 (1C, d, *J* = 64.1 Hz), 134.7, 124.7 (1C, q, *J* = 285.4 Hz), 122.9 (1C, d, *J* = 56.5 Hz), 92.8 (1C, d, *J* = 25.9 Hz), 82.1, 51.0 (1C, d, *J* = 103.8 Hz), 48.0 (1C, q, *J* = 33.6 Hz), 28.2; **IR** (neat, ν_{max} /cm^{-1}): 1705, 1446, 1406, 1384, 1368, 1268, 1224, 1145, 1091, 1019, 808; **HRMS** (ESI): calc for $C_{10}H_9BrF_3INO_2$ $(M - {}^t\text{Bu} + 2H)^+$ 437.8813, found 437.8813.

tert-Butyl (2-bromo-5-(4-hydroxypent-1-yn-1-yl)benzyl)(2,2,2-trifluoroethyl) carbamate (187)

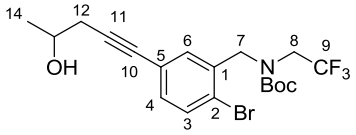

A solution of $Pd(PPh_3)_2Cl_2$ (1.29 g, 1.834 mmol), copper(I) iodide (0.349 g, 1.834 mmol), pent-4-yn-2-ol **(140)** (1.73 mL, 18.34 mmol),and *tert*-butyl (2-bromo-5-iodobenzyl)(2,2,2-trifluoroethyl)carbamate **(183)** (9.06 g, 18.34 mmol) in DMF (100 mL) under nitrogen was stirred for 2 h, after which the orange coloured solution was diluted with EtOAc (150 mL) and 10 % aqueous lithium chloride solution (150 mL) and the layers were separated. The organic layer was washed with 10 % aqueous lithium chloride solution (150 mL) and then filtered through a hydrophobic frit and concentrated *in vacuo*. The crude product was purified using a 120 g silica column, eluting with 0 – 50 % EtOAc:cyclohexane, and the desired fractions were combined and concentrated *in vacuo* to furnish *tert*-butyl (2-bromo-5-(4-hydroxypent-1-yn-1-yl)benzyl)(2,2,2-trifluoroethyl)carbamate (5.79 g, 12.86 mmol, 70 % yield) **(187)** as a yellow coloured oil.

LCMS t_R = 1.40 min (system B), 96 %, *no parent mass ion observed*; **^{1}H NMR** (400 MHz, DMSO-d_6): δ = 7.60 (1H, d, *J* = 7.8 Hz, H_3), 7.23 (1H, dd, *J* = 8.3, 2.0 Hz, H_4), 7.11 (1H, br s, H_6), 4.82 (1H, d, *J* = 4.9 Hz, OH), 4.48 (2H, s, H_7), 4.19 (2H, br s, H_8), 3.87 – 3.75 (1H, m, H_{13}), 2.56 – 2.38 (2H, m, H_{12}), 1.48 – 1.22 (9H, br d, *J* = 74.8 Hz, ^{t}BuH), 1.17 (3H, d, *J* = 5.9 Hz, H_{14}); **^{13}C NMR** (101 MHz, DMSO-d_6): δ = 154.6 – 154.0 (1C, m), 136.8 (1C, br d, *J* = 80.0 Hz), 132.8, 131.4, 130.3, 125.0 (1C, br q, *J* = 285.4 Hz), 122.8, 121.6 – 120.8 (1C, m), 89.6, 80.6 (2C, br s), 65.0, 51.5 (1C, br d, *J* = 65.3 Hz), 48.7 – 47.4 (1C, m), 29.3, 27.5, 22.5; **IR** (neat, ν_{max} /cm^{-1}): 3431 (br), 2234, 1706, 1454, 1410, 1393, 1368, 1268, 1242, 1123, 1146, 1090, 1027, 935, 825; **HRMS** (ESI): calc for $C_{19}H_{23}BrF_3NNaO_3$ $(M + Na)^+$ 472.0711, found 472.0715.

Dimethyl (*E*)-2-(2-(((*tert*-butoxycarbonyl)(2,2,2-trifluoroethyl)amino)methyl)-4-(4-hydroxypent-1-yn-1-yl)benzylidene)succinate (184)

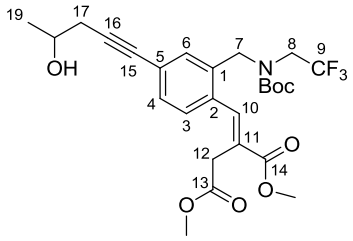

A flask containing DIPEA (8.96 ml, 51.4 mmol), *tert*-butyl (2-bromo-5-(4-hydroxypent-1-yn-1-yl)benzyl)(2,2,2-trifluoroethyl)carbamate **(187)** (5.79 g, 12.86 mmol), tri-*ortho*-tolylphosphine (0.626 g, 2.057 mmol), diacetoxypalladium (0.375 g, 1.672 mmol), and dimethyl 2-methylenesuccinate **(102)** (3.62 ml, 25.7 mmol) in propionitrile (50 mL) was purged with nitrogen and heated under reflux for 6 h, after which time the mixture was cooled to rt, and filtered through Celite®, washing the filter with EtOAc (100 mL). The filtrate was concentrated *in vacuo,* followed by purification using a 120 g silica column, eluting with 0 – 25 % EtOAc:cyclohexane, and the desired fractions were combined and concentrated *in vacuo* to furnish dimethyl (*E*)-2-(2-(((*tert*-butoxycarbonyl)(2,2,2-trifluoroethyl)amino)methyl)-4-(4-hydroxypent-1-yn-1-yl)benzylidene)succinate **(184)** (590 mg, 1.118 mmol, 9 % yield) as a yellow coloured gum.

LCMS t_R = 1.28 min (system B), 96 %, ES+ve *m/z* 428 $(M + H)^+$; **^{1}H NMR** (400 MHz, $CDCl_3$): δ = 7.89 – 7.84 (1H, m, H_{10}), 7.40 – 7.34 (1H, m, H_4), 7.27 – 7.24 (1H, m, H_6), 7.20 – 7.14 (1H, m, H_3), 4.67 – 4.44 (2H, m, H_7), 4.11 – 4.03 (1H, m, H_{18}), 3.96 – 3.66 (8H, m, OMe, OMe, H_8), 3.34 (2H, s, H_{12}), 2.69 – 2.56 (2H, m, H_{17}), 1.95 (1H, br s, OH), 1.46 (9H br s, ^{t}BuH), 1.36 – 1.33 (3H, d, *J* = 6.4 Hz, H_{19}), *nOe observed between 7.20 – 7.14 and 3.34, confirming (E) geometry*; **^{13}C NMR** (101 MHz, $CDCl_3$): δ = 171.3, 167.1, 139.8, 135.8*, 133.7*, 132.2 – 127.8* (5C, m), 124.5, 88.1, 82.4, 81.8, 66.7, 52.5, 52.3, 49.6 – 46.2* (2C, m), 33.5, 30.2, 28.2, 22.6, *carbamate C not observed*; **IR** (neat, ν_{max}

/cm^{-1}): 3500 (br), 2228, 1707, 1436, 1401, 1368, 1269, 1209, 1146, 1087, 936, 771; **HRMS** (ESI): calc for calc for $C_{26}H_{32}F_3NNaO_7$ $(M + Na)^+$ 550.2029, found 550.2028.

Dimethyl 2-(2-(((*tert*-butoxycarbonyl)(2,2,2-trifluoroethyl)amino)methyl)-4-(4-hydroxypentyl)benzyl)succinate (180)

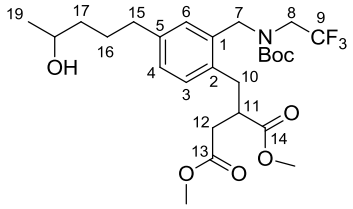

A mixture of dimethyl (*E*)-2-(2-(((*tert*-butoxycarbonyl)(2,2,2-trifluoroethyl)amino)methyl)-4-(4-hydroxypent-1-yn-1-yl)benzylidene)succinate **(184)** (540 mg, 1.024 mmol) and palladium on carbon (5 wt%) (621 mg, 0.292 mmol) in EtOH (10 mL) was stirred in the presence of hydrogen gas for 14 h, followed by filtrating through Celite®, eluting with EtOH (40 mL). The filtrate was concentrated *in vacuo,* followed by purification using a 24 g silica column, eluting with 0 – 50 % EtOAc:Cyclohexane, and the desired fractions were combined and concentrated *in vacuo* to furnish dimethyl 2-(2-(((*tert*-butoxycarbonyl)(2,2,2-trifluoroethyl)amino)methyl)-4-(4-hydroxypentyl)benzyl)succinate **(180)** (340 mg, 0.637 mmol, 62 % yield) as a colourless oil. Mixed fractions were also obtained, which were repurified using a 12 g silica column, eluting with 0 – 50 % EtOAc:cyclohexane, and the desired fractions were combined and concentrated *in vacuo* to furnish dimethyl 2-(2-(((*tert*-butoxycarbonyl)(2,2,2-trifluoroethyl)amino)methyl)-4-(4-hydroxypentyl)benzyl)succinate **(180)** (64 mg, 0.120 mmol, 12 % yield).

LCMS t_R = 1.30 min (system B), 90 %, ES+ve *m/z* 434 $(M - CO_2{}^tBu + 2H)^+$; **^{1}H NMR** (400 MHz, $CDCl_3$): δ 7.04 (2H, s, H_3, H_4), 6.91 (br s, H_6), 4.73 – 4.56 (2H, m, H_7), 3.89 – 3.58 (9H, m, H_8, H_{18}, OMe, OMe), 3.08 – 2.92 (2H, m, H_{10a}, H_{11}), 2.70 (2H, app dd, *J* = 16.6, 8.8 Hz, H_{10b}, H_{12a}), 2.58 (2H, t, *J* = 7.6 Hz, H_{15}), 2.41 (1H, dd, *J* = 16.6, 4.9 Hz, H_{12b}), 1.77

– 1.55 (2H, m, H_{16}), 1.53 – 1.40 (11H, m, ^{t}BuH, H_{17}), 1.34 (1H, br s, OH), 1.17 (3H, d, *J* = 6.4 Hz, H_{19}); **^{13}C NMR** (101 MHz, $CDCl_3$): δ = 174.7, 172.1, 155.7 – 154.8 (1C, m), 141.5, 135.1 – 133.9 (2C, m), 130.5, 129.7 – 127.3 (2C, m), 125.0 (1C, br q, *J* = 281.0 Hz), 81.6, 68.0, 52.0, 51.9, 48.8 – 46.0 (2C, m), 42.4, 38.9, 35.6 (2C, m), 34.0, 28.3, 27.5, 23.7; **IR** (neat, ν_{max} /cm^{-1}): 1736, 1704, 1437, 1407, 1368, 1269, 1214, 1145, 1086, 932, 893, 856, 826, 732; **HRMS** (ESI): calc for $C_{26}H_{38}F_3NNaO_7$ $(M + Na)^+$ 556.2498, found 556.2501.

Dimethyl 2-(2-(((*tert*-butoxycarbonyl)(2,2,2-trifluoroethyl)amino)methyl)-4-(4-oxopentyl)benzyl) succinate (179)

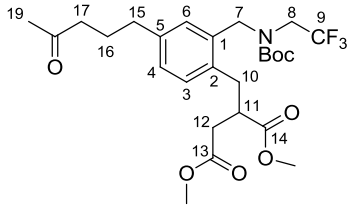

To a stirring solution of dimethyl 2-(2-(((*tert*-butoxycarbonyl)(2,2,2-trifluoroethyl)amino)methyl)-4-(4-hydroxypentyl)benzyl)succinate **(180)** (330 mg, 0.618 mmol) in CH_2Cl_2 (10 mL) was added DMP (367 mg, 0.866 mmol) and the reaction was stirred for 30 min, after which Celite® was added and the solvent was removed *in vacuo*, followed by purification using a 24 g silica column, eluting with 0 – 50 % EtOAc:cyclohexane, and the desired fractions were combined and concentrated *in vacuo* to afford 1 dimethyl 2-(2-(((*tert*-butoxycarbonyl)(2,2,2-trifluoroethyl)amino)methyl)-4-(4-oxopentyl)benzyl) succinate **(179)** (280 mg, 0.527 mmol, 85 % yield) as a colourless oil.

LCMS t_R = 1.34 min (system B), 99 %, ES+ve *m/z* 432 $(M - CO_2{}^{t}Bu + 2H)^+$; **^{1}H NMR** (600 MHz, $CDCl_3$): δ = 7.07 – 7.02 (2H, m, H_3, H_4), 6.90 (1H, br s, H_6), 4.74 – 4.57 (2H, m, H_7), 3.89 – 3.65 (2H, m, H_8), 3.63 (6H, s, OMe, OMe), 3.07 – 3.01 (1H, m, H_{11}), 3.00 – 2.93 (1H, m, H_{10a}), 2.70 (2H, app dd, *J* = 16.7, 9.0 Hz, H_{10b}, H_{12a}), 2.57 (2H, t, *J* = 7.6 Hz,

H_{15}), 2.45 – 2.39 (3H, m, H_{12b}, H_{17}), 2.11 (3H, s, H_{19}), 1.86 (2H, quin, *J* = 7.4 Hz, H_{16}), 1.50 (9H, br s, ^{t}BuH); **^{13}C NMR** (150 MHz, $CDCl_3$): δ = 208.6, 174.7, 172.1, 155.3 (1C, m), 140.8, 135.2 – 134.1 (2C, m), 130.6, 129.5 – 127.0 (2C, m), 125.0 (br q, *J* = 281.4 Hz), 81.6, 52.1, 51.9, 47.5 (1C, m), 47.0 – 46.4 (1C, m), 42.9, 42.4, 35.9 – 35.2 (1C, m), 34.8, 34.0, 30.0, 28.3, 25.3; **IR** (neat, ν_{max} /cm^{-1}): 1737, 1704, 1436, 1406, 1367, 1269, 1214, 1144, 1085, 892, 827, 771; **HRMS** (ESI): calc for $C_{26}H_{36}F_3NNaO_7$ $(M + Na)^+$ 554.2342, found 554.2341.

Dimethyl 2-(4-(3-(1,8-naphthyridin-2-yl)propyl)-2-(((*tert*-butoxycarbonyl)(2,2,2-trifluoroethyl) amino)methyl)benzyl)succinate (188)

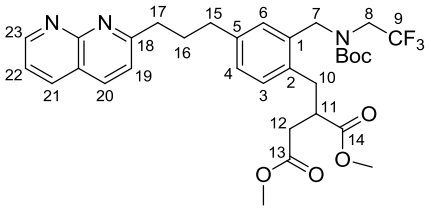

To a solution of dimethyl 2-(2-(((*tert*-butoxycarbonyl)(2,2,2-trifluoroethyl)amino)methyl)-4-(4-oxopentyl)benzyl)succinate **(179)** (280 mg, 0.527 mmol) in EtOH (6 mL) was added sulfuric acid (3 µl, 0.053 mmol), pyrrolidine (0.048 mL, 0.579 mmol) and 2-aminonicotinaldehyde **(26)** (84 mg, 0.685 mmol), and the reaction was heated under reflux for 16 h, before the yellow coloured solution was cooled to rt and the solvent was removed *in vacuo.* The crude product was purified using a 24 g silica column, eluting with 0 – 80 % EtOAc:cyclohexane, and the desired fractions were combined and concentrated *in vacuo* to yield dimethyl 2-(4-(3-(1,8-naphthyridin-2-yl)propyl)-2-(((*tert*-butoxycarbonyl)(2,2,2-trifluoroethyl)amino)methyl)benzyl)succinate **(188)** (260 mg, 0.421 mmol, 80 % yield) as a yellow coloured oil, as an inseparable mixture with the corresponding product with one ester transesterified to the ethyl ester in a 6:1 ratio.

LCMS t_R = 1.32 min (system B), 75 %, ES+ve *m/z* 618 $(M + H)^+$; **^{1}H NMR** (400 MHz, $CDCl_3$): δ = 9.08 (1H, dd, *J* = 3.9, 2.0 Hz, H_{23}), 8.15 (1H, dd, *J* = 8.3, 2.0 Hz, H_{21}), 8.08 (1H, d, *J* = 8.3 Hz, H_{20}), 7.44 (1H, dd, *J* = 8.3, 4.4 Hz, H_{22}), 7.35 (1H, d, *J* = 8.3 Hz, H_{19}), 7.10 – 7.01 (2H, m, H_3, H_4), 6.93 (1H, br s, H_6), 4.61 (2H, br s, H_7), 3.92 – 3.65 (2H, m, H_8), 3.62 (6H, s, OMe, OMe), 3.09 – 2.92 (4H, m, H_{10a}, H_{11}, H_{17}), 2.76 – 2.64 (4H, m, H_{10b}, H_{12a}, H_{15}), 2.41 (1H, dd, *J* = 16.6, 4.9 Hz, H_{12b}), 2.27 – 2.16 (2H, m, H_{16}), 1.45 (9H, br s, ^{t}BuH); **^{13}C NMR** (101 MHz, $CDCl_3$): δ = 174.7, 172.1, 166.3, 155.6 – 154.9 (1C, m), 156.2, 153.5, 141.2, 137.1, 136.8, 135.1 – 133.4 (2C, m), 130.6, 129.4 – 127.4 (2C, m), 125.0 (q, *J* = 281.4 Hz, 1C), 122.7, 121.6, 121.2, 81.5, 52.0, 51.9, 48.4 – 47.2 (1C, m), 47.1 – 45.8 (1C, m), 42.4, 38.8, 35.6 (1C, m), 35.4, 34.0, 30.8, 28.3; **IR** (neat, ν_{max} /cm^{-1}): 1734, 1702, 1608, 1451, 1436, 1405, 1367, 1269, 1206, 1144, 1086, 843, 826, 816, 775; **HRMS** (ESI): Calc for $C_{32}H_{39}F_3N_3O_6$ $(M + H)^+$ 618.2791, found 618.2802.

Dimethyl 2-(2-(((*tert*-butoxycarbonyl)(2,2,2-trifluoroethyl)amino)methyl)-4-(3-(5,6,7,8-tetrahydro-1,8-naphthyridin-2-yl)propyl)benzyl)succinate (178)

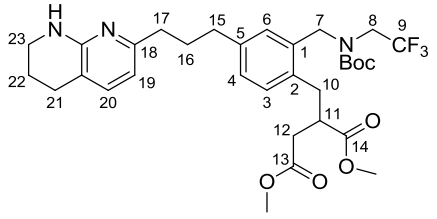

A mixture of dimethyl 2-(4-(3-(1,8-naphthyridin-2-yl)propyl)-2-(((*tert*-butoxycarbonyl)(2,2,2-trifluoroethyl)amino)methyl)benzyl)succinate **(188)** (237 mg, 0.384 mmol) and rhodium on carbon (5 wt %) (79 mg, 0.038 mmol) in EtOAc (2 mL) and EtOH (2 mL) was stirred in the presence of hydrogen gas for 14 h, followed by filtration through Celite®, washing the filter with EtOH (50 mL). The filtrate was concentrated *in vacuo*, followed by purification using a 24 g silica column, eluting with 50 – 100 % EtOAc:cyclohexane, and the desired fractions were combined and concentrated *in vacuo* to afford dimethyl 2-(2-(((*tert*-butoxycarbonyl)(2,2,2-trifluoroethyl)amino)methyl)-4-(3-(5,6,7,8-tetrahydro-1,8-naphthyridin-2-

yl)propyl)benzyl)succinate **(178)** (181 mg, 0.291 mmol, 76 % yield) as a colourless gum, as an inseparable mixture with the corresponding product with one ester transesterified to the ethyl ester.

LCMS t_R = 1.48 min (system B), 79 %, ES+ve *m/z* 622 $(M + H)^+$; **^{1}H NMR** (400 MHz, $CDCl_3$): δ = 7.07 – 7.01 (3H, m, H_3, H_4, H_{20}), 6.92 (1H, br s, H_6), 6.31 (1H, d, *J* = 7.3 Hz, H_{19}), 4.86 – 4.74 (1H, br s, NH), 4.71 – 4.56 (2H, m, H_7), 3.90 – 3.64 (2H, m, H_8), 3.64 – 3.58 (6H, m, OMe, OMe), 3.39 (2H, td, *J* = 5.6, 2.4 Hz, H_{23}), 3.08 – 2.92 (2H, m, H_{10a}, H_{11}), 2.75 – 2.65 (4H, m, H_{10b}, H_{12a}, H_{21}), 2.60 (2H, t, *J* = 7.6 Hz, H_{15}), 2.57 – 2.52 (2H, m, H_{17}), 2.40 (1H, dd, *J* = 16.6, 4.9 Hz, H_{12b}), 1.98 – 1.86 (4H, m, H_{16}, H_{22}), 1.47 (9H, br s, ^{t}BuH); **^{13}C NMR** (101 MHz, $CDCl_3$): δ = 174.7, 172.1, 158.1, 155.9, 155.7 – 154.7 (1C, m), 146.1, 141.7, 136.7, 134.9 – 134.0 (1C, m), 130.5, 129.7 – 123.6 (3C, m), 113.3, 111.5, 81.5, 52.0, 51.9, 48.7 – 45.7* (2C, m), 42.4, 41.8, 37.5, 35.6, 35.3, 34.0, 31.5, 28.3, 26.5, 21.7; **IR** (neat, ν_{max} /cm^{-1}): 3399 (br), 3250 (br), 1736, 1703, 1461, 1436, 1406, 1367, 1321, 1269, 1205, 1144, 1085, 826; **HRMS** (ESI): calc for $C_{32}H_{43}F_3N_3O_6$ $(M + H)^+$ 622.3104, found 622.3101.

Methyl 2-(3-oxo-8-(3-(5,6,7,8-tetrahydro-1,8-naphthyridin-2-yl)propyl)-2-(2,2,2-trifluoroethyl)-2,3,4,5-tetrahydro-1H-benzo[c]azepin-4-yl)acetate (189)

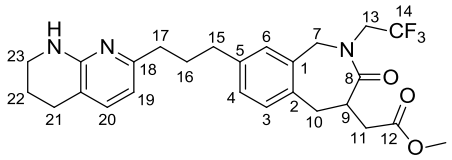

To a stirring solution of dimethyl 2-(2-(((*tert*-butoxycarbonyl)(2,2,2-trifluoroethyl)amino)methyl)-4-(3-(5,6,7,8-tetrahydro-1,8-naphthyridin-2-yl)propyl)benzyl)succinate **(178)** (134 mg, 0.216 mmol) in CH_2Cl_2 (1 mL) was added TFA (0.830 mL, 10.78 mmol) and the solution was stirred for 2 h then concentrated using a flow of nitrogen gas. The resulting oil was dissolved in PhMe (2 mL) and

heated under reflux for 6 h, followed by cooling to rt, addition of DIPEA (0.3 mL) and the removal of the solvent *in vacuo*. The resulting crude material was adsorbed onto Celite® and purified using a 12 g silica column, eluting with 40 – 100 % EtOAc:cyclohexane, and the desired fractions were combined and concentrated *in vacuo* to afford methyl 2-(3-oxo-8-(3-(5,6,7,8-tetrahydro-1,8-naphthyridin-2-yl)propyl)-2-(2,2,2-trifluoroethyl)-2,3,4,5-tetrahydro-1H-benzo[c]azepin-4-yl)acetate **(189)** (78 mg, 0.159 mmol, 74 % yield) as a yellow coloured gum, as an inseparable mixture with the corresponding ethyl ester.

LCMS t_R = 1.27 min (system B), 84 %, ES+ve *m/z* 490 $(M + H)^+$; **^{1}H NMR** (400 MHz, $CDCl_3$): δ = 7.10 (1H, d, *J* = 7.3 Hz, H_{20}), 7.08 – 7.04 (1H, m, H_4), 7.02 – 6.98 (1H, m, H_3), 6.90 (1H, s, H_6), 6.30 (1H, d, *J* = 7.3 Hz, H_{19}), 5.32 (1H, d, *J* = 16.6 Hz, H_{7a}), 4.24 – 4.10 (1H, m, H_{13a}), 4.03 – 3.90 (2H, m, H_{7b}, H_{13b}), 3.89 – 3.80 (1H, m, H_9), 3.69 (3H, s, OMe), 3.40 (2H, br t, *J* = 4.6 Hz, H_{23}), 3.08 – 2.96 (2H, m, H_{10a}, H_{11a}), 2.95 – 2.86 (1H, m, H_{10b}), 2.69 (2H, t, *J* = 6.4 Hz, H_{21}), 2.64 – 2.56 (4H, m, H_{15}, H_{17}), 2.45 (1H, dd, *J* = 16.9, 5.6 Hz, H_{11b}), 2.01 – 1.93 (2H, m, H_{16}), 1.93 – 1.85 (2H, m, H_{22}), *amine H not observed*; **^{13}C NMR** (101 MHz, $CDCl_3$): δ = 174.9, 172.6, 155.7, 155.0, 140.3, 137.7, 133.5, 133.0, 130.7, 129.1, 128.5, 124.4 (1C, q, *J* = 280.2 Hz), 114.7, 110.8, 53.2, 51.9, 47.7 (1C, q, *J* = 33.7 Hz), 41.5, 37.0, 36.7, 36.1, 35.0, 34.9, 31.2, 26.3, 21.1; **IR** (neat, ν_{max} /cm^{-1}): 3410 (br), 3255 (br), 1734, 1670, 1463, 1436, 1361, 1268, 1240, 1201, 1150, 1128, 1094; **HRMS** (ESI): calc for $C_{26}H_{31}F_3N_3O_3$ $(M + H)^+$ 490.2318, found 490.2329.

2-(3-Oxo-8-(3-(5,6,7,8-tetrahydro-1,8-naphthyridin-2-yl)propyl)-2-(2,2,2-trifluoroethyl)-2,3,4,5-tetrahydro-1H-benzo[c]azepin-4-yl)acetic acid (174)

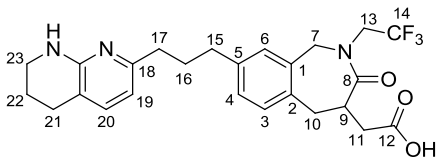

To a stirring solution of methyl 2-(3-oxo-8-(3-(5,6,7,8-tetrahydro-1,8-naphthyridin-2-yl)propyl)-2-(2,2,2-trifluoroethyl)-2,3,4,5-tetrahydro-1H-benzo[c]azepin-4-yl)acetate **(189)** (77 mg, 0.157 mmol) in MeOH (1 mL) was added sodium hydroxide (2 M in H_2O) (0.393 mL, 0.786 mmol), and the reaction stirred for 18 h. The solution was concentrated using a flow of nitrogen gas, and redissolved in H_2O (2 mL) and MeCN (1 mL), before neutralisation by dropwise addition of aqueous HCl (2 M). Due to the very limited solubility of the crude product in H_2O and MeCN, only a small portion of the solvent was purified using an Xbridge C18 column, eluting with 0 – 100 % MeCN:ammonium carbonate modified H_2O, and the desired fractions were combined and concentrated *in vacuo* to furnish 2-(3-oxo-8-(3-(5,6,7,8-tetrahydro-1,8-naphthyridin-2-yl)propyl)-2-(2,2,2-trifluoroethyl)-2,3,4,5-tetrahydro-1H-benzo[c]azepin-4-yl)acetic acid **(174)** (8.6 mg, 0.018 mmol, 12 % yield) as a pale yellow coloured gum.

LCMS t_R = 0.85 min (system B), 100 %, ES+ve *m/z* 476 $(M + H)^+$; **^{1}H NMR** (400 MHz, $CDCl_3$): δ = 10.63 (1H, br s, COOH), 7.20 (1H, d, *J* = 7.3 Hz, H_{20}), 6.91 (dd, *J* = 1.5, 7.8 Hz, H_4), 6.79 (2H, m, H_3, H_6), 6.26 (1H, d, *J* = 7.3 Hz, H_{19}), 5.18 (1H, br d, *J* = 16.6 Hz, H_{7a}), 4.29 – 4.16 (1H, m, H_{13a}), 3.93 – 3.75 (3H, m, H_{7b}, H_9, H_{13b}), 3.47 (2H, br t, *J* = 5.6 Hz, H_{23}), 3.22 (1H, dd, *J* = 17.4, 4.2, Hz, H_{10a}), 2.97 (1H, dd, *J* = 15.4, 5.1 Hz, H_{11a}), 2.88 (1H, br dd, *J* = 17.1, 13.2 Hz, H_{10b}), 2.77 – 2.67 (4H, m, H_{17}, H_{21}), 2.60 (2H, t, *J* = 8.1 Hz, H_{15}), 2.44 (1H, dd, *J* = 15.6, 8.3 Hz, H_{11b}), 2.05 – 1.88 (4H, m, H_{16}, H_{22}), *amine H not observed*; **^{13}C NMR** (101 MHz, $CDCl_3$): δ = 180.1, 176.1, 153.9, 150.9, 139.3, 139.3, 134.9, 133.4, 131.0, 128.7, 128.0, 124.6* (1C, q, *J* = 290 Hz), 117.5, 109.3, 53.1, 47.5 (1C, br d, *J* = 33.0 Hz), 40.9, 40.1, 38.3, 35.4, 35.0, 33.6, 31.2, 26.1, 20.0; **IR** (neat, ν_{max} /cm^{-1}): 3261 (br), 1667, 1627, 1395, 1321, 1267, 1211, 1148, 1128, 1093, 908, 829, 726, 675, 645; **HRMS** (ESI): calc for $C_{25}H_{29}F_3N_3O_3$ $(M + H)^+$ 476.2161, found 476.2162.

_N_-((2-Bromopyridin-3-yl)methyl)-2,2,2-trifluoroethan-1-amine (196)

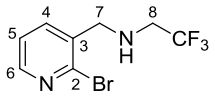

2,2,2-Trifluoroethan-1-amine (11.25 g, 114 mmol) and 2-bromonicotinaldehyde **(194)** (8.37 mL, 56.8 mmol) were combined in MeCN (100 mL) and stirred for 3 h at 80 °C, after which time sodium borohydride (2.58 g, 68.1 mmol) was added carefully, and the reaction was stirred for a further 12 h before the addition of a further portion of sodium borohydride (1.07 g, 28.4 mmol) and stirring for 2 h, followed by cooling to rt. The bright yellow coloured mixture was diluted with the addition of H_2O (100 mL) and EtOAc (100 mL). The layers were separated, and the aqueous layer was extracted with EtOAc (100 mL). The combined organic layers were filtered through a hydrophobic frit and concentrated *in vacuo.* The crude material was purified using a 120 g silica column, eluting with 0 – 30 % EtOAc:cyclohexane, and the desired fractions were combined and concentrated *in vacuo* to yield *N*-((2-bromopyridin-3-yl)methyl)-2,2,2-trifluoroethan-1-amine **(196)** (5.91 g, 22.0 mmol, 39 % yield) as a yellow coloured oil.

LCMS t_R = 0.95 min (system B), 96 %, ES+ve *m/z* 269/271 $(M + H)^+$; **^{1}H NMR** (400 MHz, $CDCl_3$): δ = 8.28 (1H, dd, *J* = 4.9, 2.0 Hz, H_6), 7.77 (1H, dd, *J* = 7.3, 2.0 Hz, H_4), 7.28 (1H, dd, *J* = 7.6, 4.6 Hz, H_5), 3.97 (2H, d, *J* = 5.9 Hz, H_7), 3.28 – 3.17 (2H, m, H_8), 1.86 (1H, br s, NH); **^{13}C NMR** (101 MHz, $CDCl_3$): δ = 148.9, 143.5, 138.0, 135.8, 123.1, 125.5 (1C, q, *J* = 279.5 Hz), 51.9, 50.0 (1C, q, *J* = 31.5 Hz); **IR** (neat, ν_{max} /cm^{-1}): 3322, 3052, 1561, 1404, 1349, 1303, 1265, 1137, 1052, 1037, 823, 794, 744, 727, 676, 663, 549; **HRMS** (ESI): calc for $C_8H_9BrF_3N_2$ $(M + H)^+$ 268.9901, found 268.9910.

tert-Butyl ((2-bromopyridin-3-yl)methyl)(2,2,2-trifluoroethyl)carbamate (193)

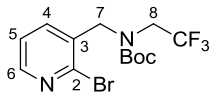

To a stirring solution of *N*-((2-bromopyridin-3-yl)methyl)-2,2,2-trifluoroethan-1-amine **(196)** (5.91 g, 21.96 mmol) and DIPEA (3.83 mL, 21.96 mmol) in CH_2Cl_2 (5 mL) was added di-*tert*-butyl dicarbonate (12.6 mL, 54.9 mmol), and the reaction was heated at 100 °C for 12 h, followed by cooling to rt, dilution with CH_2Cl_2 (100 mL), and the addition of imidazole (4.49 g, 65.9 mmol) to the stirring solution. After stirring for 1 h, the solution was diluted with 5 % aqueous citric acid (100 mL) and the layers were separated. The organic layer was washed with 5 % aqueous citric acid (100 mL), then filtered through a hydrophobic frit and concentrated *in vacuo.* The crude product was purified using an 80 g silica column, eluting with 0 – 20 % EtOAc:cyclohexane, and the desired fractions were combined and concentrated *in vacuo* to furnish *tert*-butyl ((2-bromopyridin-3-yl)methyl)(2,2,2-trifluoroethyl)carbamate **(193)** (7.14 g, 19.3 mmol, 88 % yield) as a pale yellow coloured oil.

LCMS t_R = 1.27 min (system B), 100 %, ES+ve *m/z* 369/371 $(M + H)^+$; **^{1}H NMR** (400 MHz, DMSO-d_6, 120 °C): δ = 8.30 (1H, dd, *J* = 4.6, 1.7 Hz, H_6), 7.61 – 7.56 (1H, m, H_4), 7.46 (1H, dd, *J* = 7.6, 4.6 Hz, H_5), 4.57 (2H, s, H_7), 4.14 (2H, q, *J* = 9.3 Hz, H_8), 1.40 (9H, s, ^{t}BuH); **^{13}C NMR** (101 MHz, DMSO-d_6): δ = 154.2, 148.6, 141.8 – 140.9 (1C, m), 136.0, 134.9 – 133.4 (1C, m), 125.0 (1C, br q, *J* = 280.2 Hz), 123.5, 80.7, 51.0 (1C, br d, *J* = 60.9 Hz), 48.8 – 47.6 (1C, m), 27.5; **IR** (neat, ν_{max} /cm^{-1}): 1704, 1456, 1395, 1368, 1347, 1320, 1268, 1253, 1221, 1144, 1120, 1094, 1051, 892, 828, 777; **HRMS** (ESI): calc for $C_{13}H_{17}BrF_3N_2O_2$ $(M + H)^+$ 369.0426, found 369.0432.

tert-Butyl ((2-bromo-5-hydroxypyridin-3-yl)methyl)(2,2,2-trifluoroethyl)carbamate (192)

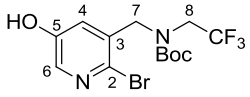

4,4,4',4',5,5,5',5'-Octamethyl-2,2'-bi(1,3,2-dioxaborolane) (3.20 g, 12.60 mmol), 4,4'-di-*tert*-butyl-2,2'-bipyridine **(197)** (0.113 g, 0.420 mmol), $[Ir(COD)OMe]_2$ (0.139 g, 0.210 mmol), and *tert*-butyl ((2-bromopyridin-3-yl)methyl)(2,2,2-trifluoroethyl)carbamate **(193)** (3.10 g, 8.40 mmol) were split equally between 2 vials, which were sealed and degassed with alternating nitrogen and vacuum. To this, *tert*-butylmethyl ether (2 x 15 mL) was added and purged with alternating nitrogen and vacuum, followed by heating to at 80 °C for 14 h, followed by cooling to rt. The solutions were combined, the solvent was removed *in vacuo* and the residue was redissolved in acetone (30 mL) and to this, tetrabutylammonium oxone (11.5 g, 13.44 mmol) in H_2O (25 mL) was added dropwise over 25 min and the red coloured solution left to stir for 3 h. Saturated aqueous sodium sulfite (50 mL) was added, followed by H_2O (30 mL) and EtOAc (150 mL). The layers were separated, and the aqueous layer was extracted with EtOAc (150 mL). The combined organic layers were filtered through a hydrophobic frit and concentrated *in vacuo*. The crude product was purified using a 120 g silica column, eluting with 0 – 30 % EtOAc:cyclohexane, and the desired fractions were combined and concentrated *in vacuo* to yield *tert*-butyl ((2-bromo-5-hydroxypyridin-3-yl)methyl)(2,2,2-trifluoroethyl)carbamate **(192)** (1.10 g, 2.86 mmol, 34 % yield) as a colourless oil, and starting material *tert*-butyl ((2-bromopyridin-3-yl)methyl)(2,2,2-trifluoroethyl)carbamate **(193)** (1.31 g, 3.55 mmol, 42 % yield) was also recovered as a colourless oil.

LCMS t_R = 0.97 min (system B), 99 %, ES+ve *m/z* 385/387 $(M + H)^+$; **^{1}H NMR** (400 MHz, DMSO-d_6, 120 °C): δ = 9.75 (1H, br s, OH), 7.87 (1H, d, *J* = 2.9 Hz, H_6), 7.04 (1H, d, *J* = 2.7 Hz, H_4), 4.48 (2H, s, H_7), 4.10 (2H, q, *J* = 9.3 Hz, H_8), 1.41 (9H, s, ^{t}BuH); **^{13}C NMR** (101 MHz, DMSO-d_6): δ = 154.3 (1C, br d, *J* = 19.8 Hz), 154.0, 136.4, 134.2 (1C, br d, *J*

= 68.2 Hz), 129.1 (1C, br d, *J* = 27.1 Hz), 124.9 (1C, br d, *J* = 283.2 Hz), 122.8 (1C, br d, *J* = 30.8 Hz), 80.7, 50.7 (1C, br d, *J* = 67.5 Hz), 48.4 – 47.6 (1C, m), 27.6; **IR** (neat, ν_{max} /cm^{-1}): 3322 (br), 1709, 1682, 1456, 1436, 1407, 1370, 1308, 1290, 1224, 1197, 1148, 1097, 1050, 884, 851, 827, 779, 633, 594, 533; **HRMS** (ESI): calc for $C_{13}H_{17}BrF_3N_2O_3$ $(M + H)^+$ 385.0375, found 385.0374.

***tert*-Butyl ((2-bromo-5-((4-methoxybenzyl)oxy)pyridin-3-yl)methyl)(2,2,2-trifluoroethyl) carbamate (198)**

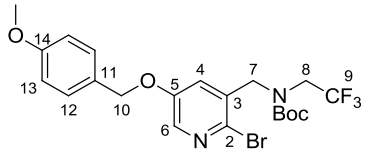

A mixture of potassium carbonate (1.184 g, 8.57 mmol), 1-(chloromethyl)-4-methoxybenzene (0.465 mL, 3.43 mmol) and *tert*-butyl ((2-bromo-5-hydroxypyridin-3-yl)methyl)(2,2,2-trifluoroethyl)carbamate **(192)** (1.10 g, 2.86 mmol) in DMF (5 mL) was heated to 80 °C for 2 h, followed by cooling to rt. The mixture was diluted with EtOAc (40 mL) and H_2O (40 mL) and the layers were separated. The organic layer was filtered through a hydrophobic frit and concentrated *in vacuo.* The crude product was purified using a 40 g silica column, eluting with 0 – 50 % EtOAc:cyclohexane, and the desired fractions were combined and concentrated *in vacuo* to furnish *tert*-butyl ((2-bromo-5-((4-methoxybenzyl)oxy)pyridin-3-yl)methyl)(2,2,2-trifluoroethyl) carbamate **(198)** (967 mg, 1.91 mmol, 67 % yield) as a colourless oil.

LCMS t_R = 1.46 min (system B), 97 %, ES+ve *m/z* 505/507 $(M + H)^+$; **^{1}H NMR** (400 MHz, DMSO-d_6, 120 °C): δ = 8.10 (1H, d, *J* = 2.9 Hz, H_6), 7.35 (2H, d, *J* = 8.8 Hz, H_{12}), 7.18 (1H, d, *J* = 2.9 Hz, H_4), 6.98 – 6.92 (2H, m, H_{13}), 5.12 (2H, s, H_{10}), 4.51 (2H, s, H_7), 4.11 (2H, q, *J* = 9.3 Hz, H_8), 3.79 (3H, s, OMe), 1.39 (9H, s, ^{t}BuH); **^{13}C NMR** (101 MHz, DMSO-d_6): δ = 159.2, 154.4 (1C, br d, *J* = 48.8 Hz), 135.9, 134.5 (1C,br d, *J* = 76.3 Hz), 131.1 (1C,br d, *J* = 15.3 Hz), 129.6, 127.8, 126.5 – 123.3 (1C, m), 123.0, 113.9, 80.7, 69.9,

55.0, 50.7 (1C, br d, *J* = 65.6 Hz), 48.6 – 47.6 (1C, m), 27.5, *carbamate C not observed*; **IR** (thin film, ν_{max} /cm^{-1}): 1708, 1515, 1445, 1430, 1396, 1369, 1291, 1250, 1224, 1145, 1095, 1032, 826; **HRMS** (ESI): calc for $C_{21}H_{25}BrF_3N_2O_4$ $(M + H)^+$ 505.0950, found 505.0953.

Dimethyl (*E*)-2-((3-(((*tert*-butoxycarbonyl)(2,2,2-trifluoroethyl)amino)methyl)-5-((4-methoxy benzyl)oxy)pyridin-2-yl)methylene)succinate (199)

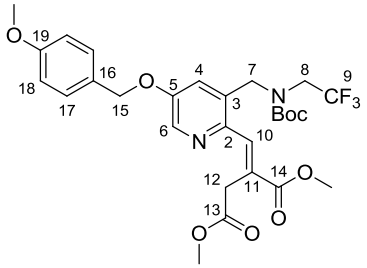

A flask containing DIPEA (1.66 mL, 9.55 mmol), *tert*-butyl ((2-bromo-5-((4-methoxybenzyl)oxy)pyridin-3-yl)methyl)(2,2,2-trifluoroethyl)carbamate **(198)** (965 mg, 1.910 mmol), tri-*ortho*-tolylphosphine (116 mg, 0.382 mmol), diacetoxypalladium (64.3 mg, 0.286 mmol) and dimethyl 2-methylenesuccinate **(102)** (806 µl, 5.73 mmol) in propionitrile (10 mL) was purged with nitrogen was heated to under reflux for 15 h, followed by cooling to rt. The orange coloured solution was concentrated *in vacuo,* followed by purification with a 80 g silica column, eluting with 0 – 40 % EtOAc:cyclohexane, and the desired fractions were combined and concentrated *in vacuo* to furnish dimethyl (*E*)-2-((3-(((*tert*-butoxycarbonyl)(2,2,2-trifluoroethyl)amino)methyl)-5-((4-methoxybenzyl)oxy)pyridin-2-yl)methylene)succinate **(199)** (425 mg, 0.730 mmol, 38 % yield) as a yellow coloured gum, as a 5:1 inseparable mixture with protodebrominated starting material pyridine.

LCMS t_R = 1.43 min (system B), 86 %, ES+ve *m/z* 583 $(M + H)^+$; **^{1}H NMR** (400 MHz, DMSO-d_6): δ = 8.35 – 8.32 (1H, m, H_6), 7.74 (1H, s, H_{10}), 7.41 – 7.36 (2H, m, H_{17}), 7.18 – 7.14 (1H, m, H_4), 6.97 – 6.93 (2H, m, H_{18}), 5.15 (2H, s, H_{15}), 4.62 (2H, s, H_7), 4.18 –

4.01 (2H, m, H_8), 3.89 (2H, s, H_{12}), 3.77 – 3.74 (6H, m, OMe, OMe), 3.58 – 3.56 (3H, m, OMe), 1.45 – 1.28 (9H, m, ^{t}BuH); **^{13}C NMR** (101 MHz, $CDCl_3$): δ = 170.8, 167.5, 159.2, 154.3, 143.9*, 135.7, 134.6*, 134.0, 129.6, 127.9, 127.3, 121.5*, 113.9, 80.7, 69.6, 55.1, 52.2, 51.4, 49.1 – 47.2* (2C, m), 32.8, 27.5, *carbamate and CF_3 shifts not observed*; **IR** (neat, ν_{max} /cm^{-1}): 1707, 1515, 1456, 1437, 1405, 1369, 1274, 1251, 1149, 1110, 1092, 1033, 826; **HRMS** (ESI): calc for $C_{28}H_{34}F_3N_2O_8$ $(M + H)^+$ 583.2267, found 583.2280.

Dimethyl 2-((3-(((*tert*-butoxycarbonyl)(2,2,2-trifluoroethyl)amino)methyl)-5-hydroxypyridin-2-yl)methyl)succinate (200)

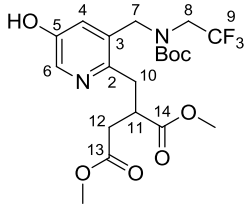

A mixture of dimethyl (*E*)-2-((3-(((*tert*-butoxycarbonyl)(2,2,2-trifluoroethyl)amino)methyl)-5-((4-methoxybenzyl)oxy)pyridin-2-yl)methylene)succinate **(199)** (376 mg, 0.645 mmol) and palladium on carbon (5 wt %) (1.37 g, 0.645 mmol) in EtOH (6 mL) was stirred in the presence of hydrogen gas for 14 h, followed by filtrating through Celite®, eluting with EtOH (40 mL). The filtrate was concentrated *in vacuo,* followed by purification using a 24 g silica column, eluting with 0 – 50 % EtOAc:cyclohexane, and the desired fractions were combined and concentrated *in vacuo* to furnish dimethyl 2-((3-(((*tert*-butoxycarbonyl)(2,2,2-trifluoroethyl)amino)methyl)-5-hydroxypyridin-2-yl)methyl)succinate **(200)** (166 mg, 0.357 mmol, 55 % yield) as a colourless oil, as an inseparable mixture with *tert*-butyl ((5-hydroxypyridin-3-yl)methyl)(2,2,2-trifluoroethyl)carbamate **(201)**, in a 5:1 ratio.

LCMS t_R = 1.04 min (system B), 85 %, ES+ve *m/z* 465 $(M + H)^+$; **^{1}H NMR** (600 MHz, $CDCl_3$): δ = 8.04 (1H, br s, H_6), 6.95 (1H, br s, H_4), 4.59 (2H, br s, H_7), 3.91 – 3.72 (2H,

m, H_8), 3.66 – 3.60 (6H, m, OMe, OMe), 3.36 (1H, quin, *J* = 7.0 Hz, H_{11}), 3.10 (1H, dd, *J* = 14.9, 7.2 Hz, H_{10a}), 2.87 (1H, br dd, *J* = 14.7, 7.3 Hz, H_{10b}), 2.76 (1H, dd, *J* = 16.5, 8.1 Hz, H_{12a}), 2.55 (1H, dd, *J* = 16.9, 5.5 Hz, H_{12b}), 1.55 – 1.36 (9H, m, ^{t}BuH), *OH not observed*; **^{13}C NMR** (150 MHz, $CDCl_3$): *δ* = 174.8, 172.4, 155.6 – 154.9 (1C, m), 152.7, 147.8 – 146.3 (1C, m), 135.7, 132.6 – 131.6 (1C, m), 124.7 (1C, q, *J* = 282.0 Hz), 122.7 (1C, br d, *J* = 219.5 Hz), 82.3, 52.2, 52.0, 48.2 – 46.9 (2C, m), 40.8, 35.6, 34.5, 28.2; **IR** (neat, ν_{max} /cm^{-1}): 3357 (br), 2625 (br), 1737, 1705, 1437, 1407, 1368, 1271, 1254, 1222, 1144, 1088, 891, 827, 733; **HRMS** (ESI): calc for $C_{20}H_{28}F_3N_2O_7$ $(M + H)^+$ 465.1849, found 465.1854.

Methyl 2-(3-hydroxy-7-oxo-6-(2,2,2-trifluoroethyl)-6,7,8,9-tetrahydro-5H-pyrido [3,2-c]azepin-8-yl)acetate (191)

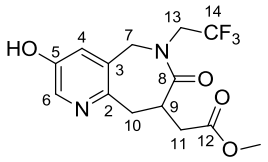

To a stirring solution of dimethyl 2-((3-(((*tert*-butoxycarbonyl)(2,2,2-trifluoroethyl)amino)methyl)-5-hydroxypyridin-2-yl)methyl)succinate **(200)** (153 mg, 0.329 mmol) in CH_2Cl_2 (5 mL) was added TFA (1.27 mL, 16.5 mmol) and the solution was stirred for 1 h, then concentrated using a flow of nitrogen gas. The resulting oil was dissolved in PhMe (5 mL) and heated under reflux for 4 h, followed by cooling to rt and removal of the solvent *in vacuo*. The crude product was purified using an Xterra® Prep RP18 OBD™ column, eluting with 0 – 100 % MeCN:ammonium carbonate modified H_2O, and the desired fractions were combined and concentrated *in vacuo* to afford methyl 2-(3-hydroxy-7-oxo-6-(2,2,2-trifluoroethyl)-6,7,8,9-tetrahydro-5H-pyrido[3,2-c]azepin-8-yl)acetate **(191)** (72.0 mg, 0.217 mmol, 66 % yield) as a colourless oil.

LCMS t_R = 0.54 min (system B), 100 %, ES+ve *m/z* 333 $(M + H)^+$; **^{1}H NMR** (400 MHz, $CDCl_3$): δ = 8.14 (1H, d, *J* = 2.9 Hz, H_6), 7.02 (1H, d, *J* = 2.9 Hz, H_4), 5.36 (1H, d, *J* = 17.1 Hz, H_{7a}), 4.29 – 4.17 (1H, m, H_{13a}), 4.05 – 3.94 (2H, m, H_{7b}, H_{13b}), 3.91 – 3.81 (1H, m, H_9), 3.71 (3H, s, OMe), 3.26 – 3.17 (1H, m, H_{10a}), 3.11 – 2.97 (2H, m, H_{10b}, H_{11a}), 2.51 (1H, dd, *J* = 17.7, 4.9 Hz, H_{11b}), *OH not observed*; **^{13}C NMR** (101 MHz, $CDCl_3$): δ = 174.5, 172.6, 151.8, 147.0, 136.1, 130.5, 124.8, 124.1* (1C, q, *J* = 281 Hz), 51.9, 51.5, 47.8 (1C, q, *J* = 33.7 Hz), 37.0, 36.2, 36.0; **IR** (neat, ν_{max} /cm^{-1}): 3319 (br), 2615 (br), 1732, 1668, 1438, 1303, 1268, 1248, 1202, 1154, 1125, 1093, 989, 910, 831, 728, 674; **HRMS** (ESI): calc for $C_{14}H_{16}F_3N_2O_4$ $(M + H)^+$ 333.1062, found 333.1061,

Methyl 2-(7-oxo-3-(2-(5,6,7,8-tetrahydro-1,8-naphthyridin-2-yl)ethoxy)-6-(2,2,2-trifluoroethyl)-6,7,8,9-tetrahydro-5H-pyrido[3,2-c]azepin-8-yl)acetate (203)

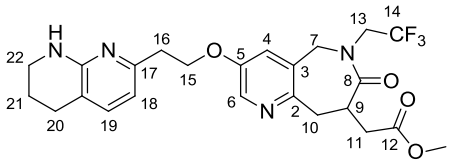

CMBP (0.170 mL, 0.650 mmol) was added to a stirring solution of *tert*-butyl 7-(2-hydroxyethyl)-3,4-dihydro-1,8-naphthyridine-1(2H)-carboxylate **(67)** (181 mg, 0.650 mmol) and methyl 2-(3-hydroxy-7-oxo-6-(2,2,2-trifluoroethyl)-6,7,8,9-tetrahydro-5H-pyrido[3,2-c]azepin-8-yl)acetate **(191)** (72 mg, 0.217 mmol) in THF (2 mL) under nitrogen, and the vial was sealed and the solution was heated at 80 °C for 2 h, followed by cooling to rt. Further portions of CMBP (0.170 mL, 0.650 mmol) and *tert*-butyl 7-(2-hydroxyethyl)-3,4-dihydro-1,8-naphthyridine-1(2H)-carboxylate **(67)** (181 mg, 0.650 mmol) were added, and the flask was purged with nitrogen gas, followed by heating at 80 °C for a further 2 h. The brown coloured solution was cooled to rt, followed by purification using a Sunfire® Prep C18 OBD™ column, eluting with 0 – 100 % MeCN:formic acid modified H_2O, and the desired fractions were combined and concentrated *in vacuo*. Partial Boc deprotection had occurred, so the resulting orange

oil was dissolved in CH_2Cl_2 (3 mL), followed by the addition of TFA (0.417 mL, 5.42 mmol). After being left to stand for 13 h, the solvent had evaporated. The resulting crude material was purified using an Xterra® Prep RP18 OBD™ column, eluting with 0 – 100 % MeCN:ammonium carbonate modified H_2O, but separation from the side product was only partially obtained, so the mixed fractions were combined and concentrated *in vacuo*, followed by further purification using a 4 g silica column, eluting with EtOAc + 1 % NEt_3, and the desired fractions were combined with previous desired fractions and concentrated *in vacuo* to furnish methyl 2-(7-oxo-3-(2-(5,6,7,8-tetrahydro-1,8-naphthyridin-2-yl)ethoxy)-6-(2,2,2-trifluoroethyl)-6,7,8,9-tetrahydro-5H-pyrido[3,2-c]azepin-8-yl)acetate **(203)** (63 mg, 0.128 mmol, 59 % yield) as a pale yellow coloured oil.

LCMS t_R = 1.04 min (system B), 99 %, ES+ve *m/z* 493 $(M + H)^+$; **^{1}H NMR** (400 MHz, $CDCl_3$): δ = 8.17 (1H, d, *J* = 2.7 Hz, H_6), 7.07 (1H, d, *J* = 7.3 Hz, H_{19}), 6.91 (1H, d, *J* = 2.2 Hz, H_4), 6.41 (1H, d, *J* = 7.3 Hz, H_{18}), 5.32 (1H, br d, *J* = 16.9 Hz, H_{7a}), 4.87 (1H, br s, NH), 4.30 (2H, t, *J* = 7.0 Hz, H_{15}), 4.18 – 3.99 (2H, m, H_{13}), 3.93 (1H, br d, *J* = 16.9 Hz, H_{7b}), 3.86 – 3.78 (1H, m, H_9), 3.43 – 3.37 (2H, m, H_{22}), 3.18 (1H, br dd, *J* = 17.7, 3.5 Hz, H_{10a}), 3.08 – 2.93 (4H, m, H_{10b}, H_{11a}, H_{16}), 2.69 (2H, br t, *J* = 6.2 Hz, H_{20}), 2.47 (1H, dd, *J* = 16.9, 5.1 Hz, H_{11b}), 1.89 (2H, quin, *J* = 5.9 Hz, H_{21}); **^{13}C NMR** (101 MHz, $CDCl_3$): δ = 174.7, 172.7, 156.1, 153.8, 153.2, 147.9, 137.2, 136.9, 129.2, 124.3 (1C, q, *J* = 280.2 Hz), 122.1, 114.3, 112.4, 68.3, 52.0, 51.8, 47.9 (1C, q, *J* = 34.2 Hz), 41.7, 38.1, 37.5, 36.5, 36.3, 26.5, 21.6; **IR** (thin film, ν_{max} /cm^{-1}): 3405 (br), 3258 (br), 1734, 1672, 1596, 1462, 1438, 1384, 1359, 1294, 1270, 1247, 1201, 1185, 1156, 1126, 1028, 732; **HRMS** (ESI): calc for $C_{24}H_{28}F_3N_4O_4$ $(M + H)^+$ 493.2063, found 493.2064.

2-(7-Oxo-3-(2-(5,6,7,8-tetrahydro-1,8-naphthyridin-2-yl)ethoxy)-6-(2,2,2-trifluoroethyl)-6,7,8,9-tetrahydro-5H-pyrido[3,2-c]azepin-8-yl)acetic acid (190)

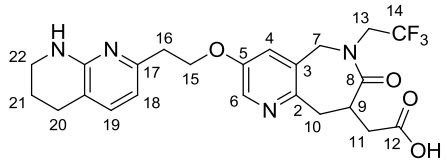

To a stirring solution of methyl 2-(7-oxo-3-(2-(5,6,7,8-tetrahydro-1,8-naphthyridin-2-yl)ethoxy)-6-(2,2,2-trifluoroethyl)-6,7,8,9-tetrahydro-5H-pyrido[3,2-c]azepin-8-yl)acetate **(203)** (32 mg, 0.065 mmol) in MeOH (1 mL) was added sodium hydroxide (2 M in H_2O) (0.065 mL, 0.130 mmol), and the reaction stirred at 35 °C for 1 h. The solution was concentrated *in vacuo*, and redissolved in H_2O (2 mL) and MeCN (1 mL), before neutralisation by dropwise addition of aqueous HCl (2 M). The resulting solution was purified using an Xbridge RP18 C18 OBD column, eluting with 0 – 100 % MeCN:ammonium carbonate modified H_2O, and the desired fractions were combined and concentrated *in vacuo* to furnish 2-(7-oxo-3-(2-(5,6,7,8-tetrahydro-1,8-naphthyridin-2-yl)ethoxy)-6-(2,2,2-trifluoroethyl)-6,7,8,9-tetrahydro-5H-pyrido[3,2-c]azepin-8-yl)acetic acid **(190)** (25.4 mg, 0.053 mmol, 82 % yield) as a colourless gum.

LCMS t_R = 0.73 min (system B), 100 %, ES+ve *m/z* 479 $(M + H)^+$; **^{1}H NMR** (400 MHz, $CDCl_3$): δ = 9.77 – 9.44 (1H, br s, COOH), 8.17 (1H, d, *J* = 2.7 Hz, H_6), 7.18 (1H, d, *J* = 7.3 Hz, H_{19}), 6.87 (1H, d, *J* = 2.7 Hz, H_4), 6.36 (1H, d, *J* = 7.1 Hz, H_{18}), 5.23 (1H, br d, *J* = 16.6 Hz, H_{7a}), 4.34 – 4.23 (2H, m, H_{15}), 4.15 – 4.03 (2H, m, H_{13}), 3.88 – 3.75 (2H, m, H_{7b}, H_9), 3.46 – 3.39 (2H, m, H_{22}), 3.29 (1H, dd, *J* = 18.0, 3.5, H_{10a}), 3.07 (2H, t, *J* = 6.7 Hz, H_{16}), 3.02 – 2.90 (2H, m, H_{10b}, H_{11a}), 2.69 (2H, br t, *J* = 6.1 Hz, H_{20}), 2.45 (1H, dd, *J* = 16.0, 7.0 Hz, H_{11b}), 1.92 – 1.82 (2H, m, H_{21}), *amine H not observed*; **^{13}C NMR** (101 MHz, $CDCl_3$): δ = 179.1, 175.7, 154.5, 152.6, 149.2, 147.8, 138.8, 136.3, 129.6, 124.5 (1C, q, *J* = 280.2 Hz), 122.3, 117.8, 111.0, 67.4, 51.6, 47.6 (1C, br q, *J* = 34.5 Hz), 41.0, 39.2, 38.3, 37.2, 34.4, 26.2, 20.1; **IR** (thin film, ν_{max} /cm^{-1}): 3330 (br), 1671, 1597, 1464,

1441, 1419, 1403, 1270, 1253, 1200, 1155, 1126, 1093, 1036, 911, 830, 731; **HRMS** (ESI): calc for $C_{23}H_{26}F_3N_4O_4$ $(M + H)^+$ 479.1906, found 479.1913.

(*S*)-Methyl 2-(3-oxo-8-(3-(pyridin-2-ylamino)propoxy)-2-(2,2,2-trifluoroethyl)-2,3,4,5-tetrahydro-1H-benzo[c]azepin-4-yl)acetate (204)

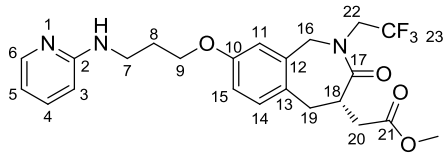

To a stirring solution of (*S*)-2-(3-oxo-8-(3-(pyridin-2-ylamino)propoxy)-2-(2,2,2-trifluoroethyl)-2,3,4,5-tetrahydro-1H-benzo[c]azepin-4-yl)acetic acid **(97)** (1.92 g, 4.25 mmol) in MeOH (40 mL) was added sulfuric acid (1.13 mL, 21.3 mmol), and the solution was heated under reflux for 1 h, after which time the pale yellow coloured solution was cooled to rt and the solvent was removed *in vacuo*. The resulting solid was diluted with CH_2Cl_2 (40 mL), H_2O (20 mL) and aqueous NaOH (2 M, 20 mL). The layers were separated and the aqueous layer was extracted with CH_2Cl_2 (40 mL), and the combined organic layers were filtered through a hydrophobic frit and concentrated *in vacuo* to yield methyl (*S*)-2-(3-oxo-8-(3-(pyridin-2-ylamino)propoxy)-2-(2,2,2-trifluoroethyl)-2,3,4,5-tetrahydro-1H-benzo[c]azepin-4-yl)acetate **(204)** (1.79 g, 3.85 mmol, 90 % yield) as a pale yellow coloured gum.

LCMS t_R = 1.11 min (system B), 96 %, ES+ve *m/z* 466 $(M + H)^+$; **^{1}H NMR** (400 MHz, $CDCl_3$): δ = 8.09 – 8.05 (1H, m, H_6), 7.41 (1H, ddd, *J* = 8.4, 6.7, 2.0 Hz, H_4), 7.02 (1H, d, *J* = 8.3 Hz, H_{14}), 6.79 (1H, dd, *J* = 8.6, 2.7 Hz, H_{15}), 6.63 (1H, d, *J* = 2.4 Hz, H_{11}), 6.57 (1H, ddd, *J* = 6.7, 5.5, 1.0 Hz, H_5), 6.41 (1H, d, *J* = 8.3 Hz, H_3), 5.33 (1H, d, *J* = 16.6 Hz, H_{16a}), 4.75 (1H, br s, NH), 4.22 – 3.92 (5H, m, H_9, H_{16b}, H_{22}), 3.89 – 3.79 (1H, m, H_{18}), 3.71 (3H, s, OMe), 3.53 – 3.47 (2H, m, H_7), 3.06 – 2.97 (2H, m, H_{19a}, H_{20a}), 2.94 – 2.85 (1H, m, H_{19b}), 2.46 (1H, dd, *J* = 16.6, 5.4 Hz, H_{20b}), 2.10 (2H, quin, *J* = 6.2 Hz, H_8); **^{13}C NMR**

(101 MHz, $CDCl_3$): δ = 175.0, 172.7, 158.8, 157.0, 148.1, 137.7, 134.3, 131.9, 128.3, 125.8*, 115.2, 114.4, 113.1, 106.9, 66.1, 53.3, 52.0, 47.9 (1C, q, *J* = 33.8 Hz), 39.5, 37.2, 36.7, 34.7, 29.3; **IR** (neat, ν_{max} /cm^{-1}): 3398 (br), 3265 (br), 1734, 1667, 1601, 1505, 1474, 1437, 1416, 1289, 1267, 1249, 1213, 1190, 1149, 1127, 1090, 1030, 984, 830, 771; **HRMS** (ESI): calc for $C_{23}H_{27}F_3N_3O_4$ 466.1954 $(M + H)^+$, found 466.1959; $[\boldsymbol{\alpha}]_D^{20}$= –95 (*c* 1.0, MeOH).

(*S*)-Methyl 2-(8-(3-((*tert*-butoxycarbonyl)(pyridin-2-yl)amino)propoxy)-3-oxo-2-(2,2,2-trifluoroethyl)-2,3,4,5-tetrahydro-1H-benzo[c]azepin-4-yl)acetate (205)

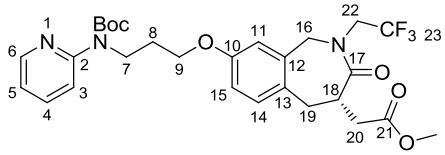

To a stirring solution of methyl (*S*)-2-(3-oxo-8-(3-(pyridin-2-ylamino)propoxy)-2-(2,2,2-trifluoroethyl)-2,3,4,5-tetrahydro-1H-benzo[c]azepin-4-yl)acetate **(204)** (742 mg, 1.59 mmol) and DIPEA (0.278 mL, 1.59 mmol) in CH_2Cl_2 (5 mL) was added di-*tert*-butyl dicarbonate (1.10 mL, 4.78 mmol), and the reaction was stirred at 100 °C for 4 h, after which time the crude product was purified using an 40 g silica column, eluting with 0 – 100 % EtOAc:cyclohexane, and the desired fractions were combined and concentrated *in vacuo* to furnish methyl (*S*)-2-(8-(3-((*tert*-butoxycarbonyl)(pyridin-2-yl)amino)propoxy)-3-oxo-2-(2,2,2-trifluoroethyl)-2,3,4,5-tetrahydro-1H-benzo[c]azepin-4-yl)acetate **(205)** (861 mg, 1.522 mmol, 95 % yield) as a pale yellow coloured oil.

LCMS t_R = 1.33 min (system B), 99 %, ES+ve *m/z* 566 $(M + H)^+$; **^{1}H NMR** (400 MHz, $CDCl_3$): δ = 8.35 – 8.32 (1H, m, H_6), 7.62 – 7.58 (2H, m, H_3, H_4), 7.01 – 6.96 (2H, m, H_5, H_{14}), 6.75 – 6.70 (1H, m, H_{15}), 6.56 (1H, d, *J* = 2.9 Hz, H_{11}), 5.31 (1H, d, *J* = 16.6 Hz, H_{16a}), 4.19 – 4.09 (3H, m, H_7, H_{22a}), 4.03 – 3.91 (3H, m, H_9, H_{22b}), 3.86 – 3.78 (1H, m, H_{18}), 3.71 (3H, s, OMe), 3.05 – 2.97 (2H, m, H_{19a}, H_{20a}), 2.93 – 2.84 (1H, m, H_{19b}), 2.46

(1H, dd, *J* = 5.6, 16.9 Hz, H_{20b}), 2.12 (2H, quin, *J* = 6.6 Hz, H_8), 1.55 (9H, s, ^{t}BuH); **^{13}C NMR** (101 MHz, $CDCl_3$): δ = 175.0, 172.8, 157.2, 154.3, 152.3, 147.8, 137.0, 134.1, 131.8, 127.9, 125.7*, 120.0, 119.7, 115.1, 114.4, 81.3, 66.1, 53.3, 52.0, 48.0*, 44.2, 37.2, 36.7, 34.7, 29.0, 28.5; **IR** (neat, ν_{max} /cm^{-1}): 1737, 1700, 1672, 1471, 1434, 1388, 1367, 1290, 1269, 1250, 1210, 1146, 1129, 1091, 988, 786; **HRMS** (ESI): calc for $C_{28}H_{35}F_3N_3O_6$ $(M + H)^+$ 566.2478, found 566.2478; $[\alpha]_D^{20}$= −70 (*c* 1.0, MeOH).

Methyl 2-((*S*)-8-(3-((*tert*-butoxycarbonyl)(pyridin-2-yl)amino)propoxy)-3-oxo-2-(2,2,2-trifluoroethyl)-2,3,4,5-tetrahydro-1H-benzo[c]azepin-4-yl)propanoate (206)

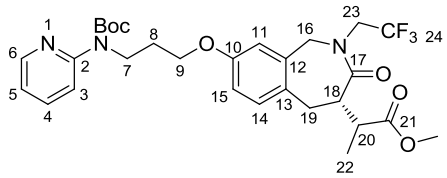

A solution of methyl (*S*)-2-(8-(3-((*tert*-butoxycarbonyl)(pyridin-2-yl)amino)propoxy)-3-oxo-2-(2,2,2-trifluoroethyl)-2,3,4,5-tetrahydro-1H-benzo[c]azepin-4-yl)acetate **(205)** (238 mg, 0.421 mmol) in THF (5 mL) under nitrogen was cooled to −78 °C and to the colourless solution was added lithium bis(trimethylsilyl)amide (0.281 mL, 0.421 mmol). The yellow coloured solution was stirred for 1 h, after followed by the addition of methyl iodide (0.026 mL, 0.421 mmol), and warming to rt. The yellow coloured mixture was stirred for 1 h, after which it was quenched by the addition of H_2O (10 mL) and diluted with EtOAc (10 mL). The layers were separated, and the aqueous layer was extracted with EtOAc (3 x 10 mL), and the combined organic layers were filtered through a hydrophobic frit and concentrated *in vacuo.* The crude product was purified using a 24 g silica column, eluting with 0 – 60 % EtOAc:cyclohexane, and the desired fractions were combined and concentrated *in vacuo* to afford methyl-2-((*S*)-8-(3-((*tert*-butoxycarbonyl)(pyridin-2-yl)amino)propoxy)-3-oxo-2-(2,2,2-trifluoroethyl)-2,3,4,5-tetrahydro-1H-benzo[c]azepin-4-yl)propanoate **(206)** (205 mg, 0.354 mmol, 84 % yield) as a pale

yellow coloured gum, as an inseparable mixture of diastereomers in a 1:1 ratio, which were used without further purification.

LCMS t_R = 1.37 min (system B), 89 %, ES+ve *m/z* 580 $(M + H)^+$; **HRMS** (ESI): calc for $C_{29}H_{37}F_3N_3O_6$ $(M + H)^+$ 580.2634, found 580.2635.

(*R*/*S*)-2-((*S*)-3-Oxo-8-(3-(pyridin-2-ylamino)propoxy)-2-(2,2,2-trifluoroethyl)-2,3,4,5-tetrahydro-1H-benzo[c]azepin-4-yl)propanoic acid, formic acid salt (207), and (*S*/*R*)-2-((*S*)-3-oxo-8-(3-(pyridin-2-ylamino)propoxy)-2-(2,2,2-trifluoroethyl)-2,3,4,5-tetrahydro-1H-benzo[c]azepin-4-yl)propanoic acid, formic acid salt (208)

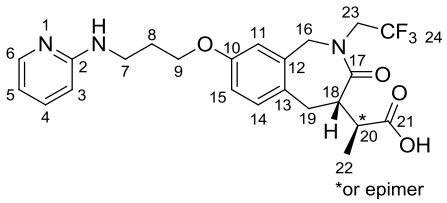

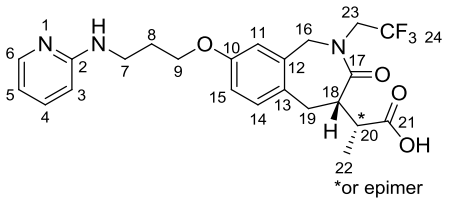

To a solution of methyl 2-((*S*)-8-(3-((*tert*-butoxycarbonyl)(pyridin-2-yl)amino)propoxy)-3-oxo-2-(2,2,2-trifluoroethyl)-2,3,4,5-tetrahydro-1H-benzo[c]azepin-4-yl)propanoate **(206)** (187 mg, 0.323 mmol) in CH_2Cl_2 (5 mL) was added TFA (124 µL, 1.613 mmol) and the colourless solution was stirred for 8 h, after which a further portion of TFA (1 mL, 12.98 mmol) was added and the colourless solution was stirred for a further 2 h before the solvent was removed under a flow of nitrogen gas. The resulting oil was dissolved in 1,4-dioxane (2.5 mL) before further dilution with H_2O (2.5 mL) and the addition of sulfuric acid (100 µL, 1.876 mmol). The colourless solution was heated to 80 °C whilst stirring for 12 h, after which the solution was cooled to rt and the solvent was removed under a flow of nitrogen gas. The crude product was purified using a Sunfire® Prep C18 OBD™ column, eluting with 0 – 100 % MeCN:formic acid modified H_2O, and the desired fractions were combined and concentrated *in vacuo* to yield (*S*/*R*)-2-((*S*)-3-oxo-8-(3-(pyridin-2-

ylamino)propoxy)-2-(2,2,2-trifluoroethyl)-2,3,4,5-tetrahydro-1H-benzo[c]azepin-4-yl)propanoic acid, formic acid salt **(207)** (16.6 mg, 0.032 mmol, 10 % yield) and (*R*/*S*)-2-((*S*)-3-oxo-8-(3-(pyridin-2-ylamino)propoxy)-2-(2,2,2-trifluoroethyl)-2,3,4,5-tetrahydro-1H-benzo[c]azepin-4-yl)propanoic acid, formic acid salt **(208)** (13.4 mg, 0.026 mmol, 8 % yield) as colourless gums.

Isomer 1 (207):

LCMS t_R = 0.72 min (system B), 95 %, ES+ve *m/z* 466 $(M + H)^+$; **^{1}H NMR** (400 MHz, $CDCl_3$): δ = 8.49 (1H, s, HCOOH), 7.88 – 7.82 (1H, m, H_6), 7.54 (1H, ddd, *J* = 8.9, 7.2, 2.0 Hz, H_4), 7.02 (1H, d, *J* = 8.3 Hz, H_{14}), 6.80 (1H, dd, *J* = 8.6, 2.7 Hz, H_{15}), 6.63 (1H, d, *J* = 2.4 Hz, H_{11}), 6.59 – 6.54 (1H, m, H_5), 6.52 (1H, d, *J* = 8.8 Hz, H_3), 5.10 (1H, d, *J* = 16.6 Hz, H_{16a}), 4.21 – 4.01 (3H, m, H_9, H_{23a}), 3.96 – 3.81 (2H, m, H_{16b}, H_{23b}), 3.49 – 3.37 (3H, m, H_7, H_{18}), 3.03 (1H, dd, *J* = 17.1, 3.9 Hz, H_{19a}), 2.95 – 2.84 (1H, m, H_{20}), 2.76 (1H, dd, *J* = 17.1, 13.1 Hz, H_{19b}), 2.11 (2H, quin, *J* = 6.2 Hz, H_8), 1.29 (3H, d, *J* = 7.3 Hz, H_{22}) *acids and amine H not observed*; **^{13}C NMR** (101 MHz, $CDCl_3$): δ = 181.0, 176.1, 169.1*, 157.4, 157.0, 143.3, 140.4, 134.5, 132.1, 128.6, 124.5 (q, *J* = 281.7 Hz), 115.1, 114.3, 111.8, 107.0, 65.3, 53.1, 47.5 (1C, q, *J* = 32.3 Hz), 43.4, 42.1, 39.0, 31.5, 28.6, 15.1; **IR** (neat, ν_{max} /cm^{-1}): 3290 (br), 1664, 1609, 1505, 1472, 1444, 1266, 1241, 1209, 1193, 1146, 1122, 1107, 1044, 829, 767, 737, 516; **HRMS** (ESI): Calc for $C_{23}H_{27}F_3N_3O_4$ $(M + H)^+$ 466.1954, found 466.1956; $[\alpha]_D^{20}$= –92 (*c* 0.5, MeCN).

Isomer 2 (208):

LCMS t_R = 0.71 min (system B), 100 %, ES+ve *m/z* 466 $(M + H)^+$; **^{1}H NMR** (400 MHz, $CDCl_3$): δ = 8.49 (1H, s, HCOOH), 7.85 (1H, dd, *J* = 5.6, 1.2 Hz, H_6), 7.57 (1H, ddd, *J* = 8.9, 7.2, 2.0 Hz, H_4), 6.90 (1H, d, *J* = 8.3 Hz, H_{14}), 6.71 (1H, dd, *J* = 8.3, 2.9 Hz, H_{15}), 6.63 – 6.57 (2H, m, H_5, H_{11}), 6.54 (1H, d, *J* = 8.8 Hz, H_3), 5.17 (1H, d, *J* = 16.6 Hz, H_{16a}), 4.35 (qd, *J* = 15.0, 9.2 Hz, H_{23a}), 4.08 (2H, t, *J* = 6.1 Hz, H_9), 3.99 (1H, d, *J* = 16.6 Hz, H_{16b}), 3.81 – 3.68 (1H, m, H_{23b}), 3.52 – 3.39 (3H, m, H_7, H_{18}), 3.11 (1H, dd, *J* = 16.9, 4.2 Hz, H_{19a}), 3.03 (1H, quin, *J* = 7.0 Hz, H_{20}), 2.88 (1H, dd, *J* = 17.1, 13.2 Hz, H_{19b}), 2.14 (2H,

quin, *J* = 6.1 Hz, H_8), 1.33 (3H, d, *J* = 7.3 Hz, H_{22}), *acids and amine H not observed;* **^{13}C NMR** (101 MHz, $CDCl_3$): δ = 179.1, 176.0, 169.1*, 157.1, 156.4, 142.9, 140.6, 134.0, 132.2, 128.5, 125.8 (1C, q, *J* = 278.8 Hz), 115.6, 113.9, 111.9, 107.3, 65.3, 53.3, 47.7 (1C, q, *J* = 33.7 Hz), 44.1, 42.5, 39.1, 32.0, 28.6, 16.7; **IR** (neat, ν_{max} /cm^{-1}): 3365 (br), 1663, 1505, 1414, 1266, 1240, 1209, 1148, 1123, 1105, 829, 766; **HRMS** (ESI): Calc for $C_{23}H_{27}F_3N_3O_4$ $(M + H)^+$ 466.1954, found 466.1956; $[\alpha]_D^{20}$= −110 (*c* 0.5, MeCN).

(*S/R)*-Methyl 2-((*S*)-8-(3-((*tert*-butoxycarbonyl)(pyridin-2-yl)amino)propoxy)-3-oxo-2-(2,2,2-trifluoroethyl)-2,3,4,5-tetrahydro-1H-benzo[c]azepin-4-yl)butanoate (209), (*R/S)*-methyl 2-((*S*)-8-(3-((*tert*-butoxycarbonyl)(pyridin-2-yl)amino)propoxy)-3-oxo-2-(2,2,2-trifluoroethyl)-2,3,4,5-tetrahydro-1H-benzo[c]azepin-4-yl)butanoate (210)

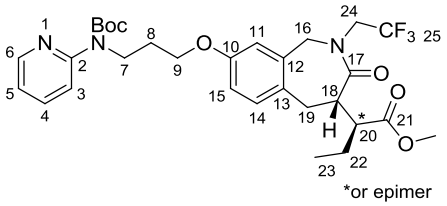

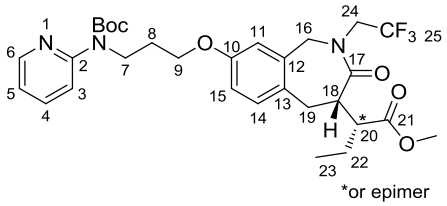

A solution of methyl (*S*)-2-(8-(3-((*tert*-butoxycarbonyl)(pyridin-2-yl)amino)propoxy)-3-oxo-2-(2,2,2-trifluoroethyl)-2,3,4,5-tetrahydro-1H-benzo[c]azepin-4-yl)acetate **(205)** (240 mg, 0.424 mmol) in THF (5 mL) under nitrogen was cooled to –78 °C and to the colourless solution was added lithium bis(trimethylsilyl)amide (0.283 mL, 0.424 mmol). The yellow coloured solution was stirred for 15 min, followed by the addition of iodoethane (0.034 mL, 0.424 mmol), and warming to rt. The yellow coloured mixture was stirred for 3 h, after which time the solution was diluted with H_2O (20 mL) and EtOAc (20 mL). The layers were separated, and the aqueous layer was extracted with EtOAc (20 mL), and the combined organic layers were filtered through a hydrophobic frit and concentrated *in vacuo. T*he crude product was purified using a 24 g silica column, eluting with 0 – 100 % EtOAc:cyclohexane, and the desired

fractions were combined and concentrated *in vacuo* to furnish (*S*/*R)*-methyl 2-((*S*)-8-(3-((*tert*-butoxycarbonyl)(pyridin-2-yl)amino)propoxy)-3-oxo-2-(2,2,2-trifluoroethyl)-2,3,4,5-tetrahydro-1H-benzo[c]azepin-4-yl)butanoate **(209)** (76.5 mg, 0.129 mmol, 30 % yield) and (*R*/*S*)-methyl 2-((*S*)-8-(3-((*tert*-butoxycarbonyl)(pyridin-2-yl)amino)propoxy)-3-oxo-2-(2,2,2-trifluoroethyl)-2,3,4,5-tetrahydro-1H-benzo[c]azepin-4-yl)butanoate **(210)** (58 mg, 0.098 mmol, 23 % yield) as colourless oils.

Isomer 1 (209):

LCMS t_R = 1.42 min (system B), 90 %, ES+ve *m/z* 594 $(M + H)^+$; **^{1}H NMR** (400 MHz, $CDCl_3$): δ = 8.33 (1H, dt, *J* = 4.9, 1.5 Hz, H_6), 7.59 (2H, m, H_3, H_4), 7.00 – 6.95 (2H, m, H_5, H_{14}), 6.71 (1H, dd, *J* = 8.3, 2.4 Hz, H_{15}), 6.55 (1H, d, *J* = 2.4 Hz, H_{11}), 5.20 (1H, d, *J* = 16.6 Hz, H_{16a}), 4.38 (1H, dq, *J* = 15.2, 9.1 Hz, H_{24a}), 4.15 – 4.10 (2H, m, H_7), 4.01 – 3.92 (3H, m, H_9, H_{16b}), 3.73 (3H, s, OMe), 3.72 – 3.61 (1H, m, H_{24b}), 3.56 – 3.48 (1H, m, H_{18}), 2.96 – 2.85 (3H, m, H_{19}, H_{20}), 2.15 – 2.07 (2H, m, H_8), 1.83 – 1.72 (1H, m, H_{22a}), 1.69 – 1.60 (1H, m, H_{22b}), 1.49 (9H, s, ^{t}BuH), 0.93 (3H, t, *J* = 7.3 Hz, H_{23}); **^{13}C NMR** (101 MHz, $CDCl_3$): δ = 175.6, 174.2, 157.1, 154.7, 154.3, 147.7, 137.0, 134.1, 132.0, 128.1, 124.5 (1C, q, *J* = 279.5 Hz), 120.0, 119.6, 115.2, 114.3, 81.3, 66.1, 53.2, 51.7, 49.4, 47.4 (1C, q, *J* = 34.2 Hz), 44.2, 43.0, 33.0, 29.0, 28.4, 24.8, 12.0; **IR** (neat, ν_{max} /cm^{-1}): 1731, 1703, 1672, 1471, 1433, 1388, 1368, 1268, 1231, 1209, 1145, 1125, 782; **HRMS** (ESI): calc for $C_{30}H_{39}F_3N_3O_6$ $(M + H)^+$ 594.2791, found 594.2793; $[\alpha]_D^{20}$= –48 (*c* 1.93, MeOH).

Isomer 2 (210):

LCMS t_R = 1.41 min (system B), 100 %, ES+ve *m/z* 594 $(M + H)^+$; **^{1}H NMR** (400 MHz, $CDCl_3$): δ = 8.34 (1H, dt, *J* = 4.9, 1.5 Hz, H_6), 7.59 (2H, m, H_3, H_4), 7.03 – 6.96 (2H, m, H_5, H_{14}), 6.73 (1H, dd, *J* = 8.3, 2.4 Hz, H_{15}), 6.56 (1H, d, *J* = 2.4 Hz, H_{11}), 5.32 (1H, d, *J* = 16.6 Hz, H_{16a}), 4.19 – 4.06 (2H, m, H_7), 4.02 – 3.86 (5H, m, H_9, H_{16b}, H_{24}), 3.69 (3H, s, OMe), 3.60 (1H, ddd, *J* = 13.3, 9.7, 3.9, H_{18}), 3.11 (1H, dd, *J* = 16.9, 3.7 Hz, H_{19a}), 2.83 – 2.73 (2H, m, H_{19b}, H_{20}), 2.12 (2H, quin, *J* = 6.6 Hz, H_8), 1.94 – 1.82 (1H, m, H_{22a}), 1.69

– 1.58 (1H, m, H_{22b}), 1.49 (9H, s, ^{t}BuH), 0.95 (3H, t, *J* = 7.6 Hz, H_{23}); **^{13}C NMR** (101 MHz, $CDCl_3$): δ = 175.8, 175.7, 157.2, 154.7, 154.3, 147.8, 137.0, 134.2, 132.0, 127.9, 124.4 (1C, q, *J* = 280.2 Hz), 120.0, 119.6, 115.1, 114.3, 81.3, 66.1, 53.3, 51.7, 48.4 – 46.9 (2C, m), 44.2, 41.8, 31.8, 29.0, 28.4, 22.5, 11.1; **IR** (neat, ν_{max} /cm^{-1}): 1701, 1671, 1612, 1588, 1506, 1471, 1433, 1367, 1269, 1208, 1143, 782; **HRMS** (ESI): calc for $C_{30}H_{39}F_3N_3O_6$ $(M + H)^+$ 594.2791, found 594.2789; $[\alpha]_D^{20}$= –82 (*c* 1.0, MeOH).

(*S*/*R*)-2-((*S*)-3-Oxo-8-(3-(pyridin-2-ylamino)propoxy)-2-(2,2,2-trifluoroethyl)-2,3,4,5-tetrahydro-1H-benzo[c]azepin-4-yl)butanoic acid (211)

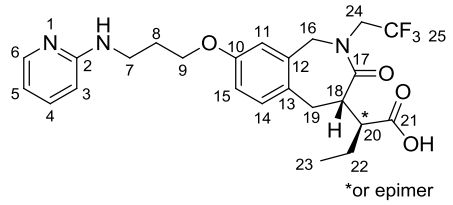

To a solution of methyl (*S*/*R*)-2-((*S*)-8-(3-((*tert*-butoxycarbonyl)(pyridin-2-yl)amino)propoxy)-3-oxo-2-(2,2,2-trifluoroethyl)-2,3,4,5-tetrahydro-1H-benzo[c]azepin-4-yl)butanoate **(209)** (84 mg, 0.141 mmol) in CH_2Cl_2 (1 mL) was added 2,2,2-trifluoroacetic acid (0.545 mL, 7.07 mmol) and the colourless solution was stirred for 12 h, during which the volatiles evaporated. The resulting oil was dissolved in 1,4-dioxane (1 mL) before further dilution with H_2O (1 mL) and the addition of sulfuric acid (0.075 mL, 1.415 mmol). The colourless solution was heated to 80 °C whilst stirring for 8 h, followed by cooling to rt. The crude product was purified using an Xbridge™ Prep C18 column, eluting with 0 – 100 % MeCN:ammonium carbonate modified H_2O, and the desired fractions were combined and concentrated *in vacuo* to yield (*S*/*R*)-2-((*S*)-3-oxo-8-(3-(pyridin-2-ylamino)propoxy)-2-(2,2,2-trifluoroethyl)-2,3,4,5-tetrahydro-1H-benzo[c]azepin-4-yl)butanoic acid **(211)** (31.2 mg, 0.065 mmol, 46 % yield) as a yellow coloured gum.

LCMS t_R = 0.74 min (system B), 100 %, ES+ve *m/z* 480 $(M + H)^+$; **^{1}H NMR** (400 MHz, $CDCl_3$): δ = 10.88 (1H, br s, COOH), 8.00 (1H, br s, NH), 7.85 (1H, d, *J* = 4.4 Hz, H_6), 7.55 (1H, app t, *J* = 7.9 Hz, H_4), 6.83 (1H, d, *J* = 8.4 Hz, H_{14}), 6.64 (1H, d, *J* = 8.4 Hz, H_{15}), 6.61 – 6.56 (2H, m, H_5, H_{11}), 6.51 (1H, d, *J* = 8.9 Hz, H_3), 5.18 (1H, d, *J* = 16.7 Hz, H_{16a}), 4.49 – 4.32 (1H, m, H_{24a}), 4.07 (2H, br d, *J* = 4.4 Hz, H_9), 3.93 (1H, d, *J* = 16.7 Hz, H_{16b}), 3.69 – 3.56 (1H, m, H_{24b}), 3.55 – 3.45 (1H, m, H_{18}), 3.41 (2H, br s, H_7), 3.17 – 3.04 (1H, m, H_{19a}), 2.96 – 2.78 (2H, m, H_{19b}, H_{20}), 2.14 (2H, br s, H_8), 1.71 (2H, t, *J* = 7.1 Hz, H_{22}), 1.02 (3H, br t, *J* = 7.1 Hz, H_{23}); **^{13}C NMR** (101 MHz, $CDCl_3$): δ = 179.9, 175.3, 157.6, 156.8, 143.5, 140.3, 134.2, 132.2, 128.6, 124.5 (1C, q, *J* = 280.8 Hz), 116.0, 113.2, 111.9, 107.0, 65.1, 53.2, 50.6, 47.4 (1C, q, *J* = 33.6 Hz), 43.0, 38.9, 32.7, 28.5, 24.8, 12.4; **IR** (neat, ν_{max} /cm^{-1}): 3258 (br), 1598, 1584, 1462, 1446, 1389, 1361, 1320, 1259, 1182, 1119, 1062, 1031, 785, 727, 701; **HRMS** (ESI): calc for $C_{24}H_{29}F_3N_3O_4$ $(M + H)^+$ 480.2110, found 480.2111; $[\alpha]_D^{20}$ = –100 (*c* 1.0, MeCN).

(*R*/*S*)-2-((*S*)-3-Oxo-8-(3-(pyridin-2-ylamino)propoxy)-2-(2,2,2-trifluoroethyl)-2,3,4,5-tetrahydro-1H-benzo[c]azepin-4-yl)butanoic acid (212)

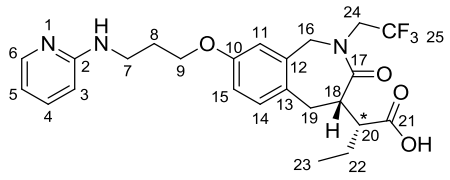

*or epimer

To a solution of (*R*/*S*)-methyl 2-((*S*)-8-(3-((*tert*-butoxycarbonyl)(pyridin-2-yl)amino)propoxy)-3-oxo-2-(2,2,2-trifluoroethyl)-2,3,4,5-tetrahydro-1H-benzo[c]azepin-4-yl)butanoate (95 mg, 0.160 mmol) **(210)** in CH_2Cl_2 (1 mL) was added 2,2,2-trifluoroacetic acid (0.62 mL, 8.00 mmol) and the colourless solution was stirred for 12 h, during which the volatiles evaporated. The resulting oil was dissolved in 1,4-dioxane (1 mL) before further dilution with H_2O (1 mL) and the addition of sulfuric acid (0.085 mL, 1.60 mmol). The colourless solution was heated to 80 °C whilst stirring for 16 h, after which time the solution was cooled to rt and the solvent was removed under a flow of nitrogen gas. The crude product was purified using an Xbridge™ Prep

C18 column, eluting with 0 – 100 % MeCN:ammonium carbonate modified H_2O, and the desired fractions were combined and concentrated *in vacuo* to yield (*R*/*S*)-2-((*S*)-3-oxo-8-(3-(pyridin-2-ylamino)propoxy)-2-(2,2,2-trifluoroethyl)-2,3,4,5-tetrahydro-1H-benzo[c]azepin-4-yl)butanoic acid **(212)** (9.8 mg, 0.020 mmol, 13 % yield) as a yellow coloured gum.

LCMS t_R = 0.75 min (system B), 96 %, ES+ve *m/z* 480 $(M + H)^+$; **^{1}H NMR** (400 MHz, $CDCl_3$): δ = 7.90 (1H, dd, *J* = 5.4, 1.0 Hz, H_6), 7.50 (1H, ddd, *J* = 8.7, 7.0, 2.0 Hz, H_4), 7.01 (1H, d, *J* = 8.4 Hz, H_{14}), 6.80 (1H, dd, *J* = 8.4, 2.5 Hz, H_{15}), 6.63 (1H, d, *J* = 2.5 Hz, H_{11}), 6.56 (1H, td, *J* = 6.2, 1.0 Hz, H_5), 6.46 (1H, d, *J* = 8.4 Hz, H_3), 5.11 (1H, br d, *J* = 16.7 Hz, H_{16a}), 4.25 – 4.02 (3H, m, H_9, H_{24a}), 3.93 – 3.79 (2H, m, H_{16b}, H_{24b}), 3.50 (1H, ddd, *J* = 13.2, 9.0, 3.9 Hz, H_{18}), 3.44 – 3.38 (2H, m, H_7), 3.05 (1H, dd, *J* = 17.0, 3.7 Hz, H_{19a}), 2.84 – 2.74 (2H, m, H_{19b}, H_{20}), 2.10 (2H, quin, *J* = 6.2 Hz, H_8), 1.90 – 1.78 (1H, m, H_{22a}), 1.74 – 1.61 (1H, m, H_{22b}), 0.95 (3H, t, *J* = 7.6 Hz, H_{23}); **^{13}C NMR** (101 MHz, $CDCl_3$): δ = 179.4, 176.4, 158.1, 157.1, 145.0, 139.5, 134.2, 132.1, 128.3, 124.5 (1C, q, *J* = 280.8 Hz), 115.2, 114.3, 112.0, 106.5, 65.5, 53.3, 48.9, 47.5 (1C, q, *J* = 33.6 Hz), 41.3, 38.9, 31.7, 28.7, 22.3, 11.2; **IR** (neat, ν_{max} /cm^{-1}): 3380 (br), 3295 (br), 1667, 1609, 1505, 1472, 1443, 1415, 1267, 1232, 1209, 1148, 1107, 1049, 985, 829, 768, 738, 672, 607, 562, 514; **HRMS** (ESI): calc for $C_{24}H_{29}F_3N_3O_4$ $(M + H)^+$ 480.2110, found 480.2109; $[\boldsymbol{\alpha}]_D^{20}$ = – 112 (*c* 0.5, MeCN).

(*S*/*R*)-Methyl 2-((*S*)-8-(3-((*tert*-butoxycarbonyl)(pyridin-2-yl)amino)propoxy)-3-oxo-2-(2,2,2-trifluoroethyl)-2,3,4,5-tetrahydro-1H-benzo[c]azepin-4-yl)-2-hydroxyacetate (214) and (*R*/*S*)-methyl 2-((*S*)-8-(3-((*tert*-butoxycarbonyl)(pyridin-2-yl)amino)propoxy)-3-oxo-2-(2,2,2-trifluoroethyl)-2,3,4,5-tetrahydro-1H-benzo[c]azepin-4-yl)-2-hydroxyacetate (215)

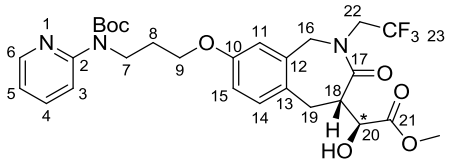

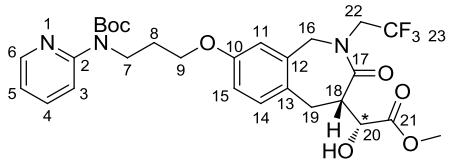

A solution of methyl (*S*)-2-(8-(3-((*tert*-butoxycarbonyl)(pyridin-2-yl)amino)propoxy)-3-oxo-2-(2,2,2-trifluoroethyl)-2,3,4,5-tetrahydro-1H-benzo[c]azepin-4-yl)acetate **(205)** (414 mg, 0.732 mmol) in THF (5 mL) under nitrogen was cooled to –78 °C and to the colourless solution was added lithium bis(trimethylsilyl)amide (1.5 M in THF, 0.488 mL, 0.732 mmol). The yellow coloured solution was stirred for 30 min, after followed by the addition of a solution of 3-phenyl-2-(phenylsulfonyl)-1,2-oxaziridine **(213)** (191 mg, 0.732 mmol) in THF (1 mL) over 1 h using a syringe pump. The colourless solution was stirred for 3 h before the addition of H_2O (20 mL) and warming to rt. The solution was further diluted with H_2O (30 mL) and EtOAc (60 mL), and the layers were separated. The aqueous layer was extracted with EtOAc (50 mL), and the combined organic layers were filtered through a hydrophobic frit and concentrated *in vacuo*. The crude product was purified using a 24 g silica column, eluting with 0 – 70 % EtOAc:cyclohexane, and the desired fractions were combined and concentrated *in vacuo*. Fractions containing a mixture of the diastereomers were recolumned using a 24 g silica column, eluting with 25 – 45 % EtOAc:cyclohexane, and the desired fractions were combined with the previously purified material and concentrated *in vacuo*. The diastereomers were separated by Andy Hobbs (GlaxoSmithKline, Stevenage), using an Xbridge™ Prep C18 column (30 x 150mm, 5 µm), eluting with 3 – 97 % MeCN:formic acid modified H_2O, and the desired fractions were combined and concentrated using a Biotage V10 evaporator to yield (*S*/*R*)-methyl 2-((*S*)-8-(3-

((*tert*-butoxycarbonyl)(pyridin-2-yl)amino)propoxy)-3-oxo-2-(2,2,2-trifluoroethyl)-2,3,4,5-tetrahydro-1H-benzo[c]azepin-4-yl)-2-hydroxyacetate **(214)** (50 mg, 0.0860 mmol, 12 % yield) and (*R*/*S*)-methyl 2-((*S*)-8-(3-((*tert*-butoxycarbonyl)(pyridin-2-yl)amino)propoxy)-3-oxo-2-(2,2,2-trifluoroethyl)-2,3,4,5-tetrahydro-1H-benzo[c]azepin-4-yl)-2-hydroxyacetate **(215)** (45 mg, 0.07704 mmol, 11 % yield) as white coloured solids, as inseparable mixtures with the corresponding Boc deprotected products, as a result of the acidic purification. These compounds were fully deprotected without further purification.

Methyl 2-((*S*)-8-(3-((*tert*-butoxycarbonyl)(pyridin-2-yl)amino)propoxy)-3-oxo-2-(2,2,2-trifluoroethyl)-2,3,4,5-tetrahydro-1H-benzo[c]azepin-4-yl)-3-hydroxypropanoate (216)

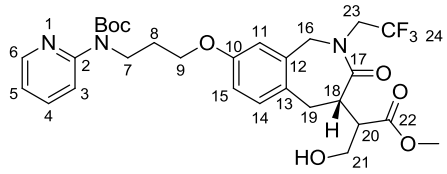

A solution of methyl (*S*)-2-(8-(3-((*tert*-butoxycarbonyl)(pyridin-2-yl)amino)propoxy)-3-oxo-2-(2,2,2-trifluoroethyl)-2,3,4,5-tetrahydro-1H-benzo[c]azepin-4-yl)acetate **(205)** (277 mg, 0.490 mmol) in THF (5 mL) under nitrogen was cooled to –78 °C and to the colourless solution was added lithium bis(trimethylsilyl)amide (0.327 mL, 0.490 mmol). The yellow coloured solution was stirred for 30 min, followed by the addition of a suspension of paraformaldehyde (14.7 mg, 0.490 mmol) in THF (1 mL), and warming to rt. The yellow coloured mixture was stirred for 4 h, after which time the solution was diluted with H_2O (20 mL), saturated aqueous sodium chloride (10 mL), and EtOAc (20 mL). The layers were separated, and the aqueous layer was extracted with EtOAc (20 mL), and the combined organic layers were filtered through a hydrophobic frit and concentrated *in vacuo.* The crude product was purified using a 24 g silica column, eluting with 0 – 100 % EtOAc:cyclohexane, and the desired fractions were combined and concentrated *in vacuo*, followed by further purification

using a 24 g silica column, eluting with 0 – 100 % EtOAc:cyclohexane, and the desired fractions were combined and concentrated *in vacuo* to furnish methyl 2-((*S*)-8-(3-((*tert*-butoxycarbonyl)(pyridin-2-yl)amino)propoxy)-3-oxo-2-(2,2,2-trifluoroethyl)-2,3,4,5-tetrahydro-1H-benzo[c]azepin-4-yl)-3-hydroxypropanoate (49.7 mg, 0.083 mmol, 17 % yield) **(216)** as a colourless oil, as an inseparable mixture of diastereomers.

LCMS t_R = 1.20/1.23 min (system B), 91 %, ES+ve *m/z* 596 $(M + H)^+$

(*S*/*R*)-2-Hydroxy-2-((*S*)-3-oxo-8-(3-(pyridin-2-ylamino)propoxy)-2-(2,2,2-trifluoroethyl)-2,3,4,5-tetrahydro-1H-benzo[c]azepin-4-yl)acetic acid (217)

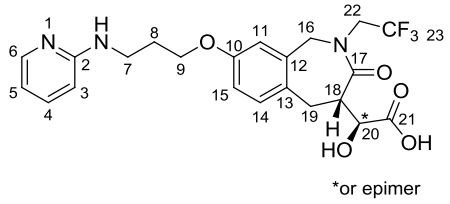

To a solution of (*S*/*R*)-methyl 2-((*S*)-8-(3-((*tert*-butoxycarbonyl)(pyridin-2-yl)amino)propoxy)-3-oxo-2-(2,2,2-trifluoroethyl)-2,3,4,5-tetrahydro-1H-benzo[c]azepin-4-yl)-2-hydroxyacetate **(214)** (47 mg, 0.081 mmol) in 1,4-dioxane (1 mL) and H_2O (1 mL) was added sulfuric acid (0.043 mL, 0.808 mmol). The colourless solution was stirred whilst heating to 50 °C for 24 h, followed by cooling to rt. The solution was partially concentrated using a flow of nitrogen gas, and the resulting colourless solution was purified using an Xbridge™ Prep C18 column, eluting with 0 – 100 % MeCN:ammonium carbonate modified H_2O, and the desired fractions were combined and concentrated in vacuo to furnish (*S*/*R*)-2-hydroxy-2-((*S*)-3-oxo-8-(3-(pyridin-2-ylamino)propoxy)-2-(2,2,2-trifluoroethyl)-2,3,4,5-tetrahydro-1H-benzo[c]azepin-4-yl)acetic acid **(217)** (24.4 mg, 0.052 mmol, 65 % yield) as a white coloured solid.

LCMS t_R = 0.72 min (system B), 100 %, ES+ve *m/z* 468 $(M + H)^+$; **^{1}H NMR** (600 MHz, DMSO-d_6): δ = 12.41 (1H, m, COOH), 7.95 (1H, dd, *J* = 5.5, 1.8 Hz, H_6), 7.37 – 7.32 (1H, m, H_4), 7.09 (1H, d, *J* = 8.4 Hz, H_{14}), 6.84 – 6.80 (2H, m, H_{11}, H_{15}), 6.54 (1H, br s, OH), 6.47 – 6.43 (2H, m, H_3, H_5), 5.73 (1H, br s, NH), 5.07 (br d, *J* = 16.5 Hz, H_{16a}), 4.31 – 4.21 (2H, m, H_{16b}, H_{22a}), 4.19 – 4.10 (2H, m, H_{20}, H_{22b}), 4.02 (2H, t, *J* = 6.4 Hz, H_9), 3.56 – 3.49 (1H, m, H_{18}), 3.36 (2H, q, *J* = 6.6 Hz, H_7), 3.11 (1H, dd, *J* = 16.9, 4.0 Hz, H_{19a}), 2.82 (1H, dd, *J* = 16.7, 13.4 Hz, H_{19b}), 1.96 (2H, quin, *J* = 6.6 Hz, H_8); **^{13}C NMR** (151 MHz, DMSO-d_6): δ = 174.6, 174.3, 159.3, 156.9, 147.9, 137.0, 135.9, 131.8, 128.8, 125.2 (1C, q, *J* = 280.9 Hz), 115.3, 114.4, 111.9, 108.6, 71.8, 66.0, 52.4, 47.2 (1C, q, *J* = 32.6 Hz), 44.7, 38.1, 30.2, 29.2; **IR** (neat, ν_{max} /cm^{-1}): 3287 (br), 1659, 1610, 1505, 1415, 1339, 1265, 1210, 1127, 909, 829, 767, 726, 513; **HRMS** (ESI): calc for $C_{22}H_{25}F_3N_3O_5$ $(M + H)^+$ 468.1746, found 468.1752; **mp**: 109 – 120 °C; $[\alpha]_D^{20}$ = *compound was insufficiently soluble in appropriate solvents for the measurement to be made.*

(*R*/*S*)-2-Hydroxy-2-((*S*)-3-oxo-8-(3-(pyridin-2-ylamino)propoxy)-2-(2,2,2-trifluoroethyl)-2,3,4,5-tetrahydro-1H-benzo[c]azepin-4-yl)acetic acid (218)

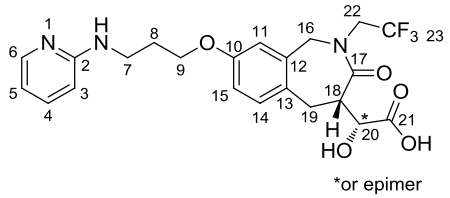

To a solution of (*R*/*S*)-methyl 2-((*S*)-8-(3-((*tert*-butoxycarbonyl)(pyridin-2-yl)amino)propoxy)-3-oxo-2-(2,2,2-trifluoroethyl)-2,3,4,5-tetrahydro-1H-benzo[c]azepin-4-yl)-2-hydroxyacetate **(215)** (42 mg, 0.072 mmol) in 1,4-dioxane (1 mL) and H_2O (1 mL) was added sulfuric acid (0.038 mL, 0.722 mmol). The colourless solution was stirred whilst heating to 50 °C for 48 h, followed by cooling to rt. The solution was partially concentrated using a flow of nitrogen gas, and the resulting colourless solution was purified using an Xbridge™ Prep C18 column, eluting with 0

– 100 % MeCN:ammonium carbonate modified H_2O, and the desired fractions were combined and concentrated in vacuo to furnish (*R*/*S*)-2-hydroxy-2-((*S*)-3-oxo-8-(3-(pyridin-2-ylamino)propoxy)-2-(2,2,2-trifluoroethyl)-2,3,4,5-tetrahydro-1H-benzo[c]azepin-4-yl)acetic acid **(218)** (23.9 mg, 0.051 mmol, 71 % yield) as a white coloured solid, an inseparable mixture (8:1) with an unidentified impurity.

LCMS t_R = 0.73 min (system B), 100 %, ES+ve *m/z* 468 $(M + H)^+$; **^{1}H NMR** (600 MHz, DMSO-d_6): δ = 7.95 (1H, dd, *J* = 5.3, 1.7 Hz, H_6), 7.33 (1H, dt, *J* = 7.7, 1.8 Hz, H_4), 7.08 (1H, d, *J* = 8.4 Hz, H_{14}), 6.87 – 6.78 (2H, m, H_{11}, H_{15}), 6.53 – 6.49 (1H, m, OH), 6.46 – 6.42 (2H, m, H_3, H_5), 4.88 (1H, d, *J* = 15.8 Hz, H_{16a}), 4.36 (1H, br d, *J* = 16.5 Hz, H_{16b}), 4.27 – 4.08 (3H, m, H_{22}, H_{20}), 4.02 (1H, td, *J* = 6.1, 2.4 Hz, H_9), 3.42 – 3.33 (3H, m, H_7, H_{18}), 3.00 (1H, br dd, *J* = 16.5, 4.4 Hz, H_{19a}), 2.92 – 2.85 (1H, m, H_{19b}), 1.96 (2H, quin, *J* = 6.5 Hz, H_8); **^{13}C NMR** (151 MHz, DMSO-d_6): δ = 174.2, 173.5, 158.8, 156.4, 147.5, 136.4, 136.0, 130.8, 128.9, 124.7 (1C, br d, *J* = 281.4 Hz), 114.8, 113.8 111.32, 108.0, 71.9, 65.5, 51.6, 47.0 (1C, br d, *J* = 32.6 Hz), 45.9, 37.6, 30.2, 28.7; **IR** (neat, ν_{max} /cm^{-1}): 3225 (br), 1656, 1610, 1407, 1348, 1266, 1245, 1225, 1166, 1130, 1098, 1075, 1052, 1037, 905, 764, 613, 574, 549, 519; **HRMS** (ESI): calc for $C_{22}H_{25}F_3N_3O_5$ $(M + H)^+$ 468.1746, found 468.1760; **mp**: 124 – 138 °C; $[\alpha]_D^{20}$ = *compound was insufficiently soluble in appropriate solvents for the measurement to be made.*

Methyl (*S*)-2-(8-hydroxy-3-oxo-2-(2,2,2-trifluoroethyl)-2,3,4,5-tetrahydro-1H-benzo[c]azepin-4-yl)acetate (105)

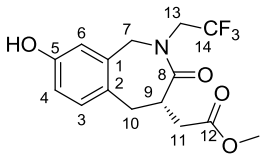

To a stirred mixture of (*S*)-2-(3-oxo-8-(3-(pyridin-2-ylamino)propoxy)-2-(2,2,2-trifluoroethyl)-2,3,4,5-tetrahydro-1H-benzo[c]azepin-4-yl)acetic acid **(97)** (2.12 g,

4.70 mmol) in CH_2Cl_2 (30 mL) under nitrogen was added BBr_3 (1 M in CH_2Cl_2, 11.7 mL, 11.7 mmol) at 0 °C dropwise over 30 mins. The pale-yellow coloured mixture was stirred whilst warming to rt for 62 h, followed by quenching by the addition of MeOH (15 mL). The solution was concentrated *in vacuo*, followed by purification using a 40 g silica column, eluting with 0 – 100 % EtOAc + 1 % NEt_3):cyclohexane, and the desired fractions were combined and concentrated *in vacuo* to furnish methyl (*S*)-2-(8-hydroxy-3-oxo-2-(2,2,2-trifluoroethyl)-2,3,4,5-tetrahydro-1H-benzo[c]azepin-4-yl)acetate **(105)** (1.42 g, 4.29 mmol, 91 % yield) as a white coloured gum.

LCMS t_R = 0.86 min (system B), 97 %, ES+ve *m/z* 332 $(M + H)^+$; **^{1}H NMR** (400 MHz, $CDCl_3$): δ = 6.96 (1H, d, *J* = 8.3 Hz, H_3), 6.72 (1H, dd, *J* = 8.3, 2.4 Hz, H_4), 6.57 (1H, d, *J* = 2.4 Hz, H_6), 5.30 (1H, d, *J* = 16.6 Hz, H_{7a}), 5.17 (1H, s, OH), 4.20 – 4.08 (1H, m, H_{13a}), 4.06 – 3.91 (2H, m, H_{7b}, H_{13b}), 3.90 – 3.78 (1H, m, H_9), 3.70 (3H, s, OMe), 3.05 – 2.96 (2H, m, H_{10a}, H_{11a}), 2.93 – 2.83 (1H, m, H_{10b}), 2.51 – 2.42 (1H, m, H_{11b}); **^{13}C NMR** (101 MHz, $CDCl_3$): δ = 175.1, 172.8, 153.8, 134.4, 132.1, 128.1, 124.4 (1C, q, *J* = 281.0 Hz), 115.8, 115.5, 53.1, 52.0, 47.9 (1C, q, *J* = 33.7 Hz), 37.2, 36.7, 34.6; **IR** (neat, ν_{max} /cm^{-1}): 3286 (br), 1732, 1651, 1614, 1440, 1366, 1299, 1267, 1213, 1125, 1091, 970, 830, 674, 564; **HRMS** (ESI): calc for $C_{15}H_{17}F_3NO_4$ $(M + H)^+$ 332.1110, found 332.1111; $[\alpha]_D^{20}$= –102 (*c* 0.5, MeOH).

Methyl (*S*)-2-(8-((*tert*-butyldimethylsilyl)oxy)-3-oxo-2-(2,2,2-trifluoroethyl)-2,3,4,5-tetrahydro-1H-benzo[c]azepin-4-yl)acetate (221)

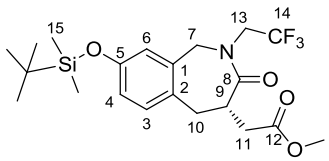

To a stirring solution of methyl (*S*)-2-(8-hydroxy-3-oxo-2-(2,2,2-trifluoroethyl)-2,3,4,5-tetrahydro-1H-benzo[c]azepin-4-yl)acetate **(105)** (1.40 g, 4.23 mmol) at 0 °C

in CH_2Cl_2 (20 mL) was added *tert*-butylchlorodimethylsilane (0.955 g, 6.34 mmol) and imidazole (0.719 g, 10.6 mmol), and the solution was warmed to rt while stirring for 30 min, followed by dilution with CH_2Cl_2 (20 mL) and H_2O (50 mL). The layers were separated, and the aqueous layer was extracted with CH_2Cl_2 (50 mL). The combined layers were filtered through a hydrophobic frit and concentrated *in vacuo.* The crude product was purified using a 40 g silica column, eluting with 0 – 50 % EtOAc:cyclohexane, and the desired fractions were combined and concentrated *in vacuo* to furnish methyl (*S*)-2-(8-((*tert*-butyldimethylsilyl)oxy)-3-oxo-2-(2,2,2-trifluoroethyl)-2,3,4,5-tetrahydro-1H-benzo[c]azepin-4-yl)acetate **(221)** (1.77 g, 3.97 mmol, 94 % yield) as a white coloured gum.

LCMS t_R = 1.51 min (system B), 100 %, ES+ve *m/z* 446 $(M + H)^+$; **^{1}H NMR** (400 MHz, $CDCl_3$): δ = 6.96 (1H, d, *J* = 8.3 Hz, H_3), 6.72 (1H, dd, *J* = 8.3, 2.9 Hz, H_4), 6.56 (1H, d, *J* = 2.4 Hz, H_6), 5.35 – 5.27 (1H, d, *J* = 16.6 Hz, H_{7a}), 4.17 – 3.98 (2H, m, H_{13}), 3.94 (1H, d, *J* = 17.1 Hz, H_{7b}), 3.89 – 3.78 (1H, m, H_9), 3.70 (3H, s, OMe), 3.05 – 2.97 (2H, m, H_{10a}, H_{11a}), 2.94 – 2.84 (1H, m, H_{10b}), 2.45 (1H, dd, *J* = 16.9, 5.6 Hz, H_{11b}), 0.98 (9H, s, ^{t}BuH), 0.18 (6H, s, H_{15}); **^{13}C NMR** (101 MHz, $CDCl_3$): δ = 175.0, 172.8, 153.8, 134.2, 131.9, 128.8, 124.4 (1C, q, *J* = 280.2 Hz), 120.6, 120.0, 53.2, 52.0, 47.9 (1C, q, *J* = 33.7 Hz), 37.2, 36.7, 34.8, 25.8, 18.4, -4.3; **IR** (neat, ν_{max} /cm^{-1}): 1733, 1674, 1501, 1473, 1435, 1413, 1363, 1298, 1252, 1214, 1183, 1153, 1128, 1090, 983, 860, 838, 801, 781, 673; **HRMS** (ESI): calc for $C_{21}H_{31}F_3NO_4Si$ $(M + H)^+$ 446.1974, found 446.1974; $[\alpha]_D^{20}$= –70 (*c* 0.5, MeOH).

(*S*)-2-(8-Hydroxy-3-oxo-7-(4,4,5,5-tetramethyl-1,3,2-dioxaborolan-2-yl)-2-(2,2,2-trifluoroethyl)-2,3,4,5-tetrahydro-1H-benzo[c]azepin-4-yl)acetate (222)

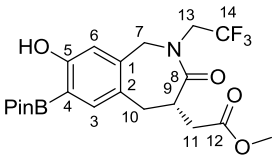

To a vial containing 4,4,4',4',5,5,5',5'-octamethyl-2,2'-bi(1,3,2-dioxaborolane) (863 mg, 3.40 mmol), 4,4'-di-tert-butyl-2,2'-bipyridine **(197)** (68.4 mg, 0.255 mmol), $[Ir(COD)OMe]_2$ (113 mg, 0.170 mmol), and methyl (*S*)-2-(8-hydroxy-3-oxo-2-(2,2,2-trifluoroethyl)-2,3,4,5-tetrahydro-1H-benzo[c]azepin-4-yl)acetate **(105)** (563 mg, 1.699 mmol) under nitrogen was added TBME (20 mL) and the flask was purged with alternating nitrogen and vacuum, followed by heating to at 100 °C in a microwave reactor for 5 h, followed by cooling to rt. The solution was adsorbed onto Celite® and purified using a 40 g silica column, eluting with 0 – 100 % EtOAc:cyclohexane, and the desired fractions were combined and concentrated *in vacuo* to yield methyl (*S*)-2-(8-hydroxy-3-oxo-7-(4,4,5,5-tetramethyl-1,3,2-dioxaborolan-2-yl)-2-(2,2,2-trifluoroethyl)-2,3,4,5-tetrahydro-1H-benzo[c]azepin-4-yl)acetate **(222)** (642 mg, 1.404 mmol, 83 % yield) as a yellow coloured gum, which was used without further purification.

(*S*)-Methyl 2-(8-((*tert*-butyldimethylsilyl)oxy)-3-oxo-6-(4,4,5,5-tetramethyl-1,3,2-dioxaborolan-2-yl)-2-(2,2,2-trifluoroethyl)-2,3,4,5-tetrahydro-1H-benzo[c]azepin-4-yl)acetate (223)

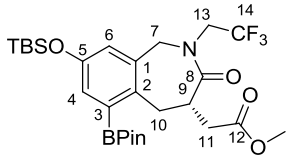

A sealed vial containing 4,4,4',4',5,5,5',5'-octamethyl-2,2'-bi(1,3,2-dioxaborolane) (814 mg, 3.20 mmol), $[Ir(COD)OMe]_2$ (212 mg, 0.320 mmol), 4,4'-di-tert-butyl-2,2'-bipyridine **(197)** (143 mg, 0.534 mmol) and methyl (*S*)-2-(8-((*tert*-

butyldimethylsilyl)oxy)-3-oxo-2-(2,2,2-trifluoroethyl)-2,3,4,5-tetrahydro-1H-benzo[c]azepin-4-yl)acetate **(221)** (476 mg, 1.068 mmol) was sealed and purged with nitrogen gas. TBME (20 mL) was added and nitrogen gas was bubbled through the resulting solution for 10 min, after which time it was sealed, and the vial was heated at 100 °C for 14 h, followed by cooling to rt. The red-brown mixture was adsorbed onto Celite® and purified using a 40 g silica column, eluting with 0 – 50 % EtOAc:cyclohexane, and the desired fractions were combined and concentrated *in vacuo* to yield methyl (*S*)-2-(8-((*tert*-butyldimethylsilyl)oxy)-3-oxo-6-(4,4,5,5-tetramethyl-1,3,2-dioxaborolan-2-yl)-2-(2,2,2-trifluoroethyl)-2,3,4,5-tetrahydro-1H-benzo[c]azepin-4-yl)acetate **(223)** (364 mg, 0.637 mmol, 60 % yield) as an orange coloured oil, as an inseparable mixture (2:3 ratio) with unreacted starting material **(221)**, which was used without further purification.

Methyl (*S*)-2-(8-hydroxy-6-methyl-3-oxo-2-(2,2,2-trifluoroethyl)-2,3,4,5-tetra hydro-1H-benzo[c]azepin-4-yl)acetate (224)

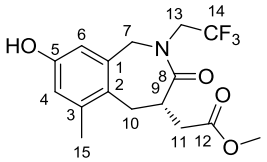

To a flask containing potassium carbonate (63.7 mg, 0.461 mmol), $Pd(Ph_3P)_4$ (53.2 mg, 0.046 mmol), methyl iodide (0.048 mL, 0.768 mmol), and methyl (*S*)-2-(8-((*tert*-butyldimethylsilyl)oxy)-3-oxo-6-(4,4,5,5-tetramethyl-1,3,2-dioxaborolan-2-yl)-2-(2,2,2-trifluoroethyl)-2,3,4,5-tetrahydro-1H-benzo[c]azepin-4-yl)acetate **(223)** (231 mg, 0.154 mmol, a 1:2 mixture with **221**) was purged with nitrogen and DMF (2 mL), EtOH (0.2 mL) and H_2O (0.2 mL) were added, followed by heating to 80 °C for 1 h followed by cooling to rt. The mixture was diluted with EtOAc (10 mL) and H_2O (10 mL) and the layers were separated. The organic layer was washed with 10 % aqueous lithium chloride solution (10 mL), filtered through a hydrophobic frit and

concentrated *in vacuo*. The crude product was purified using a 24 g silica column, eluting with 0 – 50 % EtOAc:cyclohexane, and the desired fractions were combined and concentrated *in vacuo*, before redissolution in THF (2 mL), followed by the addition of TBAF (1 M in THF, 0.350 mL, 0.350 mmol). The solution was stirred for 30 mins, followed by dilution with sat. aq. ammonium chloride solution (6 mL), H_2O (5 mL) and EtOAc (15 mL). The layers were separated, and the aqueous layer was extracted with EtOAc (15 mL). The combined organic layers were filtered through a hydrophobic frit and concentrated *in vacuo*. The crude product was purified using a 12 g silica column, eluting with 0 – 40 % EtOAc:cyclohexane, and the desired fractions were combined and concentrated *in vacuo*, followed by further purification using an Xbridge™ Prep C18 column, eluting with 0 – 100 % MeCN:ammonium carbonate modified H_2O, and the desired fractions were combined and concentrated *in vacuo* to furnish methyl (*S*)-2-(8-hydroxy-6-methyl-3-oxo-2-(2,2,2-trifluoroethyl)-2,3,4,5-tetrahydro-1H-benzo[c]azepin-4-yl)acetate **(224)** (19.8 mg, 0.057 mmol, 20 % yield over 2 steps) as a colourless gum, as an inseparable mixture with **105** (19:1 ratio).

LCMS t_R = 0.91 min (system B), 91 %, ES+ve *m/z* 346 $(M + H)^+$; **^{1}H NMR** (400 MHz, $CDCl_3$): δ = 6.63 (1H, d, *J* = 2.5 Hz, H_4), 6.45 (1H, d, *J* = 2.5 Hz, H_6), 5.34 (1H, d, *J* = 16.7 Hz, H_{7a}), 4.27 – 4.14 (1H, m, H_{13a}), 3.97 – 3.79 (3H, m, H_{7b}, H_9, H_{13b}), 3.70 (3H, s, OMe), 3.05 (1H, dd, *J* = 16.7, 8.4 Hz, H_{11a}), 2.82 (1H, dd, *J* = 17.2, 3.9 Hz, H_{10a}), 2.59 (1H, dd, *J* = 17.0, 13.5 Hz, H_{10b}), 2.50 (1H, dd, *J* = 17.0, 5.7, Hz, H_{11b}), 2.12 (3H, s, H_{15}), *OH not observed*; **^{13}C NMR** (101 MHz, $CDCl_3$): δ = 175.1, 173.0, 153.7, 139.8, 134.2, 126.2, 124.4 (1C, q, *J* = 280.8 Hz), 117.4, 114.1, 53.4, 52.1, 47.6 (1C, q, *J* = 34.6 Hz), 37.0, 36.9, 32.8, 20.3; **IR** (neat, ν_{max} /cm^{-1}): 3341 (br), 1732, 1650, 1614, 1481, 1439, 1305, 1268, 1225, 1187, 1150, 1126, 1104, 1028, 1005, 860, 830, 674; **HRMS** (ESI): calc for $C_{16}H_{19}F_3NO_4$ $(M + H)^+$ 346.1266, found 346.1259; $[\alpha]_D^{20}$= –86 (*c* 1.0, MeOH).

Methyl (*S*)-2-(8-hydroxy-6-methoxy-3-oxo-2-(2,2,2-trifluoroethyl)-2,3,4,5-tetra hydro-1H-benzo[c]azepin-4-yl)acetate (225)

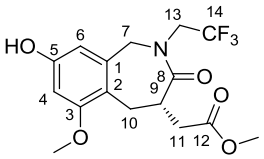

A flask containing 4-dimethylaminopyridine (DMAP) (33.8 mg, 0.277 mmol), diacetoxycopper hydrate (30.4 mg, 0.152 mmol), activated 4 Å molecular sieves and methyl (*S*)-2-(8-((*tert*-butyldimethylsilyl)oxy)-3-oxo-6-(4,4,5,5-tetramethyl-1,3,2-dioxaborolan-2-yl)-2-(2,2,2-trifluoroethyl)-2,3,4,5-tetrahydro-1H-benzo[c]azepin-4-yl)acetate **(223)** (208 mg, 0.138 mmol, a 1:2 mixture with **221**) in MeOH (5 mL) was stirred in an open flask for 5 h, followed by removal of the solvent using a flow of nitrogen. The resulting solid was redissolved in EtOAc (20 mL) and H_2O (10 mL) and filtered through Celite®, eluting with EtOAc (30 mL) and H_2O (10 mL), and the filtrate was further diluted with H_2O (20 mL) and the layers were separated. The aqueous layer was extracted with EtOAc (40 mL) and the combined organic layers were filtered through a hydrophobic frit and concentrated *in vacuo*. The crude product was purified using a 24 g silica column, eluting with 0 – 50 % EtOAc:cyclohexane, and the desired fractions were combined and concentrated *in vacuo*. To a solution of the resulting oil in THF (2 mL) was added TBAF (1 M in THF, 0.338 mL, 0.338 mmol), and the solution was stirred for 30 mins, followed by dilution with sat. aq. ammonium chloride solution (6 mL), H_2O (5 mL) and EtOAc (15 mL). The layers were separated, and the aqueous layer was extracted with EtOAc (15 mL). The combined organic layers were filtered through a hydrophobic frit and concentrated *in vacuo*. The crude product was purified using a 12 g silica column, eluting with 0 – 40 % EtOAc:cyclohexane, and the desired fractions were combined and concentrated *in vacuo,* followed by further purification using an Xbridge™ Prep C18 column, eluting with 0 – 50 % MeCN:ammonium carbonate modified H_2O, and the desired fractions were combined and concentrated to yield methyl (*S*)-2-(8-hydroxy-6-methoxy-3-oxo-2-(2,2,2-trifluoroethyl)-2,3,4,5-tetrahydro-1H-benzo[c]azepin-4-yl)acetate **(225)**

(20.1 mg, 0.056 mmol, 20 % yield over 2 steps) as a white coloured gum, as an inseparable mixture with **105** (19:1 ratio).

LCMS t_R = 0.90 min (system B), 95 %, ES+ve *m/z* 362 $(M + H)^+$; **^{1}H NMR** (400 MHz, $CDCl_3$): δ = 6.36 (1H, d, *J* = 2.5 Hz, H_4), 6.19 (1H, d, *J* = 2.0 Hz, H_6), 5.30 (1H, br d, *J* = 16.7 Hz, H_{7a}), 4.17 (1H, dq, *J* = 15.1, 8.9 Hz, H_{13a}), 3.93 – 3.79 (3H, m, H_{7b}, H_9, H_{13b}), 3.74 (3H, s, OMe), 3.69 (3H, s, OMe), 3.03 (1H, dd, *J* = 17.0, 8.6, Hz, H_{11a}), 2.91 (1H, dd, *J* = 17.7, 3.4 Hz, H_{10a}), 2.61 – 2.46 (2H, m, H_{10b}, H_{11b}), *OH not observed*; **^{13}C NMR** (101 MHz, $CDCl_3$): δ = 175.5, 173.1, 159.1, 155.0, 134.7, 124.4 (1C, q, *J* = 279.2 Hz), 116.6, 107.7, 98.6, 55.5, 53.1, 52.0, 47.7 (1C, q, *J* = 34.1 Hz), 37.0, 36.6, 29.2; **IR** (neat, ν_{max} /cm^{-1}): 3261 (br), 1734, 1642, 1595, 1443, 1363, 1262, 1202, 1157, 1127, 1085, 996, 829, 758, 675, 636, 466; **HRMS** (ESI): calc for $C_{16}H_{19}F_3NO_5$ $(M + H)^+$ 362.1215, found 362.1212; $[\boldsymbol{\alpha}]_D^{20}$= –78 (*c* 1.0, MeOH).

Methyl (*S*)-2-(6-methyl-3-oxo-8-(2-(5,6,7,8-tetrahydro-1,8-naphthyridin-2-yl)ethoxy)-2-(2,2,2-trifluoroethyl)-2,3,4,5-tetrahydro-1H-benzo[c]azepin-4-yl)acetate (227)

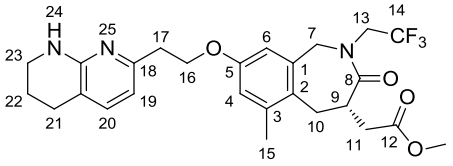

CMBP (0.022 mL, 0.085 mmol) was added to a stirring solution of 2-(5,6,7,8-tetrahydro-1,8-naphthyridin-2-yl)ethan-1-ol **(65)** (12.1 mg, 0.068 mmol) and methyl (*S*)-2-(8-hydroxy-6-methyl-3-oxo-2-(2,2,2-trifluoroethyl)-2,3,4,5-tetrahydro-1H-benzo[c]azepin-4-yl)acetate **(224)** (19.5 mg, 0.056 mmol) in THF (1 mL) under nitrogen, and the vial was sealed and the solution was heated at 80 °C for 4 h, followed by cooling to rt. Further portions of CMBP (0.022 mL, 0.085 mmol) and 2-(5,6,7,8-tetrahydro-1,8-naphthyridin-2-yl)ethan-1-ol **(65)** (12.1 mg, 0.068 mmol) were added and the solution heated for a further 3 h. The brown coloured solution

was cooled, adsorbed onto Celite® and purified using a 4 g silica column, eluting with 0 – 80 % (EtOAc + 1 % NEt_3):cyclohexane, and the desired fractions were combined and concentrated *in vacuo*, followed by further purification using an Xbridge™ Prep C18 column, eluting with 0 – 100 % MeCN:ammonium carbonate modified H_2O, and the desired fractions were combined and concentrated *in vacuo* to furnish methyl (*S*)-2-(6-methyl-3-oxo-8-(2-(5,6,7,8-tetrahydro-1,8-naphthyridin-2-yl)ethoxy)-2-(2,2,2-trifluoroethyl)-2,3,4,5-tetrahydro-1H-benzo[c]azepin-4-yl)acetate **(227)** (8.2 mg, 0.016 mmol, 29 % yield) as a colourless gum.

LCMS t_R = 1.24 min (system B), 100 %, ES+ve *m/z* 506 $(M + H)^+$; **^{1}H NMR** (400 MHz, $CDCl_3$): δ = 7.07 (1H, d, *J* = 7.3 Hz, H_{20}), 6.70 (1H, d, *J* = 2.4 Hz, H_4), 6.50 (1H, d, *J* = 2.9 Hz, H_6), 6.44 (1H, d, *J* = 7.3 Hz, H_{19}), 5.36 (1H, d, *J* = 16.6 Hz, H_{7a}), 4.75 (1H, br s, NH), 4.33 – 4.19 (3H, m, H_{13a}, H_{16}), 3.96 – 3.86 (2H, m, H_{7b}, H_8), 3.85 – 3.73 (1H, m, H_{13b}), 3.71 (3H, s, OMe), 3.40 (2H, td, *J* = 5.6, 2.4 Hz, H_{23}), 3.05 (1H, dd, *J* = 16.6, 8.3 Hz, H_{11a}), 2.99 (2H, t, *J* = 7.1 Hz, H_{17}), 2.84 (1H, dd, *J* = 17.1, 3.9 Hz, H_{10a}), 2.70 (2H, t, *J* = 6.1 Hz, H_{21}), 2.60 (1H, dd, *J* = 17.1, 13.2 Hz, H_{10b}), 2.48 (1H, dd, *J* = 16.9, 5.6 Hz, H_{11b}), 2.15 (3H, s, H_{15}), 1.95 – 1.87 (2H, m, H_{22}); **^{13}C NMR** (101 MHz, $CDCl_3$): δ = 174.8, 172.7, 156.7, 156.1, 154.5, 139.5, 136.8, 134.1, 126.5, 124.4 (1C, q, *J* = 281.0 Hz), 116.7, 114.1, 113.5, 112.4, 67.7, 53.6, 52.0, 47.5 (1C, q, *J* = 33.7 Hz), 41.8, 37.8, 37.1, 36.9, 32.9, 26.5, 21.6, 20.5; **IR** (neat, ν_{max} /cm^{-1}): 3412 (br), 3252 (br), 1671, 1599, 1587, 1478, 1462, 1435, 1344, 1308, 1269, 1230, 1216, 1186, 1149, 1126, 1104, 1064, 1048, 1031, 830; **HRMS** (ESI): calc for $C_{26}H_{31}F_3N_3O_4$ $(M + H)^+$ 506.2267, found 506.2267; $[\boldsymbol{\alpha}]_D^{20}$= –72 (*c* 0.5, MeOH).

Methyl (*S*)-2-(6-methoxy-3-oxo-8-(2-(5,6,7,8-tetrahydro-1,8-naphthyridin-2-yl)ethoxy)-2-(2,2,2-trifluoroethyl)-2,3,4,5-tetrahydro-1H-benzo[c]azepin-4-yl)acetate (228)

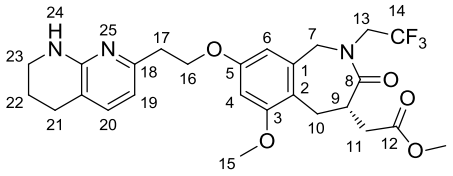

CMBP (0.036 mL, 0.138 mmol) was added to a stirring solution of 2-(5,6,7,8-tetrahydro-1,8-naphthyridin-2-yl)ethan-1-ol **(65)** (17.8 mg, 0.100 mmol) and methyl (*S*)-2-(8-hydroxy-6-methoxy-3-oxo-2-(2,2,2-trifluoroethyl)-2,3,4,5-tetrahydro-1H-benzo[c]azepin-4-yl)acetate **(225)** (20 mg, 0.055 mmol) in THF (1 mL) under nitrogen, and the vial was sealed and the solution was heated at 80 °C for 4 h, followed by cooling to rt. Further portions of CMBP (0.036 mL, 0.138 mmol) and 2-(5,6,7,8-tetrahydro-1,8-naphthyridin-2-yl)ethan-1-ol **(65)** (17.8 mg, 0.100 mmol) were added and the solution heated for a further 3 h. The brown coloured solution was cooled, adsorbed onto Celite® and purified using a 4 g silica column, eluting with 0 – 80 % (EtOAc + 1 % NEt_3):cyclohexane, and the desired fractions were combined and concentrated *in vacuo*, followed by further purification using an Xbridge™ Prep C18 column, eluting with 0 – 100 % MeCN:ammonium carbonate modified H_2O, and the desired fractions were combined and concentrated *in vacuo* to furnish methyl (*S*)-2-(6-methoxy-3-oxo-8-(2-(5,6,7,8-tetrahydro-1,8-naphthyridin-2-yl)ethoxy)-2-(2,2,2-trifluoroethyl)-2,3,4,5-tetrahydro-1H-benzo[c]azepin-4-yl)acetate **(228)** (11.4 mg, 0.022 mmol, 40 % yield) as a colourless oil.

LCMS t_R = 1.22 min (system B), 100 %, ES+ve *m/z* 522 $(M + H)^+$; **^{1}H NMR** (400 MHz, $CDCl_3$): δ = 7.08 (1H, d, *J* = 7.3 Hz, H_{20}), 6.44 (1H, d, *J* = 7.3 Hz, H_{19}), 6.40 (1H, d, *J* = 2.4 Hz, H_4), 6.24 (1H, d, *J* = 2.4 Hz, H_6), 5.34 (1H, d, *J* = 16.6 Hz, H_{7a}), 4.75 (1H, br s, NH), 4.30 – 4.15 (3H, m, H_{13a}, H_{16}), 3.95 – 3.78 (3H, m, H_{7b}, H_8, H_{13b}), 3.76 (3H, s, OMe_{15}), 3.70 (3H, s, OMe), 3.40 (2H, td, *J* = 5.5, 2.7 Hz, H_{23}), 3.07 – 2.98 (3H, m, H_{11a}, H_{17}), 2.92 (1H, dd, *J* = 17.9, 3.2 Hz, H_{10a}), 2.70 (2H, t, *J* = 6.4 Hz, H_{21}), 2.57 (1H, dd, *J* = 17.6, 13.2

Hz, H_{10b}), 2.46 (1H, dd, *J* = 16.9, 5.1 Hz, H_{11b}), 1.95 – 1.87 (2H, m, H_{22}); **^{13}C NMR** (101 MHz, $CDCl_3$): δ = 175.1, 172.9, 159.0, 158.0, 156.1, 154.4, 136.8, 134.7, 124.5 (1C, q, *J* = 281.0 Hz), 117.2, 114.1, 112.4, 106.3, 98.5, 67.9, 55.6, 53.3, 51.9, 47.6 (1C, q, *J* = 34.5 Hz), 41.8, 37.8, 37.0, 36.6, 29.3, 26.5, 21.6; **IR** (neat, ν_{max} /cm^{-1}): 3417 (br), 3252 (br), 1732, 1669, 1588, 1463, 1435, 1421, 1352, 1319, 1269, 1230, 1183, 1149, 1127, 1082, 1042, 1030, 995, 830; **HRMS** (ESI): calc for $C_{26}H_{31}F_3N_3O_5$ $(M + H)^+$ 522.2216, found 522.2217; $[\boldsymbol{\alpha}]_D^{20}$= –76 (*c* 0.5, MeOH).

(*S*)-2-(6-Methyl-3-oxo-8-(2-(5,6,7,8-tetrahydro-1,8-naphthyridin-2-yl)ethoxy)-2-(2,2,2-trifluoroethyl)-2,3,4,5-tetrahydro-1H-benzo[c]azepin-4-yl)acetic acid (219)

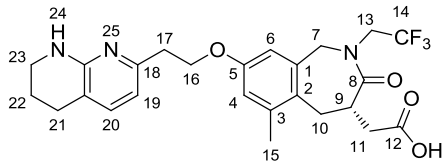

To a stirring solution of methyl (*S*)-2-(6-methyl-3-oxo-8-(2-(5,6,7,8-tetrahydro-1,8-naphthyridin-2-yl)ethoxy)-2-(2,2,2-trifluoroethyl)-2,3,4,5-tetrahydro-1H-benzo[c]azepin-4-yl)acetate **(227)** (8.2 mg, 0.016 mmol) in MeOH (1 mL) was added sodium hydroxide (2 M in H_2O, 50 µl, 0.100 mmol), and the reaction stirred at 35 °C for 1 h, followed by removal of the solvent using a flow of nitrogen gas. The residue was redissolved in H_2O (0.5 mL) and MeCN (0.5 mL), before neutralisation by dropwise addition of aqueous HCl (2 M). The resulting solution was purified using an XBridge™ Prep C18 column, eluting with 0 – 100 % MeCN:ammonium carbonate modified H_2O, and the desired fractions were combined and concentrated *in vacuo* to furnish (*S*)-2-(6-methyl-3-oxo-8-(2-(5,6,7,8-tetrahydro-1,8-naphthyridin-2-yl)ethoxy)-2-(2,2,2-trifluoroethyl)-2,3,4,5-tetrahydro-1H-benzo[c]azepin-4-yl)acetic acid **(219)** (8.0 mg, 0.016 mmol, 100 % yield) as a pale yellow coloured gum, contaminated with a small quantity of triphenylphosphine oxide.

LCMS t_R = 0.82 min (system B), 97 %, ES+ve *m/z* 492 $(M + H)^+$; **^{1}H NMR** (600 MHz, DMSO-d_6): δ = 7.05 (1H, d, *J* = 7.3 Hz, H_{20}), 6.70 (1H, d, *J* = 2.2 Hz, H_4), 6.65 (1H, d, *J* = 2.6 Hz, H_6), 6.35 (1H, d, *J* = 7.3 Hz, H_{19}), 6.28 (1H, br s, NH), 5.31 (1H, d, *J* = 16.5 Hz, H_{7a}), 4.22 – 4.07 (5H, m, H_{7b}, H_{13}, H_{16}), 3.86 – 3.78 (1H, m, H_9), 3.25 – 3.22 (2H, m, H_{23}), 2.89 – 2.81 (3H, m, H_{10a}, H_{17}) 2.68 (1H, br dd, *J* = 16.7, 8.6 Hz, H_{11a}), 2.61 (2H, t, *J* = 6.1 Hz, H_{21}), 2.44 – 2.34 (2H, m, H_{10b}, H_{11b}), 2.11 (3H, s, H_{15}), 1.75 (2H, dt, *J* = 11.6, 6.0 Hz, H_{22}); **^{13}C NMR** (150 MHz, DMSO-d_6): δ = 174.6, 173.1, 155.9, 155.6, 153.8, 138.6, 135.9, 135.0, 126.6, 124.7 (1C, q, *J* = 281.4 Hz), 115.7, 113.0, 112.9, 110.7, 66.9, 52.3, 46.5 (1C, q, *J* = 33.2 Hz, 1C), 40.7, 37.1, 37.0, 36.0, 31.9, 26.0, 21.0, 19.8; **IR** (neat, ν_{max} /cm^{-1}): 3270 (br), 1667, 1394, 1306, 1270, 1231, 1187, 1149, 1126, 1049, 727, 541; **HRMS** (ESI): calc for $C_{25}H_{29}F_3N_3O_4$ $(M + H)^+$ 492.2110, found 492.2111; $[\alpha]_D^{20}$ *could not be measured due to product insolubility in appropriate solvents.*

(*S*)-2-(6-Methoxy-3-oxo-8-(2-(5,6,7,8-tetrahydro-1,8-naphthyridin-2-yl)ethoxy)-2-(2,2,2-trifluoroethyl)-2,3,4,5-tetrahydro-1H-benzo[c]azepin-4-yl)acetic acid (226)

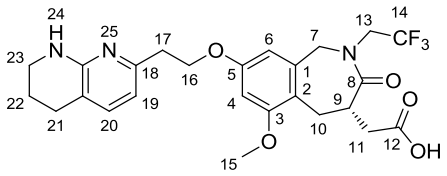

To a stirring solution of methyl (*S*)-2-(6-methoxy-3-oxo-8-(2-(5,6,7,8-tetrahydro-1,8-naphthyridin-2-yl)ethoxy)-2-(2,2,2-trifluoroethyl)-2,3,4,5-tetrahydro-1H-benzo[c]azepin-4-yl)acetate **(228)** (11.4 mg, 0.022 mmol) in MeOH (1 mL) was added sodium hydroxide (2 M in H_2O, 50 µl, 0.100 mmol), and the reaction stirred at 35 °C for 1 h, followed by removal of the solvent using a flow of nitrogen gas. The residue was redissolved in H_2O (0.5 mL) and MeCN (0.5 mL), before neutralisation by dropwise addition of aqueous HCl (2 M). The resulting solution was purified using an XBridge™ Prep C18 column, eluting with 0 – 100 % MeCN:ammonium carbonate modified H_2O, and the desired fractions were combined and concentrated *in vacuo*

to furnish (*S*)-2-(6-methoxy-3-oxo-8-(2-(5,6,7,8-tetrahydro-1,8-naphthyridin-2-yl)ethoxy)-2-(2,2,2-trifluoroethyl)-2,3,4,5-tetrahydro-1H-benzo[c]azepin-4-yl)acetic acid **(226)** (8.5 mg, 0.017 mmol, 77 % yield) as a colourless gum.

LCMS t_R = 0.81 min (system B), 100 %, ES+ve *m/z* 508 $(M + H)^+$; **^{1}H NMR** (700 MHz, DMSO-d_6): δ = 12.17 (1H, br s, COOH), 7.06 (1H, d, *J* = 7.3 Hz, H_{20}), 6.45 (1 H, d, *J* = 2.6 Hz, H_4), 6.43 (1H, d, *J* = 2.2 Hz, H_6), 6.36 (1H, d, *J* = 6.9 Hz, H_{19}), 6.31 (1H, br s, NH), 5.30 (1H, br d, *J* = 16.8 Hz, H_{7a}), 4.20 (2H, t, *J* = 7.1 Hz, H_{16}), 4.18 – 4.13 (2H, m, H_{13}), 4.10 (1H, br d, *J* = 16.8 Hz, H_{7b}), 3.77 (1H, ddt, *J* = 13.7, 8.9, 4.6 Hz, H_9), 3.73 (3H, s, H_{15}), 3.26 – 3.21 (2H, m, H_{23}), 2.89 – 2.83 (3H, m, H_{10a}, H_{17}), 2.67 (1H, dd, *J* = 16.8, 9.0 Hz, H_{11a}), 2.61 (2H, t, *J* = 6.2 Hz, H_{21}), 2.39 (1H, dd, *J* = 16.6, 4.5 Hz, H_{11b}), 2.29 (2H, dd, *J* = 17.6, 13.8 Hz, H_{10b}), 1.75 (2H, dt, *J* = 11.5, 6.1 Hz, H_{22}); **^{13}C NMR** (176 MHz, DMSO-d_6): δ = 174.7, 173.1, 158.1, 157.0, 155.9, 153.7, 136.0, 135.6, 124.7 (1C, q, *J* = 281.1 Hz), 116.4, 113.0, 110.7, 106.3, 97.8, 67.2, 55.5, 52.1, 46.6 (1C, q, *J* = 32.8 Hz), 40.7, 37.0, 36.8 (br s, 1C), 35.5, 28.8, 26.0, 21.0; **IR** (neat, ν_{max} /cm^{-1}): 3286 (br), 1667, 1606, 1416, 1319, 1270, 1229, 1183, 1149, 1127, 1081, 1044, 829, 729; **HRMS** (ESI): calc for $C_{25}H_{29}F_3N_3O_5$ $(M + H)^+$ 508.2059, found 508.2063; $[\alpha]_D^{20}$ *could not be measured due to product insolubility in appropriate solvents.*

Methyl (*S*)-2-(8-hydroxy-3-oxo-2-(2,2,2-trifluoroethyl)-6-vinyl-2,3,4,5-tetrahydro-1H-benzo[c]azepin-4-yl)acetate (229)

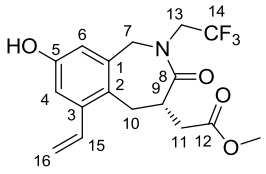

To a flask containing potassium carbonate (98 mg, 0.710 mmol), $Pd(Ph_3P)_4$ (82 mg, 0.071 mmol), bromoethene (1 M in THF, 1.18 mL, 1.18 mmol), and methyl (*S*)-2-(8-((*tert*-butyldimethylsilyl)oxy)-3-oxo-6-(4,4,5,5-tetramethyl-1,3,2-dioxaborolan-2-yl)-2-(2,2,2-trifluoroethyl)-2,3,4,5-tetrahydro-1H-benzo[c]azepin-4-yl)acetate **(223)**

(520 mg, 0.237 mmol) (a 1:3.7 mixture with **221**) was purged with nitrogen and DMF (2 mL), EtOH (0.2 mL) and H_2O (0.2 mL) was added, followed by heating to 80 °C for 2 h followed by cooling to rt. The solution was diluted with EtOAc (50 mL) and filtered through Celite®, eluting with EtOAc (70 mL). The solution was washed with H_2O (60 mL) and 10 % aqueous lithium chloride solution (50 mL), filtered with a hydrophobic frit and concentrated *in vacuo*. The crude product was purified using a 24 g silica column. eluting with 0 – 40 % EtOAc:cyclohexane, and the desired fractions were combined and concentrated *in vacuo* to furnish methyl (*S*)-2-(8-hydroxy-3-oxo-2-(2,2,2-trifluoroethyl)-6-vinyl-2,3,4,5-tetrahydro-1H-benzo[c]azepin-4-yl)acetate **(229)** (45.7 mg, 0.128 mmol, 54 % yield) as a pale yellow coloured gum, which was used without further purification.

Methyl (*S*)-2-(6-ethyl-8-hydroxy-3-oxo-2-(2,2,2-trifluoroethyl)-2,3,4,5-tetrahydro-1H-benzo[c]azepin-4-yl)acetate (230)

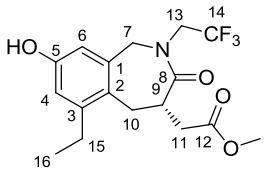

A mixture of methyl (*S*)-2-(8-hydroxy-3-oxo-2-(2,2,2-trifluoroethyl)-6-vinyl-2,3,4,5-tetrahydro-1H-benzo[c]azepin-4-yl)acetate **(229)** (45 mg, 0.126 mmol) and palladium on carbon (5 wt%) (53.6 mg, 0.025 mmol) in EtOH (6 mL) was stirred in the presence of hydrogen gas for 6 h, followed by filtrating through Celite®, eluting with EtOH (40 mL). The filtrate was concentrated *in vacuo,* followed by purification using a 24 g silica column, eluting with 0 – 50 % EtOAc:cyclohexane, and the desired fractions were combined and concentrated *in vacuo,* followed by further purification using an Xbridge™ Prep C18 column, eluting with 0 – 100 % MeCN:ammonium carbonate modified H_2O, and the desired fractions were combined and concentrated *in vacuo* to furnish methyl (*S*)-2-(6-ethyl-8-hydroxy-3-oxo-2-(2,2,2-trifluoroethyl)-2,3,4,5-

tetrahydro-1H-benzo[c]azepin-4-yl)acetate **(230)** (23 mg, 0.064 mmol, 51 % yield) as a colourless gum.

LCMS t_R = 0.97 min (system B), 97 %, ES+ve *m/z* 360 $(M + H)^+$; **^{1}H NMR** (400 MHz, $CDCl_3$): δ = 6.67 (1H, d, *J* = 2.4 Hz, H_4), 6.45 (1H, d, *J* = 2.9 Hz, H_6), 5.30 (1H, br d, *J* = 16.6 Hz, H_{7a}), 4.28 – 4.12 (1H, m, H_{13a}), 3.98 – 3.78 (3H, m, H_{7b}, H_9, H_{13b}), 3.70 (3H, s, OMe), 3.04 (1H, dd, *J* = 16.9, 8.1 Hz, H_{11a}), 2.92 (1H, dd, *J* = 16.6, 3.9 Hz, H_{10a}), 2.68 (1H, dd, *J* = 16.9, 13.4 Hz, H_{10b}), 2.55 – 2.40 (3H, m, H_{11b}, H_{15}), 1.16 (3H, t, *J* = 7.6 Hz, H_{16}); **^{13}C NMR** (101 MHz, $CDCl_3$): δ = 175.1, 172.9, 154.0, 145.5, 134.4, 125.5, 124.4 (1C, q, *J* = 280.2 Hz), 115.5, 114.0, 53.6, 52.1, 47.6 (1C, q, *J* = 34.0 Hz), 37.1, 37.1, 32.0, 25.8, 14.0; **IR** (neat, ν_{max} /cm^{-1}): 3445 (br), 1732, 1650, 1614, 1439, 1268, 1224, 1186, 1151, 1126, 1104, 987, 831; **HRMS** (ESI): calc for $C_{17}H_{21}F_3NO_4$ $(M + H)^+$ 360.1423, found 360.1420; $[\boldsymbol{\alpha}]_D^{20}$ = –87 (*c* 1.0, MeOH).

(*S*)-2-(6-Chloro-8-hydroxy-3-oxo-2-(2,2,2-trifluoroethyl)-2,3,4,5-tetrahydro-1H-benzo[c]azepin-4-yl)acetate (231)

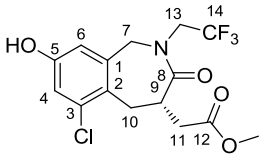

A to solution of methyl (*S*)-2-(8-((*tert*-butyldimethylsilyl)oxy)-3-oxo-6-(4,4,5,5-tetramethyl-1,3,2-dioxaborolan-2-yl)-2-(2,2,2-trifluoroethyl)-2,3,4,5-tetrahydro-1H-benzo[c]azepin-4-yl)acetate **(223)** (190 mg, 0.153 mmol) (a 2:3 mixture with **221**) in MeOH (5 mL) was added a solution of copper(II) chloride dihydrate (78 mg, 0.459 mmol) in H_2O (0.5 mL) and the solution was heated at 80 °C for 2 h, followed by cooling to rt. The solvent was removed *in vacuo,* and the residue was redissolved in THF (3 mL), followed by the addition of TBAF (1 M in THF, 0.382 mL, 0.382 mmol) and stirring for 1 h. The green coloured mixture was diluted with EtOAc (10 mL) and H_2O (10 mL) and the layers were separated. The aqueous layer was extracted with EtOAc

(10 mL), and the combined organic phases were filtered through a hydrophobic frit and concentrated *in vacuo*. The crude product was purified using a 12 g silica column, eluting with 0 – 50 % EtOAc:cyclohexane, and the desired fractions were combined and concentrated *in vacuo,* followed by further purification using an Xbridge™ Prep C18 column, eluting with 0 – 100 % MeCN:ammonium carbonate modified H_2O, and the desired fractions were combined and concentrated *in vacuo* to furnish methyl (*S*)-2-(6-chloro-8-hydroxy-3-oxo-2-(2,2,2-trifluoroethyl)-2,3,4,5-tetrahydro-1H-benzo[c]azepin-4-yl)acetate **(231)** (27.2 mg, 0.074 mmol, 49 % yield over 2 steps) as a colourless gum.

LCMS t_R = 0.95 min (system B), 96 %, ES+ve *m/z* 366 $(M + H)^+$; **^{1}H NMR** (400 MHz, $CDCl_3$): δ = 6.86 (1H, d, *J* = 2.5 Hz, H_4), 6.53 (1H, d, *J* = 2.5 Hz, H_6), 5.31 (1H, br d, *J* = 16.7 Hz, H_{7a}), 4.19 – 4.06 (1H, m, H_{13a}), 3.98 – 3.81 (3H, m, H_{7b}, H_8, H_{13b}), 3.70 (3H, s, OMe), 3.07 – 2.98 (2H, m, H_{10a}, H_{11a}), 2.68 (1H, dd, *J* = 17.5, 13.5 Hz, H_{10b}), 2.53 (1H, dd, *J* = 17.0, 5.2 Hz, H_{11b}); **^{13}C NMR** (101 MHz, $CDCl_3$): δ = 175.0, 173.1, 154.9, 136.2, 135.6, 125.0, 124.2 (1C, q, *J* = 280.8 Hz), 116.9, 115.4, 53.2, 52.2, 47.7 (1C, q, *J* = 34.6 Hz), 36.8, 36.7, 32.9; **IR** (neat, ν_{max} /cm^{-1}): 3329 (br), 1735, 1654, 1611, 1437, 1365, 1268, 1225, 1156, 1129, 1093, 991, 908, 855, 831, 730; **HRMS** (ESI): calc for $C_{15}H_{16}ClF_3NO_4$ $(M + H)^+$ 366.0720, found 366.0720; $[\alpha]_D^{20}$ = –93 (*c* 1.0, MeOH).

Methyl (*S*)-2-(6-cyano-8-hydroxy-3-oxo-2-(2,2,2-trifluoroethyl)-2,3,4,5-tetrahydro-1H-benzo[c]azepin-4-yl)acetate (232)

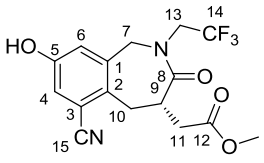

A to solution of methyl (*S*)-2-(8-((*tert*-butyldimethylsilyl)oxy)-3-oxo-6-(4,4,5,5-tetramethyl-1,3,2-dioxaborolan-2-yl)-2-(2,2,2-trifluoroethyl)-2,3,4,5-tetrahydro-1H-benzo[c]azepin-4-yl)acetate **(223)** (430 mg, 0.150 mmol) (a 1:5 mixture with **221**) in

DMF (3 mL) was added a solution of copper(I) cyanide (33.7 mg, 0.376 mmol) and potassium carbonate (104 mg, 0.752 mmol), and the solution was heated at 60 °C for 4 h, followed by cooling to rt. The black coloured mixture was diluted with EtOAc (30 mL) and H_2O (30 mL). The layers were separated, and the organic layer was washed with 10 % aqueous lithium chloride solution (30 mL), followed by filtration through a hydrophobic frit and concentration *in vacuo*. The crude product was purified using an Xbridge™ Prep C18 column, eluting with 0 – 100 % MeCN:ammonium carbonate modified H_2O, and the desired fractions were combined and concentrated *in vacuo* to furnish methyl (*S*)-2-(6-cyano-8-hydroxy-3-oxo-2-(2,2,2-trifluoroethyl)-2,3,4,5-tetrahydro-1H-benzo[c]azepin-4-yl)acetate **(232)** (4.5 mg, 0.013 mmol, 8 % yield) as a brown coloured gum, which was used without further purification.

Methyl (*S*)-2-(6-ethyl-3-oxo-8-(2-(5,6,7,8-tetrahydro-1,8-naphthyridin-2-yl)ethoxy) -2-(2,2,2-trifluoroethyl)-2,3,4,5-tetrahydro-1H-benzo[c]azepin-4-yl)acetate (234)

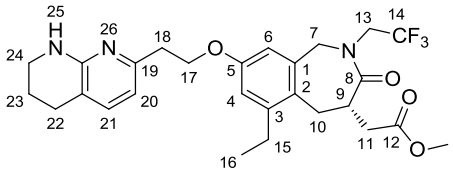

CMBP (0.033 mL, 0.125 mmol) was added to a stirring solution of 2-(5,6,7,8-tetrahydro-1,8-naphthyridin-2-yl)ethan-1-ol **(65)** (16.7 mg, 0.094 mmol) and methyl (*S*)-2-(6-ethyl-8-hydroxy-3-oxo-2-(2,2,2-trifluoroethyl)-2,3,4,5-tetrahydro-1H-benzo[c]azepin-4-yl)acetate **(230)** (22.4 mg, 0.062 mmol) in THF (1 mL) under nitrogen, and the vial was sealed and the solution was heated at 80 °C for 2 h, followed by the addition of further portions of CMBP (0.033 mL, 0.125 mmol) and 2-(5,6,7,8-tetrahydro-1,8-naphthyridin-2-yl)ethan-1-ol **(65)** (16.7 mg, 0.094 mmol) and heating for a further 2 h. The brown coloured solution was cooled, adsorbed onto Celite® and purified using a 4 g silica column, eluting with 0 – 80 % (EtOAc + 1 % NEt_3):cyclohexane, and the desired fractions were combined and concentrated *in vacuo*, followed by further purification using an Xbridge™ Prep C18 column, eluting

with 0 – 100 % MeCN:ammonium carbonate modified H_2O, and the desired fractions were combined and concentrated *in vacuo* to furnish methyl (*S*)-2-(6-ethyl-3-oxo-8-(2-(5,6,7,8-tetrahydro-1,8-naphthyridin-2-yl)ethoxy)-2-(2,2,2-trifluoroethyl)-2,3,4,5-tetrahydro-1H-benzo[c]azepin-4-yl)acetate **(234)** (17.1 mg, 0.033 mmol, 53 % yield) as a yellow coloured gum.

LCMS t_R = 1.28 min (system B), 98 %, ES+ve *m/z* 520 $(M + H)^+$; **^{1}H NMR** (400 MHz, $CDCl_3$): δ = 7.08 (1H, d, *J* = 7.3 Hz, H_{21}), 6.73 (1H, d, *J* = 2.4 Hz, H_4), 6.50 (1H, d, *J* = 2.4 Hz, H_6), 6.44 (1H, d, *J* = 7.3 Hz, H_{20}), 5.33 (1H, d, *J* = 16.6 Hz, H_{7a}), 4.77 (1H, br s, NH), 4.33 – 4.20 (3H, m, H_{13a}, H_{17}), 3.96 (1H, d, *J* = 16.6 Hz, H_{7b}), 3.92 – 3.75 (2H, m, H_9, H_{13b}), 3.70 (3H, s, OMe), 3.40 (2H, td, *J* = 5.4, 2.4 Hz, H_{24}), 3.08 – 2.98 (3H, m, H_{11a}, H_{18}), 2.93 (1H, dd, *J* = 17.1, 3.9 Hz, H_{10a}), 2.74 – 2.65 (3H, m, H_{10b}, H_{22}), 2.54 – 2.45 (3H, m, H_{11b}, H_{15}), 1.95 – 1.87 (2H, m, H_{23}), 1.17 (3H, t, *J* = 7.6 Hz, H_{16}); **^{13}C NMR** (101 MHz, $CDCl_3$): δ = 174.8, 172.7, 157.0, 156.1, 154.5, 145.2, 136.8, 134.3, 125.8, 124.4 (1C, q, *J* = 281.0 Hz), 114.9, 114.1, 113.2, 112.4, 67.7, 53.7, 51.9, 47.5 (1C, q, *J* = 33.7 Hz), 41.8, 37.8, 37.1, 37.0, 32.1, 26.5, 26.0, 21.6, 14.1; **IR** (neat, ν_{max} /cm^{-1}): 3425 (br), 3254 (br), 1739, 1671, 1601, 1587, 1463, 1447, 1436, 1207, 1230, 1186, 1152, 1128, 1105, 908, 727; **HRMS** (ESI): calc for $C_{27}H_{33}F_3N_3O_4$ $(M + H)^+$ 520.2423, found 520.2427; $[\boldsymbol{\alpha}]_D^{20}$ = –66 (*c* 0.5, MeOH).

Methyl (*S*)-2-(6-chloro-3-oxo-8-(2-(5,6,7,8-tetrahydro-1,8-naphthyridin-2-yl)ethoxy)-2-(2,2,2-trifluoroethyl)-2,3,4,5-tetrahydro-1H-benzo[c]azepin-4-yl)acetate (236)

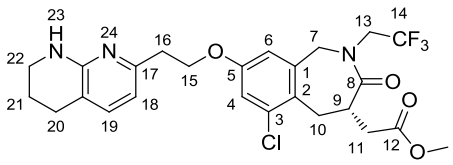

CMBP (0.028 mL, 0.107 mmol) was added to a stirring solution of 2-(5,6,7,8-tetrahydro-1,8-naphthyridin-2-yl)ethan-1-ol **(65)** (14.3 mg, 0.080 mmol) and methyl

(*S*)-2-(6-chloro-8-hydroxy-3-oxo-2-(2,2,2-trifluoroethyl)-2,3,4,5-tetrahydro-1H-benzo[c]azepin-4-yl)acetate **(231)** (19.5 mg, 0.053 mmol) in THF (1 mL) under nitrogen, and the vial was sealed and the solution was heated at 80 °C for 90 mins. The brown coloured solution was cooled, adsorbed onto Celite® and purified using a 4 g silica column, eluting with 0 – 80 % (EtOAc + 1 % NEt_3):cyclohexane, and the desired fractions were combined and concentrated *in vacuo*, followed by further purification using an Xbridge™ Prep C18 column, eluting with 0 – 100 % MeCN:ammonium carbonate modified H_2O, and the desired fractions were combined and concentrated *in vacuo* to furnish methyl (*S*)-2-(6-chloro-3-oxo-8-(2-(5,6,7,8-tetrahydro-1,8-naphthyridin-2-yl)ethoxy)-2-(2,2,2-trifluoroethyl)-2,3,4,5-tetrahydro-1H-benzo[c]azepin-4-yl)acetate **(236)** (16.7 mg, 0.032 mmol, 60 % yield) as a yellow coloured gum.

LCMS t_R = 1.29 min (system B), 100 %, ES+ve *m/z* 526 $(M + H)^+$; **^{1}H NMR** (400 MHz, $CDCl_3$): δ = 7.07 (1H, d, *J* = 7.3 Hz, H_{19}), 6.92 (1H, d, *J* = 2.9 Hz, H_4), 6.57 (1H, d, *J* = 2.4 Hz, H_6), 6.42 (1H, d, *J* = 7.3 Hz, H_{18}), 5.34 (1H, d, *J* = 16.6 Hz, H_{7a}), 4.75 (1H, br s, NH), 4.24 (2H, t, *J* = 7.1 Hz, H_{15}), 4.21 – 4.12 (1H, m, H_{13a}), 3.98 – 3.81 (3H, m, H_{7b}, H_9, H_{13b}), 3.71 (3H, s, OMe), 3.40 (2H, td, *J* = 5.6, 2.4 Hz, H_{22}), 3.10 – 2.96 (4H, m, H_{10a}, H_{11a}, H_{16}), 2.77 – 2.67 (3H, m, H_{10b}, H_{20}), 2.49 (1H, dd, *J* = 16.9, 5.1 Hz, H_{11b}), 1.91 (2H, dt, *J* = 11.9, 6.1 Hz, H_{21}); **^{13}C NMR** (101 MHz, $CDCl_3$): δ = 174.4, 172.6, 157.2, 156.1, 154.1, 136.8, 136.3, 135.7, 125.7, 124.3 (1C, q, *J* = 281.0 Hz), 115.6, 114.9, 114.2, 112.4, 68.1, 53.3, 52.0, 47.5 (1C, q, *J* = 34.5 Hz), 41.8, 37.6, 36.8, 36.6, 33.1, 26.5, 21.6; **IR** (neat, ν_{max} /cm^{-1}): 3409 (br), 3260 (br), 1732, 1672, 1600, 1463, 1434, 1414, 1270, 1227, 1187, 1151, 1125, 1094, 1029, 998, 830; **HRMS** (ESI): calc for $C_{25}H_{28}ClF_3N_3O_4$ $(M + H)^+$ 526.1720, found 526.1724; $[\alpha]_D^{20}$ = –54 (*c* 0.5, MeOH).

Methyl (*S*)-2-(6-cyano-3-oxo-8-(2-(5,6,7,8-tetrahydro-1,8-naphthyridin-2-yl) ethoxy)-2-(2,2,2-trifluoroethyl)-2,3,4,5-tetrahydro-1H-benzo[c]azepin-4-yl)acetate (238)

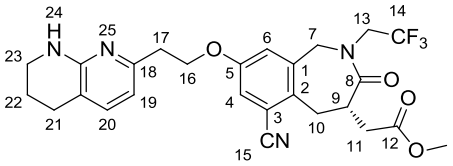

CMBP (9.9 µl, 0.038 mmol) was added to a stirring solution of 2-(5,6,7,8-tetrahydro-1,8-naphthyridin-2-yl)ethan-1-ol **(65)** (5.6 mg, 0.032 mmol) and methyl (S)-2-(6-cyano-8-hydroxy-3-oxo-2-(2,2,2-trifluoroethyl)-2,3,4,5-tetrahydro-1H-benzo[c]azepin-4-yl)acetate **(232)** (4.5 mg, 0.013 mmol) in THF (1 mL) under nitrogen, and the vial was sealed and the solution was heated at 80 °C for 2 h, followed by cooling to rt. The brown coloured solution was cooled, and purified using an Xbridge™ Prep C18 column, eluting with 0 – 100 % MeCN:ammonium carbonate modified H_2O, and the desired fractions were combined and concentrated *in vacuo* to furnish methyl (*S*)-2-(6-cyano-3-oxo-8-(2-(5,6,7,8-tetrahydro-1,8-naphthyridin-2-yl)ethoxy)-2-(2,2,2-trifluoroethyl)-2,3,4,5-tetrahydro-1H-benzo[c]azepin-4-yl)acetate **(238)** (4.7 mg, 9.10 µmol, 72 % yield) as a yellow coloured gum, which was used without further purification.

(*S*)-2-(6-Ethyl-3-oxo-8-(2-(5,6,7,8-tetrahydro-1,8-naphthyridin-2-yl)ethoxy)-2-(2,2,2-trifluoroethyl)-2,3,4,5-tetrahydro-1H-benzo[c]azepin-4-yl)acetic acid (233)

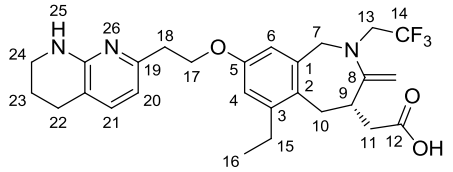

To a stirring solution of methyl (*S*)-2-(6-ethyl-3-oxo-8-(2-(5,6,7,8-tetrahydro-1,8-naphthyridin-2-yl)ethoxy)-2-(2,2,2-trifluoroethyl)-2,3,4,5-tetrahydro-1H-benzo[c]azepin-4-yl)acetate **(234)** (17.1 mg, 0.033 mmol) in MeOH (1 mL) was added sodium hydroxide (2 M in H_2O, 50 µl, 0.100 mmol), and the reaction stirred at 35 °C

for 2 h, followed by removal of the solvent using a flow of nitrogen gas. The residue was redissolved in H_2O (0.5 mL) and MeCN (0.5 mL), before neutralisation by dropwise addition of aqueous HCl (2 M). The resulting solution was purified using an XBridge™ Prep C18 column, eluting with 0 – 100 % MeCN:ammonium carbonate modified H_2O, and the desired fractions were combined and concentrated *in vacuo* to furnish (*S*)-2-(6-ethyl-3-oxo-8-(2-(5,6,7,8-tetrahydro-1,8-naphthyridin-2-yl)ethoxy)-2-(2,2,2-trifluoroethyl)-2,3,4,5-tetrahydro-1H-benzo[c]azepin-4-yl)acetic acid **(233)** (16.5 mg, 0.033 mmol, 99 % yield) as a pale yellow coloured gum.

LCMS t_R = 0.85 min (system B), 100 %, ES+ve *m/z* 506 $(M + H)^+$; **^{1}H NMR** (600 MHz, DMSO-d_6): δ = 12.13 (1H, br s, COOH), 7.05 (1H, d, *J* = 7.0 Hz, H_{21}), 6.67 (2H, s, H_4, H_6), 6.36 (1H, d, *J* = 7.3 Hz, H_{20}), 6.28 (1H, s, NH), 5.30 (1H, br d, *J* = 16.5 Hz, H_{7a}), 4.23 – 4.11 (5H, m, H_{7b}, H_{13}, H_{17}), 3.79 (1H, ddt, *J* = 13.3, 8.8, 4.5 Hz, H_9), 3.26 – 3.22 (2H, m, H_{24}), 2.93 (1H, dd, *J* = 16.9, 4.0 Hz, H_{10a}), 2.86 (2H, t, *J* = 7.0 Hz, H_{18}), 2.71 (2H, dd, *J* = 16.9, 8.8 Hz, H_{11a}), 2.61 (2H, t, *J* = 6.2 Hz, H_{22}), 2.54 – 2.38 (4H, m, H_{10b}, H_{11b}, H_{15}), 1.75 (2H, quin, *J* = 6.0 Hz, H_{23}), 1.10 (3H, t, *J* = 7.5 Hz, H_{16}); **^{13}C NMR** (151 MHz, DMSO-d_6): δ = 174.5, 173.1, 156.0, 155.9, 153.8, 144.2, 136.0, 135.2, 125.8, 124.7 (1C, q, *J* = 280.8 Hz), 114.0, 112.9, 112.8, 110.7, 66.9, 52.4, 46.5 (1C, q, *J* = 32.6 Hz), 40.7, 37.0, 36.8, 36.0, 30.9, 26.0, 25.1, 21.0, 14.0; **IR** (neat, ν_{max} /cm^{-1}): 3265 (br), 1667, 1605, 1269, 1229, 1187, 1147, 1125, 1077, 1045, 908, 830, 726, 673, 645, 490; **HRMS** (ESI): calc for $C_{26}H_{31}F_3N_3O_4$ $(M + H)^+$ 506.2267, found 506.2270; $[\alpha]_D^{20}$ = +52 (*c* 1.0, $CHCl_3$).

(*S*)-2-(6-Chloro-3-oxo-8-(2-(5,6,7,8-tetrahydro-1,8-naphthyridin-2-yl)ethoxy)-2-(2,2,2-trifluoroethyl)-2,3,4,5-tetrahydro-1H-benzo[c]azepin-4-yl)acetic acid (235)

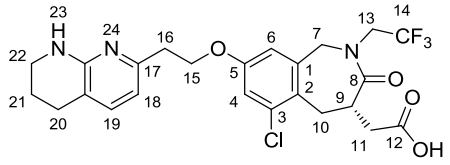

To a stirring solution of methyl (*S*)-2-(6-chloro-3-oxo-8-(2-(5,6,7,8-tetrahydro-1,8-naphthyridin-2-yl)ethoxy)-2-(2,2,2-trifluoroethyl)-2,3,4,5-tetrahydro-1H-benzo[c]azepin-4-yl)acetate **(236)** (15.1 mg, 0.029 mmol) in MeOH (1 mL) was added sodium hydroxide (2 M in H_2O, 50 µl, 0.100 mmol), and the reaction stirred at 35 °C for 1 h, followed by removal of the solvent using a flow of nitrogen gas. The residue was redissolved in H_2O (0.5 mL) and MeCN (0.5 mL), before neutralisation by dropwise addition of aqueous HCl (2 M). The resulting solution was purified using an XBridge™ Prep C18 column, eluting with 0 – 100 % MeCN:ammonium carbonate modified H_2O, and the desired fractions were combined and concentrated *in vacuo* to furnish (*S*)-2-(6-chloro-3-oxo-8-(2-(5,6,7,8-tetrahydro-1,8-naphthyridin-2-yl)ethoxy)-2-(2,2,2-trifluoroethyl)-2,3,4,5-tetrahydro-1H-benzo[c]azepin-4-yl)acetic acid **(235)** (14 mg, 0.027 mmol, 95 % yield) as a pale yellow coloured gum.

LCMS t_R = 0.85 min (system B), 100 %, ES+ve *m/z* 512 $(M + H)^+$; **^{1}H NMR** (600 MHz, DMSO-d_6): δ = 12.20 (1H, br s, COOH), 7.05 (1H, d, *J* = 7.3 Hz, H_{19}), 6.98 (1H, d, *J* = 2.6 Hz, 1=H_4), 6.86 (1H, d, *J* = 2.6 Hz, H_6), 6.35 (1H, d, *J* = 7.3 Hz, H_{18}), 6.28 (1H, br s, NH), 5.36 (1H, br d, *J* = 16.5 Hz, H_{7a}), 4.25 – 4.14 (5H, m, H_{7b}, H_{13}, H_{15}), 3.85 (1H, ddt, *J* = 13.5, 8.9, 4.5 Hz, H_9), 3.26 – 3.22 (2H, m, H_{22}), 3.01 (1H, dd, *J* = 17.6, 4.0 Hz, H_{10a}), 2.87 (2H, t, *J* = 6.8 Hz, H_{16}), 2.70 (1H, dd, *J* = 16.7, 9.0 Hz, H_{11a}), 2.61 (2H, t, *J* = 6.2 Hz, H_{20}), 2.47 – 2.42 (2H, m, H_{10b}, H_{11b}), 1.75 (2H, quin, *J* = 5.9 Hz, H_{21}); **^{13}C NMR** (151 MHz, DMSO-d_6): δ = 174.1, 172.9, 156.4, 155.9, 153.5, 137.2, 136.0, 134.6, 125.5, 124.6 (1C, q, *J* = 280.9 Hz), 114.9, 114.5, 113.0, 110.7, 67.5, 51.8, 46.5 (1C, q, *J* = 32.6 Hz), 40.6, 36.7, 36.5, 35.5, 32.4, 26.0, 20.9; **IR** (neat, ν_{max} /cm^{-1}): 3265 (br), 1668, 1603, 1393, 1269, 1228, 1151, 1123, 1093, 1040, 907, 830, 727, 677, 646; **HRMS** (ESI): calc for $C_{24}H_{26}ClF_3N_3O_4$ $(M + H)^+$ 512.1564, found 512.1566; $[\alpha]_D^{20}$ = +56 (*c* 0.5, $CHCl_3$).

(*S*)-2-(6-Cyano-3-oxo-8-(2-(5,6,7,8-tetrahydro-1,8-naphthyridin-2-yl)ethoxy)-2-(2,2,2-trifluoroethyl)-2,3,4,5-tetrahydro-1H-benzo[c]azepin-4-yl)acetic acid (237)

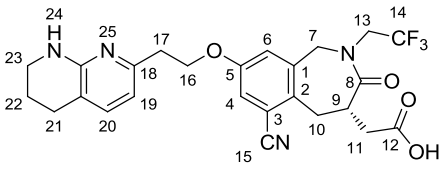

To a stirring solution of methyl (*S*)-2-(6-cyano-3-oxo-8-(2-(5,6,7,8-tetrahydro-1,8-naphthyridin-2-yl)ethoxy)-2-(2,2,2-trifluoroethyl)-2,3,4,5-tetrahydro-1H-benzo[c]azepin-4-yl)acetate **(238)** (4.7 mg, 9.10 µmol) in MeOH (0.5 mL) was added lithium hydroxide (2 M in H_2O, 0.023 mL, 0.045 mmol), and the reaction stirred at 35 °C for 2 h, followed by removal of the solvent using a flow of nitrogen gas. The residue was redissolved in H_2O (0.5 mL) and MeCN (0.5 mL), before adjustment of the pH to 3 using 5 % aqueous citric acid solution. The resulting solution was purified using an XBridge^{TM} Prep C18 column, eluting with 0 – 100 % MeCN:ammonium carbonate modified H_2O, and the desired fractions were combined and concentrated *in vacuo* to furnish (*S*)-2-(6-cyano-3-oxo-8-(2-(5,6,7,8-tetrahydro-1,8-naphthyridin-2-yl)ethoxy)-2-(2,2,2-trifluoroethyl)-2,3,4,5-tetrahydro-1H-benzo[c]azepin-4-yl)acetic acid **(237)** (2.9 mg, 5.77 µmol, 63 % yield) as a pale yellow coloured gum.

LCMS t_R = 0.80 min (system B), 100 %, ES+ve *m/z* 503 $(M + H)^+$; **^{1}H NMR** (600 MHz, $CDCl_3$): δ = 7.21 (1H, d, *J* = 7.3 Hz, H_{20}), 7.00 (1H, d, *J* = 2.2 Hz, H_4), 6.79 (1H, d, *J* = 2.2 Hz, H_6), 6.35 (1H, d, *J* = 7.0 Hz, H_{19}), 5.07 (1H, br d, *J* = 16.5 Hz, H_{7a}), 4.34 – 4.26 (1H, m, H_{16a}), 4.17 – 4.12 (1H, m, H_{16b}), 4.11 – 3.99 (2H, m, H_{13}), 3.92 (1H, br d, *J* = 16.9 Hz, H_{7b}), 3.75 – 3.67 (1H, m, H_9), 3.45 (2H, br d, *J* = 2.9 Hz, H_{23}), 3.31 (1H, br dd, *J* = 17.8, 3.5 Hz, H_{10a}), 3.10 (2H, br t, *J* = 7.2 Hz, H_{17}), 2.99 – 2.88 (2H, m, H_{10b}, H_{11a}), 2.71 (2H, br t, *J* = 5.9 Hz, H_{21}), 2.48 (1H, br dd, *J* = 16.0, 6.8 Hz, H_{11b}), 1.90 (2H, quin, *J* = 5.9 Hz, H_{22}); **^{13}C NMR** (151 MHz, $CDCl_3$): δ = 179.2, 175.2, 156.2, 154.3, 146.8, 139.0, 136.6, 133.3, 124.4 (1C, q, *J* = 280.8 Hz), 120.5, 118.4, 117.1, 117.1, 115.1, 110.7, 67.5, 52.7, 47.6 (1C, q, *J* = 33.7 Hz), 41.0, 39.2, 37.8, 33.9, 33.6, 26.2, 20.0; **IR** (neat, ν_{max} /cm^{-1}): 3330 (br), 2230, 1671, 1603, 1465, 1395, 1308, 1270, 1151, 1127, 1100, 1042, 912,

830, 729; **HRMS** (ESI): calc for $C_{25}H_{26}F_3N_4O_4$ $(M + H)^+$ 503.1906, found 503.1912; $[\alpha]_D^{20}$ = +26 (*c* 0.1, CH_2Cl_2).

Methyl (*S*)-2-(8-((*tert*-butyldimethylsilyl)oxy)-6-((4-methoxybenzyl)oxy)-3-oxo-2-(2,2,2-trifluoroethyl)-2,3,4,5-tetrahydro-1H-benzo[c]azepin-4-yl)acetate (239)

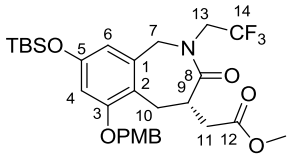

A flask containing DMAP (62.3 mg, 0.510 mmol), diacetoxycopper hydrate (56.0 mg, 0.281 mmol), activated 4 Å MS and methyl (*S*)-2-(8-((*tert*-butyldimethylsilyl)oxy)-3-oxo-6-(4,4,5,5-tetramethyl-1,3,2-dioxaborolan-2-yl)-2-(2,2,2-trifluoroethyl)-2,3,4,5-tetrahydro-1H-benzo[c]azepin-4-yl)acetate **(223)** (486 mg, 0.255 mmol) (a 1:3 mixture with **221**) in 4-methoxybenzyl alcohol (5 mL) was stirred in an open flask for 24 h, followed by the addition of Celite®, and purification using a 40 g silica column, eluting with 0 – 50 % EtOAc:cyclohexane. The desired fractions were combined and concentrated *in vacuo*, followed by dissolution of the resulting oil in EtOAc (5 mL) and cyclohexane (30 mL). The solution was cooled in an ice bath, and the remaining solution was separated from the precipitate, washing the precipitate with cyclohexane (10 mL). This process was repeated with the filtrate, to leave a colourless oil that was concentrated *in vacuo*. The resulting oil was purified using a 40 g silica column, eluting with 0 – 50 % EtOAc:cyclohexane, and the desired fractions were combined and concentrated *in vacuo*. The resulting oil was dissolved in MeOH (2 mL) and purified in two portions using an Xbridge™ Prep C18 column, eluting with 0 – 100 % MeCN:ammonium carbonate modified H_2O, and the desired fractions were combined and concentrated *in vacuo* to furnish methyl (*S*)-2-(8-((*tert*-butyldimethylsilyl)oxy)-6-((4-methoxybenzyl)oxy)-3-oxo-2-(2,2,2-trifluoroethyl)-2,3,4,5-tetrahydro-1H-benzo[c]azepin-4-yl)acetate **(239)** (45 mg, 0.077 mmol, 30 % yield) as a pale orange coloured gum which was used without further purification.

Methyl (*S*)-2-(8-hydroxy-6-((4-methoxybenzyl)oxy)-3-oxo-2-(2,2,2-trifluoroethyl)-2,3,4,5-tetrahydro-1H-benzo[c]azepin-4-yl)acetate (240)

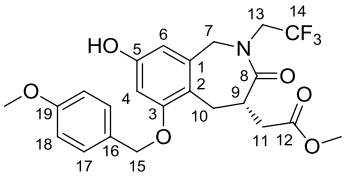

To a solution of methyl (*S*)-2-(8-((*tert*-butyldimethylsilyl)oxy)-6-((4-methoxybenzyl)oxy)-3-oxo-2-(2,2,2-trifluoroethyl)-2,3,4,5-tetrahydro-1H-benzo[c]azepin-4-yl)acetate **(239)** (45 mg, 0.077 mmol) in THF (3 mL) was added TBAF (1 M in THF, 0.093 mL, 0.093 mmol) and the solution was stirred for 30 min, followed by dilution with saturated aqueous ammonium chloride solution (10 mL) and EtOAc (10 mL). The layers were separated, and the aqueous layer was extracted with EtOAc (10 mL). The combined organic layers were filtered through a hydrophobic frit and concentrated *in vacuo*. The crude product was purified using a 4 g silica column, eluting with 0 – 50 % EtOAc:cyclohexane, and the desired fractions were combined and concentrated *in vacuo* to afford methyl (*S*)-2-(8-hydroxy-6-((4-methoxybenzyl)oxy)-3-oxo-2-(2,2,2-trifluoroethyl)-2,3,4,5-tetrahydro-1H-benzo[c]azepin-4-yl)acetate **(240)** (30.7 mg, 0.066 mmol, 85 % yield) as a white coloured solid.

LCMS t_R = 1.10 min (system B), 97 %, ES+ve *m/z* 468 $(M + H)^+$; **^{1}H NMR** (400 MHz, $CDCl_3$): δ = 7.30 – 7.26 (2H, m, H_{17}), 6.92 – 6.88 (2H, m, H_{18}), 6.42 (1H, d, *J* = 2.4 Hz, H_4), 6.19 (1H, d, *J* = 2.4 Hz, H_6), 5.94 (1H, br s, OH), 5.31 (1H, br d, *J* = 16.6 Hz, H_{7a}), 4.95 – 4.86 (2H, m, H_{15}), 4.23 – 4.08 (1H, m, H_{13a}), 3.93 – 3.79 (6H, m, OMe, H_{7b}, H_9, H_{13b}), 3.67 (3H, s, OMe), 3.02 (1H, dd, *J* = 16.9, 9.0 Hz, H_{11a}), 2.95 (1H, dd, *J* = 18.1, 3.4 Hz, H_{10a}), 2.61 (1H, dd, *J* = 17.6, 13.7 Hz, H_{10b}), 2.46 (1H, dd, *J* = 17.1, 4.9 Hz, H_{11b}); **^{13}C NMR** (101 MHz, $CDCl_3$): δ = 175.5, 173.1, 159.6, 158.3, 154.8, 134.9, 129.0, 128.9, 124.4 (1C, q, *J* = 280.2 Hz), 117.0, 114.2, 108.0, 99.9, 70.0, 55.4, 53.2, 52.0, 47.7 (1C, q, *J* = 34.5 Hz), 37.0, 36.6, 29.3; **IR** (neat, ν_{max} /cm^{-1}): 3323 (br), 1732, 1645, 1510,

1519, 1446, 1249, 1228, 1208, 1178, 1151, 1125, 1103, 1079, 1030, 1012, 830; **HRMS** (ESI): calc for $C_{23}H_{25}F_3NO_6$ $(M + H)^+$ 468.1634, found 468.1629; $[\alpha]_D^{20}$ = –58 (*c* 1.0, MeCN); **mp** 125 – 129 °C.

Methyl (*S*)-2-(6-((4-methoxybenzyl)oxy)-3-oxo-8-(2-(5,6,7,8-tetrahydro-1,8-naphthyridin-2-yl)ethoxy)-2-(2,2,2-trifluoroethyl)-2,3,4,5-tetrahydro-1H-benzo[c]azepin-4-yl)acetate (241)

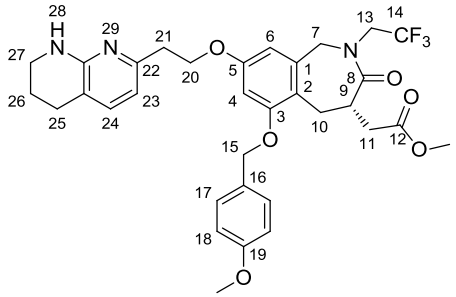

CMBP (0.031 mL, 0.117 mmol) was added to a stirring solution of 2-(5,6,7,8-tetrahydro-1,8-naphthyridin-2-yl)ethan-1-ol **(65)** (15.7 mg, 0.088 mmol) and methyl (*S*)-2-(8-hydroxy-6-((4-methoxybenzyl)oxy)-3-oxo-2-(2,2,2-trifluoroethyl)-2,3,4,5-tetrahydro-1H-benzo[c]azepin-4-yl)acetate **(240)** (27.4 mg, 0.059 mmol) in THF (1 mL) under nitrogen, and the vial was sealed and the solution was heated at 80 °C for 90 mins, followed by cooling to rt. Further portions of CMBP (0.031 mL, 0.117 mmol) and 2-(5,6,7,8-tetrahydro-1,8-naphthyridin-2-yl)ethan-1-ol **(65)** (15.7 mg, 0.088 mmol) were added, followed by heating for a further 2 h. The brown coloured solution was cooled, adsorbed onto Celite® and purified using a 4 g silica column, eluting with 0 – 80 % (EtOAc + 1 % NEt_3):cyclohexane, and the desired fractions were combined and concentrated *in vacuo*, followed by further purification using an Xbridge™ Prep C18 column, eluting with 0 – 100 % MeCN:ammonium carbonate modified H_2O, and the desired fractions were combined and concentrated *in vacuo* to furnish methyl (*S*)-2-(6-((4-methoxybenzyl)oxy)-3-oxo-8-(2-(5,6,7,8-tetrahydro-1,8-naphthyridin-2-yl)ethoxy)-2-(2,2,2-trifluoroethyl)-2,3,4,5-tetrahydro-1H-

benzo[c]azepin-4-yl)acetate **(241)** (19.6 mg, 0.031 mmol, 53 % yield) as a yellow coloured gum.

LCMS t_R = 1.34 min (system B), 100 %, ES+ve *m/z* 628 $(M + H)^+$; **^{1}H NMR** (400 MHz, $CDCl_3$): δ = 7.32 – 7.27 (2H, m, H_{17}), 7.08 (1H, d, *J* = 7.3 Hz, H_{24}), 6.93 – 6.89 (2H, m, H_{18}), 6.48 (1H, d, *J* = 2.4 Hz, H_4), 6.43 (1H, d, *J* = 7.3 Hz, H_{23}), 6.26 (1H, d, *J* = 2.0 Hz, H_6), 5.35 (1H, d, *J* = 16.6 Hz, H_{7a}), 4.96 – 4.89 (2H, m, H_{15}), 4.77 (1H, br s, NH), 4.30 – 4.18 (3H, m, H_{13a}, H_{20}), 3.94 – 3.78 (6H, m, OMe, H_{7b}, H_9 H_{13b}), 3.68 (3H, s, OMe), 3.40 (2H, td, *J* = 5.5, 2.7 Hz, H_{27}), 3.06 – 2.92 (4H, m, H_{10a}, H_{11a}, H_{21}), 2.70 (2H, t, *J* = 6.4 Hz, H_{25}), 2.62 (1H, dd, *J* = 17.9, 13.4 Hz, H_{10b}), 2.44 (dd, *J* = 16.9, 5.1 Hz, H_{11b}), 1.94 – 1.87 (2H, m, H_{26}); **^{13}C NMR** (101 MHz, $CDCl_3$): δ = 175.1, 172.8, 159.6, 158.1, 157.8, 156.1, 154.4, 136.8, 134.8, 129.0, 129.0, 124.5 (1C, q, *J* = 281.0 Hz), 117.5, 114.2, 114.1, 112.4, 106.7, 99.7, 70.1, 67.9, 55.4, 53.4, 51.9, 47.6 (1C, q, *J* = 34.5 Hz), 41.8, 37.8, 37.0, 36.6, 29.5, 26.5, 21.6; **IR** (neat, ν_{max} /cm^{-1}): 3411 (br), 3261 (br), 1734, 1673, 1587, 1514, 1462, 1435, 1381, 1350, 1321, 1267, 1249, 1181, 1127, 1072, 1030, 994, 828, 516; **HRMS** (ESI): calc for $C_{33}H_{37}F_3N_3O_6$ $(M + H)^+$ 628.2634, found 628.2637; $[\alpha]_D^{20}$ = –47 (*c* 0.5, MeCN).

Methyl (*S*)-2-(6-hydroxy-3-oxo-8-(2-(5,6,7,8-tetrahydro-1,8-naphthyridin-2-yl)ethoxy)-2-(2,2,2-trifluoroethyl)-2,3,4,5-tetrahydro-1H-benzo[c]azepin-4-yl)acetate (242)

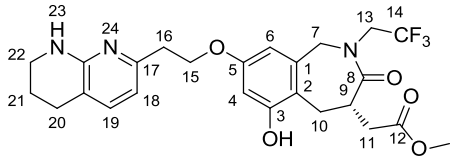

A mixture of methyl (*S*)-2-(6-((4-methoxybenzyl)oxy)-3-oxo-8-(2-(5,6,7,8-tetrahydro-1,8-naphthyridin-2-yl)ethoxy)-2-(2,2,2-trifluoroethyl)-2,3,4,5-tetrahydro-1H-benzo[c]azepin-4-yl)acetate **(241)** (14.7 mg, 0.023 mmol) and palladium on carbon (5 wt %) (50 mg, 0.023 mmol) in EtOH (5 mL) and MeCN (1 mL) was stirred in the

presence of hydrogen gas for 14 h, followed by filtration through Celite®, eluting with EtOH (40 mL). The filtrate was concentrated *in vacuo,* followed by purification using an XBridge™ Prep C18 column, eluting with 0 – 100 % MeCN:ammonium carbonate modified H_2O, and the desired fractions were combined and concentrated *in vacuo* to furnish methyl (*S*)-2-(6-hydroxy-3-oxo-8-(2-(5,6,7,8-tetrahydro-1,8-naphthyridin-2-yl)ethoxy)-2-(2,2,2-trifluoroethyl)-2,3,4,5-tetrahydro-1H-benzo[c]azepin-4-yl)acetate **(242)** (5.8 mg, 0.011 mmol, 49 % yield) as a colourless gum.

LCMS t_R = 1.09 min (system B), 95 %, ES+ve *m/z* 508 $(M + H)^+$; **^{1}H NMR** (600 MHz, $CDCl_3$): δ = 7.13 (1H, d, *J* = 7.3 Hz, H_{19}), 6.48 (1H, d, *J* = 7.3 Hz, H_{18}), 6.38 (1H, d, *J* = 2.2 Hz, H_4), 6.18 (1H, d, *J* = 2.2 Hz, H_6), 5.31 (1H, br d, *J* = 16.5 Hz, H_{7a}), 5.01 (1H, br s, OH), 4.31 - 4.22 (1H, m, H_{13a}), 4.13 - 4.07 (2H, m, H_{15}), 3.90 - 3.77 (3H, m, H_{7b}, H_9, H_{13b}), 3.69 (3H, s, OMe), 3.37 (2H, br t, *J* = 5.3 Hz, H_{22}), 3.04 (1H, dd, *J* = 16.9, 8.4 Hz, H_{11a}), 3.01 - 2.94 (3H, m, H_{10a}, H_{16}), 2.70 (2H, t, *J* = 6.2 Hz, H_{20}), 2.63 (1H, dd, *J* = 17.4, 13.8 Hz, H_{10b}), 2.47 (1H, dd, *J* = 17.1, 5.3 Hz, H_{11b}), 1.89 (2H, dt, *J* = 11.6, 6.1 Hz, H_{21}); **^{13}C NMR** (151 MHz, $CDCl_3$): δ = 175.2, 172.9, 157.6, 156.6, 155.8, 153.6, 137.6, 135.1, 124.5 (1C, q, *J* = 280.3 Hz), 116.0, 115.0, 112.5, 107.3, 101.1, 67.7, 53.3, 51.9, 47.5 (1C, q, *J* = 33.7 Hz), 41.7, 37.2, 37.0, 36.7, 29.5, 26.5, 21.2; **IR** (neat, ν_{max} /cm^{-1}): 3414 (br), 1732, 1667, 1591, 1513, 1464, 1436, 1354, 1320, 1269, 1183, 1150, 1126, 1105, 1053, 1028, 908, 831, 728, 647; **HRMS** (ESI): calc for $C_{25}H_{29}F_3N_3O_5$ $(M + H)^+$ 508.2059, found 508.2060; $[\alpha]_D^{20}$ = –51 (*c* 0.33, $CHCl_3$).

(*S*)-2-(6-Hydroxy-3-oxo-8-(2-(5,6,7,8-tetrahydro-1,8-naphthyridin-2-yl)ethoxy)-2-(2,2,2-trifluoroethyl)-2,3,4,5-tetrahydro-1H-benzo[c]azepin-4-yl)acetic acid (220)

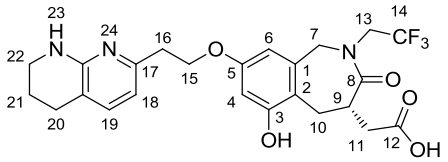

To a stirring solution of methyl (*S*)-2-(6-hydroxy-3-oxo-8-(2-(5,6,7,8-tetrahydro-1,8-naphthyridin-2-yl)ethoxy)-2-(2,2,2-trifluoroethyl)-2,3,4,5-tetrahydro-1H-benzo[c]azepin-4-yl)acetate **(242)** (5.8 mg, 0.011 mmol) in MeOH (1 mL) was added sodium hydroxide (2 M in H_2O, 0.029 mL, 0.057 mmol), and the reaction stirred at 35 °C for 2 h, followed by removal of the solvent using a flow of nitrogen gas. The residue was redissolved in H_2O (0.5 mL) and MeCN (0.5 mL), before neutralisation by dropwise addition of aqueous HCl (2 M). The resulting solution was purified using an XBridge™ Prep C18 column, eluting with 0 – 100 % MeCN:ammonium carbonate modified H_2O, and the desired fractions were combined and concentrated *in vacuo* to furnish (*S*)-2-(6-hydroxy-3-oxo-8-(2-(5,6,7,8-tetrahydro-1,8-naphthyridin-2-yl)ethoxy)-2-(2,2,2-trifluoroethyl)-2,3,4,5-tetrahydro-1H-benzo[c]azepin-4-yl)acetic acid **(220)** (4.0 mg, 8.11 µmol, 71 % yield) as a white coloured solid.

LCMS t_R = 0.76 min (system B), 100 %, ES+ve *m/z* 494 $(M + H)^+$; **^{1}H NMR** (600 MHz, DMSO-d_6): δ = 9.60 (1H, br s, COOH), 7.06 (1H, d, *J* = 7.3 Hz, H_{19}), 6.64 (1H, br s, NH), 6.35 (1H, d, *J* = 7.3 Hz, H_{18}), 6.33 (1H, d, *J* = 2.6 Hz, H_4), 6.28 (2H, app d, *J* = 2.6 Hz, H_6, OH), 5.27 (1H, br d, *J* = 16.5 Hz, H_{7a}), 4.22 – 4.11 (4H, m, H_{13}, H_{15}), 4.04 (1H, br d, *J* = 16.9 Hz, H_{7b}), 3.78 – 3.71 (1H, m, H_9), 3.26 – 3.24 (2H, m, H_{22}), 2.87 – 2.82 (3H, m, H_{10}, H_{16}), 2.67 (1H, br dd, *J* = 16.7, 8.6 Hz, H_{11a}), 2.62 (2H, br t, *J* = 6.1 Hz, H_{20}), 2.36 (1H, br dd, *J* = 16.5, 4.4 Hz, H_{11b}), 2.30 (1H, br dd, *J* = 17.6, 13.6 Hz, H_{10b}), 1.76 (2H, app dt, *J* = 11.6, 6.0, Hz, H_{21}); **^{13}C NMR** (151 MHz, DMSO-d_6): δ = 174.8, 173.1, 156.5, 156.3, 155.9, 153.8, 136.0, 135.7, 124.7 (1C, q, *J* = 280.8 Hz), 115.1, 112.9, 110.7, 109.5, 105.8, 100.8, 66.9, 52.2, 46.6 (1C, q, *J* = 32.1 Hz), 40.7, 36.9, 35.8, 28.8, 26.0, 20.9; **IR** (neat, ν_{max} /cm^{-1}): 3343 (br), 1649, 1591, 1555, 1353, 1320, 1269, 1185, 1143, 1124, 1054, 831, 753, 677, 617, 490; **HRMS** (ESI): calc for $C_{24}H_{27}F_3N_3O_5$ $(M + H)^+$ 494.1903, found 494.1917; $[\alpha]_D^{20}$ *could not be measured due to product insolubility in appropriate solvents*; **mp** 175 – 179 °C.

Methyl (*S*)-2-(8-hydroxy-7-methyl-3-oxo-2-(2,2,2-trifluoroethyl)-2,3,4,5-tetrahydro-1H-benzo[c]azepin-4-yl)acetate (244), Methyl (*S*)-2-(8-hydroxy-3-oxo-7-phenyl-2-(2,2,2-trifluoroethyl)-2,3,4,5-tetrahydro-1H-benzo[c]azepin-4-yl)acetate (246)

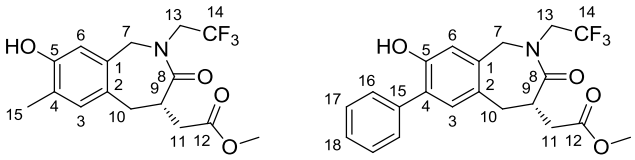

To a flask containing potassium phosphate dibasic (457 mg, 2.62 mmol), $Pd(Ph_3P)_4$ (152 mg, 0.131 mmol), methyl iodide (0.082 mL, 1.312 mmol), and methyl (*S*)-2-(8-hydroxy-3-oxo-7-(4,4,5,5-tetramethyl-1,3,2-dioxaborolan-2-yl)-2-(2,2,2-trifluoroethyl)-2,3,4,5-tetrahydro-1H-benzo[c]azepin-4-yl)acetate **(222)** (600 mg, 1.312 mmol) was purged with nitrogen and DMF (9 mL), EtOH (1 mL) and H_2O (1 mL) was added, followed by heating to 80 °C for 2 h followed by cooling to rt. The mixture was diluted with EtOAc (50 mL) and H_2O (50 mL) and the layers were separated. The organic layer was washed with 10 % aqueous lithium chloride solution (2 x 50 mL), filtered through a hydrophobic frit and concentrated *in vacuo*. The crude product was purified using a 24 g silica column, eluting with 0 – 50 % EtOAc:cyclohexane, and the desired fractions were combined and concentrated *in vacuo*, followed by further purification using an Xbridge™ Prep C18 column, eluting with 0 – 100 % MeCN:ammonium carbonate modified H_2O, and the desired fractions were combined and concentrated *in vacuo* to yield methyl (*S*)-2-(8-hydroxy-7-methyl-3-oxo-2-(2,2,2-trifluoroethyl)-2,3,4,5-tetrahydro-1H-benzo[c]azepin-4-yl)acetate **(244)** (70 mg, 0.203 mmol, 15 % yield) as a yellow coloured gum, and side product methyl (*S*)-2-(8-hydroxy-3-oxo-7-phenyl-2-(2,2,2-trifluoroethyl)-2,3,4,5-tetrahydro-1H-benzo[c]azepin-4-yl)acetate **(246)** (13 mg, 0.032 mmol, 2 % yield) as a pale yellow coloured oil.

244:

LCMS t_R = 0.95 min (system B), 88 %, ES+ve *m/z* 346 $(M + H)^+$; **^{1}H NMR** (400 MHz, $CDCl_3$): δ = 6.83 (1H, s, H_3), 6.51 (1H, s, H_6), 5.91 (1H, br s, OH), 5.25 (1H, d, *J* = 17.1

Hz, H_{7a}), 4.21 – 4.08 (1H, m, H_{13a}), 3.99 – 3.87 (2H, m, H_{7b}, H_{13b}), 3.86 – 3.78 (1H, m, H_9), 3.69 (3H, s, OMe), 3.05 – 2.91 (2H, m, H_{10a}, H_{11a}), 2.89 – 2.79 (1H, m, H_{10b}), 2.46 (2H, dd, *J* = 16.9, 5.6 Hz, H_{11b}), 2.17 (3H, s, H_{15}); **^{13}C NMR** (101 MHz, $CDCl_3$): δ = 175.4, 172.9, 152.4, 133.2, 131.5, 127.3, 124.4, 124.4 (1C, q, *J* = 280.7 Hz), 115.3, 52.8, 52.0, 47.8 (1C, q, *J* = 33.7 Hz), 37.2, 36.7, 34.5, 15.5; **IR** (neat, ν_{max} /cm^{-1}): 3284 (br), 1732, 1643, 1616, 1448, 1413, 1356, 1259, 1224, 1177, 1162, 1114, 1075, 1029, 880, 830, 773, 582; **HRMS** (ESI): calc for $C_{16}H_{19}F_3NO_4$ $(M + H)^+$ 346.1266, found 346.1266; $[\alpha]_D^{20}$ = –100 (*c* 1.0, MeOH).

246:

LCMS t_R = 1.12 min (system B), 95 %, ES+ve *m/z* 408 $(M + H)^+$; **^{1}H NMR** (400 MHz, $CDCl_3$): δ = 7.51 – 7.46 (2H, m, H_{17}), 7.44 – 7.37 (3H, m, H_{16}, H_{18}), 6.99 (1H, s, H_3), 6.73 (1H, s, H_6), 5.34 (1H, d, *J* = 16.6 Hz, H_{7a}), 5.29 (1H, s, OH), 4.20 (1H, dq, *J* = 15.2, 8.8 Hz, H_{13a}), 4.07 – 3.93 (2H, m, H_{7b}, H_{13b}), 3.91 – 3.81 (1H, m, H_9), 3.70 (3H, s, OMe), 3.08 – 2.98 (2H, m, H_{10a}, H_{11a}), 2.97 – 2.87 (1H, m, H_{10b}), 2.47 (1H, dd, *J* = 16.6, 5.9 Hz, H_{11b}); **^{13}C NMR** (101 MHz, $CDCl_3$): δ = 175.0, 172.7, 150.6, 136.4, 133.9, 132.5, 129.5, 129.0, 128.3, 128.3, 128.2, 124.4 (1C, q, *J* = 280.2 Hz), 116.3, 52.9, 52.0, 47.9 (1C, q, *J* = 33.7 Hz), 37.2, 36.7, 34.6; **IR** (neat, ν_{max} /cm^{-1}): 3334 (br), 1733, 1651, 1407, 1339, 1266, 1242, 1196, 1151, 1122, 1096, 772, 729, 699; **HRMS** (ESI): calc for $C_{21}H_{21}F_3NO_4$ $(M + H)^+$ 408.1423, found 408.1424; $[\alpha]_D^{20}$ = –86 (*c* 0.5, MeOH).

Methyl (*S*)-2-(7-methyl-3-oxo-8-(2-(5,6,7,8-tetrahydro-1,8-naphthyridin-2-yl)ethoxy)-2-(2,2,2-trifluoroethyl)-2,3,4,5-tetrahydro-1H-benzo[c]azepin-4-yl)acetate (245)

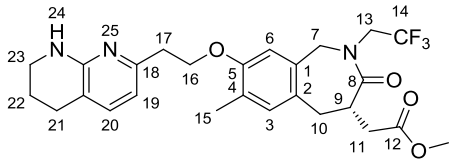

CMBP (0.130 mL, 0.495 mmol) was added to a stirring solution of 2-(5,6,7,8-tetrahydro-1,8-naphthyridin-2-yl)ethan-1-ol **(65)** (73.6 mg, 0.413 mmol) and methyl (*S*)-2-(8-hydroxy-7-methyl-3-oxo-2-(2,2,2-trifluoroethyl)-2,3,4,5-tetrahydro-1H-benzo[c]azepin-4-yl)acetate **(244)** (57 mg, 0.165 mmol) in THF (1 mL) under nitrogen, and the solution was heated at 80 °C for 1.5 h, followed by cooling to rt. The brown coloured solution was cooled, and purified using an Xbridge™ Prep C18 column, eluting with 0 – 100 % MeCN:ammonium carbonate modified H_2O, and the desired fractions were combined and concentrated *in vacuo* to furnish methyl (*S*)-2-(7-methyl-3-oxo-8-(2-(5,6,7,8-tetrahydro-1,8-naphthyridin-2-yl)ethoxy)-2-(2,2,2-trifluoroethyl)-2,3,4,5-tetrahydro-1H-benzo[c]azepin-4-yl)acetate **(245)** (42 mg, 0.083 mmol, 50 % yield) as a yellow coloured gum.

LCMS t_R = 1.28 min (system B), 96 %, ES+ve *m/z* 506 $(M + H)^+$; **^{1}H NMR** (400 MHz, $CDCl_3$): δ = 7.08 (1H, d, *J* = 7.3 Hz, H_{20}), 6.83 (1H, s, H_6), 6.51 (1H, s, H_3), 6.45 (1H, d, *J* = 7.3 Hz, H_{19}), 5.30 (1H, d, *J* = 16.6 Hz, H_{7a}), 5.06 (1H, br s, NH), 4.27 – 4.12 (3H, m, H_{13a}, H_{16}), 3.98 – 3.86 (2H, m, H_{7b}, H_{13b}), 3.81 (1H, ddt, *J* = 13.1, 8.2, 5.0 Hz, H_9), 3.69 (3H, s, OMe), 3.42 – 3.37 (2H, m, H_{23}), 3.05 – 2.91 (4H, m, H_{10a}, H_{11a}, H_{17}), 2.89 – 2.79 (1H, m, H_{10b}), 2.69 (2H, t, *J* = 6.4 Hz, H_{21}), 2.43 (1H, dd, *J* = 16.9, 5.6 Hz, H_{11b}), 2.10 (3H, s, H_{15}), 1.95 – 1.86 (2H, m, H_{22}); **^{13}C NMR** (101 MHz, $CDCl_3$): δ = 175.0, 172.7, 155.9, 155.2, 154.1, 136.9, 132.9, 131.2, 127.4, 127.1, 124.4 (1C, q, *J* = 280.2 Hz), 114.3, 112.4, 111.8, 67.9, 53.2, 51.9, 47.8 (1C, q, *J* = 34.0 Hz), 41.7, 37.7, 37.1, 36.7, 34.6, 26.5, 21.5, 15.8; **IR** (neat, ν_{max} /cm^{-1}): 3402 (br), 3253 (br), 1736, 1668, 1587, 1511, 1462, 1321, 1268, 1245, 1193, 1149, 1130, 1087, 1057, 1031, 1007, 830, 764; **HRMS** (ESI): calc for $C_{26}H_{31}F_3N_3O_4$ $(M + H)^+$ 506.2267, found 506.2273; $[\boldsymbol{\alpha}]_D^{20}$ = –76 (*c* 0.5, MeOH).

(*S*)-2-(7-Methyl-3-oxo-8-(2-(5,6,7,8-tetrahydro-1,8-naphthyridin-2-yl)ethoxy)-2-(2,2,2-trifluoroethyl)-2,3,4,5-tetrahydro-1H-benzo[c]azepin-4-yl)acetic acid (243)

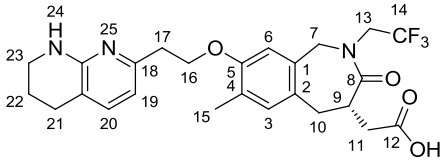

To a stirring solution of methyl (*S*)-2-(7-methyl-3-oxo-8-(2-(5,6,7,8-tetrahydro-1,8-naphthyridin-2-yl)ethoxy)-2-(2,2,2-trifluoroethyl)-2,3,4,5-tetrahydro-1H-benzo[c]azepin-4-yl)acetate **(245)** (39.5 mg, 0.078 mmol) in MeOH (2 mL) was added sodium hydroxide (2 M in H_2O, 0.195 mL, 0.391 mmol), and the reaction stirred at 35 °C for 2 h, followed by removal of the solvent using a flow of nitrogen gas. The residue was redissolved in H_2O (0.5 mL) and MeCN (0.5 mL), before adjustment of the pH to 3 using 2 M aqueous hydrochloric acid. The resulting solution was purified using an XBridge^{TM} Prep C18 column, eluting with 0 – 100 % MeCN:ammonium carbonate modified H_2O, and the desired fractions were combined and concentrated *in vacuo* to furnish (*S*)-2-(7-methyl-3-oxo-8-(2-(5,6,7,8-tetrahydro-1,8-naphthyridin-2-yl)ethoxy)-2-(2,2,2-trifluoroethyl)-2,3,4,5-tetrahydro-1H-benzo[c]azepin-4-yl)acetic acid **(243)** (38 mg, 0.077 mmol, 99 % yield) as a pale orange coloured gum.

LCMS t_R = 0.83 min (system B), 100 %, ES+ve *m/z* 492 $(M + H)^+$; **^{1}H NMR** (400 MHz, DMSO-d_6): δ = 12.11 (1H, s, COOH), 7.07 (1H, d, *J* = 7.3 Hz, H_{20}), 6.84 (1H, s, H_3), 6.79 (1H, s, H_6), 6.37 (1H, d, *J* = 7.3 Hz, H_{19}), 6.30 (1H, br s, OH), 5.26 (1H, br d, *J* = 16.6 Hz, H_{7a}), 4.24 – 4.09 (5H, m, H_{7b}, H_{13}, H_{16}), 3.80 – 3.70 (1H, m, H_9), 3.27 – 3.21 (2H, m, H_{23}), 2.95 (1H, br dd, *J* = 17.4, 3.7 Hz, H_{10a}), 2.89 (2H, t, *J* = 6.8 Hz, H_{17}), 2.72 – 2.56 (4H, m, H_{10b}, H_{11a}, H_{21}), 2.37 (1H, dd, *J* = 17.1, 4.9 Hz, H_{11b}), 2.02 (3H, s, H_{15}), 1.75 (2H, quin, *J* = 5.9 Hz, H_{22}); **^{13}C NMR** (101 MHz, DMSO-d_6): δ = 174.7, 173.0, 155.8, 154.1, 153.7, 136.0, 132.3, 132.1, 127.4, 125.0, 124.7 (1C, q, *J* = 281.0 Hz), 113.0, 112.1, 110.8, 67.4, 51.8, 46.7 (1C, q, *J* = 33.0 Hz), 40.7, 37.0, 36.4, 36.1, 33.7, 26.0, 20.9, 15.3; **IR** (neat, ν_{max} /cm^{-1}): 3301 (br), 1668, 1511, 1397, 1321, 1266, 1193, 1151, 1129, 1086,

748, 666; **HRMS** (ESI): calc for $C_{25}H_{29}F_3N_3O_4$ $(M + H)^+$ 492.2110, found 492.2110; $[\alpha]_D^{20}$ = –59 (*c* 1.0, $CHCl_3$).

4.4.2 Computational details

The first homology model for the $\alpha_V\beta_1$ integrin was developed by co-worker Pal in our laboratories, and has been detailed in a previously published study.[202] For the α_V part of the receptor, the crystal structure of the extracellular portion of the $\alpha_V\beta_6$ integrin was used, complexed to an RGD-containing peptide (accessed from the Protein Data Bank, ID: 4UM9). For the β_1 part of the receptor, the crystal structure of the $\alpha_5\beta_1$ integrin (accessed from the Protein Data Bank, ID: 3VI4) was used.

The structures were imported into MOE, the amino acid sequences were aligned, and the structures of the two proteins were superposed. Unwanted chains were removed (α_5 for 3VI4, β_6 for 4UM9), and the protein was truncated to retain only proteins in and surrounding the binding pocket for grid calculation. Calcium atoms, one of the ligands, and H_2O molecules were also deleted. The structure was protonated using the Protonate3D function in MOE, using default settings, then the model was imported into Maestro in Schrödinger. The receptor grid was then calculated for this protein using the originally crystallised RGD-containing peptides to define the binding site. This grid was then used in subsequent docking calculations.

With the grid having been generated, the prospective ligands were imported into Maestro and prepared for docking using LigPrep.[259] A tautomer with the correct ionisation (anion at the carboxylate, cation at the aminopyridine or tetrahydronaphthyridine) was selected from the LigPrep output. If no such tautomers had the required azepine ring conformation, then one tautomer was used as the input for a conformation search using MacroModel (using the OPLS3 forcefield, H_2O as the solvent).[163]

From the output of this conformation search, a conformation with the correct azepine ring conformation was selected, and docked into the previously prepared grid using Glide, creating up to ten poses per ligand, without allowing for sampling of the azepine ring conformation during the docking.[204] If the result of this docking did not appear to fit the receptor well, the best-fitting conformer was re-docked using the same approach in order attempt to find a better-fitting ligand pose. After an appropriate conformation was found, the conformation, along with the receptor, was exported to MOE for creation of the visualisations used herein.

The second homology model for the $\alpha_V\beta_1$ integrin was created by co-worker Pal in a similar fashion.[238] This homology used an alternative crystal structure of the $\alpha_5\beta_1$ integrin (accessed from the Protein Data Bank, ID: 4WK4) for the β_1 part of the receptor, but used the $\alpha_V\beta_6$ crystal structure with compound **1** bound, which has not been added to the Protein Data Bank, for the α_V part of the receptor.

For the dockings into the $\alpha_V\beta_3$ integrin, a receptor grid was calculated as described above, but using a $\alpha_V\beta_3$ crystal structure (accessed from the Protein Data Bank, ID:1L5G) with an RGD-containing peptide bound in the active site.

The docking grid files as well as SD files for the docked poses of all compounds, are included in the electronic supporting information.

For the dihedral angle analyses, the searches of the Cambridge structural database (CSD) were carried out using the Mogul software.[209] The substructures detailed in the figures in the main text were inputted, and the appropriate dihedral angles searched. The databases searched were the CSD version 5.40, the CSD February 2019 update, and the GSK internal structure database (November 2017 update), and the contributions of each of these were coloured green and included in the distribution of dihedral angles shown in the figures in the main text.

4.5 Biological and physicochemical measurements

4.5.1 Integrin cell adhesion assay (using $\alpha_V\beta_6$ as a representative example)

The integrin cell adhesion assays were carried out by co-worker Rowedder within our laboratories. Compounds were screened using a cell adhesion assay format using a modified K562 cell line that expresses $\alpha_V\beta_6$ on the cell surface. Using the glutathione S-transferase fusion proteins, the minimal RGD integrin binding loop in LAP β1 (Ace-His-Gly-Arg-Gly-Asp-Leu-Gly-Arg-Leu-Lys-Lys-NH_2) was coated onto the surface of the plastic well, followed by coating with 3 % bovine serum albumin solution to fill any gaps, hence avoiding non-specific binding. Once added to the well, a $MgCl_2$ solution was added, followed by the compounds being tested. The cells were incubated with a fluorescent indicator, BCECF-AM, for 10 min, to label the cells, then added to the plates and incubated for 30 min. After washing to remove any cells no longer bound to the LAP ligand, the remaining cells were lysed to release the fluorescent dye, and a fluorescent read out was made on the Envision plate reader.

4.5.2 AMP assay

AMP assay measurements were performed by co-worker Johnson within our laboratories. The artificial membrane permeability is a high throughput plate-based assay that measures the speed of permeation of a compound through a phospholipid membrane at pH 7.4.The lipid is egg phosphatidyl choline (1.8 %) and cholesterol (1 %) dissolved in ^{n}decane. This was applied to the bottom of the microfiltration filter inserts in a Transwell plate. Phosphate buffer (50mM Na_2HPO_4 with 0.5 % 2-hydroxypropyl-b-cyclodextrin), pH 7.4 was added to the top and bottom of the plate. The lipids are allowed to form bilayers across the small holes in the filter. The

permeation experiment was initiated by adding the compound to the bottom well and stopped after a pre-determined time had elapsed. The compound permeates through the membrane to enter the acceptor well. The compound concentration in both the donor and acceptor compartments was determined by liquid chromatography after 3 h incubation at rt.[273,102] The permeability (log $_{Papp}$) measuring how fast molecules pass through the black lipid membrane was expressed in nm/s. Each value is an average of the rate measured on two different plates.[116]

4.5.3 MDCK permeability assay

The MDCK permeability assay was performed by Cyprotex Limited. The permeability across an MDCK-MDR1 cell monolayer was measured at a starting concentration of 3 µM in the presence of GF120918, an efflux inhibitor. The pH of the donor and receiver compartments was 7.4 (Hanks' balanced salt solution). Incubations were carried out in an atmosphere of 5 % CO_2 with a relative humidity of 95 % at 37 °C for 1 h. Apical and basolateral samples were diluted for analysis by LC-MS/MS. The S39 integrity of the monolayers throughout the experiment was checked by monitoring Lucifer yellow permeation using fluorometric analysis. The values recorded herein are the permeabilities measured in the apical to basolateral direction.

4.5.4 pK_a determination and logD measurement

Measurements made on the Sirius T3 were carried out by co-worker Reid within our laboratories. The Sirius T3 (first Sirius Analytical Inc., UK, now Pion, Inc, US) instrument was used for pK_a determination of the compounds and subsequent logD measurement.[173] The pK_a determination was based on acid-base titration (using 1 M HCl and 1 M NaOH solutions to adjust the pH) and the protonation/deprotonation of

the molecule was measured either by UV spectroscopy or potentiometrically. The pK_a value was calculated from the pH where the 50 % of the protonated and unprotonated form of the molecules were present.

The UV-metric method provided pK_a results for samples with chromophores whose UV absorbance changed as a function of pH. The UV absorbance is monitored over 54 pH values in a buffered solution in 5 min. When the ionization centre was far from the UV chromophore, pH-metric method based on potentiometric acid-base titration was used. The pH of each point in the titration curve was calculated using equations that contain the pK_a, and the calculated points were fitted to the measured curve by manipulating the pK_a. The pK_a that provided the best fit was taken to be the measured pK_a. If the compound precipitated at some point during the pH titration, a co-solvent method using methanol is applied using various concentration of co-solvent. The pK_a in H_2O was calculated using the Yasuda-Shedlovsky extrapolation method. [274,275]

For the logD measurements, the potentiometric titration was carried out in the same manner as for the pK_a measurement, except that it was carried out in the presence of various ratios of water and organic co-solvent. To a vial containing the weighed solid was added water-saturated octanol and an aqueous KCl solution. The titration was then carried out, collecting 71 data points between pH 1.5 and 12.5. For each data point, the calculated pH was compared to the measured pH of the solution. The pH electrode responds only to the species in the aqueous phase, and ionisation of the compound being measured affects the measured pH of the solution. The pK_a of the compound is perturbed by the presence of the octanol or other hydrocarbon in the vial, and so the pH-metric method is capable of using mass balance and charge balance equations which include the aqueous pK_a and D values for the compound.[276] The pK_a value having already been measured, the D value is varied to fit the predicted pH of the solution to the measured value, and the fitted D value is taken to generate the logD of the compound at that pH.

4.5.5 ChromlogD measurement

ChromlogD measurements were carried out by co-worker Reid within our laboratories. The Chromatographic hydrophobicity index (CHI) values were measured using reversed phase HPLC column (50 x 2 mm 3 µM Gemini NX C18, Phenomenex, UK) with fast MeCN gradient at starting mobile phase of pHs 2, 7.4 and 10.5.[277] CHI values were derived directly from the gradient retention times by using a calibration line obtained for standard compounds. The CHI value approximates to the volume % organic concentration when the compound elutes. CHI was linearly transformed into ChromlogD by least-square fitting of experimental CHI values to calculated ClogP values for over 20,000 research compounds using the following formula: ChromlogD = 0.0857CHI-2.00.[174]

4.5.6 Cell concentration assay measurement

The cell concentration assay was performed by co-worker Johnson within our laboratories. The protocol for this assay has been described in detail elsewhere,[278] but it first involved the treatment of HeLa cells with the compound, followed by incubation for 2.5 h at 37 °C, 5 % CO_2 and 85 % humidity. Other no-cell controls were also incubated for comparison. After, the samples containing cells were washed to remove any compound that had not penetrated into the cells. The cells were lysed using MPER detergent, centrifuged, and the appropriate fractions analysed using Rapidfire-MS/MS. The data is reported as PΔC, which is equal to the log(concentration of compound in the cell/concentration of compound in the no-cell control).

4.5.7 *In vivo* rat pharmacokinetics

All animal studies were ethically reviewed and carried out in accordance with Animals (Scientific Procedures) Act 1986 and the GSK Policy on the Care, Welfare and Treatment of Animals, and were carried out by co-workers Barrett and Hogg within our laboratories.[117,192] The animal studies detailed herein were carried out on Wistar-Han rats. For the AUC measurements of compounds **1** and **15**, the values were the mean of measurement on three animals in each case. For compounds **107** and **108**, the values are the result of measurements on a single animal in each case (performed in an IV/*per os* (PO) crossover experiment). For compounds **1** (2 mg / kg dosing) and **15** (1 mg / kg dosing), the compounds were dissolved in 0.5 % hydroxypropyl methylcellulose at a concentration of 0.1 mg / mL (the formulation of compound **15** was also contained 0.2 % Tween80), and dosed by oral gavage. Blood samples were collected up to 7 h *via* a tail vein cannula, and additional sampling up to 24 h *via* direct tail venepuncture. For compound **1**, these measurements were carried out as a part of an IV/PO crossover experiment, whereas for **15** the compound was only administered orally.

For compounds **107** and **108** (both 1 mg / kg dosing), the compounds were first dosed IV, at 0.2 mg / mL, in a saline solution, *via* the femoral cannula. Blood samples were collected from the jugular cannula up to 24 h. After a minimum of three days, the animals were then dosed PO. The compounds were dosed dissolved in 0.5 % hydroxypropyl methylcellulose at a concentration of 0.1 mg / mL, and dosed by oral gavage. Blood samples were taken from the jugular cannula.

For all cases, blood samples were centrifuged to obtain plasma, which was stored frozen at –20 °C prior to analysis. The plasma samples were diluted with MeCN containing an internal standard, and centrifuged. Supernatants were concentrated under nitrogen and redissolved in MeCN:H_2O (1:9), and the concentrations of the compounds were determined by LC/MS-MS. For compounds **1** and **15**, the mean

AUCs were calculated, and dose-adjusted for comparison of the two values. For compounds **107** and **108**, the other PK parameters were calculated from the IV and PO blood concentrations.

Chapter 5: Appendices

5.1 Appendix A: Manufacturing route to 98

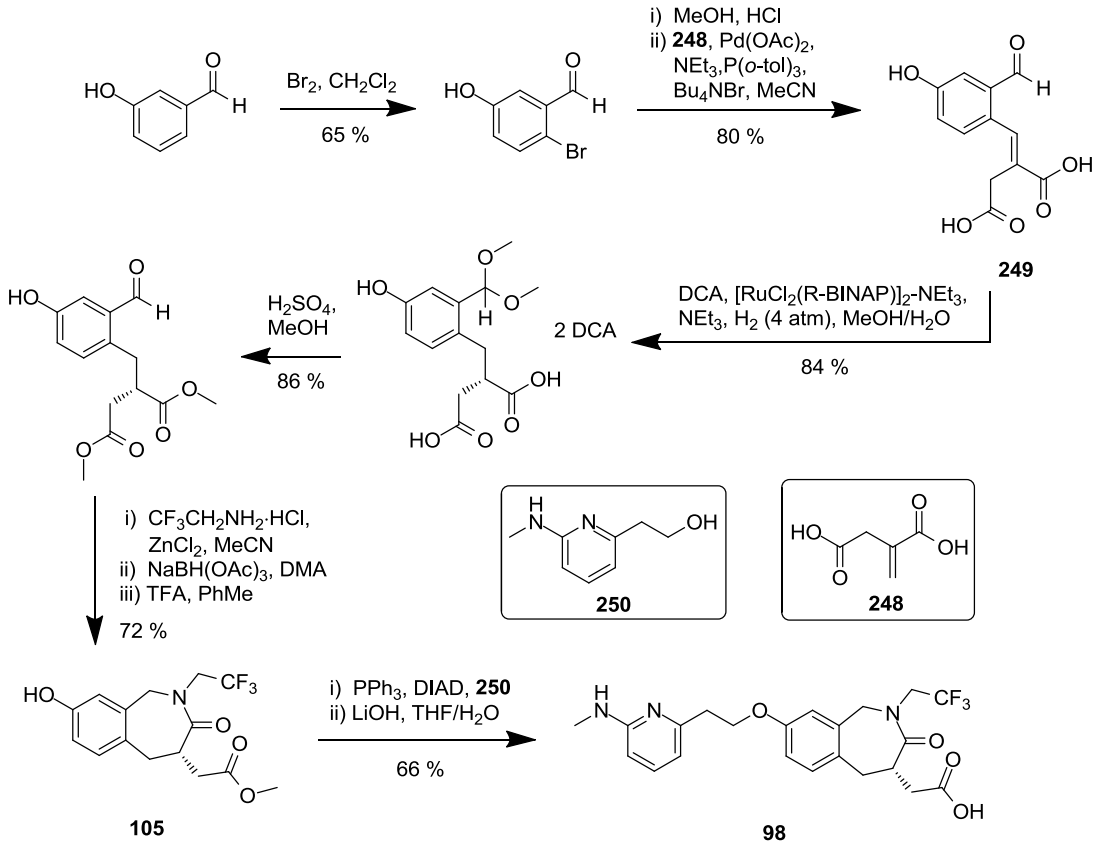

Scheme 100 *The manufacturing route to **98**, also involving a Heck reaction, followed by enantioselective reduction of **249**, followed by cyclisation and Mitsunobu reaction with alcohol **250***

This route began on 100 kg scale, and achieved the synthesis of **98** as a single enantiomer in seven steps, with a 15 % overall yield.[189] Like the medicinal chemistry route to similar analogues, the approach involved a Heck reaction with itaconic acid **(248)** to give **249** in high yield and with high selectivity for the *E*-product **(Scheme 100)**. The reaction itself was carried out on the dimethyl acetal, which was formed *in situ*, rather than on the aldehyde substrate itself, since Heck reaction of the aldehyde led to intramolecular aldol reaction of the product. The

acetal was then deprotected upon work up. A novel stereoselective reduction of alkene **249** was carried out, yielding the product in 90 – 95 % *ee*. A screen of crystallisation conditions then showed that recrystallisation of the dicyclohexylamine (DCA) salt could give the product at >99 % *ee*. Directly adding the DCA to the reaction mixture was found to give the crude salt in 98 % *ee*. The final compound **98** was then delivered in a similar way to the medicinal chemistry route to **97**, after a zinc-promoted reductive amination reaction. It was hoped that the Mitsunobu reaction could be avoided on scale, but alcohol **250**, as well as corresponding primary alkyl halides and sulfonates **(251)**, proved susceptible to elimination to form the undesired vinyl pyridine **252** when reacted with a range of alkoxide salts of alcohol **105 (Scheme 101)**. This meant that Williamson etherification was not possible and the Mitsunobu was required instead.[279] A final crystallisation after the final ester hydrolysis gave **98**.

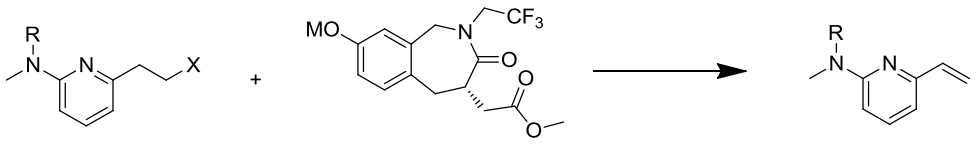

251 **252**

R = H, Boc
X = Cl, Br, I, Ms, Ts, Ns, OTf

M = Li, Na, K, Cs, Ce, Mg, Ba, Ca, pyridine-H, Et_3NH, DIPEA-H

Scheme 101 *The problematic attempted Williamson etherification using* ***251****, which often eliminated to give vinyl pyridine* ***252*** *as an undesired side product, meaning that the reaction was not superior to the Mitsunobu reaction, despite a range of alkoxide salts and leaving groups on* ***251*** *being tried in the reaction*

Chapter 6: References

(1) Wynn, T. A. *J. Pathol.* **2008**, *214*, 199–210.

(2) Nanthakumar, C. B.; Hatley, R. J. D.; Lemma, S.; Gauldie, J.; Marshall, R. P.; Macdonald, S. J. F. *Nat. Rev. Drug Discov.* **2015**, *14*, 693–720.

(3) Rockey, D. C.; Bell, P. D.; Hill, J. A. *N. Engl. J. Med.* **2015**, *372*, 1138–1149.

(4) Ellis, E.; Mann, D. *J. Hepatol.* **2012**, *56*, 1171–1180.

(5) Hosenpud, J.; Bennett, L.; Keck, B. *Lancet* **1998**, *351*, 24–27.

(6) Caminati, A.; Cassandro, R.; Torre, O.; Harari, S. *Eur. Respir. Rev.* **2017**, *26*, 170047.

(7) Drakopanagiotakis, F.; Xifteri, A.; Polychronopoulos, V.; Bouros, D. *Eur. Respir. J.* **2008**, *32*, 1631–1638.

(8) Liu, Y.-M.; Nepali, K.; Liou, J.-P. *J. Med. Chem.* **2017**, *60*, 527–533.

(9) Xaubet, A.; Ancochea, J.; Molina-Molina, M. *Med. Clínica English Ed.* **2017**, *148*, 170–175.

(10) Raghu, G.; Collard, H. R.; Egan, J. J.; Martinez, F. J.; Behr, J.; Brown, K. K.; Colby, T. V.; Cordier, J.-F.; Flaherty, K. R.; Lasky, J. A.; Lynch, D. A.; Ryu, J. H.; Swigris, J. J.; Wells, A. U.; Ancochea, J.; Bouros, D.; Carvalho, C.; Costabel, U.; Ebina, M.; Hansell, D. M.; Johkoh, T.; Kim, D. S.; King, T. E.; Kondoh, Y.; Myers, J.; Müller, N. L.; Nicholson, A. G.; Richeldi, L.; Selman, M.; Dudden, R. F.; Griss, B. S.; Protzko, S. L.; Schünemann, H. J. *Am. J. Respir. Crit. Care Med.* **2011**, *183*, 788–824.

(11) Coultas, D. B.; Zumwalt, R. E.; Black, W. C.; Sobonya, R. E. *Am. J. Respir. Crit. Care Med.* **1994**, *150*, 967–972.

(12) Thannikal, V. J.; Toews, G. B.; White, E. S.; Lynch, J. P.; Martinez, F. J. *Annu. Rev. Med.* **2004**, *55*, 395–417.

(13) Gribbin, J.; Hubbard, R. B.; Le Jeune, I.; Smith, C. J. P.; West, J.; Tata, L. J. *Thorax* **2006**, *61*, 980–985.

(14) Raghu, G.; Weycker, D.; Edelsberg, J.; Bradford, W. Z.; Oster, G. *Am. J. Respir. Crit. Care Med.* **2006**, *174*, 810–816.

(15) Schwartz, D. A.; Helmers, R. A.; Galvin, J. R.; Van-Fossen, S.; Frees, K. L.; Drayton, C. S.; Burmeister, L. F.; Hunninghake, G. W. *Am. J. Respir. Crit. Care Med* **1994**, *149*, 450–454.

(16) Collard, H. R.; Chen, S.-Y.; Yeh, W.-S.; Li, Q.; Lee, Y.-C.; Wang, A.; Raghu, G. *Ann. Am. Thorac. Soc.* **2015**, *12*, 981–987.

(17) Datta, A.; Scotton, C. J.; Chambers, R. C. *Br. J. Pharmacol.* **2011**, *163*, 141–172.

(18) Maher, T. M.; Evans, I. C.; Bottoms, S. E.; Mercer, P. F.; Thorley, A. J.; Nicholson, A. G.; Laurent, G. J.; Tetley, T. D.; Chambers, R. C.; McAnulty, R. J. *Am. J. Respir. Crit. Care Med.* **2010**, *182*, 73–82.

(19) Friedman, S. L.; Sheppard, D.; Duffield, J. S.; Violette, S. *Sci. Transl. Med.* **2013**, *5*, 167.

(20) Levental, K.; Yu, H.; Kass, L.; Lakins, J. *Cell* **2009**, *139*, 891–906.

(21) Grinnell, F.; Zhu, M.; Carlson, M. A.; Abrams, J. M. *Exp. Cell Res.* **1999**, *248*, 608–619.

(22) Liu, F.; Mih, J. D.; Shea, B. S.; Kho, A. T.; Sharif, A. S.; Tager, A. M.; Tschumperlin, D. J. *J. Cell Biol.* **2010**, *190*, 693–706.

(23) Nicholson, A. G.; Fulford, L. G.; Colby, T. V.; du Bois, R. M.; Hansell, D. M.; Wells, A. U. *Am. J. Respir. Crit. Care Med.* **2002**, *166*, 173–177.

(24) Hinz, B.; Phan, S. H.; Thannickal, V. J.; Galli, A.; Bochaton-Piallat, M.; Gabbiani,

G. *Am. J. Pathol.* **2007**, *170*, 1807–1816.

(25) Rock, J. R.; Barkauskas, C. E.; Cronce, M. J.; Xue, Y.; Harris, J. R.; Liang, J.; Noble, P. W.; Hogan, B. L. M. *Proc. Natl. Acad. Sci. U. S. A.* **2011**, *108*, 1475–1483.

(26) Khalil, N.; O'Connor, R. *Am. J. Respir. Cell Mol. Biol.* **1996**, *14*, 131–138.

(27) Munger, J. S.; Huang, X.; Kawakatsu, H.; Griffiths, M. J. D.; Dalton, S. L.; Wu, J.; Pittet, J.-F.; Kaminski, N.; Garat, C.; Matthay, M. A.; Rifkin, D. B.; Sheppard, D. *Cell* **1999**, *96*, 319–328.

(28) Malhotra, N.; Kang, J. *Immunology* **2013**, *139*, 1–10.

(29) Ishida, W.; Mori, Y.; Lakos, G.; Sun, L.; Shan, F.; Bowes, S.; Josiah, S.; Lee, W.-C.; Singh, J.; Ling, L. E.; Varga, J. *J. Invest. Dermatol.* **2006**, *126*, 1733–1744.

(30) Horan, G.; Wood, S.; Ona, V. *Am. J. Respir. Crit. Care Med* **2008**, *177*, 56–65.

(31) Raghow, R.; Postlethwaite, A. E.; Keski-Oja, J.; Moses, H. L.; Kang, A. H. *J. Clin. Invest.* **1987**, *79*, 1285–1288.

(32) Callahan, J. F.; Burgess, J. L.; Fornwald, J. A.; Gaster, L. M.; Harling, J. D.; Harrington, F. P.; Heer, J.; Kwon, C.; Lehr, R.; Mathur, A.; Olson, B. A.; Weinstock, J.; Laping, N. J. *J. Med. Chem.* **2002**, *45*, 999–1001.

(33) Burgess, H. A.; Daugherty, L. E.; Thatcher, T. H.; Lakatos, H. F.; Ray, D. M.; Redonnet, M.; Phipps, R. P.; Sime, P. J. *Am. J. Physiol. - Lung Cell. Mol. Physiol.* **2005**, *288*, 1146–1153.

(34) Sime, P.; Xing, Z.; Graham, F. *J. Clin. Invest.* **1997**, *100*, 768–776.

(35) Shull, M. M.; Ormsby, I.; Kier, A. B.; Pawlowski, S.; Diebold, R. J.; Yin, M.; Allen, R.; Sidman, C.; Proetzel, G.; Calvin, D.; Annunziata, N.; Doetschman, T. *Nature* **1992**, *359*, 693–699.

(36) Wynn, T. A.; Cheever, A. W.; Malley, J. D.; Donaldson, D. D.; Wynn, T. A. *J. Clin. Invest.* **2007**, *117*, 524–529.

(37) Piguet, P. F. *Am. J. Respir. Crit. Care Med.* **2003**, *167*, 1037–1037.

(38) Gauldie, J. *Am. J. Respir. Crit. Care Med.* **2002**, *165*, 1205–1206.

(39) Sime, P. J.; Xing, Z.; Graham, F. L.; Csaky, K. G.; Gauldie, J. *J. Clin. Invest.* **1997**, *100*, 768–776.

(40) Schultz-Cherry, S.; Murphy-Ullrich, J. *J. Cell Biol.* **1993**, *122*.

(41) Harburger, D. S.; Calderwood, D. A. *J. Cell Sci.* **2009**, *122*, 159–163.

(42) Humphries, J.; Byron, A.; Humphries, M. *J. Cell Sci.* **2006**, *119*, 3901–3903.

(43) Xiao, T.; Takagi, J.; Coller, B.; Wang, J.; Springer, T. *Nature* **2004**, *432*, 59–67.

(44) Xiong, J. P.; Stehle, T.; Zhang, R. *Science.* **2002**, *296*, 151–155.

(45) Xia, W.; Springer, T. A. *Proc. Natl. Acad. Sci. U. S. A.* **2014**, *111*, 17863–17868.

(46) Dong, X.; Hudson, N. E.; Lu, C.; Springer, T. A. *Nat. Struct. Mol. Biol.* **2014**, *21*, 1091–1096.

(47) Chu, F. M.; Picus, J.; Fracasso, P. M.; Dreicer, R.; Lang, Z.; Foster, B. *Invest. New Drugs* **2011**, *29*, 674–679.

(48) Reardon, D.; Neyns, B.; Weller, M.; Tonn, J. *Futur. Med.* **2011**, *7*, 339–354.

(49) Henderson, N.; Sheppard, D. *Biochim. Biophys. Acta - Mol. Basis Dis.* **2013**, *1832*, 891–896.

(50) Breuss, J.; Gallo, J. *J. Cell Sci.* **1995**, *108*, 2241–2251.

(51) Sheppard, D.; Cohen, D. S.; Wang, A.; Busk, M. *J. Biol. Chem.* **1992**, *267*, 17409.

(52) Puthawala, K.; Hadjiangelis, N.; Jacoby, S. C.; Bayongan, E.; Zhao, Z.; Yang, Z.; Devitt, M. L.; Horan, G. S.; Weinreb, P. H.; Lukashev, M. E.; Violette, S. M.; Grant, K. S.; Colarossi, C.; Formenti, S. C.; Munger, J. S. *Am. J. Respir. Crit. Care Med.* **2008**, *177*, 82–90.

(53) Kaminski, N.; Allard, J. D.; Pittet, J. F.; Zuo, F.; Griffiths, M. J.; Morris, D.; Huang,

X.; Sheppard, D.; Heller, R. A. *Proc. Natl. Acad. Sci. U. S. A.* **2000**, *97*, 1778–1783.

(54) Wipff, P.-J.; Hinz, B. *Eur. J. Cell Biol.* **2008**, *87*, 601–615.

(55) Zhang, Z.; Morla, A. O.; Vuori, K.; Bauer, J. S.; Juliano, R. L.; Ruoslahti, E. *J. Cell Biol.* **1993**, *122*, 235–242.

(56) Chang, Y.; Lau, W. L.; Jo, H.; Tsujino, K.; Gewin, L.; Reed, N. I.; Atakilit, A.; Nunes, A. C. F.; DeGrado, W. F.; Sheppard, D. *J. Am. Soc. Nephrol.* **2017**, *28*, 1998–2005.

(57) Reed, N. I.; Jo, H.; Chen, C.; Tsujino, K.; Arnold, T. D.; DeGrado, W. F.; Sheppard, D. *Sci. Transl. Med.* **2015**, *7*, 288ra79.

(58) Wilkinson, A. L.; Barrett, J. W.; Slack, R. J. *Eur. J. Pharmacol.* **2019**, *842*, 239–247.

(59) Hall, E. R.; Bibby, L. I.; Slack, R. J. *Biochem. Pharmacol.* **2016**, *117*, 88–96.

(60) Roper, J. Unpublished Results, GlaxoSmithKline **2018**.

(61) Aryal, S.; Nathan, S. D. *Expert Opin. Emerg. Drugs* **2018**, *23*, 159–172.

(62) Hilberg, F.; Roth, G. J.; Krssak, M.; Kautschitsch, S.; Sommergruber, W.; Tontsch-Grunt, U.; Garin-Chesa, P.; Bader, G.; Zoephel, A.; Quant, J.; Heckel, A.; Rettig, W. J. *Cancer Res.* **2008**, *68*, 4774–4782.

(63) Hisatomi, K.; Mukae, H.; Sakamoto, N.; Ishimatsu, Y.; Kakugawa, T.; Hara, S.; Fujita, H.; Nakamichi, S.; Oku, H.; Urata, Y.; Kubota, H.; Nagata, K.; Kohno, S. *BMC Pulm. Med.* **2012**, *12*, 24.

(64) Oku, H.; Nakazato, H.; Horikawa, T.; Tsuruta, Y.; Suzuki, R. *Eur. J. Pharmacol.* **2002**, *446*, 167–176.

(65) Misra, H. P.; Rabideau, C. *Mol. Cell. Biochem.* **2000**, *204*, 119–126.

(66) BNF: British National Formulary - NICE

https://bnf.nice.org.uk/drug/nintedanib.html (accessed Dec 26, **2018**).

(67) BNF: British National Formulary - NICE https://bnf.nice.org.uk/drug/pirfenidone.html (accessed Dec 26, **2018**).

(68) Allison, M. *Nat. Biotechnol.* **2012**, *30*, 375–376.

(69) An Efficacy and Safety Study of BG00011 in Participants With Idiopathic Pulmonary Fibrosis (SPIRIT) https://clinicaltrials.gov/ct2/show/NCT03573505 (accessed Dec 26, **2018**).

(70) A Clinical Study to Test How Effective and Safe GLPG1690 is for Subjects With Idiopathic Pulmonary Fibrosis (IPF) When Used Together With Standard Medical Treatment https://clinicaltrials.gov/ct2/show/NCT03711162 (accessed Dec 26, **2018**).

(71) Desroy, N.; Housseman, C.; Bock, X.; Joncour, A.; Bienvenu, N.; Cherel, L.; Labeguere, V.; Rondet, E.; Peixoto, C.; Grassot, J.-M.; Picolet, O.; Annoot, D.; Triballeau, N.; Monjardet, A.; Wakselman, E.; Roncoroni, V.; Le Tallec, S.; Blanque, R.; Cottereaux, C.; Vandervoort, N.; Christophe, T.; Mollat, P.; Lamers, M.; Auberval, M.; Hrvacic, B.; Ralic, J.; Oste, L.; van der Aar, E.; Brys, R.; Heckmann, B. *J. Med. Chem.* **2017**, *60*, 3580–3590.

(72) Maher, T. M.; van der Aar, E. M.; Van de Steen, O.; Allamassey, L.; Desrivot, J.; Dupont, S.; Fagard, L.; Ford, P.; Fieuw, A.; Wuyts, W. *Lancet Respir. Med.* **2018**, *6*, 627–635.

(73) Tager, A. M.; LaCamera, P.; Shea, B. S.; Campanella, G. S.; Selman, M.; Zhao, Z.; Polosukhin, V.; Wain, J.; Karimi-Shah, B. A.; Kim, N. D.; Hart, W. K.; Pardo, A.; Blackwell, T. S.; Xu, Y.; Chun, J.; Luster, A. D. *Nat. Med.* **2008**, *14*, 45–54.

(74) Xu, M. Y.; Porte, J.; Knox, A. J.; Weinreb, P. H.; Maher, T. M.; Violette, S. M.; McAnulty, R. J.; Sheppard, D.; Jenkins, G. *Am. J. Pathol.* **2009**, *174*, 1264–1279.

(75) Webster, A. C.; Lee, V. W. S.; Chapman, J. R.; Craig, J. C. *Transplantation* **2006**,

81, 1234–1248.

(76) Mercer, P. F.; Woodcock, H. V; Eley, J. D.; Platé, M.; Sulikowski, M. G.; Durrenberger, P. F.; Franklin, L.; Nanthakumar, C. B.; Man, Y.; Genovese, F.; McAnulty, R. J.; Yang, S.; Maher, T. M.; Nicholson, A. G.; Blanchard, A. D.; Marshall, R. P.; Lukey, P. T.; Chambers, R. C. *Thorax* **2016**, *71*, 701–711.

(77) Double-blind Placebo-controlled Pilot Study of Sirolimus in Idiopathic Pulmonary Fibrosis (IPF) https://clinicaltrials.gov/ct2/show/NCT01462006 (accessed Dec 26, **2018**).

(78) Bravi, G.; Hobbs, H.; Inglis, G. G. A.; Nicolle, S.; Peace, S. WO 2019115640A1, **2019**.

(79) Hobbs, H.; Bravi, G.; Campbell, I.; Convery, M.; Davies, H.; Inglis, G.; Pal, S.; Peace, S.; Redmond, J.; Summers, D. *J. Med. Chem.* **2019**, *62*, 6972–6984.

(80) Proof of Mechanism Study With GSK2126458 in Patients With Idiopathic Pulmonary Fibrosis (IPF) https://clinicaltrials.gov/ct2/show/NCT01725139 (accessed Aug 12, **2019**).

(81) CleanUP IPF for the Pulmonary Trials Cooperative (CleanUp-IPF) https://clinicaltrials.gov/ct2/show/NCT02759120 (accessed Aug 12, **2019**).

(82) Allen, J. T.; Knight, R. A.; Bloor, C. A.; Spiteri, M. A. *Am. J. Respir. Cell Mol. Biol.* **1999**, *21*, 693–700.

(83) Evaluate the Safety and Efficacy of FG-3019 in Patients With Idiopathic Pulmonary Fibrosis https://clinicaltrials.gov/ct2/show/NCT01890265 (accessed Aug 12, **2019**).

(84) Hinz, B. *Proc. Am. Thorac. Soc.* **2012**, *9*, 137–147.

(85) Study to Assess the Efficacy and Safety of Simtuzumab (GS-6624) in Adults With Idiopathic Pulmonary Fibrosis (IPF) (RAINIER) https://clinicaltrials.gov/ct2/show/NCT01769196 (accessed Aug 12, **2019**).

(86) Anderson, N. A.; Fallon, B. J.; Pritchard, J. M. WO2014154725, **2016**.

(87) Procopiou, P. A.; Anderson, N. A.; Barrett, J.; Barrett, T. N.; Crawford, M. H. J.; Fallon, B. J.; Hancock, A. P.; Le, J.; Lemma, S.; Marshall, R. P.; Morrell, J.; Pritchard, J. M.; Rowedder, J. E.; Saklatvala, P.; Slack, R. J.; Sollis, S. L.; Suckling, C. J.; Thorp, L. R.; Vitulli, G.; Macdonald, S. J. F. *J. Med. Chem.* **2018**, *61*, 8417–8443.

(88) Anderson, N. A.; Campbell, I. B.; Fallon, B. J.; Lynn, S. M.; Macdonald, S. J. F.; Pritchard, J. M.; Procopiou, P. A.; Sollis, S. L.; Thorp, L. R. *Org. Biomol. Chem.* **2016**, *14*, 5992–6009.

(89) Single Doses of GSK3008348 in Idiopathic Pulmonary Fibrosis (IPF) Participants Using Positron Emission Tomography (PET) Imaging https://clinicaltrials.gov/ct2/show/NCT03069989 (accessed Jan 3, **2019**).

(90) Anderson, N. A.; Campbell-Crawford, M. H. J.; Hancock, A. P.; Pritchard, J. M.; Redmond, J. M. WO2016046225, **2016**.

(91) Goodman, S. L.; Picard, M. *Trends Pharmacol. Sci.* **2012**, *33*, 405–412.

(92) Adams, J.; Anderson, E. C.; Blackham, E. E.; Chiu, Y. W. R.; Clarke, T.; Eccles, N.; Gill, L. A.; Haye, J. J.; Haywood, H. T.; Hoenig, C. R.; Kausas, M.; Le, J.; Russell, H. L.; Smedley, C.; Tipping, W. J.; Tongue, T.; Wood, C. C.; Yeung, J.; Rowedder, J. E.; Fray, M. J.; McInally, T.; Macdonald, S. J. F. *ACS Med. Chem. Lett.* **2014**, *5*, 1207–1212.

(93) Kell, D. B.; Dobson, P. D.; Oliver, S. G. *Drug Discov. Today* **2011**, *16*, 704–714.

(94) Mälkiä, A.; Murtomäki, L.; Urtti, A.; Kontturi, K. *Eur. J. Pharm. Sci.* **2004**, *23*, 13–47.

(95) Pagliara, A.; Carrupt, P. A.; Caron, G.; Gaillard, P.; Testa, B. *Chem. Rev.* **1997**, *97*, 3385.

(96) Evans, D. F.; Pye, G.; Bramley, R.; Clark, A. G.; Dyson, T. J.; Hardcastle, J. D. *Gut*

1988, *29*, 1035–1041.

(97) Fallingborg, J. *Dan. Med. Bull.* **1999**, *46*, 183–196.

(98) Guimarães, C. R. W.; Mathiowetz, A. M.; Shalaeva, M.; Goetz, G.; Liras, S. *J. Chem. Inf. Model.* **2012**, *52*, 882–890.

(99) Shultz, M. D. *J. Med. Chem.* **2019**, *62*, 1701–1714.

(100) Naylor, M. R.; Ly, A. M.; Handford, M. J.; Ramos, D. P.; Pye, C. R.; Furukawa, A.; Klein, V. G.; Noland, R. P.; Edmondson, Q.; Turmon, A. C.; Hewitt, W. M.; Schwochert, J.; Townsend, C. E.; Kelly, C. N.; Blanco, M.-J.; Lokey, R. S. *J. Med. Chem.* **2018**, *61*, 11169–11182.

(101) Lipinski, C. A.; Lombardo, F.; Dominy, B. W.; Feeney, P. J. *Adv. Drug Deliv. Rev.* **2001**, *46*, 3–26.

(102) Veber, D. F.; Johnson, S. R.; Cheng, H.-Y.; Smith, B. R.; Ward, K. W.; Kopple, K. D. *J. Med. Chem.* **2002**, *45*, 2615–2623.

(103) Matsson, P.; Doak, B. C.; Over, B.; Kihlberg, J. *Adv. Drug Deliv. Rev.* **2016**, *101*, 42–61.

(104) Giordanetto, F.; Kihlberg, J. *J. Med. Chem.* **2014**, *57*, 278–295.

(105) Whitty, A.; Zhong, M.; Viarengo, L.; Beglov, D.; Hall, D. R.; Vajda, S. *Drug Discov. Today* **2016**, *21*, 712–717.

(106) Matsson, P.; Kihlberg, J. *J. Med. Chem.* **2017**, *60*, 1662–1664.

(107) Rossi Sebastiano, M.; Doak, B. C.; Backlund, M.; Poongavanam, V.; Over, B.; Ermondi, G.; Caron, G.; Matsson, P.; Kihlberg, J. *J. Med. Chem.* **2018**, *61*, 4189–4202.

(108) Rezai, T.; Bock, J. E.; Zhou, M. V.; Kalyanaraman, C.; Lokey, R. S.; Jacobson, M. P. *J. Am. Chem. Soc.* **2006**, *128*, 14073.

(109) Caron, G.; Ermondi, G. *Future Med. Chem.* **2017**, *9*, 1–5.

(110) Witek, J.; Keller, B. G.; Blatter, M.; Meissner, A.; Wagner, T.; Riniker, S. *J. Chem. Inf. Model.* **2016**, *56*, 1547–1562.

(111) Carrupt, P.-A.; Testa, B.; Bechalany, A.; El Tayar, N.; Descas, P.; Perrissoud, D. *J. Med. Chem.* **1991**, *34*, 1272–1275.

(112) Caron, G.; Vallaro, M.; Ermondi, G. *Medchemcomm* **2017**, *8*, 1143–1151.

(113) Over, B.; McCarren, P.; Artursson, P.; Foley, M.; Giordanetto, F.; Grönberg, G.; Hilgendorf, C.; Lee, M. D.; Matsson, P.; Muncipinto, G.; Pellisson, M.; Perry, M. W. D.; Svensson, R.; Duvall, J. R.; Kihlberg, J. *J. Med. Chem.* **2014**, *57*, 2746–2754.

(114) Tyagi, M.; Poongavanam, V.; Lindhagen, M.; Pettersen, A.; Sjö, P.; Schiesser, S.; Kihlberg, J. *Org. Lett.* **2018**, *20*, 5737–5742.

(115) Pritchard, J. M.; Hancock, A. P.; Procopiou, P. A.; Macdonald, S. J. F. Unpublished Results, GlaxoSmithKline, **2014**.

(116) Johnson, T. Unpublished Results, GlaxoSmithKline, **2016**.

(117) Barrett, J. W. Unpublished Results, GlaxoSmithKline, **2015**.

(118) Johnson, T. Unpublished Results, GlaxoSmithKline, **2019**.

(119) Sakai, M.; Hayashi, H.; Miyaura, N. *Organometallics* **1997**, *16*, 4229–4231.

(120) Hayashi, T.; Yamasaki, K. *Chem. Rev.* **2003**, *103*, 2829–2844.

(121) Beeson, T. D.; MacMillan, D. W. C. *J. Am. Chem. Soc.* **2005**, *127*, 8826–8828.

(122) Dormer, P. G.; Eng, K. K.; Farr, R. N.; Humphrey, G. R.; McWilliams, J. C.; Reider, P. J.; Sager, J. W.; Volante, R. P. *J. Org. Chem.* **2003**, *68*, 467–477.

(123) Marco-Contelles, J.; Pérez-Mayoral, E.; Samadi, A.; Carreiras, M. do C.; Soriano, E. *Chem. Rev.* **2009**, *109*, 2652–2671.

(124) Goodreid, J. D.; Duspara, P. A.; Bosch, C.; Batey, R. A. *J. Org. Chem.* **2014**, *79*,

943–954.

(125) Sollis, S. L. Unpublished Results, GlaxoSmithKline, **2015**.

(126) Briggs, C. R. S.; Allen, M. J.; O'Hagan, D.; Tozer, D. J.; Slawin, A. M. Z.; Goeta, A. E.; Howard, J. A. K. *Org. Biomol. Chem.* **2004**, *2*, 732–740.

(127) Zajac, M. A. *J. Org. Chem.* **2008**, *73*, 6899–6901.

(128) Anderson, N. J.; Fallon, B. J.; Valverde, E.; MacDonald, S. J. F.; Pritchard, J. M.; Suckling, C. J.; Watson, A. J. B. *Synlett* **2012**, *23*, 2817–2821.

(129) Hindley, S.; Hortense, E. Unpublished Results, GlaxoSmithKline, **2016**.

(130) Thompson, J. Unpublished Results, GlaxoSmithKline, **2016**.

(131) Jia, X.; Huang, Q.; Li, J.; Li, S.; Yang, Q. *Synlett* **2007**, 806–808.

(132) Lampe, J. W.; Chou, Y. L.; Hanna, R. G.; Di Meo, S. V.; Erhardt, P. W.; Hagedorn, A. A.; Ingebretsen, W. R.; Cantor, E. *J. Med. Chem.* **1993**, *36*, 1041–1047.

(133) Meyer, S. D.; Schreiber, S. L. *J. Org. Chem.* **1994**, *59*, 7549–7552.

(134) Fadeyi, O. O.; Lindsley, C. W. *Org. Lett.* **2009**, *11*, 943–946.

(135) Thompson, J. Unpublished Results, GlaxoSmithKline, **2017**.

(136) Olofson, R. A.; Martz, J. T.; Senet, J. P.; Piteau, M.; Malfroot, T. *J. Org. Chem.* **1984**, *49*, 2081–2082.

(137) Sollis, S. L. Unpublished Results, GlaxoSmithKline, **2015**.

(138) Alex, A.; Millan, D. S.; Perez, M.; Wakenhut, F.; Whitlock, G. A. *Medchemcomm* **2011**, *2*, 669.

(139) Sterbenz, J. Unpublished Results, GlaxoSmithKline, **2015**.

(140) Koehorst, R. B. M.; Spruijt, R. B.; Vergeldt, F. J.; Hemminga, M. A. *Biophys. J.* **2004**, *87*, 1445–1455.

(141) Upton, R. Unpublished Results, GlaxoSmithKline, **2017**.

(142) Appavoo, S. D.; Kaji, T.; Frost, J. R.; Scully, C. C. G.; Yudin, A. K. *J. Am. Chem. Soc.* **2018**, *140*, 8763–8770.

(143) Wishart, D. S.; Sykes, B. D.; Richards, F. M. *Biochemistry* **1992**, *31*, 1647–1651.

(144) Marek, R.; Lycka, A. *Curr. Org. Chem.* **2002**, *6*, 35–66.

(145) Semenov, V. A.; Samultsev, D. O.; Krivdin, L. B. *Magn. Reson. Chem.* **2015**, *53*, 433–441.

(146) Duthaler, R. O.; Roberts, J. D. *J. Am. Chem. Soc.* **1978**, *100*, 4969–4973.

(147) Levy, G. C.; Lichter, R. L. Wiley: New York, **1979**.

(148) Cai, Z.-L.; Reimers, J. R. *J. Phys. Chem* **2000**, *104*, 8389–8408.

(149) Richards, S. A.; Hollerton, J. C. Wiley-Blackwell: New Jersey, **2010**.

(150) Richards, S. A. Unpublished Results, GlaxoSmithKline, **2018**.

(151) Gray, H.; Barrett, T. N.; Hancock, A. P.; Macdonald, S. J. F.; Pritchard, J. M.; Hatley, R. J. D. Unpublished Results, GlaxoSmithKline, **2017**.

(152) Gray, H. Unpublished Results, GlaxoSmithKline, **2018**.

(153) He, Y. Unpublished Results, GlaxoSmithKline, **2017**.

(154) Copley, R. Unpublished Results, GlaxoSmithKline, **2015**.

(155) Chen, I.-J.; Foloppe, N. *Bioorg. Med. Chem.* **2013**, *21*, 7898–7920.

(156) Over, B.; Matsson, P.; Tyrchan, C.; Artursson, P.; Doak, B. C.; Foley, M. A.; Hilgendorf, C.; Johnston, S. E.; Lee, M. D.; Lewis, R. J.; McCarren, P.; Muncipinto, G.; Norinder, U.; Perry, M. W. D.; Duvall, J. R.; Kihlberg, J. *Nat. Chem. Biol.* **2016**, *12*, 1065–1074.

(157) Binkley, J. S.; Pople, J. A.; Hehre, W. J. *J. Am. Chem. Soc.* **1979**, *102*, 939–947.

(158) Hariharan, P. C.; Pople, J. A. *Theor. Chim. Acta* **1973**, *28*, 213–222.

(159) Francl, M. M.; Pietro, W. J.; Hehre, W. J.; Binkley, J. S.; Gordon, M. S.; DeFrees, D. J.; Pople, J. A. *J. Chem. Phys.* **1982**, *77*, 3654–3665.

(160) Lee, C.; Yang, W.; Parr, R. G. *Phys. Rev. B* **1988**, *37*, 785–789.

(161) Becke, A. D. *J. Chem. Phys.* **1993**, *98*, 5648–5652.

(162) Grimme, S.; Antony, J.; Ehrlich, S.; Krieg, H. *J. Chem. Phys.* **2010**, *132*, 154104.

(163) MacroModel, Schrödinger, LLC; Schrödinger Release 2018-1, New York, NY **2018**.

(164) Jaguar, Schrödinger, LLC; Schrödinger Release 2018-1: New York, NY **2018**.

(165) Molecular Operating Environment (MOE) https://www.chemcomp.com (accessed Feb 17, **2019**).

(166) Nadin, A. Unpublished Results, GlaxoSmithKline, **2018**.

(167) Gillis, E. P.; Eastman, K. J.; Hill, M. D.; Donnelly, D. J.; Meanwell, N. A. *J. Med. Chem.* **2015**, *58*, 8315–8359.

(168) Spitznagel, G. W.; Clark, T.; von Ragué Schleyer, P.; Hehre, W. J. *J. Comput. Chem.* **1987**, *8*, 1109–1116.

(169) Hehre, W. J. Wavefunction, Inc., Irvine, California, **2003**.

(170) Papajak, E.; Zheng, J.; Xu, X.; Leverentz, H. R.; Truhlar, D. G. *J. Chem. Theory Comput.* **2011**, *7*, 3027–3034.

(171) Shalaeva, M.; Caron, G.; Abramov, Y. A.; O'Connell, T. N.; Plummer, M. S.; Yalamanchi, G.; Farley, K. A.; Goetz, G. H.; Philippe, L.; Shapiro, M. J. *J. Med. Chem.* **2013**, *56*, 4870–4879.

(172) Caron, G.; Vallaro, M.; Ermondi, G. *Drug Discov. Today. Technol.* **2018**, *27*, 65–70.

(173) Sirius T3 https://pion-inc.com/physchem-analysis/logp/siriust3/ (accessed Sep 23, **2019**).

(174) Young, R. J.; Green, D. V. S.; Luscombe, C. N.; Hill, A. P. *Drug Discov. Today* **2011**, *16*, 822–830.

(175) Miller, D. H.; Khan, O. A.; Sheremata, W. A.; Blumhardt, L. D.; Rice, G. P. A.; Libonati, M. A.; Willmer-Hulme, A. J.; Dalton, C. M.; Miszkiel, K. A.; O'Connor, P. W. *N. Engl. J. Med.* **2003**, *348*, 15–23.

(176) Miller, W. H.; Alberts, D. P.; Bhatnagar, P. K.; Bondinell, W. E.; Callahan, J. F.; Calvo, R. R.; Cousins, R. D.; Erhard, K. F.; Heerding, D. A.; Keenan, R. M.; Kwon, C.; Manley, P. J.; Newlander, K. A.; Ross, S. T.; Samanen, J. M.; Uzinskas, I. N.; Venslavsky, J. W.; Yuan, C. C.-K.; Haltiwanger, R. C.; Gowen, M.; Hwang, S.-M.; James, I. E.; Lark, M. W.; Rieman, D. J.; Stroup, G. B.; Azzarano, L. M.; Salyers, K. L.; Smith, B. R.; Ward, K. W.; Johanson, K. O.; Huffman, W. F. *J. Med. Chem.* **2000**, *43*, 22–26.

(177) Keenan, R. M.; Miller, W. H.; Kwon, C.; Ali, F. E.; Callahan, J. F.; Calvo, R. R.; Hwang, S.-M.; Kopple, K. D.; Peishoff, C. E.; Samanen, J. M.; Wong, A. S.; Chuan-Kui Yuan; Huffman, W. F. *J. Med. Chem.* **1997**, *40*, 2289–2292.

(178) Miller, W. H.; Ali, F. E.; Bondinell, W. E.; Callahan, J. F.; Calvo, R. R.; Drake, S.; Haltiwanger, R. C.; Huffman, W. F.; Hwang, S.; Jakas, D. R.; Richard, M.; Koster, P. F.; Ku, T. W.; Kwon, C.; Newlander, K. A.; Nichols, A. J.; Parker, F.; Samanen, J. M.; Southall, L. S.; Takata, D. T.; Uzinskas, I. N.; Richard, E.; Vasko-moser, J. A.; Wong, A. S.; Yellin, T. O.; Yuan, C. C. K. *Bioorg. Med. Chem. Lett.* **1996**, *6*, 2481–2486.

(179) Keenan, R. M.; Miller, W. H.; Lago, M. A.; Ali, F. E.; Bondinell, W. E.; Callahan, J. F.; Calvo, R. R.; Cousins, R. D.; Hwang, S.-M.; Jakas, D. R.; Ku, T. W.; Kwon, C.; Nguyen, T. T.; Reader, V. A.; Rieman, D. J.; Ross, S. T.; Takata, D. T.; Uzinskas, I. N.; Yuan, C. C. K.; Smith, B. R. *Bioorg. Med. Chem. Lett.* **1998**, *8*, 3165–3170.

(180) Keenan, R. M.; Miller, W. H.; Barton, L. S.; Bondinell, W. E.; Cousins, R. D.; Eppley, D. F.; Hwang, S.-M.; Kwon, C.; Lago, M. A.; Nguyen, T. T.; Smith, B. R.; Uzinskas, I. N.; Yuan, C. C. K. *Bioorg. Med. Chem. Lett.* **1999**, *9*, 1801–1806.

(181) Barrett, J. W. Unpublished Results, GlaxoSmithKline, **2019**.

(182) Johnson, T. W.; Gallego, R. A.; Edwards, M. P. *J. Med. Chem.* **2018**, *61*, 6401–6420.

(183) Smith, D. A.; Beaumont, K.; Maurer, T. S.; Di, L. *J. Med. Chem.* **2018**, *61*, 4273–4282.

(184) Rehm, S.; Thomas, R. A.; Smith, K. S.; Mirabile, R. C.; Gales, T. L.; Eustis, S. L.; Boyce, R. W. *Toxicol. Pathol.* **2007**, *35*, 958–971.

(185) Blake, S. Unpublished Results, GlaxoSmithKline, **2003**.

(186) Brigandi, R. Unpublished Results, GlaxoSmithKline, **2007**.

(187) Dieck, H. A.; Heck, R. F. *J. Am. Chem. Soc.* **1974**, *96*, 1133–1136.

(188) Mitsunobu, O.; Yamada, M. *Bull. Chem. Soc. Jpn.* **1967**, *40*, 2380–2382.

(189) Wallace, M. D.; McGuire, M. A.; Yu, M. S.; Goldfinger, L.; Liu, L.; Dai, W.; Shilcrat, S. *Org. Proc. Res. Dev.* **2004**, *8*, 738−743.

(190) Hatley, R. J. D. Unpublished Results, GlaxoSmithKline, **2017**.

(191) Taylor, J. A. Unpublished Results, GlaxoSmithKline, **2016**.

(192) Barrett, J. W.; Hogg, M. Unpublished Results, GlaxoSmithKline, **2017**.

(193) Bondinell, W. E.; Miller, W. H. US1999006008213A, **1999**.

(194) Bondinell, W. E.; Callahan, J. F.; Human, W. F.; Ku, T. .-F.; Newlander, K. A. US5693636A, **1997**.

(195) Heerding, D.; Samanen, J. M. US20020055499A1, **2002**.

(196) Ali, F. E.; Bondinell, W.; Huffman, W. F.; Lago, M. A.; Keenan, R. M.; Kwon, C.;

Miller, W. T.; Nguyen, T.; Takata, D. T. US19995977101A, **1999**.

(197) Bondinell, W. E. US2002/0019387 A1, **2002**.

(198) Heerding, D. US2001/0014737 A1, **2001**.

(199) Callahan, J. F.; Cousins, R. D.; Keenan, R. M.; Kwon, C.; Miller, W. H.; Uzinskas, I. N. US2003/0125317 A1, **2003**.

(200) Askew, B. C. US6232308B1, **2001**.

(201) Suzuki, N.; Tsuzaki, Y.; Yoshimura, K.; Hagihara, M.; Wada, Y.; Maruyama, M.; Fujii, N.; Aga, Y. US 2010/0249396 A1, **2010**.

(202) Hatley, R. J. D.; Barrett, T. N.; Slack, R. J.; Watson, M. E.; Baillache, D. J.; Gruszka, A.; Washio, Y.; Rowedder, J. E.; Pogány, P.; Pal, S.; Macdonald, S. J. F. *ChemMedChem* **2019**, *14*, 1315–1320.

(203) Nagae, M.; Re, S.; Mihara, E.; Nogi, T.; Sugita, Y.; Takagi, J. *J. Cell Biol.* **2012**, *197*, 131–140.

(204) Glide, Schrödinger, LLC; Schrödinger Release 2018-3, New York, NY **2018**.

(205) Williams, A. Unpublished Results, GlaxoSmithKline, **2015**.

(206) Taylor, J. A.; Thorp, L. R.; Chan, K.; Pritchard, J. M. Unpublished Results, GlaxoSmithKline, **2017**.

(207) Taylor, J. A. Unpublished Results, GlaxoSmithKline, **2017**.

(208) Allinger, N. L.; Burkert, U.; Profeta, S. *J. Comput. Chem.* **1980**, *1*, 281–284.

(209) Mogul https://www.ccdc.cam.ac.uk/solutions/csd-system/components/mogul/ (accessed Aug 29, **2019**).

(210) Kilbourn, R. *Nucl. Med. Biol.* **1989**, *16*, 681–686.

(211) Seefeld, M. A.; Rouse, M. B.; McNulty, K. C.; Sun, L.; Wang, J.; Yamashita, D. S.; Luengo, J. I.; Zhang, S.; Minthorn, E. A.; Concha, N. O.; Heerding, D. A. *Bioorg.*

Med. Chem. Lett. **2009**, *19*, 2244–2248.

(212) Stavber, G.; Časar, Z. *Appl. Organomet. Chem.* **2013**, *27*, 159–165.

(213) Cannon, R. J.; Curto, N. L.; Esposito, C. M.; Payne, R. K.; Janczuk, A. J.; Agyemang, D. O.; Cai, T.; Tang, X.-Q.; Chen, M. Z. *J. Agric. Food Chem.* **2017**, *65*, 5690–5699.

(214) Milne, J. E.; Buchwald, S. L. *J. Am. Chem. Soc.* **2004**, *126*, 13028–13032.

(215) Barder, T. E.; Walker, S. D.; Martinelli, J. R.; Buchwald, S. L. *J. Am. Chem. Soc.* **2005**, *127*, 4685–4696.

(216) Du, K.; Guo, P.; Chen, Y.; Cao, Z.; Wang, Z.; Tang, W. *Angew. Chem. Int. Ed.* **2015**, *54*, 3033–3037.

(217) Molander, G. A.; Sandrock, D. L. *Curr. Opin. Drug Discov. Devel.* **2009**, *12*, 811–823.

(218) Lennox, A. J. J.; Lloyd-Jones, G. C. *Angew. Chemie Int. Ed.* **2012**, *51*, 9385–9388.

(219) Bruno, N. C.; Buchwald, S. L. *Org. Lett.* **2013**, *15*, 2876–2879.

(220) Cambridge Crystallographic Database https://www.ccdc.cam.ac.uk/ (accessed May 17, **2019**).

(221) Miyaura, N.; Suzuki, A. *J. Chem. Soc., Chem. Commun.* **1979**, No. 19, 866.

(222) Sonogashira, K. *J. Organomet. Chem.* **2002**, *653*, 46–49.

(223) Seyferth, D.; Marmor, R. S.; Hilbert, P. *J. Org. Chem.* **1971**, *36*, 1379–1386.

(224) Gilbert, J. C.; Weerasooriya, U. *J. Org. Chem.* **1982**, *47*, 1837–1845.

(225) Koga, Y.; Maeno, K.; Sato, I.; Imamura, Y.; Hanazawa, T.; Iida, M.; Ohne, K.; Imamura, K.; Watanabe, T.; Nozawa, E.; Shibata, H. US201488080 A1, **2013**.

(226) Jeffery, T. *J. Chem. Soc., Chem. Comm.* **1984**, 1287–1289.

(227) Muller, S.; Liepold, B.; Roth, G. J.; Bestmann, H. J. *Synlett* **1996**, 521–522.

(228) Wu, X.; Fors, B. P.; Buchwald, S. L. *Angew. Chem. Int. Ed.* **2011**, *50*, 9943–9947.

(229) Lu, S.-C.; Li, H.-S.; Gong, Y.-L.; Zhang, S.-P.; Zhang, J.-G.; Xu, S. *J. Org. Chem.* **2018**, *83*, 15415–15425.

(230) Bulatov, T. M.; Pugachev, M. V.; Shtyrlin, N. V.; Shtyrlin, Y. G. *Tetrahedron Lett.* **2018**, *59*, 3220–3222.

(231) Tsunoda, T.; Ozaki, F.; Itô, S. *Tetrahedron Lett.* **1994**, *35*, 5081–5082.

(232) Harris, C. S.; Germain, H.; Pasquet, G. *Tetrahedron Lett.* **2008**, *49*, 5946–5949.

(233) Lippa, R. Unpublished Results, GlaxoSmithKline, **2017**.

(234) Davis, F. A.; Lamendola, J.; Nadir, U.; Kluger, E. W.; Sedergran, T. C.; Panunto, T. W.; Billmers, R.; Jenkins, R.; Turchi, I. J.; Watson, W. H.; Chen, J. S.; Kimura, M. *J. Am. Chem. Soc.* **1980**, *102*, 2000–2005.

(235) Hobbs, A. Unpublished Results, GlaxoSmithKline, **2019**.

(236) Wang, L.; Chen, H.; Duan, Z. *Chem. – An Asian J.* **2018**, *13*, 2164–2173.

(237) Kano, S.; Yuasa, Y.; Yokomatsu, T.; Shibuya, S. *Synthesis (Stuttg).* **1983**, 585–587.

(238) Pal, S. Unpublished Results, GlaxoSmithKline, **2018**.

(239) De Vivo, M.; Masetti, M.; Bottegoni, G.; Cavalli, A. *J. Med. Chem.* **2016**, *59*, 4035–4061.

(240) Fulmer, G. R.; Miller, A. J. M.; Sherden, N. H.; Gottlieb, H. E.; Nudelman, A.; Stoltz, B. M.; Bercaw, J. E.; Goldberg, K. I. *Organometallics* **2010**, *29*, 2176–2179.

(241) Tipping, W. J.; Tshuma, N.; Adams, J.; Haywood, H. T.; Rowedder, J. E.; Fray, M. J.; McInally, T.; Macdonald, S. J. F.; Oldham, N. J. *ACS Med. Chem. Lett.* **2015**, *6*, 221–224.

(242) Byrne, P. A.; Gilheany, D. G. *J. Am. Chem. Soc.* **2012**, *134*, 9225–9239.

(243) Sollis, S. L. Unpublished Results, GlaxoSmithKline, **2016**.

(244) Manley, P. J.; Miller, W. H.; Uzinskas, I. N. EP1218005 A2, **2002**.

(245) Penning, T. D.; Khilevich, A.; Chen, B. B.; Gandhi, P.; Wang, Y.; Downs, V.; Boys, M. L.; Russell, M.; Spangler, D. P.; Huff, R. M. WO2004058761 A1, **2004**.

(246) Leonard, K.; Pan, W.; Anaclerio, B.; Gushue, J. M.; Guo, Z.; DesJarlais, R. L.; Chaikin, M. A.; Lattanze, J.; Crysler, C.; Manthey, C. L.; Tomczuk, B. E.; Marugan, J. J. *Bioorg. Med. Chem. Lett.* **2005**, *15*, 2679–2684.

(247) Cookson, R. Unpublished Results, GlaxoSmithKline, **2018**.

(248) Barnett, H. Unpublished Results, GlaxoSmithKline, **2016**.

(249) Campbell-Crawford, M. H. J. Unpublished Results, GlaxoSmithKline, **2013**.

(250) Fallon, B. J. Unpublished Results, GlaxoSmithKline, **2012**.

(251) Hounslea, E. Unpublished Results, GlaxoSmithKline, **2016**.

(252) Tame, C. Unpublished Results, GlaxoSmithKline, **2013**.

(253) Redmond, J. M. Unpublished Results, GlaxoSmithKline, **2011**.

(254) Anderson, N. A. Unpublished Results, GlaxoSmithKline, **2012**.

(255) Wellaway, N. Unpublished Results, GlaxoSmithKline, **2012**.

(256) Fallon, B. J. Unpublished Results, GlaxoSmithKline, **2011**.

(257) Sollis, S. L. Unpublished Results, GlaxoSmithKline, **2014**.

(258) Smart, L. Unpublished Results, GlaxoSmithKline, **2013**.

(259) LigPrep, Schrödinger, LLC; Schrödinger Release 2018-1, New York, NY **2018**.

(260) Harder, E.; Damm, W.; Maple, J.; Wu, C.; Reboul, M.; Xiang, J. Y.; Wang, L.; Lupyan, D.; Dahlgren, M. K.; Knight, J. L.; Kaus, J. W.; Cerutti, D. S.; Krilov, G.;

Jorgensen, W. L.; Abel, R.; Friesner, R. A. *J. Chem. Theory Comput.* **2016**, *12*, 281–296.

(261) Qiu, D.; Shenkin, P. S.; Hollinger, F. P.; Still, W. C. *J. Phys. Chem.* **1997**, *101*, 3005–3014.

(262) Kelley, L. A.; Gardner, S. P.; Sutcliffe, M. J. *Protein Eng. Des. Sel.* **1996**, *9*, 1063–1065.

(263) Bochevarov, A. D.; Harder, E.; Hughes, T. F.; Greenwood, J. R.; Braden, D. A.; Philipp, D. M.; Rinaldo, D.; Halls, M. D.; Zhang, J.; Friesner, R. A. *Int. J. Quantum Chem.* **2013**, *113*, 2110–2142.

(264) Elstner, M.; Hobza, P.; Frauenheim, T.; Suhai, S.; Kaxiras, E. *J. Chem. Phys.* **2001**, *114*, 5149–5155.

(265) Cortis, C. M.; Langlois, J.; Beachy, M. D.; Friesner, R. A. *J. Chem. Phys.* **1998**, *105*, 5472.

(266) Jurcak, J. G.; Barrague, M.; Gillespy, T. A.; Edwards, M. L.; Musick, K. Y.; Weintraub, P. M.; Du, Y.; Dharanipragada, R. M.; Parkar, A. A. WO2005026175 A1, **2005**.

(267) Doušová, H.; Růžičková, Z.; Šimůnek, P. *J. Heterocycl. Chem.* **2018**, *55*, 670–684.

(268) Petroski, R. *Synth. Commun.* **2002**, *32*, 449–455.

(269) Levine, D. R.; Siegler, M. A.; Tovar, J. D. *J. Am. Chem. Soc.* **2014**, *136*, 7132–7139.

(270) Ewbank, P. C.; Nuding, G.; Suenaga, H.; McCullough, R. D.; Shinkai, S. *Tetrahedron Lett.* **2001**, *42*, 155–157.

(271) Jiang, L.; Morgans, D. J.; Bergne, G.; Chen, C.; Li, H.; Andre, P.; Halcomb, R. L.; Cha, J.; Hom, T. WO201849068 A1, **2018**.

(272) Luliński, S.; Serwatowski, J.; Szczerbińska, M. *Eur. J. Org. Chem.* **2008**, 1797–

1801.

(273) Kansy, M.; Senner, F.; Gubernator, K. *J. Med. Chem.* **1998**, *41*, 1007–1010.

(274) Reid, I. Unpublished Results, GlaxoSmithKline, **2017**.

(275) Yasuda, M. *Bull. Chem. Soc. Jpn.* **1959**, *32*, 429–432.

(276) Dyrssen, D. *Sven. Kem. Tidskr.* **1952**, *64*, 213–224.

(277) Valkó, K.; Bevan, C.; Reynolds, D. *Anal. Chem.* **1997**, *69*, 2022–2029.

(278) Gordon, L. J.; Allen, M.; Artursson, P.; Hann, M. M.; Leavens, B. J.; Mateus, A.; Readshaw, S.; Valko, K.; Wayne, G. J.; West, A. *J. Biomol. Screen.* **2016**, *21*, 156–164.

(279) Williamson, A. *London, Edinburgh, Dublin Philos. Mag. J. Sci.* **1850**, *37*, 350–356.